



Étude de la variation de la direction et de l'intensité du champ géomagnétique en Espagne durant les deux derniers millénaires

Miriam Gomez Paccard

► To cite this version:

Miriam Gomez Paccard. Étude de la variation de la direction et de l'intensité du champ géomagnétique en Espagne durant les deux derniers millénaires. Géologie appliquée. Université Rennes 1, 2006. Français. NNT : . tel-00130481

HAL Id: tel-00130481

<https://theses.hal.science/tel-00130481>

Submitted on 12 Feb 2007

HAL is a multi-disciplinary open access archive for the deposit and dissemination of scientific research documents, whether they are published or not. The documents may come from teaching and research institutions in France or abroad, or from public or private research centers.

L'archive ouverte pluridisciplinaire **HAL**, est destinée au dépôt et à la diffusion de documents scientifiques de niveau recherche, publiés ou non, émanant des établissements d'enseignement et de recherche français ou étrangers, des laboratoires publics ou privés.

N° Ordre : 3350

THÈSE

présentée

DEVANT L'UNIVERSITÉ DE RENNES 1 et L'UNIVERSITÉ COMPLUTENSE DE MADRID

pour obtenir

le grade de : ***DOCTEUR DE L'UNIVERSITÉ DE RENNES 1 et
DE L'UNIVERSITÉ COMPLUTENSE DE MADRID***

Mention Sciences de la Terre

Par

Miriam Gómez Paccard

Équipe d'accueil : Géosciences Rennes, Université de Rennes 1
Facultad de Ciencias Físicas, Universidad Complutense de
Madrid

École doctorale : Sciences de la matière

Composante universitaire : UFR Structure et Propriétés de la matière

Titre de la thèse :

**Étude de la variation de la direction et de l'intensité du
champ géomagnétique en Espagne durant les deux
derniers millénaires**

Soutenue le 10 Mars devant la commission d'examen composée de :

COMPOSITION DU JURY

Yves Gallet	Rapporteur
Gregg McIntosh	Rapporteur
Cathy Batt	Rapporteur
Dominique Gibert	Examinateur
Miquel Torta	Examinateur
Annick Chauvin	Directeur de thèse
María Luisa Osete	Directeur de thèse
Miguel Garcés	Membre invité

Remerciements / Agradecimientos

Ce travail a été réalisé à Géosciences Rennes ainsi qu'au Departament de Física de la Tierra, Astronomía y Astrofísica I de la Universidad Complutense de Madrid. J'exprime toute ma gratitude envers celles et ceux qui, de part et d'autre des Pyrénées, ont contribués de quelque manière que ce soit, à la réalisation de ce travail. Merci à tous.

Je remercie tout d'abord Yves Gallet, Gregg McIntosh, Cathy Batt, Miquel Torta, Dominique Gibert et Miguel Garcés pour avoir accepté de juger et d'évaluer ce travail. Merci pour votre participation dans le jury lors de la soutenance et/ou pour vos remarques constructives.

Ce travail n'est pas le résultat d'un travail individuel, mais le fruit d'un travail d'équipe. Pour cette raison, je voudrais particulièrement remercier Annick Chauvin pour son enthousiasme et son optimisme tout au long de cette thèse, pour ses nombreux conseils et pour tout le temps qu'elle y a consacré. Merci beaucoup pour ton excellente direction et pour m'avoir communiqué ta rigueur afin d'aboutir à un travail sérieux et précis. Cette thèse n'aurait vu le jour sans Philippe Lanos et Marisa Osete. Merci Philippe pour l'aide apportée au cours de cette recherche, particulièrement dans le monde compliqué! (eh, oui...) de la modélisation Bayésienne. *Y gracias también a Marisa Osete, por haberme permitido conocer en qué consiste esto de investigar y por tus consejos a lo largo de los últimos cinco años.* Je vous remercie tous les trois pour votre encadrement. Je voudrais aussi remercier Philippe Dufresne, Bruno Kergosien, Pierrick Roperch et Mimi Hill pour leur aide au laboratoire de Rennes. Je ne peux oublier l'aide de Jacques Thiriot, qui m'a appris à prélever les structures archéologiques et qui m'a permis de comprendre les difficultés auxquelles font face les archéologues pour obtenir des datations rigoureuses. Merci, pour le temps que tu m'as consacré, et merci pour les aventures dans le sud de l'Espagne. Sans ton immense travail, cette thèse (mais aussi l'archéomagnétisme en Espagne) ne serait pas la même. Je remercie aussi tous les archéologues avec qui j'ai collaboré pendant ces trois années. Merci pour la part de votre temps que vous avez dédié à l'archéomagnétisme.

Le travail présenté dans ce mémoire a été effectué dans le cadre du projet européen AARCH (Archaeomagnetic Applications for the Rescue of Cultural Heritage: HPRN-CT-

2002-00219), projet qui a financé la totalité du travail. Merci à tous les membres de ce projet pour leurs discussions et échanges (scientifiques, culturels et festifs !).

Un abrazo especial para la PGF de Madrid (¡que sigue creciendo!). Ya sé que, al fin y al cabo, una tesis no es para tanto, pero mil gracias por vuestro apoyo y amistad a lo largo de este tiempo, estando allá e incluso ¡jacá! (gracias por venir, de verdad). Y a los Alcalainos, cuya representante, mi prima Elena, es mi más fiel “fan”. Gracias Elena, espero que muy pronto sea al revés, y vaya yo a oírte hablar de “champiñones”. Gracias Nuria, por los años madrileños (y los de antes, que no son pocos; y los que quedan, que son más) y por animarme a venir aquí a empezar de nuevo. Y gracias a todos los compañeros paleomagnetas de la UCM, con los que me inicié en el magnetismo y demás parientes.

Beaucoup de personnes m'ont permis de passer trois ans formidables à Rennes. Je ne souhaite pas énumérer chacun d'entre vous les uns après les autres mais merci à tous, en particulier aux (ex)thésards du labo et à tous les copains que j'ai pu rencontrer au cours de ces trois années. Je n'oublie pas la famille « Babo » qui m'a toujours accueillie les bras ouverts. Spéciale dédicace à Blaze, Catherine et Casper(ita), des Bretons en Bretagne, et à Małgorzata, une autre étrangère en Bretagne...

Enfin, je remercie mes parents et mes frères (Pablo et Clara. *Sí, Pablo; tu nombre aparece en los agradecimientos* ;-)) pour leurs encouragements quotidiens tout au long des ces années (presque 30!, sauf pour Clara évidemment...), pour tout ce qu'ils ont fait pour moi auparavant. Vous avez toujours su m'encourager dans tout ce que j'ai pu entreprendre. Merci aussi à Julien de m'avoir fait beaucoup rire au quotidien (*¡cómo pasa el tiempo que de pronto son años!*), de m'avoir si bien soutenu pendant la réalisation de cette thèse (et pas uniquement par un soutien graphique ;-)), mais aussi de me l'avoir fait oublier quand il était nécessaire. Mais ce n'est pas encore fini, l'histoire continue...

...à Barcelona

Je vous dédie, à tous les cinq, ce travail.

Résumé

Des données directionnelles et d'intensité du champ magnétique terrestre (CMT) ont été acquises sur 28 sites archéomagnétiques d'Espagne en utilisant la méthode de Thellier. Une synthèse des données (de -1000 à 2000 AD) a permis de calculer la courbe bayésienne de variation séculaire (VS) pour la Péninsule Ibérique. Elle présente les mêmes caractéristiques que les VS allemande et française. La comparaison faite avec la VS au Japon et au SO des Etats-Unis suggère que les caractéristiques de la VS en Europe de l'Ouest ont un caractère local. Nos résultats d'intensité ont été combinés avec ceux déjà publiés pour l'Europe de l'Ouest (de -100 à 2000 AD). La courbe bayésienne obtenue indique que l'intensité du CMT aurait peu varié, du 1^{ère} au 5^{ème}, et du 13^{ème} au 15^{ème} siècles (valeurs à Paris proches de 65 et 57 μ T respectivement) alors que sa décroissance est forte sur les 5 derniers siècles. Enfin l'évolution de l'intensité du CMT durant le Haut Moyen age demeure encore mal contrainte.

Abstract

Directional and intensity data of the Earth's magnetic field (EMF) from 28 Spanish archeomagnetic sites have been obtained by Thellier method. A data compilation (from -1000 BC to 2000 AD) has been used to calculate the secular variation (SV) curve for the Iberian Peninsula, which presents the same characteristics than the French and German curves. The comparison with the SV for Japan and SW USA suggests that the characteristics of the SV in Western Europe have a local character. Our new intensity results together with previous data for Western Europe (between -100 and 2000 AD), have been treated by Bayesian modelling. The obtained curve indicate that the geomagnetic intensity remain more or less constant between the 1st and 4th centuries, and between the 13th and 15th centuries (mean values around 65 and 57 μ T respectively), whereas an important decrease occurs during the last 5 centuries. Finally, the evolution of the EMF intensity during High Middle Ages remains uncertain.

Table de matières

<i>Resumen en Español</i>	i
<i>Introduction générale: Le champ magnétique terrestre, les mesures magnétiques et leur relation avec l'archéologie et les sciences de la terre</i>	1
Chapitre 1: Une introduction à l'archéomagnétisme	3
1.1. Le champ magnétique terrestre, l'aimantation rémanente et l'archéomagnétisme	3
1.2. Présentation de cette étude et objectifs	14
1.3. Un coup d'oeil sur l'histoire d'Espagne	16
Chapitre 2: Courbe de variation séculaire pour la Péninsule Ibérique	23
Introduction	23
2.1. Article : A catalogue of Spanish archaeomagnetic data	31
2.2. Article: The first Secular Variation Curve for the Iberian Peninsula. Comparison with other data from Western Europe and with geomagnetic field global models	73
Chapitre 3. Variation de l'intensité du champ magnétique terrestre en Europe de l'Ouest pendant les deux derniers millénaires	109
Introduction	109
3.1. Article: Archeomagnetic study of seven contemporaneous kilns from Murcia (Spain)	115
3.2. Article : Evolution of the geomagnetic field intensity in Western Europe for the last 2000 years inferred from Bayesian statistics: 17 new archeointensity data from seven Spanish archaeological sites	135
3.3. Essai de détermination de l'archéointensité en utilisant la désaimantation par microondes	175
Conclusion	183
Références bibliographiques	187
Annexes (CD)	195

Estudio de la variación de la dirección e intensidad del campo geomagnético en España durante los últimos dos mil años

Resumen

El estudio de la evolución del campo magnético terrestre (CMT) requiere la obtención de registros de alta resolución de éste, distribuidos en las distintas regiones de la tierra. Las primeras medidas directas del campo geomagnético fueron llevadas a cabo en observatorios a principios del siglo XVII (en España se dispone de registros sistemáticos de las distintas componentes del campo geomagnético desde tan sólo la segunda mitad del s.XIX). Para épocas anteriores, este objetivo puede alcanzarse estudiando la magnetización remanente de lavas, de sedimentos lacustres o de materiales arqueológicos. El material volcánico presenta en numerosas ocasiones baja estabilidad magnética durante los experimentos de desimanación térmica realizados para determinar la dirección y/o la intensidad del campo magnético terrestre en el pasado. Esta inestabilidad se traduce muchas veces en resultados difíciles de interpretar (especialmente en los estudios de paleointensidad) y en tasas de éxito a menudo muy bajas. Por otro lado, los sedimentos lacustres pueden proporcionarnos registros continuos, pero el establecimiento de una escala temporal absoluta es todavía difícil. Por el contrario, el material arqueomagnético presenta una gran estabilidad durante los experimentos de desimanación, lo que da lugar a resultados de fácil interpretación y a altos índices de éxito (a menudo más del 80% en estudios direccionales o de intensidad). Por ello, el estudio de material arqueológico bien datado constituye el método más eficaz para obtener registros fiables de la dirección y de la intensidad del CMT en los últimos milenios. Estos datos pueden

ser utilizados para obtener la variación temporal y espacial del CMT durante los últimos milenios. El conjunto de datos arqueo-paleomagnéticos (observaciones) permite obtener la evolución de los coeficientes de Gauss del desarrollo en armónicos esféricos utilizado para describir matemáticamente el CMT. Para ello, se utiliza un procedimiento de “inversión” de las observaciones mediante el cual tratamos de obtener la combinación de coeficientes (modelo de campo global) capaz de reproducir mejor las observaciones. Estos modelos (Hongre, 1998; Korte y Constable, 2005) pueden ser utilizados para estudiar las variaciones temporales y espaciales de las distintas componentes del CMT.

El origen del arqueomagnetismo está en los primeros trabajos de E. Thellier (Thellier, 1938; Thellier y Thellier, 1959), quien propuso la primera curva de variación secular (VS) del campo geomagnético en Francia durante los últimos dos mil años (Thellier, 1981). Desde entonces la técnica arqueomagnética se ha desarrollado y, actualmente, se han publicado varias curvas de VS en Europa, como por ejemplo en Francia (Gallet et al., 2002; última actualización de la curva francesa), Alemania (Schnepp y Lanos, 2005), Hungría (Márton, 2003), Bulgaria (Kovacheva et al., 1998) o Inglaterra (Batt, 1997).

En España, a pesar del gran potencial arqueológico presente, se dispone de un número insuficiente de datos (si lo comparamos con otras regiones). La tesis de Núñez (2004), presentada en la Universidad Complutense de Madrid, constituye el primer estudio sistemático de la variación direccional del CMT en España. En este trabajo, se propone una primera curva de VS para Iberia obtenida a través del método de ventanas móviles variables (Le Goff et al., 2002). En lo que se refiere a la intensidad, sólo un dato ha sido publicado en esta región (Kovacheva et al., 1995).

En el *primer capítulo* de esta tesis se exponen las nociones básicas de magnetismo y del CMT necesarias para la compresión general de este trabajo, así como el estado actual de la técnica arqueomagnética en España. El tema de investigación de esta tesis, la “**variación de la dirección e intensidad del campo geomagnético en España durante los últimos dos mil años**” tiene como objetivo principal obtener nuevos datos arqueomagnéticos para permitir una mejor caracterización de la variación de la dirección del CMT en la Península Ibérica durante los últimos milenios y de la variación de la intensidad del CMT en Europa Occidental. Este trabajo, constituye el primer estudio sistemático de la intensidad del CMT durante los últimos milenios para la Península Ibérica.

Para ello, 26 hornos arqueológicos, un lote de ladrillos y un lote de fragmentos de tinajas han sido analizados en el laboratorio siguiendo el método propuesto por Thellier (Thellier y Thellier, 1959). En cada una de las muestras se ha investigado también el efecto de la anisotropía de la magnetización termorremanente (TRM) y el efecto de la velocidad de enfriamiento sobre la adquisición de dicha magnetización. Los resultados muestran la necesidad de realizar estas correcciones para la obtención de resultados fiables de paleointensidad. La corrección de anisotropía de la TRM es particularmente importante para las muestras provenientes de los lotes de fragmentos de tinajas y de ladrillos. Los factores de corrección relacionados con el efecto de la velocidad de enfriamiento sobre la adquisición de la TRM alcanzan valores de hasta un 20%. El análisis de laboratorio, según el procedimiento descrito anteriormente, ha permitido obtener 26 nuevas direcciones arqueomagnéticas y 24 nuevos datos de paleointensidad para la Península Ibérica.

Los 26 datos direccionales obtenidos en este trabajo, junto con nuevos datos obtenidos en la Universidad Complutense de Madrid, así como los datos previos existentes para España (esencialmente los de Núñez (2004)), han permitido elaborar el primer catálogo arqueomagnético español. 63 direcciones arqueomagnéticas están incluidas en este trabajo, además se expone y analiza en detalle la información arqueológica existente para cada una de las estructuras estudiadas, con el objetivo de permitir una futura revisión de las dataciones propuestas, en caso necesario. Este trabajo se expone en la primera parte del *capítulo 2* en forma de artículo: “**A catalogue of Spanish archaeomagnetic data**”.

La base de datos arqueomagnética realizada ha permitido obtener la curva de VS para la Península Ibérica. Para ello, hemos comparado el método clásico de ventanas móviles con el nuevo método desarrollado por Lanos (2004), basado en la estadística bayesiana. Este método tiene como ventajas poder tratar simultáneamente los datos en tres dimensiones (declinación, inclinación y tiempo), permitir la movilidad de los datos dentro del intervalo de edad propuesto por los arqueólogos, y tener en cuenta el orden estratigráfico entre distintas estructuras. La curva de VS de Iberia es muy similar a las curvas alemana y francesa. La comparación de las curvas europeas con las curvas de VS de Japón y del sudoeste de Estados Unidos permite poner en evidencia el carácter local de las curvas europeas. Finalmente, se ha comparado la curva de VS de Iberia con las predicciones de los modelos globales de campo geomagnético de Korte y Constable (2005) y Hongre et al. (1998). Los modelos predicen razonablemente bien la curva obtenida. Aún así los dos modelos son muy diferentes. El

momento dipolar obtenido a través del modelo de Korte y Constable (2005) es anómalamente bajo. Por el contrario, el modelo de Hogre et al. (1998) parece mucho más realista. Este trabajo se expone en la segunda parte del *capítulo 2* en forma de artículo: “**The first Secular Variation Curve for the Iberian Peninsula. Comparison with other data from Western Europe and with geomagnetic field global models**”.

Los resultados de intensidad se presentan y analizan en el *capítulo 3* de esta tesis. En una primera fase, se han obtenido siete datos de paleointensidad a partir del estudio de siete hornos arqueológicos contemporáneos, datados entre 1100 y 1200 dC, y muestrados en la misma excavación arqueológica. Estos resultados nos permiten discutir y analizar la dispersión obtenida. Esta dispersión se ve reducida en un 50% gracias a la corrección del efecto de la velocidad de enfriamiento sobre la adquisición de la magnetización termorremanente. Este hecho confirma la necesidad de realizar este tipo de corrección para obtener datos precisos de arqueointensidad. La sección primera del *capítulo tres* expone este trabajo en forma de artículo: “**Archeomagnetic study of seven contemporaneous kilns from Murcia (Spain)**”

En una segunda fase, se ha determinado la intensidad del campo geomagnético en el pasado a partir del estudio de 17 hornos, un lote de fragmentos de tinajas y un lote de ladrillos. Los resultados, así como una recopilación de los datos de intensidad fiables existentes en Europa Occidental, nos han permitido obtener la evolución del campo geomagnético en esta región durante los últimos milenios, también utilizando la técnica bayesiana. La evolución obtenida ha sido comparada con los modelos globales de Korte y Constable (2005) y de Hongre et al. (1998). Las predicciones del modelo de Korte y Constable (2005) están contenidas dentro del margen de error (determinados a un nivel de confianza del 95%) de la curva obtenida para Europa Occidental. Por el contrario, las predicciones del modelo de Hongre et al. (1998) difieren significativamente de nuestros resultados. Finalmente, se ha utilizado la base global de datos recientemente publicada por Korte et al. (2005) para obtener las curvas de variación de la intensidad del CMT utilizando la técnica bayesiana para distintas regiones de Europa. La dispersión de los datos de intensidad presentes en dicha base de datos es, por lo general, muy grande. Este hecho está claramente relacionado con el uso de técnicas poco precisas para la determinación de la intensidad y/o con el uso de muy pocas muestras (muchas veces una o dos) para obtener la intensidad media por estructura. Una primera conclusión de este análisis es la necesidad de obtener datos de

intensidad de alta precisión, es decir, obtenidos a partir de técnicas fiables (especialmente la técnica de Thellier) y corregidos del efecto de la anisotropía de la magnetización termorremanente y de la velocidad de enfriamiento sobre la adquisición de dicha magnetización. Los resultados de este estudio se exponen en la sección segunda del *capítulo tres*: “**Evolution of the geomagnetic field intensity in Western Europe for the last 2000 years inferred from Bayesian statistics: 17 new archeointensity data from seven Spanish archaeological sites**”.

Finalmente, se ha utilizado la desimanación por microondas para estudiar la paleointensidad en una treintena de muestras provenientes de nuestros hornos. Los resultados se exponen en la sección 3.3. Como conclusión general de este trabajo podemos señalar que la técnica propuesta por Thellier y Thellier (1959) es, por el momento, la más eficaz para la determinación de la paleointensidad en este tipo de muestras.

Le champ magnétique terrestre, les mesures magnétiques et leurs relations avec les sciences de la terre et l'archéologie

La découverte du champ magnétique terrestre est liée aux origines de la physique moderne. C'est par l'existence d'un besoin spécifique de la société lié à la navigation, le raisonnement suivi par William Gilbert et le « mystère » de l'action à distance, dont les aimants étaient pendant très longtemps les seuls exemples scientifiques, qu'a été découvert le champ magnétique terrestre. La démonstration en 1600 de William Gilbert, médecin de la reine Isabelle I d'Angleterre, sur l'origine interne du champ magnétique terrestre à travers la similitude des lignes du champ (en utilisant le langage scientifique actuel) autour de la terre et autour d'une sphère de magnétite naturellement aimanté, est considérée par un grand nombre de scientifiques comme la première publication de la physique moderne. Ses études lui ont permis d'affirmer que « *magnus magnes ipse est globus terrestris* » (la terre est en soi même un aimant géant). Ces travaux, qui arrivent comme la culmination des expériences faites en géomagnétisme pendant des siècles, mettent aussi fin aux spéculations qui ont toujours entouré le magnétisme. Il faudra encore attendre près d'un siècle pour que la loi de la gravité de Newton soit quant à elle découverte.

Aujourd'hui, grâce à l'étude du champ magnétique terrestre et à l'étude des propriétés magnétiques de matériaux naturels, on sait que le champ magnétique de la Terre varie dans le temps. Ces deux disciplines, en partie grâce à l'apport emblématique des travaux de Néel dans les années 50, ont maintenant de nombreuses applications principalement en Sciences de la Terre, mais aussi en Sciences de l'Univers, de la Vie et de l'Environnement.

Quel type d'information peuvent nous apporter les mesures magnétiques en Sciences de la Terre et en l'Archéologie?

En effet, le champ magnétique de la Terre varie dans le temps à des échelles très différentes. *Les variations lentes du champ magnétique terrestre, à l'échelle de l'année ou plus, constituent ce qu'on appelle la variation séculaire.* Elle est, ni uniforme dans le temps, ni dans l'espace. Il faut donc analyser ses caractéristiques dans les différentes régions du globe. L'archéomagnétisme est l'étude de l'aimantation thermorémanente (ATR) acquise par des terres cuites au cours de leur dernier refroidissement. Cette aimantation, stable à des échelles de temps très longues, a pour caractéristique d'être parallèle à la direction locale du champ magnétique terrestre, et une relation linéaire relie sa norme à l'intensité du champ magnétique terrestre. La datation des échantillons par l'archéologie ou par les méthodes géochronologiques permet de lier les mesures faites en laboratoire aux caractéristiques du champ magnétique terrestre à un instant donné. Ainsi, l'archéomagnétisme a une importante application géophysique car elle permet de retrouver le comportement du champ magnétique terrestre au cours des derniers millénaires et ainsi de mieux préciser son origine. En retour une fois établies, ces courbes de référence, constituent un outil de datation du matériel archéologique.

Bien qu'il existe une grande variété chronologique de fouilles archéologiques en Espagne, l'archéomagnétisme est en cours de développement et seuls quelques résultats directionnels (la majorité d'entre eux obtenus par Núñez (2004)) et une donnée d'intensité (Kovacheva et al., 1995) existent. Ce travail de thèse présente des résultats archéomagnétiques nouveaux pour l'Espagne. Ils ont été obtenus, en appliquant la méthode développée par Thellier (Thellier et Thellier, 1959), à partir de l'étude de 26 fours archéologiques, d'un lot de briques et d'un lot de céramiques. Ces résultats ont permis d'améliorer la courbe de variation séculaire en Péninsule Ibérique présenté par Núñez en 2004. Cette courbe a été obtenue en utilisant la méthode bayésienne développé par Philippe Lanos (2004). D'autre part, cette thèse présente la première étude systématique des variations d'intensité du champ géomagnétique en Espagne au cours des deux derniers millénaires. Ce travail de thèse a donc permis de mieux caractériser les variations à la fois, de l'intensité, et de la direction du champ géomagnétique dans l'Ouest de l'Europe. L'archéomagnétisme devient ainsi, par ce travail et celui de Nuñez (2004), un nouvel outil de datation des structures archéologiques en Espagne.

Chapitre 1. Une introduction à l'archéomagnétisme

1.1. Le champ magnétique terrestre, l'aimantation rémanente et l'archéomagnétisme

L'existence du champ magnétique terrestre (CMT) est connue depuis longtemps par ses applications à la navigation à travers la boussole. Son utilisation apparaît pour la première fois en Occident au tour du XII siècle, mais il est fortement possible qu'il ait été utilisée en Chine plusieurs siècles avant. Le CMT a un caractère vectoriel et sa présence peut être visualisée à l'aide d'une aiguille aimantée : l'aiguille va s'orienter dans la ligne géographique nord-sud, mais cela seulement d'une façon approximative. En fait, l'aiguille de la boussole est déviée du Nord Géographique et, libre de rotation horizontale ou verticale, s'oriente tangentiellement aux lignes de champ magnétique. Le décalage angulaire entre la projection sur l'horizontal du vecteur champ et la direction du Nord géographique est appelé déclinaison magnétique (D). Cet angle est mesuré du Nord géographique au Nord magnétique, et par convention est considérée positive dans le sens horaire. L'angle entre la projection horizontale du vecteur CMT, dirigé vers le Nord magnétique, et la direction du vecteur CMT est appelé l'inclinaison magnétique (I). Par convention cette valeur est comptée positivement lorsque le vecteur pointe vers l'intérieur de la planète, ce qui est le cas dans l'hémisphère nord. Ces deux angles, la déclinaison et l'inclinaison magnétiques, avec l'intensité du champ magnétique F décrivent ensemble le vecteur CMT (voir Figure 1), qui varie spatialement.

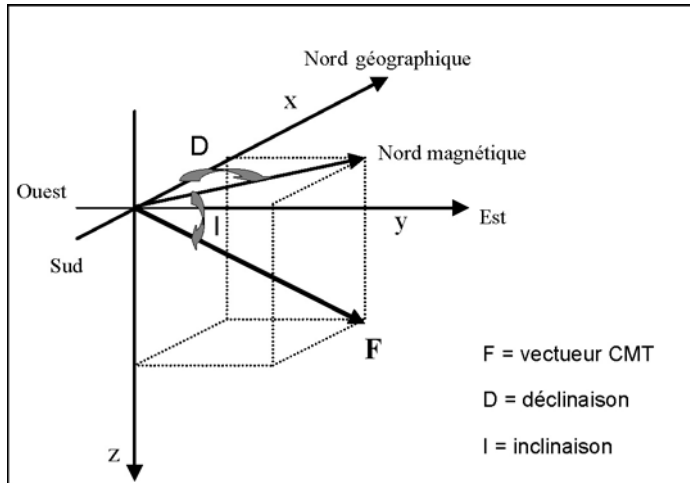


Figure 1 : Décomposition du vecteur champ magnétique terrestre, qui peut être décrit par la déclinaison, inclinaison et l'intensité ou par x , y , z dans le repère $Oxyz$.

On sait que le champ magnétique de la Terre varie également dans le temps à des échelles très différentes. Pour comprendre l'origine de ses variations il faut analyser les caractéristiques du CMT dans les différentes régions du globe. Pour cela on dispose des enregistrements directs du champ depuis les années 1830. Au-delà, on a besoin de faire appel à un des phénomènes qui a contribué le plus à la connaissance des variations du CMT dans le passé et qui a permis de révolutionner nos idées sur la tectonique globale : à savoir l'aimantation rémanente. La capacité d'acquérir une aimantation rémanente est due aux minéraux ferromagnétiques qui sont (dans certaines roches ou dans des matériaux archéologiques) dispersés dans une matrice dia ou paramagnétiques. Pour que le magnétisme de la roche ou de matériaux archéologique puisse nous apporter des renseignements sur le CMT du passé cette aimantation doit être stable et être conservée depuis la formation de la roche. Une brève explication des divers mécanismes d'acquisition et de « conservation » de l'aimantation est nécessaire pour comprendre les travaux de cette thèse. Nous introduisons les notions de temps de relaxation et d'aimantation thermorémanente :

a) le temps de relaxation

Sans la présence d'un champ magnétique, un matériel ferromagnétique formé par des particules monodomaines sans interaction, avec une aimantation résultante M_0 , subit au cours du temps une perte d'aimantation due à l'agitation thermique qui peut s'exprimer selon :

$$M = M_0 \exp\left(\frac{-t}{\tau}\right) \quad [1.1]$$

où t est le temps et τ est le temps de relaxation donné par :

$$\tau = \left(\frac{1}{C}\right) \exp\left(\frac{KV}{kT}\right) \quad [1.2]$$

et qui est le temps nécessaire pour que l'aimantation décroisse jusqu'au M_0/e , et où k est la constante de Boltzmann; K , l'énergie d'anisotropie magnétique par unité de volume, T , la température, et V , le volume de la particule. La valeur de τ est déterminée par la compétition entre l'énergie d'anisotropie magnétique (KV) et l'énergie thermique (kT). La constante C de cette équation est une fréquence qui donne la probabilité de dépasser la barrière de potentiel (KV) grâce à l'énergie thermique (kT). Cette constante est de l'ordre de 10^8 s^{-1} . Un aspect important de cette équation est que le temps de relaxation τ varie fortement avec V/T . Cette équation exprime une relation entre le temps de relaxation, la température T et le volume V qui est essentiel pour la compréhension des processus d'acquisition des aimantations thermorémanentes. L'équation [1.2] est la base de la théorie de Néel (Néel, 1955).

A température ambiante, les petits grains se comportent de manière instable due à l'agitation thermique et atteignent l'équilibre rapidement si un petit champ magnétique est présent. Dans cette situation tous les domaines ne sont pas alignés avec le champ. Si le champ disparaît, la rémanence acquise par ces grains disparaît. Ce comportement est appelé superparamagnétisme. Pour les grains plus grands l'aimantation est plus stable et ils ont un moment magnétique bloqué. C'est important de voir comment une augmentation par deux du coefficient V/T donne lieu à une augmentation du temps de relaxation de 10^8 , cela fait que la transition entre l'état superparamagnétique et celle du moment bloqué est très brusque. Pour un matériel il existe un volume critique V_c (qui dépend de la température) qui sépare ces deux comportements. Les grains avec $V < V_c$ ont de τ petits et ils atteignent rapidement la situation d'équilibre en s'orientant selon la direction du champ magnétique. Les moments magnétiques de grains avec $V > V_c$ restent bloqués. De la même façon, on appelle température de blocage T_b , la température à laquelle le temps de relaxation est petit. Pour $T > T_b$ le grain est superparamagnétique et pour $T < T_b$ le moment magnétique du grain est bloqué. Ces deux

concepts sont essentiels pour comprendre les processus d'acquisition de l'aimantation thermorémanente.

b) l'aimantation thermorémanente.

On appelle aimantation thermorémanente (ATR) l'aimantation acquise par une roche au cours de son refroidissement de la température de Curie jusqu'à la température ambiante en présence d'un champ magnétique. Pendant le refroidissement (au delà de la Température de Curie) l'aimantation spontanée apparaît. Si la température diminue, dépassant les températures de blocage des grains, le temps de relaxation τ augmente très rapidement et l'aimantation acquise reste bloquée (la barrière d'énergie entre les différents états d'aimantations est plus grande que l'énergie thermique disponible). Les grains sont maintenant dans l'état de moment bloqué et, les changements postérieurs du champ magnétique extérieur à des températures au dessous de T_b , ne produisent aucun changement sur l'aimantation des grains.

Néel établit les bases théoriques pour comprendre comment l'ATR peut rester stable à l'échelle des temps géologiques. Il démontre que pour un instant donné t , l'aimantation totale d'un ensemble de grains monodomaines sans interactions et en présence d'un champ magnétique H_0 est contrôlée par les transitions entre les deux états où les moments des grains sont parallèles ou antiparallèles à H_0 . L'évolution de l'aimantation totale vers l'équilibre est donnée par:

$$M = M_0 \exp\left(\frac{-t}{\tau}\right) + M_{eq} \left(1 - e^{\frac{-t}{\tau}}\right) \quad [1.3]$$

où M_{eq} est l'aimantation d'équilibre :

$$M_{eq} = M_s \tanh \frac{\mu_0 V M_s H_0}{kT} \quad [1.4]$$

où M_s est l'aimantation à saturation et où le temps de relaxation est :

$$\tau^{-1} = \tau_0^{-1} \exp\left[-\left(\frac{KV}{kT}\right)\left(1 - \frac{H_0}{H_k}\right)^2\right] \quad [1.5]$$

où τ_0 est de l'ordre de 10^{-9} s et H_k est la force microscopique coercitive.

D'après l'équation [1.3], l'aimantation totale serait similaire à l'aimantation d'équilibre M_{eq} après un temps t de l'ordre de τ . De petits changements en température ont un effet énorme sur les temps de relaxations. Par exemple, pour des particules monodomaine de magnétite, si le τ d'un grain est de l'ordre de 1 s à une température de 550°C (30° inférieur à la T de Curie de la magnétite) après un refroidissement jusqu'à la température ambiante, le τ est plus grand que l'âge de la Terre. Même des grains avec de T_b de l'ordre de 330°C ont de τ de l'ordre de 10^9 années après leur refroidissement à température ambiante. Quand les grains se refroidissent au-dessous de leur T_b , M_{eq} reste donc bloqué. On appelle cette aimantation l'aimantation thermorémanente (ATR) et elle est donnée par l'éq. [1.4]. Pour des champs faibles, comme celui de la Terre,

$$\tanh(\alpha) \approx \alpha \quad \text{où } \alpha = \frac{\mu_0 V M_s H_0}{kT}$$

et cette ATR est proportionnelle à H_0 et elle est relativement intense. L'ATR peut être désaimantée seulement en chauffant à des températures de déblocage T_{ub} similaires à sa T_b originale (en Accord avec l'éq. [1.5], quand $H_0 \ll H_k$, $T_{ub} \approx T_b$). Cette ATR est stable à l'échelle des temps géologiques. Ce fait est la base des études paléomagnétiques et archéomagnétiques.

L'archéomagnétisme étudie l'ATR acquise par les terres cuites durant leur dernier refroidissement. Cette aimantation, stable à des échelles de temps très longues, a pour caractéristiques d'être parallèle à la direction locale du champ magnétique terrestre, et une relation linéaire relie sa norme à l'intensité du champ (Néel, 1955; Thellier, 1938). Ainsi, l'étude de l'aimantation des terres cuites permet de retrouver le comportement du CMT au cours des derniers millénaires, en permettant d'explorer les variations temporelles du CMT à l'échelle de siècles.

Le CMT découle d'un potentiel magnétique, dont on fournit un développement en harmoniques sphériques. Cette analyse avait été introduite par Laplace et Legendre pour étudier des problèmes gravitationnels, et il a été appliqué au CMT par Gauss en 1839. Le développement en harmoniques sphériques permet d'écrire le potentiel géomagnétique Φ comme une fonction scalaire définie en tout point qui peut se diviser en deux parties: une partie qui trouve son origine dans l'intérieur de la Terre, c'est la source du champ interne, et une autre partie qui a une origine externe liée à la ionosphère et à la magnétosphère (voir Figure 2). La contribution des sources externes au champ total en surface de la Terre est très faible, de l'ordre de 1%. Le reste du champ trouve son origine à l'intérieur de la terre, deux champs magnétiques (champ principal et champ d'anomalie ou champ crustal) donnent lieu au champ interne.

Origine du champ magnétique terrestre

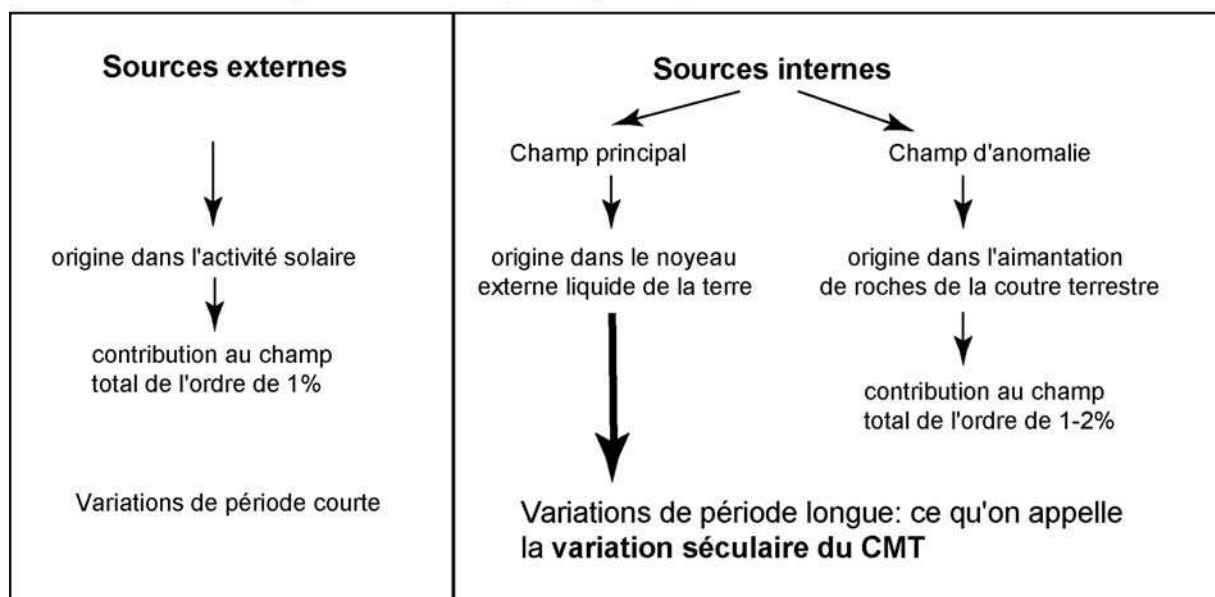


Figure 2 : Sources principales, externes et internes, à l'origine du champ magnétique terrestre.

On peut donc séparer le potentiel géomagnétique Φ comme somme des deux potentiels qui correspondent aux sources internes (Φ_i) et aux sources externes (Φ_e):

$$\Phi = \Phi_i + \Phi_e \quad [1.6]$$

et pour la région libre de sources électromagnétiques près de la surface de la Terre le potentiel vérifie l'équation de Laplace :

$$\nabla^2 \Phi = 0 \quad [1.7]$$

La résolution de cette équation permet d'écrire les potentiels interne et externe sous la forme d'une somme d'harmoniques sphériques, fonctions des coordonnées sphériques (r, θ, λ) du point d'observation (où r est le rayon, θ la colatitude et λ la longitude):

$$\Phi_i = a \sum_{n=1}^{\infty} \left(\frac{a}{r} \right)^{n+1} S_n(\theta, \lambda) \quad [1.8]$$

$$\Phi_e = a \sum_{n=1}^{\infty} \left(\frac{r}{a} \right)^n S_n(\theta, \lambda) \quad [1.9]$$

où a est le rayon de la Terre, r la distance du point d'observation au centre de la terre, et $S_n(\theta, \lambda)$ sont les harmoniques sphériques de surface qui peuvent s'exprimer comme :

$$S_n(\theta, \lambda) = \sum_{m=0}^n P_n^m(\cos \theta) (g_n^m \cos m\lambda + h_n^m \sin m\lambda) \quad [1.10]$$

où g_n^m et h_n^m sont les coefficients de Gauss et P_n^m sont les fonctions associés de Legendre de degré n et ordre m . Les coefficients g_n^m et h_n^m peuvent être déterminés à partir des composantes observées du champ magnétique terrestre. Pour cela, on cherche à déterminer les coefficients qui sont capables de reproduire le mieux possible les observations. Cette procédure donne lieu aux modèles de champ global (IGRF) qui peuvent être utilisés ensuite pour reproduire les différents composants du CMT au cours des temps.

L'analyse par harmoniques sphériques permet d'écrire le spectre d'énergie du CMT d'origine interne à la surface de la Terre. On observe que le spectre est dominé par les termes de degré 1, qu'il décrit une pente négative jusqu'aux degrés 14-15 (partie dominée par le champ principal) et il devient constant pour des termes supérieurs (partie dominée par champ crustal). On peut voir dans la Figure 3 le spectre d'énergie obtenu par Hulot et al. (2002) à partir de la modélisation des observations de satellites Oersted et Magsat. Cette étude montre

comment le champ principal domine le signal pour des degrés jusqu'à 13 et le champ d'anomalie domine le signal pour des degrés supérieurs à 15.

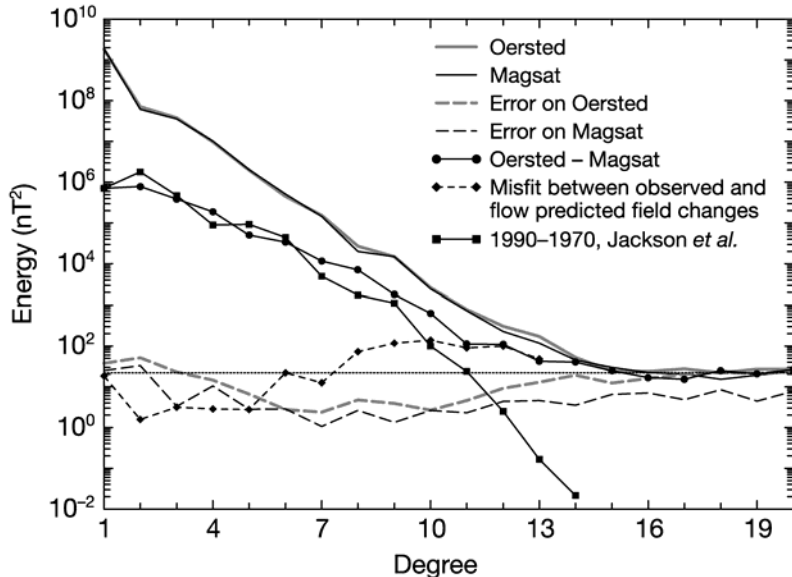


Figure 3 : Spectre d'énergie du CMT obtenue du Oersted et Magsat models (Hulot et al. 2002)

Comme on peut voir dans la Figure 3 le degré 1 domine très largement le spectre d'énergie du champ principal. En effet on peut décrire les termes associés au degré 1 comme :

$$\Phi_i = \frac{a^3}{r^2} (g_1^0 2 \cos \theta + \sin \theta 2\sqrt{2} (g_1^1 \cos \lambda + h_1^1 \sin \lambda)) \quad [1.11]$$

Si on examine les valeurs des trois premiers coefficients on peut voir que, sur la surface de la Terre, g_1^0 prédomine sur le reste (il est approximativement 5 fois plus grand que les autres). Ce coefficient représente le champ d'un dipôle centré et orienté dans la direction de l'axe de rotation de la Terre. Si on tient compte des deux coefficients suivants g_1^1 et h_1^1 l'axe du dipôle est incliné de 11.5° par rapport à l'axe de rotation. Un tel dipôle développe un champ magnétique auquel nous pouvons assimiler une grande partie (autour du 90%) de CMT. Cette partie est appelée champ dipolaire avec une valeur de moment dipolaire m :

$$m = \frac{4\pi a^3}{\mu_0} \sqrt{(g_1^0)^2 + (g_1^1)^2 + (h_1^1)^2} \quad [1.12]$$

Les autres termes, pour $n \geq 2$, sont des termes du CMT qui représentent le champ non dipolaire qui rend compte des 10% restant.

Les modèles de champ global nous permettent de séparer la partie dipolaire et non dipolaire du champ géomagnétique et de tracer la variation des différentes composantes du CMT. Par exemple, ils permettent de retrouver les variations directionnelles du pôle nord géomagnétique au cours de derniers millénaires (voir Figure 4) ou de déterminer la variation spatiale et temporelle de la composante radiale (B_r) du CMT à la surface du noyau. L'étude des variations des maxima et des minima de la composante B_r à la surface du noyau peut nous renseigner sur les mouvements du fluide du noyau au toit du noyau (voir Figure 5).

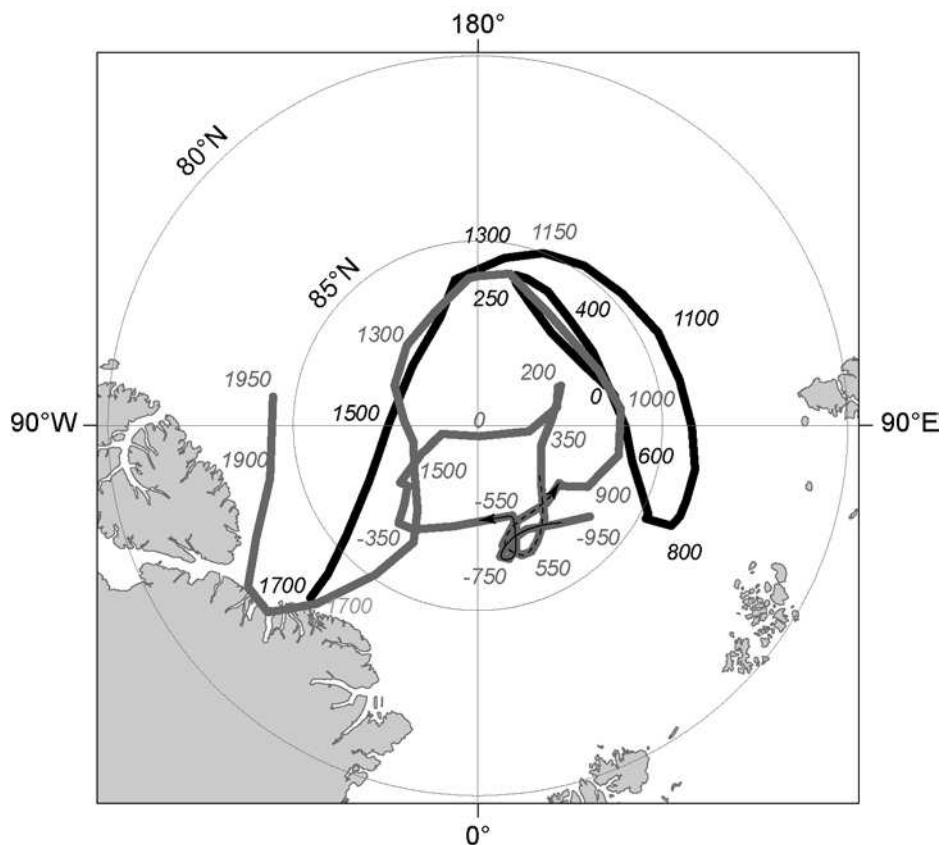


Figure 4 : Variation du pôle nord géomagnétique au cours de derniers millénaires selon le modèle de Korte et Constable (2005) en gris dans la figure, et le modèle de Hongre et al. (1998) en noir.

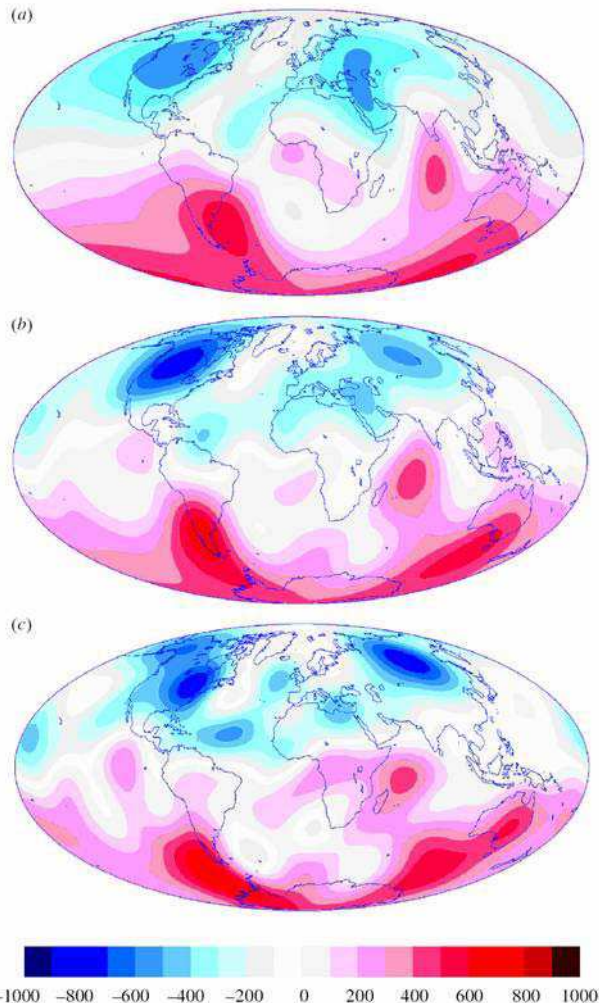


Figure 5 : Composante radiale du champ géomagnétique terrestre à la surface du noyau (a) en 1590 (b) 1690 et (c) 1790 AD. D'après Jackson et al. (2000).

Comme on peut voir dans la Figure 4, les modèles globaux existant donnent lieu à des résultats sensiblement différents. Cela peut être dû au faible nombre des données archéo-paléomagnétiques disponibles et aussi à la distribution inhomogène des sites étudiés. En effet, si on observe la disposition des sites archéo-paléomagnétiques mondiaux étudiés (Korte et Constable, 2005) on peut voir que la majorité des données proviennent de l'Hémisphère Nord (Figure 6). En ce qui concerne l'archéointensité la majorité de données proviennent de l'Europe.

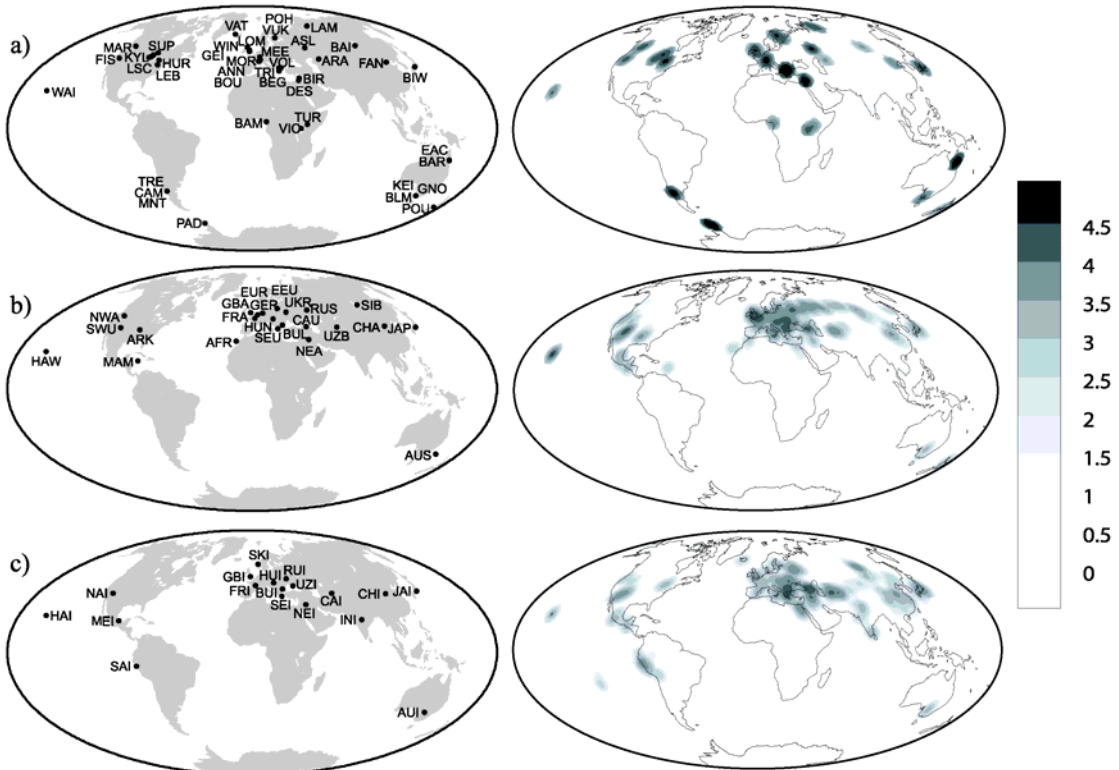


Figure 6 : Disposition des sites étudiés compilés par Korte et al. (2005) pour les sept derniers millénaires. a) lacs, b) données directionnelles archéomagnétiques, et c) données d'intensité archéomagnétique. A droite concentration des données.

Un autre problème lié aux données d'intensité est la forte dispersion observée dans les résultats disponibles pour les différentes régions (voir aussi Korte et al. (2005)). Cette forte dispersion est probablement liée à l'utilisation de méthodes de détermination de la paléointensité peu précises.

Il est donc nécessaire, pour améliorer notre connaissance de la variation séculaire du CMT dans le passé, d'obtenir plus de données directionnelles et d'intensité et, à la fois des données d'intensité plus précises. Cette thèse essaie de combler le manque de données d'archéointensité pour l'Espagne, et de compléter la base de données directionnelles pour cette région.

Notez que les modèles IGRF et autres modèles utilisés dans le cadre de cette thèse (basés sur l'analyse en harmoniques sphériques) représentent les sources d'origine interne du champ magnétique terrestre.

1.2. Présentation de cette étude et objectifs

Comme on l'a déjà signalé les composantes du champ magnétique varient dans le temps. Les variations temporelles du CMT constituent ce qu'on appelle la variation séculaire. Celle-ci n'est uniforme ni dans le temps ni dans l'espace, et il est nécessaire d'analyser ses caractéristiques dans différentes régions du globe. On cherche donc à établir des courbes de référence des variations temporelles de la direction et de l'intensité du champ géomagnétique. L'étude des structures en place (comme les fours ou les sols brûlés) est susceptible de nous apporter une description complète du vecteur champ géomagnétique. Les objets déplacés (comme les briques, les tuiles ou de céramiques) permettent seulement d'obtenir des informations sur l'intensité du champ magnétique ancien si on ne connaît pas leurs positions de cuisson. Dans certain cas on peut faire des hypothèses sur la position de cuisson des objets ce qui permet de déterminer aussi l'inclinaison du CMT (Lanos, 1987). Ainsi, en étudiant des structures bien datées d'âges différents réparties dans une région du globe on peut établir une courbe de variation séculaire valide pour cette région. En retour une fois établies ces courbes de référence, elles peuvent être utilisées comme outil de datation du matériel archéologique, en comparant l'aimantation acquise pour la structure à dater avec la courbe de référence valide pour la région de la structure.

En Europe, plusieurs courbes de référence, pas toujours parfaitement établies à l'échelle des 2 ou 3 derniers millénaires sont disponibles par exemple, pour la France (Gallet et al., 2002), l'Allemagne (Schnepp and Lanos, 2005), la Bulgarie (Kovacheva et al., 1998) et la Hongrie (Márton, 2003). En ce qui concerne l'Espagne, même s'il existe une grande variété chronologique de fouilles archéologiques, l'archéomagnétisme est en cours de développement et seuls quelques résultats sont disponibles. Thellier (1981), publie la première étude archéomagnétique menée sur des structures espagnoles, c'est l'étude d'un four à Ampurias, il calcule la moyenne directionnelle à partir de 4 échantillons. Une dizaine d'années après, Parés et al. (1992) présente l'étude, aussi directionnelle d'un four à poterie romain et comparent la direction moyenne obtenue avec la courbe Françaises à la latitude de Paris. Quelques années plus tard, ce même four fait l'objet d'une étude d'intensité (Kovacheva et

al., 1995), c'est d'ailleurs la seule étude d'archéointensité connue jusqu'à présent pour la Péninsule Ibérique. Oyamburu et al. (1996) étudient aussi deux fours romains et obtiennent leur direction moyenne. Un autre four romain fait l'objet d'une étude directionnelle à Arva (Evans, personal communication). La première étude systématique des directions du champ magnétique ancien en Espagne pendant les derniers millénaires est la thèse de Juan Ignacio Núñez Aguilar « Estudio arqueomagnético de la Península Ibérica, primera curva de variación secular de los últimos tres milenios » présenté en 2004 à l'Université Complutense de Madrid (Nuñez, 2004).

Considérant ce faible nombre d'études archéomagnétiques pour l'Espagne, surtout d'archéointensité (avec une seule donnée publiée à ce jour), nous avons décidé d'étudier 28 sites archéomagnétiques, tout en ayant comme objectifs principaux :

Objectif 1 (Chapitre 2) : L'amélioration de la courbe de variation séculaire pour l'Espagne obtenue dans les travaux de thèse de Núñez (2004). Pour accomplir cet objectif nous avons réuni et révisé les données déjà existantes pour l'Espagne, tout en apportant de nouvelles directions à partir de l'étude archéomagnétique de structures archéologiques. Les résultats sont exposés dans la section 2.1. de cette thèse : « **A catalogue of Spanish archaeomagnetic data** ». Une fois établi le catalogue archéomagnétique pour l'Espagne nous avons cherché à établir la meilleure courbe de référence pour cette région. Pour cela nous avons fait une comparaison des différentes méthodes de construction des courbes. La méthode bayésienne proposée par Lanos (2004) est la méthode choisie pour la présentation de la courbe directionnelle pour la Péninsule Ibérique. Ainsi ce travail a permis de mieux préciser les variations directionnelles du CMT en Europe de l'Ouest, et de comparer la courbe avec deux autres courbes déjà établies, à savoir les courbes française et allemande. Les résultats sont exposés dans la section 2.2 de cette thèse : « **The first archaeomagnetic secular variation curve for the Iberian Peninsula. Comparison with other data from Western Europe and with global geomagnetic field models** ».

Objectif 2 (Chapitre 3) : La mesure des valeurs d'intensité du CMT en Espagne pendant les deux derniers millénaires ce qui permettra de mieux caractériser l'évolution de l'intensité du CMT en Europe de l'Ouest ainsi que de discuter de la qualité des données d'archéointensité disponibles jusqu'à présent. Dans une première étape nous avons étudié sept fours contemporains prélevés dans la même fouille et tous datés entre 1100 et 1200 AD. L'étude

comparative de ces fours a permis d'abord, d'apporter sept nouvelles données d'intensité pour l'Espagne, et ensuite de discuter les causes possibles qui jouent sur la dispersion observée dans les études d'intensité. Les résultats sont exposés dans la section 3.1 : « **Archeomagnetic study of seven contemporaneous kilns from Murcia (Spain)** ». Ensuite nous avons procédé à l'étude systématique de 15 fours, un lot de briques et un lot de céramiques. Grâce aux données obtenues une courbe d'intensité pour l'Europe de l'Ouest établie avec la méthode bayésienne est proposée (Lanos, 2004). La courbe obtenue est comparée avec les modèles globaux de champ géomagnétique récemment publiés par Korte et Constable (2005) et Hongre et al. (1998), et avec les courbes d'intensité obtenues en utilisant aussi la méthode bayésienne pour d'autres régions du monde. Les résultats sont exposés dans la section 3.2: «**Evolution of the geomagnetic field intensity in Western Europe for the last 2000 years inferred from Bayesian statistics: 17 new archeointensity data from seven Spanish archaeological sites**». Enfin, nous avons testé la validité de la technique microondes pour la détermination de l'archéointensité dans les terres cuites. Pour cela, 29 échantillons ont été étudiés en utilisant le system à 8.2 GHz de laboratoire de Liverpool. Les résultats sont exposés dans la section 3.3.

Objectif 3 : Un nouvel outil de datation. Cette thèse constitue la première étude systématique des variations d'intensité en Espagne pendant les deux derniers millénaires. Les données d'intensité obtenues ainsi que l'amélioration et l'établissement de la courbe directionnelle de référence pour la Péninsule Ibérique constituent en eux-mêmes un nouvel outil de datation pour l'archéologie en Espagne.

1.3. Un coup d'oeil sur l'histoire de l'Espagne

Comme on l'a déjà signalé, pour connaître les variations du CMT au cours des derniers millénaires, l'archéomagnétisme repose sur l'étude des structures qui ont acquis une aimantation thermorémanente (ATR) et qui sont bien datées par les contraintes de l'archéologie ou par des méthodes géochronologiques (C14, dendrochronologie, etc). Malheureusement, les datations des structures archéologiques ne sont pas toujours faciles, et une analyse minutieuse de tous les renseignements sur les dates d'utilisation et d'abandon des

structures (correspondant au dernier refroidissement) doit être accomplie pour chacune des structures archéomagnétiques étudiées. Dans cette thèse, nous avons étudié des structures archéologiques espagnoles, et un coup d'oeil sur l'histoire de l'Espagne reste nécessaire pour bien comprendre les contraintes archéologiques qui servent de base à la datation des structures étudiées. J'aimerais bien signaler aussi la nécessité d'une réelle collaboration entre deux groupes de chercheurs: les géophysiciens, qui vont mesurer le signal ancien dans les terres cuites, et les archéologues, qui vont proposer une datation ce qui nous permettra d'établir la relation directe avec les mesures faites au laboratoire. Il est nécessaire d'avoir des datations les plus fiables possibles pour les structures, car, les erreurs de datation peuvent donner lieu à de mauvaises estimations des variations du CMT.

Voici un bref résumé de l'histoire de l'Espagne de l'époque Romaine jusqu'au XVI^{ème} siècle, intervalle dans lequel sont comprises la grande majorité des structures archéologiques étudiées dans le cadre de cette thèse.

Carrefour entre l'Europe et l'Afrique, entre les civilisations païennes, chrétiennes et musulmanes, l'Espagne fut pendant des siècles un pays de conflits, de conquêtes et de reconquêtes. Après la victoire de Rome contre Carthage, au III^e siècle avant JC, les Romains arrivèrent, et mirent deux siècles pour imposer leur culture dans la *quasi* totalité de la péninsule. Ainsi Hispania est devenue une province de l'Empire Romain pendant sept siècles, rythmés par la « Pax Romana » et l'essor de la culture et civilisation latine. Rappelons ainsi que des Empereurs comme Trajan et Hadrien ou penseurs comme Sénèque, étaient d'origine ibérique. Pendant ce temps Hispania se couvre d'aqueducs, théâtres, cirques, ponts et thermes. C'est pourquoi, de nombreux fours à céramiques, domestiques ou forges datant de cette époque ont été découverts par les archéologues. Dans cette thèse un four romain a été étudié (DENA).

Pendant le haut Moyen-âge, la péninsule Ibérique a vu l'arrivée de plusieurs peuples germaniques, ce qui sert à accélérer la crise sociale de l'Empire Romain. Si les Vandales, poursuivant leur route vers l'Afrique du Nord, ne firent pas que traverser le pays, les Suèves s'installèrent dans le nord-ouest et les Visigoths établirent dans le reste du pays un royaume puissant qui s'étendait au-delà des Pyrénées. Finalement ils se replièrent dans la péninsule, se convertirent aux christianisme, et vont dominer le pays jusqu'au début du VIII^e siècle. De

cette époque, très peu de vestiges de l'activité industrielle et de surcroît mal datés ont été trouvés.

En 711 se produit l'arrivée des Musulmans en provenance de l'Afrique par le détroit de Gibraltar et la défaite du dernier roi visigoth Rodéric (Don Rodrigo). Les Musulmans s'établirent sous le mandat du calife de Damasco. Même s'il y avait des noyaux de résistance dans le nord, la culture arabe fut florissante dans le reste de la péninsule et les Arabes développèrent les arts, les sciences, les techniques agricoles et créèrent de nombreux palais, mosquées, écoles et bains publics. Al-Andalus, la nouvelle appellation de la péninsule musulmane, devient le foyer incontournable de la culture occidentale à cette époque, c'est grâce aux philosophes et scientifiques ibero-árabes que nous ont été transmises les œuvres les plus importantes de l'antiquité grecque et romaine. Les Musulmans en s'installant dans la péninsule vont renforcer l'importance des concentrations urbaines déjà existantes au lieu de fonder des villes nouvelles, particulièrement au cours du IX et X siècles. A l'exception du palais de l'époque califale de Madina-al-Azhara et Madina-al-Zahira, le reste des 22 villes créées par les Arabes en Espagne répondent, au début, à des raisons stratégiques. Plusieurs d'entre elles ont donné lieu après à des concentrations urbaines stables. Six, sur la route qui reliait Córdoba à Toledo et à Zaragoza; les plus importantes étant Calatayud, la ville hispano-musulmane la plus ancienne, créée en 716, et qui est considérée comme la plus importante forteresse de l'ouest de Al-Andalus; Calatrava, dans la vallée du Guadiana, étape sur le chemin des troupes entre Córdoba et Toledo; Madrid, emplacement des troupes qui surveillaient l'accès septentrional à la vallée du Tajo; et Medinaceli, qui a été créée au cours de la moitié du IX siècle pour être le point de départ des troupes musulmanes contre la Castilla de Fernán González. Mise à part cette importante voie de communication, mais aussi en suivant des critères stratégiques, les villes de Murcia et Tudela ont été créées après la destruction des anciennes villes rebelles contre le pouvoir de Córdoba au début du IX siècle. Tudela, servira ensuite de base avancée pour les Musulmans de Zaragoza afin de contrôler cette région (García de Cortázar, 2001). En 929, Umayyad Abd-al-Rahman III autoproclame son propre califat, lequel est politiquement indépendant du monde islamique oriental. A cette époque, Córdoba était le centre culturel de cette région avec plus d'un million d'habitants. Après deux siècles et demi relativement stables, les disputes pour la succession et la lutte pour le pouvoir parmi les tribus arabes du Nord de l'Afrique qui arrivent en Al-Andalus entraînèrent l'effondrement de la dynastie Umayyad au début du XI siècle. La proximité de l'Afrique du Nord et de l'Al-Andalus facilita l'arrivée continue de berbères, à la

recherche d'une amélioration de leur qualité de vie ainsi que de leur sécurité sur les terres de la Péninsule Ibérique. La guerre civile éclate et l'Al-Andalus se divise en plusieurs petits états indépendants, appelés Taifas, comme par exemple Toledo, Badajoz, Sevilla, Valencia, Cordoba, Granada, Murcia. Pendant les XI et XII siècles la population africaine de l'Al-Andalus augmenta avec l'arrivée des « Almorávides », berbères nomades du Sahara, et les « Almohades », qui venaient de l'Atlas marocain. Cette période correspond aussi à un important développement culturel et économique des petits royaumes chrétiens du nord de la Péninsule. Durant le XI siècle, quelques-uns de ces royaumes commencent à s'agrandir, et sous le règne d'Alfonso VI, Toledo est reconquis. Cette période est appelée par les Chrétiens *la reconquête*. Il faut noter aussi la présence importante de la communauté juive tant dans Al-Andalus que dans l'Espagne chrétienne, avec une grande influence dans le commerce et l'artisanat et en général de bonnes relations de coexistence entre les trois cultures. Une autre preuve de l'interrelation des cultures est l'existence de l'art mudéjar (ou mozárabe), créé par des artisans arabes (chrétiens) dans des territoires chrétiens (arabes), où les différentes caractéristiques architecturales coexistent. Au XIII siècle, les conquêtes chrétiennes mirent fin à la domination musulmane dans le sud de la péninsule sauf l'important sultanat de Granada qui dura jusqu'au XV siècle.

La majorité des fours étudiés (Murcia: MURG, MURO, MURN, MURM, MURL, MURI, MURH, MURK; Calatrava la Vieja: CALA, CALB, CALC et le lot de céramiques CERCALB produites en CALB; Valencia: VALN, VALI, VALK, VALM) correspond à la période comprise entre les X et XV siècles.

L'union en 1469 entre Isabel de Castilla et Fernando d'Aragon, réunit deux des plus importants royaumes chrétiens d'Espagne et fut un moment décisif pour l'unification sous le pouvoir chrétien de la péninsule. En 1492, la reddition d'Abu Abdallah (Boabdil) face à Isabel et Fernando supposa la perte du dernier sultanat de Granada et marqua définitivement la fin de la domination musulmane. A cette époque un décret imposa l'expulsion des Juifs des royaumes d'Espagne, des milliers de Juifs étaient contraints ou à se convertir ou bien à abandonner leurs possessions. Pendant des siècles ces juifs d'origine espagnole, les Sefardies, ont conservé dans la diaspora, la langue espagnole telle qu'on la parlait au XV siècle. Après la découverte de l'Amérique par Cristobal Colon, en 1492, l'Espagne devient l'une des nations les plus puissantes d'Europe. Juana, dite « la loca » (fille des Rois Catholiques), se maria avec Felipe, dit « el Hermoso » (petit-fils de l'empereur germanique Maximilien), avec qui elle eut

un fils, Carlos Quinto, qui devint roi d'Espagne et Empereur de l'Empire Romano-Germanique. Il introduisit ainsi la maison d'Autriche (les Habsbourg) en Espagne et passa à la tête de l'empire le plus puissant de l'ancien monde. Bien que le XVI siècle voit donc la puissance espagnole atteindre son apogée par la force de ses armées, et malgré l'obtention de richesses par l'exploitation du continent américain et la politique matrimoniale des Habsbourg (son union avec le Portugal), l'économie va à la catastrophe. Toute une littérature extrêmement critique où les « Picaros, Hidalgos, Licenciados » essayaient de survivre et de se débrouiller dans un monde d'apparences, est la meilleure illustration d'un géant aux pieds d'argile tel que l'était l'Empire espagnol.

Quelques fours étudiées appartiennent aussi aux XV et XVI siècles (PATH, PATA, PATB, PATJ)

Le pouvoir des Habsbourg prit fin lorsque Carlos II, dit « el Embrujado », meurt sans descendance et qu'une guerre de Succession eut lieu au terme de laquelle le Bourbon Philippe V (neveu du roi soleil, Louis XIV) devint roi d'Espagne en abandonnant ses droits sur la couronne de France. Actuellement un de ses descendants Juan Carlos est le roi d'Espagne.

Deux fours et un lot de briques étudiées appartiennent aux XVII (VALL), XIX (le briques GUA2) et XX siècles (YUS2).

La Figure 7 illustre les événements postérieurs à cette date ainsi qu'une vue générale des différentes périodes de l'histoire de la péninsule Ibérique. Il s'agit, bien sûr, comme la brève introduction ci-dessus, d'une approche très générale. Le lecteur pourra se référer aux livres d'histoire comme par exemple la collection « Historia de España dirigida por Miguel Artola, Alianza Editorial » pour avoir une vision plus approfondie de l'histoire espagnole.

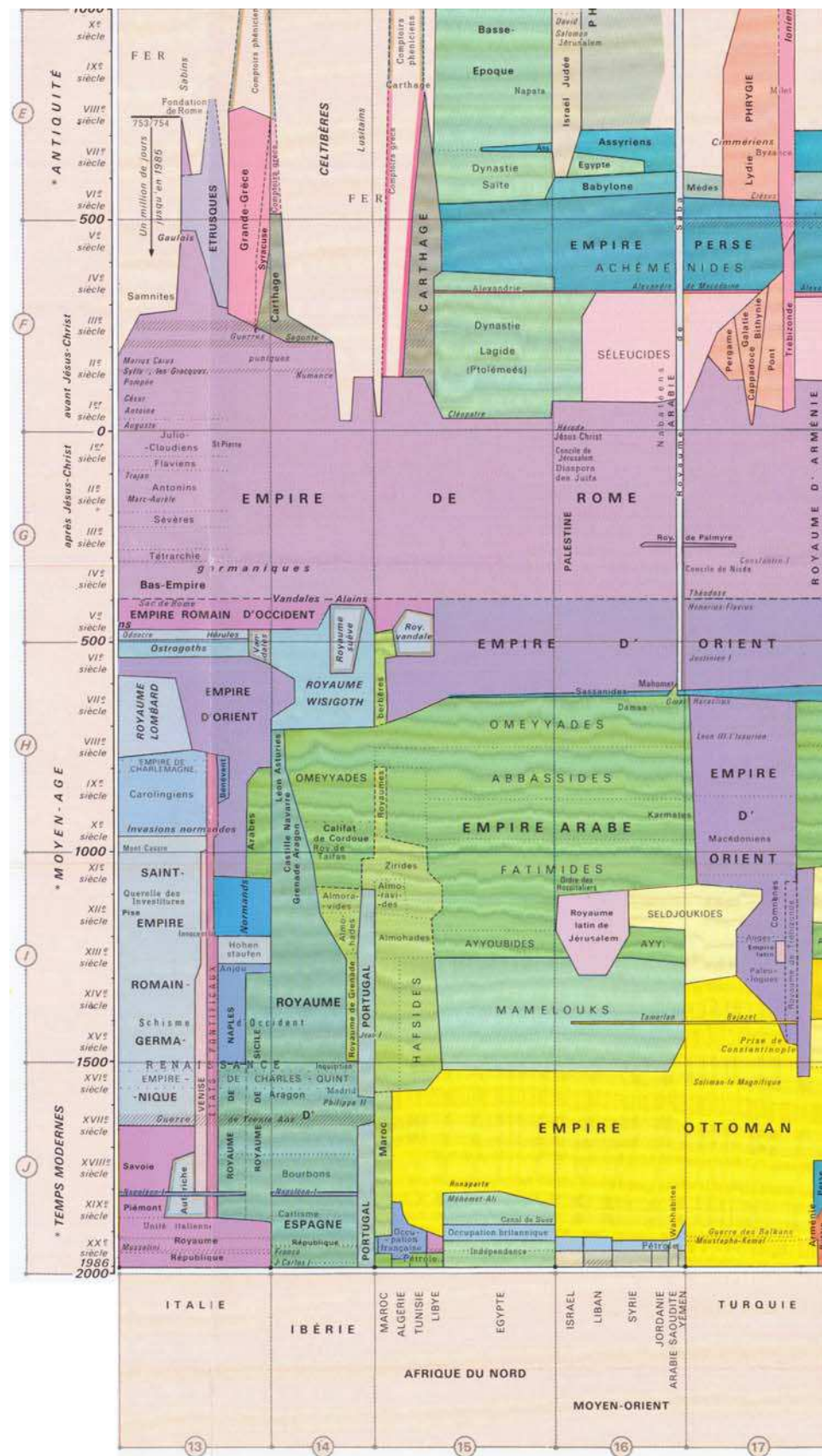


Figure 7: Tableau synoptique de l'histoire de la Péninsule Ibérique (d'après le tableau synoptique de l'histoire du Monde pendant les cinquante derniers siècles de L. H. Fournet édité par SIDES)

Chapitre 2. Courbe de variation séculaire pour la Péninsule Ibérique

Introduction

Comme nous l'avons déjà signalé, l'étude de la variation du champ magnétique dans les différentes régions du globe est essentielle pour mieux comprendre les variations du CMT au cours des derniers millénaires. En Espagne, nous disposons de peu de données (voir 1.2 de cette thèse), pour cette raison, nous avons cherché à les compléter en étudiant 26 fours archéologiques (structures en place qui nous permet d'obtenir la direction et l'intensité du champ magnétique ancien), une d'entre elles étant un four romain daté entre 200-220 après JC, les autres datés du XI^e au XIX^e siècles. Les structures étudiées proviennent en majorité de l'Est de l'Espagne. Une rigoureuse analyse sur l'âge des structures apporté par les renseignements archéologiques est présentée dans l'Annexe V de cette thèse, étape capitale dans la reconstruction de CMT. La technique utilisée pour la détermination à la fois de la direction et de l'intensité du CMT ancien est celle qu'a développé Thellier (1959). En plus, les corrections d'anisotropie de l'ATR ont été calculées pour chaque échantillon (Annexes I et II). Les analyses d'anisotropie montrent que pour l'argile cuite de nos fours, la correction d'anisotropie n'est pas cruciale. Les faibles valeurs d'anisotropie trouvées dans la majorité des échantillons et la distribution erratique des axes principaux des tenseurs de l'anisotropie de l'ATR ne modifient quasiment pas les directions moyennes par site (voir Annexe I). Les résultats directionnels par échantillon et par site, ainsi que les diagrammes de Zijderveld, sont réunis dans l'Annexe I.

La section 2.1 présente l'article « **A catalogue of Spanish archeomagnetic data** », dans lequel nous avons compilé et mis à jour les résultats archéomagnétiques par les études antérieures pour la Péninsule Ibérique (la majorité de données proviennent de Núñez (2004)). Nous y avons obtenu aussi de nouveaux résultats, qui sont décrits dans cet article.

La section 2.2 présente l'article « **The first Secular Variation Curve for the Iberian Peninsula. Comparison with other data from Western Europe and with geomagnetic field global models** ». Les données espagnoles, ainsi que une compilation des données françaises et marocaines situées à moins de 900 km de Madrid, ont permis de calculer la courbe de variation séculaire en Péninsule Ibérique pour les derniers millénaires. Nous avons comparé la méthode classique par fenêtres mobiles à la méthode bayésienne. Cette méthode a l'avantage de traiter les données en 3D simultanément (déclinaison, inclinaison et temps), de permettre aux données d'être mobiles dans l'intervalle de temps proposé par les archéologues et de tenir compte des contraintes stratigraphiques. Enfin, nous discutons la comparaison de nos résultats avec les courbes française et allemande et les modèles globaux de champ proposés par Korte et Constable (2005) et Hongre et al. (1998).

Dans la partie suivante nous présentons un bref résumé de la méthode bayésienne utilisée dans le cadre de ce travail de thèse (sections 2.2 y 3.2) afin d'en faciliter la compréhension. L'intérêt de cette méthode réside dans ses applications en archéomagnétisme. C'est Philippe Lanos qui les a développées. Il a notamment écrit un code numérique permettant de dater par l'archéomagnétisme des structures archéologiques et de construire des courbes d'étalonnage (courbes de références) en archéomagnétisme (Lanos, 2004; Lanos et al. 2005).

L'approche bayésienne en chronométrie applications à l'archéomagnétisme (Lanos, 2004 ; Lanos et al. 2005)

La statistique bayésienne permet une amélioration significative de la méthode de construction des courbes de variation séculaire du CMT. En effet, au niveau des points de référence servant à la construction des courbes d'étalonnage, il est possible de tenir compte, de façon probabiliste, non seulement des erreurs expérimentales mais aussi des erreurs sur les calages chronologiques ainsi que des informations de chronologie relative fournies par la stratigraphie. D'autre part, cette statistique fournit un cadre théorique et pratique pour le calcul des dates calendaires. Elle permet de calculer des dates archéomagnétiques pour toute combinaison des variables inclinaison, déclinaison et intensité du champ magnétique terrestre,

et d'associer un niveau de fiabilité à chaque datation, compte tenu des mesures réalisées (Dehling and Van der Plicht, 1993 ; Buck et al., 1996 ; Lanos, 2004).

La construction bayésienne des courbes d'étalonnage en archéomagnétisme

L’Inclinaison I et la Déclinaison D sont, avec la variable Intensité F, les trois composantes qui permettent de décrire complètement le CMT à un instant donné en un point donné (repéré en longitude et latitude, à la surface de la Terre). A un instant donné, ces trois composantes du CMT varient en fonction de la localisation géographique. De plus, en un point donné, ces trois composantes varient au cours du temps. La construction des courbes de variation séculaire de I, D et F en fonction du temps pour une région donnée repose sur l’idée que des structures contemporaines doivent fournir les mêmes valeurs de I, D et F aux erreurs expérimentales près, et sur l’idée que le champ magnétique varie de façon “ lisse ” à l’échelle de la décennie. Ce dernier point est justifié par l’allure des courbes de variation du champ géomagnétique enregistré dans les observatoires en particulier en France au cours des derniers siècles.

Il existe actuellement plusieurs méthodes statistiques de construction des courbes qui mettent en œuvre ces idées. On part de la formalisation suivante: à un instant donné t , ou bien pour un intervalle de temps donné $[t_1, t_2]$, correspondant à un point de référence (structure de terre cuite de type four, foyer ou matériaux de construction), on détermine une valeur de I, D ou F, qui sera exprimée sous la forme d'une moyenne Y , et d'une erreur d'estimation σ sur cette moyenne. La difficulté du tracé de courbes en archéomagnétisme réside dans l'existence des erreurs sur les mesures et sur le temps, et dans le fait que les points de référence sont le plus souvent irrégulièrement répartis sur le temps. Les méthodes statistiques les plus couramment utilisées reposent sur l'usage de la moyenne mobile à fenêtre de largeur variable, appliquée dans le cas uni-dimensionnel (on traite séparément I, D et F) (Batt, 1997) ou dans le cas bi-dimensionnel (par exemple on traite simultanément I et D) (Le Goff et al., 1992, 2002). Ces outils présentent cependant l'inconvénient de supposer que la courbe est en moyenne une droite dans chaque fenêtre considérée (Lanos et al., 2005). Ceci produit un lissage plus ou moins accentué selon la largeur de la fenêtre choisie, qui peut produire des erreurs notables sur l'estimation de l'inclinaison du champ.

Une autre méthode, adaptée et développée par Lanos (2004), repose sur l'approche bayésienne “ pénalisée ”. Elle consiste à faire passer à travers l'ensemble des points de référence une courbe qui a la propriété de s'ajuster aux données de telle sorte que sa courbure soit continue quel que soit le temps t . La fonction inconnue g sera estimée dans le cadre de la théorie de l'inférence bayésienne (Dudewicz et Mishra, 1988 ; Tassi, 1992 ; Droebecke et al., 2002) à partir de la formule des probabilités conditionnelles qui relie les observations Y et les paramètres du modèle. D'où g sera estimé par l'estimateur bayésien g_B donné par:

$$g_B = \int g p(Y | g, \alpha, \sigma_\alpha^2, t, S) p(g | \alpha, \sigma_\alpha^2, t, S) p(\alpha | \sigma_\alpha^2, t, S) p(\sigma_\alpha^2 | t, S) p(t | S) dg_1 \dots dg_n dt_1 \dots dt_n d\alpha d\sigma_\alpha^2$$

[1.1]

L'estimateur g_B est une espérance conditionnelle a posteriori sachant les observations Y . Les variables Y , g et t sont des vecteurs aléatoires, de dimension n égal au nombre de nœuds sur le temps. Le nombre de points de référence N est égal ou supérieur au nombre de nœuds selon qu'il y a un ou plusieurs sites Y_{ij} ayant une même date t_i . Pour chaque nœud t_i , on détermine une valeur moyenne Y_i (d'où le vecteur Y). Le vecteur t est le vecteur temps associé aux structures de référence. Le scalaires α correspond au coefficient de lissage et le scalaire σ_α^2 correspond à la variance globale des points de référence par rapport à la courbe (leur densités seront définies plus loin).

La densité conditionnelle $p(t | S)$ est le produit des densités a priori des temps des structures de référence supposées indépendantes, d'où le produit des densités :

$$p(t | S) = \prod_{i=1}^n \left(\frac{1}{(t_{i2} - t_{i1})} \right) \cdot 1_S(t) \quad [1.2]$$

La fonction indicatrice $1_S(t)$ est égale à 1 si tous les temps t_i sont dans les intervalles définis et si les éventuelles relations stratigraphiques entre les t_i (ce peut être des relations partielles entre les t_i) sont vérifiées, à 0 sinon. C'est donc à ce niveau que l'on introduit les informations archéologiques de type stratigraphique pour la construction de la courbe. Par exemple, dire qu'un four de potier a cessé de fonctionner durant le second siècle ap. J.-C. du

fait d'avoir retrouvé dans son remplissage des tessons de céramique datés de ce siècle pourra se traduire par un intervalle de date $[t_1, t_2] = [100, 200]$. Mais ceci introduit implicitement de nombreuses hypothèses sur l'histoire de la structure. La notion chronologique vraiment fiable est en fait le *Terminus Post Quem* (TPQ), qui se traduit par un intervalle de temps fermé à gauche et ouvert à droite. Dans notre exemple, l'arrêt du four a eu lieu en toute rigueur après 100 ap. J.C. Seules des informations d'ordre stratigraphique peuvent alors permettre de fermer l'intervalle à droite. La mise en place d'une base de données archéomagnétiques, consiste non seulement à accumuler des mesures archéomagnétiques, mais aussi à définir entre les structures de référence un ensemble de contraintes chronologiques telles que les intervalles de date de référence $[t_1, t_2]$ puissent se fermer avec suffisamment de précision. Un moyen efficace d'y parvenir est évidemment d'étudier des structures de terre cuite mises en relation stratigraphique au sein d'un même site archéologique. En définitive, TPQ et relations d'ordre stratigraphique peuvent être pris en compte sans difficulté grâce à l'approche bayésienne.

La densité conditionnelle a priori $p(\mathbf{g} | \alpha, \sigma_\alpha^2, S, \mathbf{t})$ permet de définir le type de fonction \mathbf{g} que l'on admet : en particulier, il paraît “raisonnable”, au vu des données récentes d'observatoire, de donner plus de poids aux fonctions présentant un caractère plus lissant (avec courbure “continue”). Cela revient à pénaliser les fonctions plus “agitées” par rapport au moins agitées. La conséquence de ce choix est que la fonction \mathbf{g} sera de type “Spline cubique naturelle pénalisée” (Wahba, 1990 ; Green et Silverman, 1994). On remarque ici que l'on ne choisit un type particulier de fonction a priori. C'est uniquement sur l’“allure” de la fonction que se porte le choix a priori.

$$p(\mathbf{g} | \alpha, \sigma_\alpha^2, S, \mathbf{t}) = \frac{\det^+(\alpha \mathbf{K})}{(2\pi)^{\frac{n-2}{2}}} \exp \left[-\frac{1}{2} \mathbf{g}^T (\alpha \mathbf{K}) \mathbf{g} \right] \quad [1.3]$$

La matrice \mathbf{K} dépend uniquement des intervalles entre les temps t_i . Le paramètre α est le coefficient de lissage. Si $\alpha = 0$, la fonction de lissage sera une spline cubique naturelle passant par tous les points de \mathbf{Y} . Si $\alpha = \infty$, alors la fonction de lissage sera une droite de régression linéaire. Le meilleur coefficient de lissage est celui qui va établir le meilleur équilibre (au sens du maximum de vraisemblance) entre l'ajustement de la fonction aux points observés \mathbf{Y} et le lissage de la fonction \mathbf{g} (élimination des variations trop rapides liées aux erreurs). Ce choix peut être effectué par une minimisation du risque quadratique par la méthode de « validation

croisée généralisée » (Wahba, 1990 ; Green and Silverman, 1994). Il peut aussi être effectué de façon bayésienne en introduisant une mesure a priori de type « Jeffrey » répondant à un critère d'invariance (Droesbecke et al., 2002) : $p(\alpha | \sigma_\alpha^2, S, t) \propto 1/\alpha^2$. D'autre part, la densité a priori sur la variance globale est définie par $p(\sigma_\alpha^2 | S, t) \propto 1_{[0, \infty]}$ (Lanos et al., 2005).

Enfin, les observations Y suivent une loi d'échantillonnage Gaussienne (Lanos 2004) :

$$p(Y | g, \alpha, \sigma_\alpha^2, S, t) = \sqrt{\frac{\det(W)}{(2\pi)^n}} \exp \left[-\frac{1}{2} (Y-g)^T W (Y-g) \right] \quad [1.4]$$

où la matrice diagonale de précision W est définie par les termes:

$$W_i = \frac{1}{m_i} \sum_{j=1}^{m_i} \left(\sigma_\alpha^2 + \frac{\alpha_{95ij}^2}{2.45^2} \right)^{-1} \quad [1.5]$$

Le nombre de points de référence par noeud de temps t_i est m_i et l'erreur quadratique associée à chaque point est α_{95ij}^2 (Lanos et al., 2005) dans le cas directionnel, ou bien l'erreur quadratique d'estimation dans le cas de l'intensité.

Dans cette approche générale, il n'y a plus de fenêtre mobile de largeur fixée arbitraire, mais il y a une réelle prise en compte de la variation de la densité de points sur le temps. L'hypothèse de linéarité locale de la courbe se transforme en une contrainte beaucoup plus souple : on cherche une fonction présentant une courbure continue qui s'adapte aux données de telle sorte que le retrait de tout point modifie le moins possible la courbe globale. L'approche n'est plus une estimation ponctuelle de g , mais devient une estimation fonctionnelle. Par ailleurs, on n'est plus contraint de considérer les centres d'intervalles de date des points de référence, mais on donne la possibilité aux temps de se déplacer dans ces intervalles, en fonction de la densité de probabilité a priori $p(t | S)$, qui tient compte des connaissances archéologiques. La courbe moyenne est tracée avec une spline cubique naturelle passant par l'ensemble des points estimés g_B . Dans le cas des données directionnelles, nous utilisons les splines sphériques qui permettent d'estimer une courbe à la surface de la sphère en tenant compte à la fois de l'inclinaison et de la déclinaison (Jupp and Kent, 1987 ; Lanos, 2004), puisque ces deux variables sont liées.

Enfin, la méthode permet de définir une enveloppe d'erreur qui tient compte de toutes les erreurs intervenant dans les différents niveaux de l'analyse. On définit la variance a posteriori conditionnelle par :

$$\sigma_{g_B}^2 = E[g^2] - g_B^2$$

Une enveloppe de plus forte densité a posteriori à 95% sur la courbe est tracée en utilisant aussi une spline cubique d'interpolation. Dans le cas directionnel, les courbes marginales d'inclinaison g_{B_I} et de déclinaison g_{B_D} sont obtenues par enroulement sur la sphère des courbes paramétriques Bayésiennes déterminées dans le plan de projection azimutal (Jupp and Kent, 1987 ; Lanos 2004). Dans ce cas, l'erreur sur g_{B_I} est donnée par

$$\sigma_{g_B} \text{ et l'erreur sur } g_{B_D} \text{ par } \sigma_{g_B} / \cos g_{B_I}$$

En définitive, la statistique Bayésienne permet d'introduire avec une grande souplesse la discussion archéologique dans l'outil statistique et de prendre en compte toutes les erreurs à la fois analytiques et temporelles. La datation par archéomagnétisme est une méthode relative fondée sur la connaissance préalable de courbes d'étalonnage construites point par point, à partir de structures datées par d'autres moyens, le plus souvent archéologiques ou historiques, quelquefois chronométriques (^{14}C , TL...). Ceci constitue une originalité, en réalité une difficulté, par rapport à l'ensemble des autres grandes méthodes de datation utilisées en archéologie. La mise en œuvre des outils statistiques Bayésiens doit donc obligatoirement s'accompagner d'une discussion (régulière) des critères de datation retenus pour l'élaboration des bases de données archéomagnétiques.

2.1 Article : A catalogue of Spanish archeomagnetic data (Geophysical Journal International, in press)

M. Gómez-Paccard^(1,2,3), G. Catanzariti⁽²⁾, V.C. Ruiz-Martínez⁽²⁾, G. McIntosh⁽²⁾, J.I. Nuñez⁽²⁾, M.L. Osete⁽²⁾, A. Chauvin⁽¹⁾, Ph. Lanos⁽³⁾, D.H. Tarling⁽⁴⁾, D. Bernal-Casasola⁽⁵⁾, J. Thiriot⁽⁶⁾ and “archaeological working group”

where “archaeomagnetic working group” is composed by:

A. Sáez-Espigares, I. García-Villanueva, J.A. Gisbert-Santonja, M.A. Hervás, P. Jiménez-Castillo, M. Mesquida-García, I. Navarro, M. Orfila-Pons, I. Ramírez-González, M. Retuerce, D. Urbina and C. Urquijo

⁽¹⁾ Géosciences-Rennes, CNRS, UMR 6118, Campus de Beaulieu, 35042, Rennes, Cedex, France.

⁽²⁾ Facultad de Ciencias Físicas, Universidad Complutense de Madrid, Ciudad Universitaria, 28040, Madrid, Spain.

⁽³⁾ Civilisations Atlantiques et Archéosciences, CNRS, UMR 6566, Campus de Beaulieu, 35042, Rennes, Cedex, France.

⁽⁴⁾ Dept. Geological Sciences, Univ. Plymouth, Drake Circus, Plymouth, PL4 8AA, U.K,

⁽⁵⁾ Facultad de Filosofía y Letras, Universidad de Cádiz, 11003 Cádiz, Spain.

⁽⁶⁾ Laboratoire d'archéologie médiévale méditerranéenne, CNRS, UMR 6572, Maison méditerranéenne de Sciences de l'Homme, 13094, Aix-en-Provence, Cedex 2, France.

Accepted date. Received date; in original form date

Abbreviated title: Spanish Archaeomagnetic Catalogue

Corresponding author: Miriam Gómez-Paccard, phone: 0033 2 23 23 67 59/ fax: 0033 2 23 23 60 40/ e-mail: miriam.gomez@univ-rennes1.fr

Summary

A total of 58 new archaeomagnetic directions has been determined from archaeological structures in Spain. Together with 5 previous results they allow the compilation of the first archaeomagnetic catalogue for Spain, which includes 63 directions with ages ranging between the 2nd century BC and the 20th century AD. Characteristic remanence directions have been obtained from stepwise thermal and alternating field demagnetisation. The hierarchical structure has been respected in the calculation of the mean site directions. Rock magnetic experiments reveal that the main magnetic carrier is magnetite or titano-magnetite with different titanium contents. The age estimate of the studied structures is generally well justified by archaeological constraints. For 6 structures the proposed date is also supported by physical methods. The data are in close agreement with the French secular variation curve. This catalogue represents the first step in the construction of a secular variation curve for the Iberian Peninsula, which will be of much use in archaeomagnetic dating and in modelling of the earth's magnetic field in Western Europe.

Keywords: Archaeomagnetism, Geomagnetic secular variation, Spain, Western Europe,

1. Introduction

In order to use archaeomagnetism as a dating tool a reliable reference curve has to be constructed for the region in question. For this purpose, the study of well dated archaeological structures is required. Such structures include kilns, ovens, thermal baths and burnt walls, or any heated material that has recorded the earth's magnetic field during its cooling and thus acquired a thermoremanent magnetisation (TRM) parallel to the ambient field. The reference curves - called secular variation (SV) curves - can be used as a dating tool by comparing the archaeomagnetic field information (direction and/or intensity) of archaeological material with the known secular variation curve of the earth's magnetic field for this area. More or less well defined SV curves covering the last millennia are available for different countries in Europe (Schnepp & Lanos 2005, Gallet *et al.* 2002, Kovacheva & Toshkov 1994, Batt 1997) and this dating method is currently in use. The large number of excavations carried out in the past or that are now in progress in Spain means that the potential of this technique in the Iberian Peninsula is great. However, despite such potential there is a lack of archaeomagnetic data available for the region, a deficit addressed here.

This study consists of a compilation of previously available results for Spain, along with the results of the study of 58 new structures, giving rise to a catalogue of 63 archaeomagnetic directions. The principal information related to each individual study has been detailed, including the field sampling and laboratory treatment, and the criteria used in the determination of the characteristic directions, at the specimen, sample and site level. Rock magnetic studies have been carried out to identify the main magnetic minerals carrying the archaeomagnetic signal. The archaeological and chronological information has also been compiled and analysed, and is presented as an appendix.

This work is the first example of an intensive cooperation between archaeologists and geophysicists in Spain in the field of archaeomagnetism and establishes the basis of future archaeomagnetic research. The catalogue presented represents the first step in the construction of a reliable SV curve for the Iberian Peninsula. The data set further contributes to better constraining the variation of the earth's magnetic field in Western Europe during the two last millennia.

2. Previous archaeomagnetic studies in Spain

The first published result from Spain was from Ampurias, Cataluña (Thellier 1981). The pioneer of archaeomagnetism studied one Spanish kiln dated between 200 BC and 100 AD and provided the first archaeomagnetic direction for this region. The next results were from La Maja, in La Rioja, and Villa del Pañuelo, in Madrid. At La Maja, Parés *et al.* (1992) studied a Roman pottery kiln, whose abandonment was dated by archaeological constraints as being in the 1st century AD. They confirmed the previous archaeological date by referring the obtained inclination to the French SV curve, giving an age of 30-78 AD. The archaeological date (1st century AD) has been retained in this catalogue. Kovacheva *et al.* (1995) conducted an archaeointensity study using the same sample collection and confirm, by comparison with archaeointensity data from neighbouring countries, the date estimated by Parés *et al.* (1992). Two Roman kilns were studied at Villa del Pañuelo, Madrid (Oyamburu *et al.* 1996), which were also dated using the French SV curve, giving ages of 0-150 AD and 150-350 AD. The results obtained are consistent with later archaeological dating. The archaeological date has been retained in this catalogue. There are unpublished results available from the Roman ovens of Arva and Celti (in Seville), studied by Evans (private communication). Although not well dated at the time of their study, the archaeomagnetic results demonstrated that these ovens were not coeval and that a difference of approximately 50-100 years existed between their

use. Recent archaeological studies now place the Arva oven between 150 and 250 AD (Remesal, private communication). These 5 directions have been included in the catalogue. Nachasova *et al.* (2002) published an archaeointensity study of ceramic fragments from Valencia dated between the 5th and 2nd centuries BC. These data, concerning only archaeointensity determinations, are not included in the catalogue but can be found in Korte *et al.* (2005).

3. New archaeomagnetic studies

3.1. Sampling

The locations of the new structures that have been investigated are shown in Fig. 1. Most of the structures are kilns, but one furnace, two thermal baths, two burnt walls and a burnt floor have also been studied. The types of material sampled include burnt clay, bricks and native rock, depending on the construction of the particular structures. Three types of independently oriented samples were taken in the field. For well-consolidated structures oriented core samples were taken using portable rock drills of the type commonly used in palaeomagnetic studies (drill samples in Table 1). Alternatively, especially for less well-consolidated structures, large block samples were taken by preparing a flat surface using gypsum plaster, which was then oriented (block samples in Table 1). In the case of poorly-consolidated material the samples were completely encased in plaster before removal. Smaller hand samples were occasionally taken using the method described by Tarling (1983). Here small, wooden cylinders were fixed to the material to be sampled. These were oriented and removed, with a small amount of material staying fixed to the cylinders (hand samples in Table 1). Orientation in the vertical plane was achieved using a compass and/or inclinometer, and in the horizontal plane using spirit levels, magnetic and solar compasses. At least 4, but generally more than 8, independently oriented samples were taken from each archaeological structure (N' in Table 1).

In the laboratory, standard cylindrical specimens (volume = 10.8 cm³) were prepared from the cored and block samples. Poorly consolidated samples from 5 sites were treated using sodium silicate (“waterglass”) or ethyl silicate (“Silbond 40”,) prior to taking the specimens. Several treatment techniques were used. The first involved cutting slices from the sample (from sites CDAJ, CDAH, CDAU and CDAP in Table 1), followed by a 2-step impregnation using first 50-50 % then 20-80 % water-sodium silicate solution, both under vacuum. 2×2×2 cm³ cubic specimens were then cut from the dried sample slice. Alternatively, the samples (from site

GUA1 in Table 1) were immersed in ethyl silicate over a period of days, then taken out and dried (at room temperature). Standard cylindrical specimens were then drilled from the sample. Previous studies carried out in baked clays show that the impregnation with water glass does not significantly affect the remanence during heating experiments (Kostadinova *et al.* 2004).

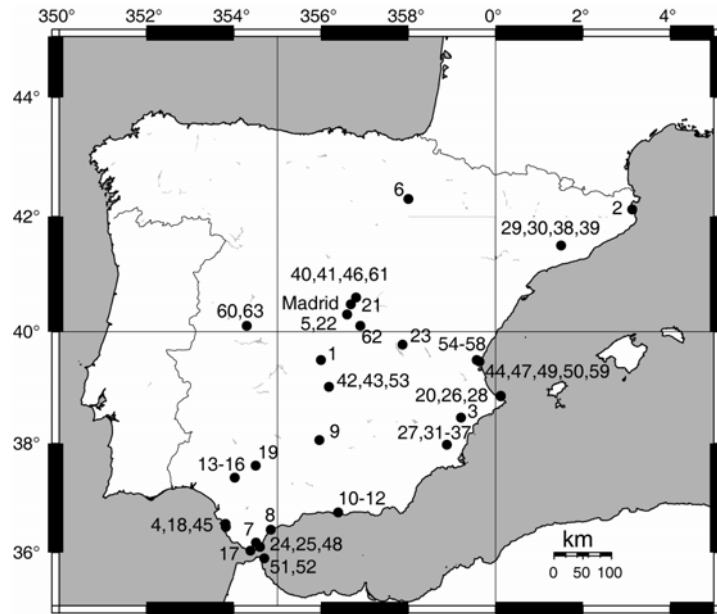


Figure 1. Map showing the location of archaeomagnetic sites included in the catalogue. Madrid (40.4 °N, 3.7 °W) has been chosen as the reference site for Spain.

3.2. Magnetic measurements

Measurements were performed in the palaeomagnetic and archaeomagnetic laboratories of the University Complutense de Madrid (Spain), Géosciences Rennes (France) and the University of Plymouth (UK). Remanent magnetisation was measured using Molspin, JR5 (Agico) or Digico large sample spinner magnetometers. Stepwise alternating field (AF) demagnetisation was carried out using Schonstedt or Molspin large demagnetisers, with 5 or more steps up to the maximum available field (100 or 150 mT). Stepwise thermal (Th) demagnetisation was conducted using MMTD or Schonstedt ovens with 5 or more steps until more than 80 % of natural remanent magnetisation (NRM) had been removed, unless thermally induced alteration took place, at which point demagnetisation was halted. For the structures analysed

at Rennes, the classical Thellier paleointensity method (Thellier and Thellier, 1959), with pTRM checks, based on the comparison between natural remanent magnetization (NRM) lost and partial thermoremanent magnetization (pTRM) gained in a known laboratory field was used. The thermal demagnetisation data were obtained from these experiments, denoted as TH in Table 1.

Low field magnetic susceptibility (K) was measured for all specimens using Bartington or Kappabridge (KLY3, Agico) susceptibility meters. K was also measured after each heating step during Th and TH demagnetisation in order to monitor mineralogical alteration. Thermomagnetic curves were measured in air using a KLY3 susceptibility meter with fitted furnace. Magnetic hysteresis was measured using a coercivity meter (Jasonov *et al.* 1998) with a maximum applied field of 500 mT. This instrument also generated stepwise acquisition and reverse-field acquisition of isothermal remanence (IRM).

TRM anisotropy has been determined for all specimens from 21 of the 25 structures measured in Rennes (AT in Table 1). To achieve this, TRM acquisition in 6 directions was carried out after demagnetising the NRM to 70 % of its initial value, followed by a thermal stability check along the specimen cylindrical axis. The NRM and TRM measurements were corrected for anisotropy using the method described by Veitch *et al.* (1984) and Chauvin *et al.* (2000). All specimens used to calculate mean directions of magnetisation from these 21 structures have been corrected for TRM anisotropy.

4. New results

4.1. Archaeological dating

In order to propose an interval of age for each structure a critical analysis of the compiled archaeological information was carried out. The *terminus post-quem* (TPQ) and the *terminus ante-quem* (TAQ), proposed by archaeologists or by radiocarbon studies, are given where available. The TPQ (TAQ) refers to the date after (before) which the structure may have been in use. The TPQ, generally easier to determine than the TAQ, is commonly determined on the basis of the age of the oldest objects found in the same stratigraphic unit as the analysed structure. The TAQ is generally established on the basis of the abandonment of the site, ceramics and/or burial/infilling of the abandoned structure. These two parameters are the principal support of the proposed ages. A description of each archaeological site and structure is given in an Appendix, together with some references that may be useful for future archaeomagnetic studies. The ages ascribed to each of the structures included in the catalogue are shown in Table 1.

Six of the analysed structures have been dated by the radiocarbon method. At the Plaza de Moros site (1, PLM, in Table 1), conflictive radiocarbon dates were obtained from samples from the same burnt wooden beam used in the dating experiment. The younger of the dates (200 BC – 20 AD) is consistent with the archaeologically-determined date (150-50 BC). The archaeological date has been retained in the catalogue. At the Avenida Blas de Infante site (48, BI, in Table 1) the year of the fire associated with the sampled structure is precisely controlled by historical documents, whereas at the Yuste site (63, YUS2, in Table 1) anecdotal evidence describes a modern kiln used in 1959 AD. A further 15 structures include some form of historical constraints on the definition of their TPQ/TAQ. The remaining structures are dated on the basis of archaeological information. Great care has been taken in collecting and assessing this information and the basis of the archaeological constraints for each site and structure is set out in the Appendix. In future studies it would be of great interest to constrain archaeological information by other physical dating techniques, and to describe the stratigraphic constraints between the studied structures. Lanos (2004) demonstrate that such information may be taken into account in the construction of SV curves.

4.2. Demagnetisation of NRM

NRM demagnetisation results were visually inspected using orthogonal and stereographic projections. In many cases a variable, unstable component was removed at low temperatures or fields (< 200 °C or < 2-10 mT). This is interpreted as a viscous overprint and is not

considered further. Specimens from all but 5 structures exhibited a single stable component. Well-defined, linear trajectories trending to the origin of the orthogonal projection were isolated by both Th/TH and AF demagnetisation and remanence directions were calculated using principal component analysis (Kirschvink 1980). Two types of behaviour could be distinguished within this group of specimens on the basis of the NRM intensity decay curves. The first type of behaviour, called group 1A in Fig. 2, includes specimens exhibiting a single unblocking temperature (T_{ub}) or coercivity spectrum. AF demagnetisation produced monotonic NRM intensity decay curves and more than 90 % of NRM was demagnetised by 100 mT (CARI.06A, HIP.01A, Fig. 2). Thermal demagnetisation revealed monotonic intensity decays, with a range of maximum T_{ubs} of between 300 and 625 °C. In most cases a maximum T_{ub} of between 500-600 °C was observed (eg. MURH.5A, Fig. 2). T_{ubs} of 290-320 °C were also common, as were T_{ubs} of around 400-450 °C (eg. CARI.03A, Fig. 2). In all of these cases there is no evidence of a further, higher-temperature component and the NRM vector passes through the origin of the orthogonal vector plots.

The second type of behaviour (called group 1B in Fig. 2) includes specimens with two T_{ub} /coercivity spectra. Here there are 2 magnetic phases carrying the single, stable component. AF demagnetisation lead to NRM decreases up to 100 mT, but with more than 20 % remaining undemagnetised (eg. L2.02A, LLD.11M, LLD.14M, Fig. 2). This type of specimen is considered as having a low coercivity phase and an (undefined) high coercivity phase. Th/TH demagnetisation defined two spectra at different temperatures. Different spectra were recognised on the basis of clear slope changes on the intensity decay plot (eg. L2.01A, Fig. 2).

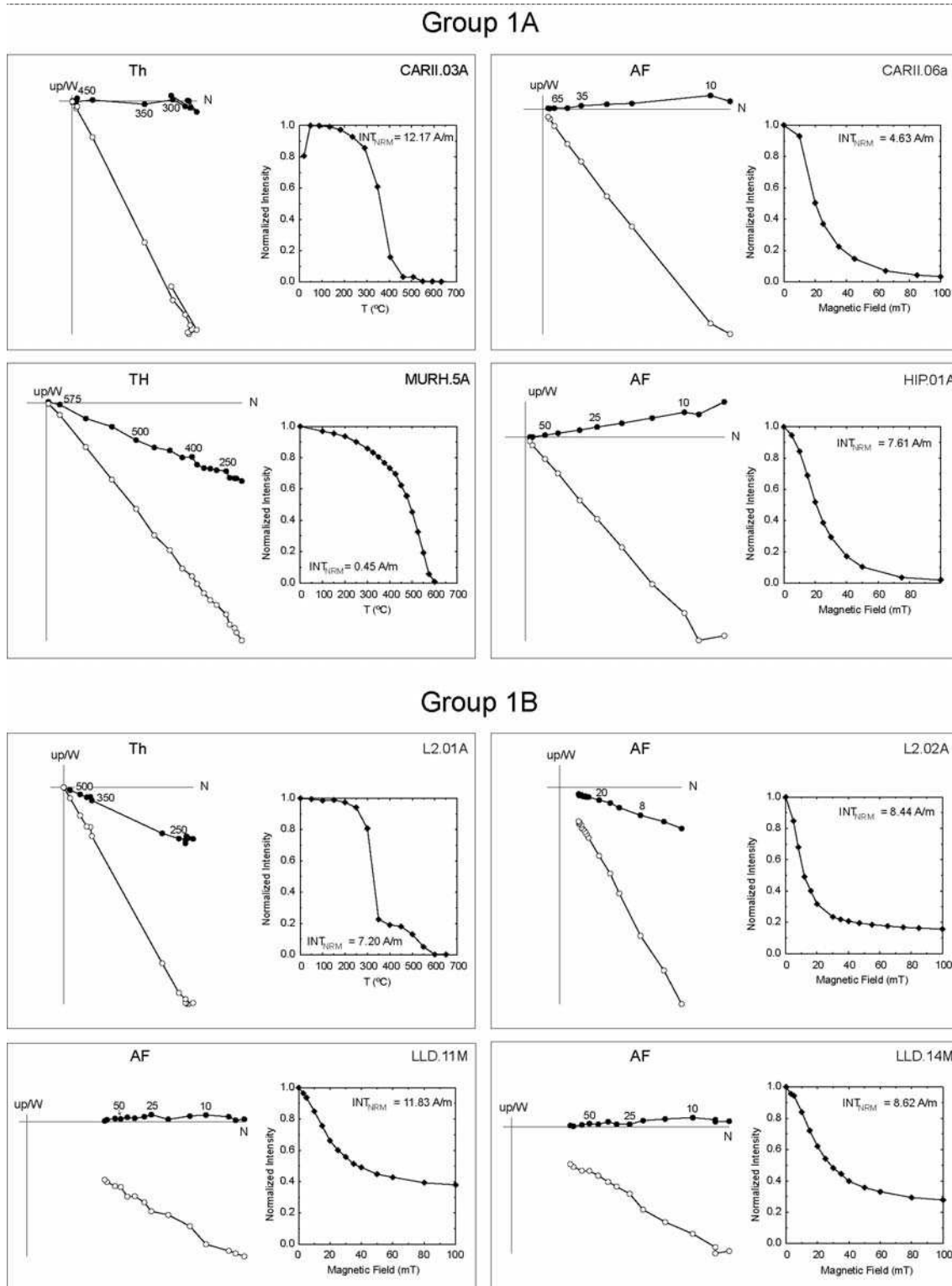


Figure 2. Representative plots for Type 1 and Type 2 NRM demagnetisation behaviour (see text for explanation). Orthogonal vector plots (solid (open) symbols: projection upon horizontal (vertical) plane) and normalised intensity decay plots are shown on the left and right resp. TH/Th/AF refer to thermal demagnetisation from Thellier-type palaeointensity experiments/thermal demagnetisation/alternating field demagnetisation respectively.

Five structures exhibited complex NRM demagnetisation behaviour, with two stable components of magnetisation (MAGII.5, VAL.13A, Fig. 3). Th/TH demagnetisation was generally better than AF at isolating the two components. Where linear segments of both components could be isolated on the orthogonal projection, remanence directions were calculated as previously described. This wasn't generally possible, as in most cases there was considerable overlap of the T_{ub} /coercivity spectra associated with the two directions. Here the low temperature or low coercivity phase was defined by great-circle analysis of the stereographic projection of the NRM vector (Fig. 3), calculating a pole direction defining the best-fit plane of the great-circle traced by the vector endpoint after each demagnetisation step.

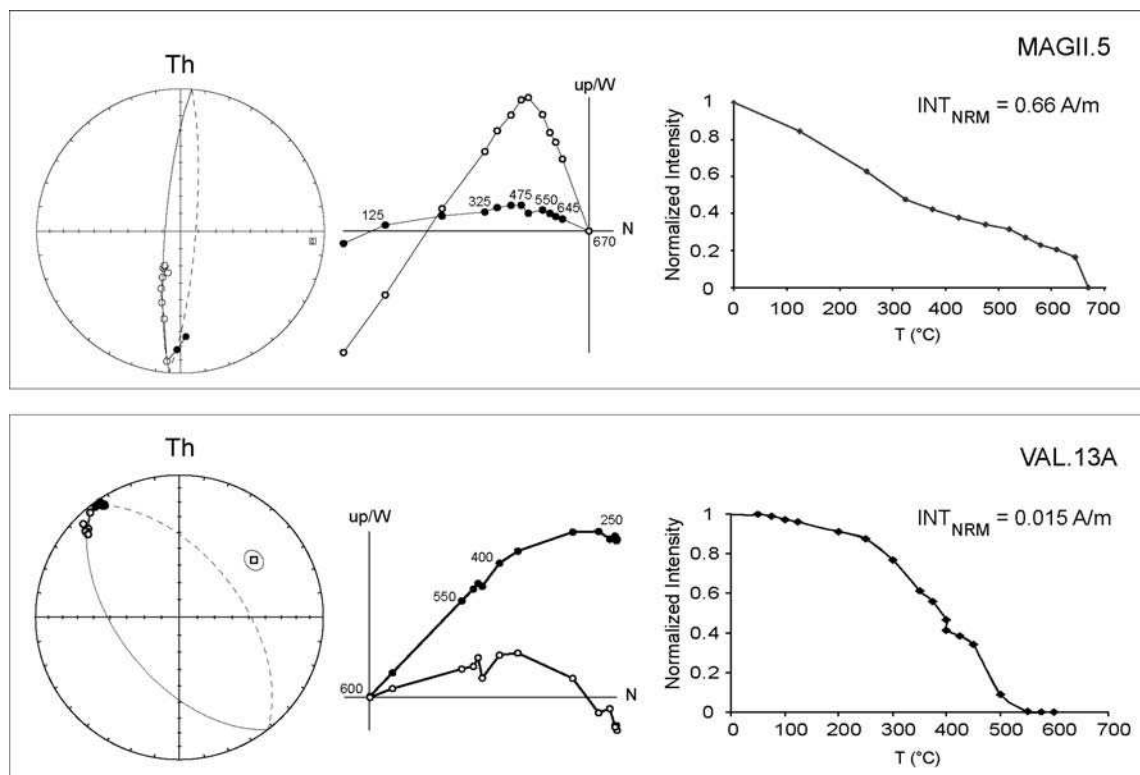


Figure 3. Representative plots for complex NRM demagnetisation behaviour (see text for explanation). Stereographic projections (solid symbols: projection on the lower hemisphere), orthogonal vector plots and normalised intensity decay plots are shown from left to right. The great circles used to calculate directions are shown on the stereographic projections.

4.3. Rock magnetic properties

4.3.1. NRM-K

Fig. 4 shows the intensity of the NRM (A/m) plotted versus K (SI), indicating Koenigsberger ratio (Q) isolines. The specimens have been divided into two groups: specimens from structures heated to low temperatures (eg. burnt walls/floors, VAL, BI and ALG in Table 1, open circles in Fig. 4) and specimens from well-heated structures (all remaining structures, solid circles in Fig. 4). Both NRM and K vary by several orders of magnitude, giving values of Q generally between 1 and 100. This high variability is due to the different materials used in the construction of the structures. The specimens corresponding to the less heated materials generally present lower NRM and K values.

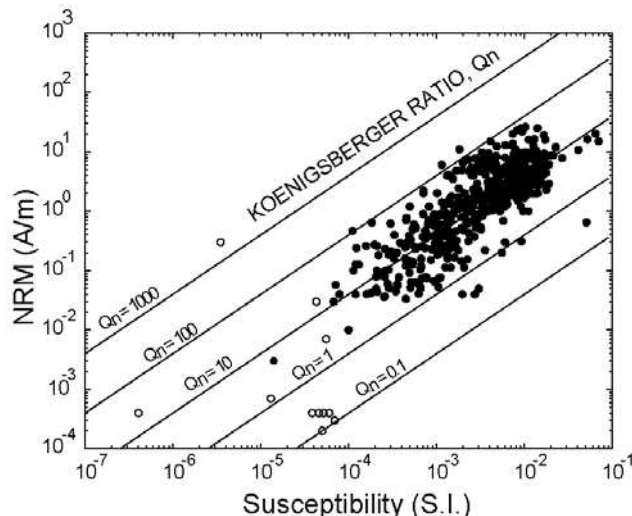


Figure 4. NRM intensity (A/m) versus bulk susceptibility (SI) for specimens from partially-heated (white circles, structures 23, 50 and 62 in Table 1) and well-heated (black circles) structures. Koenigsberger ratio isolines are shown.

4.3.2. Thermomagnetic curves

The variation of bulk susceptibility with temperature (KT curve) was determined for more than 140 samples from 26 structures (C in Table 1), from which the Curie temperatures (T_c) have been calculated using the first and second derivative method described by Tauxe (1998). In some cases smoothing of the data was needed due to the low K values and subsequent bad signal to noise ratio. Occasionally T_c could not be determined because of the low K values.

Representative thermomagnetic curves are given in Fig. 5, along with a histogram of T_{cS} s obtained.

The majority of the KT curves are relatively reversible, showing that the magnetic carriers are thermally stable. An unstable magnetic phase is sometimes observed around 200°C on the heating curve, which is absent on the cooling curve (eg. MURI.5, Fig. 5). This may point to the presence of goethite. The T_{cS} s obtained are in agreement with the unblocking temperatures found in the thermal demagnetisation of NRM. Four types of behaviour, but two principal types, were found. In most cases T_{cS} s of between 540 and 585 °C were observed (eg. CALB.9, Fig. 5), suggesting that the principal magnetic carrier is magnetite or Ti-poor titanomagnetite. The other main group of samples exhibited T_{cS} s of between 270 and 420 °C (eg. MURI.5, Fig. 5), and these phases dominate even if a high T_c phase is also present (eg. MURM.2, Fig. 5). Similar low Curie temperatures have been also observed by other authors (Casas *et al.* 2005, Schnepp *et al.* 2004, Chauvin *et al.* 2000) in bricks and baked clays. Another less important group of samples gives T_{cS} s between 435 and 510 °C, suggesting that in this case the magnetic carrier is titanomagnetite with higher Ti content. The last group of samples shows T_{cS} s higher than 585 °C, reaching up to 630 °C (eg. DENA.83, Fig. 5), which can be interpreted in terms of partially oxidised (titano)magnetite or (titano)maghemite. The reversibility of these curves indicates that this is thermally stable. Clear indication of the presence of hematite was rarely encountered in the KT curves.

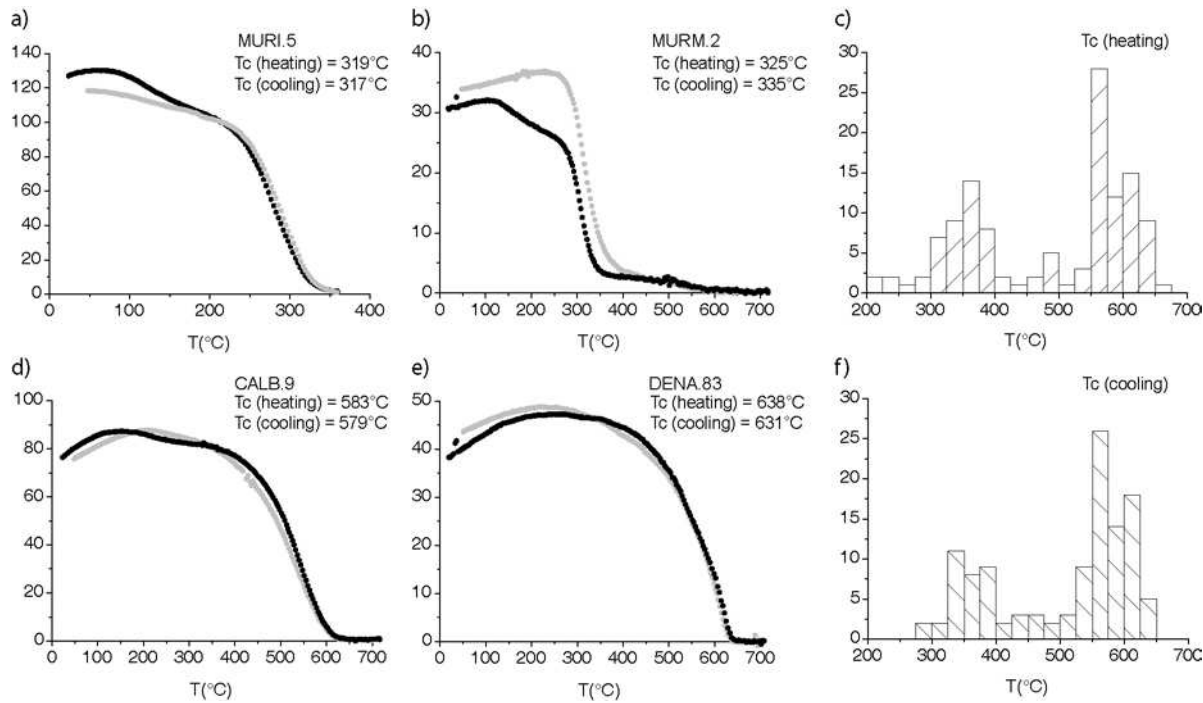


Figure 5. Representative thermomagnetic curves. Susceptibility is plotted on the y axis in arbitrary units. Heating/cooling are shown in black/grey. The distributions of Curie temperatures (T_c), calculated from the heating (c) and cooling (f) branches of the curves, are shown.

4.3.3. Hysteresis and IRM measurements

Magnetic hysteresis and IRM acquisition curves have been measured for a selection of samples spanning the range of material encountered in the studied structures (H in Table 1). Some typical curves are shown in Fig. 6. In most cases saturation is approached by 300 mT and the hysteresis curves have a simple, narrow shape. IRM acquisition curves are square-shaped and also reach saturation at fields below 300 mT. This all indicates the dominance of low coercivity minerals (eg. (titano)magnetite and/or maghemite). The ascending and descending branches of the hysteresis curves are indistinguishable and linear at fields > 300 mT, indicating a dominant control by paramagnetic (most probably clay) minerals. Hysteresis parameters (coercivity, H_c , saturation magnetisation, M_s) have been calculated after correcting for the paramagnetic contribution. Saturation remanence (M_{rs}) and the coercivity of remanence (H_{cr}) have been calculated from the IRM acquisition curves. The influence of high coercivity minerals, most probably hematite, is seen in a minority of samples. IRM acquisition curves do not reach saturation by 500 mT, the maximum applied field. Here,

wasp-waisted hysteresis loops attest to the presence of mixtures of low and high coercivity minerals.

The magnetisation and coercivity ratios have been plotted on a Day plot (Day *et al.* 1977) (Fig. 6). Most of the data fall within the ‘pseudosingle domain’ region of the plot, with a trend parallel to the single and multidomain magnetite mixing curves as given by Dunlop (2002). The results are interpreted in terms of mixtures of singledomain and multidomain material. Whilst the former probably dominates the stable NRM properties, multidomain material is present in significant amounts. Similar results have been seen in other archaeomagnetic studies (eg. Schnepp *et al.* 2004). The various material types are not differentiated, indicating uniform magnetic mineralogy across most of the sampled structures. A group of samples exhibit H_{cr}/H_c ratios > 5 . They correspond to samples with wasp-waisted loops and unsaturated IRM curves, caused by the presence of a mixture of high and low coercivity minerals. In such mixtures the high coercivity material has a greater effect on H_{cr} and gives rise to the elevated H_{cr}/H_c values. This data cannot be used to infer domain states.

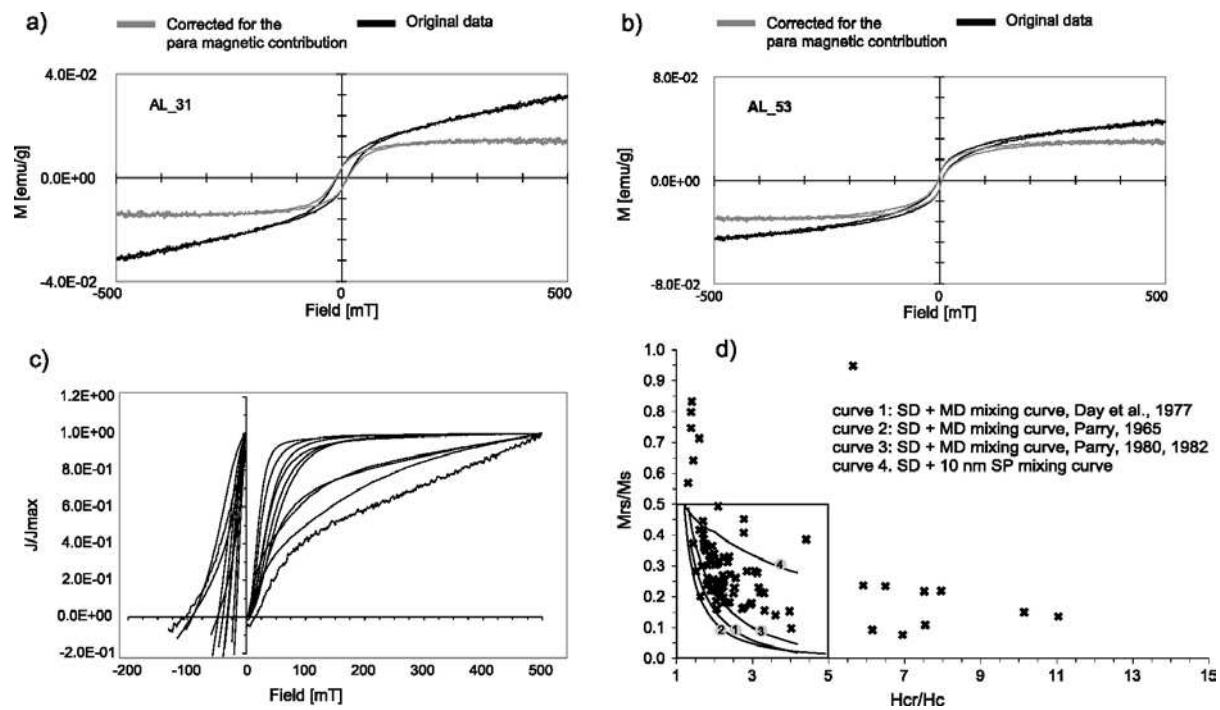


Figure 6. (a-c) Representative hysteresis and isothermal remanent magnetisation and backfield curves. The curves after correcting for the paramagnetic contribution are shown in grey. (d) Day plot of hysteresis ratios. The mixing models of Dunlop (2002) are shown.

4.3.4. TRM anisotropy

Chauvin *et al.* (2000) demonstrated that the correction of NRM and TRM measurements using the TRM anisotropy tensor is needed in order to obtain accurate archaeomagnetic results from tiles or bricks studied by Thellier-style experiments. For this reason, TRM anisotropy has been studied for 21 of the 25 structures studied in Rennes (AT in Table 1). The results show that the degree of anisotropy (the ratio of maximum and minimum axes of the TRM anisotropy tensor, k_1/k_3) is usually < 15 %, and that the principal axes do not show any systematic directional properties. Correcting for TRM anisotropy leads to little or no change in the mean ChRM directions, due to the random distribution of the TRM anisotropy axes and the low degree of anisotropy. For all the studied structures there is no clear dominance of magnetic lineation or foliation, except for the kiln MURO where foliation dominates. However, the characteristic directions of this kiln remains similar before and after TRM anisotropy correction. Typical behaviour is illustrated in Fig. 7 (PATH, structure 57 in Table 1). The directions of the principal TRM anisotropy axes are randomly distributed (Fig. 7a) and the Flinn diagram (magnetic lineation L (k_1/k_3), versus the magnetic foliation F (k_2/k_3)) shows no clear dominance of either L or F (Fig. 7b). For the structures studied here correction for TRM anisotropy is not important. This can be explained by the fact that the majority of sampled material is composed of baked clay or a mixture of bricks and baked clay. Nonetheless, all of the results labelled AT in Table 1 have been corrected for TRM anisotropy.

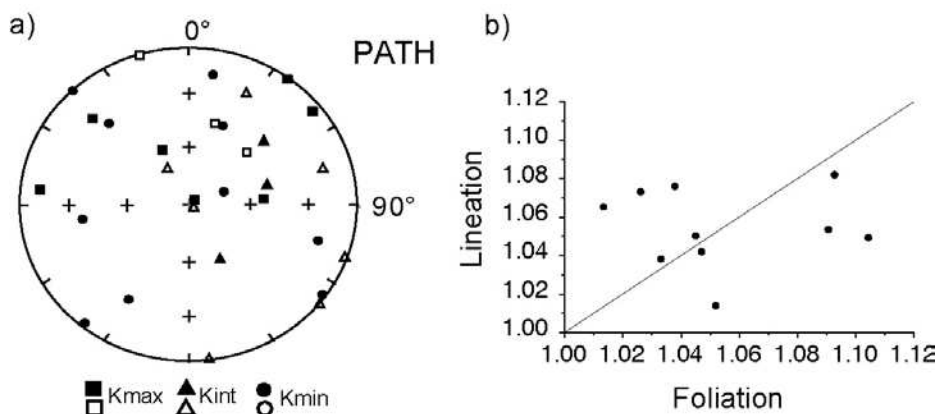


Figure 7. (a) Stereoplot of TRM anisotropy directions and (b) Flinn diagram for structure PATH (structure 57 in Table 1).

Courbe de variation séculaire pour la Péninsule Ibérique

Table 1

No	Name	t _{min}	t _{max}	t _{mean}	Meth.	N'/(n'/n)/N	D _s	I _s	D _m	I _m	k	a ₉₅	Site	Structure	Samples	Lat (°N)	Long (°E)	Treat.	ChRM	RM	Lab.	Reference
1	PLM	-150	-50	-100	arch/C1 4	8/(9/9)/8	-4.0	58.2	-4.1	59.0	182	4.1	Plaza de Moros	pottery kiln	drill	39.50	-4.00	AF/Th	PCA		M	
2	AMP	-200	100	-50	arch	4	-8.5	63.5	-7.7	62.7	2592	1.5	Ampurias	kiln	block	42.12	3.13	NRM	PCA			Thellier, 1981
3	MON	-50	35	-7.5	arch	21/(12/9)/9	0.3	57.3	0.3	59.1	546	2.2	El Monastil	pottery kiln	drill	38.47	-0.79	AF	PCA		M	
4	GA	40	50	45	arch	11/(10/7)/7	3.8	53.4	4.1	57.4	150	4.9	El Gallinero	pottery kiln	hand	36.53	-6.19	AF/Th	PCA		P	
5	VIL1	0	100	50	arch	25	-5.5	57.1	-5.5	57.2	116	2.6	Villa del Pañuelo I	kiln	drill	40.30	-3.40	Th	PCA		M	Oyamburu, 1996
6	LMA	0	100	50	arch	29	-0.8	58.4	-0.9	56.6	128	2.1	Calahorra, La Maja	pottery kiln	drill	42.27	-2.02	AF/Th	PCA			Parés, 1992
7	COS	0	100	50	arch	14/(23/14)/14	3.7	54.3	4.0	58.2	46	6.0	Costalita	kiln	drill	36.42	-5.15	AF/Th	PCA		M	
8	VC	80	90	85	arch	31/(34/27)/27	2.1	46.7	2.5	51.6	146	2.3	Venta del Carmen	pottery kiln	hand/ drill	36.18	-5.49	AF/Th	PCA		P/M	
9	VIA	50	150	100	arch	10/(10/9)/9	1.4	50.5	1.5	53.0	259	3.2	Villares Andujar	pottery kiln	drill	38.06	-4.04	AF	PCA		M	
10	CAR-HI	50	150	100	arch	7/(8/8)/7	-1.7	55.3	-1.8	58.4	293	3.5	Cartuja I	pottery kiln	drill	37.18	-3.10	AF/Th	PCA		M	
11	CAR-HII	50	150	100	arch	9/(11/9)/7	-3.1	52.2	-3.3	55.5	125	5.4	Cartuja II	pottery kiln	drill	37.18	-3.10	AF/Th	PCA		M	
12	CAR-HIII	50	150	100	arch	5/(8/7)/5	2.9	52.3	3.0	55.6	392	3.9	Cartuja III	pottery kiln	drill	37.18	-3.10	AF/Th	PCA		M	
13	PAR1	90	130	110	arch	14/(10/10)/10	-2.4	53.0	-2.3	56.1	484	2.2	Patio Cardenal I	pottery kiln	drill	37.38	-5.98	AF	PCA		M	
14	PAR3	90	130	110	arch	13/(6/6)/6	-4.1	54.1	-4.1	56.9	324	3.7	Patio Cardenal III	pottery kiln	drill	37.38	-5.98	AF	PCA		M	
15	PAR4	90	130	110	arch	13/(8/7)/7	-2.7	53.3	-2.4	56.3	1026	1.9	Patio Cardenal IV	pottery kiln	drill	37.38	-5.98	AF	PCA		M	
16	PAR5	90	130	110	arch	20/(17/17)/17	-4.3	53.5	-4.3	56.4	193	2.6	Patio Cardenal V	pottery kiln	drill	37.38	-5.98	AF	PCA		M	
17	BC	100	150	125	arch	16/(16/14)/14	-2.2	46.7	-2.0	51.6	145	3.6	Baelo Claudia	baths	drill	36.03	-5.62	AF	RC+PCA(6)		M	
18	GAL	100	220	160	arch	11/(12/8)/7	-0.1	55.8	-0.1	59.4	176	4.6	Gallineras	pottery kiln	drill	36.47	-6.18	AF/Th	PCA		M	
19	ARV	150	250	200	arch	17	-3.7	51.8	-3.6	54.6	682	1.3	Arva	kiln		37.60	-5.50					Evans, pers.comm.
20	DENA	220	250	235	arch	13/(10/10)/10	-4.5	52.6	-5.0	54.5	669	1.9	Setla Mirarosa Miraflor	kiln	block	38.86	0.02	TH	PCA	AT, C	R	
21	HIP	225	325	275	arch	22/(23/18)/18	-4.0	52.6	-4.1	52.5	104	3.4	Hippolytus	baths	drill	40.48	-3.32	AF/Th	PCA		M	
22	VIL2	250	350	300	arch	31	-2.7	51.7	-2.6	51.7	131	2.2	Villa del Pañuelo II	kiln	drill	40.30	-3.40	Th	PCA		M	Oyamburu, 1996
23	VAL	270	330	300	arch	18/(24/7)/7	-5.4	48.0	-5.8	48.9	58	9.7	Valeria	burnt wall	drill	39.77	-2.13	AF/Th	RC		M	
24	PG1	400	410	405	arch	14/(14/13)/13	-14.1	46.4	-14.3	50.8	33	7.3	Puente Grande I	pottery kiln	drill	36.18	-5.49	AF	PCA		M	
25	PG2	400	410	405	arch	23/(18/15)/15	0.3	52.5	0.4	56.7	129	3.4	Puente Grande II	pottery kiln	drill	36.18	-5.49	AF	PCA		M	
26	RO2	1000	1050	1025	arch	15/(18/14)/14	17.3	50.9	16.8	51.6	100	4.0	Ramon Ortega II	pottery kiln	hand	38.86	0.12	AF	PCA		P	
27	MURG	1000	1100	1050	arch	21/(8/8)/8	21.7	51.3	21.8	52.9	1437	1.5	Murcia c/Sagasta	glass making	block	37.98	-1.12	TH	PCA	AT, C	R	

Courbe de variation séculaire pour la Péninsule Ibérique

kiln																				
28	RO1	1050	1100	1075	arch	20/(20/16)/16	15.8	47.9	15.2	48.7	380	1.9	Ramon Ortega I	pottery kiln	hand	38.86	0.12	AF	PCA	P
29	CDAP	1010	1220	1115	C14	11/(17/8)/8	3.6	50.6	2.5	49.1	236	3.6	Cabrera d'Anoia	pottery kiln	block	41.50	1.50	AF/TH	PCA	C R
30	CDAU	1029	1203	1116	C14	14/(12/6)/6	9.6	45.7	8.0	43.6	2765	1.3	Cabrera d'Anoia	pottery kiln	block	41.50	1.50	AF/TH	PCA	C R
31	MURO	1100	1200	1150	arch/his	6/(7/6)/6	13.6	44.7	13.2	47.1	308	3.8	Murcia c/Puxmarina	kiln	block	37.98	-1.12	TH	PCA	AT, C R
32	MURN	1100	1200	1150	arch/his	19/(7/6)/6	14.0	45.1	13.7	47.3	1038	2.1	Murcia c/Puxmarina	kiln	block	37.98	-1.12	TH	PCA	AT, C R
33	MURM	1100	1200	1150	arch/his	15/(10/7)/7	14.9	45.5	14.6	47.7	811	2.1	Murcia c/Puxmarina	kiln	block	37.98	-1.12	TH	PCA	AT, C R
34	MURL	1100	1200	1150	arch/his	16/(9/9)/9	16.2	44.2	15.8	46.4	1842	1.2	Murcia c/Puxmarina	kiln	block	37.98	-1.12	TH	PCA	AT, C R
35	MURI	1100	1200	1150	arch/his	15/(13/7)/7	15.2	41.7	14.8	44.0	215	4.1	Murcia c/Puxmarina	kiln	block	37.98	-1.12	TH	PCA	AT, C R
36	MURK	1100	1200	1150	arch/his	16/(13/9)/9	14.1	45.2	13.8	47.4	547	2.2	Murcia c/Puxmarina	kiln	block	37.98	-1.12	TH	PCA	AT, C R
37	MURH	1100	1200	1150	arch/his	15/(20/10)/10	17.3	46.4	17.1	48.4	330	2.7	Murcia c/Puxmarina	kiln	block	37.98	-1.12	TH	PCA	AT, C R
38	CDAJ	1056	1262	1159	C14	12/(11/8)/8	9.0	45.2	7.4	43.1	416	2.7	Cabrera d'Anoia	pottery kiln	block	41.50	1.50	AF/TH	PCA	C R
39	CDAH	1043	1281	1162	C14	10/(11/5)/5	10.7	46.4	9.1	44.3	3461	1.3	Cabrera d'Anoia	pottery kiln	block	41.50	1.50	AF/TH	PCA	C R
40	MAGI	1250	1300	1275	arch	14/(14/5)/5	11.5	42.6	11.3	42.2	500	4.8	Magisterio I	pottery kiln	drill	40.63	-3.16	Th	RC	M
41	MAGII	1250	1300	1275	arch	16/(16/6)/6	4.1	47.3	4.0	47	179	6.1	Magisterio II	pottery kiln	drill	40.63	-3.16	Th	RC+PCA(1)	M
42	CALA	1275	1300	1287.5	arch/his	16/(9/8)/8	11.4	44.9	11.6	46.5	356	2.9	Calatrava la Vieja	pottery kiln	block	39.02	-3.82	TH	PCA	AT, C R
43	CALB	1275	1300	1287.5	arch/his	14/(12/10)/10	7.1	44.4	7.2	46.2	284	2.9	Calatrava la Vieja	pottery kiln	block	39.02	-3.82	TH	PCA	AT, C R
44	VALN	1238	1350	1294	arch	20/(12/9)/9	2.1	46.6	1.3	47.7	1859	1.2	Valencia Velluters	bricks making kiln	block	39.47	-0.37	TH	PCA	AT, C R
45	CSR			1300	arch	10/(11/3)/3	8.1	46.0	8.9	51.0	298	7.2	Castillo de San Romualdo	kiln	drill	36.3	-6.1	AF/TH	PCA	H M
46	GUA1	1275	1325	1300	arch	4/(16/16)/4	14.3	57.8	14.2	57.5	1104	2.8	SUE-10	pottery kiln	hand	40.60	-3.20	AF/Th	PCA	H M
47	VALI	1238	1400	1319	arch	21/(13/11)/11	4.4	46.4	3.6	47.3	725	1.7	Valencia Velluters	bricks making kiln	block	39.47	-0.37	TH	PCA	AT, C R
48	BI	1369	1369	1369	hist	28/(30/12)/10	0.4	41.9	0.8	47.3	206	3.4	Av. Blas de Infante	burnt wall	drill	36.13	-5.45	AF/Th	PCA	M
49	VALK	1300	1450	1375	arch	15/(9/9)/9	3.0	44.2	2.2	45.2	1606	1.3	Valencia Velluters	glass making kiln	block	39.47	-0.37	TH	PCA	AT. C R
50	VALM	1300	1450	1375	arch	16/(9/9)/9	7.2	47.0	6.5	47.8	2733	1.0	Valencia Velluters	glass making kiln	block	39.47	-0.37	TH	PCA	AT, C R
51	LLD	1400	1415	1407.5	arch/his	14/(15/15)/14	9.6	37.0	10.4	43.4	98	4.0	Llano las Damas	pottery kiln	hand	35.89	-5.30	AF/Th	PCA	M
52	HR	1400	1415	1407.5	arch/his	8/(8/7)/7	7.8	35.9	8.6	42.4	417	3.1	Huerta Rufino	pottery kiln	drill	35.89	-5.30	AF/Th	RC+PCA(5)	M
53	CALC	1400	1420	1410	arch/his	18/(9/8)/8	3.0	47.0	3.1	48.6	790	2.0	Calatrava la Vieja	pottery kiln	block	39.02	-3.82	TH	PCA	AT, C R
54	PATA	1450	1500	1475	arch	15/(18/10)/10	3.6	56.4	3.5	57.1	792	1.7	Paterna c/Huertos	pottery kiln	block	39.50	-0.43	TH	PCA	AT, C R
55	TMO	1490	1540	1515	arch	18/(18/16)/16	7.5	55.7	7.4	56.2	343	2.0	Paterna Testar del Moli	pottery kiln	drill	39.50	-0.43	AF	PCA	M

Courbe de variation séculaire pour la Péninsule Ibérique

56	PATJ	1429	1611	1520	C14	22/(17/16)/16	6.6	62.2	6.9	62.7	1201	1.1	Paterna Testar del Moli	pottery kiln	block	39.50	-0.43	TH	PCA	AT, C	R
57	PATH	1450	1600	1525	arch	12/(15/10)/10	7.3	53.5	7.0	54.1	831	1.7	Paterna Testar del Moli	pottery kiln	block	39.50	-0.43	TH	PCA	AT, C	R
58	PATB	1525	1650	1587.5	arch	20/(13/11)/11	5.8	64.1	6.4	64.6	827	1.6	Paterna c/Huertos	pottery kiln	block	39.50	-0.43	TH	PCA	AT, C	R
59	VALL	1575	1625	1600	arch	19/(13/11)/11	9.1	56.6	9.0	57.1	557	1.9	Valencia Velluters	kiln	block	39.47	-0.37	TH	PCA	AT, C	R
60	YUS1	1784	1814	1799	arch/his	8/(22/17)/7	-14.3	55.5	-14.3	55.5	173	4.6	Monastery at Yuste	kiln	hand/drill	40.10	-5.70	Th	PCA		M
61	GUA2	1825	1845	1835	arch/his	13/(16/16)/13	-21.1	61.5	-21.1	61.4	238	2.7	Huertas del Carmen	furnace	drill	40.60	-3.20	AF	PCA	H	M
62	AL	1830	1910	1870	arch/his	7/(20/11)/6	-14.2	63.0	-14.3	63.3	159	5.3	Palacio de Perales	burnt floor	hand	40.10	-3.10	Th	PCA	H	M
63	YUS2	1959	1959	1959	his	5/(19/15)/5	-11.1	58.2	-11.0	58.2	138	6.5	Monastery at Yuste	kiln	hand	40.10	-5.70	Th	PCA	C	M

Table 1. Archaeomagnetic directions from Spanish sites. Columns from left to right:

No, structure number; Name, name of the structure; t_{min} , minimum age of the structure in years AD; t_{max} , maximum age of the structure in years AD; t_{mean} , mean age of the structure in years AD; Meth., method of dating (arch.: archaeological age estimate, hist: historical document, C14: conventional ^{14}C ; TL: thermoluminescence); $N'/(n'/n)/N$: number of independently oriented samples taken from the site (N')/specimens analysed (n')/taken into account in the calculation of the mean sample directions(n)/samples taken into account in the calculation of the mean site direction (N); D_s and I_s , declination and inclination in situ; D_m and I_m , declination and inclination at the latitude of Madrid (40.4, -3.7); k and α_{95} , precision parameter and 95 % confidence limit of characteristic remanent magnetisation; Site: site name; Structure, kind of structure; Samples, type of samples (drill: drilled samples, hand: hand samples, block: large block samples); Lat and Long, site latitude and longitude; Treat., laboratory treatment (AF: alternating field demagnetisation, Th: Thermal demagnetisation, TH: Thermal demagnetisation from Thellier palaeointensity experiments); ChRM, ChRM determination method (RC: remagnetisation circles, PCA: principal component analysis - with number of PCA analyses when mixed with RC given in brackets); RM, rock magnetic experiments (AT: anisotropy of TRM, C: Curie temperature determination, H: hysteresis and IRM measurements); Lab., laboratory where measurements were made (M: Madrid, R: Rennes, P: Plymouth); Reference, blank space indicates this study.

5. New archaeomagnetic directions

Site-mean directions have in all cases been calculated following a hierarchical structure (ie. specimen → independently oriented sample → site). When more than one specimen was available from an independently oriented sample (drilled core or block sample), a mean sample direction was calculated using all of the specimens (for sites Th and AF in Table 1) or the most reliable demagnetisation experiment was retained (for sites TH in Table 1). This choice was made on the basis of the larger fraction of NRM lost during Thellier experiments. As can be seen in Table 1, the number of individual directions retained for mean computation (N) is often lower than the number of independently oriented samples collected (N'). This is related mostly to drilled samples that have been discarded because of potential orientation errors, and in some cases to samples that were lost due to the difficulty in preparing specimens from poorly-consolidated blocks.

The mean directions for each structure were calculated using Fisher (1953) statistics. Generally, more than 7 mean (independently oriented) sample directions have been used in the calculation of the mean site direction. For the 5 structures that exhibited 2 stable directions, the mean of the common (ie. archaeomagnetic) directions was calculated using the remagnetisation circle method or by a combination of this technique and principal component analysis (McFadden & McElhinny 1988).

For every site or structure the sample directions have been tested to see if they show a Fisherian distribution. Deviations from a Fisher distribution are assumed to arise through undetected orientation errors (of the structure itself or during its sampling) or to incomplete resolution of the ChRM (due to partial heating). In those structures showing non-Fisherian distributions, the sample direction showing the largest angular distance from the mean was discarded and the distribution recalculated, the process being repeated until Fisherian conditions were met. The results from 12 structures (and a total of only 4 % of the samples measured) have been modified in this way. In only 4 structures have more than 2 samples been discarded, corresponding to those that have suffered partial heating. Therefore all site mean directions have been calculated from Fisher distributed directions. The resulting directional distributions are shown in Fig. 8.

a)

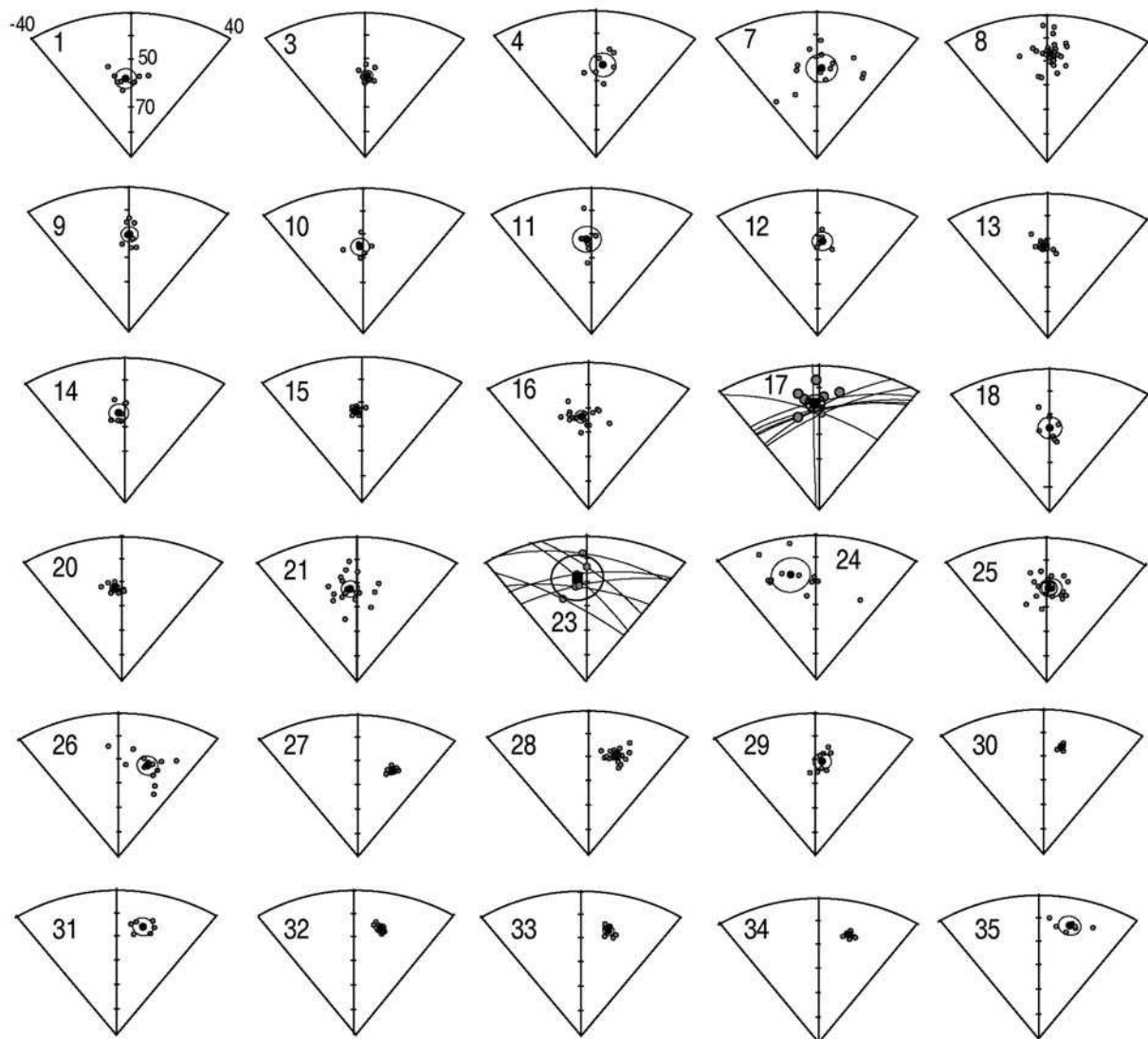


Figure 8. a and b) Stereoplots of ChRM directions at the sample level (grey symbols), together with the mean direction and α_{95} (in black) for each of the new structures studied. Where remagnetisation circles have been used to determine site directions, the great circles used in the calculation are shown.

b)

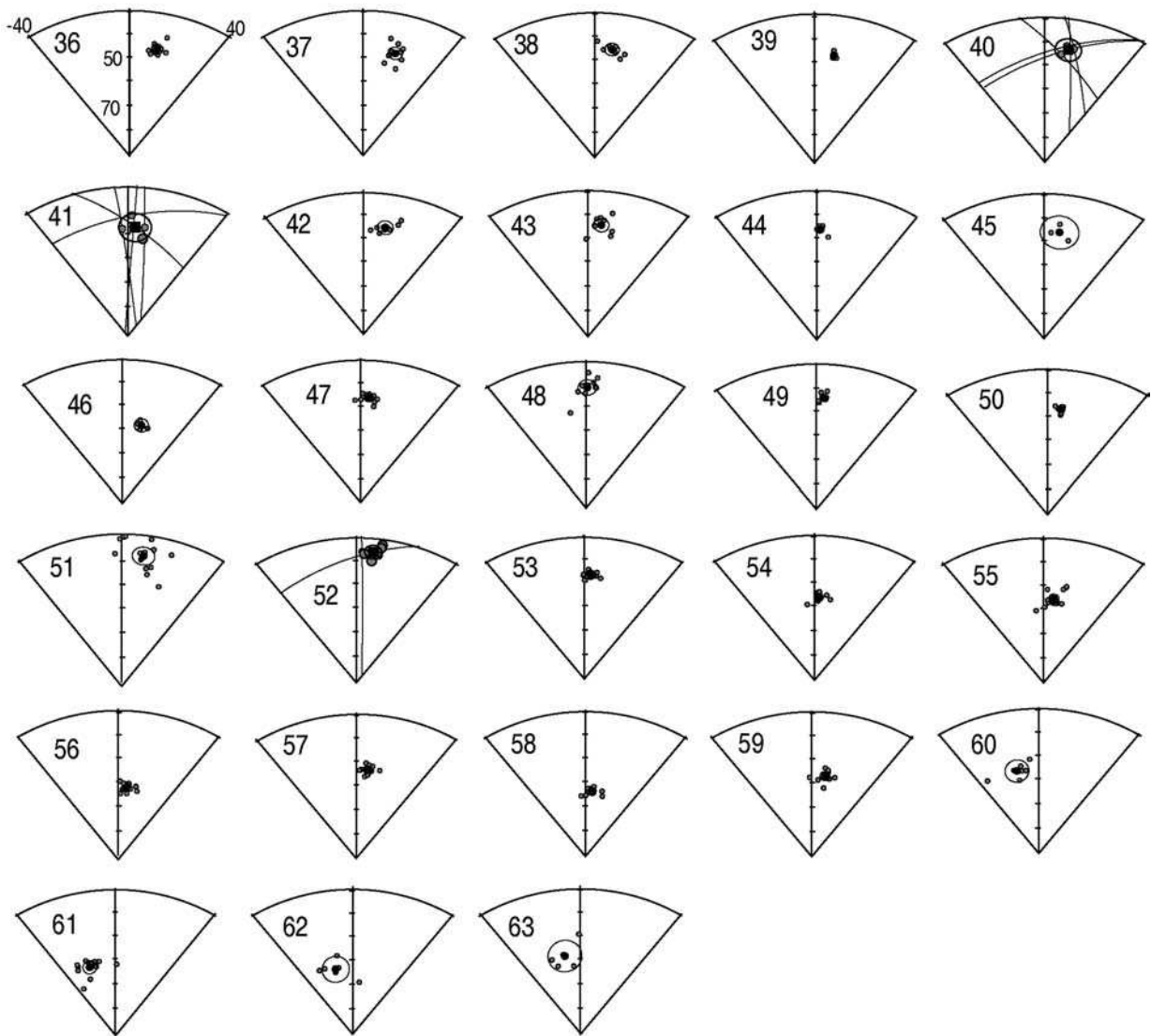


Figure 8. a and b) Stereoplots of ChRM directions at the sample level (grey symbols), together with the mean direction and α_{95} (in black) for each of the new structures studied. Where remagnetisation circles have been used to determine site directions, the great circles used in the calculation are shown.

The 58 new directions are shown in Table 1, along with the previously published data described earlier. Each site direction has been transferred to Madrid (40.4°N , 3.7°W) via the virtual geomagnetic pole (VGP). The age distribution of the data set spans approximately 2000 years. The oldest studied structure is dated at between 150 and 50 BC and the youngest at 1959 AD, and there is a gap between the 6th and 10th centuries where no data are available.

For Roman, Medieval and Modern times several archaeomagnetic directions per century are available.

All of the data are represented in Fig. 9. Structure 45, which has no available dating error information, has been plotted with an arbitrary error of ± 200 years. Structures coming from the same site and with the same age estimation give very similar results, for example the 4 pottery kilns from Patio Cardenal (structures 9 to 12, Table 1) or the 7 kilns from Murcia c/Puxmarina (structures 31 to 37, Table 1). There is a very good agreement for the declination values. However, inclination sometimes shows a higher between-site dispersion, for example between 1500 and 1600 AD.

Six structures have been studied for this period (54-59, Table 1), 4 of which give very similar results, whereas 2 (PATJ, 56, and PATB, 58, Table 1) exhibit higher inclinations which are more consistent with later periods. These structures have relatively large uncertainties associated with their archaeological age estimates (see Appendix), and considering their true age as being nearer the 17th century (rather than in the middle of the proposed interval) might explain the high inclinations. Alternatively, the structures may have suffered post-abandonment local movements, although archaeological observations and the large size of the structures do not support this idea. Irrespective of the explanation of the inclination variation, it should be noted that the dispersion observed in the inclination data is similar to that seen in other archaeological data (eg. Schnepf *et al.* 2004).

The data from GUA1 (structure 46 in Table 1) is offset from the other data from the 14th century AD. This discrepancy may be explained by the lack of archaeological information (see Appendix). The age of the kiln is placed at 1300 ± 25 AD, but no information is available to propose a reliable TPQ or TAQ for the structure. The mean value from PG1 (structure 24 in Table 1) is offset from the mean value of PG2 (number 25 in Table 1), but taking into account the large errors of PG1 the data are in agreement. These two structures, from the same archaeological site, are considered coeval on the basis of the archaeological information (see Appendix). Direct observations of the geomagnetic field for the Iberian Peninsula since 1858 obtained at the magnetic observatories of Lisboa, Coimbra and San Fernando (see Gaibar-Puertas 1953, for the data obtained at San Fernando) are also plotted on Fig. 9. They agree well with the modern archaeomagnetic directions for structures 62 and 63, taking into account the errors in the archaeomagnetic data.

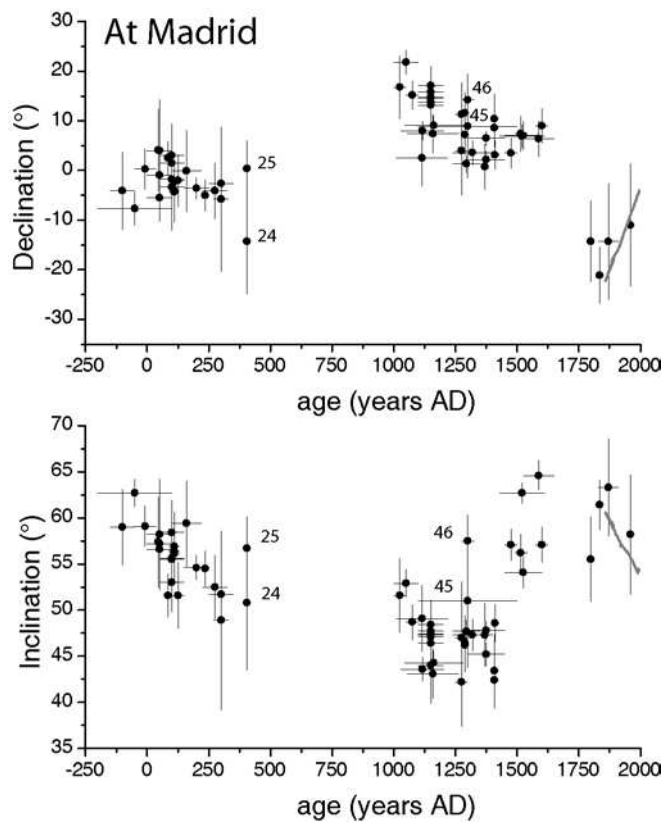


Figure 9. Declination and inclination versus age (reduced to Madrid). One site (structure 45 in Table 1) where no age error is available is plotted with an error of 200 years, although there are no archaeological constraints. Direct observations from the Iberian Peninsula are plotted in grey.

In order to compare the Spanish data with the French SV curve (Gallet *et al.* 2002), the Spanish data have been recalculated for the latitude of Paris and plotted together with the French data (Fig. 10). The anomalous inclination obtained for GUA1 is also in disagreement with the inclination values given by the French SV curve, suggesting that the assigned archaeological age of 1300 AD may be questionable. For the rest of the data a good agreement with the French SV is observed.

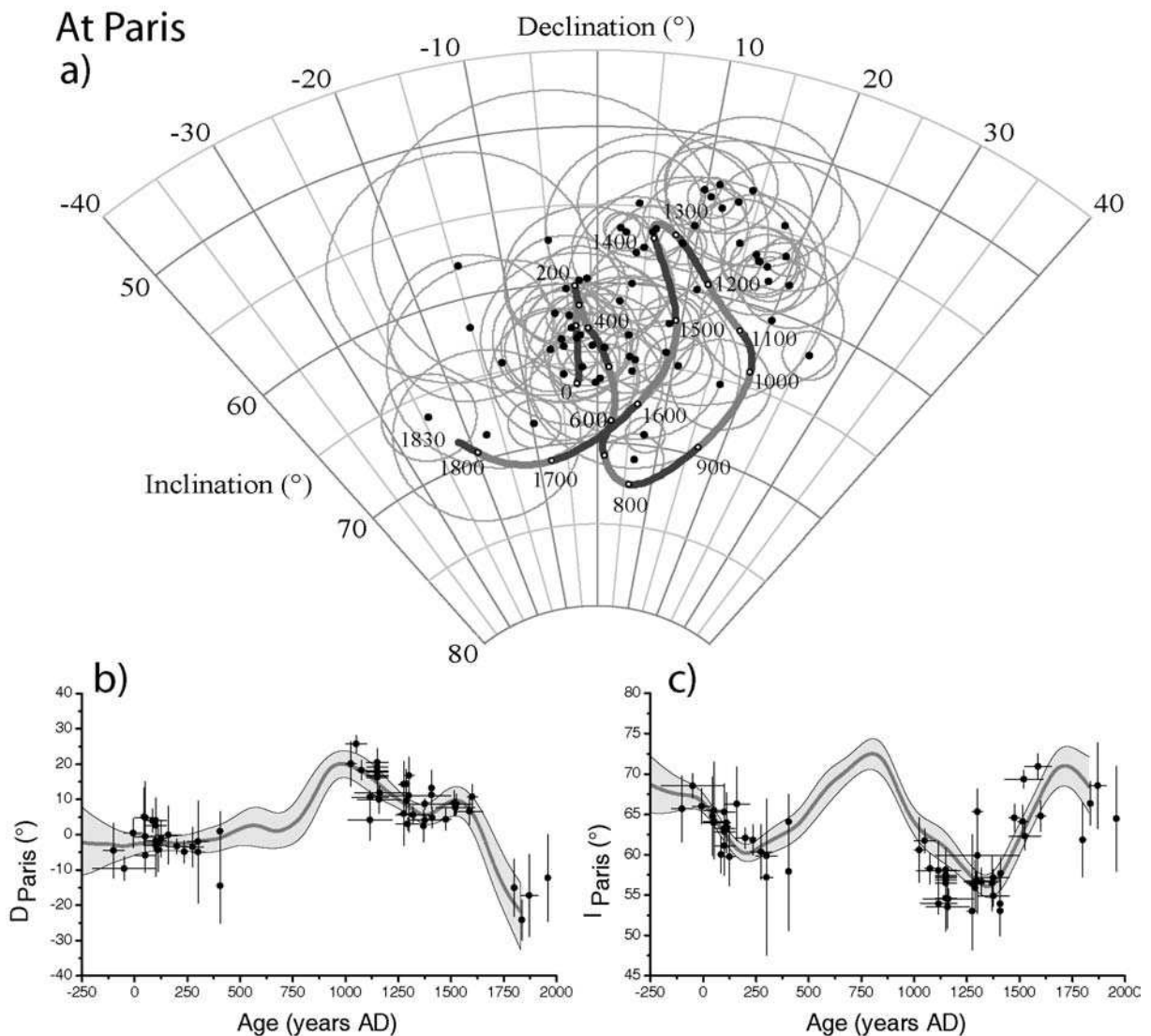


Figure 10. Comparison of the Spanish data with the French Secular Variation curve (Gallet et al. 2002) obtained by Bayesian modelling. The Spanish data have been reduced to Paris. a) Stereographic plot, b) declination, c) inclination. The French SV curve is given in grey.

6. Conclusions

A compilation of 63 archaeomagnetic directions has been presented, comprising 5 previous results and 58 new results. The types of archaeological structures range from ceramic and brick making kilns and furnaces, ovens, burnt walls and burnt floors. All have yielded stable and well defined site-mean directions that have been calculated following a hierarchical structure. The use of remagnetisation circle analysis for partially heated structures has improved the definition of the archaeomagnetic direction associated with relatively low

temperature heating. Rock magnetic studies indicate that the magnetic signal is dominated by magnetite or Ti-poor titanomagnetite. Thermally stable (titano)maghemite or partially oxidised magnetite has also been recognised, and in a few cases the influence of hematite has been observed.

The compiled data span approximately 2000 years, from 100 BC to 1959 AD. Throughout most of the record several directions per century are available, although there is a gap in the data between the 6th and 10th century. The data are in broad agreement with the French SV curve of Gallet *et al.* (2002). There is a need to extend the data, and to improve the precision of the periods covered. However, the results represent the first step in the construction of a SV curve for the Iberian Peninsula. This will provide an additional tool in the dating of archaeological remains in the region, and the data can be used to better constrain the behaviour of the earth's magnetic field in Western Europe during the last few millennia.

Acknowledgements

M. Gómez-Paccard and G. Catanzariti acknowledge fellowships from the AARCH Network (Archaeomagnetic Applications for the Rescue of Cultural Heritage), Contract EU: HPRN-CT-2002-00219. The authors would like to thank two anonymous reviewers for their constructive comments which improved the manuscript both in substance and style.

References

- Batt, C.M., 1997. The British archaeomagnetic calibration curve: an objective treatment. *Archaeometry*, 39, 153-168.
- Casas, Ll., Shaw, J., Gich, M. & Share, J.A., 2005. High-quality microwave archeointensity determinations from an early 18th century AD English brick kiln, *Geophys. J. Int.*, 161, 653-661.
- Chauvin, A., Garcia, Y., Lanos, Ph. & Laubenheimer, F., 2000. Paleointensity of the geomagnetic field recovered on archaeomagnetic sites from France, *Phys. Earth Planet. Inter.*, 120, 111-136.
- Day, R., Fuller, M.D. & Schmidt, V.A., 1977. Hysteresis properties of titanomagnetites: grain size and composition dependence, *Phys. Earth Planet. Inter.*, 13, 260-267.
- Dunlop, J., 2002. Theory and application of the Day plot (Mrs/Ms versus Hcr/Hc). 1. Theoretical curves and tests using titanomagnetite data, *J. Geophys. Res.*, 107, doi:10.1029/2001JB000486.
- Fisher, R.A., 1953. Dispersion on a sphere, *Proc. Roy. Soc. London A*, 217, 295.
- Gaibar-Puertas, C., 1953. Variación Secular del Campo Geomagnético, Observatorio del Ebro, Tarragona.
- Gallet, Y., Genevey, A. & Le Goff, M., 2002. Three millennia of directional variations of the Earth's magnetic field in western Europe as revealed by archaeological artefacts, *Phys. Earth Planet. Inter.*, 131, 81-89.
- Jasonov, P.G., Nurgaliev, D.K., Burov, D.V. & Heller, F., 1998. A modernized coercivity spectrometer, *Geologica Carpathica*, 49, 3, 224-225.
- Kirschvink, J.L., 1980. The least-squares line and plane and the analysis of paleomagnetic data. *Geophys. J. R. astron. Soc.*, 62, 699-718.
- Korte, M., Genevey, A., Constable, C.G., Frank, U. & Schnepp, E., 2005. Continuous geomagnetic field models for the past 7 millennia: 1. A new global data compilation. *Geochem. Geophys. Geosyst.*, 6, doi:10.1029/2004GC000800.
- Kostadinova, M., Jordanova, N., Jordanova, D. & Kovacheva, M., 2004. Preliminary study on the effect of water glass impregnation on the rock-magnetic properties of baked clay. *Stud. Geophys. Geod.*, 48, 637-646.
- Kovacheva, M. & Toshkov, A., 1994. Geomagnetic field variations as determined from Bulgarian archeomagnetic data. Part I: The last 2000 years AD. *Sur. Geophys.*, 15, 673-701.

- Kovacheva, M., Parés, J.M., Jordanova, N. & Karloukovski, V., 1995. A new contribution to the archaeomagnetic study of a Roman pottery kiln from Calahorra (Spain), *Geophys. J. Int.*, 123, 931-936.
- Lanos, Ph., 2004. Bayesian inference of calibration curves: application to archaeomagnetism, in *Tools for constructing chronologies: crossing disciplinary boundaries*, Vol. 177, pp. 43-82, eds. Buck, C. & Millard A., Springer-Verlag, London.
- McFadden, P.L. & McElhinny, M.W., 1988. The combined analysis of remagnetization circles and direct observations in paleomagnetism, *Earth planet. Sci. Lett.*, 87, 161-172.
- Nachasova, I.E., Burakov, K.S. & Bernabeu, J., 2002. Geomagnetic field intensity variations in Spain, *Phys. Solid. Earth, Engl. Transl.*, 38, 371-376.
- Oyamburu, I., Villalain, J.J., Osete, M.L., Zarzalejos, M. & Blasco, C., 1996. Estudio paleomagnético del yacimiento de Villa del Pañuelo (Villamanta, Madrid), *Geogaceta*, 20, 1044-1046.
- Parés, J.M., De Jonge, R., Pascual, J.O., Bermúdez, A., Tovar, C.J., Luezas, R.A. & Maestro, N., 1992. Archaeomagnetic evidence for the age of a Roman pottery kiln from Calahorra (Spain). *Geophys. J. Int.*, 112, 533-537.
- Schnepp, E. & Lanos, Ph., 2005. Archaeomagnetic secular variation in Germany during the past 2500 years. *Geophys. J. Int.*, 163, 479-490.
- Schnepp, E., Pucher, R., Reindeers, J., Hambach, U., Soffel, H. & Hedley, I., 2004. A German catalogue of archaeomagnetic data. *Geophys. J. Int.*, 157, 64-78.
- Tarling, D.H., 1983. *Palaeomagnetism: principles and applications in geology, geophysics and archaeology*, Chapman and Hall, London.
- Tauxe, L., 1998. *Paleomagnetic principles and practice*. Kluwer Academic Publishers, The Netherlands.
- Thellier, E., 1981. Sur la direction du champ magnétique terrestre en France durant les deux derniers millénaires. *Phys. Earth Planet. Inter.*, 24, 89-132.
- Thellier, E. & Thellier, O., 1959. Sur l'intensité du champ magnétique terrestre dans le passé historique et géologique. *Ann. Géophys.*, 15, 285-376.
- Veitch, R.J., Hedley, G. & Wagner, J.J., 1984. An investigation of the intensity of the geomagnetic field during Roman times using magnetically anisotropic bricks and tiles. *Arch. Sc. Genève*, 37, 359-373.

Appendix: Archaeological and chronological information

This provides a summary of the archaeological sites and structures sampled, briefly describing where the samples were taken and the basis on which the structures have been dated. All block samples denoted as TH in Table 1 were taken by J. Thiriot, the remaining samples were taken by members of the UCM team (Spain). The *terminus post-quem* (TPQ) and *terminus ante-quem* (TAQ) are given where available. The TPQ (TAQ) indicates that the structures could be in use after (before) the given date.

The structures from each of the sites are set out below under the following heading:

Site name (Province). Archaeologists in charge of the excavation. (structure number) laboratory structure name (archaeological structure name when different): age in years AD.

Plaza de Moros (Toledo). D. Urbina and C. Urquijo. (1) PLM: -100 ± 50.

Plaza de Moros, Toledo, is considered a typical example of a fortified human settlement from the Second Iron Age (Urbina 2004). It was destroyed following a fire which affected the whole of the site. Archaeomagnetic samples were taken from one of the burnt household walls.

The age is controlled by archaeological data and C14 dating. The general features are typical of Iron Age hillforts from central Spain. Archaeological constraints (ceramic fragments, metallic objects, decoration and painting style) place the site between the 4th and 2nd century BC (Cuadrado 1991, Fernández-Rodríguez 1987). No artefacts have been found above the stratigraphic layer associated with the fire and there is no evidence for later Roman occupation. On this basis the age of the fire has been placed at 150-50 BC (Urbina, private communication).

C14 dates have been obtained from two samples from a burnt wooden beam from one of the households, giving dates of 520-400 BC and 200 BC - 20 AD. The different dates could represent different ages during the growth of the tree from which the beam was prepared. In this case the younger of the 2 will be closer to the age of the death of the tree – ie. when it was used in the construction of the house. The archaeologically-constrained date of the fire is the preferred date (150-50 BC), pending resolution of the radiocarbon discrepancies.

El Monastil (Alicante). A.M. Poveda-Navarro. (3) MON: -7.5 ± 42.5.

Archaeological excavations in El Monastil, Alicante, revealed the remains of a pottery kiln. It has a square base, with part of the grill in situ and a semi-circular praefurnium (Poveda 1997, p482). Archaeomagnetic samples were taken from the baked floor and interior walls of the kiln.

The TPQ is based on ceramic fragments used in construction of the kiln, specifically mortar fragments and a fragment of amphora type Loma do Canho 67, providing an age of 1st century BC (Poveda 1997, p483). The TAQ is based on an amphora fragment found in the oven in-fill. The amphora, of the type Dr. 1 – sigillata italica – Conspectus 22, is dated between 10 BC and 35 AD (Poveda 1997, p484). The age of abandonment has been placed between the second half of the 1st century BC and the TAQ (50 BC – 35 AD).

El Gallinero (Cádiz). I. Fernández García. (4) GA: 45 ± 5.

The area around Puerto Real, Cádiz, is a well-known zone of ceramic production (García-Vargas & Sibón-Olano 1995, Cepillo-Galvin & Blanes 2002). Excavations revealed a circular kiln, with a deteriorated grill supported by a central pillar with radial arcs. Archaeomagnetic samples were taken from the interior walls of the kiln.

Archaeological evidence, specifically the amphora types (Dr. 7, 8 and 10) produced in the area, indicates a period of activity around the second quarter of the 1st century AD (García-Vargas 1998, p170-171), an age supported by later studies (Lagóstena & Bernal 2004, p70). The age of abandonment of the site has been placed in the middle of the 1st century AD (40-50 AD).

Costalita (Málaga). I. Navarro. (7) COS: 50 ± 50.

The Roman site of Costalita was discovered in 2002 during construction works in Estepona, Málaga. Two excavations, 50 m apart, revealed the remains of a kiln used for manufacturing ceramics and construction materials (“*Pueblo Andaluz*”), together with the remains of a thermal bath (Padilla *et al.* 2003, Suárez-Padilla *et al.* 2004). The kiln consists of a buried combustion chamber, with 4 adobe arcs supporting the grate. Each arc is in turn supported by two adobe pillars. The remains of the praefurnium have also been recognised. Archaeomagnetic samples were taken from the interior of the combustion chamber and from the praefurnium.

The age is controlled by archaeological data. Padilla *et al.* (2003) propose a chronology based on ceramic finds and on comparison with material from other Roman sites in the region. Ceramic fragments found during excavation can be ascribed to the 1st century AD. Some decorated fragments are similar to those found at the Venta del Carmen site (8, VC), which has been placed between the middle of the 1st century AD and the end of the 2nd century AD. A chronology centred in the mid-1st century AD (0-100 AD) is consistent with the materials recovered at the site and with the construction techniques of the kiln.

Venta del Carmen (Cádiz). D. Bernal-Casasola. (8) VC: 85 ± 5.

The Venta del Carmen site is located close to Los Barrios, Cádiz. Two circular kilns, with grates supported by a central pillar, were excavated. In their last phase of use they were used as boilers (Bernal 1998, Bernal & Lorenzo 1998a), to which end a series of channels and other structures were constructed. Archaeomagnetic samples were taken from the central pillar and the interior and exterior of the kiln wall.

The workshop has been placed between the Augustine and Flavian epochs (10 BC – 90 AD), following evidence provided by imported goods (Italic and Gaulish sigillata, fine-walled ceramics, volute skylights and amphorae), along with the amphorae produced by the workshop itself (Bernal & Lorenzo 1998b). The age of abandonment of the site has been placed at 80-90 AD, just before sedimentary infilling of the kiln and nearby structures which occurred at the end of the 1st century AD.

Villares Andújar (Jaén). I. Fernández-García. (9) VIA: 100 ± 50.

Several kilns have been recovered from this well-known workshop near Andújar, in Jaen. The structure available for archaeomagnetic study was not excavated during the archaeological investigation of the site. It was exposed in a vertical cross-section in a road cutting. Archaeomagnetic samples were taken from the exposed kiln walls.

Archaeological considerations place the production period of the well-studied kilns as between the middle of the 1st and 2nd centuries AD (Fernández-García 2004, p244-266). The sampled structure is considered as being coeval with the other kilns, between 50-150 AD, although this needs to be confirmed by further field investigations.

Cartuja I-III (Granada). M. Orfila-Pons. (10-12) CAR-HI, CAR-HII, CAR-HIII: 100 ± 50 .

Cartuja was an important Roman centre for manufacturing ceramic and building materials, located in the city of Granada. Excavations yielded 10 pottery kilns representing 3 phases of construction. Phase I dates from pre-1st century AD, phase II from the first half of the 1st century AD and phase III from between the second half of the 1st century and the first half of the 2nd century AD. Three kilns from phase III have been sampled for archaeomagnetic studies. Kiln HI, used in the manufacture of building material, is rectangular, with a grate supported by a double-arch structure and a well-preserved praefurnium. Archaeomagnetic samples have been taken from the interior kiln walls. Kiln HII is also rectangular, with a grate supported by 4 arches and 2 praefurniums representing different phases of construction. Archaeomagnetic samples have been taken from the interior walls of the firing chamber. Kiln HIII is rectangular, similar in structure to HI. It has a grate supported by 4 double arches and a large praefurnium with an adobe vault lined with bricks. Archaeomagnetic samples have been taken from the interior walls of the firing chamber and from the grate.

Archaeological data have been used to constrain their ages (Casado-Millán *et al.* 1999). Phases I-III have been distinguished on the basis of material recovered from the site (ceramics, building materials, coins, etc.) and on the ceramic styles produced at the site. The sampled kilns are from phase III and are considered to be coeval. An age of 50-150 AD has been ascribed to them.

Patio Cardenal I-V (Sevilla). M.A. Tabales-Rodríguez. (13-16) PAR1, PAR 3, PAR4, PAR5 (H-I, -III, -IV, -V): 110 ± 20 .

Archaeological excavations revealed one of the most important conserved workshops of Hispalis, the Roman city on which Seville now stands (Tabales-Rodríguez 2003). In ‘Patio del Cardenal’, 5 circular kilns with circular central pillars supporting their grates were found, along with the remains of some large storerooms and some later rubbish dumps. Archaeomagnetic samples were taken from 4 of the kilns: PAR1 – baked floor and interior wall of the kiln, PAR3 - baked floor, interior wall of the kiln and central pillar, PAR4 – interior wall of the kiln and central pillar, PAR5 - baked floor and interior wall of the kiln.

Archaeological data have been used to date the kilns. The workshop mainly produced amphorae (types Dr. 20, Haltern 70, Dr. 28 and Beltran IIA, García-Vargas 2003). The proposed date of infilling/burial of the kilns is the second half of the 1st century AD, although some of the ovens could have been in use during the first decades of the 2nd century AD (Chic & García 2003, p305). The kilns correspond to the final moments of the workshop, placed at 90-130 AD.

Baelo Claudia (Cádiz). A. Álvarez-Rojas. (17) BC: 125 ± 25 .

‘Baelo Claudia’ is one of the best known Hispano-Roman sites, archaeological investigations since the beginning of the 20th century revealing the remains of a Roman city with a thermal complex which includes baths. The oven associated with heating the baths has been studied archaeomagnetically. Samples were taken from the praefurnium.

The site has been dated using archaeological information. Placed in the Low Imperial epoch by its excavators (Etienne & Mayet 1971), later studies improved on the original date, changing it to the middle of the 2nd century AD, maybe during the reign of Adriano (Sillieres 1995, p161-2). The marks ‘IMP.AVG’ found on the bricks

from the hipocaust are from a similar chronological period. The studied structure has been ascribed to the first half of the 2nd century AD (100-150 AD), based on archaeological considerations.

Gallineras (Cádiz). A. Sáez-Espligares. (18) GAL: 160 ± 60.

Gallineras, located in San Fernando, close to the city of Cádiz, is known as one of the main manufacturing centres of potteries and ceramics in southern Spain during Roman times. Excavations revealed a Roman villa, amphorae and 7 kilns. Subsequent quarrying activity nearby lead to severe degradation of the site and only 2 of the 7 kilns survived, 1 of which has been studied archaeomagnetically. Samples were taken from the praefurnium and interior wall of the kiln.

The area is rich in archaeological sites whose occupation date back from the 2nd - 8th century BC and it was an important production centre well into Roman times. The kilns at Gallineras are associated with the Roman villa, and have been dated using archaeological evidence. Ample pottery and amphora fragments have been recovered and engineering works in 1989 lead to the discovery of complete amphorae. Based on the style of the amphorae, and the recovered ceramics, Sáez-Romero *et al.* (2003) have proposed a principal age of kiln production ranging from the end of the 1st century BC to the 2nd century AD. However, some fragments from the early 3rd century AD have also been found and an age of 100-220 AD has been ascribed here in order to take this into account.

Setla-Mirarrosa-Miraflor (Alicante). J.A. Gisbert-Santonja. (20) DENA (II): 235 ± 15.

The kiln sampled (Setla-Mirarosa-Miraflor) was discovered in a large handicrafts complex close to the coast (Gisbert-Santonja 1988, Gisbert-Santonja & Antoni 1991). Archaeomagnetic samples were taken from the interior walls of the kiln.

The age of this structure is archaeologically well constrained by findings of Amphorae (type Almadraba IV), 3rd century AD pottery and coins. Note that the age control of Roman ceramics is well constrained for this period, allowing the definition of an age of 220-250 AD for the structure.

Hippolytus (Madrid). S. Rascón, J. Polo. (21) HIP (horno termas): 275 ± 50.

Hippolytus, near Madrid, is a complex of thermal baths associated with the Roman city of Complutum. One of the ovens associated with heating the baths has been studied archaeomagnetically. Samples were taken from the brick walls of the praefurnium.

The structure has been dated through archaeological investigations. Following extensive studies, the thermal complex and ovens have been dated as between the late 3rd century and the early part of the 4th century AD (225-325 AD), principally through ceramic finds and pavement types (García-Moreno & Rascon 1999).

Valeria (Cuenca). A. Fuentes-Domínguez. (23) VAL (Casa de los Adobes): 300 ± 30.

The ruins of the Roman city of Valeria, located close to Cuenca, have been under investigation since the early 1970s. The burnt wall of a building affected by a fire and subsequently abandoned has been studied archaeomagnetically. Samples were taken from the limestone blocks of the lower part of the burnt wall.

The TPQ/TAQ are defined by the lifespan of the city, known through archaeological considerations. It existed in the Low Imperial epoch, from the end of the 2nd century to the beginning of the 3rd century AD (TPQ), and was

abandoned towards the end of the 4th century AD (TAQ). The date of the fire affecting the sampled builing is placed at 270-330 AD by ceramics and coins found in association with the house (Fuentes 1998, Larrañaga 1995).

Puente Grande I-II (Cádiz). D. Bernal-Casasola, L. Lorenzo. (24, 25) PG1 (Horno 1 del sector G), PG2 (Horno 2 del sector G): 405 ± 5.

A large agricultural production centre, known as the Roman Villa of Puente Grande (Bernal & Lorenzo 2002 ed), was excavated in the Los Barrios district near Algeciras Bay. The site had 2 phases of occupation, and 2 circular kilns associated with the second occupation period have been studied archaeomagnetically. For structure PG1 samples were taken from the baked floor and walls of the combustion chamber. For PG2, samples were taken from the walls of the combustion chamber.

The site has been dated through archaeological information. No TPQ is defined, whilst the TAQ is well-defined through coin finds. The first occupation phase has been placed in the 1st century AD, with subsequent abandonment during the Trajan epoch (Bernal & Lorenzo 2002a). The second phase, to which belong the excavated kilns, is placed between the 4th century and the early part of the 5th century AD (Bernal & Lorenzo 2002b). Ceramic fragments (including African and southern Hispanic amphorae) and coins dated at 330-335 AD were found during excavation of the kilns (Lagostena & Bernal 2004, p51-2), giving a period of production in the 4th century. The age of abandonment of the second occupation phase, hence the TAQ, is given by ceramic finds across the whole site, along with coins of age 348-395 AD, placing it in the first decade of the 5th century AD. There is no archaeological evidence of progressive abandonment and the studied kilns correspond with the abandonment phase of the villa, at 400-410 AD.

Ramón Ortega I-II (Alicante). J.A. Gisbert-Santonja. (26) RO2 (U.E.125): 1025 ± 25, (28) RO1 (U.E.132): 1075 ± 25.

Archaeological excavations in Denia (“Avenida Ramón Ortega”), revealed a complex of 6 Islamic, circular kilns which were found alongside a necropolis. Two of the kilns were chosen for archaeomagnetic studies. For both structures (RO1 and RO2), samples were taken from the walls of the firing chamber.

The structures have been dated through archaeological considerations (Gisbert-Santonja & Antoni 2000, Gisbert-Santonja 1997. The site is well-dated through ceramic finds, kiln types and the general archaeological context (Gisbert-Santonja, private communication). The kilns have been placed in the 11th century AD, but are not considered coeval. RO2 is dated at 1000-1050 AD and RO1 at 1050-1100 AD.

Murcia c/Sagasta (Murcia). J. Navarro-Palazón y F. Muñoz-López. (27) MURG (MUS 36.3): 1050 ± 50.

Excavations in Murcia (“Calle Sagasta”) revealed an Islamic pottery kiln. This kiln has been sampled for archaeomagnetic study, with samples taken from the interior walls of the kiln, which has been dated using archaeological data. Ceramic shards associated with the kiln have been dated as 11th century AD. The excavation of the levels overlying the kiln indicate urbanisation of the area from the beginning of the 12th century. Therefore the kiln is considered to have been in use during the 11th century (Jiménez-Castillo, private communication).

Cabrera d'Anoia (Barcelona). J.I. Padilla-Lapuente and J. Thiriot. (29) CDAP (99P): 1115 ± 105 , (30) CDAU (99U): 1116 ± 87 , (38) CDAJ (99J): 1159 ± 103 , (39) CDAH (99H): 1162 ± 119 .

Cabrera Castle is located on a hill near the Anoia river valley, 50 km north-west of Barcelona. Around 40 Medieval, grey pottery kilns laying in a parallel series were found during excavations of the hillside substrata, 4 of which were sampled for archaeomagnetic study. Samples were taken from the interior walls of the kilns.

The grey pottery produced in this area is dated between the 9th and 15th century AD, and part of the production of the kilns is considered to have been for the castle occupants. The 4 studied kilns have been dated using the C14 method at the University Claude-Bernard of Lyon and the University of Barcelona (Padilla *et al.* 1998), giving ages that range from 1115 to 1162 AD.

Murcia c/Puxmarina (Murcia). P. Jiménez-Castillo and J. Navarro-Palazón. (31) MURO (MUP99E), (32) MURN (MUP99D), (33) MURM (MUP99B) (34) MURL (MUP99A), (35) MURI (MUP131), (36) MURK (MUP185), (37) MURH (MUP22): 1150 ± 50 .

Excavations in Murcia (“Calle Puxmarina”) revealed an abandoned, Islamic “caliphal” house that had been converted into a glass-making workshop. Seven well-preserved Islamic kilns were found and all were sampled for archeomagnetic study. The samples were taken from the interior walls of the kilns.

The TAQ of these structures (1200 AD) is historically and archaeologically well constrained by the Christian conquest of the area in 1243 and by the construction of Islamic houses at the beginning of the 13th century. Ceramic finds and the general archaeological context indicate that the site was active during the 12th century but a well-defined TPQ is not available (Jiménez *et al.* 2000). The proposed abandonment date is between 1100 and 1200 AD. Note that MURL, MURM, MURN and MURO are 4 phases of the same kiln, MURL being the most recent.

Magisterio I-II (Guadalajara). I. Ramírez-González. (40, 41) MAGI (MAG1), MAGII (MAG2): 1275 ± 25 .

Two kilns were revealed during excavations at El Magisterio, in Guadalajara. Both have been studied archaeomagnetically. Samples were taken from the kiln walls.

The structures have been dated through archaeological considerations. The kilns are considered coeval, and have been dated at 1250-1300 AD, principally through ceramic fragments found during excavations (Ramírez-González 2005a).

Calatrava la Vieja (Ciudad Real). M. Retuerce and M.A. Hervás. (42, 43) CALA (CV218), CALB (CV250): 1287.5 ± 13 , (53) CALC (CV252): 1410 ± 10 .

Calatrava la Vieja is an important site due that has been the object of numerous investigations (Retuerce & Hervas 2004). Occupied by Muslims from the 8th century AD, it was conquered in 1147 and became the first Templar possession in Castilla. After a brief Muslim occupation (1195-1212), it was re-conquered and stayed in Christian hands until its abandonment at the beginning of the 15th century. Three kilns have been found at the

site, all of which have been sampled for archaeomagnetic study. The samples were taken from the interior walls of the kilns.

The age of the kilns CALA and CALB is archaeologically and historically well constrained by ceramics and by the general context of the site. Ceramic finds correspond to the domain of the Calatrava Order, which held the castle after its re-conquest in 1212, defining a TPQ for these two structures of 1212 AD. The age of abandonment is also constrained by ceramic typology and the general archaeological and historical context, and is placed at the end of the 13th century (1275-1300 AD).

The age of kiln CALC is controlled by archaeological data. It is placed between 1390 and 1420 AD on the basis of ceramic typology and the abandonment of the castle at the beginning of the 15th century (TAQ), which defines an age of abandonment of 1400-1420 AD.

Valencia Velluters (Valencia). I. García-Villanueva. (44) VALN (VVE6009): 1294 ± 56, (47) VALI (VVE3734): 1319 ± 81, (49, 50) VALK (VVE4799), VALM (VVE5418): 1375 ± 75, (59) VALL (VVE5327): 1600 ± 25.

Velluters, in Valencia, was located between the Islamic and Christian walls on the west side of Valencia. This area has been in continuous occupation since Medieval times. Several domestic, pottery and glass making kilns, related to different periods of occupation, have been discovered, 5 of which have been sampled for archaeomagnetic study. Samples were taken from the interior walls of the kilns.

The ages of the structures have been controlled primarily through archaeological considerations (García-Villanueva, private communication). Kilns VALI and VALN are probably Islamic kilns which were in use until at least the Christian conquest of the area in 1238 AD, which defines their TPQ. The ancient access to VALI was buried beneath a surface from the second half of the 14th century. This places the TAQ at 1400 AD. VALN was covered by a ground level dated at the first half of the 14th century and was also affected by two holes, one of them filled with ceramics of the first half of the 14th century, allowing the definition of a TAQ of 1350 AD.

Kilns VALK and VALM were built on a ground level from the first half of the 14th century, and stratigraphically above the kilns another layer from the middle of the 15th century was found. This constrains the TPQ and TAQ of these structures to 1300 and 1450 AD resp. VALK, built on the top of the remains of VALM, is the younger of the two structures.

VALL was probably made in second half of the 15th century, in use during the 16th century and abandoned at the end of the 16th or the beginning of the 17th century. Ceramics from the late 15th – early 16th century were found within the kiln, establishing a TPQ of 1475-1525 AD. The TAQ, constrained by a covering layer containing well-dated ceramics from the end of the 16th century and the first quarter of the 17th century, is set at 1625 AD.

Castillo de San Romualdo (Cádiz). A. Sáez-Espigares. (45) CSR: 1300 ± ?.

Castillo de San Romualdo is unique in Spain, representing an Islamic kind of building known as a “ribat” (a mixture of monastery and hillfort), supposed to have been built by Islamic masons who remained in Spain after the Christian re-conquest. It is found in San Fernando, close to Cádiz. Archaeological excavations of the castle interior

revealed 7 different floor levels and a small adobe oven containing fired bricks. The oven has been studied archaeomagnetically. Samples were taken from the fired bricks found in the oven interior.

The age has been controlled using archaeological data. Little information is available about the exact origin of the castle, though due to its particular style of construction it is supposed to have been built in the late Middle Ages (before the end of the 14th century). The various floor levels, corresponding to different occupation phases have been dated using archaeological data. The first phase is interpreted as being from the low Middle Ages on the basis of ceramics, organic remains and bronze coins. The oven has been ascribed to a late Middle Age occupation level, placed in 1300 AD (Sáez-Espligares *et al.* 2001), with a lack of data preventing the definition of any error of this date.

SUE-10 (Guadalajara). I. Ramírez-González. (46) GUA1: 1300 ± ?.

Archaeological excavations at SUE 10 – c/Ingeniero Mariño, in the city of Guadalajara, revealed the remains of a pottery kiln, 2 storage silos and domestic pottery fragments. Of the kiln, 2 pillars supporting the vault of the firing chamber and parts of the floor and walls of the combustion chamber were preserved in situ. Archaeomagnetic samples were taken from the 2 support pillars.

The kiln has been dated using archaeological data, principally through the construction technique used and the ceramics found in the silos. No strict TPQ/TAQ have been defined, and an age of 1300 ± 25 AD has been ascribed (Ramírez-González 2005b).

Av. Blas de Infante (Cádiz). A. Torremocha. (48) BI (murallas Merinies, torres T3 y T4): 1369.

The fortifications of Algeciras were destroyed during the 14th century Muslim reconquest of Algeciras. During the attack, the towers and walls were first undermined, then the newly-formed spaces were filled with wood which was then burnt, leading to the collapse of the towers and walls. Archaeomagnetic samples were taken from the fire-affected sandstone blocks from the base of the walls.

The date of the reconquest (hence the TPQ/TAQ of the burnt walls) is precisely controlled by historical documents. The chronicle of Enrique II places the year of the attack as 1369 AD. Muslim documents are more precise. The written communication of Ibn-al-Jat b states that the attack started on July 28th, 1369, and that control of the city was acquired by July 31st. A letter sent to Muhammad V al Jeque de la Meca in August 1369 supports these dates (Torremocha-Silva *et al.* 1999, Torremocha-Silva *et al.* 2000).

Llano las Damas (Ceuta). D. Bernal-Casasola, J.M. Pérez-Rivera. (51) LLD: 1407.5 ± 7.5.

Excavations in Ceuta, the Spanish enclave on the northern African coast, revealed a poorly conserved kiln. The kiln has been studied archaeomagnetically, with samples taken from the walls of the combustion chamber.

No firm TPQ is available. The kiln has been dated through historical and archaeological considerations, mainly ceramic finds. The proposed age of abandonment is between the second half of the 14th century AD and the Portuguese conquest of the city in 1415 AD (TAQ). Pending future investigations, the latter date is favoured, and an age of 1400-1415 AD has been ascribed.

Huerta Rufino (Ceuta). J.M. Hita-Ruiz, F. Villada-Paredes. (52) HR: 1407.5 AD ± 7.5.

Excavations in Ceuta, revealed an area of well-preserved Islamic houses. In one of the houses the remains of a kitchen with an oven and fireplace were identified. This oven/fireplace has been studied archaeomagnetically, with samples taken from the oven/fireplace hearth stones.

The structures have been dated through historical and archaeological considerations, although no details are available. Ceramic finds are placed between the second quarter of the 14th century and late 14th century. As with the previous site (51, LLD), the Portuguese conquest of the city in 1415 AD (TAQ) is favoured as the date of abandonment, and an age of 1400-1415 AD has been ascribed.

Paterna c/Huertos (Valencia). M. Mesquida-García. (54) PATA (H21A): 1475 ± 25, (58) PATB (H21B): 1587.5 ± 62.5.

Paterna Testar del Moli (Valencia). M. Mesquida-García. (55) TMO: 1515 ± 25, (56) PATJ (H3B): 1520 ± 91, (57) PATH (41A): 1525 ± 75.

The locality of Paterna is still known as a large pottery production centre. Two archaeological sites, at Calle de los Huertos and Testar del Moli have been studied (Mesquida-García 2002, Mesquida-García *et al.* 2001), with 5 kilns sampled for archaeomagnetic study. Samples were taken from the interior walls of the kilns.

PATA and PATB are 2 phases of the same kiln, PATB being the more recent. The phases have been dated using archaeological data. Ceramics from the 15th century have been found in association with the kiln. Archaeological constraints suggest abandonment of the first phase of the kiln took place between 1450-1500 AD, placing the TAQ at 1500 AD. The second phase of the kiln (with TPQ at 1450 AD) is said to have been in use for at least 75 years (Mesquida-García, private communication), though a well-defined TAQ is not available. In order to prevent any error in dating the last use of the structure, a large interval of 1525-1650 AD is proposed as the age of abandonment of PATB.

Archaeological data have been used to date TMO, although no details are available. The ascribed age is 1490-1540 AD.

PATH has been dated using archaeological data, ceramics from the end of the 14th century and the beginning of the 15th century giving a TPQ of 1375 AD. Archaeological constraints place the abandonment at 1450-1500 AD.

PATJ has been dated using the C14 method, giving an age of 1429-1611 AD.

Monastery at Yuste (Cáceres). I. Ramírez-González. (60) YUS1: 1799 ± 15, (63) YUS2: 1959.

The monastery at Yuste is an important historical site in Spain, being the site at which King Carlos V resided after his abdication in 1556. Archaeological investigations at the site revealed a completely preserved, large bread-making oven. Furthermore, a small oven was built by one of the monks in 1959, by the “Casa del Obispo”, next to the Monastery. This was an attempt to recreate traditional ceramic production methods. Both the historical and modern structures were sampled for archaeomagnetic study. For YUS1, samples were taken from the floor and interior walls of the cooking chamber. For YUS2, samples were taken from the walls of the firing chamber.

Both structures are well-dated through archaeological, historical and anecdotal evidence. For YUS1, historical and archaeological considerations indicate the oven was in use during the life-span of the monastery. The TPQ, associated with the date of construction of the monastery, is not defined, although the site was occupied since at least the early part of the 15th century AD. The monastery was burnt to the ground during the Spanish War of Independence (1808-1814 AD), thus fixing the TAQ. The oven is considered to have been in use in the final decades up until the destruction of the monastery, and the age has been set between 1784 and 1814 AD (Ramírez-González 2000).

In 1949 AD the monastery was restored and in 1959 the modern kiln (YUS2) was built. It was abandoned in the same year because of a failure to produce acceptable ceramics.

Huertas del Carmen (Guadalajara). I. Ramírez González. (61) GUA2: 1835 ± 10.

Excavations related to construction works revealed a large brick-making furnace associated with the Convento del Carmen in Guadalajara. A large ($>6m^3$) combustion chamber and grate are preserved in situ. Archaeomagnetic samples were taken from the (vitrified) bricks of the interior walls of the combustion chamber. The age of the furnace is controlled by archaeological and historical data. It is associated with the construction and maintenance of the Convent, which was built in 1632, which defines the TPQ. Documentary evidence of maintenance work associated with the sale of the Convent places the TAQ at 1845. The last use of the oven is considered to have been associated with this work. Ceramic finds support such a date (Ramírez-González 2005c).

Palacio de Perales (Madrid). I. Ramírez González. (62) AL: 1870 ± 40.

Archaeological excavations of the Palacio de Perales in Valdeolmos-Alalpardo, Madrid, revealed the remains of some perimeter walls, baked clay paving stones and a buried cellar with well-conserved arcs. In one of the paved areas the outline of the remains of some kind of fire has been recognised. The paving stones affected are blackened and physically altered, and are readily distinguishable from unaffected areas. The burnt area has been sampled for archaeomagnetic study, samples being taken from an area of approximately 2m².

The TPQ is well-constrained through historical documents, which state that the palace was built in 1730 AD for the Pinedo Family. After a century of occupation, the Palace suffered partial collapse and was eventually abandoned between 1830 and 1850 AD. Between the end of the 19th century AD and the beginning of the 20th century the palace was dismantled and the material recycled for use in new constructions, loosely defining the TAQ. The fire is associated with the period between the abandonment of the site and its dismantlement. It has been ascribed an age of 1830-1910 AD (Ramírez-González 2004, 2005d).

References: Appendix

- Bernal, D., 1998. Excavaciones arqueológicas en el alfar romano de la Venta del Carmen (Los Barrios, Cádiz). Una aproximación a la producción de ánforas en la Bahía de Algeciras en época altoimperial, Madrid.
- Bernal, D. & Lorenzo, L., 1998a. Los hornos y las estructuras asociadas, en Excavaciones arqueológicas en el alfar romano de la Venta del Carmen (Los Barrios, Cádiz). Una aproximación a la producción de ánforas en la Bahía de Algeciras en época altoimperial (D. Bernal ed.), Madrid, pp. 81-120.
- Bernal, D. & Lorenzo, L., 1998b. Las cerámicas importadas y la cronología del complejo alfarero, en Excavaciones arqueológicas en el alfar romano de la Venta del Carmen (Los Barrios, Cádiz). Una aproximación a la producción de ánforas en la Bahía de Algeciras en época altoimperial (D. Bernal ed.), Madrid, pp. 63-80.
- Bernal, D. & Lorenzo, L., 2002. Excavaciones arqueológicas en la villa romana del Puente Grande (Los Altos del Ringo Rango, Los Barrios, Cádiz). Una ventana al conocimiento de la explotación económica de la Bahía de Algeciras entre el s. I y el V d.C., Huelva.
- Bernal, D. & Lorenzo, L., 2002a. Las cerámicas finas (TSI, TSG, TSH, TSA A) y otras cerámicas datantes (lucernas, paredes finas, africanas de cocina y engobe rojo pompeyano), Excavaciones arqueológicas en la villa romana del Puente Grande (Los Altos del Ringo Rango, Los Barrios, Cádiz). Una ventana al conocimiento de la explotación económica de la Bahía de Algeciras entre el s. I y el V d.C., Huelva, pp. 137-187.
- Bernal, D. & Lorenzo, L., 2002b. Las cerámicas africanas (TSA C y D) y la cronología de la fase bajoimperial, en Excavaciones arqueológicas en la villa romana del Puente Grande (Los Altos del Ringo Rango, Los Barrios, Cádiz). Una ventana al conocimiento de la explotación económica de la Bahía de Algeciras entre el s. I y el V d.C., Huelva, pp. 357-368.
- Casado-Millán, P.J., Burgos-Juárez, A., Orfila-Pons, M., Alcaraz-Hernández, F., Cassinello-Roldán, S., Cevidanes-León, S., Ruiz-Torres, S., 1999. Intervención arqueológica de urgencia en el alfar romano de Cartuja (Granada). Anuario Arqueológico de Andalucía 1994, vol. III. Actividades de Urgencia, Sevilla , pp. 129-139.
- Cepillo-Galvin, J.J. & Blanes, C., 2002. Informe- memoria de la intervención arqueológica de urgencia en las obras de limpieza y consolidación del horno romano de El Gallinero, Puerto Real (Cádiz), Anuario Arqueológico de Andalucía '99, III.1, Sevilla, pp. 73-77.
- Chic-García, G. & García-Vargas, E., 2003. Alfares y producciones cerámicas en la provincia de Sevilla. Balance y perspectivas, Figlinae Baeticae. Talleres alfareros y producciones cerámicas en la Bética romana (s. II a.C. – VII d.C.), British Archaeological Reports, International Series 1266, I, Oxford, pp. 279-348.
- Cuadrado, E., 1991. La cerámica ibero-céltica de barniz rojo. Trabajos de Prehistoria, 48, 341-356.
- Etienne, R. & Mayet, F., 1971. Briques de Belo: relations entre la Maurétanie Tingitane et la Bétique au Bas Empire, Mélanges de la Casa de Velázquez VII, Madrid, pp. 59-74.
- Fernández-García, M.I., 2004. Alfares y producciones cerámicas en la provincia de Jaén. Balance y perspectivas, Figlinae Baeticae. Talleres alfareros y producciones cerámicas en la Bética romana (s. II a.C. – VII d.C.), British Archaeological Reports, International Series 1266, I, Oxford, pp. 239-272.
- Fernández-Rodríguez, M., 1987. Cerámica de barniz rojo en la Meseta. Archivo Español de Arqueología, 60, 3-20.

- Fuentes, A., 1988. La cronología del yacimiento hispanorromano de Valeria y su relación con otros análogos de la Meseta. 1º Congreso de Historia de Castilla - La Mancha. T II, Ciudad Real, 211 ss.
- García-Vargas, E., 1998. La producción de ánforas en la Bahía de Cádiz en época romana (s. II a.C. – IV d.C.), Ed. Gráficas Sol, Écija.
- García-Moreno, L.A. & Rascon, S., 1999. Complutum y las ciudades hispanas en la Antigüedad Tardía. *Acta Antiqua Complutensia*. Nº I, pp. 7-23 (ISBN 84-8138-276-0)
- García-Vargas, E., 2003. Las producciones de la figlina. Ánforas, Arqueología y rehabilitación en el Parlamento de Andalucía. Investigaciones arqueológicas en el Antiguo Hospital de las Cinco Llagas de Sevilla, Sevilla, pp. 200-219.
- García-Vargas, E. & Sibon-Olano, F., 1995. Excavaciones de urgencia en el horno romano de El Gallinero (Puerto Real, Cádiz), *Anuario Arqueológico de Andalucía '92*, III, Sevilla, pp. 124-129.
- Gisbert-Santonja, 1997. "La producción cerámica en Daniya-Dénia-en el siglo XI, *Cerâmica Medieval e Pós-Medieval. Métodos e resultados para seu estudo*. Actas das 3as jornadas, 28 a 31 de Octubre.
- Gisbert-Santonja, J.A., 1988. "L'Almadrava, Setla-Mirarosa-Miraflor, la Marina Alta, Alfar de ánforas romanas de finales del siglo I a principios del III d.C.", *Mémoires Arqueologiques de la Comunitat Valenciana*, Educació y Ciencia de la Generalitat Valenciana, Valencia, pp.21-24.
- Gisbert-Santonja, J.A. & Antoni, J., 2000. Cerámica Califal de Dénia, Universitat d'Alacant, Vicerectorat d'Extensió Universitària, Secretariat de Cultura, Alacant.
- Gisbert-Santonja, J.A. & Antoni, J., 1991. El alfar romano de l'Almadrava (Setla-Mirarosa-Miraflor) y la producción de ánforas e el territorio de Dianium, Aranegui Gascó, C., *Saguntum y el Mar*, pp.114-116.
- Jiménez, P., Muñoz-López, F. & Thiriot, J., 2000. Les ateliers urbains de verriers de Murcia au XIIe s. (C. Puxmarina et Pl. Belluga). In : Pétrequin, P., Fluzin, Ph., Thiriot, J., Benoir, P. dir.— Arts du feu et productions artisanales. XXèmes Rencontres internationales d'Antibes, 1999. Editions APDCA, Antibes, 2000, p. 433-452.
- Lagostena, L. & Bernal, D., 2004. Alfares y producciones cerámicas en la provincia de Cádiz. Balance y perspectivas, *Figlinae Baeticae. Talleres alfareros y producciones cerámicas en la Bética romana* (s. II a.C. – VII d.C.), British Archaeological Reports, International Series 1266, I, Oxford, pp. 39-124.
- Larrañaga, J., 1995. Ruinas de Valeria. N.A.H. II, 153 ss.
- Mesquida-García, M., 2002. La cerámica de Paterna, Reflejos del Mediterraneo, Museo de Bellas Artes de Valencia.
- Mesquida-García, M., López-Peris, J.E., Prados, S. & Smolka R., 2001. Las Ollerías de Paterna. Tecnología y producción, Volumen I. Siglos XII y XIII, Ajuntament de Paterna.
- Padilla, J.I., Thiriot, J., Evin, J. & Mestres, J., 1998. Datation par le radiocarbone des ateliers de potiers médiévaux de Cabrera d'Anoia en Catalogne. Actes du colloque "C14 Archéologie", pp. 419-423.
- Poveda, A., 1997. El horno romano (s. I a.C.) de El Monastil, XXIV Congreso Nacional de Arqueología, Elda, Alicante, pp. 481-493.
- Ramírez-González, I., 2000. Informe de la Intervención Arqueológica en el Monasterio de San Jerónimo de Yuste (Cuacos de Yuste, Cáceres), 2ª fase.
- Ramírez-González, I., 2004. Informe de Excavación arqueológica de la U.E.17, 18 y SAU nº 1 de Alalpardo (Madrid).

- Ramírez-González, I., 2005a. Informe de la Excavación Arqueológica de la Escuela de Magisterio de Guadalajara.
- Ramírez-González, I., 2005b. Informe de la Excavación Arqueológica en el área de afección de la SUE 10 de Guadalajara.
- Ramírez-González, I., 2005c. Informe de Excavación Arqueológica en la Intervención Arqueológica en el área de afección de la SUE 20.5. de Guadalajara.
- Ramírez-González, I., 2005d. Informe de Excavación arqueológica de la U.E.17, 18 y SAU nº 1 de Alalpardo (Madrid).
- Retuerce, M. & Hervás, M.A., 2004. Excavaciones arqueológicas en Calatrava la Vieja. Planteamientos y principales resultados. Castilla La Mancha. 1996-2002. Patrimonio Histórico-Arqueología. Castilla La Mancha, 18.
- Sáez-Espligares, A., Torremocha Silva, A. & Sáez Romero, A.M., 2001. Informes de las actividades arqueológicas desarrolladas en el castillo de San Romualdo". Campañas de 2000 y 2001. Anuario Arqueológico de Andalucía/2001, III, Sevilla, pp. 111-120.
- Sáez-Romero, A.M., Montero, R., Toboso, E.J. & Díaz, J.J., 2003. Control arqueológico en el yacimiento púnico-romano de Gallineras (San Fernando, Cádiz). Anuario Arqueológico de Andalucía/2000, III, Sevilla, pp. 166-173.
- Suárez-Padilla, J., Tomassetti Guerra, J.M., Fernández-Rodríguez, L.E. & Navarro-Luengo, I., 2003. Un Horno Romano de época Altoimperial en El Saladillo. Asociación Cilniana, n 14.
- Sillieres, P., 1995. Baelo Claudia. Une cité romaine de Bétique, Madrid.
- Suárez-Padilla, J., Tomassetti-Guerra, J.M., Bravo-Jiménez, S., Fernández-Rodríguez, L.E. & Navaro-Luengo, I., 2004. Un horno cerámico de época altoimperial en El Saladillo (Estepota, Málaga). D. Bernal/L. Lagóstena, eds., Figlinae Baeticae. Talleres alfareros y producciones cerámicas en la bética romana (siglos II a.C – VII d.C.), Cádiz.
- Tabales-Rodríguez, M.A., 2003. El complejo alfarero localizado bajo el Parlamento de Andalucía, Arqueología y rehabilitación en el Parlamento de Andalucía. Investigaciones arqueológicas en el Antiguo Hospital de las Cinco Llagas de Sevilla, Sevilla, pp. 139-162.
- Torremocha-Silva, A., Navarro Luengo, I. & Bautista Salado, J.B., 1999. Al-Binya, la ciudad palatina meriní de Algeciras. Fundación Municipal de Cultura "José Luis Cano", Algeciras.
- Torremocha-Silva, A., Navarro Luengo, I. & Bautista Salado, J.B., 2000. La Puerta de Gibraltar (Algeciras): un ejemplo de ingreso adelantado de época meriní en al-Andalus. Caetaria, 3, pp.187-207.
- Urbina, D., 2004. Plaza de Moros (Villatobas, Toledo) y los recintos amurallados de la II Edad del Hierro en el Valle Medio Tajo. Trabajos de Prehistoria, 61(2), pp. 155-166.

2.2. Article: The first Secular Variation Curve for the Iberian Peninsula. Comparison with other data from Western Europe and with geomagnetic field global models (soumis à Geochemistry, Geophysics, Geosystems)

M. Gómez-Paccard

Géosciences-Rennes, CNRS, UMR 6118, Université de Rennes 1, Campus de Beaulieu, 35042, Rennes, Cedex, France (miriam.gomez@univ-rennes1.fr, phone: 0033 2 23 23 67 59/ fax: 0033 2 23 23 60 40)

Facultad de Ciencias Físicas, Universidad Complutense de Madrid, Ciudad Universitaria, 28040, Madrid, Spain.

Civilisations Atlantiques et Archéosciences, CNRS, UMR 6566, Université de Rennes 1, Campus de Beaulieu, 35042, Rennes, Cedex, France.

Ph. Lanos

Civilisations Atlantiques et Archéosciences, CNRS, UMR 6566, Université de Rennes 1, Campus de Beaulieu, 35042, Rennes, Cedex, France (philippe.lanos@univ-rennes1.fr)

A. Chauvin

Géosciences-Rennes, CNRS, UMR 6118, Université de Rennes 1, Campus de Beaulieu, 35042, Rennes, Cedex, France (annick.chauvin@univ-rennes1.fr)

G. McIntosh

Facultad de Ciencias Físicas, Universidad Complutense de Madrid, Ciudad Universitaria, 28040, Madrid, Spain (gregc@fis.ucm.es)

M.L. Osete

Facultad de Ciencias Físicas, Universidad Complutense de Madrid, Ciudad Universitaria,
28040, Madrid, Spain (mlosete@fis.ucm.es)

G. Catanzariti

Facultad de Ciencias Físicas, Universidad Complutense de Madrid, Ciudad Universitaria,
28040, Madrid, Spain (gcatanza@fis.ucm.es)

V.C. Ruiz-Martínez

Facultad de Ciencias Físicas, Universidad Complutense de Madrid, Ciudad Universitaria,
28040, Madrid, Spain (vcarlos@fis.ucm.es)

J.I. Nuñez

Facultad de Ciencias Físicas, Universidad Complutense de Madrid, Ciudad Universitaria,
28040, Madrid, Spain (jnuneza.hgugm@salud.madrid.org)

Abstract

A first secular variation (SV) curve for the Iberian Peninsula was computed by hierarchical Bayesian method using a total of 134 archaeomagnetic directions with ages ranging from -775 to 1959 AD. A general agreement is observed between the Iberian curve and the French and German SV curves, although some interesting differences were found, such as the occurrence of lower inclinations between the 11th and 14th centuries in the Iberian curve. The analysis of these three reference curves indicates that SV in Western Europe is characterised by three major directional changes at -125, 200 and 1350 AD. It is suggested that these cusps are regional features of the geomagnetic field. The Iberian curve has been compared with the predictions of the CALS3K.2, CALSK7K.2 and Hongre global models. Despite large differences recognised between these models, even for the dipolar terms, they predict reasonably well the Iberian archaeomagnetic SV.

Keywords: Archaeomagnetism, Geomagnetic Secular Variation, Bayesian statistics, Iberian Peninsula

Index terms: 1503 Geomagnetism and Paleomagnetism: Archeomagnetism; 1522 Geomagnetism and Paleomagnetism: Paleomagnetic secular variation; 1532 Geomagnetism and Paleomagnetism: References fields: regional, global.

1. Introduction

The variation of the geomagnetic field in the archaeological past can be obtained from palaeomagnetic directions determined from heated and well dated archaeological structures. Archaeomagnetic data are the only palaeomagnetic data of high resolution for the last millennia (data from lakes and sediments may be smoothed and/or offset due to the magnetisation acquisition process and to sedimentation gaps). These data are used to build secular variation (SV) reference curves that provide knowledge of geomagnetic field variations at regional and global scales for periods covering the last few millennia. Along with historical data, detailed SV curves can also be used for dating purposes. Several SV curves are now available for Europe, including Great Britain [Batt, 1997], Bulgaria [Kovacheva *et al.*, 1998], France [Gallet *et al.*, 2002], Hungary [Márton, 2003] and Germany [Schnepp and Lanos, 2005]. Despite the high number of archaeological excavations carried out in Spain only limited data are available for this region. In a recent work, Gómez-Paccard *et al.* (in press, 2006) provide a compilation of 5 previous results and present 58 new archaeomagnetic directions. In the present study this data set is used, along with data from southern France and northern Morocco, to propose a first SV curve for the Iberian Peninsula. The French and Moroccan data can be used in constructing the SV curve due to their geographical proximity to the Iberian Peninsula. The hierarchical bivariate method by moving average technique [Le Goff, 1990; Le Goff *et al.*, 1992; Daly and Le Goff, 1996; Lanos, 2005] and the hierarchical Bayesian modelling [Lanos, 2004] are implemented in order to determine the best way to calculate the Iberian curve. To determine the characteristics of the geomagnetic SV in Western Europe over the last two millennia, the Iberian curve has been compared with the French and German archaeomagnetic reference curves. Finally, a comparison between available geomagnetic field global models [Hongre *et al.*, 1998; Korte and Constable, 2005] has been conducted in order to test the reliability of their predictions.

2. Available data from Spain, France and Morocco

Spanish data

Gómez-Paccard *et al.* (in press, 2006) compiled the available data for Spain and presented 58 new archaeomagnetic directions, carefully describing the sampling, experimental procedures and dating constraints of the new directions. Samples were taken as oriented blocks or drilled directly from the archaeological heated structures. Classical thermal or alternating field demagnetisation or Thellier method were applied in order to determine the characteristic

directions for each structure. In most cases high quality, single component remanence vectors were obtained. For some structures, which were heated to relatively low temperatures, more than 1 component could be recognised and great circle analysis was required. The characteristic directions and their statistical parameters were calculated using principal component [Kirschvink, 1980] or great circle [McFadden and McElhinny, 1988] analysis and Fisher [1953] statistics. As proposed by *Lanos et al.* [2005], a hierarchical structure was followed in the calculation of the 58 new directions. Together with 5 previous data from Spain [*Thellier*, 1981; *Parés et al.*, 1992; *Oyamburu et al.*, 1996], a total of 63 archaeomagnetic directions are available from Spain (see Table 1 and Figure 1).

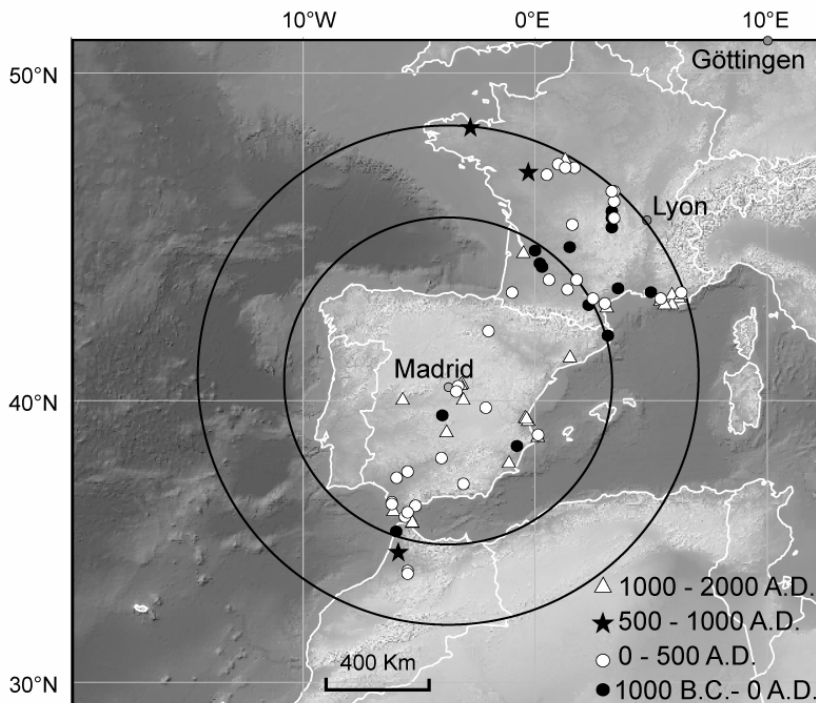


Figure 1: Map showing locations of archaeomagnetic sites (plotted in different symbols for the different age ranges) compiled for the construction of the secular variation curve for the Iberian Peninsula. Madrid (40.4°N , 3.7°W) has been chosen as the reference site. Two circles of radii 600 km and 900 km are shown.

French and Moroccan data

Archaeomagnetic research started in France with the work of E. Thellier [*Thellier*, 1938], who later published the first SV curve for France for the last two millennia [*Thellier*, 1981]. This curve has been revised, completed and extended by *Bucur* [1994]. Since then, new archaeomagnetic directional results have been collected by *Moutmir* [1995], *Chauvin et al.* [2000] and *Gallet et al.* [2002], who presented a new SV curve for France. Together they provide a high quality collection of archaeomagnetic data. In this study, only the data from sites with a geographical proximity to the Iberian Peninsula (within a 900 km radius of Madrid) have been considered (see Figure 1). This includes data from *Gallet et al.* [2002] (which itself includes a selection of well-dated results (called PC) from *Bucur* [1994], data from *Moutmir* [1995] and some new archaeomagnetic directions), together with the directional results of *Chauvin et al.* [2000]. A total of 63 archaeomagnetic directions from France have been compiled (see Table 1).

In contrast, very few archaeomagnetic studies have been performed in Morocco. The first concerned the study of six structures coming from three localities [*Kovacheva*, 1984], in which 4 reliable archaeomagnetic directions were given. Five directions from *Najid* [1986] are also available in the archaeomagnetic databases Archeo00 of Don Tarling (<http://www.ngdc.noaa.gov/seg/geomag/>) and *Korte et al.* [2005], giving a total of 9 archaeomagnetic directions from Morocco (Figure 1). They correspond to sites within a 900 km radius of Madrid (see Table 1).

Courbe de variation séculaire pour la Péninsule Ibérique

Name	t _{min}	t _{max}	t _{mean}	t _{bayesian}	I _s (°)	D _s (°)	N	α_{95}	k	Lat. (°N)	Long. (°E)	Stratigraphic constraints	Reference
Sites (Spain)													
Plaza de Moros (PLM)	-150	-50	-100	-98.7	58.2	-4.0	8	4.1	182	39.50	-4.00		
Ampurias (AMP)	-200	100	-50	-98.7	63.5	-8.5	4	1.5	2592	42.12	3.13		Thellier, 1981
El Monastil (MON)	-50	35	-7.5	-5.6	57.3	0.3	9	2.2	546	38.47	-0.79		
El Gallinero (GA)	40	50	45	45.0	53.4	3.8	7	4.9	150	36.53	-6.19		
Villa del Pañuelo I (VILI)	0	100	50	51.4	57.1	-5.5	25	2.6	116	40.30	-3.40		Oyamburu, 1996
Calahorra, La Maja (LMA)	0	100	50	54.9	58.4	-0.8	29	2.1	128	42.27	-2.02		Parés, 1992
Costalita (COS)	0	100	50	46.8	54.3	3.7	14	6.0	46	36.42	-5.15		
Venta del Carmen (VC)	80	90	85	85.3	46.7	2.1	27	2.3	146	36.18	-5.49		
Villares Andújar (VIA)	50	150	100	109.2	50.5	1.4	9	3.2	259	38.06	-4.04		
Cartuja I (CAR-HI)	50	150	100	86.3	55.3	-1.7	7	3.5	293	37.18	-3.10		
Cartuja II (CAR-HII)	50	150	100	100.1	52.2	-3.1	7	5.4	125	37.18	-3.10		
Cartuja III (CAR-HIII)	50	150	100	96.5	52.3	2.9	5	3.9	392	37.18	-3.10		
Patio Cardenal I (PARI)	90	130	110	109.0	53.0	-2.4	10	2.2	484	37.38	-5.98		
Patio Cardenal III (PAR3)	90	130	110	108.6	54.1	-4.1	6	3.7	324	37.38	-5.98		
Patio Cardenal IV (PAR4)	90	130	110	109.1	53.3	-2.7	7	1.9	1026	37.38	-5.98		
Patio Cardenal V (PAR5)	90	130	110	109.0	53.5	-4.3	17	2.6	193	37.38	-5.98		
Baelo Claudia (BC)	100	150	125	128.2	46.7	-2.2	14	3.6	145	36.03	-5.62		
Gallineras (GAL)	100	220	160	140.5	55.8	-0.1	7	4.6	176	36.47	-6.18		
Arva (ARV)	150	250	200	199.1	51.8	-3.7	17	1.3	682	37.60	-5.50		Evans, pers.comm.
Setla Mirarosa Miraflor (DENA)	220	250	235	234.9	52.6	-4.5	10	1.9	669	38.86	0.02		
Hyppolytus (HIP)	225	325	275	274.4	52.6	-4.0	18	3.4	104	40.48	-3.32		
Villa del Pañuelo II (VIL2)	250	350	300	296.6	51.7	-2.7	31	2.2	131	40.30	-3.40		Oyamburu, 1996
Valeria (VAL)	270	330	300	299.7	48.0	-5.4	7	9.7	58	39.77	-2.13		
Puente Grande I (PG1)	400	410	405	404.9	46.4	-14.1	13	7.3	33	36.18	-5.49		
Puente Grande II (PG2)	400	410	405	405.0	52.5	0.3	15	3.4	129	36.18	-5.49		
Ramon Ortega II (RO2)	1000	1050	1025	1027.7	50.9	17.3	14	4.0	100	38.86	0.12		
Murcia c/Sagasti (MURG)	1000	1100	1050	1033.2	51.3	21.7	8	1.5	1437	37.98	-1.12		
Ramon Ortega I (RO1)	1050	1100	1075	1079.0	47.9	15.8	16	1.9	380	38.86	0.12		

Courbe de variation séculaire pour la Péninsule Ibérique

Cabrera d'Anoia (CDAP)	1010	1220	1115	1174.4	50.6	3.6	8	3.6	236	41.50	1.50
Cabrera d'Anoia (CDAU)	1029	1203	1116	1180.0	45.7	9.6	6	1.3	2765	41.50	1.50
Murcia c/Puxmarina (MURO)	1100	1200	1150	1119.6	44.7	13.6	6	3.8	308	37.98	-1.12
Murcia c/Puxmarina (MURN)	1100	1200	1150	1135.8	45.1	14.0	6	2.1	1038	37.98	-1.12
Murcia c/Puxmarina (MURM)	1100	1200	1150	1151.7	45.5	14.9	7	2.1	811	37.98	-1.12
Murcia c/Puxmarina (MURL)	1100	1200	1150	1170.8	44.2	16.2	9	1.2	1842	37.98	-1.12
Murcia c/Puxmarina (MURI)	1100	1200	1150	1157.4	41.7	15.2	7	4.1	215	37.98	-1.12
Murcia c/Puxmarina (MURK)	1100	1200	1150	1146.4	45.2	14.1	9	2.2	547	37.98	-1.12
Murcia c/Puxmarina (MURH)	1100	1200	1150	1134.3	46.4	17.3	10	2.7	330	37.98	-1.12
Cabrera d'Anoia (CDAJ)	1056	1262	1159	1217.0	45.2	9.0	8	2.7	416	41.50	1.50
Cabrera d'Anoia (CDAH)	1043	1281	1162	1215.1	46.4	10.7	5	1.3	3461	41.50	1.50
Magisterio I (MAGI)	1250	1300	1275	1270.6	42.6	11.5	5	4.8	500	40.63	-3.16
Magisterio II (MAGII)	1250	1300	1275	1275.9	47.3	4.1	6	6.1	179	40.63	-3.16
Calatrava la Vieja (CALA)	1275	1300	1287.5	1286.6	44.9	11.4	8	2.9	356	39.02	-3.82
Calatrava la Vieja (CALB)	1275	1300	1287.5	1287.4	44.4	7.1	10	2.9	284	39.02	-3.82
Valencia Velluters (VALN)	1238	1350	1294	1310.6	46.6	2.1	9	1.2	1859	39.47	-0.37
Guadalajara (GUA1)	1275	1325	1300	not used	57.8	14.3	4	2.8	1104	40.60	-3.20
Castillo de San Romualdo (CSR)	1100	1500	1300	1334.0	46.0	8.1	3	7.2	298	36.30	-6.10
Valencia Velluters (VALI)	1238	1400	1319	1329.6	46.4	4.4	11	1.7	725	39.47	-0.37
Av. Blas de Infante (BI)	1369	1369	1369	1369.0	41.9	0.4	10	3.4	206	36.13	-5.45
Valencia Velluters (VALM)	1300	1450	1375	1342.8	47.0	7.2	9	1.0	2733	39.47	-0.37
Valencia Velluters (VALK)	1300	1450	1375	1383.5	44.2	3.0	9	1.3	1606	39.47	-0.37
Llano las Damas (LLD)	1400	1415	1407.5	1407.2	37.0	9.6	14	4.0	98	35.89	-5.30
Huerta Rufino (HR)	1400	1415	1407.5	1407.0	35.9	7.8	7	3.1	417	35.89	-5.30
Calatrava la Vieja (CALC)	1400	1420	1410	1410.3	47.0	3.0	8	2.0	790	39.02	-3.82
Paterna c/Huertos (PATA)	1450	1500	1475	1487.6	56.4	3.6	10	1.7	792	39.50	-0.43
Paterna Testar del Moli (TMO)	1490	1540	1515	1520.1	55.7	7.5	16	2.0	343	39.50	-0.43
Paterna Testar del Moli (PATJ)	1429	1611	1520	1593.6	62.2	6.6	16	1.1	1201	39.50	-0.43
Paterna Testar del Moli (PATH)	1450	1600	1525	1515.7	53.5	7.3	10	1.7	831	39.50	-0.43
Paterna c/Huertos (PATB)	1525	1650	1587.5	1625.6	64.1	5.8	11	1.6	827	39.50	-0.43
Valencia Velluters (VALL)	1575	1625	1600	1591.5	56.6	9.1	11	1.9	557	39.47	-0.37
Monastery at Yuste (YUS1)	1784	1814	1799	1835.2	55.5	-14.3	7	4.6	173	40.10	-5.70

Courbe de variation séculaire pour la Péninsule Ibérique

Huertas del Carmen (GUA2)	1825	1845	1835	1800.4	61.5	-21.1	13	2.7	238	40.60	-3.20
Palacio de Perales (AL)	1830	1910	1870	1865.5	63.0	-14.2	6	5.3	159	40.10	-3.10
Monastery at Yuste (YUS2)	1959	1959	1959	1959.0	58.2	-11.1	5	6.5	138	40.10	-5.70

Sites r < 600 km (France and Morocco)

Saint Florence	-325	-275	-300.0	-299.4	66.4	-2.8	11	2.2	386	44.8	0.0	Bucur 1994
Dchar Jdid. the citadel	-300	-100	-200.0	-186.9	53.0	1.8	10	5.1	75	35.5	-6.0	Kovacheva 1984
Aiguillon F1+2+3	-120	-80	-100.0	-99.5	62.4	-2.4	45	1.1	1825	44.3	0.3	Bucur 1994
Aiguillon F4	-120	-80	-100.0	-99.7	64.1	2.6	19	0.8	1607	44.3	0.3	Bucur 1994
Montans 4	-100	-80	-90.0	-90.0	63.5	-2.6	11	1.0	1696	43.9	1.8	Bucur 1994
Lagrere	-80	-40	-60.0	-59.9	62.9	-3.7	14	0.9	1797	44.4	0.2	Bucur 1994
Limoux II (four II)	-20	-5	-12.5	-12.6	62.0	-0.3	7	2.1	625	43.1	2.3	Bucur 1994
Montans 6	20	30	25.0	24.9	62.3	-1.2	7	1.2	2054	43.9	1.8	Bucur 1994
Al Kouass (Chkakra)	-100	0	-50.0	-49.3	54.3	-6.1	5	3.3	360	35.5	-6.0	Kovacheva 1984
Montans I	140	160	150.0	150.1	56.0	-0.1	12	1.6	673	43.9	1.8	Bucur 1994
Abrens (Laure Minervois)	175	225	200.0	200.0	56.8	-0.3	16	1.1	1031	43.3	2.5	Bucur 1994
Barat de Vin	400	400	400.0	400.5	59.6	-1.0	8	1.5	1079	43.5	-1.0	Bucur 1994
Lectoure	375	425	400.0	397.9	57.5	-4.3	20	1.7	311	43.9	0.6	Bucur 1994
Toulouse Place St. Etienne	450	550	500.0	508.7	63.4	1.0	9	0.6	5769	43.6	1.4	Bucur 1994
Sadirac SB4	1350	1400	1375.0	1373.6	51.0	1.9	10	0.8	2865	44.8	-0.5	Bucur 1994
Sadirac SB3	1500	1525	1512.5	1512.2	57.9	10.0	8	1.0	2331	44.8	-0.5	Bucur 1994

Sites r < 900 km (France and Morocco)

Gannat	-850	-700	-775.0	-744.2	65.1	14.0	10	2.9	237	46.2	3.3	Moutmir 1995
Lignat	-850	-700	-775.0	-762.9	67.7	29.4	24	2.4	146	45.8	3.3	Moutmir 1995
St. Blaise	-575	-550	-562.5	-561.6	65.6	0.5	11	0.9	2355	43.5	5.0	Bucur 1994
Issoire 1	-750	-250	-500.0	-662.7	69.1	21.6	21	1.4	961	45.5	3.3	Moutmir 1995
Aspiran. AFR 6186	-525	-475	-500.0	-501.1	69.5	9.9	17	1.8	398	43.6	3.6	Gallet 2002
Aspiran. AFR 6416	-525	-475	-500.0	-501.4	69.4	9.6	13	1.5	728	43.6	3.6	Gallet 2002
Issoire 2	-700	-600	-650.0	-648.0	73.0	22.0	8	1.6	483	45.5	3.3	Moutmir 1995
Loupiac. Loup-01	-850	-700	-775.0	-777.6	64.5	27.0	14	1.3	889	44.9	1.5	Gallet 2002
Loupiac. Loup-03	-850	-700	-775.0	-814.6	62.4	36.2	14	2.6	242	44.9	1.5	Gallet 2002

Courbe de variation séculaire pour la Péninsule Ibérique

Loupiac. Loup-12	-850	-700	-775.0	-742.0	66.7	19.7	9	3.4	236	44.9	1.5	Gallet 2002
Loupiac. Loup-16	-850	-700	-775.0	-794.2	62.4	27.4	17	3.2	123	44.9	1.5	Gallet 2002
Petit et grand Lezat	-100	-50	-75.0	-75.9	65.7	-7.9	10	1.5	931	46.0	3.3	Bucur 1994
Sallèles d'Aude F10	-30	30	0.0	-1.3	62.5	0.2	8	1.8	756	43.2	3.0	Chauvin 2000
Marseille	-30	40	5.0	-2.3	63.7	-2.4	46	0.6	1215	43.3	5.4	Bucur 1994
Lezoux F3	-25	50	12.5	6.8	64.5	-2.4	14	1.1	1243	45.8	3.4	Bucur 1994
Lezoux LAS65	15	20	17.5	17.5	63.5	-1.3	22	1.3	684	45.8	3.4	Bucur 1994
Gievres II sol brûlé	40	40	40.0	40.5	64.1	-0.5	6	0.8	5047	47.3	1.7	Bucur 1994
Mougon II	40	60	50.0	50.9	61.4	-3.3	20	1.1	1698	47.1	0.5	Bucur 1994
Sallèles d'Aude F12	50	90	70.0	71.6	57.8	-1.6	18	1.2	756	43.2	3.0	Chauvin 2000
Yseure (Le Pavillon)	79	80	80.0	80.0	61.0	-1.5	17	0.7	2265	46.6	3.4	Bucur 1994
Amboise	75	125	100.0	103.0	60.2	-5.5	14	1.7	474	47.4	1.0	Bucur 1994
Pouillé les Bordes (four 5)	75	150	112.5	101.4	64.6	-6.3	8	1.8	771	47.3	1.3	Bucur 1994
Pouillé les Bordes (four 6)	75	150	112.5	116.2	60.4	-1.1	7	1.5	1248	47.3	1.3	Bucur 1994
Sallèles d'Aude F13	100	160	130.0	130.4	56.7	-5.1	8	1.0	2450	43.2	3.0	Chauvin 2000
Sallèles d'Aude F15	120	180	150.0	150.9	55.9	-5.6	10	1.7	678	43.2	3.0	Chauvin 2000
La Croiselle/Briance	150	200	175.0	176.1	56.9	1.1	10	2.3	372	45.6	1.6	Bucur 1994
Varennes/Allier	150	210	180.0	180.6	58.8	-1.5	8	1.8	749	46.3	3.4	Bucur 1994
Lezoux (Hôpital)	160	200	180.0	181.3	53.7	-2.5	11	1.7	548	45.8	3.4	Bucur 1994
Toulon/Allier	180	180	180.0	180.5	57.9	-2.5	17	1.0	4012	46.6	3.3	Bucur 1994
Lezoux 85	175	190	182.5	182.5	58.2	-5.3	15	0.6	3206	45.8	3.4	Bucur 1994
Sallèles d'Aude F3	190	230	210.0	210.2	56.1	0.2	20	1.7	339	43.2	3.0	Chauvin 2000
Sallèles d'Aude F9	195	235	215.0	215.2	56.9	0.3	16	2.0	306	43.2	3.0	Chauvin 2000
Volubilis. the big furnace	200	300	250.0	252.6	50.3	-7.8	10	3.6	151	34.0	-5.5	Kovacheva 1984
Sallèles d'Aude F7	235	295	265.0	264.5	58.8	1.2	15	2.3	907	43.2	3.0	Chauvin 2000
Volubilis. NE	200	390	295.0	283.2	44.7	0.1	3	1.8	2016	34.1	-5.5	Najid 1986
Volubilis. palais Justice	200	390	295.0	295.7	47.2	-8.4	4	8.5	68	34.1	-5.5	Najid 1986
Sallèles d'Aude F8	280	340	310.0	309.9	56.5	-2.8	10	2.8	250	43.2	3.0	Chauvin 2000
Sallèles d'Aude F14	280	340	310.0	310.0	56.5	-3.3	9	2.1	494	43.2	3.0	Chauvin 2000
Volubilis. S thermal bath	250	390	320.0	320.0	47.5	-1.8	9	3.1	227	34.1	-5.5	Najid 1986
Lezoux III Jardin de l'Hospice	385	450	417.5	418.8	61.1	-2.0	7	1.3	1622	45.8	3.4	Bucur 1994
Le Thoronet (Abbaye)	400	500	450.0	443.9	58.5	2.0	7	1.5	1333	43.5	6.3	Bucur 1994

Courbe de variation séculaire pour la Péninsule Ibérique

Volubilis. the furnace in the S of the site	400	500	450.0	444.7	51.7	-6.7	5	2.5	627	34.0	-5.5	Kovacheva 1984
Masmolene I	500	600	550.0	547.1	62.9	4.4	11	0.6	4360	44.0	4.5	Bucur 1994
El Basra	600	1000	800.0	864.8	51.9	22.5	28	2.3	132	34.8	-5.9	Najid 1986
El Basra	600	1000	800.0	858.2	51.5	18.1	8	3.4	212	34.8	-5.9	Najid 1986
Peran en Pledran	910	930	920.0	919.8	65.6	23.3	12	1.0	1776	48.5	-2.8	Bucur 1994
Douè la Fontaine (cellule II)	900	1000	950.0	949.7	63.1	20.3	10	1.8	607	47.2	-0.3	Bucur 1994
Moulins/Cephons	1032	1068	1050.0	1050.5	59.3	15.7	15	1.1	1138	47.0	1.6	Bucur 1994
Cabasse	1100	1150	1125.0	1115.4	58.5	15.8	10	1.1	1608	43.4	6.2	Bucur 1994
Planier	1250	1300	1275.0	1277.2	53.7	6.9	14	1.0	1372	43.2	5.9	Bucur 1994
Sainte Barbe (Marseille)	1280	1320	1300.0	1301.7	49.2	4.6	15	1.7	460	43.3	5.4	Bucur 1994
Cadrix	1365	1385	1375.0	1374.7	48.9	7.2	14	1.3	841	43.5	5.9	Bucur 1994
Tintaine (four à chaux)	1550	1590	1570.0	1568.9	60.5	9.0	7	1.8	985	43.1	3.1	Bucur 1994
Blois	1578	1578	1578.0	1578.5	60.4	6.7	15	0.7	2562	47.6	1.3	Bucur 1994
La Madrague (St. Cyr./Mer)	1680	1720	1700.0	1702.8	67.1	-11.5	7	1.3	1796	43.2	5.6	Bucur 1994
Thoronet Four de l'âne	1829	1831	1830.0	1830.0	62.9	-18.3	6	1.4	1626	43.5	6.3	Bucur 1994

Table 1: Archeomagnetic directions from Spanish, French and Moroccan sites. The first set include Spanish archaeomagnetic sites, the second sites from Morocco and France inside a circle around Madrid of 600 km, and the third sites from Morocco and France between the circles described by two circles of 600 and 900 km. Columns from left to right:

Name, name of the structure; t_{min} , minimum age of the abandon of the structure; t_{max} , maximum age of the abandon of the structure; t_{mean} , mean age of the interval proposed for the abandon of the structures in years AD; $t_{bayesian}$, time at which the maximum of probability is obtained (using Bayesian modelling);

I_s and D_s , inclination and declination of the mean site direction in situ;

N , number of samples used for the calculation of the archaeomagnetic mean direction;

α_{95} and k , 95 % confidence limit and precision parameter from Fisher statistics;

Lat. and Long., site latitude and longitude;

Stratigraphic constraints, stratigraphic constraints between the structures

Reference, reference for each archaeomagnetic direction, for the Spanish data blank space means Gómez-Paccard et al. (in press, 2006).

3. The reference curve data set

The reference curves have been established assuming that within a restricted region the SV curves can be represented by a single curve assigned to a fixed reference site. Madrid is close to the geographic centre of the Iberian Peninsula (40.4°N , 3.7°W) and has been chosen as the reference point. It is generally assumed that for regions with a radius of about 600 km the earth's magnetic field behaviour is dominated by the dipole part of the field [Tarling, 1983], so that no significant errors are introduced in relocating the directions to a central reference point. A total of 63 Spanish archaeomagnetic directions are available from within the 600 km radius, with a further 16 from Morocco and southern France. One of the Spanish directions (GUA1 in Table 1) is offset from the general trend displayed by the other data. Recent results of radiocarbon dating cast doubt on the age assigned to the structure and so the direction has not been used in calculating SV curves.

The data set (called the 600 km data set) contains 78 directions, which are shown in Figure 2, after relocation to Madrid via the virtual geomagnetic pole (VGP) method. They are generally very well defined. Around 60 % have α_{95} values less than 3° , and only 5 have values bigger than 5° . The different sources of errors related to archaeomagnetic studies have been widely discussed in the literature and a recent analysis can be found in *Lanos et al.* [2005]. Uncertainties related to the ages of the structures can differ depending on the archaeological information available, but for the Spanish data set it is generally around 50 years. The compiled data span approximately 2000 years, from -100 to 1959 AD. Throughout most of the record several directions per century are available, although there is a gap in the data between the 6th and 10th centuries.

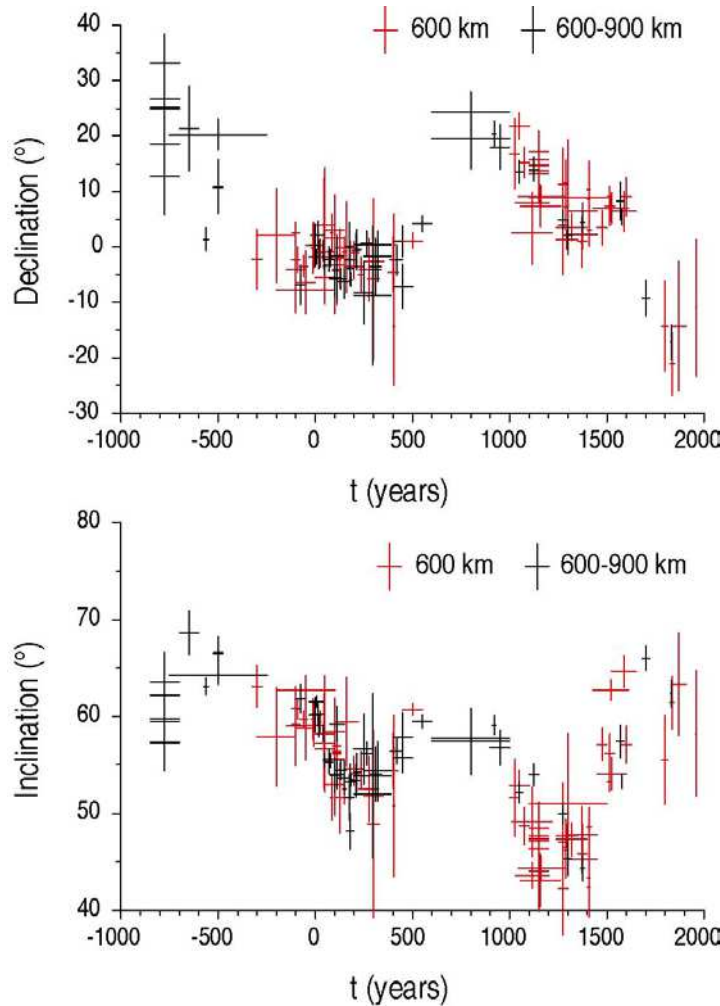


Figure 2: Declination and inclination of the archaeomagnetic directions available for the two reference areas, relocated to Madrid. Data coming from localities less than 600 km from Madrid are plotted in red, and data coming from localities between 600 and 900 km in black.

In southern France or northern Morocco several data can help to cover this gap, but they are from localities more than 600 km from Madrid (see Figure 1). Using data from such distal sources may introduce errors due to the process of relocation to the central reference point. To investigate this question the angular errors introduced during the relocation process via the VGP method have been estimated in the same way as by *Noel and Batt* [1990]. These results were obtained by *Núñez* [2004] for the Iberian Peninsula using the IGRF (1900) and the IGRF (2000) models. The IGRF values have been calculated for an area described by 30°N , 50°N and 15°W , 10°E , relocated to Madrid, and the results are compared with the Madrid IGRF values. The obtained angular differences in declination and inclination have been plotted as isolines every 0.5° in Figure 3. For an area of radius 900 km, inclination errors are less than

2° and declination errors are less than 3°. Assuming that the harmonic content of the field has been similar throughout archaeological time, then similar error values can be expected in the past. Angular relocation errors of 2-3° are of the same order as the typical α_{95} values of the Spanish archaeomagnetic directions, and if the marginal errors on the estimated SV curve are bigger, then these errors would not be significant.

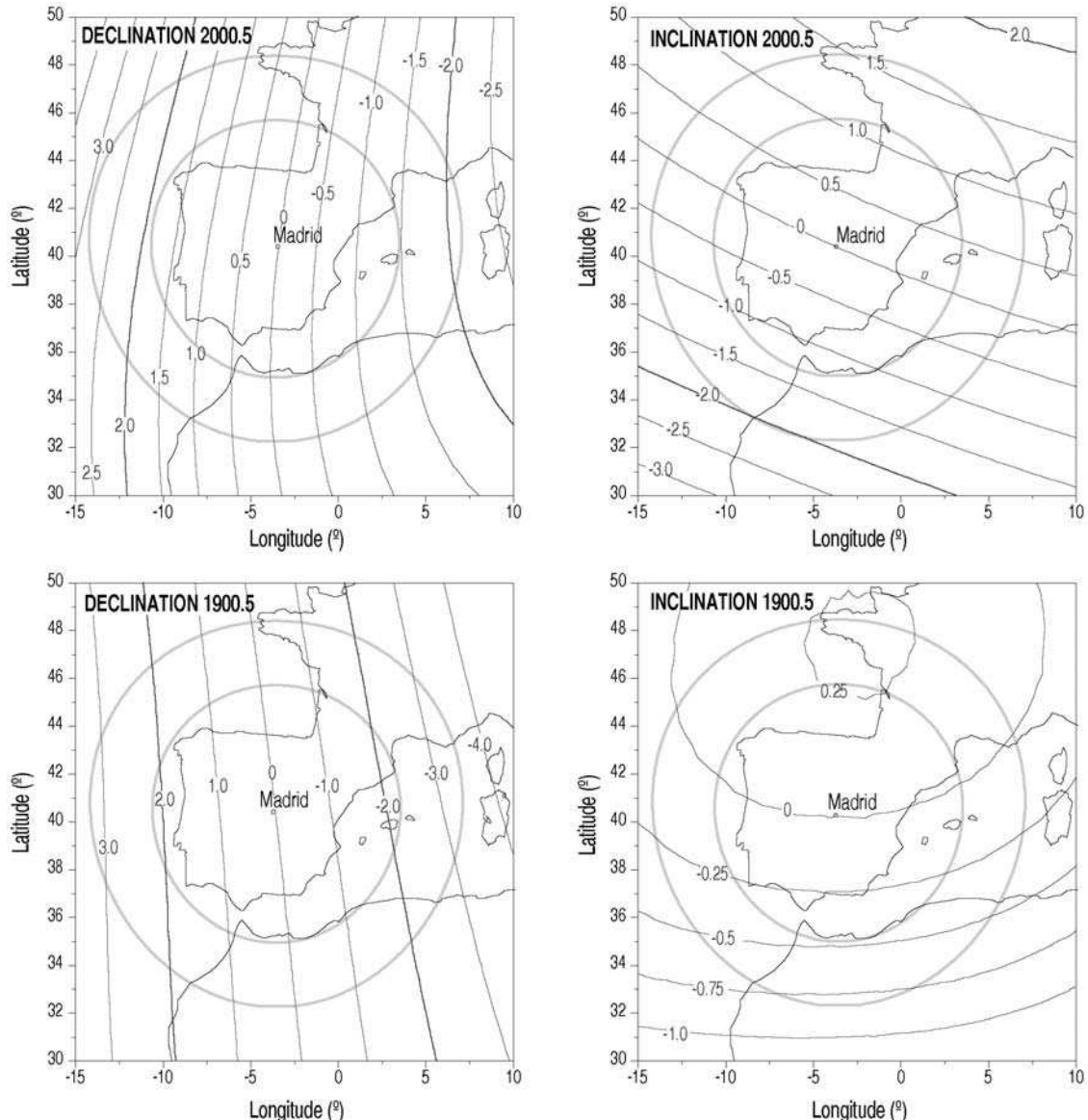


Figure 3: Isolines of the errors in declination and inclination introduced during the VGP relocation between any point on the plot and Madrid. The errors have been calculated using the IGRF 2000 model. Two circles centred at Madrid with 600 and 900 km radii are shown.

The assumption of almost constant harmonic content of the field during archaeological times has been tested using the global model CALSK3.2 of *Korte and Constable* [2005]. The Gauss coefficients have been calculated each 25 years for the last 3000 years. Then the magnetic energy at the Earth surface of each degree, defined as

$$R_n(t) = (n+1) \sum_n^m (g_n^m(t)^2 + h_n^m(t)^2) \quad (1)$$

has been calculated [*Lowes*, 1966]. The results indicate that the ratio of the magnetic energy of the non-dipole (from degree 2 up to degree 10) to the energy of the dipole, has remained almost constant with a mean value of 0.02 ± 0.005 . Based on these calculations the harmonic content appears more or less constant over the considered archaeological times and the assumption seems valid.

Another problem to be considered is that archaeomagnetic errors (sample orientation, measurement procedures) are not systematic, whereas errors introduced by relocating directions at any given time to a central reference point are. To see if such systematic errors influence on the SV curve estimation two archaeomagnetic directional data sets have been compiled. The first data set corresponds to sites which fall within a 600 km radius circle centred on Madrid (the 600 km data set described before, Table 1). The second data set (900 km data set) includes an additional 56 (“foreign”) archaeomagnetic directions corresponding to sites situated between 600 and 900 km from Madrid (the black symbols in Figure 2), giving a total of 134 data (see Table 1). It can be seen that the relocated directions from the two data sets are similar over the same time periods, and that there is no observable systematic error associated with the data between 600-900 km from Madrid.

As the accuracy of any calculated SV curve depends principally on the number of reference points and on their associated dating errors, the use of the 900 km data set should increase the reliability of a curve obtained for the Iberian Peninsula. Furthermore, the 900 km data set includes data that partially fill the gap between the 6th and 10th centuries AD in the 600 km data set. It also includes data from the -6th to -8th centuries, which are not represented in the 600 km data set, thus extending coverage over a longer time period.

4. The First SV curve for Iberia

In order to determine the best SV curve for Iberia the two compiled data sets (600 and 900 km) were treated using the hierarchical bivariate [Lanos *et al.*, 2005] and the hierarchical Bayesian modelling based on roughness penalty [Lanos, 2004]. A comparison between the classical stratified bivariate [Le Goff, 1990; Le Goff *et al.*, 1992; Daly and Le Goff, 1996] and the hierarchical bivariate approaches has been presented by Lanos *et al.* [2005]. The principal difference found was in the estimation of the marginal errors. In the stratified approach these errors are divided by the total number of samples contributing to the window, whilst in the hierarchical approach these errors are divided by the number of sites contributing to the window. As demonstrated by Lanos *et al.* [2005], a hierarchical approach should be used in archaeomagnetic curve estimation. Therefore this approach has been retained here.

In order to determine the best window widths to use with hierarchical bivariate statistics several values were tested (50, 80, 100 and 120 years). No significant differences were found, therefore it was decided to use a window width of 80 years, plotted in 25 year steps, with at least four reference points per window.

Bayesian modelling [Lanos, 2004] puts some prior knowledge on the global nature of the curve to be estimated, i.e. it is assumed that the studied physical phenomena vary in a smooth way, and it allows the window width to be automatically adapted to the density of points along the time axis, making the points movable within their respective dating error ranges. This approach allows the fitting of a spherical spline function based on roughness penalty to the data in three dimensions (declination, inclination and time), calculating the weight on the construction of the SV curve of all of the possible three-dimensional data. The results are expressed as a mean curve and an envelope (error) at a 95 % confidence level. The “real” curve will lie somewhere inside the error band. In addition, this method takes into account stratigraphic constraints provided by archaeological investigations, some of which are known for the Spanish data (Table 1 and Gómez-Paccard *et al.* (in press, 2006)).

Figures 4 a) and b) shows the curves obtained for the 600 and 900 km data sets calculated using Bayesian methods and the comparison between the hierarchical bivariate and Bayesian modelling for the 900 km data set. The hierarchical bivariate curves are not continuous because some time windows contain less than four reference points (Figure 4b). It is noticeable that the mean values obtained with the two methods are very similar, although the hierarchical bivariate mean curve and corresponding errors seem a little choppy.

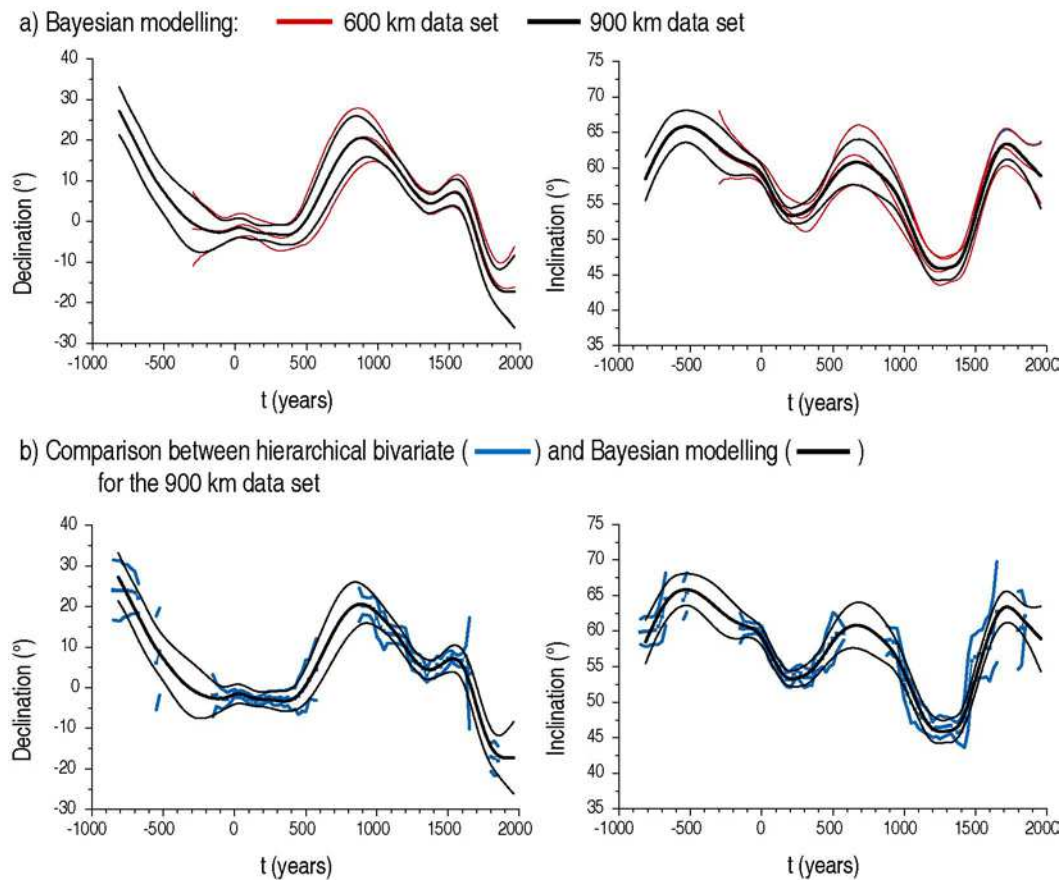


Figure 4: Comparison between the hierarchical bivariate and the Bayesian modelling:

(a) the results from Bayesian modelling for the 600 and 900 km data set and (b) a comparison between the results obtained by hierarchical bivariate (calculated using 25 year steps with a least four reference points per window) and Bayesian modelling for the 900 km data set. All curves have been calculated at Madrid and are plotted with their 95 % confidence level error bands.

The archaeomagnetic data sets are unevenly distributed in time. For this reason, Bayesian modelling has been retained in order to calculate the best SV curve for Iberia. The Bayesian curves, and their error envelopes, calculated with the 600 and 900 km data sets are very similar between -350 and 2000 AD (Figure 4a). As previously discussed, the maximum error due to the VGP relocation process from any point inside a reference area of 900 km (Figure 3) to Madrid is approximately 3° (estimated by the IGRF (1900) and the IGRF (2000)). This error is lower than the errors of declination and inclination at the 95 % confidence level obtained for the Bayesian curve (of about 5° , Figure 4a). Therefore it is considered that the

error introduced during relocation is included in the error inherent to the archaeomagnetic data.

Taking into account all of the previous discussions, Bayesian modelling of the 900 km data set has been used to calculate the curve most representative of the SV for the Iberian Peninsula. It is shown in Figure 5. Table 2 gives the results obtained for inclination and declination (in steps of approximately 25 years), together with their marginal errors. In Table 1, t_{bayesian} indicates the most probable ages (at the 95 % confidence level) obtained by Bayesian modelling for each structure.

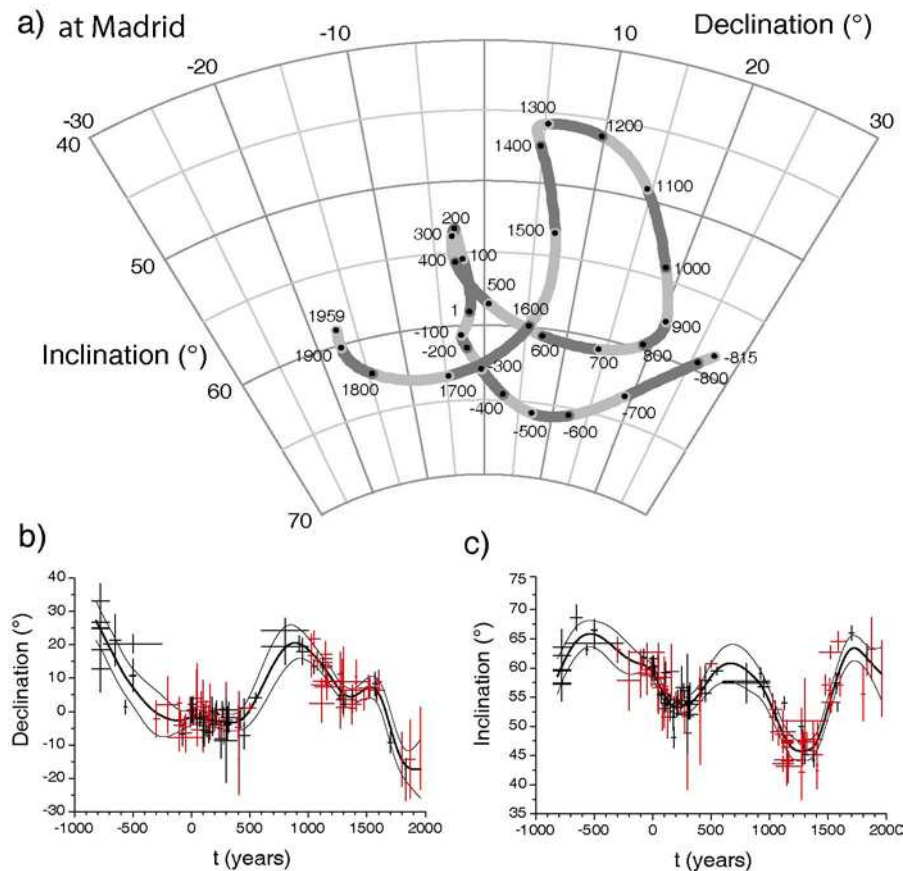


Figure 5: The first SV curve for Iberia obtained by Bayesian modelling of the 900 km data set. a) stereo-plot of declination and inclination, dark and light grey indicate century timescales, b) declination versus time and c) inclination versus time. In figures b) and c) data coming from localities less than 600 km from Madrid are plotted in red and data located between 600 and 900 km from Madrid are plotted in black.

The age of the reference archaeomagnetic data used ranges from -775 to 1959 AD. Throughout most of the record several directions per century are available, although there is a need to extend the data, especially between the 6th and 10th centuries AD and prior to 0 AD, where the majority of the data come from neighbouring countries.

t (years)	I (°)	I _{min} (°)	I _{max} (°)	D (°)	D _{min} (°)	D _{max} (°)
-815	58.5	55.4	61.6	27.2	21.3	33.1
-790	59.6	56.8	62.5	25.6	19.8	31.3
-767	60.6	57.9	63.4	24.1	18.4	29.6
-745	61.5	58.9	64.2	22.5	16.9	28.1
-723	62.4	59.8	65.0	21.0	15.3	26.6
-698	63.2	60.7	65.9	19.3	13.5	25.0
-673	64.0	61.5	66.6	17.6	11.6	23.4
-650	64.6	62.1	67.1	16.0	10.0	21.8
-626	65.1	62.6	67.6	14.4	8.5	20.1
-601	65.4	63.1	67.8	12.8	6.9	18.4
-576	65.7	63.4	68.0	11.2	5.5	16.7
-556	65.8	63.5	68.1	10.0	4.5	15.5
-531	65.9	63.6	68.1	8.7	3.2	14.2
-506	65.8	63.5	68.1	7.5	1.9	13.0
-490	65.7	63.4	68.0	6.8	1.1	12.4
-465	65.5	63.1	67.9	5.6	-0.2	11.4
-440	65.3	62.7	67.8	4.5	-1.6	10.5
-415	64.9	62.3	67.6	3.5	-2.9	9.6
-390	64.6	61.8	67.3	2.5	-4.0	8.9
-365	64.2	61.2	67.0	1.5	-5.1	8.1
-340	63.7	60.7	66.7	0.7	-6.0	7.4
-315	63.3	60.2	66.3	0.0	-6.7	6.7
-293	62.9	59.9	65.9	-0.6	-7.2	6.0
-268	62.5	59.5	65.4	-1.1	-7.5	5.3
-243	62.1	59.2	64.9	-1.5	-7.6	4.5
-218	61.7	59.1	64.4	-1.9	-7.5	3.7
-193	61.4	59.0	63.9	-2.2	-7.3	2.9
-171	61.2	58.9	63.4	-2.4	-7.1	2.2
-146	61.0	59.0	63.0	-2.6	-6.7	1.5
-121	60.8	59.1	62.5	-2.7	-6.3	0.8
-100	60.6	59.1	62.2	-2.7	-5.9	0.5
-65	60.4	59.0	61.7	-2.5	-5.2	0.2
-49	60.2	58.9	61.5	-2.3	-4.9	0.3
-24	59.8	58.5	61.0	-2.0	-4.5	0.5
-5	59.3	58.1	60.5	-1.7	-4.2	0.7
13	58.8	57.5	60.0	-1.6	-4.0	0.8
31	58.2	56.9	59.4	-1.5	-3.9	0.8
48	57.5	56.2	58.7	-1.6	-3.9	0.7
65	56.8	55.5	58.0	-1.7	-4.0	0.5
86	56.0	54.7	57.2	-2.0	-4.2	0.2
110	55.1	53.9	56.3	-2.3	-4.4	-0.2
131	54.5	53.3	55.6	-2.5	-4.5	-0.6
151	53.9	52.8	55.0	-2.7	-4.6	-0.8
183	53.4	52.4	54.5	-2.8	-4.6	-1.0
200	53.3	52.2	54.4	-2.9	-4.7	-1.1
216	53.3	52.2	54.4	-2.9	-4.7	-1.0
236	53.3	52.2	54.5	-2.9	-4.9	-1.0

Courbe de variation séculaire pour la Péninsule Ibérique

258	53.4	52.2	54.7	-3.0	-5.1	-0.9
280	53.6	52.3	54.9	-3.1	-5.3	-0.9
311	53.9	52.5	55.3	-3.2	-5.6	-0.9
336	54.2	52.8	55.6	-3.3	-5.7	-0.9
361	54.7	53.2	56.1	-3.3	-5.8	-0.8
386	55.2	53.8	56.7	-3.2	-5.8	-0.5
406	55.7	54.2	57.3	-2.9	-5.7	-0.1
424	56.3	54.6	57.9	-2.5	-5.5	0.5
446	56.9	55.1	58.8	-1.9	-5.2	1.5
466	57.5	55.6	59.5	-1.1	-4.8	2.6
491	58.2	56.1	60.4	0.0	-4.0	4.2
515	58.9	56.6	61.3	1.4	-3.2	6.0
540	59.5	56.9	62.0	2.9	-2.1	8.0
563	59.9	57.2	62.6	4.4	-0.9	9.9
588	60.3	57.5	63.2	6.1	0.4	12.0
613	60.6	57.6	63.6	7.9	1.9	14.1
638	60.8	57.6	63.9	9.7	3.4	16.2
663	60.8	57.6	64.0	11.5	5.0	18.1
688	60.8	57.5	64.1	13.2	6.5	20.0
713	60.7	57.3	64.0	14.8	8.1	21.6
738	60.5	57.1	63.8	16.2	9.5	23.0
763	60.2	56.9	63.5	17.5	10.9	24.2
788	59.8	56.6	63.1	18.6	12.2	25.1
813	59.4	56.3	62.6	19.4	13.3	25.7
838	59.0	55.9	62.0	20.1	14.2	26.0
861	58.6	55.6	61.4	20.4	14.9	26.0
883	58.1	55.4	60.8	20.6	15.5	25.7
908	57.5	55.0	60.0	20.5	15.8	25.2
931	56.9	54.5	59.2	20.2	15.9	24.5
952	56.2	53.9	58.4	19.8	15.8	23.8
977	55.2	53.0	57.3	19.2	15.5	22.9
1002	54.1	52.0	56.1	18.5	15.0	21.9
1027	53.0	51.0	54.8	17.6	14.4	20.8
1044	52.1	50.2	54.0	17.0	13.9	20.0
1067	51.0	49.2	52.8	16.1	13.2	18.9
1091	49.9	48.1	51.6	15.2	12.4	17.8
1116	48.8	47.0	50.5	14.1	11.5	16.7
1137	48.0	46.2	49.7	13.2	10.5	15.8
1153	47.4	45.6	49.2	12.4	9.7	15.0
1171	46.9	45.0	48.7	11.5	8.8	14.1
1192	46.4	44.6	48.2	10.5	7.7	13.0
1216	46.1	44.3	47.9	9.2	6.6	11.7
1239	45.9	44.2	47.6	8.1	5.6	10.4
1264	45.9	44.3	47.4	6.9	4.6	9.2
1278	45.9	44.3	47.4	6.4	4.1	8.6
1298	45.9	44.3	47.5	5.7	3.3	7.9
1321	46.0	44.3	47.7	5.0	2.6	7.4
1338	46.1	44.4	47.8	4.7	2.2	7.2
1362	46.3	44.7	48.0	4.5	2.1	6.8
1381	46.7	45.1	48.3	4.5	2.2	6.8
1402	47.3	45.8	48.9	4.7	2.4	7.0
1416	47.9	46.4	49.5	4.9	2.6	7.2
1441	49.2	47.7	50.9	5.4	3.0	7.9
1466	50.8	49.2	52.5	6.0	3.4	8.7
1488	52.3	50.6	54.1	6.5	3.7	9.4
1513	54.0	52.3	55.9	7.0	3.9	10.1
1531	55.3	53.5	57.2	7.1	3.9	10.4
1556	57.0	55.2	58.8	7.1	3.6	10.4

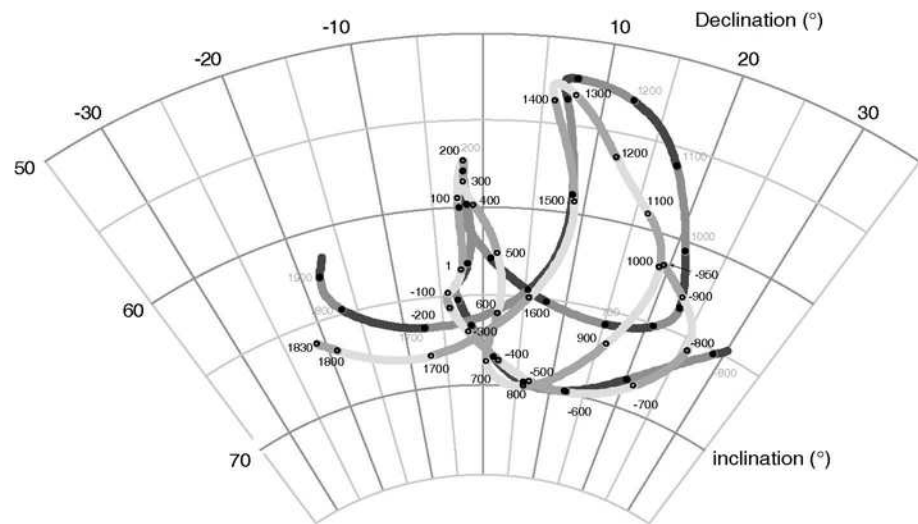
1580	58.4	56.7	60.4	6.5	2.9	10.0
1600	59.7	57.8	61.7	5.6	1.6	9.3
1625	61.0	59.0	63.1	3.8	-0.5	7.9
1647	62.0	59.9	64.1	1.7	-2.9	6.1
1672	62.8	60.6	65.0	-1.1	-6.0	3.6
1697	63.3	61.0	65.5	-4.1	-9.1	0.7
1719	63.4	61.2	65.6	-6.8	-11.7	-1.9
1744	63.3	61.2	65.4	-9.6	-14.4	-4.9
1769	63.0	60.9	65.1	-12.0	-16.7	-7.5
1794	62.5	60.4	64.6	-14.0	-18.6	-9.6
1817	62.0	59.9	64.1	-15.4	-20.0	-10.9
1836	61.6	59.4	63.8	-16.2	-20.9	-11.6
1861	61.1	58.5	63.5	-16.9	-22.0	-11.8
1882	60.6	57.8	63.4	-17.2	-22.9	-11.5
1907	60.1	56.7	63.3	-17.4	-24.0	-10.7
1932	59.5	55.6	63.4	-17.4	-25.0	-9.7
1959	59.0	54.5	63.5	-17.3	-26.0	-8.5

Table 2: Secular variation curve for the Iberian Peninsula at Madrid: t , age in years AD; I (D), inclination (declination); I_{\min} - I_{\max} (D_{\min} - D_{\max}), marginal errors for inclination (declination).

5. Comparison with French and German Secular Variation Curves

In order to compare the Iberian SV curve with the French and German curves, the Bayesian curves for these two countries have been plotted. The German archaeomagnetic curve was published by *Schnepp and Lanos* [2005], relocated to Göttingen. It includes a total of 166 archeomagnetic directions. The French SV curve was calculated by Bayesian modelling, the reference data set used is the same as that of *Gallet et al.* [2002], together with the 12 archaeomagnetic directions determined by *Chauvin et al.* [2000]. The archaeomagnetic directions were relocated to Paris. The velocities and curvatures of the curves have been calculated directly from the obtained spherical spline functions. In order to visually compare the curves they have been plotted in Figures 6 and 7, after relocation to a common point, Lyon (45.46 °N, 4.50 °E, Figure 1), chosen because of its central location between Madrid and Göttingen. However, and in order to avoid relocation errors, the calculation of the velocities and changes in curvatures of the curves has been performed using the spherical splines obtained for Madrid (Iberian curve), Paris (French curve) and Göttingen (German curve). It is worth pointing out that the French and German data sets have only 25 archeomagnetic directions in common.

a) Iberian (—) and French (—) SV curves, at Lyon



b) Iberian (—) and German (—) SV curves, at Lyon

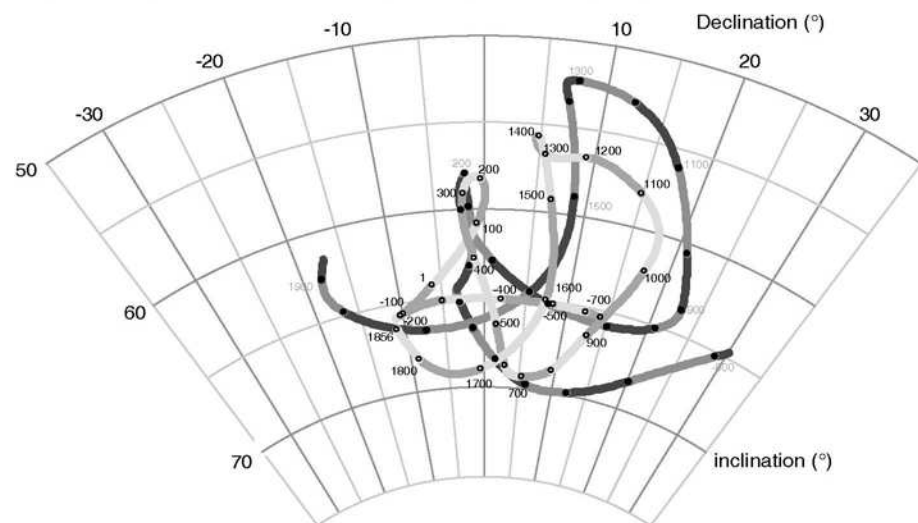


Figure 6: SV curves for a) Iberia and France and b) Iberia and Germany at Lyon (45.46°N , 4.50°E). All have been calculated by Bayesian modelling. Ages are plotted in black for the French and Germany SV curves and in italic grey for the Iberian SV curve.

The three SV curves look similar during most of the past three millennia, especially the French and Iberian curves. However, closer inspection reveals some significant differences in the details of the curves. Lower inclinations are seen in the Iberian curve between the 11th and 14th century and between the 16th and 19th century (Figures 6 and 7). These two differences are constrained by a relatively large number of Spanish data and may be related to features of

the local geomagnetic field. If the Iberian and German SV curves are characterised by a period of two centuries (from 1200 to 1400) with low inclinations, this period of low inclinations seems shorter in the French SV curve. The trend of the Iberian SV curve between the 10th and 15th centuries is very similar to that obtained for Italy recorded in historical lava flows [Tanguy *et al.*, 1999; Arrighi *et al.*, 2004]. It is noticeable that the lowest inclinations observed for France and Iberia do not have exactly the same values as for Germany. The differences between the three curves observed during the 6-9th centuries can be explained by the small number of data available for this period in the Iberian curve.

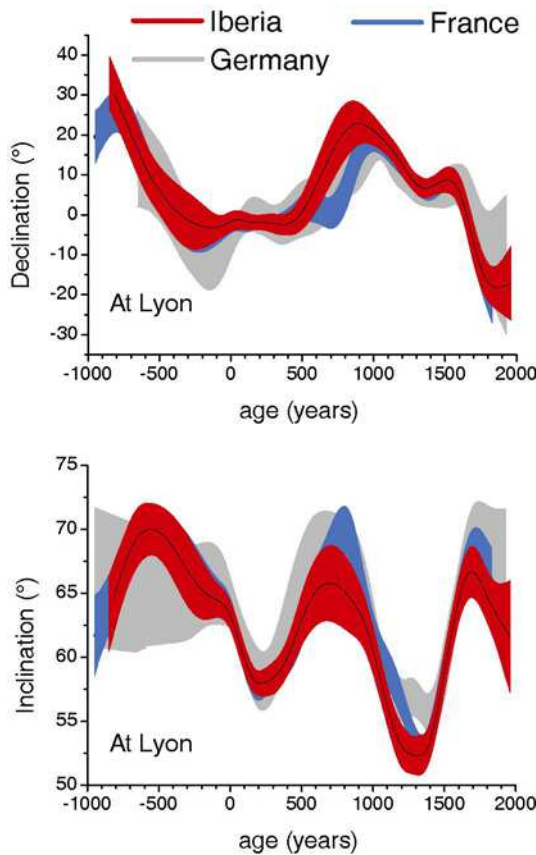


Figure 7: Declination and inclination values together with the marginal errors versus time for the Iberian, French and German SV curves at Lyon. All obtained by Bayesian modelling.

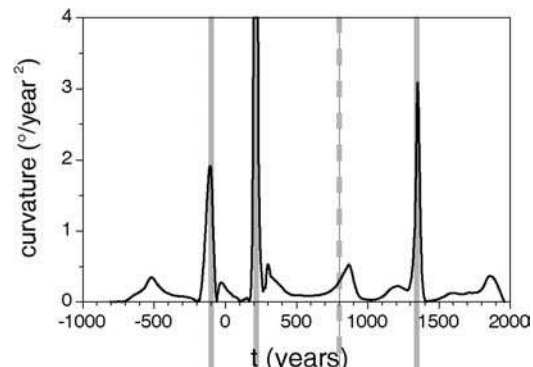
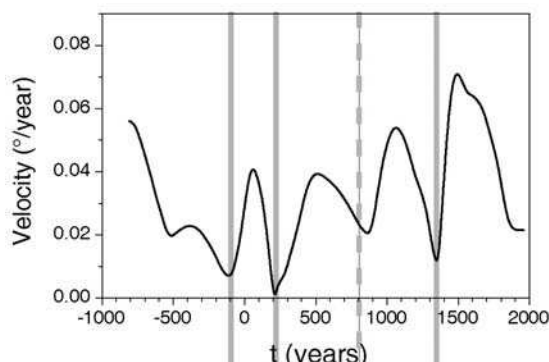
The same analysis can be done taking into account the marginal errors of the curves (Figure 7). They are generally lower for the French SV curve than for the Iberian or German curves, due to the larger number of archaeomagnetic data available for France. However, the error

margins of the Iberian curve for the period between the 10th and 17th centuries are small and the differences discussed before are well constrained for this region.

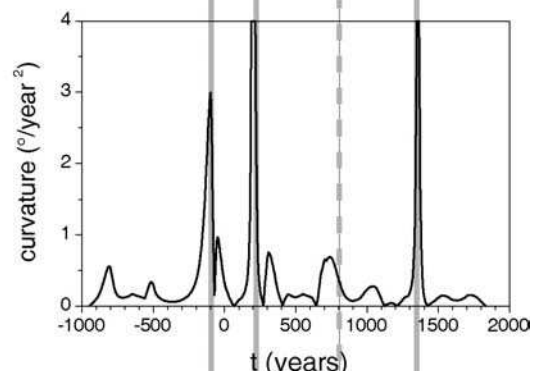
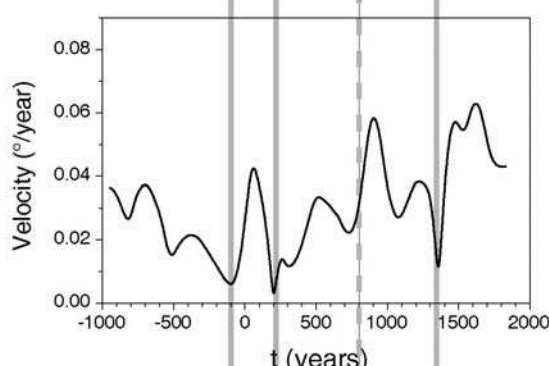
Figure 8 shows the rate of the secular variation (velocity) and curvature values computed using Iberian, French and German Bayesian curves. The general trend of the obtained values of velocity and curvature is very similar. Three major directional cusps, related with velocity minima, are observed in each of the curves, the first around -125 AD, the second around 200 AD and the third around 1350 AD. Two of these major directional changes (at 200 and 1350) are in agreement with those found by *Gallet et al.* [2003] (200 and 1400) and seem to occur a little later in the German curve. A further change in curvature is seen at around 600-700 AD for the German curve, which is suggested in the French curve but poorly expressed in the Iberian curve (Figure 8). This last directional cusp could be related to the one derived by *Gallet et al.* [2003] and identified at around 800 AD. The weak temporal resolution of this last directional change could be explained by the lack of data in the European records between the 5th and the 10th centuries (the so-called Dark Ages).

It is concluded that the SV for Western Europe over the last three millennia is characterised by 3 major directional changes associated with low secular variation rates. In order to see if these characteristics have a regional or a global significance, archaeomagnetic data from other regions have been analysed. In the global archaeomagnetic data set built by *Korte et al.* [2005] the records from Japan and Southwest USA are the most continuous (outside Europe), both in declination and inclination, and are also the less scattered over the last 1500 years. After relocation of the data to a common point (35.3 °N, 136.8 °E for Japan and 39.5 °N, 250.7 °E for Southwest USA), SV curves for these two regions have been calculated using Bayesian modelling (Figure 9a). The only difference with the previous analysis is that the number of samples per site used to calculate the mean directional data is not taken into account, because this information is not reported in the data set published by *Korte et al.* [2005].

Iberian Peninsula



France



Germany

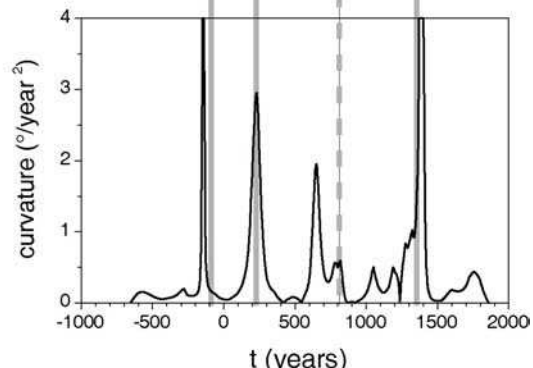
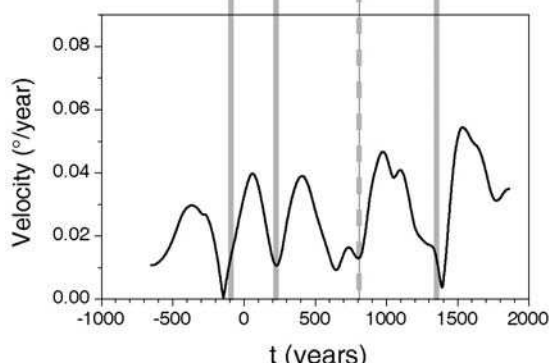
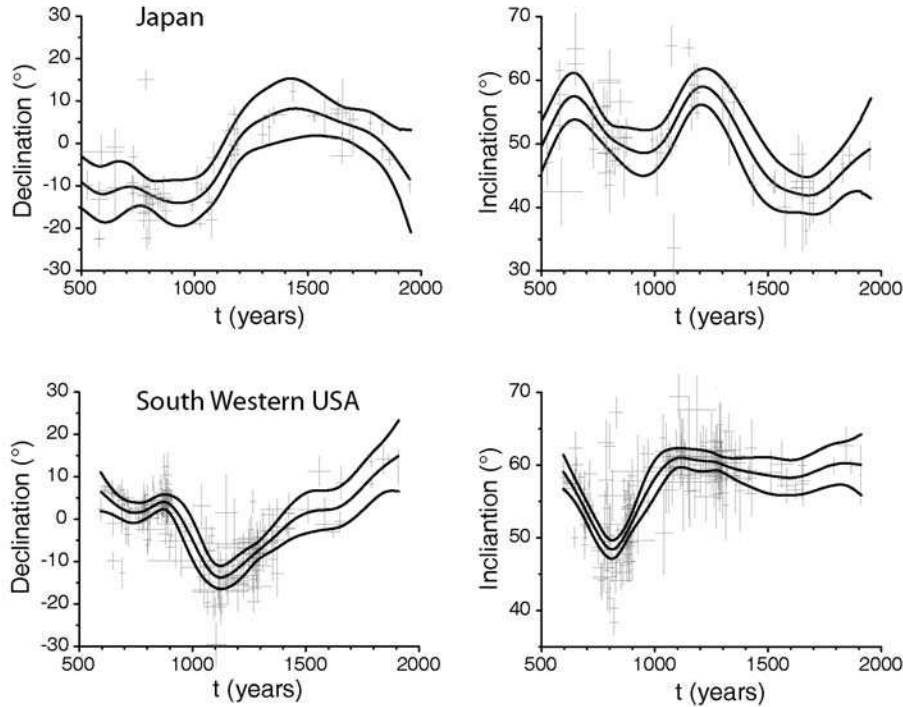


Figure 8: Comparison of the velocity and changes in curvature of the Iberian, French and German SV curves, calculated by Bayesian modelling.

a) Bayesian curves



b) velocities and changes in curvature

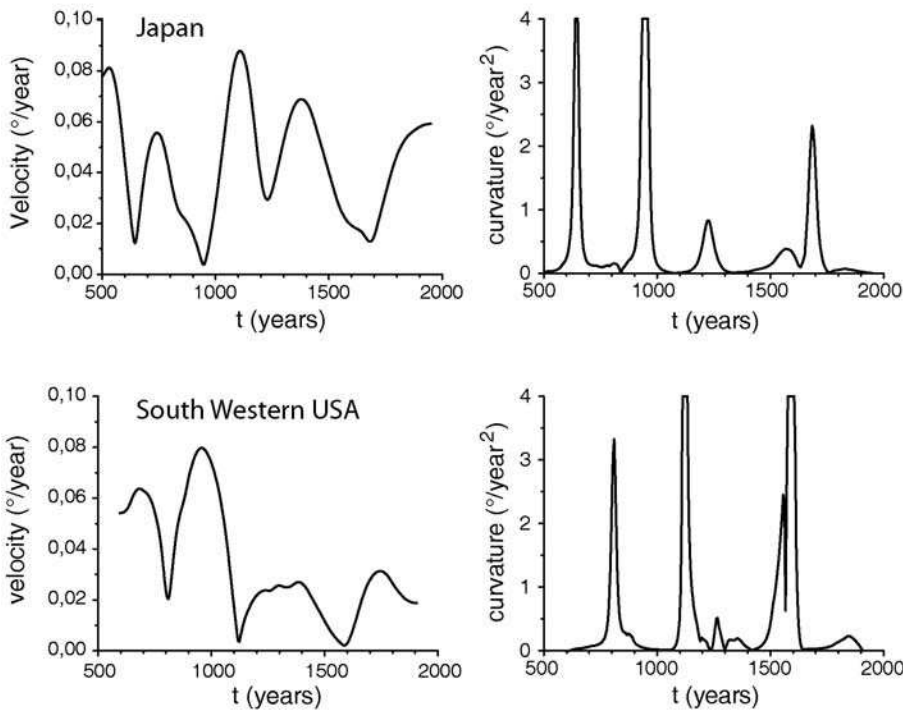


Figure 9: a) Declination and inclination values together with the marginal errors versus time for Japan and Southwest USA, b) corresponding velocities and changes in curvature. All obtained by Bayesian modelling.

The secular variation rates and changes in curvature obtained are shown in Figure 9b. Three (for Southwest USA) and four (for Japan) major directional changes can be observed, occurring at different time periods. Moreover, the ages of these cusps are not in agreement with those observed in Europe, except perhaps the one present for the period 650-800 AD. This seems to indicate that major directional changes are a regional feature of the geomagnetic field, even though more detailed and longer records are clearly needed.

6. Comparison with global models

The Iberian SV curve presented here has also been compared with the new CALS3K.2 and CALS7K.2 global models of *Korte and Constable* [2005] and the model of *Hongre et al.* [1998]. The *Hongre et al.* [1998] model is derived with Gauss coefficients up to degree two plus degree three order three. The models of *Korte and Constable* [2005] are derived with Gauss coefficients up to order ten. For the last two millenia there is little difference between the CALS3K.2 and CALS7K.2 models, so the CALS3K.2 model has been used here. It should be pointed out that the higher degree terms provided by the *Korte and Constable* [2005] models must be rather uncertain due to the inhomogeneous palaeo-archaeointensity database that is available.

Differences between the Hongre and CALS3K.2 models can be seen in Figure 10. This gives the corresponding positions of the north geomagnetic pole (Figure 10a), the variations of the dipole moment (Figure 10b) and the variations of the ratio of the magnetic energy at the Earth surface between the quadrupole (terms of degrees two) and the dipole (terms of degrees one) during the last two millennia (Figure 10c). It was expected that the dipole terms would be the most robust and should be similar for the *Korte and Constable* [2005] and *Hongre et al.* [1998] models, but this is clearly not the case. Also plotted are the DGRF-1950 dipole moment (Figure 10b) and the ratio of the magnetic energy between the quadrupole and the dipole for the year 1950 (Figure 10c). In the CALS3K.2 model, the ratio of the magnetic energy between the quadrupole and the dipole is very different from the value obtained using the DGRF-1950 model.

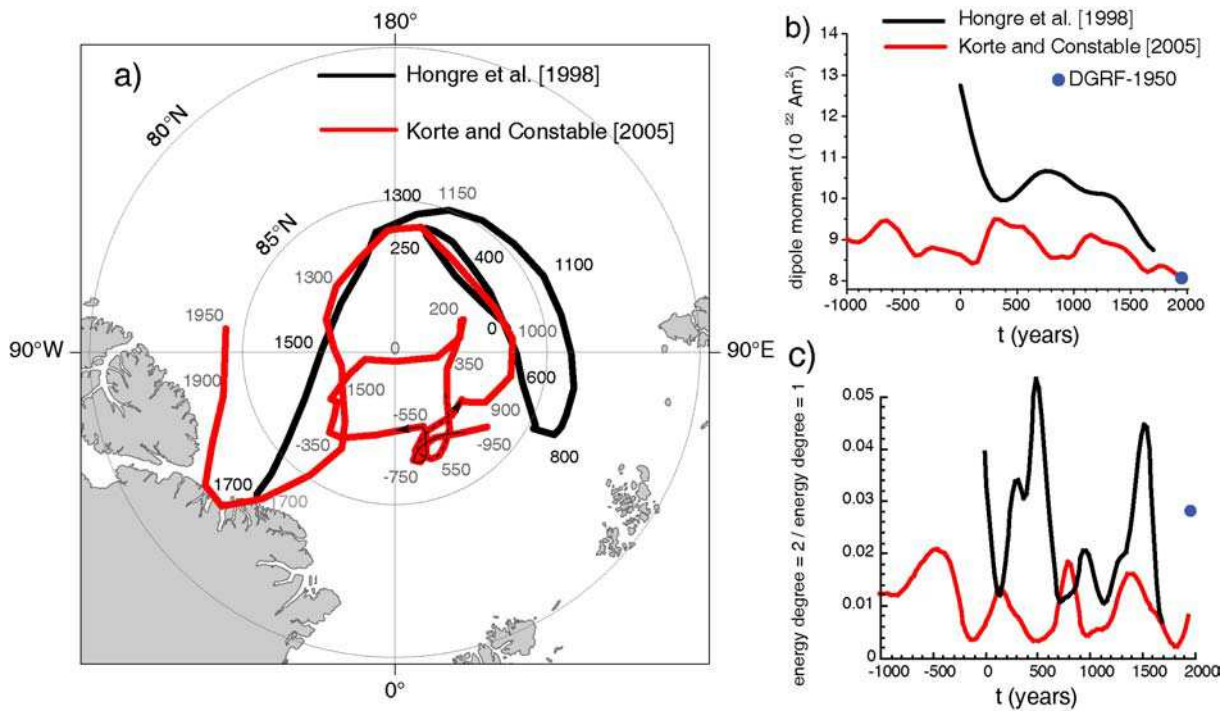


Figure 10: a) Location of the north magnetic pole as computed from CALS3K.2 [Korte and Constable, 2005] and from Hongre et al. [1998] global models and b) Dipole moment (10^{22} Am^2) and ratio of degree 2 energy divided by degree 1 energy, as computed from CALS3K.2 [Korte and Constable, 2005] and from Hongre et al. [1998] global models.

Model predictions of declination and inclination at Madrid have been calculated. The results are displayed in Figure 11, together with the Iberian SV curve. The directional changes expected at Madrid when only dipole terms are included (Figure 11a), when terms up to order two (Figure 11b) and three (Figure 11c) are used and when all Gauss coefficients are used (Figure 11d) are shown. It can be seen how the results for the dipole directional changes are quite different for both models, the curves obtained with Hongre et al. [1998] model being smoother. However, the dipole part predictions of declination and inclination show the same overall shape and features as the archaeomagnetic SV curve for Iberia, although the amplitudes are very different. When non dipole terms are included, the amplitudes of the fluctuations of the predicted SV curves increase considerably and the models fit reasonably well the archaeomagnetic curve, showing the same fluctuations with time. However, there is a discrepancy between some of the amplitudes of these fluctuations (in both declination and inclination). The declination results obtained using the models from Korte and Constable [2005] agree very well with the results from Hongre et al. [1998], except before 600 AD

where the declination values are generally more easterly for the CALS3K.2 model. In contrast, for inclination, the amplitudes are clearly more important for the *Hongre et al.* [1998] model when all the coefficients are used. The best fit is obtained with the *Hongre et al.* [1998] model, up to degree 2 (Fig 11b).

In spite of their differences, both models predict reasonably well the Iberian archaeomagnetic SV. To improve knowledge of the evolution of the dipole, more data are clearly needed in order to increase the accuracy of global models. The Iberian data used in this article could be used for future global modelling and will increase their resolution.

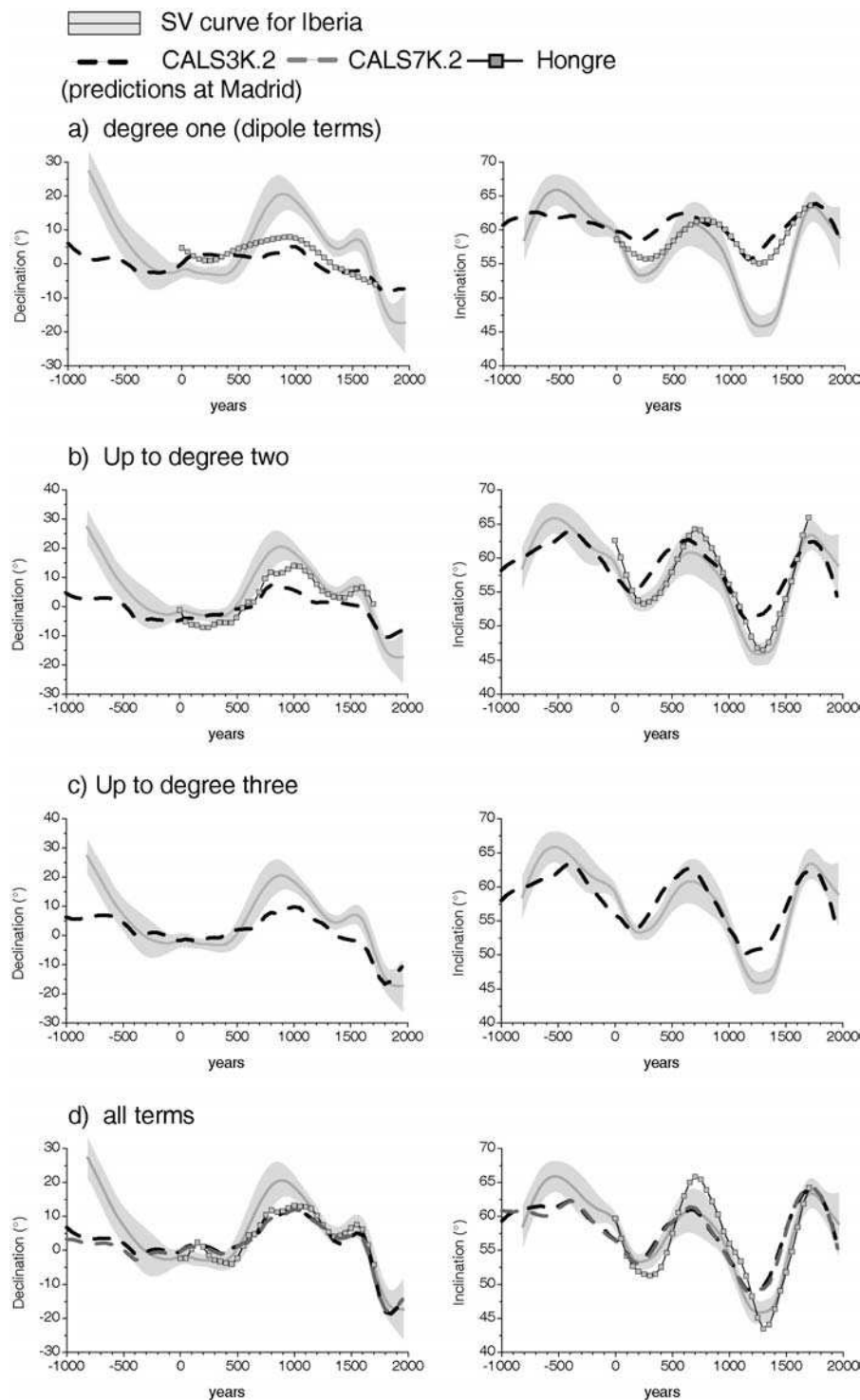


Figure 11: Comparison between the declination and inclination of the SV reference curve obtained for Iberia (in grey) and prediction values from the CALS3 (7)K.2 [Korte and Constable, 2005] and Hongre et al. global models [Hongre et al., 1998] using the Gauss coefficients up to different degrees, calculated at Madrid: a) degree one, b) degree two, c) degree three and d) all Gauss coefficients provided by the models. Results from CALSK3.2 are very similar to those from CALSK3.2 and are not plotted.

7. Conclusions

This study presents the first archaeomagnetic SV reference curve for Iberia. It has been calculated using Bayesian modelling. The age of the reference archaeomagnetic data used ranges from -775 to 1959 AD. Throughout most of the record several directions per century are available, although there is a need to extend the data, especially before 0 AD and between the 6th and 10th centuries (where the majority of the data comes from neighbouring countries). However, the first SV for Iberia is now available.

Compared to French and German SV curves the same general patterns are found but significant differences can be observed between the 11th and 14th centuries AD and the last few centuries, where lower inclinations are found for the Iberian curve. Analysis of the Iberian, French and German reference curves indicates that SV in Western Europe is characterised by three cusps or major directional changes associated with low SV rates (at -125, 200 and 1350 AD). The SV curves and corresponding rates and changes in curvature for Japan and Southwest USA have also been calculated using Bayesian modelling. The results suggest that the observed cusps are representing a regional feature of the geomagnetic field. Longer and more detailed records are clearly needed in order to test this idea.

Differences between the new CALS3K.2 and CALS7K.2 global models of *Korte and Constable* [2005] and the model of *Hongre et al.* [1998] are clearly observed. Even the lowest terms (i.e. the dipole) are quite different for both models. Despite these differences, both models predict reasonably well the Iberian archaeomagnetic SV curve.

The SV curve obtained extends the archaeomagnetic dating technique to Spain and Portugal. This provides a valuable tool for archaeologists working in the region, which has a rich and increasingly studied archaeological past. Finally, the Iberian curve contributes to the increase in the knowledge of the earth's magnetic field, and the data can be used for future modelling of geomagnetic field behaviour.

Acknowledgements

M. Gómez-Paccard and G. Catanzariti acknowledge their fellowships from the AARCH Network (Archaeomagnetic Applications for the Rescue of Cultural Heritage), Contract EU: HPRN-CT-2002-00219.

References

- Arrighi, S., M. Rosi, J.C. Tanguy, and V. Courtillot (2004), Recent eruptive history of Stromboli (Aeolian Islands, Italy) determined from high-accuracy archeomagnetic dating, *Geophys. Res. Lett.*, 31, L19603, doi:10.1029/2004GL020627.
- Batt, C.M. (1997), The British archaeomagnetic calibration curve: an objective treatment, *Archaeometry*, 39, 153-168.
- Bucur, I. (1994), The direction of the terrestrial magnetic field in France during the last 21 centuries, *Phys. Earth Planet. Inter.*, 87, 95-109.
- Chauvin, A., Y. Garcia, Ph. Lanos, and F. Laubenheimer (2000), Paleointensity of the geomagnetic field recovered on archaeomagnetic sites from France, *Phys. Earth Planet. Inter.*, 120, 111-136.
- Daly, L., and M. Le Goff (1996), An updated and homogeneous world secular variation data base. 1. smoothing of the archaeomagnetic results, *Phys. Earth Planet. Inter.*, 93, 159-190.
- Fisher, R.A. (1953), Dispersion on a sphere, *Proc. Roy. Soc. London A*, 217, 295-305.
- Gallet, Y., A. Genevey, and V. Courtillot (2003), On the possible occurrence of 'archaeomagnetic jerks' in the geomagnetic field over the past three millennia, *Earth Planet. Sci. Lett.*, 214, 237-242.
- Gallet, Y., A. Genevey, and M. Le Goff (2002), Three millennia of directional variations of the Earth's magnetic field in western Europe as revealed by archaeological artefacts, *Phys. Earth Planet. Inter.*, 131, 81-89.
- Gómez-Paccard, M., G. Catanzariti, V. Ruiz, G. McIntosh, J. Nuñez, M. Osete, Ph. Lanos, A. Chauvin, D. Tarling, D. Bernal-Casasola, J. Thiriot, and "archaeological working group" (2006), A catalogue of Spanish archaeomagnetic data, *Geophys. J. Int.*, *in press*.
- Hongre, L., G. Hulot, and A. Khokhlov, (1998), An analysis of the geomagnetic field over the past 2000 years, *Phys. Earth Planet. Inter.*, 106, 311-335.
- Kirschvink, J.L. (1980), The least-squares line and plane and the analysis of palaeomagnetic data, *Geophys. J. R. astron. Soc.*, 62, 699-718.
- Korte, M., and C.G. Constable (2005), Continuous geomagnetic field models for the past 7 millenia: 2. CALS7K, *Geochem. Geophys. Geosyst.*, 6, Q02H16, doi:10.1029/2004GC000801.

- Korte, M., A. Genevey, C.G. Constable, U. Frank, and E. Schnepp (2005), Continuous geomagnetic field models for the past 7 millennia: 1. A new global data compilation. *Geochem. Geophys. Geosyst.*, 6, Q02H15, doi:10.1029/2004GC000800.
- Kovacheva, M. (1984), Some archaeomagnetic conclusions from three archaeological localities in north-west Africa, *C. R. Acad. Sci. Bulgaria*, 37, 171-174.
- Kovacheva, M., N. Jordanova, and V. Karloukovski (1998), Geomagnetic field variations as determined from Bulgaria Archaeomagnetic data. Part II: The last 8000 years, *Sur. Geophys.*, 19, 431-460.
- Lanos, Ph. (2004), Bayesian inference of calibration curves: application to archaeomagnetism, in *Tools for constructing chronologies: crossing disciplinary boundaries*, Vol. 177, edited by C. Buck, and A. Millard, pp. 43-82, Springer-Verlag, London.
- Lanos, Ph., M. Le Goff, M. Kovacheva, and E. Schnepp, (2005), Hierarchical modelling of archaeomagnetic data and curve estimation by moving average technique, *Geophys. J. Int.*, 160, 440-476.
- Le Goff, M. (1990), Lissage et limites d'incertitude des courbes de migration polaire: pondération des données et extension bivariate de la statistique de Fisher, *C. R. Acad. Sci. Paris*, 311(Serie II), 1191-1198.
- Le Goff, M., B. Henry, and L. Daly (1992), Practical method for drawing VGP path, *Phys. Earth Planet. Inter.*, 70, 201-204.
- Lowes, F. J. (1966), Mean square values on the sphere of spherical harmonic vector fields, *J. Geophys. Res.*, 71, 2179.
- McFadden, P.L., and M.W. McElhinny (1988), The combined analysis of remagnetization circles and direct observations in paleomagnetism, *Earth planet. Sci. Lett.*, 87, 161-172.
- Márton, P. (2003), Recent achievements in archaeomagnetism in Hungary, *Geophys. J. Int.*, 153, 675-690.
- Moutmir, M. (1995), Analyses magnétiques de terres cuites protohistoriques en France. Apports en archéomagnétisme (Premier millénaire avant J.C.) et en archéologie, PhD thesis, Muséum National d'histoire Naturelle, Paris.
- Najid, D. (1986), Palaeomagnetic studies in Morocco, PhD thesis, Univ. of Newcastle upon Tyne, Newcastle upon Tyne, UK.
- Noel, M. and C.M. Batt (1990), A method for correcting geographically separated remanence directions for the purpose of archeomagnetic dating, *Geophys. J. Int.*, 102, 753-756.

- Núñez, J.I. (2004), Estudio arqueomagnético de la Península Ibérica: Primera curva de variación secular de los últimos tres milenios, PhD thesis, Universidad Complutense de Madrid, Madrid.
- Oyamburu, I., J.J. Villalain, M.L Osete, M. Zarzalejos, and C. Blasco, (1996), Estudio paleomagnético del yacimiento de Villa del Pañuelo (Villamanta, Madrid), *Geogaceta*, 20, 1044-1046.
- Parés, J.M., R. De Jonge, J.O. Pascual, A. Bermúdez, C.J. Tovar, R.A. Luezas, and N. Maestro (1992), Archaeomagnetic evidence for the age of a Roman pottery kiln from Calahorra (Spain), *Geophys. J. Int.*, 112, 533-537.
- Schnepp, E. and Ph. Lanos (2005), Archaeomagnetic secular variation in Germany during the past 2500 years, *Geophys. J. Int.*, 163, 479-490.
- Tanguy, J.C., M. Le Goff, V. Chillemi, A. Paiotti, C. Principe, S. La Delfa, and G. Patanè (1999), Variation séculaire de la direction du champ géomagnétique enregistrée par les laves de l'Etna et du Vésuve pendant les deux derniers millénaires, *C. R. Acad. Sci Paris., Ser.IIa. Terre Planètes*, 329, 557-564.
- Tarling, D.H. (1983), *Palaeomagnetism: Principles and applications in geology, geophysics and archaeology*, pp 279, Chapman and Hall, London.
- Thellier, E. (1938), Sur l'aimantation des terres cuites et ses applications géophysiques, *Ann. Inst. Phys. Globe Univ. Paris*, 16, 157-302.
- Thellier, E. (1981), Sur la direction du champ magnétique terrestre en France durant les deux derniers millénaires, *Phys. Earth Planet. Inter.*, 24, 89-132.

Chapitre 3. Variation de l'intensité du champ magnétique terrestre en Europe de l'Ouest pendant les deux derniers millénaires

Introduction

Un des objectifs de cette thèse est d'obtenir de nouvelles mesures d'intensité du CMT en Espagne pendant les deux derniers millénaires. Cela permettra de mieux caractériser l'évolution de l'intensité du CMT en Europe de l'Ouest ainsi que de comparer les résultats obtenus avec les données d'intensité disponibles pour d'autres régions du globe. Dans une première étape, nous avons utilisé la base des données mondiale publiée par Korte et al. (2005). Dans cet article, une compilation de données d'archéointensité pour différentes régions et pour les derniers millénaires est disponible. Nous avons traité les données pour chaque région par la méthode bayésienne (voir chapitre 2). Les résultats sont montrés à la Figure 1. Plusieurs méthodes de détermination de l'archéointensité ont été utilisées pour obtenir ces données: des méthodes à chauffes successives (Thellier et Thellier (1959), Coe (1967)), et d'autres méthodes comme la méthode de Shaw (1974), de Rolph et Shaw (1986), de Tanguy (1975), de Burakov (1981) ou Burakov et Nachasova (1985). Ces méthodes ont été appliquées avec ou sans tests de stabilité magnétique. Il faut signaler aussi que les corrections de l'anisotropie de l'ATR et de l'effet de la vitesse de refroidissement sur l'acquisition de

l'ATR ne sont pas systématiquement appliquées. Nous remarquons que dans cette base de données aucune sélection n'est faite par rapport à la méthode utilisée pour la détermination de l'intensité. Pour chacune des régions, les données ainsi que la courbe bayésienne obtenue, sont présentées à la latitude et longitude moyennes des sites étudiés (voir Korte et al., 2005).

Comme on peut voir à la Figure 1, la dispersion entre les données est en général très forte. Cette dispersion est probablement liée à l'utilisation de méthodes de détermination de la paléointensité peu précises ou à un faible nombre d'échantillons par site (voir Chauvin et al. 2000). Elle peut être due également à des mauvaises datations. En plus, dans certaines régions un faible nombre de données est disponible. Nous voulons faire remarquer aussi que la majorité des données d'archéointensité proviennent de l'Hémisphère Nord (essentiellement de l'Europe).

Il est donc nécessaire, pour améliorer notre connaissance de la variation de l'intensité du CMT dans le passé, d'obtenir plus de données d'intensité et, à la fois, des données plus précises. En ce qui concerne la Péninsule Ibérique, une seule étude d'intensité du CMT (Kovacheva, 1995) existe pour les deux derniers millénaires. Cette thèse essaie de combler ce manque de données. Les 24 fours étudiés dans la détermination de la courbe de variation séculaire (Chapitre 2), complétés par des lots de céramiques et de briques, nous ont également permis d'obtenir l'intensité du CMT ancien en utilisant la méthode de Thellier (1959). Les valeurs d'intensité ont été corrigées de l'effet d'anisotropie de l'aimantation thermorémanente ainsi que de l'effet de la vitesse de refroidissement sur l'acquisition de l'aimantation thermorémanente.

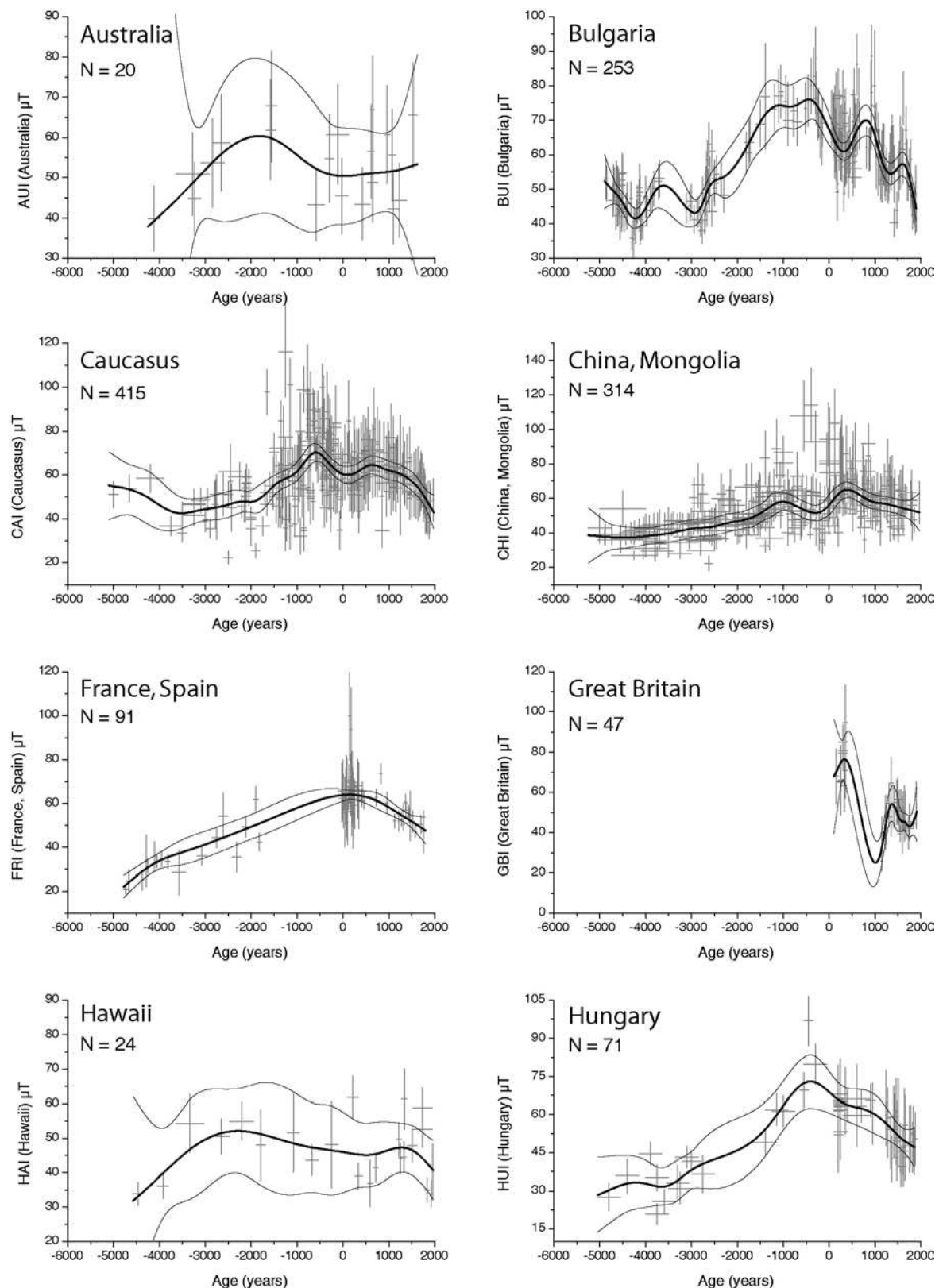


Figure 1a: Données d'archéointensité pour les différentes régions du globe (Korte et al., 2005) et courbes bayésiennes obtenues. N, nombre de données disponibles pour chaque région.

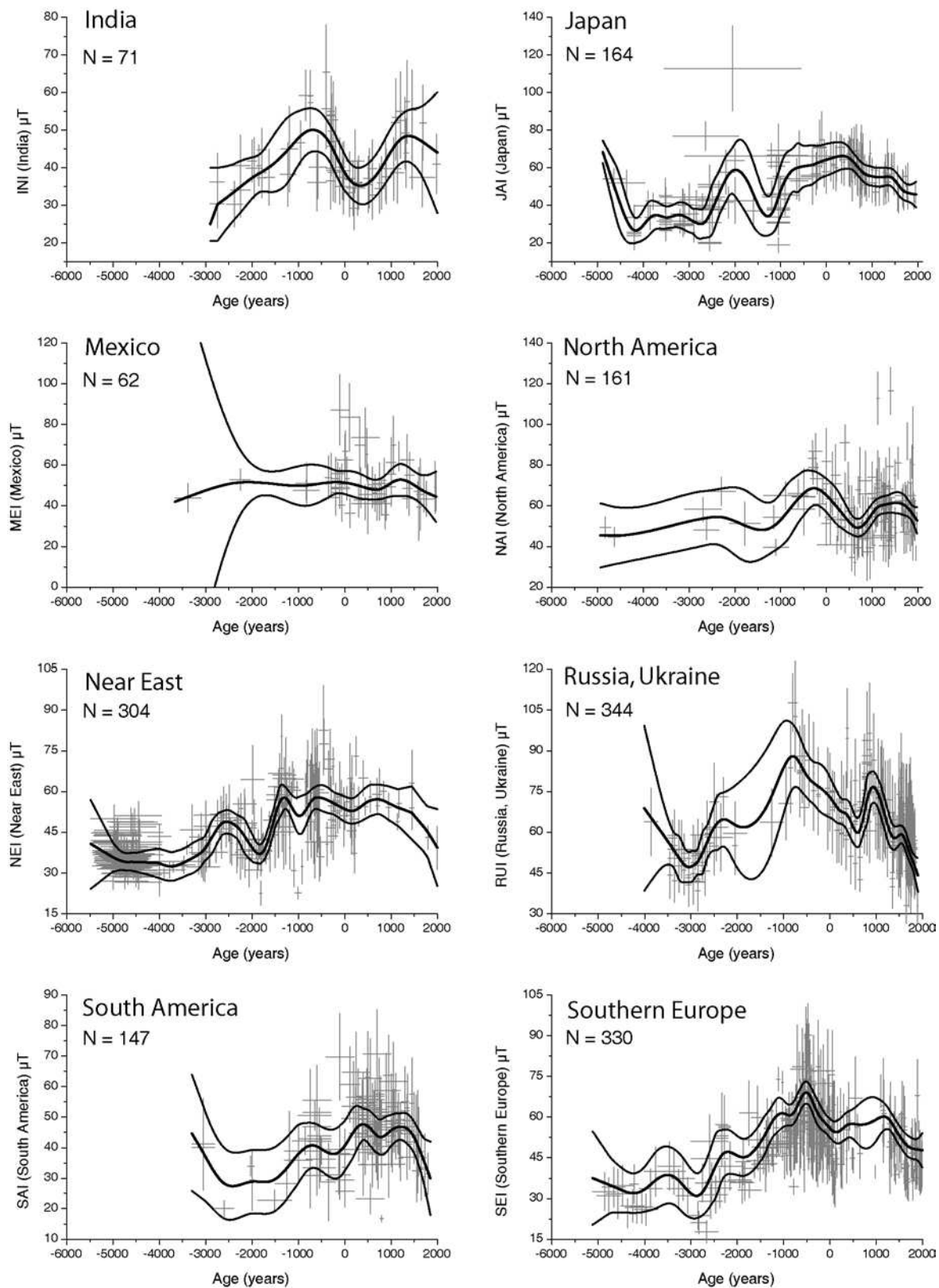


Figure 1b : Données d'archéointensité pour les différentes régions du globe (Korte et al., 2005) et courbes bayésiennes obtenues. N, nombre de données disponibles pour chaque région.

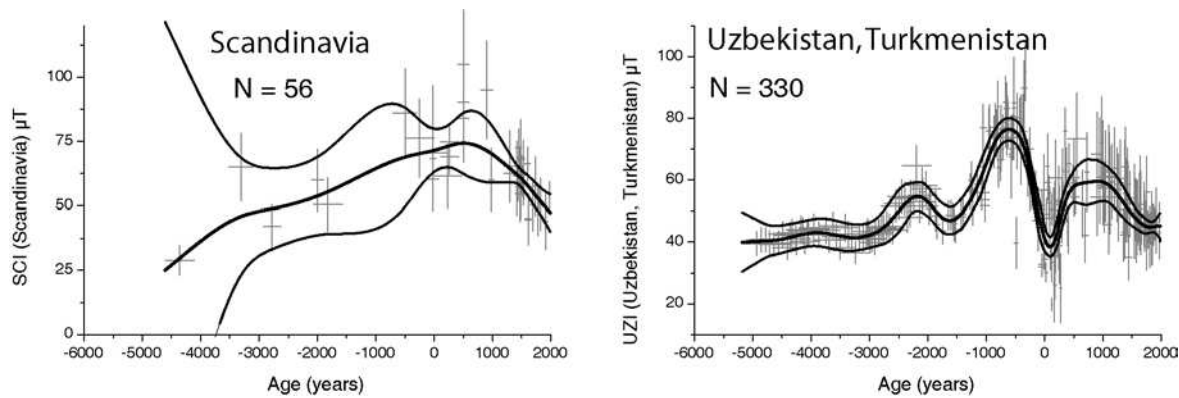


Figure 1c : Données d'archéointensité pour les différentes régions du globe (Korte et al., 2005) et courbes bayésiennes obtenues. N, nombre de données disponibles pour chaque région.

Dans la première partie de ce chapitre, nous présentons sous forme d'article intitulé « **Archeomagnetic study of seven contemporaneous kilns from Murcia (Spain)** », sept valeurs d'intensité obtenues à travers l'étude de sept fours contemporains datés entre 1100 et 1200 et prélevés sur un même site archéologique à Murcia. Après correction de l'effet de la vitesse de refroidissement sur l'acquisition de l'ATR acquise, la dispersion des données d'intensité inter-sites est réduite de 50%. Bien que la dispersion demeure toujours élevée, ces résultats confirment le besoin de corriger l'effet de la vitesse de refroidissement pour une détermination précise de l'intensité du CMT ancien. Nous discutons par la suite l'origine de cette dispersion et enfin nous comparons nos résultats à ceux obtenus en France.

Dans un deuxième article intitulé « **Evolution of the geomagnetic field intensity in Western Europe for the last 2000 years inferred from Bayesian statistics: 17 new archeointensity data from seven Spanish archaeological sites** », la détermination de l'intensité du champ magnétique est obtenue par l'étude de 15 fours, d'un lot de briques et d'un lot de céramiques. Ces résultats, ainsi qu'une compilation des données d'intensité fiables déjà publiées, nous permettent d'obtenir par la méthode bayésienne, l'évolution du CMT en Europe de l'Ouest pour les derniers millénaires. Nous comparons ensuite la courbe d'évolution prédictive par les modèles globaux du CMT de Korte et Constable (2005) et de Hongre et al. (1998) avec nos résultats. L'enveloppe d'erreurs de notre courbe (au niveau de confiance 95%) contient les prédictions à Paris du modèle de Korte et Constable (2005). Les prédictions du modèle de Hongre et al. (1998) sont assez différentes de la courbe obtenue. Par contre, l'évolution de l'intensité du champ dipolaire au cours des deux derniers millénaires paraît plus réaliste pour le modèle de Hongre et al. (1998). Enfin, nous comparons la courbe

obtenue avec les courbes de variation d'intensité dans différentes régions d'Europe (Bulgarie, Russie, Caucase, Uzbekistan et Hongrie), obtenues aussi par la méthode bayésienne.

Comme nous le verrons dans les sections 3.1 et 3.2, les minéraux magnétiques contenus dans les terres cuites étudiées présentent, en général, une très bonne stabilité aux expositions thermiques qui sont nécessaires à la détermination de l'intensité. Par conséquent, l'application de la méthode de Thellier et Thellier (1959) donne lieu à des taux de réussite très élevés (plus de 80% dans la majorité de sites étudiés). Cependant pour les quatre fours de Cabrera d'Anoia étudiés (voir section 2.1), la méthode de Thellier ne permet pas d'obtenir des valeurs d'intensité fiables à cause de la forte altération magnéto-chimique observée. Pour cette raison, ainsi que pour tester la validité de la technique microondes pour la détermination de l'archéointensité dans les terres cuites, nous avons étudié 29 échantillons provenant des sites étudiés en utilisant la désaimantation par microondes. Les résultats d'archéointensité obtenus sont présentés dans la troisième partie de ce chapitre. Les résultats montrent que la désaimantation par microondes est peu efficace pour ces échantillons. Cependant quelques valeurs cohérentes ont été obtenues bien que les moyennes par site montrent une forte dispersion.

3.1. Article : Archeomagnetic study of seven contemporaneous kilns from Murcia (Spain) (Physics of the Earth and Planetary Interiors, in press)

M. Gómez-Paccard ^{a, b, c *}, A. Chauvin ^a, Ph. Lanos ^b, J. Thiriot^d, P. Jiménez Castillo^e.

^a Géosciences-Rennes, CNRS, UMR 6118, Université de Rennes 1, Campus de Beaulieu, 35042, Rennes, Cedex, France.

^b Civilisations Atlantiques et Archéosciences, CNRS, UMR 6566, Université de Rennes 1, Campus de Beaulieu, 35042, Rennes, Cedex, France.

^c Facultad de Ciencias Físicas, Universidad Complutense de Madrid, Ciudad Universitaria, 28040, Madrid, Spain.

^d Laboratoire d'archéologie médiévale méditerranéenne, Maison méditerranéenne de Sciences de l'Homme, CNRS, UMR 6572, 13094, Aix-en-Provence, Cedex 2, France.

^e Escuela de Estudios Árabes (CSIC), 18009, Granada, Spain.

* Corresponding author: Tel.: +33-2-23-236759. Fax: +33-2-23-236040. E-mail address: miriam.gomez@univ-rennes1.fr



Available online at www.sciencedirect.com



Physics of the Earth and Planetary Interiors xxx (2006) xxx–xxx

 PHYSICS
OF THE EARTH
AND PLANETARY
INTERIORS

www.elsevier.com/locate/pepi

Archeomagnetic study of seven contemporaneous kilns from Murcia (Spain)

M. Gómez-Paccard^{a,b,c,*}, A. Chauvin^a, Ph. Lanos^b,
J. Thiriot^d, P. Jiménez-Castillo^e

^a Géosciences-Rennes, CNRS, UMR 6118, Université de Rennes 1, Campus de Beaulieu, 35042 Rennes, Cedex, France

^b Civilisations Atlantiques et Archéosciences, CNRS, UMR 6566, Université de Rennes 1, Campus de Beaulieu, 35042 Rennes, Cedex, France

^c Facultad de Ciencias Físicas, Universidad Complutense de Madrid, Ciudad Universitaria, 28040 Madrid, Spain

^d Laboratoire d'archéologie médiévale méditerranéenne, Maison méditerranéenne de Sciences de l'Homme, CNRS,
UMR 6572, 13094 Aix-en-Provence, Cedex 2, France

^e Escuela de Estudios Árabes (CSIC), 18009 Granada, Spain

Received 10 November 2005; received in revised form 27 February 2006; accepted 8 March 2006

Abstract

New archeointensity values have been determined from seven Spanish kilns sampled at the same archeological site and dated by archeological constraints as between 1100 and 1200 A.D. The directions of the characteristic remanent magnetization and paleointensities have been obtained from classical Thellier experiments conducted on 69 samples collected from the walls of the kilns. Thermoremanent magnetization (TRM) anisotropy and the cooling rate effect upon TRM intensity acquisition have been investigated in all the samples. Differences between mean archeointensities per site, before and after corrections for cooling rate are between 3 and 17%. The study of these seven “contemporaneous” kilns coming from the same archeological site and treated in the same way in the laboratory allows us to discuss the different factors that can cause the dispersion between sites generally observed in archeointensity studies. The results confirm, on one hand, the need for cooling rate corrections in this kind of study and, on the other hand, the need to obtain several archeointensity determinations per century in order to construct a reliable archeointensity curve. Finally, the new data provide a robust mean intensity ($60.3 \pm 3.3 \mu\text{T}$ at the latitude of Paris) for the middle of the XII century in Western Europe and constrain better the evolution of the geomagnetic field intensity during medieval times in this area.

© 2006 Elsevier B.V. All rights reserved.

Keywords: Archeomagnetism; Paleointensity; Thellier method; Cooling rate corrections; Dispersion between sites; Western Europe

1. Introduction

Research in archeomagnetism has provided some archeomagnetic reference curves that relate the time variations of the directions of the Earth's magnetic field

in Europe (i.e. Schnepp and Lanos, 2005; Márton, 2003; Gallet et al., 2002; Kovacheva et al., 1998; Batt, 1997). These data have been used in global models of the secular variation (Korte et al., 2005). However more paleointensity data are clearly needed in order to constraint these models. The intensity variations of the geomagnetic field during the last 2000 years have been previously investigated in Western Europe, in particular in France (Gallet et al., 2005; Genevey and Gallet, 2002; Chauvin et al., 2000). However, few archeointensity studies are avail-

* Corresponding author. Tel.: +33 223 236759; fax: +33 223 236040.

E-mail address: miriam.gomez@univ-rennes1.fr
(M. Gómez-Paccard).

able in Spain for this period (Kovacheva et al., 1995). These data are obtained from archeologically dated fired materials such as kilns, pottery fragments or bricks, and many more archeointensity studies are needed to construct a reliable intensity variation curve for Western Europe. A reference curve of the field intensity time variations should also be useful for future archeomagnetic dating, especially in the case of pottery and for displaced objects such as tiles, where only the paleoinclination and the paleointensity can be determined.

Spain has a rich historical past that has been the subject of intensive archeological research which makes this country a favorable place to obtain detailed records of the variation of the Earth's magnetic field during historical time. One example of this is the excavation at Murcia, "calle Puxmarina", where several structures suitable for archeomagnetic studies were found. This city became one of the most important in Al-Andalus (the Muslim area of the Iberian Peninsula), together with Sevilla and Valencia, during the XII and the first half of the XIII centuries. In this study we present new archeointensity results from seven kilns collected in a single archeological site, "calle Puxmarina", in Murcia, all of them archeologically dated between 1100 and 1200 A.D. The determination of the paleointensity on these seven kilns from the same site allows us to discuss the dispersion obtained for different structures dated during the same interval of time. On the other hand, these data better constrain the evolution of the Earth's magnetic field in Western Europe during medieval times.

2. Archeological dating and sampling

Our samples were collected at Murcia (latitude: 37.98°N and longitude: 1.12°E), calle Puxmarina, by Jacques Thiriot. The archeological excavation, directed by Pedro Jiménez Castillo and Julio Navarro Palazón, revealed that during the XI century a big caliphal house was abandoned and in its place was built a glass workshop. The overall excavation was located on horizontal ground and the surface area of this workshop was around 150 m². Seven well-preserved Islamic kilns were found during excavations and were sampled for archeomagnetism. The strict upper age – *Terminus Ante Quem* (TAQ) – of the structures (1200 A.D.) is archeologically and historically well constrained by the construction of a Islamic house (that was built above the workshop that was partially destroyed for the construction of the house), with a TAQ for the construction determined at 1200 A.D. on the basis of well dated ceramics found at the construction level of the house. The Christian conquest of the area in 1243 A.D., provides another date after which

the kilns could not have been in use. The ceramics found during the archeological excavation and the general context of the site indicated that it was active during the XII century. This suggests that the second half of the XII century is the interval most probably containing the real date of the abandonment of the studied structures. However, as the archeological constraints did not reveal the exact lower strict limit on age – *Terminus Post Quem* – of the structures, we decided to consider a larger interval, between 1100 and 1200 A.D.

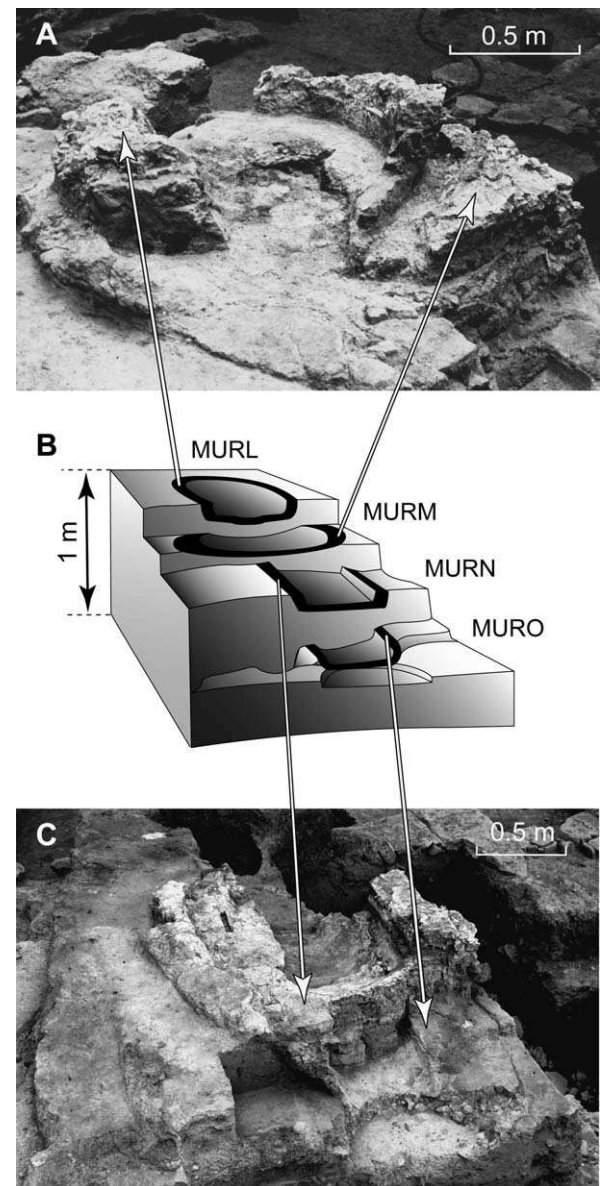


Fig. 1. Reconstitution and pictures of four of the seven kilns sampled at Murcia. The oven MURL, situated at the top, is the youngest one and MURO, at the bottom, the oldest. The well baked walls are shown in black.

Three of the seven kilns sampled (MURI, MURH and MURK) were independent, whereas the other four (MURO-N-M-L) were different phases of the same structure. Several consecutive phases, more or less well defined, were archeologically observed in this structure, each one built upon the previous one. In order to avoid possible remagnetizations, only well-defined phases far away from the firing chamber of the predecessor kiln were sampled for archeomagnetism. The vertical distance between each sampled phase is approximately 30 cm (Fig. 1). Typical distances between the four independent archeological structures sampled (MURI, MURK, MURH and MURO-N-M-L) are about 3 m.

The stratigraphic constraints (MURO, MURN, MURM and MURL from the oldest to the youngest kilns) can be taken into account in the construction of secular variation reference curves (Lanos, 2004). Archeologists support the idea that MURL and MURM were built for metallurgical purposes and MURO and MURN were glass making kilns. The archeologically determined baked walls or floors (in black in Fig. 1), as well as the distance between each sampled phase and the relatively low firing temperature, assure that the magnetic signals acquired for each superposed kiln were independent. The independent structures MURH and MURK, approximately 150 cm × 40 cm size, were also constructed for glass working, and MURI, the biggest structure approximately 170 cm × 130 cm size, was a glass making and melting kiln.

Between 6 and 19 independently oriented samples were collected per kiln. The samples taken from the walls were composed of burnt clay, bricks or a mixture of both and were oriented by the magnetic and solar compass on the horizontal plane of plaster coverage. In the laboratory, standard cores (10.8 cm³) were drilled within the archeomagnetic material collected.

3. Experimental procedure

3.1. Magnetic measurements

Remanent magnetization and low field susceptibility were measured with a Molspin spinner or JRS (AGICO) magnetometers and a Bartington susceptibility meter, respectively, in the paleomagnetic laboratory of Géosciences-Rennes. Thermomagnetic curves were performed in air using a KLY3 (Agico) susceptibility meter with fitted furnace. Isothermal remanent magnetization (IRM) was obtained using an ASC Scientific impulse magnetizer. Magnetic hysteresis loop was measured using a coercivity meter (Jasonov et al., 1998) with a maximum applied field of 500 mT in the pale-

omagnetic laboratory of the University Complutense of Madrid. This instrument also generated stepwise acquisition and reverse-field acquisition of isothermal remanence (IRM). Scanning electron microscopy (SEM) and energy dispersive X-ray analysis were carried out using a conventional SEM JSM 6400 and an energy-dispersion spectrometer OXFORD Link Isis in the C.M.E.B.A. at the University of Rennes 1. The classical Thellier paleointensity method (Thellier and Thellier, 1959), based on the comparison between natural remanent magnetization (NRM) lost and partial thermoremanent magnetization (pTRM) gained in a known laboratory field was used. A laboratory field, of 50 or 60 µT, was applied along the cylindrical axis Z of the samples. Samples were heating in air in a magnetic measurements oven, from 100 °C to temperatures at which more than the 85% of the initial NRM was lost, using between 6 and 17 temperature steps. In addition to the low field susceptibility measurements and also in order to detect possible alteration in the magnetic mineralogy of the samples pTRM checks were made every two-temperature step.

3.2. TRM anisotropy

On each sample the TRM anisotropy tensor was determined and all NRM and TRM measurements were corrected for TRM anisotropy (Chauvin et al., 2000; Veitch et al., 1984). This tensor was obtained from the acquisition of a TRM in six different directions, in sample coordinates Z, -Z, X, -X, Y and -Y. Finally, a last remagnetization was performed along the +Z axis of the samples in order to check their thermal stability. If no or few (less than 10%) modifications of the TRM acquisition capacity are observed, all the NRM and TRM measurements are corrected for anisotropy. Chauvin et al. (2000) demonstrated that the correction of the NRM and TRM measurements using the tensor of TRM anisotropy is clearly needed in order to obtain precise values of paleointensity on tiles or bricks. Garcia (1996) and Genevey and Gallet (2002) measured the anisotropy correction factors at two different temperatures and showed that they do not depend on the temperature at which they were determined. In order to avoid magneto-chemical changes the TRM anisotropy tensor was measured during the Thellier experiment at temperatures at which around 70% of the NRM intensity is lost.

3.3. Effect of cooling rate upon the TRM intensity

The cooling rate dependence of TRM intensity was first reported by Néel (1955) for an assemblage of identical single domain magnetic grains. With the use of

both cryogenic magnetometers and smaller samples with quicker cooling times this problem appeared important and some theoretical models (McClelland-Brown, 1984; Halgedahl et al., 1980; Walton, 1980) and experimental data were published (Genevey and Gallet, 2002; Chauvin et al., 2000; Biquand, 1994; Fox and Aitken, 1980). The main conclusion of all these studies is the increase of TRM intensity as the cooling rate decreases for assemblies of single domain (SD) or pseudo-single domain (PSD) grains. As our samples cooled quicker in our archeointensity experiments (typical cooling time of 45 min) than during the original cooling at the archeological site this effect must be investigated.

In order to quantify the cooling rate effect for our samples, we carried out on each sample a supplementary cycle of measurements consisting of four TRM acquisition steps after the end of the Thellier experiments. These four steps allow us to quantify the correction factor for the effect of cooling rate upon TRM intensity as a percentage defined by $(\text{TRM}_{s+} - \text{TRM}_{r+})/\text{TRM}_{r+}$, where r and s denote the rapid (45 min) and slow cooling time used, and + and – the directions of the applied magnetic field along the +Z or –Z axes of the samples (Fig. 2). Two slow linear cooling times, of 24 and 48 h, were used. Archeological information suggests that the real cooling time related to the acquisition of the ancient TRM is most probably contained between these two values.

Changes in TRM acquisition capacity of the samples could be detected by an alteration factor defined as a percentage $(\text{TRM}_{r2-} - \text{TRM}_{r1-})/\text{TRM}_{r1-}$ (see Fig. 2). This alteration factor estimates the amount of magnetochemical changes which occur during the third (slow

cooling) and/or the fourth (rapid cooling) heatings. Such changes could introduce an error in the correction factor which is estimated by comparing TRMs acquired during the third and the first heatings. For this reason, we have decided to correct archeointensity determinations for cooling rate effect only when the correction factors were bigger than the alteration factors.

Note that a little (less than 15%) NRM was, in some cases, still remaining in our samples when the cooling rate experiments were carried out but as we compare the vertical components of magnetization related to steps with the applied field in the same sense, this is not a problem.

4. Magnetic mineralogy

NRM intensity and low field susceptibility are scattered both between and within sites (Fig. 3). The material studied is characterized by a NRM lower than 10 A/m and low field susceptibility between 10^{-4} and 10^{-2} SI units. The Königsberger ratios (for an ambient field of 50 µT) range from 3 to 30, with a mean value of 13.3 (see Table 2).

4.1. Thermomagnetic curves

In order to investigate the magnetic carriers in our samples a total of 48 variation curves of the low field susceptibility versus temperature were determined ($K-T$ curves). Almost all the $K-T$ curves were relatively reversible, showing that no important mineralogical changes occurred during heating (Fig. 4). The Curie temperatures, T_c , were calculated using the method of the second derivative described by Tauxe (1998).

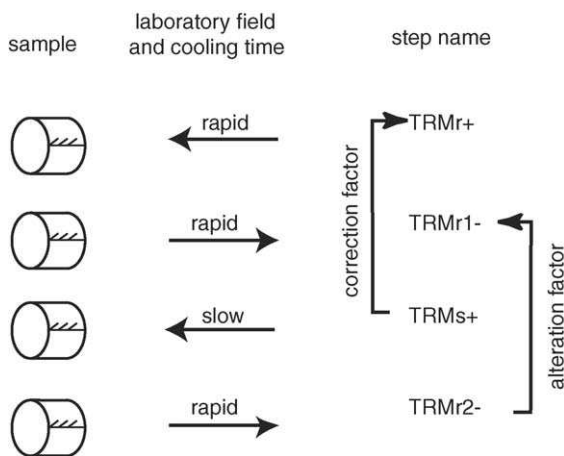


Fig. 2. Diagram showing the four thermal steps carried out at the same temperature in order to determine the cooling rate effect upon the TRM intensity. The correction and alteration factors were calculated using steps 1 and 3, and steps 2 and 4, respectively.

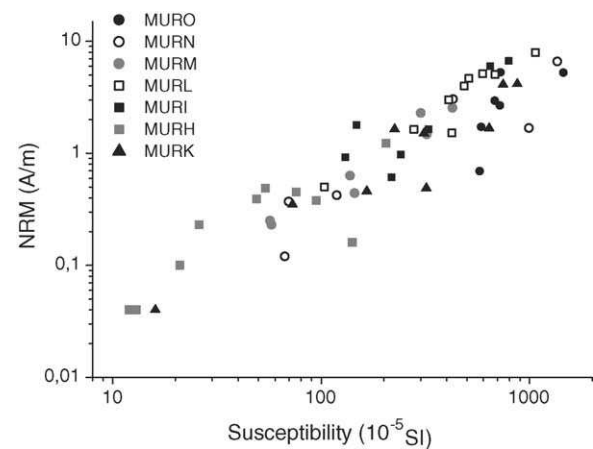


Fig. 3. NRM intensity (A/m) vs. susceptibility (10^{-5} SI units) for all our samples.

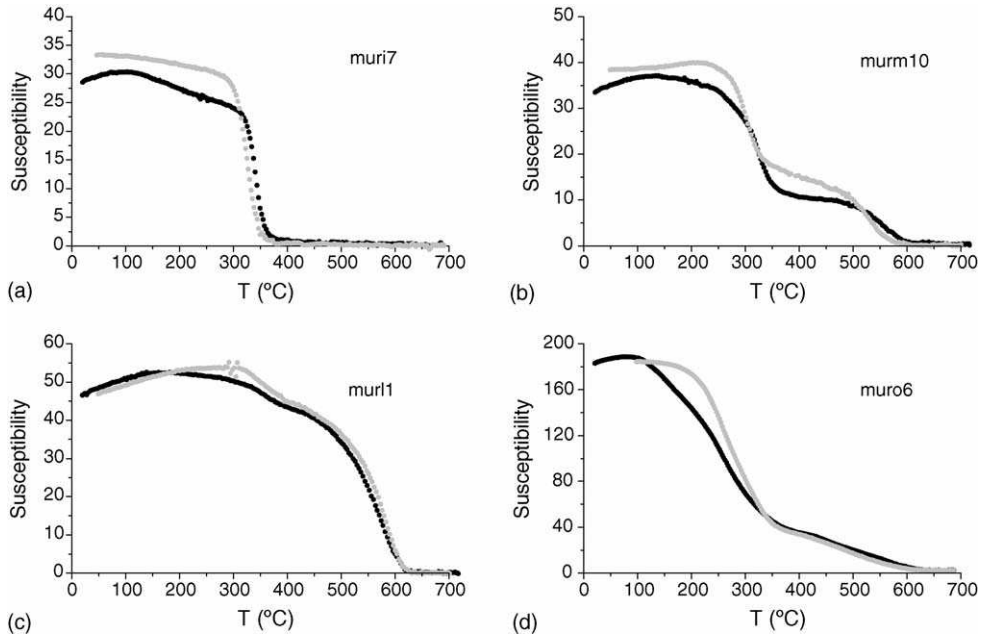


Fig. 4. Examples of typical susceptibility vs. temperature curves ($K-T$ curves). Temperatures are in degrees Celsius and susceptibilities in arbitrary units. Heating (cooling) branches are plotted in black (grey) circles.

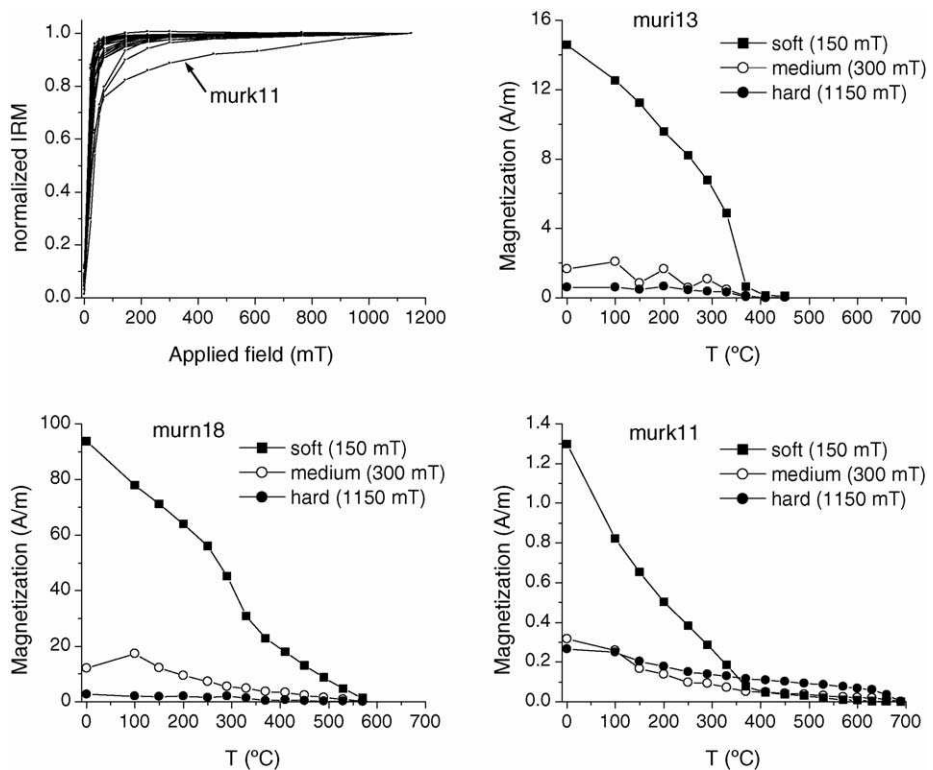


Fig. 5. Isothermal remanent magnetization acquisition curves (IRM) and thermal demagnetization of three-axes IRM for representative samples (see text).

A low Curie temperature magnetic phase (with T_c between 300 and 400 °C) dominates the signal in the majority of the samples (Fig. 4a). A higher T_c phase (with T_c of around 580 °C) is also recognized in almost all samples of the sites MURO, MURM, MURN, MURH and MURK (Fig. 4b and d). In a few samples only this high T_c phase is present (Fig. 4c). In some cases we found T_c higher than 585 °C, which can be interpreted in terms of partially oxidized (titano)magnetite or (titano)maghemitite. Maghemite is not supposed to be stable during heating, and in air, it should transform into hematite. In our samples a very good thermal stability has been observed during Thellier experiments and during thermomagnetic analysis. However, Al-, Na- or Mg-substituted maghemites are stable at high temperatures (Stacey and Bajernee, 1974). Thermomagnetic curves suggest that the principal magnetic phases present in our samples are titanomagnetite with high Ti content or a

very stable Al-, Na- or Mg-substituted maghemite. Magnetic minerals with low T_c were also found in bricks by Casas et al. (2005) and Chauvin et al. (2000). The determined Curie points are in agreement with the unblocking temperatures observed in the Thellier experiments. This, together with the single vector components observed (see Section 6.1), demonstrates that the NRM of the samples is a full TRM.

4.2. Hysteresis and IRM acquisition curves

We have performed experiments on the acquisition of isothermal remanent magnetization (IRM) on 23 representative cylindrical samples of the seven studied kilns (Fig. 5). Hysteresis measurements and progressive IRM acquisition up to 500 mT have also been carried out on five pulverized samples selected from the same collection (Fig. 6). In most cases samples show a rapid increase

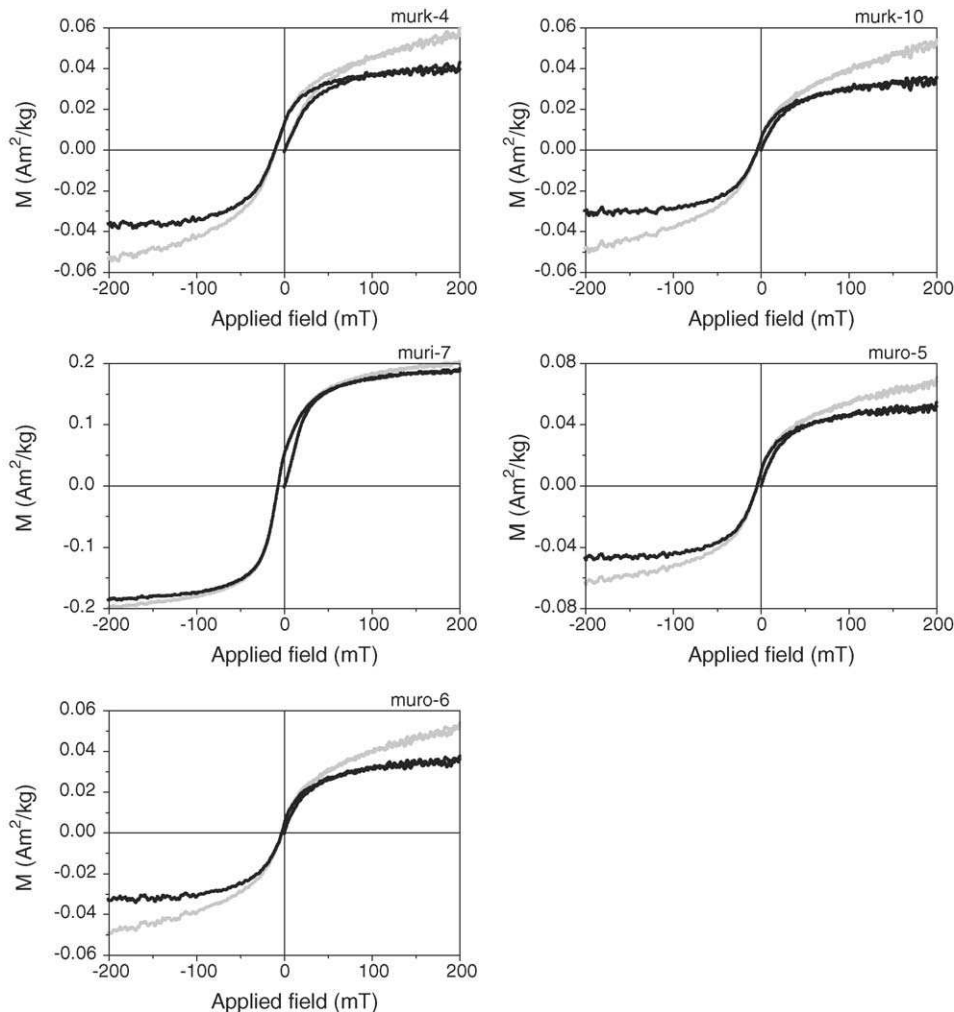


Fig. 6. Hysteresis loops of representative samples. Grey lines, original data and black lines, corrected for the paramagnetic contribution.

of IRM intensity and saturation is reached between 50 and 150 mT. This suggests that magnetization is carried by low coercivity magnetic minerals such as titanomagnetite or magnetite. A gradual increase of the intensity of the IRM up to the maximum magnetizing field of 1150 mT is observed for only one sample (murmurk11, Fig. 5) suggesting the presence of hematite.

Thermal demagnetization of three-axes composite IRM was conducted on 22 from the 23 cylindrical samples using the method proposed by Lowrie (1990). IRM acquisitions were performed in three steps. First, the samples were remagnetized in a field of 1150 mT along their Z axis, then a second IRM was given along their X axis in a field of 300 mT, and finally a third IRM was given along their Y axis in a field of 150 mT. The thermal demagnetization of each orthogonal component is then analyzed separately. In all samples IRM along the Y axis has the highest intensity and unblocking tempera-

tures usually lower than 400 °C are associated with this component of magnetization (Fig. 5). On some samples this Y component is demagnetized at temperature close to 570 °C.

These experiments suggest again that the main magnetic carrier in our samples is titanomagnetite. Magnetite or Ti-poor titanomagnetite is also observed (sample murmurk18, Fig. 5), while hematite is recognized in only one sample (murmurk11, Fig. 5).

The five hysteresis curves (Fig. 6) have been corrected for the linear paramagnetic signal that dominates the magnetization at applied fields higher than 50–100 mT. The values of H_{cr} obtained ranges between 12.7 and 24.6 mT and intensities of the magnetization at saturation (J_s) between 0.04 and 0.10 A m²/kg. H_{cr}/H_c ratios range from 1.81 to 6.15 and the J_{rs}/J_s ratios from 0.09 to 0.31. These values are in agreement with the values proposed in the literature for titanomagnetites (Peters

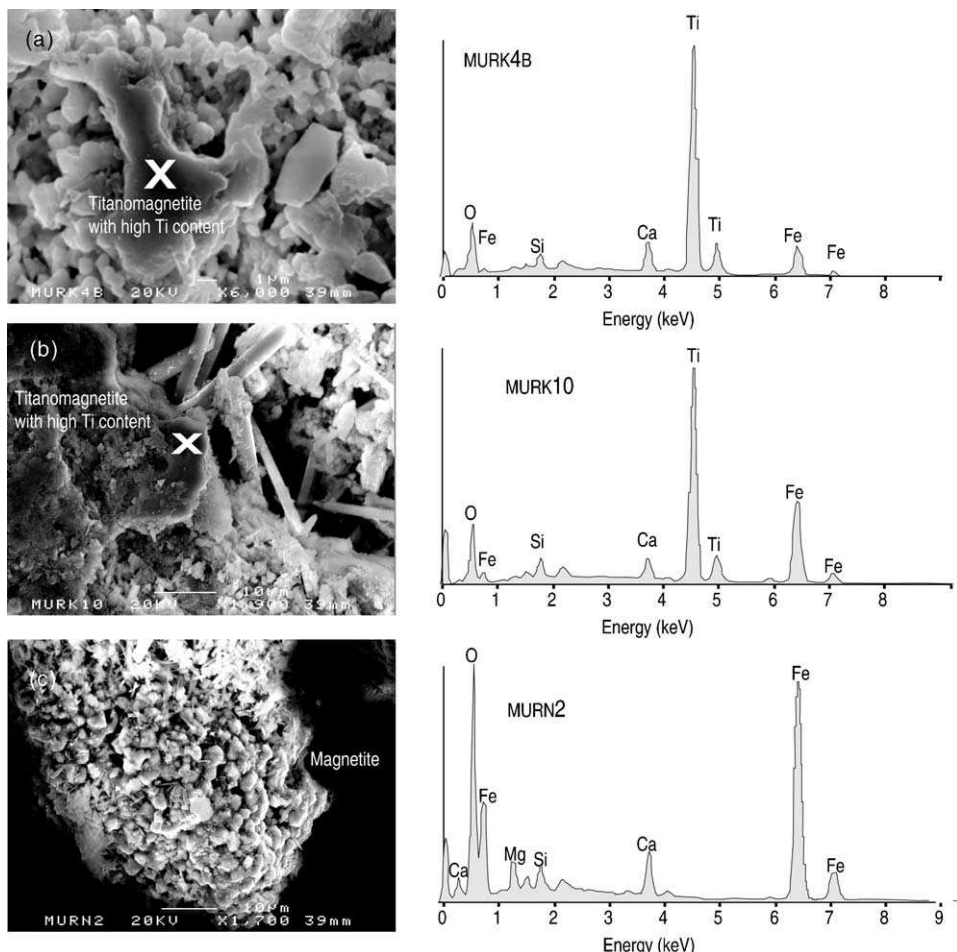


Fig. 7. Three representative examples of scanning electron microscopy observations. Points where energy dispersive X-ray analyses were done are marked by white crosses (see text).

Table 1

Studied structures at Murcia and compilation of the directional results in situ and at the latitude of Paris

Name	Stratigraphic constraints	<i>n</i>	D_s	I_s	α_{95}	<i>k</i>	D_{pa}	I_{pa}
MURO	Older than MURN	6	13.6	44.7	3.8	308	16.2	56.9
MURN	Younger than MURO and older than MURM	6	14.0	45.1	2.1	1038	16.7	57.1
MURM	Younger than MURN and older than MURL	7	14.9	45.5	2.1	811	17.7	57.5
MURL	Younger than MURM	9	16.2	44.2	1.2	1842	19.1	56.5
MURI		7	15.2	41.7	4.1	215	18.0	54.6
MURH		10	17.3	46.4	2.7	330	20.5	58.1
MURK		9	14.1	45.2	2.2	547	16.8	57.2
Mean		7	15.0	44.7	1.3	2137	17.9	56.7

n, number of samples taking into account for the calculation of the mean; D_s , I_s , mean declination and inclination in situ; α_{95} , 95% confidence cone of mean directions in situ and *k*, precision parameter; D_{pa} , I_{pa} , mean declination and inclination relocated to Paris.

and Dekkers, 2003), and the ratios of H_{cr}/H_c and J_{rs}/J_s lie in the PSD range according to the criteria of Day et al. (1977). Such a rock-magnetic signature presumably results from a mixture of distinct populations of magnetic particles with different composition and grain size (Dunlop, 2002).

4.3. SEM observations

Scanning electron microscopy (SEM) and energy dispersive X-ray analysis were carried out on five selected samples: muro5, muro6, murk4, murk10 and murn2. Even if the number of investigated samples is low, SEM observations can provide additional information about the magnetic mineralogy and grain size distribution.

SEM experiments confirm the previous results. Several titanomagnetite with high Ti-content and with different sizes were found in the four studied samples (examples in Fig. 7a and b).

These particles are supposed to represent the low coercivity (less than 150 mT) and low T_c phase (around 300–400 °C) observed. Titanomagnetite with low Ti content and magnetite (Fig. 7c) were also found. In many cases, as shown in Fig. 7c, magnetite was found as an aggregate of magnetite spherules of different sizes. Only the smaller spherules of about 0.1 μm (Day et al., 1977) are SD and could carry the remanence.

5. Directions of magnetization

The archeomagnetic directions and paleointensities were simultaneously determined from the Thellier experiments. The mean directions of magnetization per site and their statistical parameters were calculated using principal component analysis (Kirschvink, 1980) and Fisherian statistics (Fisher, 1953). The obtained directions of magnetization (Table 1) were translated to Paris

via the virtual geomagnetic pole (VGP). All the measurements are corrected for TRM anisotropy. The very similar directions obtained, with their circles of confidence (α_{95}) overlapping, are in agreement with archeological information that proposed the same age interval for the seven structures.

Fig. 8 shows the stereographic projection of the mean directions of magnetization together with the French reference curve (Gallet et al., 2002) built using Bayesian statistics (Lanos, 2004). We can observe significant differences between the French curve and our data. Our seven structures gave lower inclinations than the French SV curve.

The distance between each one of the studied structures (about 3 m) suggests that these differences are not related to a displacement posterior to the last use of the structures. If it were the case, all the structures would have had to be displaced in the same way but an overall landslide of the horizontal ground of the workshop,

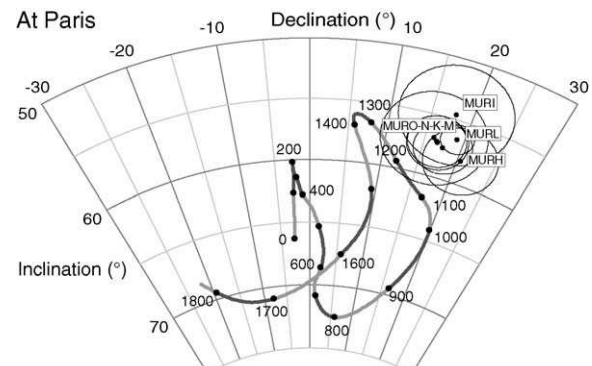


Fig. 8. Stereographic projection of the reference French curve for the directional changes of the geomagnetic field over the last two millennia (data from Gallet et al. (2002) treated by Bayesian modelling (Lanos, 2004)), without error margins, together with mean directions of magnetization with α_{95} error circles of the seven Spanish structures. All data are relocated to Paris.

where our structures were located, was not observed during the excavations. On the contrary, individual movements could not be totally discarded for the structure MURK during the archeological excavation, partially destroyed by posterior constructions, but the indistinguishable archeomagnetic direction of this structure and MURO-N-M allow us to reject this possibility.

Lower inclinations in Iberia than in France, between the XI and the XIV centuries, have been confirmed by a relatively large number of Spanish data (Gómez-Paccard et al., 2006). They are also observed on historical lava flows of the same period from Italy (Tanguy et al., 1999; Arrighi et al., 2004). These differences either are related to features of the regional geomagnetic field or they indicate that the French secular variation curve is not perfectly constrained for this period.

6. Paleointensity determination

Paleointensity determinations were attempted on 69 samples with between 6 and 13 independently oriented samples studied per structure. Only 15 samples were rejected, the different criteria used to retain or reject our paleointensity estimations are described in Section 6.1. This success rate of 80% shows the excellent phys-

ical and chemical stability of the magnetic minerals contained in our samples. Only samples corrected for TRM anisotropy and for which the cooling rate effect was investigated were retained, therefore, six samples on which such experiments were not successful, were rejected.

6.1. NRM–TRM diagrams

The quality of the obtained archeointensity data can be assessed in different ways using parameters proposed in the literature. The linear segment in the NRM–TRM diagram used to calculate the paleointensity was determined for at least five points. The last point retained is the last step before any evidence of changes in magnetic mineralogy, detected either by changes in pTRM acquisition or by the growth of a chemical remanent magnetization (CRM). Differences between the original pTRM at a given temperature step and the pTRM check at the same temperature that were more than 10% of the total TRM intensity acquired were considered as significant. The lower limit of the fraction of the NRM component retained for slope calculation (f parameter, Coe et al., 1978) was set at 40% following Chauvin et al. (2005). Note that as no secondary components of

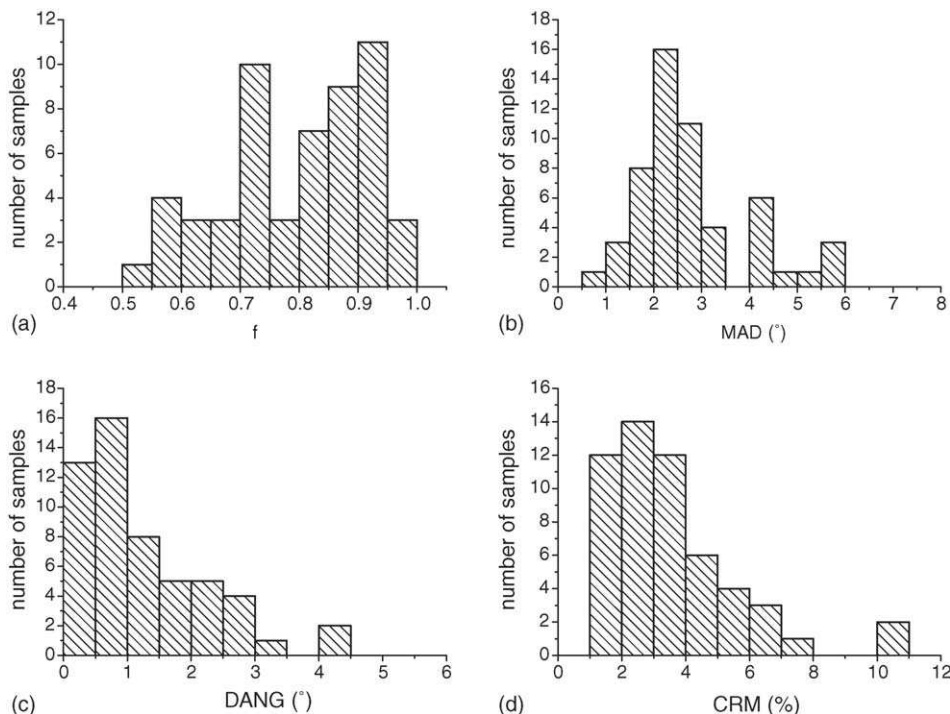


Fig. 9. Variations of some parameters used to test the quality of our archeointensity determinations. (a) f , fraction of the NRM used in the slope calculation; (b) MAD, maximum angle of deviation; (c) DANG, deviation angle; (d) CRM, acquisition of chemical remanent magnetization as a percentage of the applied field.

Table 2

Archeointensity results

Name	Spl.	NRM	χ ($\times 10^{-5}$)	Q_1	$T_{\min} - T_{\max}$	n	f	g	q	MAD	DANG	CRM	$F \pm \sigma F$	F_e	$F_m \pm S.D.$	F_{po}	ΔM	Alt (%)	ΔM	Alt (%)	F_{pocr}	F_{pa}	VDM ($\times 10^{22} A/m^2$)	VADM ($\times 10^{22} A/m^2$)	Q
MURO	1A	2.66	723	9.3	100–425	10	0.93	0.84	33.8	0.6	0.1	2.0	60.7 ± 1.4	63.8	64.7 ± 4.5	64.0	15.2	2.8	21.9	0.9	53.4 ± 5.3	61.5	11.0	9.5	149
	2A	2.94	682	10.8	100–425	10	0.83	0.85	18.8	2.0	1.3	3.1	72.8 ± 2.6	70.1			19.1	6.5	24.5	3.6					
	3A	5.27	728	18.2	100–425	10	0.60	0.83	14.8	1.9	0.4	2.5	67.4 ± 2.3	64.7			15.0	12.1	19.2	8.7					
	4A	1.72	587	7.4	100–425	10	0.84	0.82	22.4	2.3	0.6	3.5	59.6 ± 1.8	58.3			9.5	1.8	17.0	-2.1					
	5A	0.69	577	3.0	100–425	10	0.75	0.85	17.4	3.2	2.9	10.7	72.4 ± 2.7	69.5			21.6	7.3	29.9	2.3					
	6A	5.22	1455	9.0	100–425	10	0.81	0.85	41.4	2.4	1.4	5.2	64.3 ± 1.1	61.8			17.9	6.0	22.7	6.6					
MURN	2A	1.68	997	4.2	150–480	10	0.71	0.88	11.6	2.6	1.9	4.6	53.7 ± 2.6	53.7	52.3 ± 8.8	51.9	0.8	0.6	1.7	-2.9	52.7 ± 9.1	60.6	10.8	9.3	155
	7A	0.42	119	8.9	150–450	9	0.73	0.82	10.0	1.7	0.1	1.1	51.2 ± 3.3	49.8			-2.3	-0.1	-0.4	-2.6					
	13A	0.37	70	13.3	150–450	9	0.57	0.87	18.8	2.2	0.6	2.6	67.3 ± 2.0	67.6			-0.8	0.0	3.0	-4.6					
	14A	0.12	67	4.5	100–560	15	0.88	0.92	44.7	2.0	0.9	1.2	44.8 ± 0.6	43.5			4.9	-10.1	6.6	3.8					
	17A	3.03	430	17.7	100–450	9	0.64	0.76	20.5	2.0	0.8	2.1	45.1 ± 0.8	44.4			1.5	3.2	-0.4	-1.7					
	18B	6.58	1361	12.2	100–480	11	0.87	0.83	49.3	1.3	0.2	3.0	56.9 ± 0.8	55.0			-3.6	-0.4	-1.6	-1.9					
MURM	2A	0.44	145	7.6	100–330	6	0.73	0.70	18.3	2.1	2.1	4.4	54.9 ± 1.6	54.5	52.9 ± 3.3	53.5	4.2	-2.9	8.0	-2.6	50.9 ± 3.4	58.6	10.4	9.0	160
	6A	0.63	138	11.5	100–450	10	0.86	0.87	29.1	2.1	2.2	2	55.1 ± 1.6	53.8			0.8	-0.4	0.8	-0.9					
	8A	0.25	57	11.1	100–500	12	0.70	0.90	24.5	2.6	1.0	3.1	54.9 ± 1.6	50.1			3.9	-1.1	4.3	-3.9					
	9A	2.28	301	19.0	100–420	9	0.92	0.79	31.7	2.6	0.4	4.7	59.0 ± 1.6	58.1			6.7	1.0	9.2	2.0					
	10A	1.47	322	11.5	100–330	6	0.55	0.62	7.7	2.7	2.5	4.4	48.8 ± 2.0	48.1			-1.6	-1.1	-4.2	-0.5					
	12A	0.23	58	9.9	100–590	15	0.92	0.91	37.4	1.7	0.5	2.6	52.2 ± 1.3	51.1			12.1	0.6	12.1	-0.6					
MURL	1B	1.63	279	14.7	150–580	15	0.90	0.92	49.7	1.6	0.2	1.4	53.3 ± 0.8	52.1	50.7 ± 3.7	49.7	5.7	0.6	5.0	2.3	49.2 ± 3.3	56.7	10.1	8.7	685
	2A	4.64	513	22.7	100–420	9	0.92	0.71	51.0	2.2	0.4	2.6	50.3 ± 0.6	47.4			-2.0	-6.3	-2.2	-6.0					
	3A	0.50	104	12.1	100–480	11	0.80	0.89	37.9	2.2	0.8	1.8	48.9 ± 0.7	48.1			1.2	-0.4	3.1	-1.1					
	8A	1.52	425	9.0	100–390	8	0.89	0.64	19.5	3.4	0.7	3.2	57.0 ± 1.5	55.8			-2.8	-12.3	0.5	-4.5					
	10B	2.99	409	18.4	100–390	8	0.93	0.71	110.4	1.3	0.9	1.6	50.2 ± 0.3	49.8			1.5	-5.2	2.4	-2.1					
	11A	3.99	488	20.5	100–420	9	0.97	0.72	77.9	2.2	0.8	1.9	54.5 ± 0.4	52.4			0.3	-3.2	-0.4	-4.8					
MURI	13A	5.13	597	21.6	100–390	8	0.93	0.56	140.0	2.6	0.6	2.9	45.6 ± 0.2	44.8			3.3	-6.0	2.9	-3.6					
	14A	7.93	1066	18.7	100–390	8	0.93	0.80	141.7	2.5	1.1	2.4	54.2 ± 0.2	50.5			3.2	-5.1	2.8	-2.7					
	15A	5.05	686	18.5	100–420	9	0.77	0.77	57.4	2.5	0.9	1.9	57.4 ± 0.6	55.6			5.4	-0.4	10.0	2.2					
	3A	6.65	795	21.0	100–350	8	0.73	0.79	24.3	2.8	1.2	3.2	51.6 ± 1.0	52.5	49.9 ± 5.9	51.4	10.8	-2.7	10.1	-2.9	50.2 ± 6.3	57.9	10.6	8.9	219
	4A	1.78	148	30.3	100–560	15	0.86	0.91	79.7	2.7	1.6	2.5	60.1 ± 0.6	60.2			-7.4	-7.6	-7.9	-9.4					
	5A	1.63	327	12.6	100–320	7	0.78	0.82	38.4	2.6	2.3	3.6	54.1 ± 0.8	51.5			2.3	-3.7	5.4	-2.2					
MURH	6A	6.00	649	23.2	100–380	9	0.61	0.68	9.4	4.6	1.5	1.8	50.5 ± 1.9	51.8			-3.0	-7.0	0.9	-4.7					
	11A	0.97	242	10.1	100–320	7	0.71	0.75	27.3	5.6	4.1	5.4	46.9 ± 0.7	45.5			7.4	-0.6	10.8	-2.0					
	12A	0.92	131	17.7	100–320	7	0.58	0.72	16.2	4.4	2.3	4.6	45.6 ± 0.9	44.7			1.8	-6.0	5.6	-5.8					
	15A	0.61	218	7.0	100–290	6	0.74	0.78	23.7	4.3	1.1	3.9	46.2 ± 0.9	43.4			0.2	-1.7	0.9	0.9					
	2A	1.23	205	15.1	100–550	15	0.94	0.91	72.7	1.6	0.3	3.7	59.8 ± 0.8	64.7	57.6 ± 7.7	58.9	3.7	-0.1	3.5	1.1	57.6 ± 6.8	66.2	11.6	10.2	508
	3A	0.04	13	7.7	100–550	15	0.89	0.92	16.2	3.4	1.5	5.8	53.2 ± 2.8	60.7			3.0	2.7	4.6	-0.2					
MURH	5A	0.45	76	14.9	100–600	17	0.99	0.91	91.8	1.2	0.5	1.6	56.9 ± 0.6	54.4			2.8	-0.6	3.1	0.6					
	7A	0.49	54	22.8	100–475	12	0.70	0.88	34.1	2	0.4	2.9	58.5 ± 1.2	60.6			3.1	-3.8	2.9	0.5					
	8C	0.23	26	22.2	100–600	17	0.80	0.93	57	1.6	0.7	1.7	62.2 ± 1.0	61.3			4.4	-2.3	6.2	-0.5					
	9A	0.39	49	20.0	100–525	14	0.93	0.89	75.2	2.2	0.2	2.4	61.9 ± 0.9	63.9			2.5	-6.0	12.0	9.1					
	12A	0.16	141	2.9	100–450	9	0.74	0.83	11.5	5.0	0.9	10.3	45.0 ± 2.1	42.9			-4.5	-2.2	1.3	-6.9					
	13'A	0.04	12	8.4	100–600	17	0.94	0.93	42.5	2.2	0.4	1.9	59.0 ± 1.4	60.8			1.2	-1.6	0.7	-1.0					
14A	0.10	21	12.0	100–600	17	0.97	0.92	69.5	1.7	0.4	1.3	58.0 ± 0.9	62.1			5.7	-2.8	6.8	-2.6						
	15A	0.38	95	10.1	100–450	9	0.88	0.79	37.3	1.6	0.7	2.8	47.7 ± 0.9	45.0			-0.6	-1.4	1.0	-3.2					

Table 2 (Continued)

Name	Spl.	NRM (A/m)	χ ($\times 10^{-5}$)	Q_1	$T_{\min} - T_{\max}$ (°C)	n	f	g	q	MAD (°)	DANG (°)	CRM	$F \pm \sigma_F$ (μT)	$F_{\text{in}} \pm \text{S.D.}$ (μT)	F_{po} (μT)	F_{par} (μT)	F_{poor} (μT)	Alt	ΔM	Alt	F_{VDM} ($\times 10^{22}$ A/m 2)	Q	
MURK	3B	4.17	874	12.0	100–470	12	0.81	0.88	24.7	2.7	1.7	3.9	58.6 ± 1.6	58.0	59.8 ± 4.0	60.8	8.0	2.5	7.7	5.0	54.5 ± 5.7	62.7	11.1
	4A	0.35	73	12.1	100–530	14	0.87	0.91	58.3	2.2	1.0	3.3	62.3 ± 0.8	64.2	11.7	0.5	10.0	1.0	1.0	1.0	9.6	219	
	5A	1.64	225	18.3	100–560	15	0.89	0.92	44.8	2.4	2.0	2.6	64.1 ± 1.3	60.9	6.9	-4.3	5.1	-5.6					
	7A	1.51	312	12.2	100–440	11	0.52	0.90	8.6	5.6	4.0	6.0	60.4 ± 3.3	59.3	10.9	-1.2	11.1	0.0					
	8B	0.46	166	7.0	100–380	9	0.69	0.84	11.6	3.2	0.9	4.1	64.0 ± 3.5	63.2	4.9	-0.8	10.1	-10.5					
	10B	1.68	640	6.6	100–350	8	0.73	0.86	13.7	4.0	2.7	3.6	52.8 ± 2.2	53.0	17.6	-3.7	18.4	0.0					
	11B	0.49	320	3.9	100–350	8	0.71	0.84	11.3	5.6	2.7	7.0	52.8 ± 2.5	57.1	22.0	-6.0	23.2	-0.1					
	12A	0.04	16	5.9	100–410	10	0.74	0.83	27.9	4.2	1.3	6.0	65.5 ± 1.5	65.4	11.8	-1.3	13.3	-1.1					
	14A	4.10	746	13.8	100–410	9	0.80	0.62	18.1	4.2	0.3	6.7	56.8 ± 1.5	57.2	4.3	-1.3	4.7	3.0					

Name, name of the structure; Spl., sample number; NRM, intensity of the natural remanent magnetization in A/m; χ , initial susceptibility in 10^{-5} SI units; Q_1 , Koeningberger ratio for a magnetic field of $50 \mu\text{T}$; interval temperature $T_{\min} - T_{\max}$ used for the slope calculation; n , number of data points within this temperature interval; f , fraction of the NRM component used in the slope calculation; g , gap factor; q , quality factor; MAD, maximum angle of deviation; DANG, deviation angle; CRM, potential error on the estimation of the paleointensity due to the acquisition of CRM as a percentage of the applied field; $F \pm \sigma_F$, mean intensity and standard deviation per sample without anisotropy correction; F_{in} , mean intensity per sample with correction of anisotropy; $F_{\text{in}} \pm \text{S.D.}$, anisotropy corrected mean intensity and standard deviation; F_{po} , weighted mean intensity; ΔM (24 h), ΔM (48 h), alteration factors for a cooling time of 24 h (48 h); alt (24 h) (alt (48 h)), alteration factors for a cooling time of 24 h (48 h); F_{poor} , weighted mean intensity after cooling rate correction; F_{par} , weighted mean intensity at the latitude of Paris after cooling rate correction; VDM and VADM, values of the virtual dipole moment and virtual axial dipole moment calculated using the weighted mean intensities corrected for the effect of cooling rate upon TRM acquisition; $Q = N(q)$, site quality factor.

magnetization were found in our samples, the f parameters are not overestimated (Tauxe and Staudigel, 2004). Maximum acceptable values of the maximum angle of deviation (MAD) and deviation angle (DANG) were set to 10° (Pick and Tauxe, 1993) and following Chauvin et al. (2005) maximum potential error to the paleointensity caused by CRM acquisition (R parameter) must be lower than 15%. Finally, a maximum value of 10% was assigned to alteration tests carried out during the TRM anisotropy and cooling rate correction cycles (see Sections 3.2 and 3.3). The majority of our paleointensity determinations have f factors bigger than 0.6, MAD always lower than 6° and DANG lower than 5° (Fig. 9). Two samples showed CRM values bigger than 10%, but CRM is lower than 8% for the rest of the samples (Fig. 9, Table 2).

Four examples of NRM–TRM diagrams are plotted together with their corresponding orthogonal vector plots (Fig. 10). For the majority of our samples we observed a well-defined single component of magnetization going toward the origin, which likely corresponds to the TRM acquired during the last firing of the structures, before their abandonment. Two principal behaviors were found, a first one characterized by low unblocking temperature T_{ub} , at around 400°C (Fig. 10a and b), and a second one characterized with high T_{ub} at around 580 – 600°C (Fig. 10c and d). The mean paleointensity for each structure was determined using the weighting factor w proposed by Prévot et al. (1985) for each sample and the dispersion of the mean is expressed as the standard deviation (Table 2).

6.2. TRM anisotropy

The degree of TRM anisotropy k_1/k_3 (where k_1 and k_3 are the maximum and minimum axes of the tensor of TRM anisotropy) is typically lower than 14%, except for 5 baked clays and 13 bricks (Fig. 11a and b).

There is not a dominance of magnetic lineation or foliation (Fig. 11c and d), except for the kiln MURO where the magnetic lineation dominates (Fig. 12). On all studied sites, the principal axes of the anisotropy tensors did not show systematic directions (Fig. 12). These random directions explain the similarity of the mean direction and mean intensities per site before and after anisotropy correction.

6.3. Cooling rate dependence

Cooling rate dependence of the acquisition of TRM intensity was calculated for linear cooling times of 24 and 48 h. When the alteration factors are bigger than the

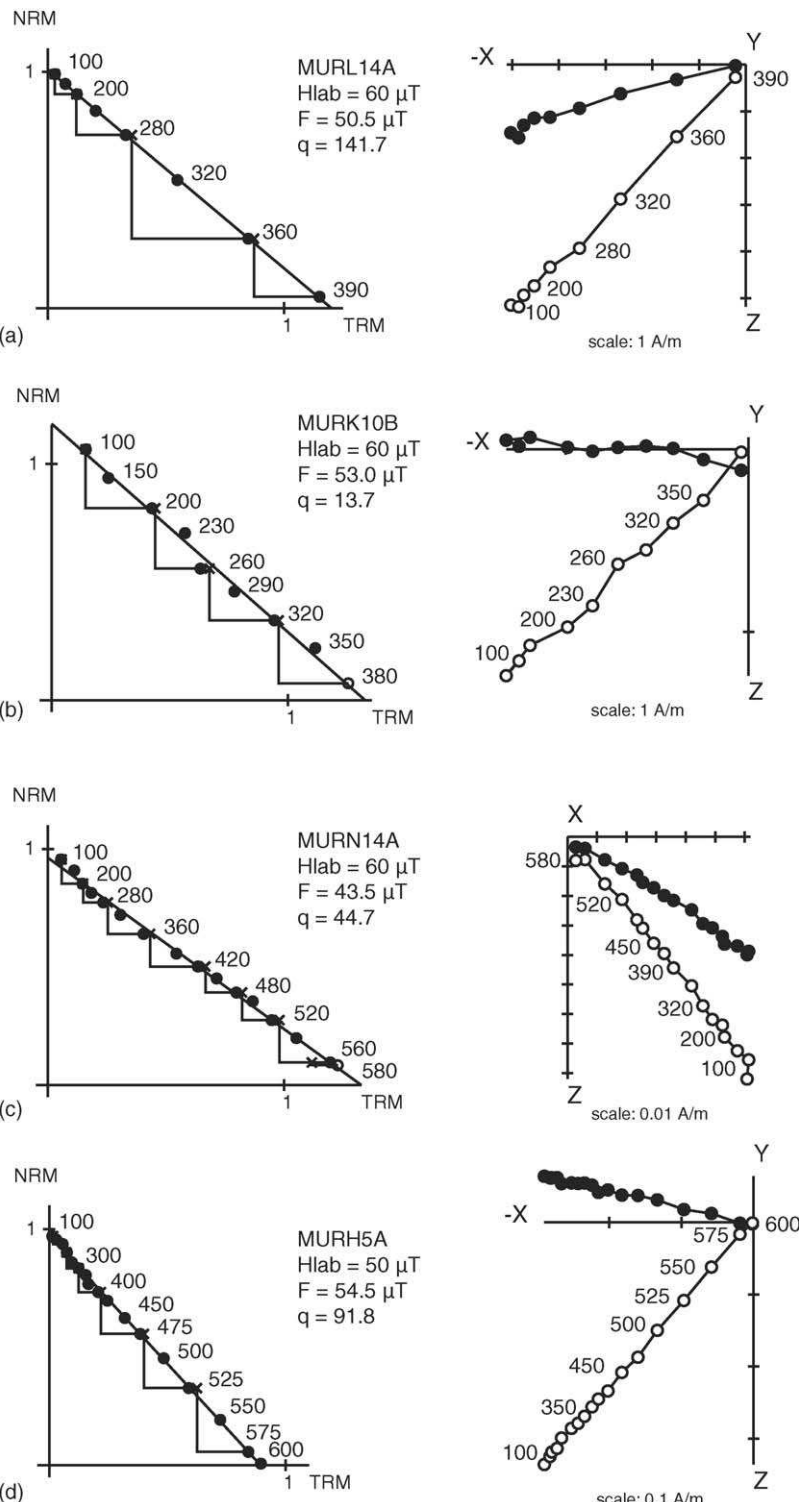


Fig. 10. Examples of NRM/TRM diagrams together with orthogonal vector projections of the remanent magnetization in sample coordinates. Open (solid) circles are projections upon vertical (horizontal) planes. Diagrams are normalized to the initial NRM intensity. Closed circles on the NRM/TRM diagrams are data used for archeointensity determinations. The laboratory field used H_{lab} during the Thellier experiments and the obtained F paleointensity together with the quality factor q are indicated. Temperatures are in °C.

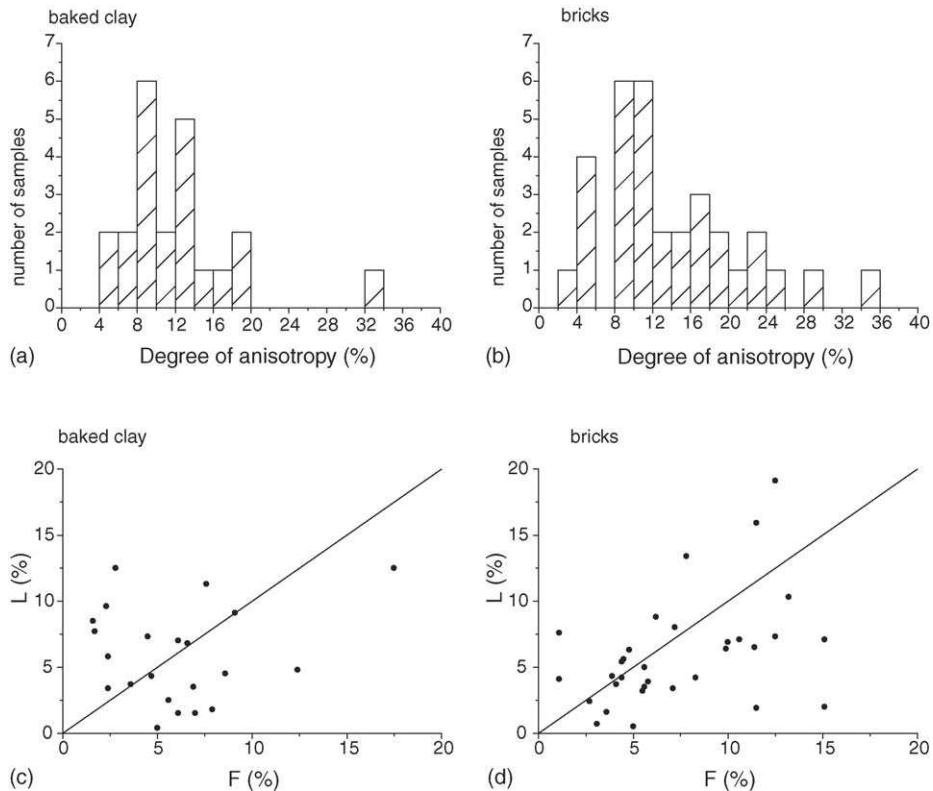


Fig. 11. Distribution of the degree of anisotropy of the TRM (a and b) and Flinn diagrams showing individual sample lineation L and foliation F data (c and d) for baked clay and for bricks.

correction factors no correction of the archeointensity determinations was applied (see Section 3.3, Table 2 and Fig. 13).

The correction upon the archeointensity for individual samples, for 24 h of cooling, is typically lower than 10% with an alteration factor lower than 5% (Table 2 and Fig. 13). This corresponds to a difference in the

mean archeointensity per kiln, which is very important for two kilns (16.7% for MURO and 10.3% for MURK), moderately significant for one kiln (4.9%, MURM) and not so significant (less than 3%) for the other four kilns (Table 2).

Generally only a very small increase in the correction factors was found when the experiments were performed

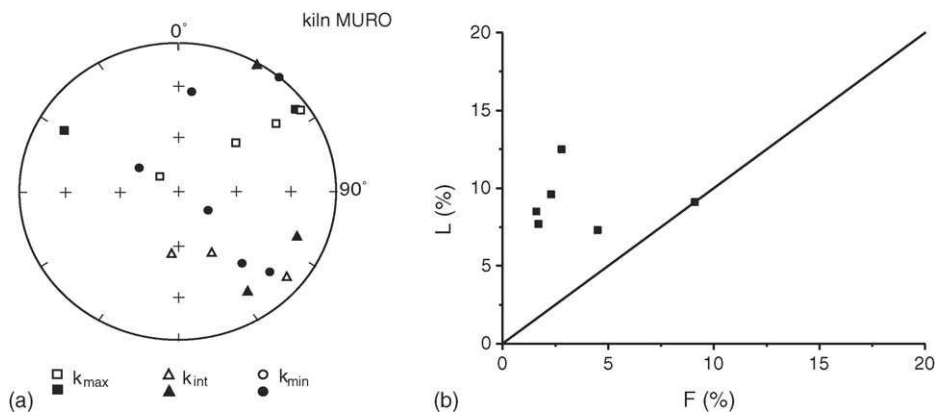


Fig. 12. (a) Kiln MURO: stereographic projection, in sample coordinates, of direction of the principal axes of the TRM anisotropy tensor, open symbols are projections on upper hemisphere; (b) Flinn diagram of individual samples, lineation and foliation data.

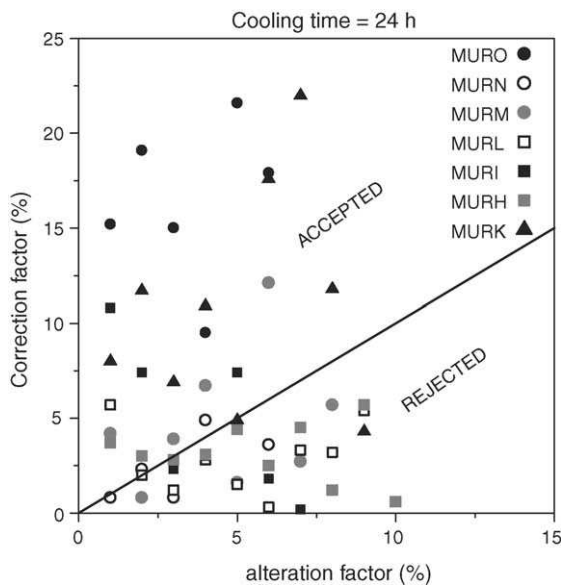


Fig. 13. Absolute values of the effect of cooling rate upon TRM intensity vs. variations of the TRM acquisition capacity (alteration factor) of our samples, for cooling times of 24 h (see text).

with a cooling time of 48 h (except for the site MURO). For this reason, and in order to retain the mean intensity values least affected by magneto-chemical changes, we believe that the mean intensity values corrected for a cooling time of 24 h are the most reliable estimates

of archeointensity. In some cases (see Table 2) negative cooling rate correction factors were found. A decrease of the TRM intensity as the cooling rate increases was previously associated to multidomain (MD) magnetic grains behavior (McClelland-Brown, 1984). However the linearity of our NRM–TRM diagrams indicates the dominance of SD grains in our samples.

No clear relationship between the cooling rate correction factor and other magnetic parameters were observed. Further investigations are needed to better understand which parameters (for example grain size, chemical composition) play an important role in the cooling rate effect, and how they act.

7. Results and discussion

Before cooling rate correction, standard deviations (S.D.) lower than 7% of the mean archeointensity are observed for four of the seven studied structures (Table 2). For the other three kilns (MURH, MURN and MURO) the S.D. of the mean intensity is greater, between 12 and 17%. The scatter within sites is not reduced after the cooling rate correction; however, the dispersion between sites is considerably reduced (Fig. 14 and Table 2). Our results also appear closer, after correction (Fig. 14b), to the other data published for the same time period.

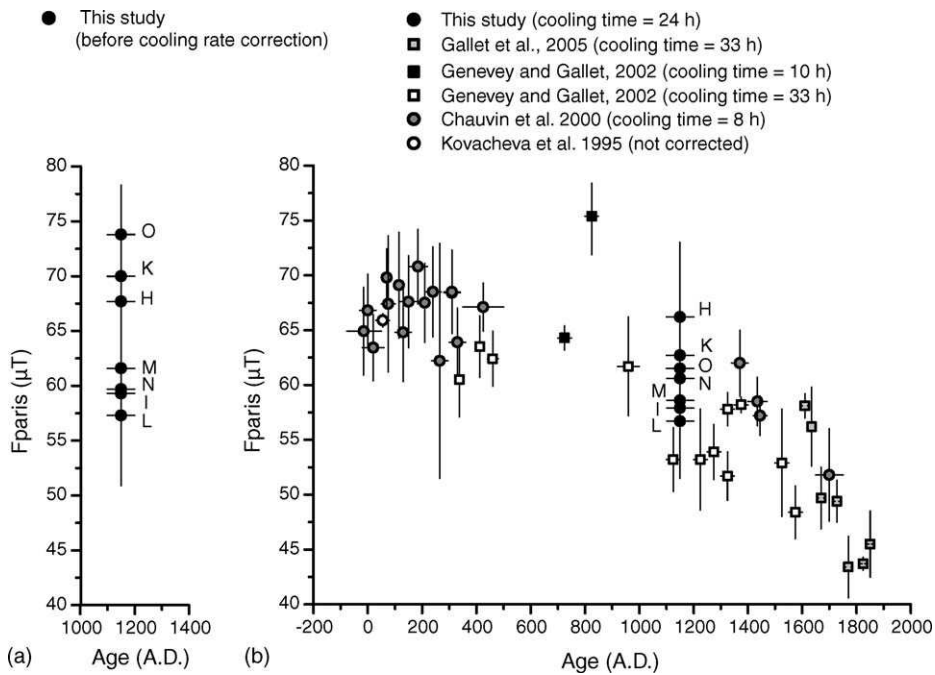


Fig. 14. Comparison between intensity data available for Western Europe and (a) our data before cooling rate correction, (b) our data corrected for the effect of cooling rate upon TRM intensity acquisition.

Assuming that all the sites have exactly the same age, the mean intensity for the seven structures and the corresponding S.D. can be calculated following the Bayesian hierarchical model described by [Lanos et al. \(2005\)](#). The uncorrected mean intensity \pm S.D. at the latitude of Paris is $64.2 \pm 5.8 \mu\text{T}$, and after cooling rate correction is $60.3 \pm 3.3 \mu\text{T}$, both at 95% confidence level. In this study the cooling rate corrections reduce by almost 45% the standard deviation of the mean intensity, suggesting the importance of such a correction.

However, even with the cooling rate correction performed, we find some differences between the seven site mean intensities (from 66.2 to $56.7 \mu\text{T}$ at the latitude of Paris). This could be explained by several factors: (a) errors due to a wrong estimate in the ancient cooling time for each structure; (b) the sites do not have the same age within the interval of age proposed by the archeologist; and/or (c) the precision of the archeointensity estimations (related to the experimental procedures used and the material studied) is not sufficient to obtain more accurate results.

The hypothesis (a) could explain part of the observed dispersion between sites. However in this study two linear cooling times (24 and 48 h) were investigated and no important differences were found for six of the seven studied structures, suggesting that the choice between these two cooling times is not fundamental.

The hypothesis (b) is clearly true for kilns MURO-N-M-L that could not be in use exactly at the same time as they are different phases of the same structure. If we take into account the stratigraphic order (MURO-N-M-L from the older to the younger one) proposed by archeologists, our mean results for these four kilns, after cooling rate correction, indicate that a decrease in the geomagnetic field intensity of around 8% (from 61.5 to $56.7 \mu\text{T}$) occurred in Spain during the XII century.

On the basis of our intensity results, as well as the variation of the geomagnetic field in Western Europe known at present ([Fig. 14](#)) we can suggest that the kiln MURH, and probably also the kiln MURK, are older than the five other structures. In order to verify the ages proposed, we tried to date our structures by comparison of the characteristic archeomagnetic directions with the French SV curve. For this purpose we calculated the age probability density at 95% confidence level. For all the structures the results obtained include the 1100–1200 interval considered in this study, suggesting that the dates proposed are rather good. However, for the kilns with higher values of α_{95} the intervals obtained are very large (1070–1324 for MURO and 1082–1355 for MURI). For the other five kilns the upper age limit found is no more than 1250 A.D. and the lower limit no less than 1050 A.D.

No differences or chronological order can be deduced from this analysis.

The archeological constraints and the very similar directions of the characteristic remanent magnetization of our seven structures ([Table 1](#)) clearly support the idea that the differences in age are not very important, and anyway always inside the period between 1100 and 1200 A.D.

Finally, the last hypothesis (c), related to the precision limit of the experimental procedure for the archeointensity determination, should not be forgotten and must be taken into account in the interpretation of intensity data. If we consider the paleointensity technique used, the type of material and the number of samples studied per site, we can attribute to our seven sites a “weighting factor of quality” of 16 (see [Chauvin et al., 2000](#)). The site quality factors Q ([Chauvin et al., 2005](#)) are quite high (see [Table 2](#)). In a recent paleointensity study of six historical lava flows from Hawaii ([Chauvin et al., 2005](#)), erupted between 1950 and 1982, the observed mean site paleointensities were typically within 10% of the Definitive Geomagnetic Reference Field and the dispersion between sites was around 15%. In our archeointensity data the between sites dispersion is of the same order of magnitude. We suggest that these values represent the precision limit of the Thellier method.

The differences between mean site intensities obtained in this study confirm the need to obtain several intensity data per century in order to construct a reliable intensity curve and to describe the evolution of the Earth's magnetic field; otherwise our knowledge of Earth's intensity evolution could be strongly biased. Care must be taken with interpretation of peaks on the intensity evolution of the Earth's magnetic field derived from a little number of data. Further investigations are needed in order to confirm the relative intensity maxima proposed by [Gallet et al. \(2005\)](#) and [Genevey and Gallet \(2002\)](#) as well as the proposed relationship between intensity changes of the Earth's magnetic field and climate changes at century scales.

[Fig. 14](#) shows the present day knowledge for the evolution of the geomagnetic field intensity in Western Europe for the last two millennia. The data confirm an important drop in the geomagnetic field intensity between the IX and the XIX centuries, changing from a possible mean of around 75 to around $45 \mu\text{T}$ at the latitude of Paris.

8. Conclusions

Variations of low field susceptibility versus temperature, hysteresis measurements, IRM acquisitions curves

and the almost ideal behavior of our samples during Thellier experiment strongly suggest that the principal carrier of the remanent magnetization in our samples is a single domain Ti-rich titanomagnetite. The possibility of a stable Al-, Na- or Mg-substituted maghemite could not be discarded. Archeological constraints and archeomagnetic mean directions of magnetization indicate that the seven sampled kilns were abandoned between 1100 and 1200 A.D. TRM anisotropy correction is not significant in the determination of the mean directions of magnetization and mean paleointensities per site in our samples, composed of burnt clay and/or bricks. In contrast, the cooling rate corrections reduce by almost 45% the standard deviation of the mean intensity between sites, suggesting the importance of such a correction in this kind of study. Our data provide a robust mean intensity ($60.3 \pm 3.3 \mu\text{T}$ at the latitude of Paris) and a VDM mean value ($10.7 \times 10^{22} \text{ A m}^2$) for the middle of the XII century in Western Europe and better constrain the evolution of the geomagnetic field intensity during medieval times in this area. We suggest that the dispersion observed between the seven mean archeointensities is not explained by errors in the age estimation of the sites or in the cooling rate used in our corrections. This dispersion seems related to the experimental procedure and sampled materials. It appears then, that even with data which satisfy all quality criteria, several archeointensity determinations per century are clearly needed in order to build a reliable reference curve.

Acknowledgements

M. Gómez-Paccard acknowledges a fellowship from the AARCH Network (Archeomagnetic Applications for the Rescue of Cultural Heritage), Contract EU: HPRN-CT-2002-00219. We wish to thank M. Hill, P. Roperech and two anonymous reviewers for their constructive comments which improved the manuscript both in substance and style. We wish to thank the paleomagnetic laboratory of the University Complutense de Madrid and the CMEBA of the University of Rennes 1 for their help with hysteresis and SEM experiments, respectively.

References

- Arrighi, S., Rosi, M., Tanguy, J.C., Courtillot, V., 2004. Recent eruptive history of Stromboli (Aeolian Islands, Italy) determined from high-accuracy archeomagnetic dating. *Geophys. Res. Lett.* 31, L19603, doi:10.1029/2004GL020627.
- Batt, C.M., 1997. The British archeomagnetic calibration curve: an objective treatment. *Archaeometry* 39, 153–168.
- Biquand, D., 1994. Effet de la vitesse de refroidissement sur l'intensité de l'aimantation thermorémanente: étude expérimentale, conséquences théoriques. *Can. J. Earth Sci.* 31, 1342–1352.
- Casas, L., Shaw, J., Gich, M., Share, J.A., 2005. High-quality microwave archaeointensity determinations from an early 18th century A.D. English brick kiln. *Geophys. J. Int.* 161, 653–661.
- Chauvin, A., Garcia, Y., Lanos, Ph., Laubenheimer, F., 2000. Paleointensity of the geomagnetic field recovered on archaeomagnetic sites from France. *Phys. Earth Planet. Inter.* 120, 111–136.
- Chauvin, A., Roperech, P., Levi, S., 2005. Reliability of geomagnetic paleointensity data: the effects of the NRM fraction and concave-up behavior on paleointensity determination by Thellier method. *Phys. Earth Planet. Inter.* 150, 265–286.
- Coe, R.S., Grommé, C.S., Mankinen, E.A., 1978. Geomagnetic paleointensities from radiocarbon-dated lava flows on Hawaii and the question of the Pacific nondipole low. *J. Geophys. Res.* 83, 1740–1756.
- Day, R., Fuller, M., Schmidt, V.A., 1977. Hysteresis properties of titanomagnetites: grain-size and compositional dependence. *Phys. Earth Planet. Inter.* 13, 260–267.
- Dunlop, D.J., 2002. Theory and application of the Day plot (Mrs/Ms versus Hcr/Hc). 1. Theoretical curves and tests using titanomagnetite data. *J. Geophys. Res.* 107 (B3), 2056, doi:10.1029/2001JB000486.
- Fisher, R.A., 1953. Dispersion on a sphere. *Proc. Roy. Soc. London, Ser. A* 217, 295–305.
- Fox, J.M.W., Aitken, M.J., 1980. Cooling rate dependence of thermoremanent magnetization. *Nature* 283, 462–463.
- Gallet, Y., Genevey, A., Le Goff, M., 2002. Three millennia of directional variation of the Earth's magnetic field in Western Europe as revealed by archeological artefacts. *Phys. Earth Planet. Inter.* 131, 81–89.
- Gallet, Y., Genevey, A., Fluteau, F., 2005. Does Earth's magnetic field secular variation control centennial climate change? *Earth Planet. Sci. Lett.* 236, 339–347.
- Garcia, Y., 1996. Variation de l'intensité du champ magnétique terrestre en France durant les deux derniers millénaires. Ph.D. Thesis. Université de Rennes 1, Rennes, France.
- Genevey, A., Gallet, Y., 2002. Intensity of the geomagnetic field in Western Europe over the past 2000 years: new data from ancient French pottery. *J. Geophys. Res.* 107 (B11), 2285, doi:10.1029/2001JB000701.
- Gómez-Paccard, M., Catanzariti, G., Ruiz, V.C., McIntosh, G., Nuñez, J.I., Osete, M.L., Lanos, Ph., Chauvin, Tarling, D.H., Bernal-Casasola, D., Thiriot, J., Archaeological Working Group, 2006. A catalogue of Spanish archaeomagnetic data. *Geophys. J. Int.*, in press.
- Halgedahl, S.L., Day, R., Fuller, M., 1980. The effect of the cooling rate on the intensity of weak-field TRM in single-domain magnetite. *J. Geophys. Res.* 85, 3690–3698.
- Jasonov, P.G., Nurgaliev, D.K., Burov, D.V., Heller, F., 1998. A modernized coercivity spectrometer. *Geol. Carpath.* 49 (3), 224–225.
- Kirschvink, J.L., 1980. The least-squares line and plane and the analysis of paleomagnetic data. *Geophys. J. Roy. Astron. Soc.* 62, 699–718.
- Korte, M., Genevey, A., Constable, C.G., Frank, U., Schnepf, E., 2005. Continuous geomagnetic field models for the past 7 millennia. 1. A new global data compilation. *Geochem. Geophys. Geosyst.* 6 (2), 1–32.
- Kovacheva, M., Parés, J.M., Jordanova, N., Karloukovski, V., 1995. A new contribution to the archaeomagnetic study of a Roman pottery kiln from Calahorra (Spain). *Geophys. J. Int.* 123, 931–936.

- Kovacheva, M., Jordanova, N., Karloukovski, V., 1998. Geomagnetic field variations as determination from Bulgarian archaeomagnetic data. Part II. The last 8000 years. *Sur. Geophys.* 19, 431–460.
- Lanos, Ph., 2004. Bayesian inference of calibration curves: application to archaeomagnetism. In: Buck, C.E., Millard, A.R. (Eds.), *Tools for Constructing Chronologies: Crossing Disciplinary Boundaries*, Lecture Notes in Statistics, Springer, London, pp. 43–82.
- Lanos, Ph., Le Goff, M., Kovacheva, M., Schnepp, E., 2005. Hierarchical modelling of archaeomagnetic data and curve estimation by moving average technique. *Geophys. J. Int.* 160, 440–476.
- Lowrie, W., 1990. Identification of ferromagnetic minerals in a rock by coercivity and unblocking temperature properties. *Geophys. Res. Lett.* 17, 159–162.
- Márton, P., 2003. Recent achievements in archaeomagnetism in Hungary. *Geophys. J. Int.* 153, 675–690.
- McClelland-Brown, E., 1984. Experiments on TRM intensity dependence on cooling rate. *Geophys. Res. Lett.* 11, 205–208.
- Néel, L., 1955. Some theoretical aspects of rock-magnetism. *Adv. Phys.* 4, 191–243.
- Peters, C., Dekkers, M.J., 2003. Selected room temperature magnetic parameters as a function of mineralogy, concentration and grain size. *Phys. Chem. Earth* 28, 659–667.
- Pick, T., Tauxe, L., 1993. Holocene paleointensities: Thellier experiments on submarine basaltic glass from the East Pacific Rise. *J. Geophys. Res.* 98 (B10), 17949–17964.
- Prévot, M., Mankinen, E.A., Coe, R.S., Grommé, C.S., 1985. The Steens Mountain (Oregon) geomagnetic polarity transition. 2. Field intensity variations and discussion of reversal models. *J. Geophys. Res.* 90, 10417–10448.
- Schnepp, E., Lanos, Ph., 2005. Archaeomagnetic secular variation in Germany during the past 2500 years. *Geophys. J. Int.* 163, 479–490.
- Stacey, F.D., Bajernee, S.K., 1974. *The Physical Principles of Rock Magnetism*. Elsevier, New York, p. 195.
- Tanguy, J.C., Le Goff, M., Chillemi, V., Paiotti, A., Principe, C., La Delfa, S., Patanè, G., 1999. Variation séculaire de la direction du champ géomagnétique enregistrée par les laves de l'Etna et du Vésuve pendant les deux derniers millénaires. *C.R. Acad. Sci. Paris* 329, 557–564.
- Tauxe, L., 1998. *Paleomagnetic Principles and Practice*. Kluwer Academic Publishers, Boston, MA, p. 299.
- Tauxe, L., Staudigel, H., 2004. Strength of the geomagnetic field in the Cretaceous normal superchron: new data from submarine basaltic glass of the Troodos Ophiolite. *Geochem. Geophys. Geosyst.* 5, doi:10.1029/2003GC000635, Q02H06.
- Thellier, E., Thellier, O., 1959. Sur l'intensité du champ magnétique terrestre dans le passé historique et géologique. *Ann. Géophys.* 15, 285–376.
- Veitch, R.J., Hedley, G., Wagner, J.J., 1984. An investigation of the intensity of the geomagnetic field during Roman times using magnetically anisotropic bricks and tiles. *Arch. Sci. (Geneva)* 37 (3), 359–373.
- Walton, D., 1980. Time–temperature relations in the magnetization of assemblies of single domain grains. *Nature* 286, 245–247.

3.2. Article: Evolution of the geomagnetic field intensity in Western Europe for the last 2000 years inferred from Bayesian statistics: 17 new archeointensity data from seven Spanish archeological sites (à soumettre à Journal Geophysical Research)

M. Gómez-Paccard ^{a, b, c *}, A. Chauvin ^a, Ph. Lanos ^b, J. Thiriot ^d

^aGéosciences-Rennes, CNRS, UMR 6118, Université de Rennes 1, Campus de Beaulieu, 35042, Rennes, Cedex, France.

^bCivilisations Atlantiques et Archéosciences, CNRS, UMR 6566, Université de Rennes 1, Campus de Beaulieu, 35042, Rennes, Cedex, France.

^cUniversidad Complutense de Madrid, Facultad de Ciencias Físicas, Ciudad Universitaria, 28040, Madrid, Spain.

^dLaboratoire d'archéologie médiévale méditerranéenne, CNRS, UMR 6572, Maison méditerranéenne de Sciences de l'Homme, 13094, Aix-en-Provence, Cedex 2, France.

* Corresponding author: Tel.: +33-2-23-236759. Fax: +33-2-23-236040. E-mail address: miriam.gomez@univ-rennes1.fr

Keywords

Thellier method; archeointensity; Bayesian statistics; Western Europe

Abstract

We studied one roman pottery kiln, 15 kilns with ages ranging between 1000 AD and 1959 AD, a group of large jars fragments dated between 1275 and 1300 AD and a group of baked bricks dated between 1825 and 1845 AD. The samples were analysed using the Thellier method. The intensity values were corrected for thermoremanent magnetization (TRM) anisotropy. In the majority of the studied sites this correction is not very important, except for the bricks for which the uncorrected mean intensity differs in more than 5% from the corrected value. The cooling rate dependence upon TRM acquisition has been also studied. Cooling rate correction factors per sample up to 15% and per site up to 7.7% have been obtained. Our new 17 data, together with 62 previous results from France, Denmark and Spain, have been used to construct the geomagnetic field intensity variation curve for Western Europe. The Bayesian model was used for this purpose. The obtained curve indicate that the geomagnetic intensity remain more or less constant between the 1st and 4th centuries, and between the 13th and 15th centuries (mean values around 65 and 57 μ T respectively), whereas an important decrease occurs during the last 5 centuries. Finally, the evolution of the EMF intensity during High Middle Ages remains uncertain. The global geomagnetic models of Hongre and Korte and Constable were used to predict the intensity evolution at Paris for the last 2000 years. The intensity predictions of Korte and Constable models agree better than Hongre predictions with our obtained curve. In contrast the dipole moment obtained using Korte and Constable models seems to be underestimated for the first millennium AD. The dipole moment evolution obtained by Hongre model agree better with the VADM evolution obtained in this work or in the archeointensity compilation of Yang for the last two millennia.

1. Introduction

The study of the evolution of the geomagnetic field requires widely distributed high-resolution magnetic records of the Earth's magnetic field. Prior to times of direct measurements (a massive compilation of historical observations of the geomagnetic field made in magnetic observatories or taken by mariners can be found in *Jackson et al.*, [2000]), this purpose could be achieved by studying the remanent magnetization of archeological material, lava flows and lake sediments. Volcanic rocks sometimes lead to low success rate or paleointensity determinations which are difficult to interpret due to the low stability of the magnetic minerals during heating. Sedimentary rocks can provide only a continuous record of the relative paleointensity changes, and the translation towards an absolute scale is not always easy. In contrast, archeomagnetic materials acquire a thermoremanent magnetization (TRM) that can be used to obtain at the same time the paleodirection and the absolute paleointensity of the Earth's magnetic field. In addition, magnetic minerals in the archeomagnetic samples generally show a good physico-chemical stability during heatings which is traduced in an easy interpretation and high success rates (often 80% or more) of the paleointensity experiments. Then, archeomagnetic studies of well-dated material can provide the highest resolution description of the full-vector Earth's magnetic field over the last millennia.

Archeomagnetic, volcanic and sedimentary paleomagnetic data can be used to compute spherical harmonic models of the geomagnetic field (see for example *Hongre et al.*, [1998]) that can offer better insight into the field evolution and underlying processes at the core mantle boundary than individual times series. A global data set of archeomagnetic and paleomagnetic data –including intensity data- covering the past 7000 years has been recently compiled by *Korte et al.* [2005]. This data set has been used to construct continuous global geomagnetic field models for the last millennia [*Korte and Constable*, 2005]. From these models, the evolution of the dipole moment during the last millennia can be obtained. The dipole moments predicted by *Korte and Constable* [2005] models are significantly lower than the dipole moment predicted by *Hongre et al.* [1998] models or the virtual axial dipole moment (VADM) variations published by *Yang et al.* [2000]. The evolution, during the last two millennia, of the geographical coordinates of the North geomagnetic pole predicted by both models is also different. These differences proved the need to obtain more directional and intensity data in order to improve our knowledge of the evolution of the Earth's magnetic field.

Archeomagnetic research started in France with the work of E. Thellier [Thellier, 1938; Thellier and Thellier, 1959] and has progressed to the stage where several directional secular variation curves are now available for Europe, including France [Gallet *et al.*, 2002], Germany [Schnepp and Lanos, 2005], Hungary [Márton, 2003], Bulgaria [Kovacheva *et al.*, 1998], Great Britain [Batt, 1997] and Spain [Gómez-Paccard *et al.*, 2006b and Gómez-Paccard *et al.*, submitted]. Archeointensity data are also available for Western Europe. Chauvin *et al.* [2000] provided 20 archeointensity data for France and compiled the archeointensity results available for Western Europe for the last two millennia. This study shows that the reliability of some of these results seems questionable because they were obtained using unreliable paleointensity techniques and/or with very few samples per site. Since then, 21 new reliable results obtained from French pottery fragments were published [Genevey and Gallet, 2002; Gallet *et al.*, 2005]. In Spain, one archeointensity data, obtained from a Roman pottery kiln, was published in 1995 [Kovacheva *et al.* 1995] and seven others were obtained from medieval kilns located in the city of Murcia [Gómez-Paccard *et al.*, 2006a].

We have investigated 15 kilns, a group of bricks and a group of large jars fragments coming from seven Spanish localities. Our study provides 17 new intensity data. They were combined with the most reliable data previously published in order to build the curve of the variations of the paleointensity of the geomagnetic field over Western Europe during the last 2000 years. This curve was inferred from Bayesian statistics [Lanos, 2004] and was calculated using 78 data. The intensity reference curve proposed should also be useful for future archeomagnetic dating in this region, especially in the case of displaced objects.

2. Archeological dating and sampling

The locations of the archaeological excavations where the material was sampled are shown in Figure 1. Fifteen kilns were sampled. Between 12 and 22 independently oriented samples were collected per kiln. The samples, taken from the walls, were composed of burnt clay, bricks or a mixture of them and were oriented by the magnetic and solar compass on the horizontal plane of plaster coverage. Nine infill bricks (bricks GUA2 found in the kiln GUA2) and 5 jars fragments (jars fragments CERCALB made on the kiln CALB) were also collected. In the laboratory, one standard paleomagnetic core was drilled per archeomagnetic sample. The dating of the structures (Table 1), mainly based on archaeological constraints, is widely

reported in Gómez-Paccard *et al.* [2006b]. The age of the studied samples ranges between the 2nd century and the 20th centuries AD.

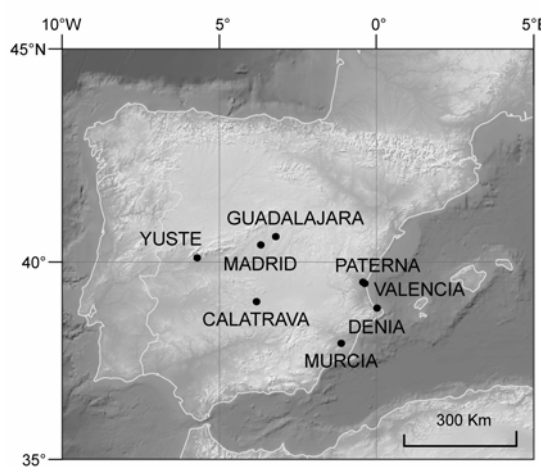


Figure 1: Map of Spain showing the location of the archeomagnetic sites where our samples were collected and Madrid

Directional results [Gómez-Paccard et al.]													
No	Name	Lat (°N)	Long (°E)	t _{min}	t _{max}	Meth.	n	D _s	I _s	k	α ₉₅	Site	Structure
1	DENA	38.86	0.02	220	250	arch	10	-4.5	52.6	669	1.9	Setla Mirarosa Miraflor	kiln
2	MURG	37.98	-1.12	1000	1100	arch	8	21.7	51.3	1437	1.5	Murcia c/Sagasta	glass making kiln
3	CALA	39.02	-3.82	1275	1300	arch/his	8	11.4	44.9	356	2.9	Calatrava la Vieja	pottery kiln
4	CALB	39.02	-3.82	1275	1300	arch/his	10	7.1	44.4	284	2.9	Calatrava la Vieja	pottery kiln
5	CERCALB (*)	39.02	-3.82	1275	1300	arch/his						Calatrava la Vieja	jars fragments made on CALB
6	VALN	39.47	-0.37	1238	1350	arch	9	2.1	46.6	1859	1.2	Valencia Velluters	bricks making kiln
7	VALI	39.47	-0.37	1238	1400	arch	11	4.4	46.4	725	1.7	Valencia Velluters	bricks making kiln
8	VALK	39.47	-0.37	1300	1450	arch	9	3.0	44.2	1606	1.3	Valencia Velluters	glass making kiln
9	VALM	39.47	-0.37	1300	1450	arch	9	7.2	47.0	2733	1.0	Valencia Velluters	glass making kiln
10	CALC	39.02	-3.82	1400	1420	arch/his	8	3.0	47.0	790	2.0	Calatrava la Vieja	pottery kiln
11	PATA	39.50	-0.43	1450	1500	arch	10	3.6	56.4	792	1.7	Paterna c/Huertos	pottery kiln
12	PATJ	39.50	-0.43	1429	1611	C14	16	6.6	62.2	1201	1.1	Paterna Testar del Moli	pottery kiln
13	PATH	39.50	-0.43	1450	1600	arch	10	7.3	53.5	831	1.7	Paterna Testar del Moli	pottery kiln
14	PATB	39.50	-0.43	1525	1650	arch	11	5.8	64.1	827	1.6	Paterna c/Huertos	pottery kiln
15	VALL	39.47	-0.37	1575	1625	arch	11	9.1	56.6	557	1.9	Valencia Velluters	kiln
not studied here	GUA2	40.60	-3.20	1825	1845	arch/his	13	-21.1	61.5	238	2.7	Guadalajara, Huertas del Carmen	furnace
16	BRICKS GUA2 (*)	40.60	-3.20	1825	1845	arch/his							Brick fragments made on GUA2
17	YUS2	40.10	-5.70	1959	1959	his	5	-11.1	58.2	138	6.5	Monastery at Yuste	kiln

Table 1: Location and ages of the different group of samples studied and archaeomagnetic directions obtained by Gómez-Paccard et al. [2006b]. Columns from left to right:

No, number; Name, name; Lat. and Long., latitude and longitude of the sampling site; t_{min}, minimum age in years AD; t_{max}, maximum age in years AD; Meth., method of dating (arch.: archaeological age estimate, hist: historical document, C14: conventional ¹⁴C); n, samples taken into account in the calculation of the mean site direction D_s and I_s, declination and inclination in situ; k and α₉₅, precision parameter and 95 % confidence limit of characteristic remanent magnetisation; Site; site name; Structure, kind of structure.

(*) number 5 are pottery fragments made on the kiln CALB (No 4) and number 16 are brick fragments made on the kiln GUA2.

3. Archeomagnetic directions

Remanent magnetization was measured with a Molspin spinner or JR5 (AGICO) magnetometers and low field susceptibility with a Bartington susceptibility meter at the paleomagnetic laboratory of Géosciences-Rennes.

Our samples are characterized by a NRM lower than 13 A/m and low field susceptibility between 10^{-4} and 10^{-2} SI units (Figure 2). NRM intensity and low field susceptibility are scattered both between and within sites.

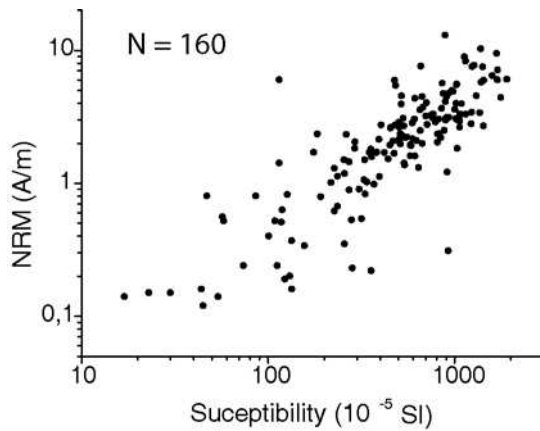


Figure 2: NRM intensity (A/m) versus susceptibility (10^{-5} SI units) for all our samples.

The original Thellier paleointensity method [Thellier and Thellier, 1959], based on the comparison between natural remanent magnetization (NRM) lost and partial thermoremanent magnetization (pTRM) gained in a known laboratory field was used in order to determine simultaneously the characteristic directions of magnetization and the paleointensities on all the sites except the site GUA2. Archeomagnetic directions of the site GUA2 were obtained by classical thermal demagnetization of samples taken from the walls of the structures where the bricks, studied for paleointensity, were manufactured and heated (see [Gómez-Paccard *et al.*, 2006b]). On all the other sites the characteristics directions and the paleointensities have been calculated using the same temperature interval.

The archeomagnetic directions obtained are described in more detail in a previous study [Gómez-Paccard *et al.*, 2006b]. The spectrum of the unblocking temperatures observed

ranges between 350°C and 600°C, except for two samples of YUS2 with unblocking temperatures up to 675°C

In most cases high quality, single component of magnetization were obtained which likely corresponds to the TRM acquired during the last firing of the structures, related to their abandon. A low temperature secondary component (probably a viscous magnetization) was observed on only 5% of the studied samples. For three samples of the kilns YUS2 (11A3, 13A3 and 23A1) two components have been detected. The direction of the low temperature component (which is not going toward the origin) is the same on the 3 samples and is similar to the directions found on the other two studied samples from YUS2 (41A2 and 43A3), where only a well defined univectorial component is observed. This low temperature component has been interpreted as the magnetization acquired during the last firing of the structure. The direction of the high temperature component is scattered and has been interpreted as the original magnetization acquired by the bricks when they were made. These 3 samples were situated at the bottom of the structure and are clearly less heated than the other two located at the top of the structure.

The characteristic directions and their statistical parameters were calculated using principal component analysis [Kirschvink, 1980] and Fisher [1953] statistics. Figure 3 and Table 1 show the results obtained together with the secular variation curve for Iberia (*Gómez-Paccard et al.*, submitted, 2006]. The archeomagnetic directions are generally well determined with α_{95} lower than 3°, except for the kiln YUS2 ($\alpha_{95}= 6.5^\circ$) where in some samples, two archeomagnetic directions were detected. However, the mean archeomagnetic direction of YUS2 agrees well with the observatory data available for the Iberian Peninsula (see Figure 3). Mean directions of magnetization for archeomagnetic structures of the same age (Table 1 and Fig. 3) are in agreement, for example CALA-B, VALN-I, or PATH-A. The structures PATB and PATJ, with large age uncertainty, seem to be contemporaneous. One can note that stratigraphic constraints observed during excavations prove also that the site PATB is younger than the site PATA (see *Gómez-Paccard et al.* [2005b]).

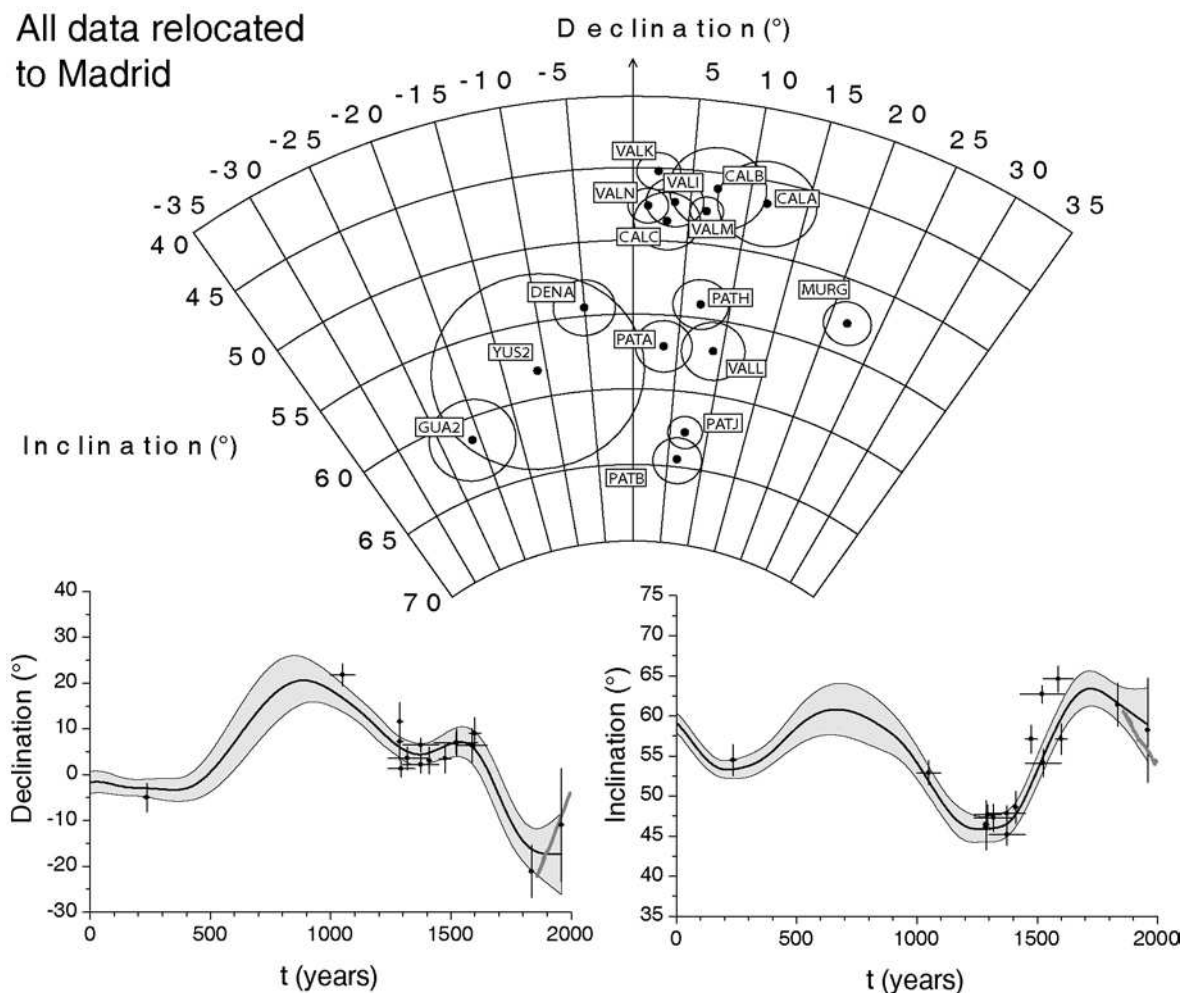


Figure 3: a) Stereographic projection of mean directions of magnetization with α_{95} error circles of the studied Spanish structures, b) and c) declination and inclination of mean direction together with the Iberian secular variation curve and its enveloppe error. Grey curve: observatory data available for the Iberian Peninsula since the middle of the 19th century [Gomez-Paccard et al., submitted, 2006]. All data are relocated to Madrid.

4. Magnetic mineralogy

Low field susceptibility versus temperature curves (K-T curves), isothermal remanent magnetization (IRM) acquisition and thermal demagnetization of composite IRM have been carried out in order to determine the principal magnetic carrier in our samples. Thermomagnetic curves were performed in air using a KLY3 (Agico) susceptibility meter with fitted furnace. Isothermal remanent magnetization (IRM) was obtained using an ASC Scientific impulse magnetizer.

One sample has been also analysed by scanning electron microscopy (SEM) and energy dispersive X-ray analysis. In next sections we describe these experiments.

4.1. KT curves

A total of 109 K-T curves up to 700°C were determined. Heating and cooling curves are reasonably reversible, suggesting that few mineralogical changes occurred during heating (Figure 4). Curie temperatures (T_c) between 350°C and 650°C were observed. In some cases only one magnetic phase is present and in others two magnetic phases, one of low T_c (around 350-400°C) and another of high T_c (see Figure 4b). Generally this high Curie Temperature range between 550 and 585°C. Some samples have a T_c higher than 585°C, which can be interpreted in terms of partially oxidised (titano)magnetite or (titano)maghemite or hematite (see Figure 4d). Thermomagnetic curves suggest that the principal magnetic phases present in our samples are magnetite or titanomagnetite with different Ti content. The determined Curie points are in agreement with the unblocking temperatures observed during Thellier experiments.

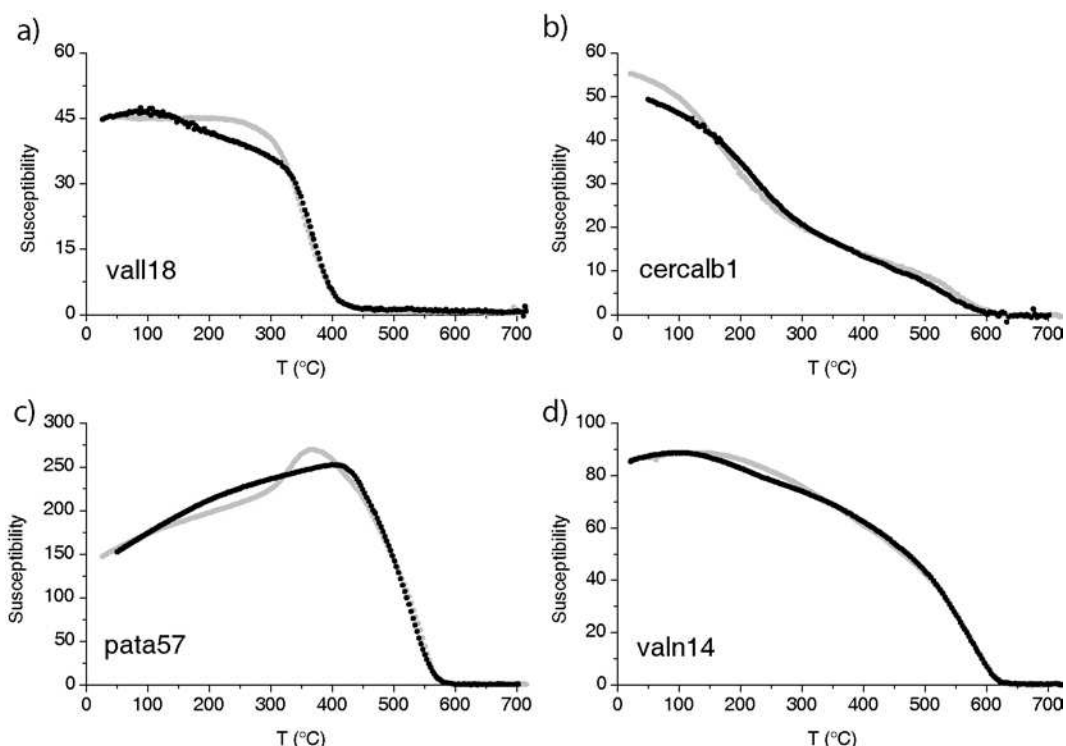


Figure 4. Examples of typical susceptibility versus temperature curves (K-T curves). Temperatures are in degrees Celsius and susceptibilities in arbitrary units. Heating (cooling) branches are plotted in black (grey) circles.

4.2. IRM acquisition and thermal demagnetization of composite IRM

Fifty-five samples (from all studied sites) were analysed by progressive acquisition of isothermal remanent magnetization (IRM). In most cases saturation is reached for fields between 50 and 150 mT (Figure 5). This suggests that magnetization is carried by low coercivity magnetic minerals such as titanomagnetite or magnetite. A gradual increase of the intensity of the IRM up to the maximum magnetizing field of 1150 mT is observed in some samples. This suggests (Figure 5e and f) the presence of hematite.

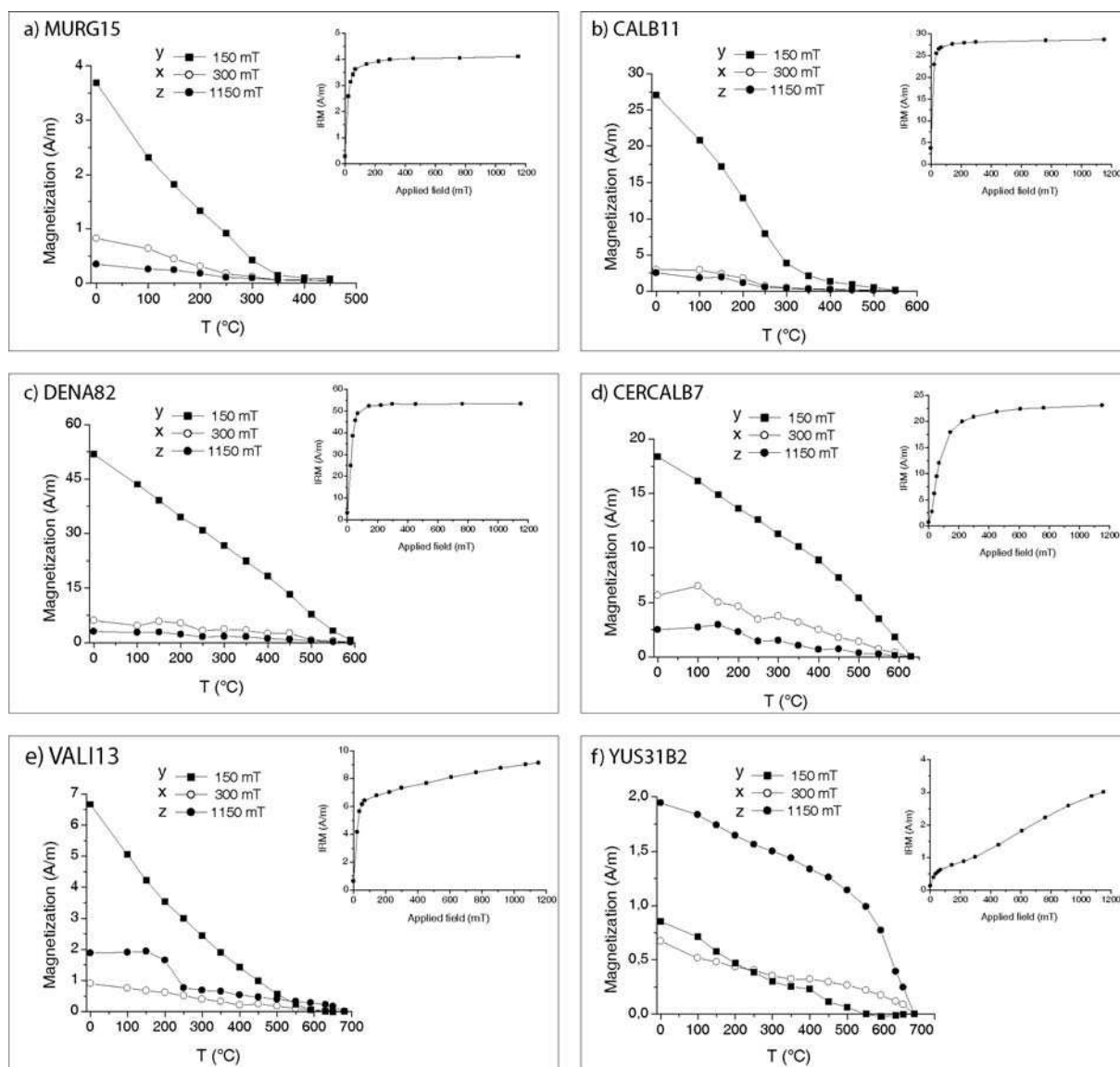


Figure 5: Isothermal remanent magnetization acquisition curves (IRM) and thermal demagnetization of three axis IRM for representatives samples (see text).

Thermal demagnetization of three-axes composite IRM [Lowrie 1990] was also conducted on the same of samples. IRM acquisitions were performed in three steps. First, the samples were remagnetized in a field of 1150 mT along their Z axis, then a second IRM was given along their X axis in a field of 300 mT, and finally a third IRM was given along their Y axis in a field of 150 mT. The thermal demagnetization of each orthogonal component is then analyzed separately (Figure 5). In almost of the samples IRM along the Y axis has the highest intensity and its unblocking temperatures range between 350°C and 600°C (Figure 5a, b, c and d). In few samples from three sites (VALI, GUA2 and YUS2) the magnetization acquired along the Z axis (in 1150 mT) has unblocking temperatures above 650°C (Figure 5e,f). This suggests the presence of hematite. Goethite was also recognized in some samples (Fifure 5e). These experiments suggest again that the main magnetic carrier in our samples is magnetite or titanomagnetite with different Ti contents.

4.3. SEM and energy dispersive X-ray analysis

Scanning electron microscopy (SEM) and energy dispersive X-ray analysis were carried out on the sample VALI13 where hematite was detected (see Figure 4e). For this purpose we used a conventional SEM JSM 6400 and an energy-dispersion spectrometer OXFORD Link Isis in the C.M.E.B.A. at the University of Rennes 1. SEM experiments confirm the previous results: titanomagnetite and hematite were found in this sample. The particle showed in Figure 6a (titanomagnetite: for this particle the X-ray analysis confirm the presence of O, Fe and Ti but the numerical results are biased by the presence of C probably contained in the matrix of the bulk sample) is supposed to represent the low coercivity (less than 150 mT) magnetic phase observed in VALI13. The particle showed in Figure 6b (hematite: 47.16% of O and 31.62% of Fe) corresponds to the magnetic phase which do not reach saturation at 1150 mT (see IRM results).

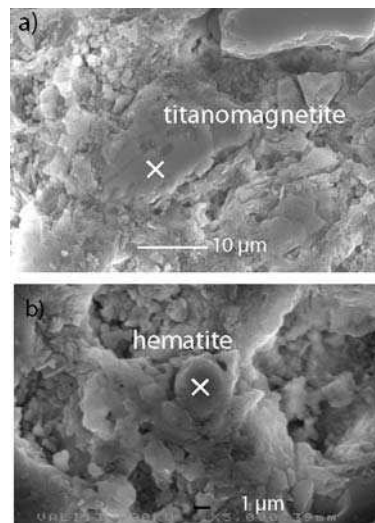


Figure 6: Examples of scanning electron microscopy observations. Points where energy dispersive X-ray analyses were done are marked by white crosses (see text).

5. Archaeointensity determinations

5.1 Experimental procedure

A laboratory field, of 50 or 60 μT was applied along the cylindrical axis Z of the samples during Thellier experiments. Heatings and coolings were performed in the applied field. Samples were heating in air in a Magnetic Measurements oven, from 100°C to temperatures at which more than the 85% of the initial NRM was lost, using between 7 and 19 temperature steps. In addition to the low field susceptibility measurements and also in order to detect possible alteration in the magnetic mineralogy of the samples pTRM checks were made every two temperature steps.

5.2. TRM anisotropy

As demonstrated by *Chauvin et al.* [2000], the correction of the NRM and TRM measurements using the tensor of TRM anisotropy is clearly needed in order to obtain precise paleointensity values on tiles or bricks. Therefore, the TRM anisotropy tensor was determined on 157 samples following the method proposed by *Chauvin et al.* [2000] and *Veitch et al.* [1984]. This tensor was obtained from the acquisition of a TRM in six different directions, in sample coordinates X, -X, Y, -Y, Z and -Z. The +Z remagnetisation step was used to check the thermal stability of the samples, by comparing this step with the measure previously

obtained during Thellier experiments. If no or few modifications (<10%) of the TRM acquisition capacity were found, all the NRM and TRM measurements were corrected for TRM anisotropy; otherwise the sample was rejected. In order to avoid magneto-chemical changes the TRM anisotropy tensor was measured during the Thellier experiment at temperatures at which around 70% of the NRM intensity is lost.

5.3. Effect of cooling rate upon the TRM intensity

The cooling rate dependence of TRM intensity was first reported by *Néel* [1955] for an assemblage of identical single-domain (SD) magnetic grains. This effect leads to the increase of TRM intensity as the cooling rate decreases for assemblies of SD or pseudo-single domain (PSD) grains. This has been also experimentally confirmed in baked clays and pottery fragments [see for example Chauvin, 2000; Genevey and Gallet, 2005]. Archeological information suggests that the real cooling time of the structures in the archeological sites is probably of one or two days. As our samples cooled quicker in our archeointensities experiments carried out in the laboratory, the cooling rate effect on the TRM intensity has been investigated using cooling times of 24 and 48 hours. In order to quantify it, we carried out on each sample a supplementary cycle of measurements consisting of four TRM acquisition steps at the end of the Thellier experiments in the same laboratory field. The four steps were carried out at the same temperature (10° higher than the last temperature step during Thellier experiments). First a TRM (TRM_{r+}) was given during a rapid cooling (45 minutes) to room temperature with the applied field along the cylindrical axes of the samples, +Z. The second step also consists on a rapid cooling but with the applied field along -Z (TRM_{r1-}). The third step involves a linear slow cooling time along the direction Z+ (TRM_{s+}), and the last step rapid along Z- (TRM_{r2-}). We decide to compare the vertical component of the magnetization (Z) acquired in the same sense of the applied field in order to avoid some possible effect of the NRM remaining in our samples (note that this value is always less than 15%). These four steps allow us to quantify the correction factor for the effect of cooling rate upon TRM intensity as a percentage

$$\text{correction factor (\%)} = (\text{TRM}_{s+} - \text{TRM}_{r+}) / \text{TRM}_{r+} \quad (1)$$

and the percentage of alteration as the ratio

$$\text{alteration (\%)} = (\text{TRM}_{r2-} - \text{TRM}_{r1-}) / \text{TRM}_{r1-} \quad (2)$$

The percentage of alteration could be related to magneto-chemical changes due to the heating performed on step 3 (slow cooling) or on step 4 (rapid cooling). We are not able to determine

in which of the two steps the sample alters. For this reason, we have decided to correct archeointensity determinations for cooling rate effect only when the correction factors were more important than the evolution factors.

5.4. NRM-TRM diagrams

Paleointensity determinations were attempted on 175 samples, 160 of them have given reliable results. The very high success rate of more than 90% shows the excellent physical and chemical stability of the magnetic minerals contained in our samples (Figure 7).

The selection criteria used to reject or retain the samples are the classical parameters proposed in the literature: a) the linear segment in the NRM-TRM diagrams used to calculate the paleointensity was determined for at least 5 points, the last point retained is the last step before any evidence of changes in magnetic mineralogy; b) pTRM checks were considered as successful when they indicated an evolution , which corresponds to less than 10% of total TRM intensity acquired; c) the lower limit of the fraction of the NRM component retained for slope calculation, f parameter from *Coe et al.* [1978], was set at 40%; c) the maximum acceptable values of the Maximum Angle of Deviation (MAD) and Deviation Angle (DANG) were set to 10° [*Pick and Tauxe*, 1993] and following *Chauvin et al.* [2005] the maximum potential error to the paleointensity caused by CRM acquisition must be lower than 15%; and d) a maximum value of 10% was assigned to alteration tests carried out during the TRM anisotropy measurements. Figure 8 shows an example of rejected sample.

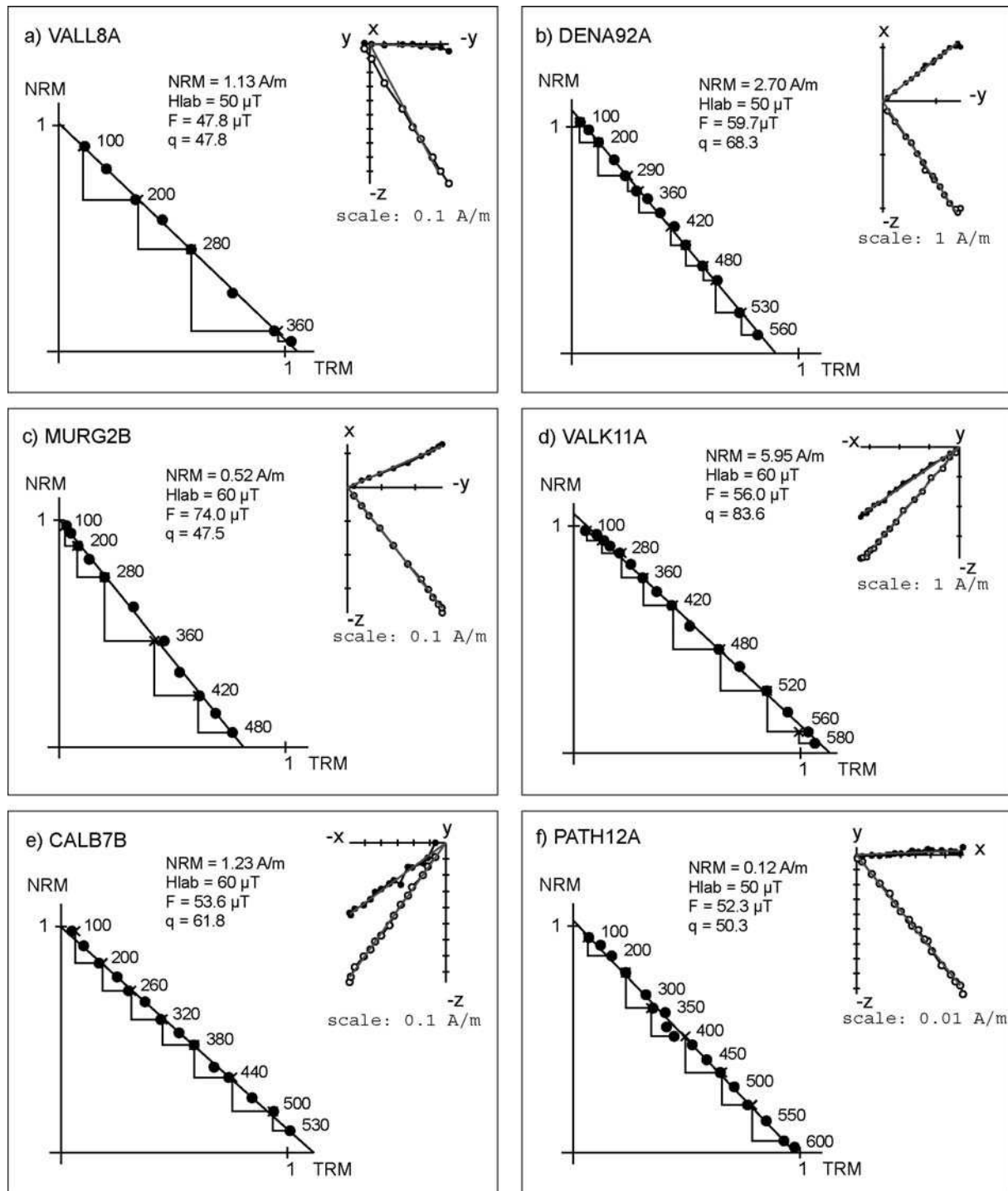


Figure 7: Examples of single component NRM/TRM diagrams together with orthogonal vector projections of the remanent magnetization in sample coordinates. Open (solid) circles are projections upon vertical (horizontal) planes. Diagrams are normalized to the initial NRM intensity. Closed circles on the NRM/TRM diagrams are data used for archeointensity determinations. The laboratory field used Hlab during the Thellier experiments and the obtained F paleointensity together with the quality factor q are indicated.

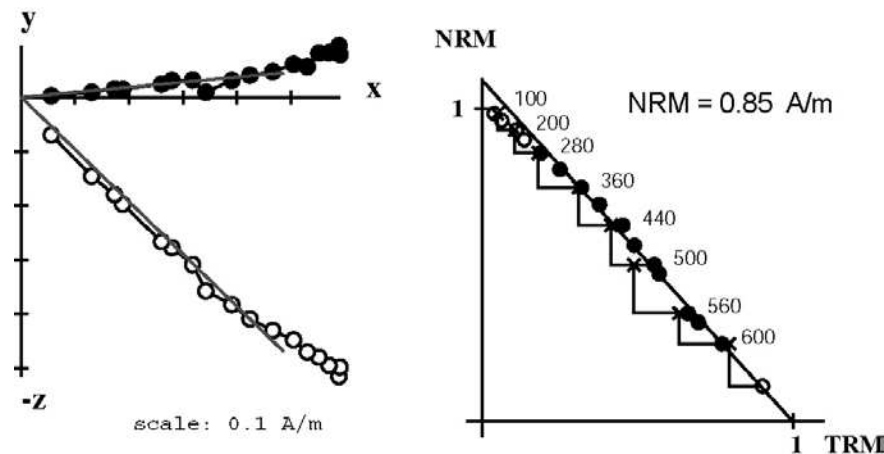


Figure 8: Example of a rejected sample: orthogonal vector projections of the remanent magnetizations together with NRM/TRM diagrams. Modifications of the direction of magnetization indicate some magneto-chemical changes.

On three samples from the sites YUS2, the paleointensities were determined on the low temperature component of magnetization (see section 3 and Figure 9).

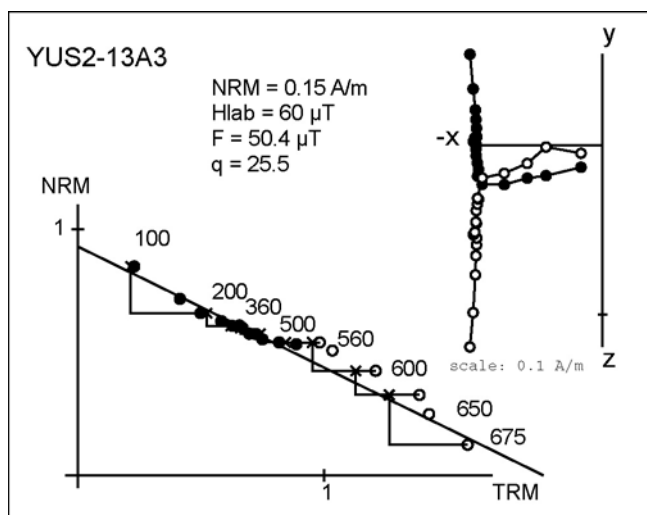


Figure 9: Example of two components NRM/TRM diagram together with orthogonal vector projections of the remanent magnetization in sample coordinates.

The generally high quality NRM-TRM diagrams observed allows us to obtain archeointensity determinations related always with f factors bigger than 0.5, MAD lower than 5.5° and DANG lower than 5° . For four samples the CRM obtained is bigger than 10% but for the rest of the samples this parameter is lower (Figure 10, Table 2). In order to calculate the mean sites intensities the weighting factors proposed by *Prévot et al.* [1985] for each sample have been used and the dispersion of the mean is expressed as the standard deviation (s.d.). For the not oriented bricks and jars fragments the archeomagnetic directions of the corresponding structures (see Table 1) have been used to calculate the virtual dipole moments (VDM). In next sections we describe the TRM anisotropy and cooling rate corrections results.

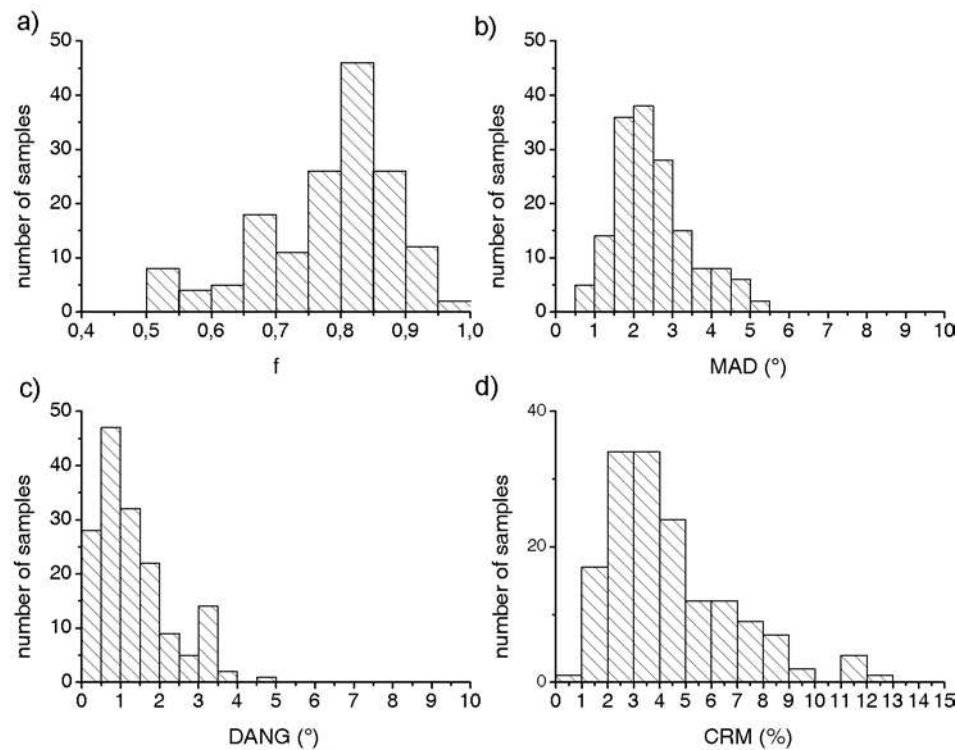


Figure 10: Variations of some parameters used to test the quality of our archeointensity determinations. (a) f , fraction of the NRM component used in the slope calculation; (b) MAD, maximum angle of deviation; (c) DANG, deviation angle and (d) CRM, acquisition of chemical remanent magnetization as a percentage of the applied field.

Variation de l'intensité du CMT en Europe de l'Ouest pendant les deux derniers millénaires

Name	Spl.	NRM	χ	Q_I	$T_{min}-T_{max}$	n	f	g	q	MAD	DANG	CRM	$F \pm \sigma F$	F_e	$Fm \pm sd$	Fpo	Fpocr	Fpa	VDM	VADM
Age		(A/m)	(10^{-5})		(°C)					(°)	(°)	(%)	(μT)	(μT)	(μT)	(μT)	(μT)	$10^{22} A/m^2$	$10^{22} A/m^2$	
DENA	82-A	3.20	700	11.50	100-560	14	0.77	0.91	56.1	1.6	0.7	4.6	58.4 ± 0.7	58.5	59.0 ± 3.1	58.8	54.4 ± 3.4	61.1	10.2	9.5
220-250	83-A	1.80	356	12.71	100-530	13	0.64	0.90	24.6	2.5	1.7	3.7	60.3 ± 1.7	64.0						
	84-A	1.97	513	9.65	100-500	12	0.68	0.91	29.5	1.9	0.3	2.4	61.2 ± 1.3	61.1						
	85-A	5.56	1029	13.59	100-560	13	0.86	0.89	48.0	2.3	1.0	3.3	58.1 ± 1.1	55.8						
	86-A	5.43	483	28.25	100-530	13	0.84	0.89	41.3	1.7	1.8	5.7	53.9 ± 1.0	53.4						
	88-A	5.94	478	31.20	100-450	10	0.68	0.87	20.0	4.9	2.5	12.2	62.1 ± 1.9	58.0						
	89-A	2.29	522	11.04	100-560	14	0.86	0.92	48.3	1.7	1.1	5.5	62.1 ± 1.0	61.3						
	90-A	1.21	913	3.32	100-530	13	0.78	0.91	45.9	2.4	0.8	2.4	58.1 ± 0.9	60.8						
	91-A	1.99	671	7.45	100-530	13	0.73	0.91	37.9	2.3	0.5	3.7	56.9 ± 1.0	57.4						
	92-A	2.70	536	12.64	100-560	14	0.87	0.92	68.3	1.6	0.7	3.6	59.5 ± 0.7	59.7						
MURG	1-B	0.31	926	0.8	150-320	5	0.51	0.73	4.0	3.3	0.4	4.2	47.2 ± 3.7	48.7	55.5 ± 9.6	58.0	58.3 ± 10.5	66.4	11.1	10.3
1000-1100	2-B	0.52	58	22.5	100-480	11	0.90	0.89	47.5	1.1	0.4	1.1	74.4 ± 1.6	74.0						
	3-B	8.25	1145	18.1	100-390	8	0.90	0.83	49.8	1.9	0.9	3.2	56.3 ± 0.8	55.0						
	10-A	0.16	134	3.0	100-360	7	0.79	0.79	31.4	2.2	0.5	2.0	55.4 ± 1.0	54.4						
	11-A	0.34	157	5.4	100-420	9	0.78	0.84	66.7	1.8	0.2	2.2	58.6 ± 0.5	56.2						
	12-A	0.4	101	10.0	100-450	10	0.79	0.79	31.4	2.2	0.5	2.0	55.8 ± 1.8	55.0						
	13-A	5.99	115	130.9	100-480	11	0.78	0.89	45.3	1.9	0.5	3.6	63.4 ± 0.9	60.4						
	17-A	0.01	10	2.5	280-420	5	0.41	0.74	9.3	1.7	2.5	3.9	41.9 ± 0.9	40.5						
CALA	2-A	5.65	859	16.5	100-530	12	0.83	0.90	38.2	2.6	0.6	3.1	58.7 ± 1.1	57.7	59.9 ± 2.8	59.3	58.4 ± 3.1	66.8	12.0	10.2
1275-1300	4-A	3.07	530	14.6	100-560	13	0.88	0.90	160.0	1.6	0.5	1.4	57.0 ± 0.3	57.6						
	6-A	2.15	597	9.1	100-560	13	0.88	0.91	56.1	2.3	0.4	4.1	60.0 ± 0.8	62.8						
	7-A	2.49	655	9.6	100-560	13	0.84	0.91	116.1	1.6	0.3	1.7	55.8 ± 0.3	58.3						
	8-A	3.03	610	12.5	100-500	11	0.88	0.89	54.7	1.4	0.4	2.0	61.4 ± 0.9	61.7						
	10-A	2.32	263	22.2	100-500	11	0.91	0.89	113.6	1.1	0.4	1.8	57.7 ± 0.3	58.7						
	11-A	1.52	441	8.7	100-560	13	0.85	0.91	45.2	2.5	0.9	3.0	57.8 ± 0.9	60.4						
	13-A	7.54	1241	15.3	100-530	12	0.85	0.90	40.6	1.9	0.5	2.2	55.8 ± 0.9	57.0						
	14-A	2.11	500	10.6	100-360	7	0.50	0.83	26.8	1.6	3.4	1.8	65.7 ± 1.1	65.3						

Variation de l'intensité du CMT en Europe de l'Ouest pendant les deux derniers millénaires

CALB		1-B	1.60	614	6.6	100-530	14	0.83	0.91	30.9	2.7	1	4.5	56.2 ± 1.4	57.1	56.6 ± 4.2	56.4	54.4 ± 3.7	62.2	11.2	9.5
1275-1300	2-B	4.89	983	12.5	100-410	10	0.75	0.86	28.7	2.8	0.2	3.2	63.9 ± 1.5	64.7							
	3-A	4.73	871	13.7	100-500	13	0.85	0.91	61.4	2.0	0.5	1.9	63.1 ± 0.8	61.0							
	4-A	2.22	555	10.1	100-500	13	0.80	0.92	45.3	3.1	1.9	2.9	55.7 ± 0.9	55.6							
	6-A	1.70	383	11.2	100-530	14	0.85	0.92	17.4	3.9	0.8	8.8	56.2 ± 2.5	55.0							
	7-B	1.18	257	11.5	100-530	14	0.87	0.92	61.8	4.1	0.5	4.1	53.5 ± 0.7	53.6							
	8-B	1.50	330	11.4	100-500	13	0.87	0.92	47.8	5.0	0.5	2.7	51.9 ± 0.8	50.4							
	9-A	3.09	766	10.1	100-560	15	0.86	0.91	69.5	3.4	1.6	3.4	58.7 ± 0.7	54.9							
	13-A	1.29	227	14.3	100-560	15	0.82	0.81	33.8	3.6	3.4	2.4	61.1 ± 1.3	60.4							
	14-B	1.61	579	7.0	100-560	15	0.83	0.92	36.9	3.2	0.4	3.5	53.4 ± 1.1	53.7							
CERCALB		1-A	0.35	257	3.4	150-470	9	0.48	0.85	5.8	3.6	1.1	7.0	46.0 ± 2.5	46.3	54.6 ± 7.0	55.9	55.6 ± 7.0	61.8	11.4	9.7
1275-1300	2-A	2.74	404	17.0	100-530	12	0.85	0.90	34.9	1.8	0.9	2.1	49.2 ± 1.0	52.4							
	4-A	1.83	292	15.8	200-440	7	0.54	0.83	9.9	4.7	1.7	3.1	51.3 ± 2.4	56.6							
	6-A	0.63	119	13.3	320-600	10	0.58	0.88	22.9	2.7	2.4	5.7	71.1 ± 1.5	62.9							
VALN		1-A	3.96	1090	9.14	100-540	13	0.77	0.91	102.1	2.7	0.4	2.7	53.1 ± 0.4	52.7	50.4 ± 3.1	50.7	48.5 ± 2.6	54.7	9.7	8.4
1238-1350	2-A	2.09	624	8.40	100-540	13	0.81	0.91	43.1	2.1	0.7	3.6	50.2 ± 0.9	49.9							
	4-A	1.71	383	11.21	100-540	13	0.83	0.91	57.2	2.0	0.9	2.1	46.2 ± 0.6	44.5							
	5-A	1.70	420	10.17	100-540	13	0.82	0.91	69.1	2.7	1.0	3.2	48.9 ± 0.5	45.6							
	6-A	2.21	536	10.36	100-540	13	0.83	0.91	68.4	1.7	0.9	2.2	49.1 ± 0.5	49.0							
	7-A	2.07	469	11.09	100-540	13	0.80	0.92	57.5	2.6	1.7	3.1	50.5 ± 0.7	50.7							
	9-A	3.12	934	8.40	100-540	13	0.78	0.90	76.7	3.5	1.5	4.6	52.6 ± 0.5	52.6							
	12-A	2.89	791	9.19	100-540	13	0.85	0.91	82.4	1.8	1.2	3.7	50.3 ± 0.5	50.9							
	14-A	3.60	1004	9.02	100-540	13	0.79	0.91	102.9	3.1	2.2	4.5	55.8 ± 0.4	54.6							
	16-A	2.80	1228	5.72	100-540	13	0.73	0.91	36.9	4.3	3.2	7.8	51.9 ± 1.0	52.2							
	18-A	2.63	1066	6.19	100-540	13	0.79	0.92	52.2	3.2	3.3	6.1	53.1 ± 0.8	51.9							
VALI		5-A	2.03	810	6.3	100-450	10	0.65	0.89	20.9	2.8	0.7	3.5	54.6 ± 1.5	52.2	54.4 ± 3.1	54.6	50.4 ± 2.0	57.9	10.2	8.8
1238-1400	6-A	1.12	396	7.1	100-540	13	0.72	0.91	22.8	2.5	1.5	4.6	57.0 ± 1.6	57.8							
	8-A	3.01	1031	7.4	100-540	13	0.77	0.91	32.2	1.6	1.9	1.7	57.5 ± 1.3	57.1							
	11-A	1.37	540	6.4	100-540	13	0.80	0.91	71.4	2.1	0.8	2.3	52.9 ± 0.5	54.2							

Variation de l'intensité du CMT en Europe de l'Ouest pendant les deux derniers millénaires

	12-A	1.01	218	11.6	100-540	13	0.76	0.91	40.7	2.3	1.0	3.1	55.9 ± 1.0	56.4								
	13-A	1.58	360	11.0	100-480	11	0.67	0.90	29.8	2.2	2.3	4.5	57.2 ± 1.1	58.3								
	14-B	2.98	898	8.3	100-510	12	0.73	0.90	24.1	5.3	4.7	7.2	58.2 ± 1.6	58.4								
	17-B	0.89	272	8.2	100-510	12	0.77	0.91	52.1	2.8	0.8	1.9	48.1 ± 0.6	49.2								
	18-A	2.20	845	6.5	100-510	12	0.78	0.91	35.1	2.3	0.9	3.2	51.7 ± 1.1	53.0								
	19-A	0.62	227	6.9	100-510	12	0.64	0.91	27.2	3.2	1.5	4.4	50.6 ± 1.1	51.8								
	21-A	0.90	308	7.3	100-510	12	0.62	0.90	31.6	2.9	3	7.1	55.0 ± 1.0	56.9								
VALK	1-A	1.94	579	8.4	100-450	10	0.52	0.87	19.9	3.5	0.8	4.0	57.6 ± 1.15	54.0	54.9 ± 3.6	55.4	51.6 ± 4.1	58.3	10.6	9.0		
1300-1450	2-A	8.91	1128	19.9	100-560	15	0.88	0.90	65.4	0.6	0.0	1.5	57.3 ± 0.63	55.9								
	4-A	0.67	236	7.1	100-560	15	0.87	0.90	53.6	0.8	0.0	2.4	60.7 ± 0.85	56.4								
	5-A	0.37	134	6.9	100-560	15	0.85	0.92	64.0	1.3	0.0	3.4	60.5 ± 0.73	56.4								
	11-A	5.95	1433	10.4	100-580	16	0.89	0.92	83.6	0.8	0.0	2.5	57.2 ± 0.51	56.0								
	12-A	0.24	74	8.2	200-560	13	0.77	0.91	59.9	1.6	0.5	2.5	61.2 ± 0.67	59.8								
	13-A	2.34	811	7.3	100-560	13	0.75	0.91	60.3	2.1	1.2	2.5	58.2 ± 0.64	57.2								
	14-B	7.51	1417	13.3	100-560	15	0.87	0.92	55.8	1.8	0.9	2.1	52.3 ± 0.63	49.6								
	15-B	2.64	505	13.1	100-500	12	0.69	0.90	34.8	2.5	1.9	2.9	51.8 ± 0.78	48.6								
VALM	1-A	0.53	281	4.7	100-450	10	0.71	0.88	12.5	4.0	1.2	6.3	58.2 ± 2.3	58.6	49.9 ± 4.3	49.9	47.1 ± 4.5	53.2	9.4	8.2		
1300-1450	2-A	1.42	537	6.6	100-420	9	0.82	0.84	33.3	1.9	1.2	3.4	46.8 ± 0.8	46.8								
	3-A	6.45	1590	10.2	100-560	15	0.76	0.92	32.8	2.5	0.4	2.5	46.2 ± 0.8	47.4								
	4-A	3.07	897	8.6	100-560	15	0.80	0.92	56.4	1.6	0.5	3.1	53.8 ± 0.7	53.9								
	6-A	1.31	642	5.1	100-560	15	0.84	0.92	65.1	1.5	0.9	2.4	54.8 ± 0.6	52.7								
	7-A	3.41	1235	6.9	100-560	15	0.86	0.93	66.3	1.9	0.9	2.5	50.4 ± 0.5	48.6								
	8-A	5.99	1695	8.9	100-560	15	0.82	0.93	54.0	2.1	0.6	2.3	49.8 ± 0.6	49.0								
	12-A	2.91	1065	6.9	100-480	11	0.68	0.89	26.8	2.6	2.0	3.5	48.6 ± 0.9	47.3								
	14-A	3.18	1067	7.5	100-480	11	0.68	0.89	21.0	2.5	3.0	4.6	47.5 ± 1.1	44.9								
CALC	1-A	1.71	176	24.4	100-530	12	0.88	0.90	62.4	2.6	0.4	1.3	50.5 ± 0.6	50.1	50.3 ± 2.5	50.2	48.7 ± 3.0	53.3	9.7	8.5		
1400-1420	2-A	0.51	118	10.9	100-530	12	0.74	0.86	50.1	3.0	1.8	3.8	53.9 ± 0.6	49.0								
	4-A	0.98	371	6.6	100-500	11	0.82	0.89	73.9	1.9	0.9	2.3	56.0 ± 0.5	54.2								
	8-A	0.83	332	6.3	100-500	11	0.83	0.89	57.3	1.7	1.2	2.3	54.9 ± 0.7	53.0								

Variation de l'intensité du CMT en Europe de l'Ouest pendant les deux derniers millénaires

	9-A	0.20	131	3.8	100-440	9	0.76	0.84	62.1	1.9	0.1	1.7	52.1 ± 0.5	51.8									
	10-A	1.06	327	8.1	100-500	11	0.82	0.90	45.8	1.8	0.2	1.1	48.5 ± 0.6	47.7									
	11-A	0.82	127	16.2	100-440	9	0.66	0.87	72.6	2.0	3.8	3.6	48.5 ± 0.3	47.2									
	16-A	0.56	57	24.7	100-500	11	0.83	0.89	75.4	1.8	0.8	1.7	52.7 ± 0.5	51.3									
	17-A	1.42	115	31.0	100-500	11	0.86	0.89	110.2	1.8	0.7	2.2	47.8 ± 0.3	48.0									
PATH		1-A	2.35	831	7.1	100-400	9	0.81	0.86	22.9	4.6	0.4	11.3	54.1 ± 1.7	54.4	55.5 ± 4.3	54.4	52.5 ± 5.3	58.7	9.8	9.1		
1450-1600		3-B	0.54	318	4.3	100-400	9	0.52	0.83	12.5	3.4	1.0	8.3	64.3 ± 2.9	64.3								
4-A		0.22	357	1.5	100-325	6	0.69	0.78	11.5	4.3	2.4	11.3	59.7 ± 3.5	62.0									
5-B		0.24	112	5.4	100-550	15	0.81	0.92	40.3	2.6	1.3	4.6	54.7 ± 1.1	54.7									
6-A		1.02	339	7.6	100-550	15	0.83	0.92	53.6	2.9	1.1	2.8	51.9 ± 0.8	51.6									
7-A		3.11	906	8.6	100-400	9	0.84	0.85	30.4	2.8	0.8	3.1	53.7 ± 1.3	54.2									
8'-A		0.16	44	9.1	100-600	17	0.88	0.93	59.5	2.5	3.2	5.1	57.1 ± 0.9	55.3									
10-A		4.13	895	11.6	100-450	10	0.88	0.87	36.5	1.2	1.5	1.8	51.3 ± 1.1	51.2									
11-A		0.14	54	6.5	100-475	12	0.67	0.90	19.0	4.9	2.3	4.3	53.8 ± 1.8	55.1									
12-A		0.12	45	6.7	100-600	17	0.92	0.93	50.3	2.0	0.6	2.5	48.9 ± 0.8	52.3									
PATA		50'-A	9.48	1683	14.2	100-525	15	0.89	0.92	64.4	2.0	0.5	4.2	55.4 ± 0.8	55.1	51.8 ± 4.9	52.7	51.2 ± 5.3	56.9	9.2	8.9		
1450-1500		51'-A	10.25	1381	18.7	100-550	17	0.68	0.92	54.8	2.9	0.8	3.8	48.4 ± 0.5	45.5								
52-A		5.75	1390	10.4	100-450	13	0.75	0.86	30.3	2.2	1.0	5.0	52.4 ± 1.2	53.6									
53-A		3.39	1366	6.2	100-425	12	0.66	0.88	28.0	3.7	2.0	6.9	50.0 ± 1.1	50.8									
54-A		4.42	1770	6.3	100-425	12	0.63	0.88	17.3	4.2	1.7	9.7	48.2 ± 1.4	45.2									
55-A		6.05	1905	8.0	100-575	18	0.88	0.86	57.9	3.8	3.1	7.9	47.2 ± 0.6	45.2									
56-A		3.30	1150	7.2	100-450	11	0.83	0.81	38.6	2.4	0.4	4.2	55.5 ± 1.1	56.3									
57-B		7.09	1702	10.5	100-350	9	0.77	0.79	45.5	1.9	0.9	5.3	56.3 ± 0.8	57.7									
58-A		5.51	1025	13.5	100-600	19	0.92	0.92	105.6	2.2	0.8	4.3	56.2 ± 0.5	56.4									
62-A		3.31	769	10.8	100-525	16	0.70	0.90	39.3	3.4	1.2	4.8	50.8 ± 0.8	51.8									
PATB		1-A	2.14	394	13.62	100-500	12	0.67	0.88	23.8	2.0	1.4	7.2	48.8 ± 1.2	47.9	51.9 ± 4.2	50.6	50.4 ± 4.0	55.1	8.2	8.8		
1525-1650		2-A	1.94	451	10.82	100-590	15	0.87	0.91	60.5	2.2	1.5	3.7	47.3 ± 0.6	47.6								
3-A		4.54	1308	8.71	100-390	8	0.52	0.85	10.4	2.1	3.2	8.4	60.4 ± 3.1	59.0									
4-A		4.74	932	12.78	100-480	11	0.83	0.88	33.0	1.3	0.8	6.3	50.6 ± 1.2	49.9									

Variation de l'intensité du CMT en Europe de l'Ouest pendant les deux derniers millénaires

	5-B	2.35	512	11.54	100-530	13	0.86	0.91	31.8	4.3	1.2	11.5	48.3 ± 1.1	46.5							
	6-A	1.83	1035	4.45	100-330	6	0.52	0.80	6.3	4.0	1.4	8.5	52.8 ± 3.7	52.3							
	7-A	4.53	520	21.89	150-390	7	0.78	0.78	41.8	1.1	1.2	3.4	49.2 ± 0.7	49.2							
	8-A	4.09	894	11.50	100-330	6	0.69	0.75	15.1	1.2	1.4	3.0	58.6 ± 2.3	58.4							
	11-A	4.97	968	12.89	100-390	8	0.55	0.85	9.6	2.1	3.2	5.7	54.3 ± 2.9	51.6							
	12-A	2.76	713	9.72	100-480	11	0.78	0.89	23.9	2.8	1.5	5.6	53.2 ± 1.6	51.9							
	14-A	4.45	904	12.36	100-480	11	0.84	0.90	34.4	3.0	1.0	6.1	50.0 ± 1.2	48.3							
	20-A	3.06	1019	3.06	100-330	6	0.74	0.79	12.0	2.9	1.3	8.0	58.1 ± 3.3	60.1							
PATJ	40-A	3.57	654	13.72	100-525	14	0.82	0.90	48.3	2.1	1.9	6.9	51.2 ± 0.8	52.8	55.5 ± 4.0	54.5	52.5 ± 4.2	57.6	8.7	9.1	
1429-1611	41-A	1.50	256	14.74	100-575	16	0.88	0.92	122.5	1.4	0.4	4.5	50.6 ± 0.4	52.6							
	42-A	1.71	350	12.26	100-475	12	0.61	0.90	41.0	1.8	2.0	6.5	51.9 ± 0.7	50.9							
	43-B	1.68	474	8.90	100-500	13	0.70	0.88	33.2	2.2	1.2	7.1	61.6 ± 1.4	58.8							
	44-A	3.31	1070	7.78	100-450	11	0.53	0.89	11.5	3.9	1.1	9.3	62.1 ± 3.2	61.9							
	45-B	1.91	584	8.24	100-550	15	0.79	0.92	44.9	2.1	1.6	4.6	53.4 ± 0.9	54.5							
	46-A	2.50	880	7.13	100-375	8	0.73	0.83	15.6	2.0	1.3	4.7	60.2 ± 2.8	58.3							
	47-B	0.79	192	10.36	100-600	17	0.89	0.92	131.8	2.3	2.5	6.0	52.7 ± 0.4	52.5							
	48-A	4.35	613	17.84	100-525	14	0.84	0.90	38.0	2.1	1.4	6.9	57.3 ± 1.3	56.9							
	49-A	0.52	109	11.99	100-600	17	0.91	0.92	95.8	2.9	0.4	5.5	52.5 ± 0.5	52.7							
	50-A	4.03	707	14.31	100-425	10	0.66	0.86	18.9	3.1	1.9	11.0	62.1 ± 2.3	62.3							
	52-A	3.73	677	13.85	100-550	15	0.85	0.91	73.1	2.1	0.7	6.1	59.5 ± 0.7	58.1							
	53-B	3.98	1020	9.81	100-525	14	0.74	0.92	27.4	2.2	1.3	7.4	53.9 ± 1.4	52.8							
	54-A	2.83	594	11.99	100-550	15	0.85	0.92	60.6	1.3	0.9	3.5	54.2 ± 0.8	52.6							
	55-A	3.04	822	9.28	100-475	12	0.60	0.90	14.9	4.2	1.4	7.2	52.5 ± 2.0	50.4							
	56-A	7.68	1274	15.14	100-425	10	0.74	0.87	33.6	2.0	0.1	6.3	62.9 ± 1.4	60.6							
VALL	1-A	2.63	456	14.51	100-390	8	0.85	0.83	69.4	1.3	2.2	5.4	61.5 ± 0.8	60.9	55.5 ± 4.0	56.4	55.4 ± 4.6	61.1	9.9	9.6	
1575-1625	2-A	2.60	454	14.38	100-420	9	0.91	0.83	26.8	2.3	3.0	5.3	54.5 ± 1.6	55.4							
	3-A	2.73	481	14.28	100-420	9	0.90	0.82	46.2	1.2	0.1	2.7	59.3 ± 1.1	59.7							
	4-A	4.47	669	16.79	100-420	9	0.90	0.83	74.0	1.2	0.4	2.0	57.3 ± 0.6	56.3							
	5-A	2.04	293	17.52	100-420	9	0.90	0.83	88.0	1.5	1.1	4.6	58.7 ± 0.6	58.1							
	7-A	1.45	272	13.38	100-420	9	0.70	0.86	38.7	4.5	1.9	4.1	56.8 ± 1.0	55.2							
	8-A	1.13	236	11.99	100-390	8	0.86	0.84	47.8	1.0	3.8	8.8	48.3 ± 0.7	47.8							

Variation de l'intensité du CMT en Europe de l'Ouest pendant les deux derniers millénaires

	14-A	2.87	503	14.33	100-420	9	0.92	0.84	33.1	1.5	0.4	3.7	55.9 ± 1.5	57.2						
	16-A	3.65	852	10.77	100-390	8	0.84	0.83	19.1	3.1	3.2	8.1	53.3 ± 1.9	51.7						
	17-A	2.70	1429	4.75	100-390	8	0.73	0.83	18.2	2.8	1.7	6.4	50.7 ± 1.7	50.9						
	18-A	3.93	518	19.07	100-390	8	0.89	0.79	50.6	2.1	3.0	5.0	55.6 ± 0.8	57.6						
Bricks GUA2	3-A	0.23	283	2.0	100-560	12	0.82	0.90	67.4	2.3	0.7	2.6	48.2 ± 0.4	44.3	47.0 ± 2.1	47.4	46.8 ± 2.9	51.0	7.9	8.0
1825-1845	4-A	2.34	184	32.0	100-400	8	0.80	0.85	59.9	1.7	0.9	0.8	49.3 ± 0.4	46.7						
	6-A	3.22	744	10.9	100-470	10	0.84	0.88	37.0	2.1	0.7	1.6	49.2 ± 0.7	45.6						
	7-A	0.15	30	12.6	100-600	15	0.85	0.91	116.7	1.9	1.6	4.5	53.7 ± 0.3	50.2						
	8-A	0.19	123	3.9	100-530	12	0.79	0.88	67.0	3.0	1.3	1.5	53.8 ± 0.4	46.7						
	9-A	7.59	659	28.9	100-400	8	0.83	0.83	68.2	0.9	0.5	1.3	49.9 ± 0.4	48.4						
YUS2	11A3	0.14	17	20.7	200-600	13	0.55	0.85	10.2	1.7	1.1		42.3 ± 1.9		45.4 ± 7.6	50.1	48.9 ± 7.7	52.2	8.6	8.4
1959	13A3	0.15	23	16.4	100-530	12	0.76	0.85	25.5	4.8	3.1		50.4 ± 1.3							
	23A1	0.8	86	23.4	100-530	12	0.99	0.83	150.0	0.8	0.1		56.8 ± 0.3	54.6						
	41A2	0.8	47	42.8	100-560	13	0.90	0.79	33.3	2.9	2.6	3.8	43.2 ± 0.6	40.5						
	43A3	13	888	36.8	100-560	13	0.97	0.85	36.1	3.3	2.5	2.6	39.4 ± 0.6	39.0						

Table 2: archeointensity results.

Name (Age), name of the group samples (age of the samples); Spl., sample number; NRM, intensity of the Natural Remanent Magnetization in A/m; χ , initial susceptibility in 10^{-5} SI units; Ql, Koenigsberger ratio for a magnetic field of $50\mu T$; interval temperature T_{min} - T_{max} used for the slope calculation; n, number of data points within this temperature interval; f, fraction of the NRM component used in the slope calculation; g, gap factor; q, quality factor; MAD, maximum angle of deviation; DANG, deviation angle; CRM, potential error on the estimation of the paleointensity due to the acquisition of CRM during Thellier experiment as a percentage of the applied field; F \pm σ F, mean intensity and standard deviation per sample without anisotropy correction; Fe, mean intensity per sample with correction of anisotropy; Fm \pm sd, anisotropy corrected mean intensity and standard deviation; Fpo, weighted mean intensity; Fpocr, weighted mean intensity after cooling rate correction, Fpa, weighted mean intensity at the latitude of Paris after cooling rate correction; VDM and VADM, values of the virtual dipole moment and virtual axial dipole moment calculated using the weighted mean intensities corrected for the effect of cooling rate upon TRM acquisition.

5.5. TRM anisotropy

TRM anisotropy has been determined on 157 samples. For the majority of the samples the degree of anisotropy k_1/k_3 (where k_1 and k_3 are the maximum and minimum axes of the tensor of TRM anisotropy) were generally lower than 10%. There is no dominance of magnetic lineation or foliation and the directions of the principal axes of the tensors are scattered within almost all the sites. Figure 11a shows an example (CALA) of this general behavior.

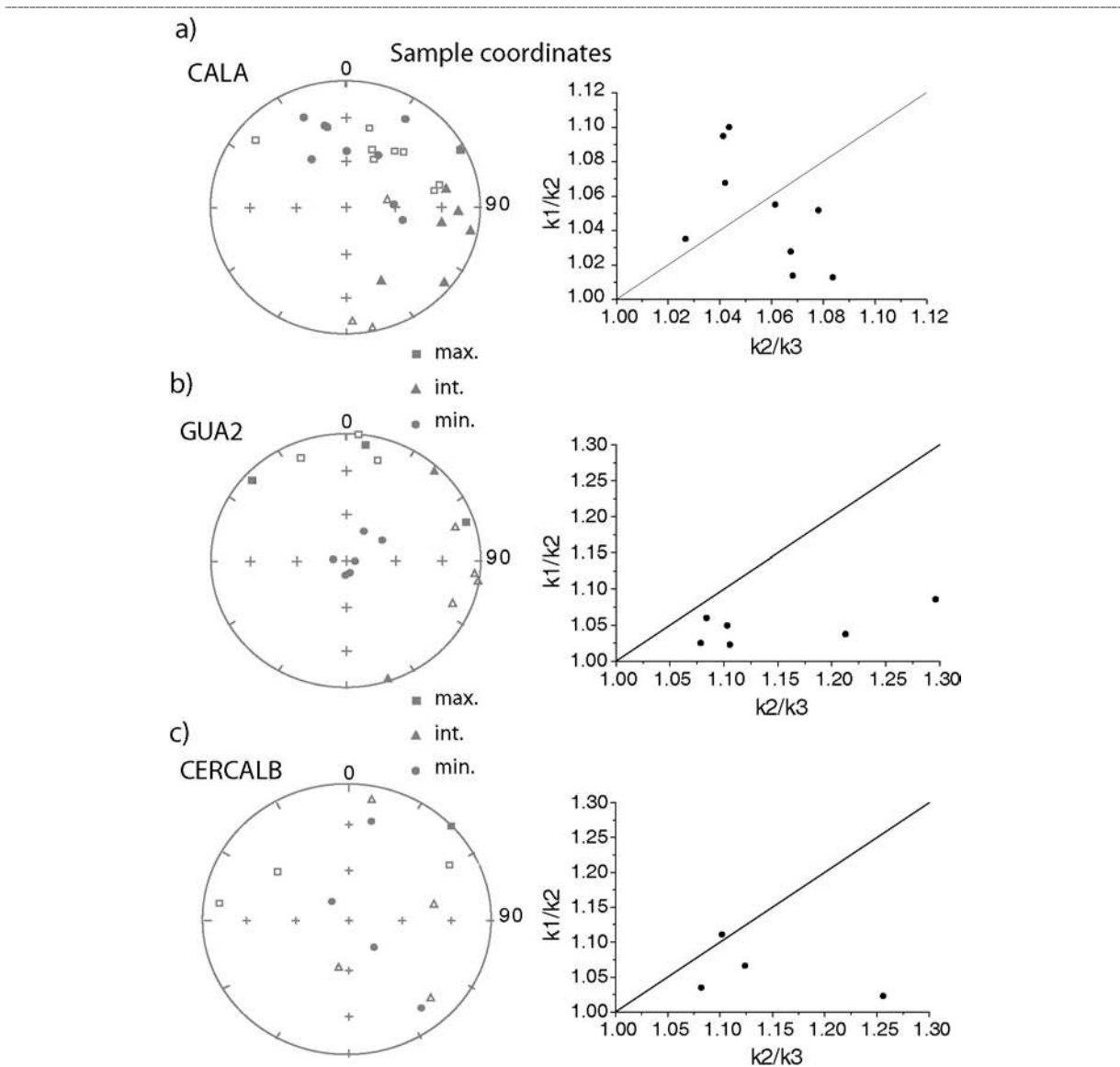


Figure 11: Example of stereographic projection, in sample coordinates, of the direction of the principal axes of the TRM anisotropy tensor and Flinn diagram of individual sample lineation and foliation data for a) kiln CALA, b) bricks from GUA2 and c) jars fragments CERCALB. Results in sample coordinates. Samples were drilled perpendicularly to the flattening plane of the samples (when present).

The infill bricks (bricks GUA2) and the jars fragments (CERCALB) are the exception. In these cases higher degrees of anisotropy, up to 40%, were found and the magnetic foliation dominates (see Figure 11b and c). The easy plane of magnetization is contained in the flattening plane (XY plane of the sample) of the bricks and the hard direction of magnetization along the Z axis of the samples.

The random directions of the principal axes of the tensors, together with the generally low degrees of anisotropy, explain the similarity of the mean intensities and mean directions of magnetization per site before and after TRM anisotropy correction (see Table 2). Only for bricks GUA2 the differences between the mean site intensity before and after TRM anisotropy corrections are significant (5.7%). For CERCALB the uncorrected and the corrected mean site intensities differ only in 0.4% but the dispersion of the mean decrease after the TRM anisotropy correction.

5.6. Dependence of cooling rate upon TRM acquisition

Following the method described in section 5.3., the correction factors and the alteration factors obtained for a linear cooling of 24 hours are shown in Figure 12a. Figure 12b shows the correction factors retained per sample and applied to the archeointensity determinations, plotted in Figure 12a in the “accepted” zone. Note that when the correction factors were lower than the alteration parameter, no correction was applied (“rejected” zone Figure 12a).

The correction upon the archeointensity applied to individual samples is typically lower than 10%, but can reach 14% (Figure 12b). A big variability between samples of the same archeological site is observed (see Figure 12a), suggesting than the cooling rate effect is highly dependent of the particular magnetic mineralogy of the samples. This correction must be investigated for each sample. The alterations are typically lower than 5% (Figure 12a).

These results correspond to mean site correction factors (overestimation of the paleointensity) which are important (bigger than 5%) for four sites; moderate (between 3 and 5%) for five, and not so significant (less than 3%) for the other 8 sites. The maximum value of overestimation (7.7%) was found for the kiln VALI. In one of the kilns, MURG, the mean site correction factor is +0.5% (the paleointensity mean is underestimate). The decrease of TRM intensity as the cooling rate decreases has been associated in the literature [McClelland-

Brown, 1984] to multi-domain (MD) grains but the linearity of the NRM-TRM diagrams clearly indicates the dominance of single-domain (SD) grains in the samples from this site.

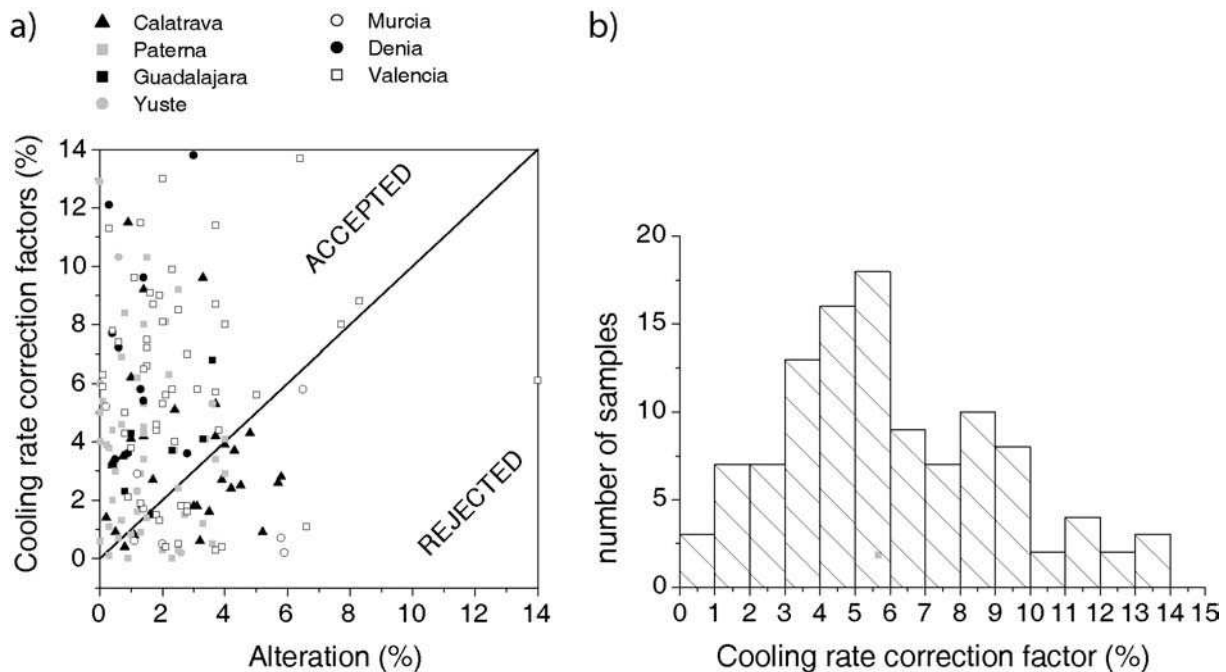


Figure 12: a) Absolute values of the effect of cooling rate upon TRM intensity versus variations of the TRM acquisition capacity (alteration) of our samples, for cooling times of 24 hours, b) histogram showing the corrections applied for this effect.

A linear cooling time of 48 hours was also applied leading generally to a very small increase in the correction factors. For this reason, and in order to retain the mean intensity values least affected by magneto-chemical alteration, we considered that the mean intensity values corrected for a cooling time of 24 h are the most reliable.

5.7. New archeointensity results

17 new mean archeointensity determinations have been obtained with standard deviation (s.d.), lower than 8% for 9 of the 17 results (Table 2). For 5 sites, s.d. around the mean intensity are between 8 and 11% (medium values), and for the other three the s.d. are greater (CERCALB, YUS2 and MURG), between 11 and 18%. Archeointensity values determined from sites dated on the same interval of time are generally close, for example VALN and VALI or VALM and CALC. The results obtained for the kiln CALB are very similar to the

result obtained for the group of jars fragments CERCALB made on this kiln. However, the mean intensity from CALA (dated at the same interval than CALB) is 4 μT higher.

6. Discussion

6.1. Reliable previous archeointensity results for Western Europe over the last 2000 years

Chauvin et al. [2000] compiled the available results for Western Europe giving different weights depending on three criteria: the paleointensity technique used, the type of materials and the number of samples per site. The authors demonstrated that some of the available results (associated low weighing factor) seems not reliable. Therefore, we have conducted the same analysis and we consider only the data related to weight factors equal or bigger to 10 (note the maximum weight possible is 16 and the minimum is 3).

Spain

One archeointensity data for Spain has been published by *Kovacheva et al.* [1995]. The authors study a Roman pottery kiln. The classical Thellier method was used but no TRM anisotropy or cooling rate corrections have been performed. Recently, seven archeointensity values were obtained from seven contemporaneous kilns from Murcia dated between 1100 and 1200 AD by archaeological constraints [*Gómez-Paccard et al.*, 2006a]. These data were obtained using the Thellier method and were corrected for TRM anisotropy and cooling rate effect using a cooling time of 24 h.

France

Data published by *Gallet et al.* [2005], *Genevey and Gallet* [2002] and *Chauvin et al.* [2000], were acquired by the Thellier method and corrected for TRM anisotropy and cooling rate effects. Using this data there are 42 reliable archeointensity results from France for the last two millennia.

Denmark and S. Norway

Gram-Jensen et al. [2000] studied 15 archeomagnetic sites in Denmark and one in South Norway. The experiments were performed using Thellier method. TRM anisotropy was investigated. No cooling rate corrections were performed in this study. Although the number of samples is low for some sites, 13 paleointensity values are available for this area.

6.2. Evolution of the intensity of the Earth's magnetic field during the last 2000 years inferred from Bayesian modelling

The 17 new data described here together with the previous results for France and Spain Denmark are shown in Figure 13. The centered dipole moment model was used to calculate the paleointensities at the latitude of Paris. This relocation process may introduce errors. To investigate this question the intensity errors introduced during the relocation process via the centered dipole model have been estimated using the IGRF 2000 model. As, in our dataset, Murcia is the locality most distant from Paris it was chosen to conduct this test. The difference between the relocated intensity and the direct intensity at Paris is 3 μT . This discrepancy is of the same order or lower than the typical error associated to the compiled mean paleointensity data (see Figure 13 or Table 2). We consider then that the relocation process does not introduce significant errors.

Some of the new results obtained agree very well with the previous published results, for example during the 3th, the 14th and the 16th centuries. In contrast big discrepancies are observed in some periods, for example the three data from Calatrava, around 1250 AD (sites CALA-B), differs in 10 μT or more from the previous results obtained by Genevey and Gallet [2002]. The IGRF at Paris for 1959 AD gives a geomagnetic field intensity of 46.6 μT . The mean intensity of YUS2 ($52.2 \pm 7.7 \mu\text{T}$) is in agreement with this value if we take into account the dispersion around the mean.

The Bayesian modelling [Lanos, 2004] based on roughness penalty has been used in order to calculate the evolution of the geomagnetic intensity in Western Europe during the last millennia. This approach puts some prior knowledge on the global nature of the curve to be estimated (it is assumed that the studied physical phenomena vary in a smooth way); it allows the window width to be automatically adapted to the density of points along the time axis, making the points movable inside the dating ranges; and it can take into account stratigraphic constraints provided by archaeological investigations. Figure 13 shows the obtained curve together with the error band at 95% confidence level at the latitude of Paris. Table 3 gives the results, every 25 year steps, of the Bayesian curve obtained. We can notice that the Bayesian curves computed with or without the data from Denmark and Norway are very similar. That suggests that the use of these uncorrected data for the cooling rate effect do not introduce a significant bias in our result.

The majority of the data available for the Roman period up to 400 AD are corrected for cooling rate effect for 8 hours of cooling [Chauvin et al., 2000] or not corrected [Kovacheva et al., 1995, Gram-Jensen, 2000]. This produces probably some of the systematic offset observed between these data and the other (corrected for 24 h or 33 h of cooling). The big dispersion observed between sites could not be only explained by errors on the estimation of the cooling time used to correct the results (note that cooling rate corrections are generally lower than 10%). However, Bayesian curve, which also takes into account age uncertainties indicates small variations of the geomagnetic field intensity during Roman times. For High Middle Ages, rapid variations ($7 \mu\text{T}$ per century) of the field strength have been proposed [Genevey and Gallet, 2002]. However, only three archeointensity data are available for this period. Consequently, the Bayesian curve is not very well constrained and more intensity data are clearly needed this time period. The smaller narrow bump in intensity proposed by [Genevey and Gallet, 2002] during the 14th and 15th centuries is not confirmed by our results. On the contrary, geomagnetic field intensity seems to be constant between the 13th and the 15th centuries, before decreasing from $58 \mu\text{T}$ to $47 \mu\text{T}$.

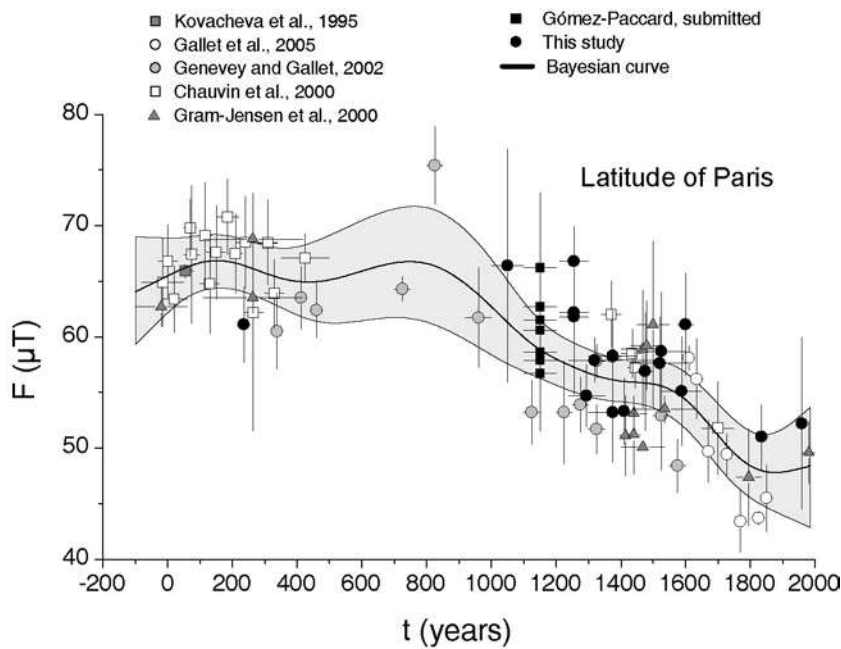


Figure 13: Seventy height intensity data compiled for Western Europe and Bayesian curve obtained in this study together with the marginal errors at 95% confidence level. All relocated at Paris.

As only high quality data have been retained in this study, the dispersion observed should not be due to unreliable archeointensity determinations. The dispersion is probably related to the precision limit of our archeointensity determinations and to some age errors of the studied sites. However, for the data set compiled several results per century are available, except for the period between 500 AD and 1000 AD. Future archeointensity research must focus on this period.

age	F (μT)	Error min.	Error max.	age	F (μT)	Error min.	Error max.
-100	64.05	59.31	69.01	950	64.04	59.24	68.69
-75	64.40	60.00	68.98	975	63.39	58.81	67.87
-50	64.76	60.73	68.95	1000	62.71	58.38	66.97
-25	65.12	61.45	68.92	1025	62.01	57.96	66.03
0	65.48	62.15	68.88	1050	61.31	57.58	65.05
25	65.83	62.81	68.88	1075	60.62	57.22	64.07
50	66.15	63.36	68.92	1100	59.97	56.90	63.12
75	66.43	63.79	69.01	1125	59.37	56.58	62.25
100	66.65	64.09	69.10	1150	58.85	56.27	61.48
125	66.79	64.29	69.16	1175	58.39	55.96	60.85
150	66.85	64.38	69.18	1200	58.01	55.65	60.33
175	66.82	64.38	69.13	1225	57.66	55.36	59.89
200	66.70	64.30	69.00	1250	57.34	55.09	59.52
225	66.51	64.13	68.84	1275	57.03	54.84	59.18
250	66.27	63.89	68.64	1300	56.74	54.62	58.86
275	66.01	63.61	68.42	1325	56.50	54.45	58.57
300	65.74	63.30	68.22	1350	56.29	54.31	58.32
325	65.49	62.98	68.05	1375	56.13	54.22	58.12
350	65.27	62.63	67.98	1400	56.02	54.15	57.97
375	65.10	62.29	67.99	1425	55.95	54.09	57.89
400	64.98	61.97	68.09	1450	55.90	54.00	57.86
425	64.92	61.69	68.27	1475	55.85	53.84	57.86
450	64.93	61.47	68.52	1500	55.76	53.61	57.84
475	65.00	61.32	68.80	1525	55.57	53.29	57.76
500	65.12	61.25	69.12	1550	55.29	52.87	57.57
525	65.28	61.24	69.45	1575	54.89	52.35	57.24
550	65.48	61.28	69.79	1600	54.35	51.73	56.78
575	65.69	61.35	70.13	1625	53.67	50.99	56.18
600	65.91	61.44	70.46	1650	52.87	50.15	55.49
625	66.13	61.54	70.77	1675	52.01	49.26	54.76
650	66.33	61.63	71.05	1700	51.14	48.36	53.99
675	66.51	61.70	71.30	1725	50.30	47.52	53.24
700	66.64	61.74	71.50	1750	49.54	46.76	52.55
725	66.73	61.72	71.64	1775	48.90	46.09	51.96
750	66.76	61.65	71.72	1800	48.40	45.53	51.52
775	66.71	61.51	71.72	1825	48.06	45.06	51.25
800	66.59	61.32	71.62	1850	47.86	44.66	51.21
825	66.37	61.07	71.41	1875	47.80	44.30	51.38
850	66.06	60.78	71.08	1900	47.84	43.96	51.72
875	65.66	60.43	70.64	1925	47.96	43.64	52.21
900	65.19	60.06	70.08	1950	48.13	43.32	52.78
925	64.64	59.66	69.43	1975	48.32	42.99	53.40

Table 3: Intensity curve obtained by Bayesian modelling each 25 years. Age. age in years; F. intensity in μT ; Error min. and error max.. minimum an maximum marginal errors in μT . All data at the latitude of Paris.

6.3. Comparison with the prediction of CALS3(7)K.2 [Korte and Constable, 2005] and Hongre et al. [1998] global models

We have then compared the Bayesian intensity curve with the predictions of the CALS3(7)K.2 [Korte and Constable, 2005] and Hongre et al. [1998] global models at Paris. The fit between the prediction of the model CALS3(7)K.2 and our curve seems very good. The prediction is practically contained inside the Bayesian error margin at 95% confidence level. The similarity of the curves could be explained by the fact that the majority of the archeointensity data used in CALS3(7)K.2 are from European studies. In contrast the intensity predictions obtained with Hongre's model are not so similar to our obtained curve, showing in general higher values than the Bayesian curve obtained.

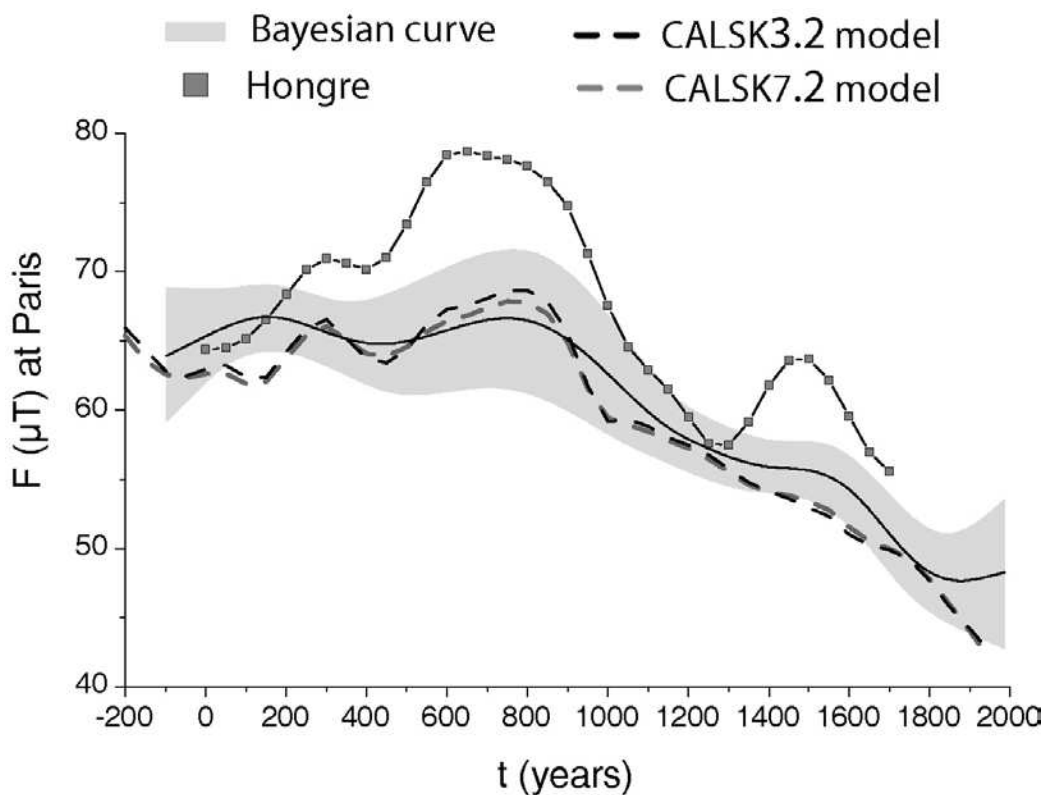


Figure 14: Comparison between the Bayesian curve obtained and the prediction of CALSK3(7).2 [Korte and Constable, 2005] and Hongre [1998] global models. All at the latitude of Paris.

Figure 15 shows dipole moment calculated using global models together with the virtual axial dipole moments (VADM) obtained by Yang et al. [2000] from archeomagnetic data. The VADM results obtained using the Western European data compiled in this work, together

with the VADM Bayesian curve, are also plotted. We can see how the dipole moment obtained by Hongre's model fit better the *Yang et al.* [2000] and our results than the dipole moment obtained with CALS3(or7)K.2 models. It seems that the Korte and Constable models underestimated the dipole part of the earth magnetic field, for ages before 1200 AD.

The comparison between Figures 14 and 15 suggest that the non dipole part of the field deduced for Korte and Constable models is very important some periods (where the dipole part seems underestimated), for example, for the period between 600 and 900 AD. During this period the dipole moment predicted is anomalously low (see Figure 15), in contrast the intensity predictions at Paris agree very well with our obtained curve (see Figure 14). The dipole moment obtained by Hongre fits better with *Yang et al.* [2000] results or our curve. Note that the dipole moment obtained by *Yang et al.* [2000] was obtained using a global compilation of archeointensity data and is supposed to eliminate the non dipole component of the Earth's magnetic field. In contrast our VADM results are obtained from Western Europe and the non dipole part is not averaged.

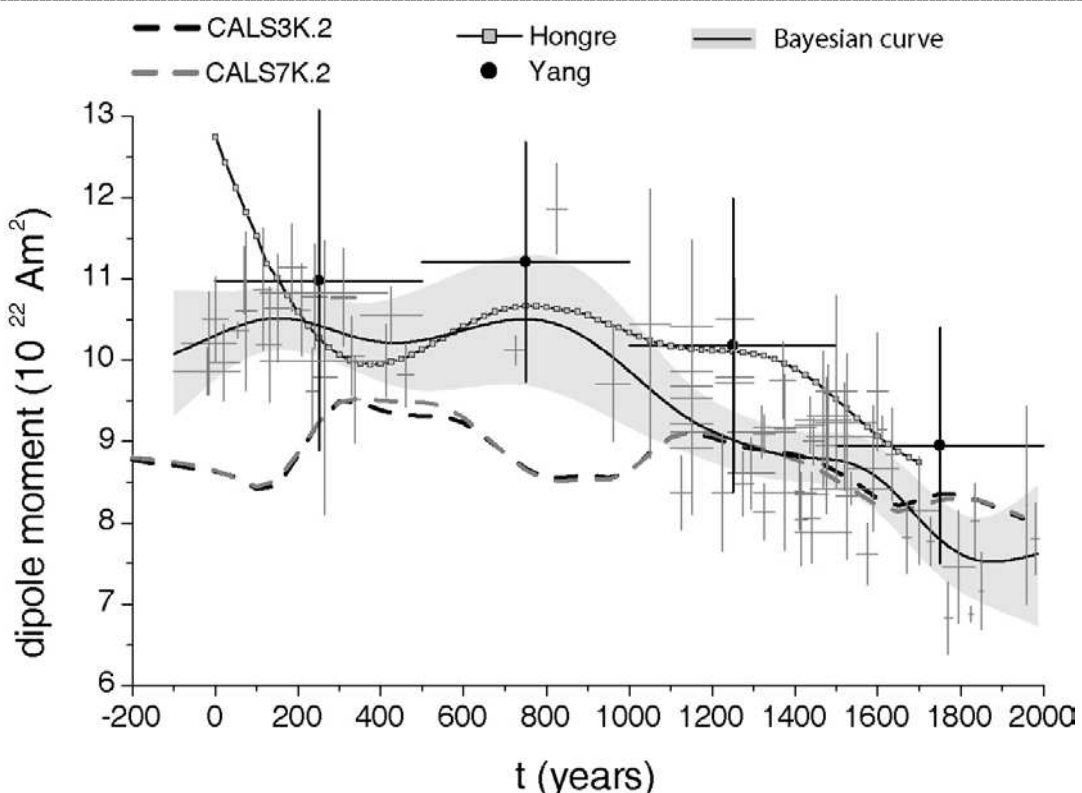


Figure 15: Comparison between dipole moment obtained with the Bayesian Western Europe curve and the dipole moment predicted by CALSK3(7).2 [Korte and Constable, 2005], Hongre [1998] global model and Yang et al. [2000] dipole moment estimations. All at Paris.

The differences observed between the models indicate the need to obtain more archeointensity data in order to better constraint the accuracy of global models.

7. Conclusions

We studied one roman pottery kiln, 15 kilns with ages ranging between 1000 AD and 1959 AD, a group of large jars fragments dated between 1275 and 1300 AD and a group of baked bricks dated between 1825 and 1845 AD. The original Thellier paleointensity method [Thellier and Thellier, 1959] was used. 160 from the 175 studied samples gave reliable results. The intensity values were corrected for thermoremanent magnetization (TRM) anisotropy. In the majority of the studied sites this correction is not significant. The cooling rate dependence upon TRM acquisition has been also studied. Cooling rate correction factors per sample up to 15% and per site up to 7.7% have been obtained. 17 new mean archeointensity determinations have been obtained with standard deviation (s.d.) lower than 8% for 9 of the 17 results. Our new data, together with 62 previous results from France, Denmark and Spain, have been used to construct the geomagnetic field intensity variation curve for Western Europe. Bayesian modelling was used for this purpose. The geomagnetic field intensity remain more or less constant between the 1st and 4th centuries, and between the 13th and 15th centuries (mean values around 65 and 57 μT respectively), whereas an important decrease occurs during the last 5 centuries. More data are clearly needed in order to establish a reliable reference curve for High Middle Ages. Differences between the new CALS3K.2 and CALS7K.2 global models of Korte & Constable (2005) and the model of Hongre *et al.* (1998) have been observed. The dipole moment obtained by Hongre *et al.* [1998] seems more realistic. The observed differences between both models indicate the need to obtain more reliable archeointensity data in order to better constraint the accuracy of global model. Our results contribute to the increase in the knowledge of the earth's magnetic field, and the data obtained can be used for future modelling of geomagnetic field behaviour. The use of the intensity reference curve obtained for dating remains very difficult for some periods due to little variation of the geomagnetic field or to the important envelope error of the curve. However, for the last five centuries the curve obtained offer a promising archeological tool.

References

- Batt, C., The British archaeomagnetic calibration curve: an objective treatment, *Archaeometry*, 39, 153-168, 1997.
- Chauvin, A., P. Roperch, and S. Levi, Reliability of Geomagnetic Paleointensity Data: The effects of the NRM fraction and concave-up behavior on paleointensity determination by Thellier method, *Phys. Earth Planet. Inter.*, 150, 265-286, 2005.
- Chauvin, A., Y. Garcia, Ph. Lanos, and F. Laubenheimer, Paleointensity of the geomagnetic field recovered on archaeomagnetic sites from France, *Phys. Earth Planet. Inter.*, 120, 111-136, 2000.
- Coe, R., C. Grommé, and E. Mankinen, Geomagnetic paleointensities from radiocarbon-dated lava flows on Hawaii and the question of the Pacific nondipole low, *J. Geophys. Res.*, 83, 1740-1756, 1978.
- Fisher, R.A., 1953. Dispersion on a sphere, *Proc. Roy. Soc. London A*, 217, 295.
- Gallet, Y., A. Genevey, and F. Fluteau, Does Earth's magnetic field secular variation control centennial climate change?, *Earth Planet. Sci. Lett.*, 236, 339-347, 2005.
- Gallet, Y., A. Genevey, and M. Le Goff, Three millennia of directional variations of the Earth's magnetic field in western Europe as revealed by archaeological artefacts, *Phys. Earth Planet. Inter.*, 131, 81-89, 2002.
- Garcia, Y., 1996. Variation de l'intensité du champ magnétique terrestre en France durant les deux derniers millénaires, Ph.D thesis, Université de Rennes 1, Rennes, France.
- Genevey, A., and Y. Gallet, Intensity of the geomagnetic field in Western Europe over the past 2000 years: new data from ancient French pottery, *J. Geophys. Res.*, 107 (B11), 2285, 2002.
- Gómez-Paccard, M., A. Chauvin, Ph. Lanos, J. Thiriot, and P. Jiménez-Castillo, Archeomagnetic study of seven contemporaneous kilns from Murcia, Spain, *Phys. Earth Planet. Int.*, *in press*, 2006a.
- Gómez-Paccard, M., G. Catanzariti, V. Ruiz, G. McIntosh, J. Nuñez, M. Osete, Ph. Lanos, A. Chauvin, D. Tarling, D. Bernal-Casasola, J. Thiriot, and “archaeological working group”, A catalogue of Spanish archaeomagnetic data, *Geophys. J. Int.*, *in press*, 2006b.
- Gómez-Paccard, M., Ph. Lanos, A. Chauvin, G. McIntosh, M.L. Osete, G. Catanzariti, V.C. Ruiz-Martínez and J.I. Nuñez, The first Secular Variation Curve for the Iberian

- Peninsula. Comparison with other data from Western Europe and with geomagnetic field global models, *Submitted to Geochemistry, Geophysics, Geosystems*, 2006.
- Hongre, L., G. Hulot, and A. Khokhlov, An analysis of the geomagnetic field over the past 2000 years, *Phys.Earth Planet. Int.*, 106, 311-335, 1998.
- Jackson, A., A. Jonkers, and M. Walker, Four centuries of geomagnetic secular variation from historical records, *Philos. Trans. R. Soc. London, Ser. A.*, 358, 957-990, 2000.
- Korte, M. and C. Constable, Continuous geomagnetic field models for the past 7 millenia: 2. CALS7K. *Geochem. Geophys. Geosyst*, 6, doi:10.1029/2004GC000801, 2005.
- Korte, M., A. Genevey, G. Constable, U. Frank, and E. Schnepp, Continuous geomagnetic field models for the past 7 millennia: 1. A new global data compilation. *Geochem. Geophys. Geosyst.*, 6(2), 1-32, 2005.
- Kovacheva, M., J. Parés, N. Jordanova, and V. Karloukovski, A new contribution to the archaeomagnetic study of a Roman pottery kiln from Calahorra (Spain), *Geophys. J. Int.*, 123, 931-936, 1995.
- Kovacheva, M., N. Jordanova, and V. Karloukovski, V., Geomagnetic field variations as determination from Bulgarian archaeomagnetic data. Part II: the last 8000 years, *Sur. Geophys.*, 19, 431-460, 1998.
- Lanos, Ph., 2004. Bayesian inference of calibration curves: application to archaeomagnetism. In: C.E. Buck and A.R. Millard (Editors). Tools for constructing chronologies: crossing disciplinary boundaries. Lecture Notes in Statistics, London, pp. 43-82.
- Lowrie, W., Identification of ferromagnetic minerals in a rock by coercivity and unblocking temperature properties, *Geophys. Res. Lett.* 17, 159-162, 1990.
- Márton, P., Recent achievements in archaeomagnetism in Hungary, *Geophys. J. Int.*, 153, 675-690, 2003.
- McClelland-Brown, E., Experiments on TRM intensity dependence on cooling rate, *J. Geophys. Res. Lett.* 11, 205-208, 1984.
- Nachasova, I., K. Burakov, and J. Bernabeu, Geomagnetic field intensity variations in Spain, *Phys. Solid. Earth, Engl. Transl.*, 38, 371-376, 2002.
- Néel, L., Some theoretical aspects of rock-magnetism, *Adv. Phys.*, 4, 191-243, 1955.
- Pick, T., and L. Tauxe, Holocene paleointensities: Thellier experiments on submarine basaltic glass from the East Pacific Rise, *J. Geophys. Res.*, 98(B10), 17949-17964, 1993.
- Prévot, M., E. Mankinen, R. Coe, and C. Grommé, The Steens Mountain (Oregon) geomagnetic polarity transition. 2. Field intensity variations and discussion of reversal models, *J. Geophys. Res.*, 90, 10417-10448, 1985.

Variation de l'intensité du CMT en Europe de l'Ouest pendant les deux derniers millénaires

- Schnepp, E. and Ph. Lanos, Archaeomagnetic secular variation in Germany during the past 2500 years, *Geophys. J. Int.*, 163, 479-490, 2005.
- Thellier, E., Sur l'aimantation des terres cuites et ses applications géophysiques. Thèse de doctorat. Paris, *Ann. Inst. Phys. Globe Paris*, 16, 157-302, 1938.
- Thellier, E., and O. Thellier, Sur l'intensité du champ magnétique terrestre dans le passé historique et géologique, *Ann. Géophys.*, 15, 285-376, 1959.
- Veitch, R., I. Hedley, and J. Wagner, An investigation of the intensity of the geomagnetic field during Roman times using magnetically anisotropic bricks and tiles, *Arch. Sc.*, 37(3), 359-373, 1984.
- Yang, S., H. Odah, and J. Shaw, Variation in the geomagnetic dipole moment over the past 12000 years, *Geophys. J. Int.*, 140, 158-162, 2000.

3.3 Essai de détermination de l'archéointensité en utilisant la désaimantation par microondes

La méthode conventionnelle développée par Thellier et Thellier (1959) pour la détermination de la paléointensité a été utilisée dans les travaux de cette thèse. Cette méthode présente plusieurs qualités, en particulier l'existence de contrôles expérimentaux qui permettent de détecter toute évolution magnéto-chimique éventuelle des échantillons. Si cette évolution vient à être décelée, l'acquisition d'une ATR par paliers de température croissante permet de conserver les résultats obtenus avant cette évolution. Cette technique, qui permet de toucher tout le spectre de températures de blocage, nous semble la plus fiable pour obtenir des déterminations précises de l'intensité du CMT ancien. En contrepartie, la méthode de Thellier et Thellier (1959) est relativement longue et l'exposition des échantillons à des chauffes répétées reste nécessaire. Cela multiplie le risque d'évolution physico-chimique.

Pour remédier à ces inconvénients (long temps d'expérience et grand nombre de chauffes subies par les échantillons) différentes techniques ont été développées. Kono et Ueno (1977) proposent une procédure à chauffe unique à chaque température, avec l'application d'un champ de laboratoire perpendiculaire à l'ARN de l'échantillon. Cette méthode ne tient pas compte de la mesure de la direction de l'ARN à chaque pallier de température et il est impossible de détecter les éventuelles (re)aimantations liées au traitement thermique.

Shaw (1974) propose une autre procédure qui repose sur la comparaison des courbes de désaimantation par champ alternatif de l'ARN et l'ARM (l'aimantation rémanente anhystérétique). L'analyse de la base de données d'intensité pour la France (Chauvin et al. 2000) indique un biais des valeurs d'intensité obtenues par cette méthode.

Dans les procédures antérieures, la désaimantation thermique est utilisée. Une nouvelle méthode basée sur la désaimantation par microondes de haute fréquence a été développée par

le groupe de paléomagnétisme de l'Université de Liverpool (Walton et al. 1992 et Walton et al. 1993). Cette technique a été appliquée avec succès à l'étude de céramiques (Shaw et al. 1996, 1999), de roches volcaniques (voir par exemple Hill et Shaw, 1999 ou Hill et al. 2005) et à l'étude d'un lot de briques (Casas et al. 2005). L'avantage principal de cette méthode est d'éviter les réchauffements successifs des échantillons à haute température. En effet, la désaimantation des échantillons est obtenue grâce à l'application des microondes de haute fréquence qui stimulent les minéraux magnétiques directement, en provoquant leur désaimantation. Le problème fondamental de cette technique est qu'il n'y a pas, à présent, une théorie bien développée pour expliquer les processus d'acquisition d'aimantation (ou désaimantation) par microondes, contrairement au cas des désaimantations ou re-aimantations thermiques.

Comme nous avons pu le voir dans le cadre de cette thèse, les minéraux magnétiques contenus dans les terres cuites étudiées présentent une très bonne stabilité aux expositions thermiques nécessaires pour la détermination de l'intensité et la méthode de Thellier et Thellier (1959) donne lieu à des taux de réussite très élevés (plus de 80% dans la majorité de sites étudiés). Cependant pour les quatre fours de Cabrera d'Anoia étudiés dans le cadre de cette thèse, la méthode de Thellier ne permet pas d'obtenir des valeurs d'intensité fiables à cause de la forte altération magnéto-chimique observée. Ces fours sont excavés dans le sol géologique du site constitué de granite plus ou moins altéré. Il est aussi intéressant de tester la validité de la technique microondes pour la détermination de l'archéointensité dans les terres cuites. Pour cela, et grâce au groupe de paléomagnétisme de l'Université de Liverpool, nous avons pu utiliser le système à 8.2 GHz de ce laboratoire. Nous remercions l'équipe de Liverpool de nous avoir permis de réaliser ces mesures. Nous décrivons ensuite les procédures utilisées et les résultats obtenus.

L'appareil utilisé permet de réaliser des expériences équivalentes aux expériences de Thellier, mais en appliquant des microondes à différentes puissances, considérés comme équivalentes aux réchauffements des échantillons à différentes températures dans les expériences conventionnelles de désaimantation thermique. Pour la détermination de la paléointensité nous avons utilisé la méthode proposée par Hill et Shaw (1999). Pour cela on détermine la direction stable de l'ARN et ensuite on applique les microondes à des puissances successivement supérieures (jusqu'à 170 W) avec un champ de laboratoire perpendiculaire à la direction de l'ARN. La valeur du champ magnétique appliqué est de 60 µT. L'analyse

vectorielle permet de déterminer les valeurs de l'ARN et de la T_MRM (aimantation acquise par l'échantillon par l'application de microondes) aux différentes étapes (puissances) et le diagramme traditionnel d'Arai peut être utilisé.

La plus forte puissance qu'on peut appliquer avec l'appareil à 8.2 GHz est de 170 W et les microondes sont appliquées généralement pendant 10 s (15 s maximum). La température maximale observée dans les échantillons pour cette puissance et une application de 10 s est inférieure à 200°C (Hill, 2000). C'est pourquoi on suppose que la technique de microondes doit provoquer des altérations magnéto-chimiques nettement inférieures aux altérations produites au cours des expériences de Thellier, où on applique des températures supérieures à 450 °C dans la majorité des cas (voir par exemple Annexe I de cette thèse). La mesure de l'aimantation est faite sur un magnétomètre SQUID (voir figure 1, pour plus de renseignements voir Hill (2000)). Les échantillons de 5 mm de diamètre ont été préparés au laboratoire de Liverpool.

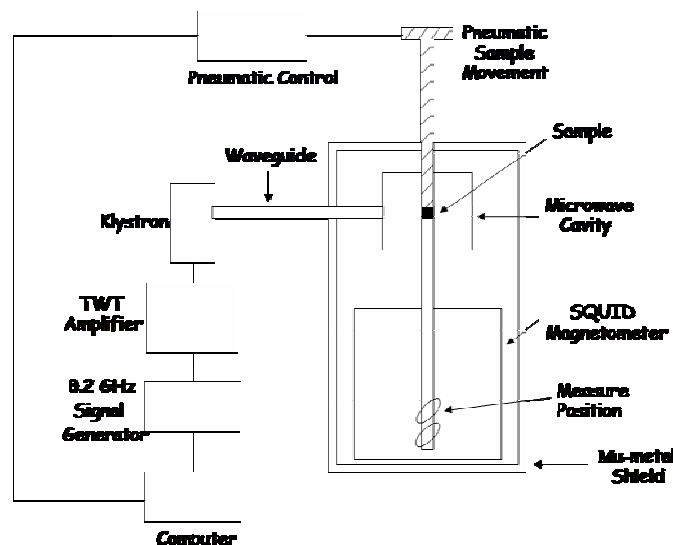
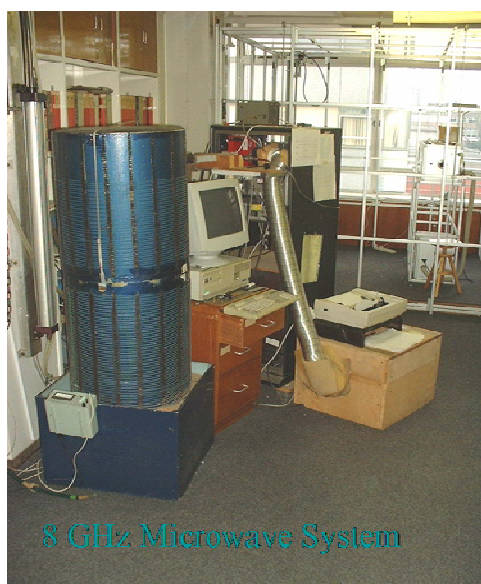


Figure 1 : système à 8 GHz utilisé

Description de résultats :

29 échantillons ont été étudiés (dena82, dena92, muri1, muri6, murk3, patb7, patb10, patj47, patj56 et 19 échantillons provenant de quatre fours CDAH, CDAJ, CDAP et CDAU de Cabrera d'Anoia; les structures associées sont décrites dans l'article : « A catalogue of

Spanish archaeomagnetic data »). Le spectre de températures de blocage des échantillons étudiés va de 350°C (pour muri1) à 560°C (pour dena92) (voir Annexe I de cette thèse).

13 des 29 échantillons étudiés ne se désaimantent pas par l'application de microondes, même en utilisant la puissance et le temps d'application les plus élevés. La désaimantation par microondes ne se montre pas efficace et plus de 70% de l'ARN initiale reste pour 45% des échantillons étudiés. Ce fait ne semble pas être lié au spectre de températures de blocage observées au cours des désaimantations thermiques. Des échantillons avec des températures de blocage basses (par exemple muri1, figure 2a) ou hautes (patj47, figure 2b) ne perdent au maximum que 30% de leur aimantation.

Pour les 17 échantillons dans lesquels nous avons obtenu une désaimantation de l'ARN supérieure à 30%, la majorité de pTRM checks réalisés donnent des résultats négatifs. Ce fait est probablement lié à la difficulté de reproduire la puissance appliquée avec l'appareil utilisé et non à une altération magnéto-chimique des échantillons (figure 2c et 2d). Dans certains cas les résultats obtenus ne donnent pas lieu à une droite dans le diagramme d'Arai (figure 2e). Seulement trois échantillons (cdau10, cdauj11 et cdaj12) présentent des taux de désaimantation supérieurs à 40% et de pTRM checks positifs (voir exemple cdau10 figure 2f).

Si on considère que les pTRM checks négatifs n'indiquent pas une altération magnéto-chimique, on peut calculer les valeurs d'archéointensité à partir de la pente, de la même manière que dans les expériences classiques de Thellier.

Pour l'échantillon patb7 la valeur d'intensité calculée à partir de la pente (voir figure 2c), avec un champ de 60 µT, est de 47.3 µT. Ce résultat est très similaire à 49.2 µT, valeur obtenue pour le même échantillon en utilisant la méthode classique de Thellier (voir Annexe 1 de cette thèse).

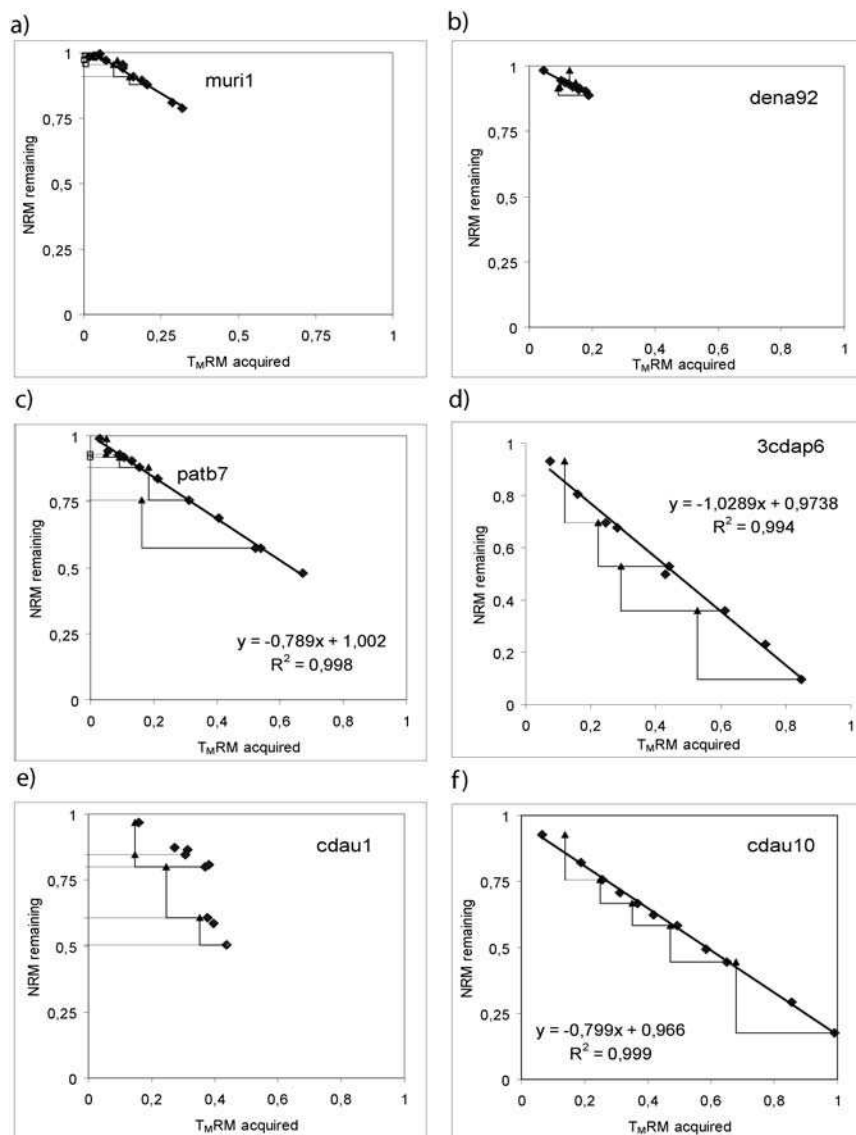


Figure 2 : résultats des échantillons représentatifs

Les 16 autres échantillons qui peuvent être analysés correspondent aux fours de Cabrera d'Anoia.

Four CDAH : trois échantillons ont été analysés, un seul se désaimante (cdah10) mais les résultats ne donnent pas lieu à une droite dans le diagramme d'Arai.

Four CDAU : trois échantillons ont été étudiés. Un seul se désaimante en donnant un diagramme d'Arai de bonne qualité avec de pTRM checks corrects (voir figure 2f). La valeur d'archéointensité obtenue est de 47.9 in situ (51.8 à Paris).

Four CDAP : Quatre des sept échantillons analysés donnent des résultats interprétables (voir figure 3). Comme on peut le constater, la dispersion de résultats obtenus est très grande. Si on considère les 4 résultats, la moyenne obtenue pour ce site est de $51.4 \pm 11.8 \mu\text{T}$ in situ, et de $55.5 \pm 11.8 \mu\text{T}$ à Paris.

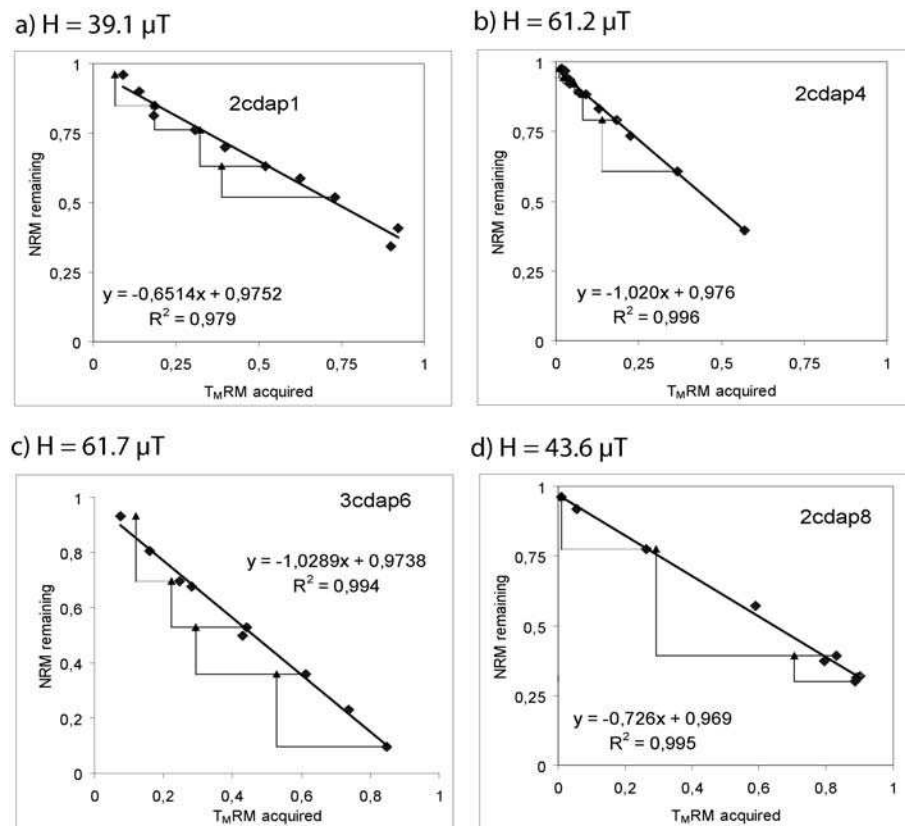


Figure 3 : résultats pour le four CDAP

Four CDAJ : Tous les échantillons de ce four se désaimantent mais seulement 8 mesures se montrent plus ou moins fiables. Les résultats sont décrits dans la figure 4. Deux échantillons ont été mesurés deux fois (cdaj2 et cdaj10) et donnent des résultats plus ou moins similaires, la moyenne des deux résultats a été utilisée pour calculer la moyenne par site qui vaut : 48.5 ± 7.5 in situ, 51.5 à Paris, avec $N = 6$ échantillons.

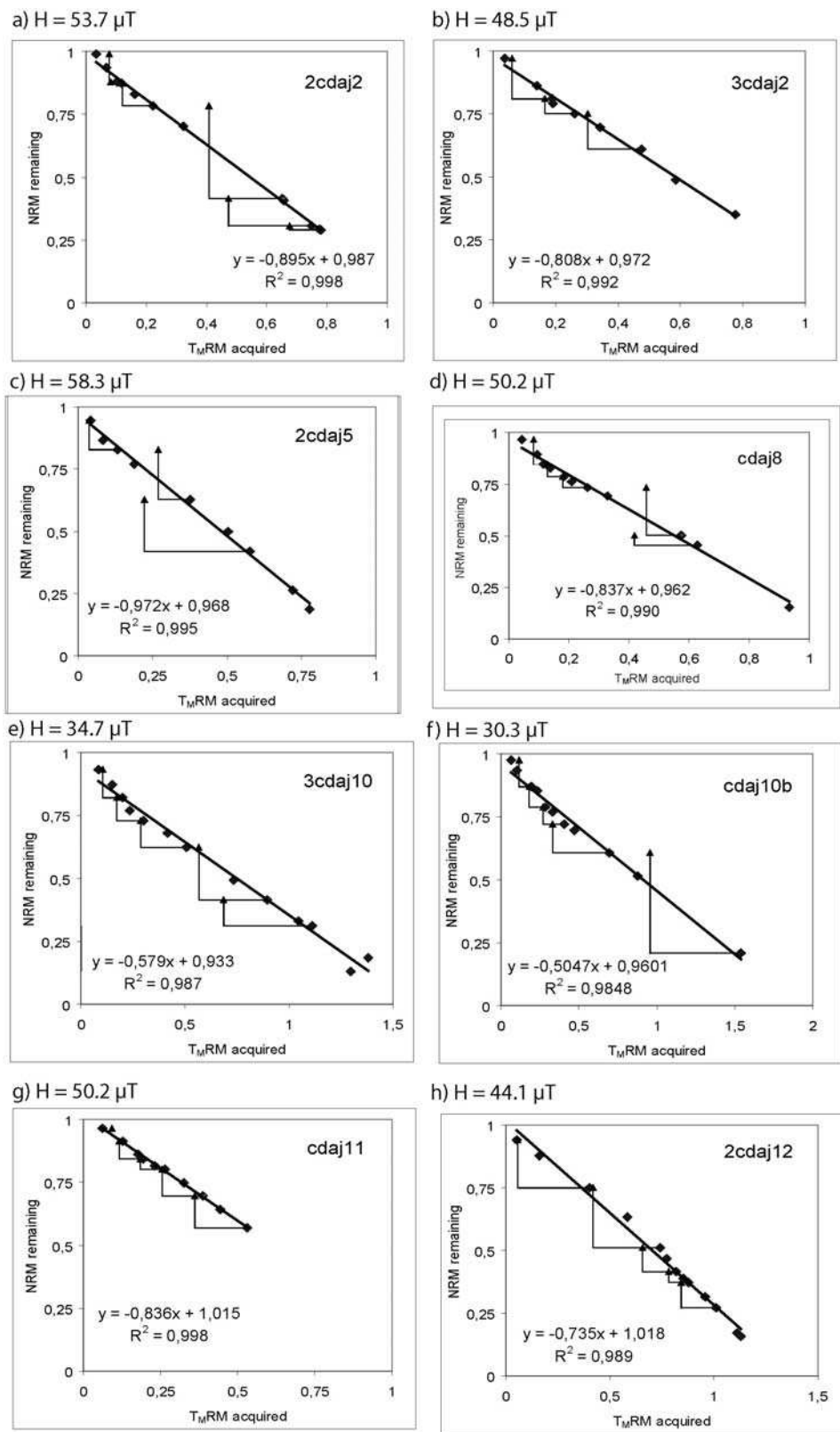


Figure 4 : résultats pour le four CDAJ

Les moyennes obtenues par site à Paris sont faibles si on les compare avec les résultats d'archéointensité d'Europe de l'Ouest (voir section 2.2 de cette thèse).

Conclusion :

La désaimantation par microondes est peu efficace pour les échantillons étudiés. La moitié des échantillons ne se désaimantent pas et seulement 12 des 29 échantillons étudiés donnent de résultats interprétables (la majorité correspond à des échantillons de granite et pas de terres cuites). En plus, la difficulté à reproduire la puissance de microondes utilisées ne permet pas de vérifier la stabilité magnéto-chimique des échantillons étudiés. L'étude des échantillons des fours de Cabrera d'Anoia, composés de granites plus ou moins altérés, a permis d'obtenir des valeurs moyennes par site. Les valeurs obtenues sont cohérentes avec les données d'intensité déjà publiées, mais il faut signaler que les moyennes par site montrent une forte dispersion.

De nouvelles expériences avec le nouvel appareil à 14 GHz, plus stable, pourraient servir à tester si, avec des microondes de fréquences supérieures, il serait possible de désaimanter un plus grand nombre d'échantillons composés de terres cuites. Il nous paraît nécessaire de comprendre pourquoi certains échantillons avec la même composition magnétique se désaimantent (par exemple, le lot de briques étudiées par Casas et al. 2005, avec des échantillons composés de titanomagnétites avec faible contenu en titane) et d'autres non (par exemple, l'échantillon muri1 de cette étude où le porteur magnétique principal est aussi de la titanomagnétite avec peu de titane, voir section 2.1 de cette thèse). La méthode Thellier et Thellier (1959) est pour l'instant la méthode la plus fiable pour l'étude de la paléointensité dans les terres cuites. En plus, le taux de réussite est très élevé..

Conclusion

L'objectif de cette thèse a été d'obtenir de nouvelles données archéomagnétiques dans le but de préciser les variations temporelles du champ magnétique terrestre (CMT) à l'échelle des derniers millénaires en Espagne. Pour atteindre cet objectif, nous avons analysé 26 fours archéologiques, un lot de briques et un lot de fragments de jarres en utilisant la méthode de Thellier et Thellier (1959). Les mesures ont été corrigées de l'effet de l'anisotropie de l'aimantation thermorémanente ainsi que de l'effet de la vitesse de refroidissement sur l'intensité de l'aimantation thermorémanente. Cette analyse nous a permis d'obtenir 26 nouvelles données directionnelles et 24 nouvelles données d'archéointensité.

La compilation des données directionnelles obtenues dans le cadre de cette thèse, des données des récents travaux archéomagnétiques menés à l'Université Complutense de Madrid et des données des travaux antérieurs nous a permis de générer le premier catalogue de données archéomagnétiques pour l'Espagne. Cette compilation comprend une description et une analyse rigoureuses des contraintes archéologiques en vue d'une éventuelle réactualisation des datations. Cette base de données nous a permis de calculer la courbe de variation directionnelle séculaire pour la Péninsule Ibérique. Pour cela nous avons comparé la méthode classique par fenêtres mobiles à la méthode bayésienne (Lanos, 2004). Cette dernière méthode a l'avantage de traiter les données en 3D simultanément (déclinaison, inclinaison et temps), de permettre aux données d'être mobiles dans l'intervalle de temps proposé par les archéologues et de tenir compte des contraintes stratigraphiques. Pour ces raisons nous avons choisi la méthode bayésienne pour présenter la courbe de variation séculaire en Péninsule Ibérique. Ensuite, nous mettons en évidence la forte similarité observée entre nos résultats et les courbes de variation séculaire française et allemande. Ces trois courbes de variation séculaire sont caractérisées par trois changements directionnels majeurs et brusques se produisant à 125BC, 200 AD et 1350 AD. Afin de comprendre si les similarités observées entre trois courbes européennes répondent à un phénomène local ou au contraire à un

phénomène global, il a été nécessaire d'analyser la variation séculaire dans un site éloigné de l'Europe. La base mondiale de données archéo-paléomagnétiques (Korte et al., 2005) offre deux régions favorables, le Japon et le sud-ouest des Etats-Unis : ces régions sont éloignées de l'Europe et de nombreuses données sont disponibles pour les derniers millénaires. Nous avons calculé les courbes de variation séculaire du CMT pour ces deux régions à partir également de la modélisation bayésienne, ainsi que leurs vitesses et changements de courbure. Les résultats obtenus nous permettent de suggérer que les caractéristiques des courbes de variation séculaire de l'Europe de l'Ouest ont un caractère régional. Cependant, il nous paraît nécessaire de densifier la base de données archéo-paléomagnétiques pour mieux contraindre les variations du CMT, à échelle régionale et globale. Nous avons aussi comparé nos résultats directionnels avec les prédictions des modèles globaux de champ proposés par Korte et Constable (2005) et Hongre et al. (1998). Bien que les modèles prédisent raisonnablement bien nos résultats, ils sont très différents, même pour la partie dipolaire du CMT. Les valeurs du moment dipolaire déduites des modèles de Korte et Constable (2005) pour les derniers millénaires paraissent sous-estimées. Le moment dipolaire déduit du modèle de Hongre et al. (1998) nous semble, quant à lui, plus réaliste.

En ce qui concerne l'intensité, nous avons obtenu, dans un premier temps, sept valeurs d'intensité en étudiant sept fours contemporains datés entre 1100 et 1200 et prélevés sur un même site archéologique à Murcia. Ces données nous permettent d'illustrer la dispersion des résultats pour des fours d'un même âge. Après correction de l'effet de la vitesse de refroidissement, la dispersion des données d'intensité est réduite de 50%. Bien que la dispersion demeure élevée, ces résultats confirment le besoin de corriger l'effet de la vitesse de refroidissement pour une détermination précise de l'intensité du CMT ancien. L'origine de cette dispersion est sans doute pour partie liée aux limites de la méthode.

Dans un deuxième temps, nous avons déterminé l'intensité du champ magnétique ancien par l'étude de 15 fours, d'un lot de briques et d'un lot de fragments de jarres. Ces résultats, ainsi qu'une compilation des données d'intensité fiables existantes en Europe de l'Ouest, nous permettent d'obtenir, par la méthode bayésienne, l'évolution du CMT au cours des derniers millénaires. La courbe obtenue indique que l'intensité du CMT aurait peu varié, du 1^{er} au 5^{ème} AD, et du 13^{ème} au 15^{ème} siècle AD (valeurs à Paris proches de 65 et 57 μ T respectivement) alors que sa décroissance est forte sur les 5 derniers siècles. Enfin l'évolution de l'intensité du CMT durant le Haut Moyen age demeure encore mal contrainte.

Nous avons testé la validité de la technique microondes pour la détermination de l'archéointensité dans les terres cuites. Pour cela, 29 échantillons ont été étudiés en utilisant le système à 8.2 GHz du laboratoire de géomagnétisme de Liverpool (UK). Les résultats montrent que la méthode Thellier et Thellier (1959) est pour l'instant la méthode la plus fiable et la plus efficace pour l'étude de la paléointensité dans des terres cuites de minéralogie magnétique variée.

La courbe de variation séculaire (directionnelle) en Péninsule Ibérique établie dans le cadre de cette thèse peut être utilisée comme outil de datation du matériel archéologique de région pour une grande partie des deux derniers millénaires. Cette courbe pourra en effet être sans doute encore améliorée entre le 5^{ème} et 11^{ème} siècles. La courbe de variation de l'intensité du CMT en Europe de l'Ouest peut également être utilisée pour des datations, combinée avec les directions (I, D) ou l'inclinaison seule (matériaux déplacés). Cependant la datation uniquement à partir des données d'intensité risque d'être difficile ou quasi impossible à cause de la faible variation du CMT durant certaines périodes (du 1^{er} au 5^{ème} AD, et du 13^{ème} au 15^{ème} siècle AD) ou bien à cause de l'importance de l'enveloppe d'erreur sur la courbe d'intensité entre le 5^{ème} et 11^{ème} siècles. Les travaux futurs doivent donc envisager de combler le faible nombre de données directionnelles et d'intensité pour cette dernière période.

Références bibliographiques

- Arrigui, S., Rosi, M., Tanguy, J.C. and Courtillot, V., 2004. Recent eruptive history of Stromboli (Aeolian Islands, Italy) determined from high-accuracy archeomagnetic dating. *Geophys. Res. Lett.*, 31, L19603, doi:10.1029/2004GL020627.
- Batt, C.M., 1997. The British archaeomagnetic calibration curve: an objective treatment, *Archaeometry*, 39, 153-168.
- Biquand, D., 1994. Effet de la vitesse de refroidissement sur l'intensité de l'aimantation thermorémanente: étude expérimentale, conséquences théoriques, *Can. J. Earth Sci.*, 31, 1342-1352.
- Buck C.E., Cavanagh W.G. and Litton C.D., 1996. *Bayesian approach to interpreting archaeological data*, Wiley, 382 p.
- Bucur, I., 1994. The direction of the terrestrial magnetic field in France during the last 21 centuries, *Phys. Earth Planet. Inter.*, 87, 95-109.
- Burakov, K. S., 1981. Determination of the ancient geomagnetic field using magnetically anisotropic samples, *Izs. Akad. Nauk SSSR, Fiz Zemli*, 11, 116-120.
- Burakov, K. S., and Nachasova, I. E., 1985. Determination of the ancient geomagnetic intensity corrected for heating related chemical alteration, *Izs. Akad. Nauk SSSR, Fiz Zemli*, 10, 93-96.
- Butler, R. F., 1992. *Paleomagnetism: Magnetic Domains to Geologic Terranes*, Blackwell Science.
- Casas, Ll., Shaw, J., Gich, M. and Share, J.A., 2005. High-quality microwave archeointensity determinations from an early 18th century AD English brick kiln, *Geophys. J. Int.*, 161, 653-661.
- Chauvin, A., Garcia, Y., Lanos, Ph. and Laubenheimer, F., 2000. Paleointensity of the geomagnetic field recovered on archaeomagnetic sites from France, *Phys. Earth Planet. Inter.*, 120, 111-136.
- Chauvin, A., Roperch, P. and Levi, S., 2005. Reliability of Geomagnetic Paleointensity Data: The effects of the NRM fraction and concave-up behavior on paleointensity determination by Thellier method, *Phys. Earth Planet. Inter.*, 150, 265-286.

- Coe, R., Paleointensities of the Earth's magnetic field determined from Tertiary and Quaternary rocks, 1967. *J. Geophys. Res.*, 72, 3247-3262.
- Coe, R., Grommé, C. and Mankinen, E., 1978. Geomagnetic paleointensities from radiocarbon-dated lava flows on Hawaii and the question of the Pacific nondipole low, *J. Geophys. Res.*, 83, 1740-1756.
- Day, R., Fuller, M.D. and Schmidt, V.A., 1977. Hysteresis properties of titanomagnetites: grain size and composition dependence, *Phys. Earth Planet. Inter.*, 13, 260-267.
- Daly, L. and Le Goff, M., 1996. An updated and homogeneous world secular variation data base. 1. Smoothing of the archaeomagnetic results, *Phys. Earth Planet. Inter.*, 93, 159-190.
- Dehling H. and Van der Plicht J., 1993, Statistical problems in calibrating radiocarbon dates, *Radiocarbon*, vol. 35, n° 1, p. 239-244
- Droesbecke J.-J., Fine J., Saporta G. (eds), 2002. *Méthodes Bayésiennes en statistique*. Ed. Technip, Paris, 418 p.
- Dudewicz E.J. and Mishra S.N., 1988. *Modern Mathematical statistics*, J. Wiley and Sons, New-York, 838 p.
- Dunlop D.J., 2002. Theory and application of the Day plot (Mrs/Ms versus Hcr/Hc) 1. Theoretical curves and tests using titanomagnetite data, *J. Geophys. Res.*, 107 (B3), 2056, 10.1029/2001JB000486.
- Dunlop, D. and Özdemir, Ö. 1997. *Rock Magnetism Fundamentals and frontiers*, Cambridge University Press.
- Fisher, R.A., 1953. Dispersion on a sphere, *Proc. Roy. Soc. London A*, 217, 295.
- Fox, J.M. and Aitken, M.J., 1980. Cooling rate dependence of thermoremanent magnetization, *Nature*, 283, 462-463.
- Gaibar-Puertas, C., 1953. Variación Secular del Campo Geomagnético, Observatorio del Ebro, Tarragona.
- Gallet, Y., Genevey, A. and Le Goff, M., 2002. Three millennia of directional variations of the Earth's magnetic field in Western Europe as revealed by archaeological artefacts, *Phys. Earth Planet. Inter.*, 131, 81-89.
- Gallet, Y., Genevey, A. and Courtillot, V., 2003. On the possible occurrence of 'archaeomagnetic jerks' in the geomagnetic field over the past three millennia, *Earth and Planet. Sci. Lett.*, 214, 237-242.
- Gallet, Y., Genevey, A. and Fluteau, F., 2005. Does Earth's magnetic field secular variation control centennial climate change?, *Earth Planet. Sci. Lett.*, 236, 339-347.

- García de Cortázar, J.A., 2001. *La época medieval*. In: S.A. Alianza Editorial (Editor), Historia de España dirigida por Miguel Artola, Madrid, pp. 426.
- Garcia, Y., 1996. *Variation de l'intensité du champ magnétique terrestre en France durant les deux derniers millénaires*, Ph. D thesis, Université de Rennes 1, Mémoires de Géosciences-Rennes, n° 74, 331p, France.
- Genevey, A. and Gallet, Y., 2002. Intensity of the geomagnetic field in Western Europe over the past 2000 years: new data from ancient French pottery, *J. Geophys. Res.*, 107 (B11), 2285.
- Gómez-Paccard, M., A. Chauvin, Ph. Lanos, J. Thiriot, and P. Jiménez-Castillo, 2006. Archeomagnetic study of seven contemporaneous kilns from Murcia, Spain, *Phys. Earth Planet. Int.*, *in press*.
- Gómez-Paccard, M., G. Catanzariti, V. Ruiz, G. McIntosh, J. Nuñez, M. Osete, Ph. Lanos, A. Chauvin, D. Tarling, D. Bernal-Casasola, J. Thiriot, and “archaeological working group”, 2006. A catalogue of Spanish archaeomagnetic data, *Geophys. J. Int.*, *in press*.
- Gómez-Paccard, M., Ph. Lanos, A. Chauvin, G. McIntosh, M.L. Osete, G. Catanzariti, V.C. Ruiz-Martínez and J.I. Nuñez, The first Secular Variation Curve for the Iberian Peninsula. Comparison with other data from Western Europe and with geomagnetic field global models, *submitted to Geochemistry, Geophysics, Geosystems*.
- Gram-Jensen, M., N. Abrahamsen, and A. Chauvin, 2000. Archaeomagnetic intensity in Denmark, *Phys. Chem. Earth (A)*, 25, 525-531.
- Green, P.J. and Silverman, B.W., 1994. *Non-parametric regression and generalized linear models, a roughness penalty approach*, Chapman and Hall, London, 182.
- Halgedahl, S.L., Day, R. and Fuller, M., 1980. The effect of the cooling rate on the intensity of weak-field TRM in single-domain magnetite, *J. Geophys. Res.*, 85, 3690-3698.
- Hill, M. J., 2000. *The microwave palaeointensity technique and its application to lava*. Unpublished thesis Univ. Liverpool.
- Hill, M. J., and Shaw, J., 1999. Palaeointensity results for historic lavas from Mt. Etna using microwave demagnetisation / remagnetisation in a modified Thellier type experiment, *Geophys. J. Int.*, 139, 583-590.
- Hill, M. J., Shaw, J. and Herrero-Bervera, 2005. Palaeointensity record through the Lower Mammoth reversal from the Waianae volcano, Hawaii, *Earth Planet. Sci. Lett.*, 230, 255-272.
- Hongre, L., Hulot, G., and Khokhlov A., 1998. An analysis of the geomagnetic field over the past 2000 years, *Phys. Earth Planet. Int.*, 106, 311-335.

- Hulot, G., Eymin, C., Langlais, B., Mandea, M. and Olsen, N., 2002. Small-scale structure of the geodynamo inferred from Oersted and Magsat satellite data, *Nature*, 416, 620-623.
- Jackson, A., Jonkers A. and Walker, M., 2000. Four centuries of geomagnetic secular variation from historical records, *Philos. Trans. R. Soc. London, Ser. A.*, 358, 957-990.
- Jasonov, P.G., Nurgaliev, D.K., Burov, D.V. and Heller, F., 1998. A modernized coercivity spectrometer, *Geologica Carpathica*, 49, 3, 224-225.
- Jupp, P.E. and Kent, J.T., 1987. Fitting smooth paths to spherical data, *Applied Statistics*, 36(1), 34-46.
- Kirschvink, J.L., 1980. The least-squares line and plane and the analysis of paleomagnetic data, *Geophys. J. R. astron. Soc.*, 62, 699-718.
- Kono, M. and Ueno, N., 1977. Paleointensity determination by a modified Thellier method, *Phys. Earth Plan. Int.*, 13, 305-314.
- Korte, M. and Constable, C., 2005. Continuous geomagnetic field models for the past 7 millenia: 2. CALS7K, *Geochem. Geophys. Geosyst.*, 6, doi:10.1029/2004GC000801.
- Korte, M., Genevey, A., Constable, C.G., Frank, U. and Schnepf, E., 2005. Continuous geomagnetic field models for the past 7 millennia: 1. A new global data compilation, *Geochem. Geophys. Geosyst.*, 6, doi:10.1029/2004GC000800.
- Kovacheva, M., 1984. Some archaeomagnetic conclusions from three archaeological localities in north-west Africa, *C. R. Acad. Sci. Bulg.*, 37, 171-174.
- Kovacheva, M., Parés, J.M., Jordanova, N. and Karloukovski, V., 1995. A new contribution to the archaeomagnetic study of a Roman pottery kiln from Calahorra (Spain), *Geophys. J. Int.*, 123, 931-936.
- Kovacheva, M., Jordanova, N. and Karloukovski, V., 1998. Geomagnetic field variations as determined from Bulgarian archeomagnetic data. Part I: The last 2000 years AD, *Surv. Geophys.*, 15, 673-701.
- Kovacheva, M., Jordanova, N. and Karloukovski, V., 1998. Geomagnetic field variations as determined from Bulgaria Archaeomagnetic data. Part II: The last 8000 years, *Surv. Geophys.*, 19, 413-460.
- Lanos, Ph., 1987. *Archéomagnétisme des matériaux déplacés; Application à la datation des matériaux de construction d'argile cuite en archéologie*, Université de Rennes 1, 317 pp.
- Lanos, Ph., 2004. *Bayesian inference of calibration curves: application to archaeomagnetism*. In: C.E. Buck and A.R. Millard (Editors). Tools for constructing chronologies:

- crossing disciplinary boundaries. Lecture Notes in Statistics, vol. 177, London, pp. 43-82.
- Lanos, Ph., Le Goff, M., Kovacheva, M. and Schnepp, E., 2005. Hierarchical modelling of archaeomagnetic data and curve estimation by moving average technique, *Geophys. J. Int.*, 160, 440-476.
- Le Goff, M., 1990. Lissage et limites d'incertitude des courbes de migration polaire: ponderation des donnees et extension bivariate de la statistique de Fisher, *C. R. Acad. Sci. Paris*, 311 (Serie II), 1991-1998.
- Le Goff, M., Henry, B. and Daly, L., 1992. Practical method for drawing VGP path, *Phys. Earth Planet. Inter.*, 70, 201-204.
- Le Goff, M., Gallet, Y. Genevey, A. and Warmé, N., 2002. On archeomagnetic secular variation curves and archeomagnetic dating, *Phys. Earth Planet. Inter.*, 134, 203-211.
- Lowes, F. J., Mean square values on the sphere of spherical harmonic vector fields, 1966. *J. Geophys. Res.*, 71, 2179.
- Lowrie, W., 1990. Identification of ferromagnetic minerals in a rock by coercivity and unblocking temperature properties, *Geophys. Res. Lett.* 17, 159-162.
- McFadden, P.L. and McElhinny, M.W., 1988. The combined analysis of remagnetization circles and direct observations in paleomagnetism, *Earth Planet. Sci. Lett.*, 87, 161-172.
- McClelland-Brown, E., 1984. Experiments on TRM intensity dependence on cooling rate, *J. Geophys. Res. Lett.*, 11, 205-208.
- Márton, P., 2003. Recent achievements in archaeomagnetism in Hungary, *Geophys. J. Int.*, 153, 675-690.
- Marton, P., 1996. Archaeomagnetic directions: the Hungarian calibration curve. In: *Palaeomagnetism and Tectonics of the Mediterranean Region*. Morris A. and Tarling D. (eds), Geological Society Special publication No 105, 385-399.
- Moutmir, A., 1995. *Analyses magnétiques de terres cuites protohistoriques en France. Apports en archéomagnétisme (Premier millénaire avant J.C.) et en archéologie*, Paris, 245 pp.
- Nachasova, I.E., Burakov, K.S. and Bernabeu, J., 2002. Geomagnetic field intensity variations in Spain, *Phys. Solid. Earth, Engl. Transl.*, 38, 371-376.
- Najid, D., 1986. *Palaeomagnetic studies in Morocco*, Newcastle upon Tyne, 287 pp.
- Néel, L., 1955. Some theoretical aspects of rock-magnetism, *Adv. Phys.*, 4, 191-243.

- Noel, M. and Batt, C.M., 1990. A method for correcting geographically separated remanence vectors for the purpose of archeomagnetic dating, *Geophys. J. Int.*, 102, 753-756.
- Núñez, J.I., 2004. *Estudio arqueomagnético de la Península Ibérica: Primera curva de variación secular de los últimos tres milenios*, Universidad Complutense de Madrid, 320 pp.
- Oyamburu, I., Villalain, J.J., Osete, M.L., Zarzalejos, M. and Blasco, C., 1996. Estudio paleomagnético del yacimiento de Villa del Pañuelo (Villamanta, Madrid), *Geogaceta*, 20, 1044-1046.
- Parés, J.M., De Jonge, R., Pascual, J.O., Bermúdez, A., Tovar, C.J., Luezas, R.A. and Maestro, N., 1992. Archaeomagnetic evidence for the age of a Roman pottery kiln from Calahorra (Spain), *Geophys. J. Int.*, 112, 533-537.
- Peters, C. and Dekkers, M.J., 2003. Selected room temperature magnetic parameters as a function of mineralogy, concentration and grain size, *Phys. Chem. Earth*, 28, 659-667.
- Pick, T., and Tauxe, L., 1993. Holocene paleointensities: Thellier experiments on submarine basaltic glass from the East Pacific Rise, *J. Geophys. Res.*, 98 (B10), 17949-17964.
- Prévot, M., Mankinen, E.A., Coe, R.S. and Grommé, C.S., 1985. The Steens Mountain (Oregon) geomagnetic polarity transition. 2. Field intensity variations and discussion of reversal models, *J. Geophys. Res.*, 90, 10417-10448.
- Rolph; T.C., Shaw, J., 1986. Variations of the geomagnetic field in Sicily, *J. Geomagn. Geoelectr.*, 38, 1269-1277.
- Schnepp, E. and Lanos, Ph. 2005, Archaeomagnetic secular variation in Germany during the past 2500 years, *Geophys. J. Int.*, 163, 479-490.
- Schnepp, E., Pucher, R., Reindeers, J., Hambach, U., Soffel, H. and Hedley, I., 2004. A German catalogue of archaeomagnetic data, *Geophys. J. Int.*, 157, 64-78.
- Shaw, J., 1974. A new method of determining the magnitude of the palaeomagnetic field application to five historic lavas and five archaeological samples, *Geophys. J. R. astr. Soc.*, 39, 133-141.
- Shaw, J., Yang, S. Rolph, T. C. and Sun, F. Y., 1999. A comparison of archaeointensity results from Chinese ceramics using microwave and conventional Thellier's and Shaw's methods, *Geophys. J. Int.*, 136, 714-718.
- Tanguy, J.C., Le Goff, M., Chillemi, V., Paiotti, A., Principe, C., La Delfa, S. and Patanè, G., 1999. Variation séculaire de la direction du champ géomagnétique enregistrée par les

- laves de l'Etna et du Vésuve pendant les deux derniers millénaires. *C. R. Acad. Sci. Paris*, 329, 557-564.
- Tanguy, J.C., 1975. Intensity of the geomagnetic field from recent Italian lavas using a new paleointensity method. *Earth. Planet. Sci. Lett.*, 27, 314-320.
- Tarling, D.H., 1983. *Palaeomagnetism: Principles and applications in geology, geophysics and archaeology*, pp 279, Chapman and Hall, London.
- Tarling, D.H., 1999. The global archaeomagnetic data base, *Geophys. Res. Abstr.*, 1, 161, <http://www.ngdc.noaa.gov/seg/potfld/paleo.shtml>
- Tassi Ph., 1992, *Méthodes statistiques*, Economica, coll. "Economie et statistiques avancées", Paris, 474 p.
- Tauxe, L., 1998. *Paleomagnetic principles and practice*. Kluwer Academic Publishers, Boston, Massachusetts, 299 pp.
- Tauxe, L. and Staudigel, H., 2004. Strength of the geomagnetic field in the Cretaceous normal superchron: new data from submarine basaltic glass of the Troodos Ophiolite, *Geochem. Geophys. Geosyst.* 5, doi: 10.1029/2003GC000635, Q02H06.
- Thellier, E., Sur l'aimantation des terres cuites et ses applications géophysiques. Thèse de doctorat. Paris, *Ann. Inst. Phys. Globe Paris*, 16, 157-302, 1938.
- Thellier, E. and Thellier, O., 1959. Sur l'intensité du champ magnétique terrestre dans le passé historique et géologique, *Ann. Géophys.*, 15, 285-376.
- Thellier, E., 1981. Sur la direction du champ magnétique terrestre en France durant les deux derniers millénaires, *Phys. Earth Planet. Inter.*, 24, 89-132.
- Udías, A. and Mezcua, J. *Fundamentos de geofísica*, Alianza Editorial, Madrid.
- Veitch, R.J., Hedley, G. and Wagner, J.J., 1984. An investigation of the intensity of the geomagnetic field during Roman times using magnetically anisotropic bricks and tiles, *Arch. Sc. Genève*, 37, 359-373.
- Wahba G., 1990. *Spline models for observational data*, Society for industrial and applied mathematics, Philadelphia, Pennsylvania, 169 p.
- Walton, D., 1980. Time-temperature relations in the magnetization of assemblies of single domain grains, *Nature*, 286, 245-247.
- Yang, S., H. Odah and J. Shaw, Variation in the geomagnetic dipole moment over the past 12000 years, *Geophys. J. Int.*, 140, 158-162, 2000.

Annexes

I. Détermination de l'archéointensité	p197
II. Anisotropie de l'aimantation thermorémanente	p299
III. Détermination de températures de Curie	p305
IV. Acquisition d'aimantation rémanente isotherme (ARI) et désaimantation thermique des ARI croisées	p319
V. Fiches archéologiques des fours étudiés	p329

Annexe I: Détermination de l'archéointensité

22 fours, un lot de briques et un lot de céramiques ont été étudiés. Pour chaque site étudié, les résultats par échantillons, ainsi que les différents paramètres utilisés pour déterminer l'archéointensité sont réunis dans un tableau dans lequel est reporté également les moyennes par site. Les résultats sont donnés sous forme de tableaux résumant les différents paramètres utilisés pour déterminer l'archéointensité. Dans ces tableaux : Spl., référence de l'échantillon; NRM, aimantation rémanente de l'échantillon; χ , susceptibilité mesurée en champ faible et à température ambiante; $\Delta\chi$, variations maximales de la susceptibilité magnétique au cours des expériences de Thellier; Ql, rapport de Koenigsberger; Tmin-Tmax, intervalle de température utilisé pour le calcul de la pente; n, nombre d'étapes utilisées; f, fraction de l'aimantation rémanente utilisée; g, facteur de distance moyenne entre les points; q, facteur de qualité, mad, angle maximal de déviation (Kirschvink, 1980); dang, angle de déviation (Pick et Tauxe, 1993); crm, erreur potentielle maximale sur la détermination de l'intensité liée à l'acquisition d'une aimantation rémanente chimique; I et D (Ie et De), inclinaison et déclinaison avant (après) la correction d'anisotropie; $F \pm \sigma_F$, estimation de l'intensité et son erreur standard avant la correction d'anisotropie; Fe, estimation de l'intensité après la correction d'anisotropie; Tan, température à laquelle l'anisotropie a été mesurée; dMan, évolution magnéto chimique de l'aimantation pendant les cycle de mesures d'anisotropie; k1/k3, degré d'anisotropie; ki (I, D) avec i= 1, 2, 3, directions des axes principaux du tenseur d'anisotropie; ΔM et dz (pour 24 ou 48 h), facteur de correction lié à l'effet de la vitesse de refroidissement sur l'acquisition d'aimantation thermorémanente et l'évolution liée au cycle de mesures pour cette correction.

L'ordre de présentation des résultats obtenus par site est le suivant :

DENA	p199
MURG	p202
MURO	p205
MURN	p208
MURM	p211
MURL	p214
MURI	p217
MURH	p221
MURK	p227
CALA	p231
CALB	p235
CERCALB	p238
VALN	p241
VALI	p245
VALK	p249
VALM	p252
CALC	p255
PATH	p258
PATA	p264
PATB	p270
PATJ	p274
VALL	p280
GUA2	p284
YUS2	p288
CDAP	p291
CDAU	p293
CDAJ	p295
CDAH	p297

DENA: 220-250 A.D.

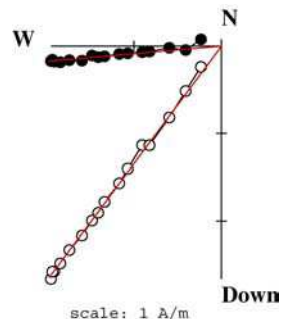
Latitude = 38° 52' N Longitude = 0° 1' E

 $H_{lab} = 50.0 \mu T$

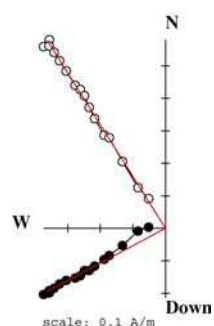
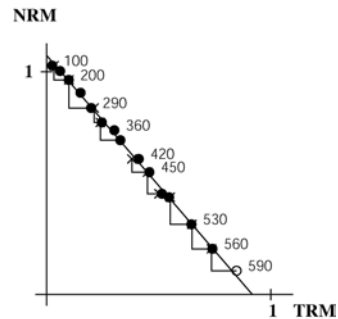
Spl	NRM (A/m)	χ (10^{-5})	$\Delta\chi$ (%)	Q _I	T _{min-T_{max}} (°C)	n	f	g	q	mad	dang	crm	anisotropy				F _e (μT)	T _{an} (°C)	dM _{an} (%)	k _{1/k₃} (%)	Direction of anisotropy axes				Cooling rate gain						
													no		yes		no		yes		k1		k2		k3		24 h		48 h		
													I	D	I _e	D _e	F ± σF	(μT)	I	D	I	D	I	D	ΔMz ₂₄ (%)	dz ₂₄ (%)	ΔMz ₄₈ (%)	dz ₄₈ (%)			
82-A	3.20	700	-4.4	11.50	100-560	14	0.77	0.91	56.1	1.6	0.7	4.6	53.6	-5.1	53.3	0.9	58.4 ± 0.7	58.5	500	-4.2	14.5	-22.1	29.0	59.7	75.0	19.7	-52.7	13.8	3.0	16.9	3.8
83-A	1.80	356	5.1	12.71	100-530	13	0.64	0.90	24.6	2.5	1.7	3.7	53.7	-4.2	51.1	-4.5	60.3 ± 1.7	64.0	500	-3.2	17.7	-9.3	-36.8	71.2	24.7	16.3	236.0	9.6	1.4	9.0	0.3
84-A	1.97	513	-7.0	9.65	100-500	12	0.68	0.91	29.5	1.9	0.3	2.4	53.5	-4.1	53.9	-2.1	61.2 ± 1.3	61.1	500	-3.5	7.0	21.9	59.5	56.4	186.6	24.2	-40.9	5.8	1.3	4.2	-1.8
85-A	5.56	1029	-8.6	13.59	100-560	13	0.86	0.89	48.0	2.3	1.0	3.3	52.6	-4.7	54.6	-2.4	58.1 ± 1.1	55.8	500	-1.5	12.1	-16.8	41.5	65.9	89.1	16.8	-43.3	7.2	-0.6	7.5	-2.1
86-A	5.43	483	16.8	28.25	100-530	13	0.84	0.89	41.3	1.7	1.8	5.7	53.3	0.1	53.9	1.4	53.9 ± 1.0	53.4	500	-2.7	6.2	-6.7	38.4	65.3	113.5	23.6	-48.7	3.6	2.8	3.5	-0.7
88-A	5.94	478	7.7	31.20	100-450	10	0.68	0.87	20	4.9	2.5	12.2	49.5	-5.8	49.9	-4.3	62.1 ± 1.9	58.0	390	-6.4	15.0	-43.9	-14.7	-17.9	93.4	40.7	19.5	3.4	-0.5	6.0	-3.7
89-A	2.29	522	-9.4	11.04	100-560	14	0.86	0.92	48.3	1.7	1.1	5.5	54.2	-3.4	54.4	-7.3	62.1 ± 1.0	61.3	500	-2.1	10.2	-27.2	42.7	-61.4	203.2	8.2	128.5	5.4	-1.4	5.2	-0.9
90-A	1.21	913	-9.0	3.32	100-530	13	0.78	0.91	45.9	2.4	0.8	2.4	53.3	-10.8	51.2	-12.6	58.1 ± 0.9	60.8	500	-1.1	11.3	-25.3	48.8	-57.4	186.4	19.2	129.3	3.6	-0.9	1.1	-2.0
91-A	1.99	671	-11.6	7.45	100-530	13	0.73	0.91	37.9	2.3	0.5	3.7	53.5	-3.4	52.8	-4.7	56.9 ± 1.0	57.4	500	-1.6	4.1	-51.4	46.3	38.5	49.6	1.6	-41.7	12.1	0.3	8.8	1.0
92-A	2.70	536	-5.2	12.64	100-560	14	0.87	0.92	68.3	1.6	0.7	3.6	50.8	-7.5	50.0	-8.1	59.5 ± 0.7	59.7	500	-5.6	4.9	-47.9	11.4	38.0	41.7	15.4	-60.8	7.7	0.4	2.5	0.0

Without anisotropy correction. 10 samples:										With anisotropy and cooling rate corrections. 10 samples:									
82-A . 83-A. 84-A. 85-A. 86-A. 88-A. 89-A. 90-A. 91-A. 92-A										82-A. 83-A. 84-A. 85-A. 86-A. 88-A. 89-A. 90-A. 91-A. 92-A									
F _m ± sd	F _{po}	I _{ms}	D _{ms}	F _{pa}	I _{pa}	D _{pa}	VDM	VADM	F _m ± sd	F _{po}	F _{pocr}	I _{ms}	D _{ms}	F _{pa}	I _{pa}	D _{pa}	VDM	VADM	
(μT)	(μT)	($^{\circ}$)	($^{\circ}$)	(μT)	($^{\circ}$)	($^{\circ}$)	($10^{22} A/m$)	($10^{22} A/m$)	(μT)	(μT)	(μT)	($^{\circ}$)	($^{\circ}$)	(μT)	($^{\circ}$)	($^{\circ}$)	($10^{22} A/m$)	($10^{22} A/m$)	
59.1 ± 2.5	58.8	52.8	-4.9	66.0	61.9	-5.3	11.0	10.3	59.0 ± 3.1	58.8	54.4 ± 3.4	52.6	-4.5	61.1	61.8	-4.8	10.2	9.5	
$\alpha_{95} = 1.4$ k = 1274										$\alpha_{95} = 1.9$ k = 669									
F_{ma} (μT)										I_{ma} ($^{\circ}$)									
60.1										D _{ma} ($^{\circ}$)									

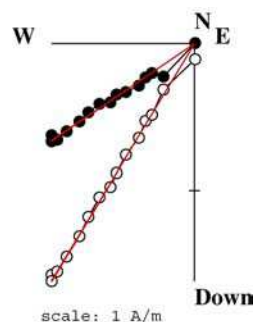
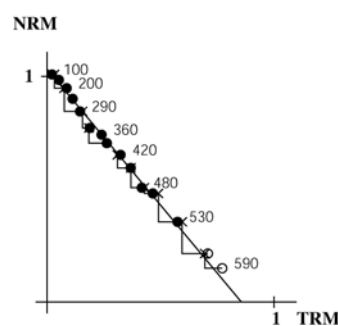
DENA. Age of the structure: 220-250 A.D.
 $H_{lab} = 50 \mu T$. Sample coordinates.



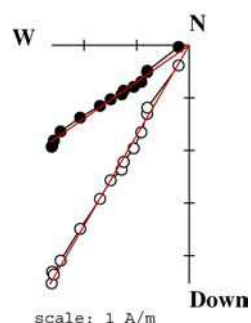
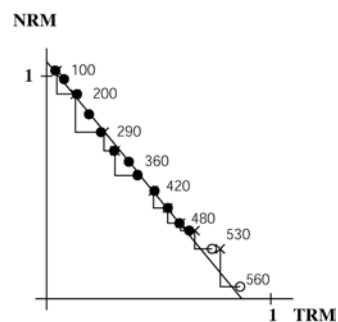
DENA82A
 With correction of anisotropy
 $NRM_0 = 3.20 \text{ A/m}$
 $F = 58.5 \mu T$
 $q = 56.1$



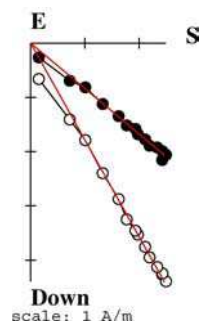
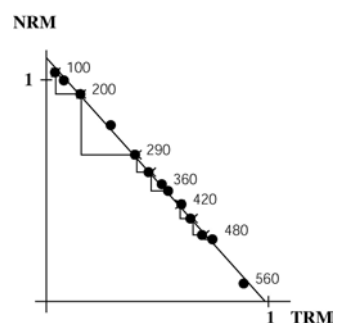
DENA83A
 With correction of anisotropy
 $NRM_0 = 1.80 \text{ A/m}$
 $F = 63.0 \mu T$
 $q = 24.6$



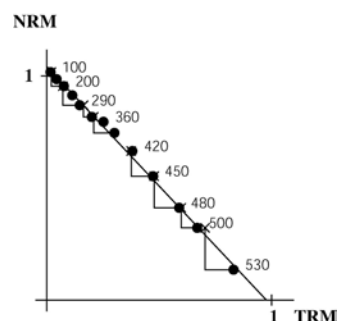
DENA84A
 With correction of anisotropy
 $NRM_0 = 1.97 \text{ A/m}$
 $F = 61.1 \mu T$
 $q = 29.5$

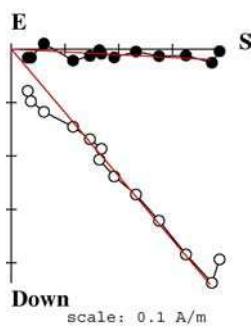


DENA85A
 With correction of anisotropy
 $NRM_0 = 5.56 \text{ A/m}$
 $F = 55.8 \mu T$
 $q = 48.0$

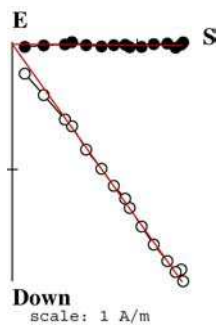
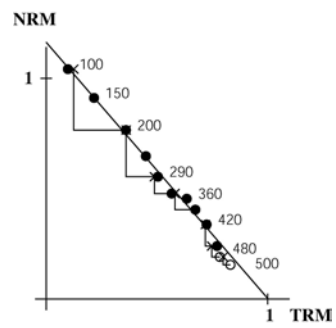


DENA86A
 With correction of anisotropy
 $NRM_0 = 5.43 \text{ A/m}$
 $F = 53.4 \mu T$
 $q = 41.3$

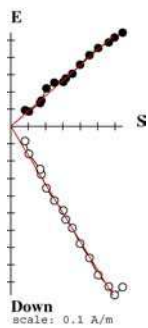
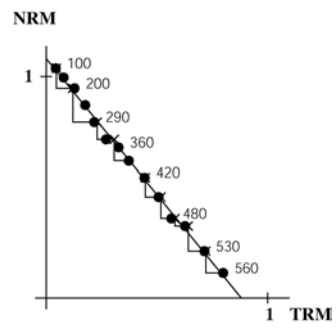




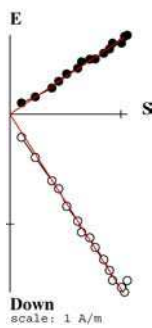
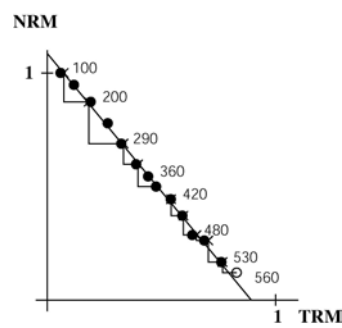
DENA88A
With correction of anisotropy
 $NRM_0 = 5.94 \text{ A/m}$
 $F = 58.0 \mu\text{T}$
 $q = 20.0$



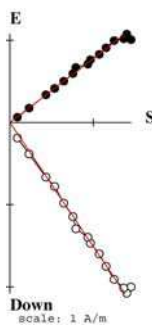
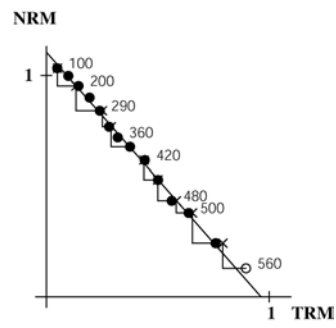
DENA89A
With correction of anisotropy
 $NRM_0 = 2.29 \text{ A/m}$
 $F = 61.3 \mu\text{T}$
 $q = 48.3$



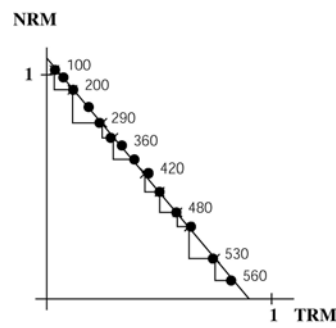
DENA90A
With correction of anisotropy
 $NRM_0 = 1.21 \text{ A/m}$
 $F = 60.8 \mu\text{T}$
 $q = 45.9$



DENA91A
With correction of anisotropy
 $NRM_0 = 1.99 \text{ A/m}$
 $F = 57.4 \mu\text{T}$
 $q = 37.9$



DENA92A
With correction of anisotropy
 $NRM_0 = 2.70 \text{ A/m}$
 $F = 59.7 \mu\text{T}$
 $q = 68.3$



MURG: 1000-1100 A.D.

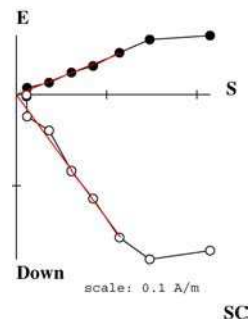
Latitude = $37^{\circ} 59' N$ Longitude = $1^{\circ} 07' W$

$$H_{lab} = 60.0 \text{ } \mu\text{T}$$

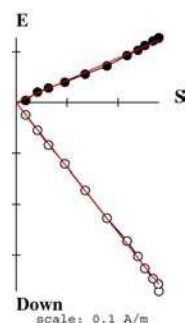
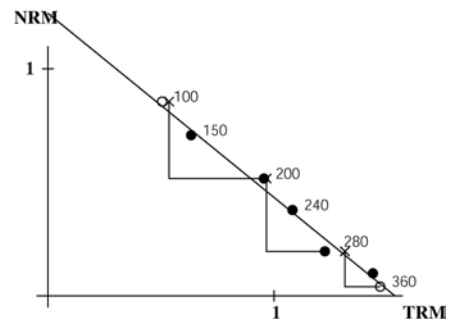
H _{lab} = 60.0 μT															anisotropy				Direction of anisotropy axes				Cooling rate gain									
Spl	NRM (A/m)	χ		Δχ		Q _i	T _{min} -T _{max} (°C)	n	f	g	q	mad	dang	crm	no		yes		no		yes		k1		k2		k3		24 h		48 h	
		(10 ⁻⁵)	(%)	(%)	(%)										(°)	(°)	(°)	(°)	(%)	(%)	(%)	(%)	(°)	(°)	(°)	(°)	(%)	(%)	(%)	(%)		
1-B	0.31	926	-14.0	0.8	150-320	5	0.51	0.73	4.0	3.3	0.4	4.2	53.4	25.2	51.7	22.8	47.2 ± 3.7	48.7	360	3.9	15.3	-17.6	67.5	-69.3	214.5	10.6	154.1	5.8	6.5	15.4	-5.1	
2-B	0.52	58	-27.6	22.5	100-480	11	0.90	0.89	47.5	1.1	0.4	1.1	49.5	19.4	49.5	19.8	74.4 ± 1.6	74.0	360	-6.4	9.2	22.3	-53.8	-62.5	-15.6	15.3	42.7	-1.7	-1.4			
3-B	8.25	1145	-15.0	18.1	100-390	8	0.90	0.83	49.8	1.9	0.9	3.2	50.1	26.0	50.4	24.1	56.3 ± 0.8	55.0	360	0.4	9.0	-40.3	62.0	16.0	137.9	45.4	31.0	0.2	-5.9	3.2	-1.0	
10-A	0.16	134	-10.4	3.0	100-360	7	0.79	0.79	31.4	2.2	0.5	2.0	52.1	22.8	52.6	21.4	55.4 ± 1.0	54.4	360	1.8	8.4	-23.0	74.5	26.1	152.5	54.0	20.2	-0.7	-5.8	6.5	1.0	
11-A	0.34	157	-11.5	5.4	100-420	9	0.78	0.84	66.7	1.8	0.2	2.2	49.0	21.2	51.9	18.5	58.6 ± 0.5	56.2	360	-2.9	13.5	-14.5	34.3	-8.1	126.4	73.3	64.8	-0.5	2.0			
12-A	0.4	101	-13.9	10.0	100-450	10	0.79	0.79	31.4	2.2	0.5	2.0	49.5	26.9	50.5	24.8	55.8 ± 1.8	55.0	450	-3.1	6.9	-27.1	59.5	-6.2	152.7	62.1	74.5	0.6	-1.1			
13-A	5.99	115	-13.9	130.9	100-480	11	0.78	0.89	45.3	1.9	0.5	3.6	52.1	22.1	53.8	18.5	63.4 ± 0.9	60.4	360	-5.8	14.3	-18.4	31.8	24.8	112.9	58.3	-25.6	-2.9	-1.2	broken		
17-A	0.01	10	30.0	2.5	280-420	5	0.41	0.74	9.3	1.7	2.5	3.9	48.5	25.8	49.9	23.2	41.9 ± 0.9	40.5	360	-1.3	9.5	-31.8	22.6	-13.7	121.3	54.7	51.5	5.2	-0.2			

Without anisotropy correction. 8 samples:								With anisotropy and cooling rate corrections. 8 samples:										
$F_m \pm sd$	F_{po}	I_{ms}	D_{ms}	F_{pa}	I_{pa}	D_{pa}	VDM	$F_m \pm sd$	F_{po}	F_{pocr}	I_{ms}	D_{ms}	F_{pa}	I_{pa}	D_{pa}	VDM	VADM	
(μT)	(μT)	($^\circ$)	($^\circ$)	(μT)	($^\circ$)	($^\circ$)	($10^{22} A/m$)	(μT)	(μT)	(μT)	($^\circ$)	($^\circ$)	(μT)	($^\circ$)	($^\circ$)	($10^{22} A/m$)	($10^{22} A/m$)	
56.6 ± 9.8	59.5	50.6	23.7	68.2	61.1	27.9	11.4	10.5	55.5 ± 9.6	58.0	58.3 ± 10.5	51.3	21.7	66.4	61.7	25.6	11.1	10.3
$\alpha_{95} = 1.7$				F_{ma}	I_{ma}	D_{ma}		$\alpha_{95} = 1.5$				F_{ma}	I_{ma}	D_{ma}				
$k = 1081$				(μT)	($^\circ$)	($^\circ$)		$k = 1437$				(μT)	($^\circ$)	($^\circ$)				
				60.6	52.1	23.8						59.4	52.9	21.8				

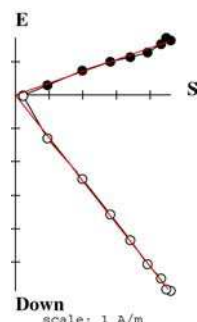
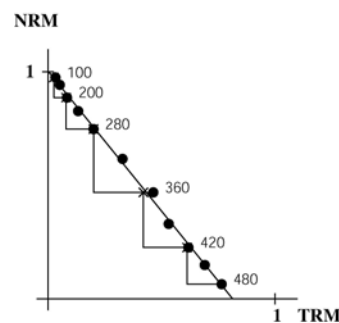
MURG. Age of the structure: 1000-1100 A.D.
 $H_{lab} = 60 \mu T$. Sample coordinates.



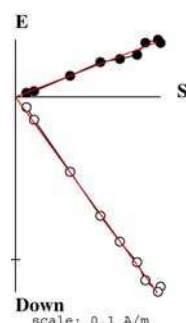
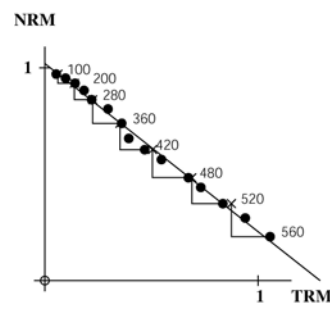
MURG1B
 With correction of anisotropy
 $NRM_0 = 0.31 \text{ A/m}$
 $F = 48.7 \mu T$
 $q = 4.0$



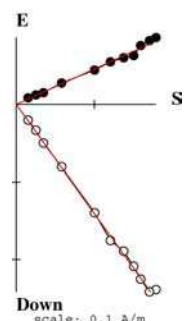
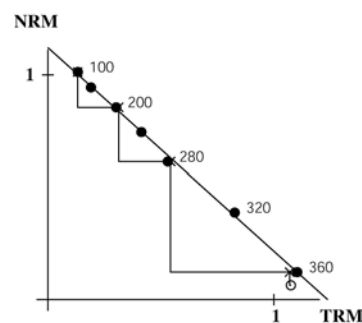
MURG2B
 With correction of anisotropy
 $NRM_0 = 0.52 \text{ A/m}$
 $F = 74.0 \mu T$
 $q = 47.5$



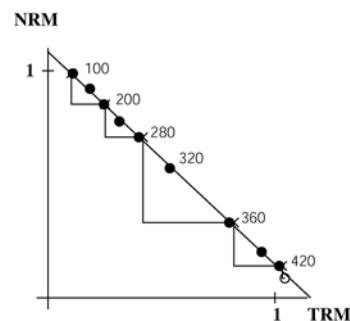
MURG3B
 With correction of anisotropy
 $NRM_0 = 8.25 \text{ A/m}$
 $F = 55.0 \mu T$
 $q = 49.8$

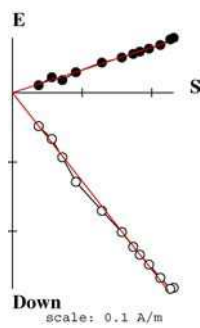


MURG10A
 With correction of anisotropy
 $NRM_0 = 0.16 \text{ A/m}$
 $F = 54.4 \mu T$
 $q = 31.4$

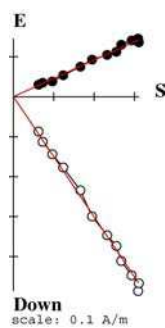


MURG11A
 With correction of anisotropy
 $NRM_0 = 0.34 \text{ A/m}$
 $F = 56.2 \mu T$
 $q = 66.7$

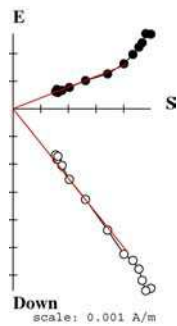




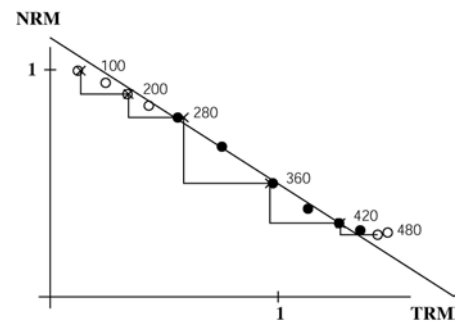
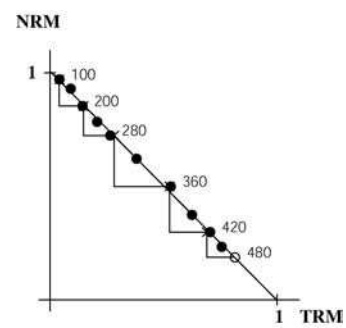
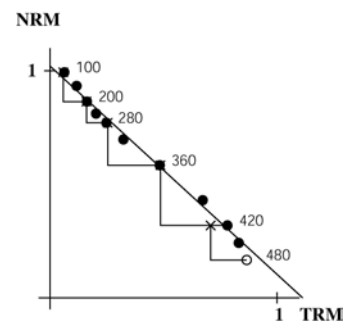
MURG12A
With correction of anisotropy
 $NRM_0 = 0.40 \text{ A/m}$
 $F = 55.0 \mu\text{T}$
 $q = 20.7$



MURG13A
With correction of anisotropy
 $NRM_0 = 5.99 \text{ A/m}$
 $F = 60.4 \mu\text{T}$
 $q = 45.3$



MURG17A
With correction of anisotropy
 $NRM_0 = 0.01 \text{ A/m}$
 $F = 40.5 \mu\text{T}$
 $q = 9.3$



MURO: 1100-1200 A.D.

Latitude = 37° 59' N Longitude = 1° 07' W

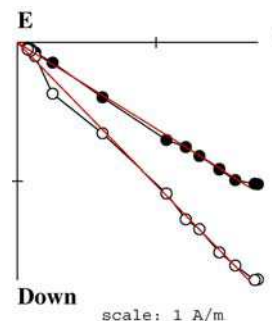
 $H_{lab} = 50.0 \mu T$

Spl	NRM (A/m)	anisotropy												Direction of anisotropy axes						Cooling rate gain											
		No			yes			no			yes			k ₁			k ₂			k ₃			24 h		48 h						
		χ (10 ⁻⁵)	$\Delta\chi$ (%)	Q _I	T _{min-T_{max}} (°C)	n	f	g	q	mad	dang	crm	I	D	I _e	D _e	F ± σF	F _e (μT)	T _{an} (°C)	dM _{an} (%)	k _{1/k₃} (%)	I	D	I	D	I	D	ΔMz ₂₄ (%)	dz ₂₄ (%)	ΔMz ₄₈ (%)	dz ₄₈ (%)
1-A	2.66	723	-11.3	9.25	100-425	10	0.93	0.84	33.8	0.6	0.1	2.0	43.8	16.4	41.1	17.5	60.7 ± 1.4	63.8	350	-10.5	10.3	-77.5	-48.7	-12.5	129.6	0.4	39.6	15.2	2.8	21.9	0.9
2-A	2.94	682	-20.5	10.83	100-425	10	0.83	0.85	18.8	2.0	1.3	3.1	44.3	20.3	43.7	19.3	72.8 ± 2.6	70.1	400	-3.0	9.5	-49.4	48.3	21.1	111.6	32.8	7.2	19.1	6.5	24.5	3.6
2-B	2.09	625	-13.3	8.39	100-425	10	0.65	0.85	11.3	1.5	1.2	2.8	44.8	18.5	43.3	19.0	69.3 ± 3.4	71.4	400	3.0	12.5	-0.3	-53.1	85.3	33.5	4.7	216.9	13.5	8.5	19.9	2.5
3-A	5.27	728	-12.6	18.19	100-425	10	0.60	0.83	14.8	1.9	0.4	2.5	43.9	18.4	46.6	18.2	67.4 ± 2.3	64.7	400	0.8	12.1	8.3	53.4	21.9	146.8	66.4	-56.2	15.0	12.1	19.2	8.7
4-A	1.72	587	-21.5	7.36	100-425	10	0.84	0.82	22.4	2.3	0.6	3.5	46.6	11.7	48.6	9.5	59.6 ± 1.8	58.3	300	4.5	19.0	18.4	-60.3	1.2	30.1	71.6	123.7	9.5	1.8	17.0	-2.1
5-A	0.69	577	-20.1	3.01	100-425	10	0.75	0.85	17.4	3.2	2.9	10.7	41.0	14.4	43.2	9.7	72.4 ± 2.7	69.5	300	7.0	15.6	-5.9	54.8	-52.3	152.5	37.1	140.3	21.6	7.3	29.9	2.3
6-A	5.22	1455	-26.6	9.02	100-425	10	0.81	0.85	41.4	2.4	1.4	5.2	43.7	11.4	44.5	7.2	64.3 ± 1.1	61.8	300	1.1	12.1	-24.2	53.4	-56.3	185.7	22.0	133.0	17.9	6.0	22.7	6.6

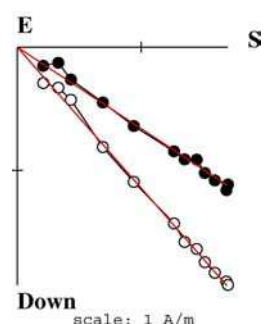
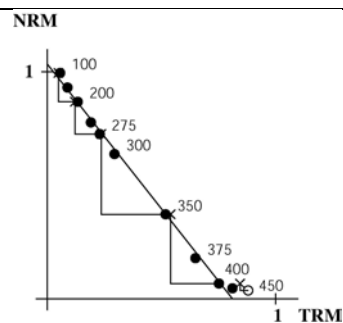
Without anisotropy correction. 6 samples:										With anisotropy and cooling rate corrections. 6 samples:									
I-A. 2-A. 3-A. 4-A. 5-A. 6-A										I-A. 2-A. 3-A. 4-A. 5-A. 6-A									
F _m ± sd	F _{po}	I _{ms}	D _{ms}	F _{pa}	I _{pa}	D _{pa}	VDM	VADM	F _m ± sd	F _{po}	F _{pocr 24 h}	F _{pocr 48 h}	I _{ms}	D _{ms}	F _{pa 24h}	I _{pa}	D _{pa}	VDM _{24h}	VADM _{24h}
(μT)	(μT)	(°)	(°)	(μT)	(°)	(°)	(10 ²² A/m)	(10 ²² A/m)	(μT)	(μT)	(μT)	(μT)	(°)	(°)	(μT)	(°)	(°)	(10 ²² A/m)	(10 ²² A/m)
66.2 ± 5.7	65.1	43.9	15.4	75.1	56.3	18.2	13.5	11.5	64.7 ± 4.5	64.0	53.4 ± 5.3	49.1 ± 5.9	44.7	13.6	61.5	56.9	16.2	11.0	9.5
$\alpha_{95} = 2.6$ k = 677										$\alpha_{95} = 3.8$ k = 308									

MURO. Age of the structure: 1100-1200 A.D.

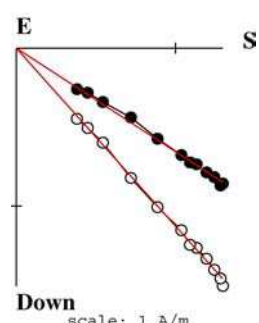
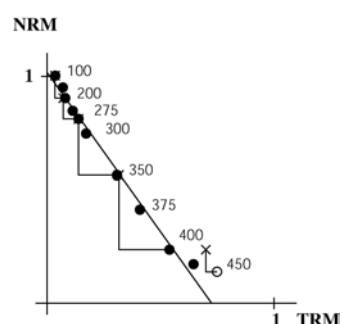
$H_{lab} = 50 \mu T$. Sample coordinates.



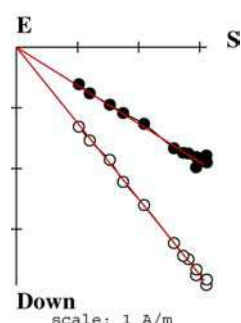
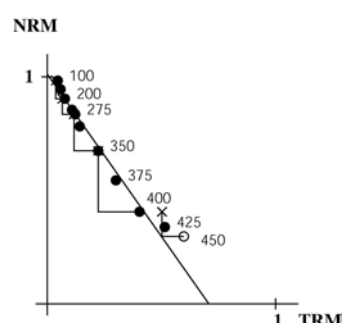
MURO1A
With correction of anisotropy
 $NRM_0 = 2.66 \text{ A/m}$
 $F = 63.8 \mu T$
 $q = 33.8$



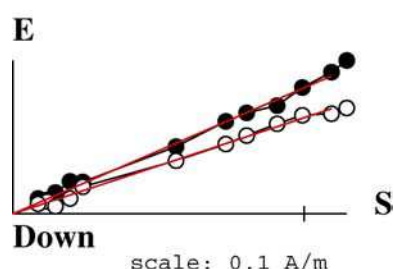
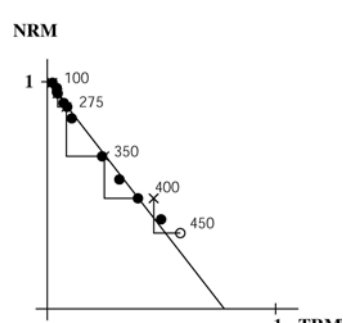
MURO2A
With correction of anisotropy
 $NRM_0 = 2.94 \text{ A/m}$
 $F = 70.1 \mu T$
 $q = 18.8$



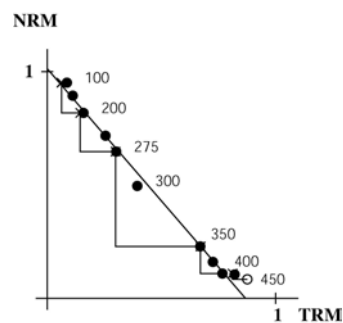
MURO2B
With correction of anisotropy
 $NRM_0 = 2.09 \text{ A/m}$
 $F = 71.4 \mu T$
 $q = 11.3$

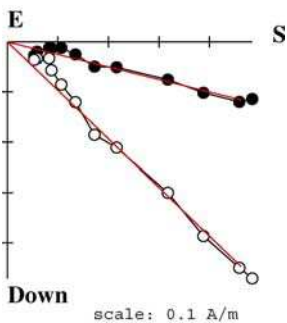


MURO3A
With correction of anisotropy
 $NRM_0 = 5.27 \text{ A/m}$
 $F = 64.7 \mu T$
 $q = 14.6$

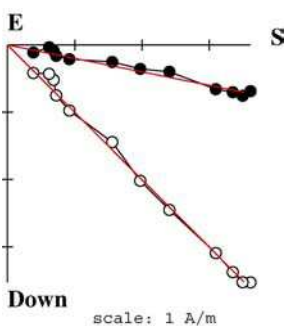


MURO4A
With correction of anisotropy
 $NRM_0 = 1.72 \text{ A/m}$
 $F = 58.3 \mu T$
 $q = 22.4$

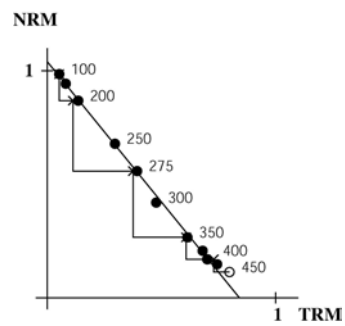
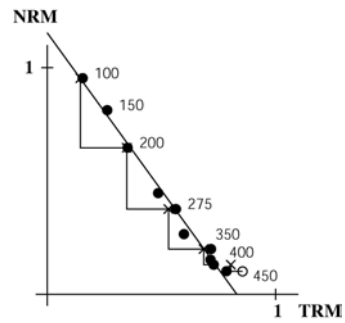




MURO5A
With correction of anisotropy
 $NRM_0 = 0.69 \text{ A/m}$
 $F = 69.5 \mu\text{T}$
 $q = 17.4$



MURO6A
With correction of anisotropy
 $NRM_0 = 5.22 \text{ A/m}$
 $F = 61.8 \mu\text{T}$
 $q = 41.4$



MURN: 1100-1200 A.D.

Latitude = $37^{\circ} 59' N$ Longitude = $1^{\circ} 07' W$

$$H_{lab} = 60.0 \text{ } \mu T$$

H _{lab} = 60.0 μT															anisotropy								Direction of anisotropy axes								Cooling rate gain							
Spl	NRM (A/m)	χ (10 ⁻⁵)	Δχ (%)	Q _I	T _{min} -T _{max} (°C)	n	f	g	q	mad	dang	crm	no		yes		no		yes		T _{an} (°C)	dM _{an} (%)	k ₁ /k ₃ (%)	k1		k2		k3		24 h		48 h						
															I	D	I _e	D _e	F ± σF	F _e (μT)			I	D	I	D	ΔMz ₂₄ (%)	dz ₂₄ (%)	ΔMz ₄₈ (%)	dz ₄₈ (%)								
2-A	1.68	997	-21.8	4.2	150-480	10	0.71	0.88	11.6	2.6	1.9	4.6	43.4	10.7	42.7	11.2	53.7 ± 2.6	53.7	360	-3.3	5.2	-31.7	-58.9	-47.2	72.8	25.6	13.9	0.8	0.6	1.7	-2.9							
7-A	0.42	119	-21.8	8.9	150-450	9	0.73	0.82	10.0	1.7	0.1	1.1	45.0	17.2	47.2	15.5	51.2 ± 3.3	49.8	450	2.7	10.3	3.8	63.0	-10.4	152.3	78.9	172.7	-2.3	-0.1	-0.4	-2.6							
8-B	0.25	69	-11.6	9.1	100-420	9	0.6	0.81	14.3	3.3	0.6	2.9	43.6	17.8			52.5 ± 1.6										-3.3	0.0										
13-A	0.37	70	-8.6	13.3	150-450	9	0.57	0.87	18.8	2.2	0.6	2.6	44.7	14.6	45.9	16.5	67.3 ± 2.0	67.6	450	2.2	15.8	-7.0	-51.6	24.5	35.2	64.4	233.1	-0.8	0.0	3.0	-4.6							
14-A	0.12	67	-13.4	4.5	100-560	15	0.88	0.92	44.7	2.0	0.9	1.2	44.9	15.1	46.3	15.9	44.8 ± 0.6	43.5	500	-3.2	12.9	-2.3	39.7	67.5	124.2	22.3	-49.4	4.9	-10.1	6.6	3.8							
17-A	3.03	430	18.1	17.7	100-450	9	0.64	0.76	20.5	2.0	0.8	2.1	43.1	14.0	44.0	15.2	45.1 ± 0.8	44.4	450	-0.2	10.8	-14.4	-33.2	-26.9	64.3	58.9	31.5	1.5	3.2	-0.4	-1.7							
18-B	6.58	1361	-15.4	12.2	100-480	11	0.87	0.83	49.3	1.3	0.2	3.0	43.6	9.7	44.2	10.3	56.9 ± 0.8	55.0	360	-2.1	8.9	-1.8	-39.6	-38.2	51.8	51.8	48.1	-3.6	-0.4	-1.6	-1.9							

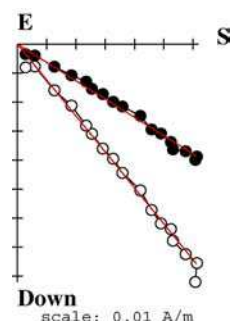
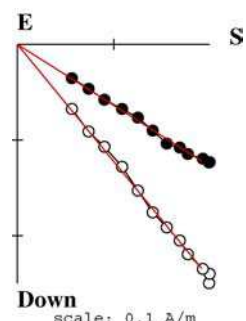
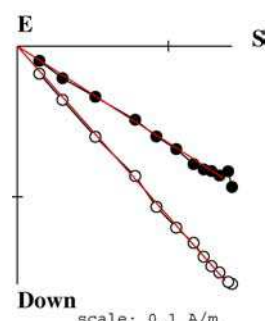
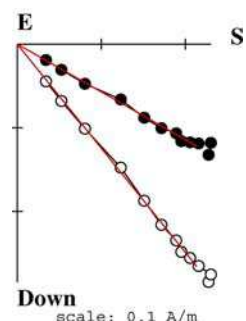
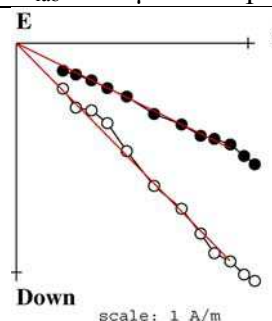
Without anisotropy correction. 7 samples:									With anisotropy and cooling rate correction. 6 samples:											
F _m ± sd	F _{po}	I _{ms}	D _{ms}	F _{pa}	I _{pa}	D _{pa}	VDM	VADM	F _m ± sd	F _{po}	F _{po} cr 24 h	F _{po} cr 48 h	I _{ms}	D _{ms}	F _{pa} 24h	I _{pa}	D _{pa}	VDM _{24h}	VADM _{48h}	
(μT)	(μT)	(°)	(°)	(μT)	(°)	(°)	(10 ²² A/m)	(10 ²² A/m)	(μT)	(μT)	(μT)	(μT)	(°)	(°)	(μT)	(°)	(°)	(10 ²² A/m)	(10 ²² A/m)	
53.1 ± 7.7	52.9	44.1	14.1	60.9	56.4	16.8	10.9	9.4	52.3 ± 8.8	51.9	52.0 ± 9.7	51.2 ± 8.8	45.1	14.0	59.8	57.1	16.7	10.6	9.0	
$\alpha_{95} = 1.7$			F_{ma}	I_{ma}	D_{ma}				$\alpha_{95} = 2.1$			F_{ma} 24h	I_{ma}	D_{ma}						
k = 1214			(μT)	(°)	(°)				k = 1038			(μT)	(°)	(°)				53.2	47.3	13.7
			54.2	46.4	13.7															

Samples rejected:

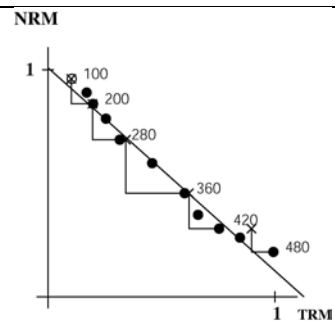
8B: (o correction of anisotropy).

MURN. Age of the structure: 1100-1200 A.D.

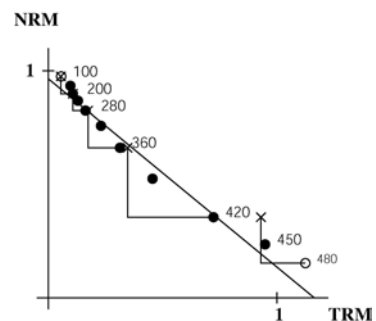
$H_{lab} = 60 \mu T$. Sample coordinates.



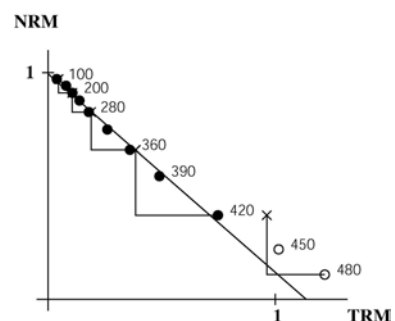
MURN2A
With correction of anisotropy
 $NRM_0 = 1.68 \text{ A/m}$
 $F = 53.7 \mu T$
 $q = 11.6$



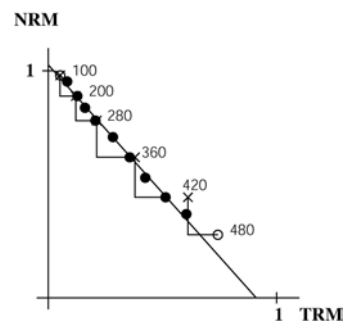
MURN7A
With correction of anisotropy
 $NRM_0 = 0.42 \text{ A/m}$
 $F = 49.8 \mu T$
 $q = 10.0$



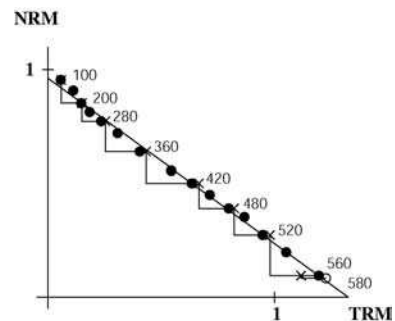
MURN8B
Without correction of anisotropy
 $NRM_0 = 0.25 \text{ A/m}$
 $F = 52.5 \mu T$
 $q = 14.3$

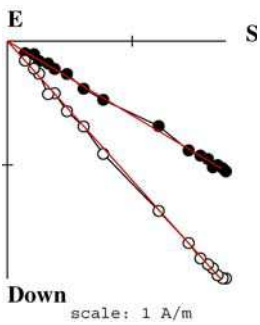


MURN13A
With correction of anisotropy
 $NRM_0 = 0.37 \text{ A/m}$
 $F = 67.6 \mu T$
 $q = 18.8$

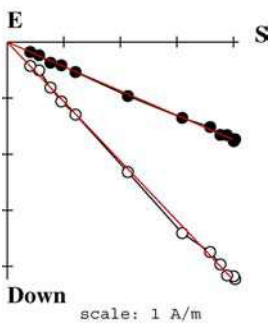


MURN14A
With correction of anisotropy
 $NRM_0 = 0.12 \text{ A/m}$
 $F = 43.5 \mu T$
 $q = 44.7$

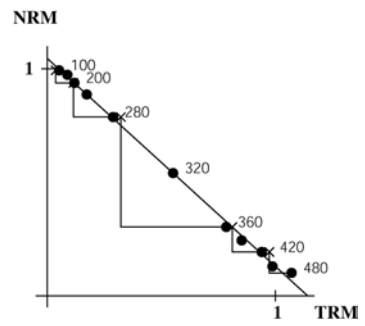
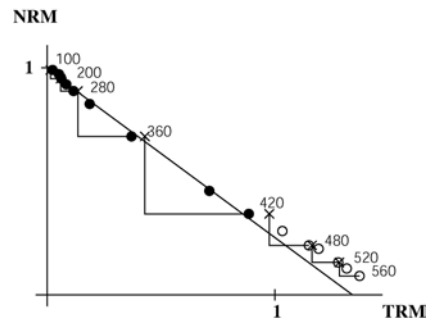




MURN17A
With correction of anisotropy
 $NRM_0 = 3.03 \text{ A/m}$
 $F = 44.4 \mu\text{T}$
 $q = 20.5$



MURN18B
With correction of anisotropy
 $NRM_0 = 6.58 \text{ A/m}$
 $F = 55.0 \mu\text{T}$
 $q = 49.3$



MURM: 1100-1200 A.D.

Latitude = 37° 59' N Longitude = 1° 07' W

 $H_{lab} = 50.0 \mu T$

Spl	NRM (A/m)	anisotropy														T_{an} (°C)	dM_{an} (%)	k_1/k_3 (%)	Direction of anisotropy axes				Cooling rate gain								
		no		yes		no		yes		k1		k2		k3						24 h		48 h									
		I	D	I_e	D_e	$F \pm \sigma F$	F_e	(°)	(°)	(°)	(°)	(°)	(°)	(°)	(°)				(%)		(%)										
2-A	0.44	145	-15.2	7.55	100-330	6	0.73	0.70	18.3	2.1	2.1	4.4	42.1	15.9	43.6	14.9	54.9 ± 1.6	54.5	330	0.4	13.5	18.4	-38.2	7.4	54.3	70.1	165.4	4.2	-2.9	8.0	-2.6
6-A	0.63	138	-10.9	11.49	100-450	10	0.86	0.87	29.1	2.1	2.2	2.0	45.9	18.0	48.0	18.4	55.1 ± 1.6	53.8	330	0.6	9.9	-3.5	-50.5	7.9	39.0	81.3	242.8	0.8	-0.4	0.8	-0.9
6-B	0.61	168	-11.3	9.15	100-390	8	0.61	0.84	11.7	2.8	3.0	5.4	49.0	18.4	48.6	18.5	53.2 ± 2.8	52.0	330	-2.0	14.0	4.0	-47.6	-54.8	36.7	34.9	45.2	0.3	0.0		
8-A	0.25	57	-10.5	11.05	100-500	12	0.70	0.90	24.5	2.6	1.0	3.1	44.2	16.5	46.3	19.3	54.9 ± 1.6	50.1	500	0.1	17.8	-31.3	-4.7	-0.5	85.6	58.7	-3.6	3.9	-1.1	4.3	-3.9
9-A	2.28	301	-9.0	19.00	100-420	9	0.92	0.79	31.7	2.6	0.4	4.7	43.4	15.1	44.6	12.7	59.0 ± 1.6	58.1	390	-4.0	7.7	-20.8	87.7	-25.4	188.1	56.2	143.2	6.7	1.0	9.2	2.0
10-A	1.47	322	-3.1	11.47	100-330	6	0.55	0.62	7.7	2.7	2.5	4.4	43.5	15.3	44.6	13.4	48.8 ± 2.0	48.1	330	-1.1	8.0	2.0	48.8	-66.0	134.4	23.9	139.7	-1.6	-1.1	-4.2	-0.5
12-A	0.23	58	-20.7	9.90	100-590	15	0.92	0.91	37.4	1.7	0.5	2.6	46.7	14.6	48.2	13.6	52.2 ± 1.3	51.1	500	-1.9	8.4	1.3	43.6	-84.6	120.0	5.3	133.7	12.1	0.6	12.1	-0.6
13-B	2.54	428	2.1	14.92	100-330	6	0.64	0.66	11.9	4.0	3.4	5.9	44.8	15.1	43.1	12.3	52.6 ± 1.8	54.5	330	-7.1	13.8	72.7	-81.7	11.1	47.3	13.1	139.9	2.7	-1.4	5.1	-1.1
14-A	0.66	67	-4.5	24.70	rejected																										
15-A	1.16	131	-6.1	22.22	100-360	7	0.41	0.58	4.9	6.2	1.9	6.9	44.4	13.8	39.3	14.0	48.8 ± 1.9	52.7	390	-34.0	21.4	-80.4	9.7	4.4	72.7	8.5	-17.9	5.7	-1.2	6.0	-2.5

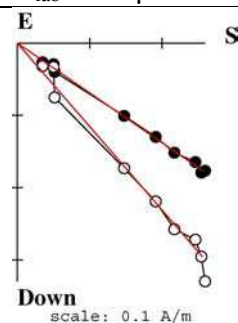
Without anisotropy correction. 7 samples:							With anisotropy and cooling rate corrections. 7 samples:												$F_m \pm sd$		F_{po}		$F_{po cr 24\text{ h}}$		$F_{po cr 48\text{ h}}$		I_{ms}		D_{ms}		$F_{pa 24\text{ h}}$		I_{pa}		D_{pa}		$VDM_{24\text{ h}}$		$VADM_{24\text{ h}}$	
(μT)	(μT)	(°)	(°)	(μT)	(°)	(°)	(μT)	(μT)	(μT)	(μT)	(μT)	(°)	(°)	(μT)	(μT)	(μT)	(μT)	(°)	(°)	(μT)	(μT)	(°)	(°)	(μT)	(μT)	(°)	(°)	(10 ²² A/m)	(10 ²² A/m)											
53.9 ± 3.2	54.6	44.4	15.8	62.9	56.6	18.7	11.2		9.7					52.9 ± 3.3	53.5	50.9 ± 3.4	50.2 ± 2.9	45.5	14.9	58.6	57.5	17.7	10.4							9.0										
$\alpha_{95} = 1.3$		F_{ma}	I_{ma}	D_{ma}										$\alpha_{95} = 2.1$						$F_{ma 24\text{ h}}$	I_{ma}	D_{ma}																		
$k = 2110$		(μT)	(°)	(°)										$k = 811$						(μT)	(°)	(°)																		
		55.9	46.6	15.5																52.1	47.7	14.6																		

Rejected samples:

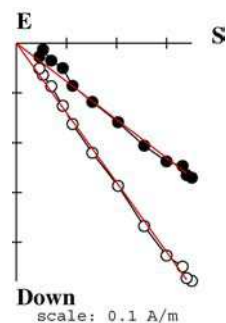
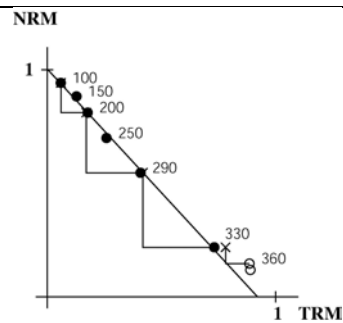
6B (sister specimen of 6A); 14A (not going through the origin); 15A (Tan bigger than the interval of T retained).

MURM. Age of the structure: 1100-1200 A.D.

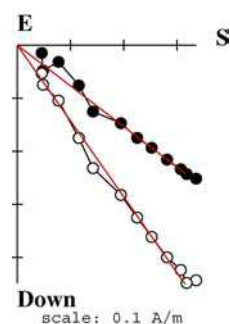
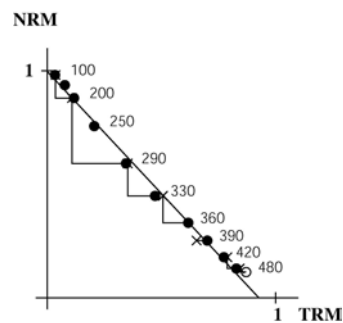
$H_{lab} = 50 \mu T$. Sample coordinates.



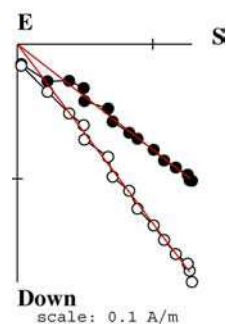
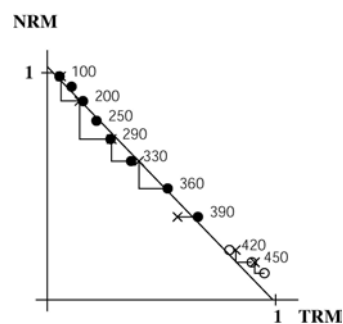
MURM2A
With correction of anisotropy
 $NRM_0 = 0.44 \text{ A/m}$
 $F = 54.5 \mu T$
 $q = 18.3$



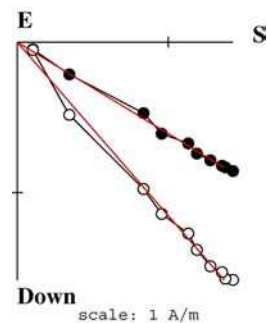
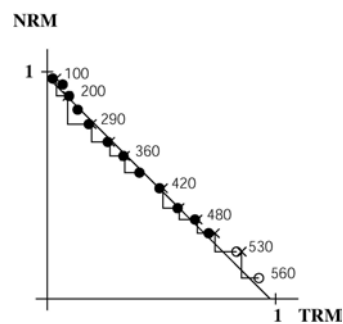
MURM6A
With correction of anisotropy
 $NRM_0 = 0.63 \text{ A/m}$
 $F = 53.8 \mu T$
 $q = 29.1$



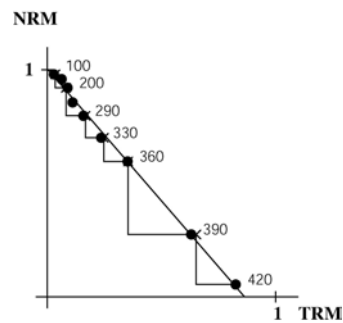
MURM6B
With correction of anisotropy
 $NRM_0 = 0.61 \text{ A/m}$
 $F = 52.0 \mu T$
 $q = 11.7$

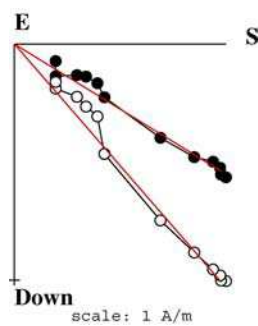


MURM8A
With correction of anisotropy
 $NRM_0 = 0.25 \text{ A/m}$
 $F = 50.1 \mu T$
 $q = 24.5$

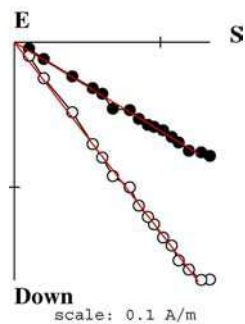
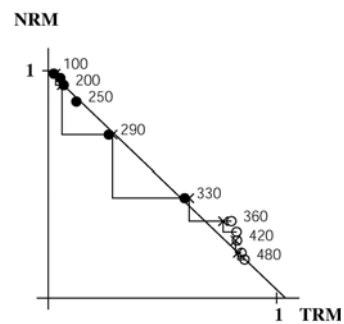


MURM9A
With correction of anisotropy
 $NRM_0 = 2.28 \text{ A/m}$
 $F = 58.1 \mu T$
 $q = 31.7$

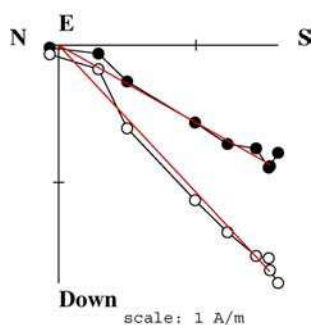
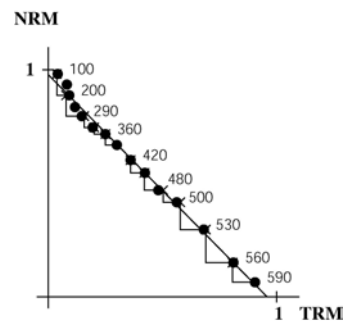




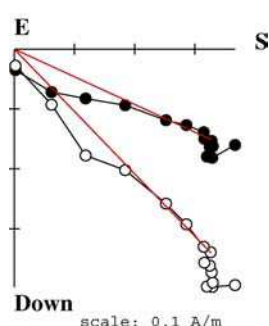
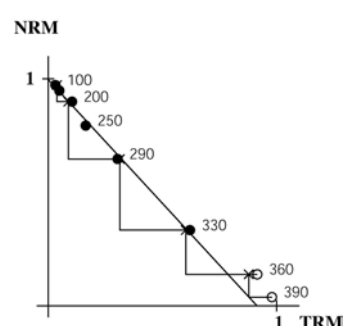
MURM10A
With correction of anisotropy
 $NRM_0 = 1.47 \text{ A/m}$
 $F = 48.1 \mu\text{T}$
 $q = 7.7$



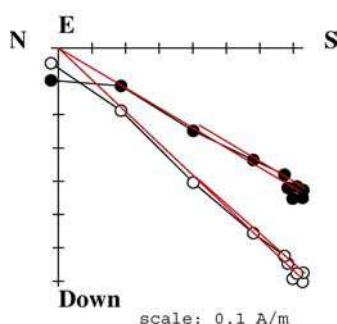
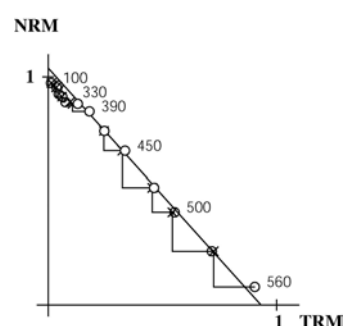
MURM12A
With correction of anisotropy
 $NRM_0 = 0.23 \text{ A/m}$
 $F = 51.1 \mu\text{T}$
 $q = 37.4$



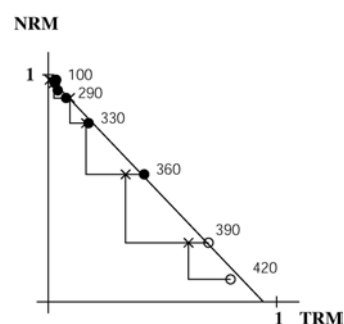
MURM13B
With correction of anisotropy
 $NRM_0 = 2.54 \text{ A/m}$
 $F = 54.5 \mu\text{T}$
 $q = 11.9$



MURM14A
With correction of anisotropy
 $NRM_0 = 0.66 \text{ A/m}$
Rejected



MURM15A
With correction of anisotropy
 $NRM_0 = 1.16 \text{ A/m}$
 $F = 52.7 \mu\text{T}$
 $q = 4.9$



MURL: 1100-1200 A.D.

Latitude = 37° 59' N Longitude = 1° 07' W

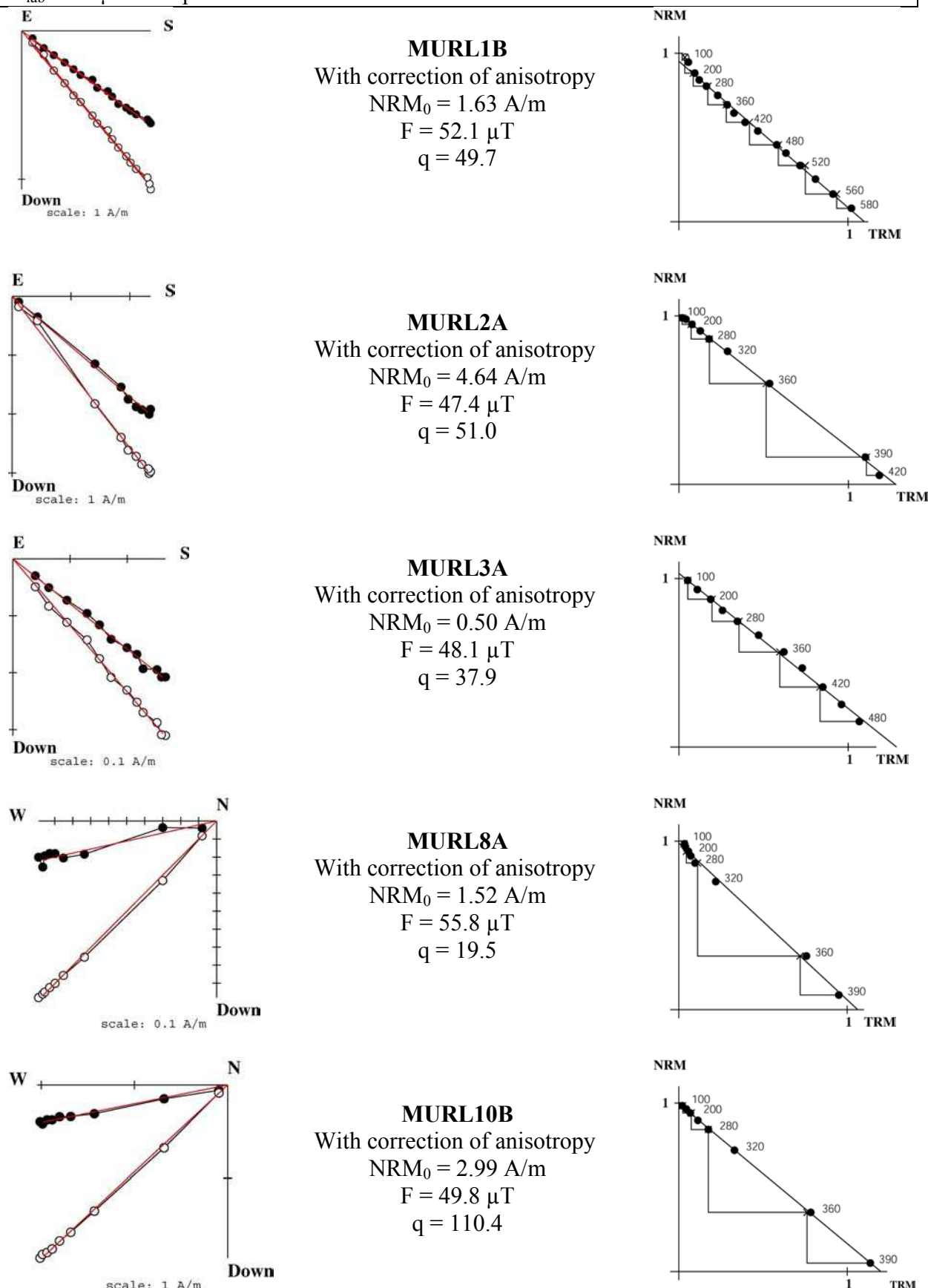
 $H_{lab} = 60.0 \mu T$

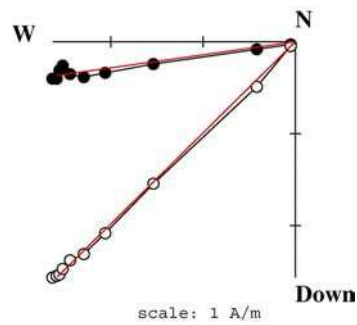
Spl	NRM (A/m)	anisotropy												Direction of anisotropy axes						Cooling rate gain											
		no			yes			no			yes			k1			k2			k3			24 h		48 h						
		I	D	I_e	D_e	$F \pm \sigma F$	F_e	T_{an}	dM_{an}	k_1/k_3	I	D	I_e	D_e	$F \pm \sigma F$	F_e	T_{an}	dM_{an}	k_1/k_3	I	D	I_e	D_e	$F \pm \sigma F$	F_e	T_{an}	dM_{an}	k_1/k_3	ΔMz_{24}	dz_{24}	ΔMz_{48}
1-B	1.63	279	-10.4	14.7	150-580	15	0.90	0.92	49.7	1.6	0.2	1.4	42.9	14.3	44.2	15.1	53.3 ± 0.8	52.1	450	0.9	5.4	8.5	60.8	18.6	153.7	69.5	-52.7	5.7	0.6	5.0	2.3
2-A	4.64	513	-4.3	22.7	100-420	9	0.92	0.71	51.0	2.2	0.4	2.6	42.2	18.3	44.4	18.8	50.3 ± 0.6	47.4	390	-3.4	9.2	-13.0	30.3	-2.3	120.9	76.8	40.7	-2.0	-6.3	-2.2	-6.0
3-A	0.50	104	-9.6	12.1	100-480	11	0.80	0.89	37.9	2.2	0.8	1.8	42.0	16.3	42.5	16.5	48.9 ± 0.7	48.1	450	-1.5	5.8	-5.5	-54.3	-14.9	37.2	74.0	15.9	1.2	-0.4	3.1	-1.1
8-A	1.52	425	-2.6	9.0	100-390	8	0.89	0.64	19.5	3.4	0.7	3.2	43.3	13.7	44.4	14.5	57.0 ± 1.5	55.8	360	0.1	10.7	-1.2	76.2	76.8	161.3	13.2	-13.5	-2.8	-12.3	0.5	-4.5
10-B	2.99	409	-8.8	18.4	100-390	8	0.93	0.71	110.4	1.3	0.9	1.6	42.4	16.9	42.4	16.1	50.2 ± 0.3	49.8	360	2.0	8.5	-16.7	-67.8	-65.1	62.6	17.9	16.6	1.5	-5.2	2.4	-2.1
11-A	3.99	488	-4.9	20.5	100-420	9	0.97	0.72	77.9	2.2	0.8	1.9	43.6	18.2	44.5	19.5	54.5 ± 0.4	52.4	390	-5.5	7.4	-19.6	36.8	-18.5	133.7	62.5	83.7	0.3	-3.2	-0.4	-4.8
13-A	5.13	597	-5.7	21.6	100-390	8	0.93	0.56	140.0	2.6	0.6	2.9	45.4	14.1	45.9	16.9	45.6 ± 0.2	44.8	390	-4.1	13.4	-43.2	-15.3	-10.6	84.8	44.9	5.5	3.3	-6.0	2.9	-3.6
14-A	7.93	1066	-7.7	18.7	100-390	8	0.93	0.80	141.7	2.5	1.1	2.4	43.2	17.9	45.5	13.1	54.2 ± 0.2	50.5	360	-3.3	8.2	19.0	-47.4	-1.5	42.1	71.0	127.6	3.2	-5.1	2.8	-2.7
15-A	5.05	686	-8.5	18.5	100-420	9	0.77	0.77	57.4	2.5	0.9	1.9	42.9	14.7	43.8	14.8	57.4 ± 0.6	55.6	390	-8.7	19.8	7.3	32.4	-42.0	115.9	47.1	130.3	5.4	-0.4	10.0	2.2

Without anisotropy correction. 9 samples:												With anisotropy and cooling rate correction. 9 samples:												
I-B, 2-A, 3-A, 8-A, 10-B, 11-A, 13-A, 14-A, 15-A												I-B, 2-A, 3-A, 8-A, 10-B, 11-A, 13-A, 14-A, 15-A												
$F_m \pm sd$	F_{po}	I_{ms}	D_{ms}	F_{pa}	I_{pa}	D_{pa}	VDM	VADM	$F_m \pm sd$	F_{po}	F_{pocr}	I_{ms}	D_{ms}	F_{pa}	I_{pa}	D_{pa}	VDM	VADM						
(μT)	(μT)	($^\circ$)	($^\circ$)	(μT)	($^\circ$)	($^\circ$)	($10^{22} A/m$)	($10^{22} A/m$)	(μT)	(μT)	(μT)	($^\circ$)	($^\circ$)	(μT)	($^\circ$)	($^\circ$)	($10^{22} A/m$)	($10^{22} A/m$)						
52.4 ± 3.9	51.9	43.1	16.1	59.8	55.6	19.0	10.8	9.2	50.7 ± 3.7	49.7	48.6 ± 3.9	44.2	16.2	56.0	56.5	19.1	10.0	8.4						
$\alpha_{95} = 1.1$	F_{ma}	I_{ma}	D_{ma}						$\alpha_{95} = 1.2$	$F_{ma\ 24h}$	I_{ma}	D_{ma}												
$k = 2274$	(μT)	($^\circ$)	($^\circ$)						$k = 1842$	(μT)	($^\circ$)	($^\circ$)												
	53.1	45.4	15.7							49.7	46.4	15.8												

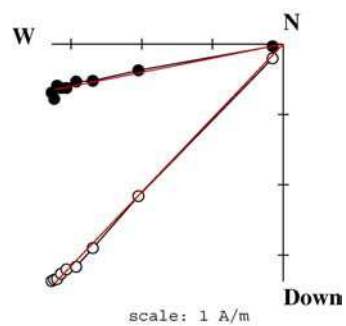
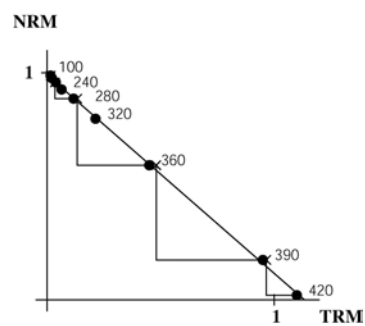
MURL. Age of the structure: 1100-1200 A.D.

$H_{lab} = 60 \mu T$. Sample coordinates.

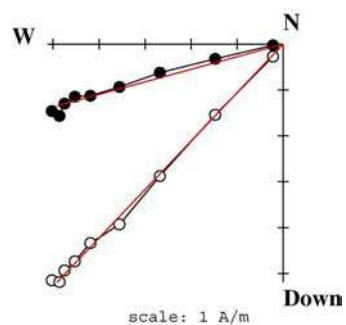
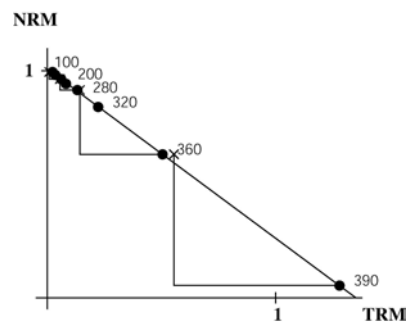




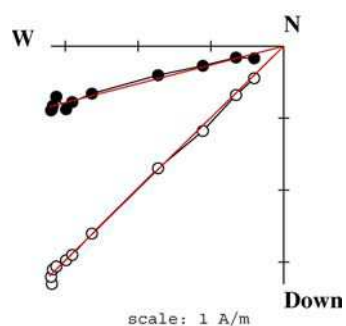
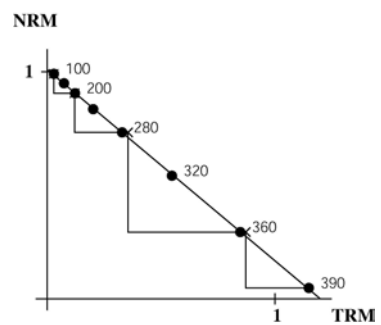
MURL11A
With correction of anisotropy
 $NRM_0 = 3.99 \text{ A/m}$
 $F = 52.4 \mu\text{T}$
 $q = 77.9$



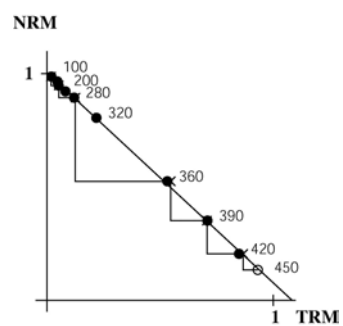
MURL13A
With correction of anisotropy
 $NRM_0 = 5.13 \text{ A/m}$
 $F = 44.8 \mu\text{T}$
 $q = 140.0$



MURL14A
With correction of anisotropy
 $NRM_0 = 7.93 \text{ A/m}$
 $F = 50.5 \mu\text{T}$
 $q = 141.7$



MURL15A
With correction of anisotropy
 $NRM_0 = 5.05 \text{ A/m}$
 $F = 55.6 \mu\text{T}$
 $q = 57.4$



MURI: 1100-1200 A.D.

Latitude = 37° 59' N Longitude = 1° 07' W

 $H_{lab} = 60.0 \mu T$

Spl	NRM (A/m)	χ (10^{-5})	$\Delta\chi$ (%)	Q _i	T _{min} -T _{max} (°C)	n	f	g	q	mad	dang	crm	anisotropy				F _e (μT)	T _{an} (°C)	dM _{an} (%)	k ₁ /k ₃ (%)	Direction of anisotropy axes				Cooling rate gain						
													no		yes		no		yes		k1		k2		k3		24 h		48 h		
													I	D	I _e	D _e	F ± σF	F _e	T _{an}	dM _{an}	k ₁ /k ₃	I	D	I	D	I	D	ΔMz ₂₄	dz ₂₄	ΔMz ₄₈	dz ₄₈
1-A	1.83	300	-11.0	15.3	100-320	7	0.79	0.83	33.4	2.4	0.4	2.4	42.6	10.1	39.1	8.8	60.0 ± 1.2	63.9	290	-18.4	15.7	-84.3	13.4	-3.1	135.7	4.9	46.0	3.3	-1.2	6.6	-3.1
2-A	4.45	443	-5.0	25.3	100-350	8	0.73	0.80	30.6	3.3	1.3	3.5	42.3	14.9	32.2	14.7	55.3 ± 1.0	58.1	320	-11.1	14.1	79.3	-36.8	-0.7	49.4	10.6	139.3	5.8	-3.5	4.6	-4.1
3-A	6.65	795	-8.1	21.0	100-350	8	0.73	0.79	24.3	2.8	1.2	3.2	41.0	22.6	38.9	25.9	51.6 ± 1.0	52.5	320	-4.7	17.4	-55.8	69.5	-32.2	227.5	10.2	144.1	10.8	-2.7	10.1	-2.9
4-A	1.78	148	7.4	30.3	100-560	15	0.86	0.91	79.7	2.7	1.6	2.5	41.3	16.9	40.6	16.2	60.1 ± 0.6	60.2	410	-4.0	5.5	-69.2	73.4	9.5	137.2	18.3	44.0	-7.4	-7.6	-7.9	-9.4
5-A	1.63	327	-5.5	12.6	100-320	7	0.78	0.82	38.4	2.6	2.3	3.6	41.2	15.0	42.0	18.3	54.1 ± 0.8	51.5	290	-2.5	15.6	-9.6	48.1	-62.6	157.2	25.4	133.5	2.3	-3.7	5.4	-2.2
6-A	6.00	649	-5.5	23.2	100-380	9	0.61	0.68	9.4	4.6	1.5	1.8	43.0	17.3	41.3	17.9	50.5 ± 1.9	51.8	380	-7.8	8.4	-57.6	5.7	-27.6	151.3	15.5	69.6	-3.0	-7.0	0.9	-4.7
7-B	3.84	454	-3.5	21.3	100-350	8	0.50	0.74	14.5	4.8	5.1	3.5	43.6	18.2			49.9 ± 1.0										7.9	0.0	2.4	-1.8	
8-A	7.44	830	-3.0	22.5	100-350	8	0.52	0.80	31.6	4.2	3.2	5.4	44.0	11.2			49.8 ± 0.5														
11-A	0.97	242	-7.4	10.1	100-320	7	0.71	0.75	27.3	5.6	4.1	5.4	42.9	7.3	43.2	8.8	46.9 ± 0.7	45.5	320	-0.2	10.0	-3.4	36.8	-61.0	132.9	28.7	125.0	7.4	-0.6	10.8	-2.0
12-A	0.92	131	-6.1	17.7	100-320	7	0.58	0.72	16.2	4.4	2.3	4.6	41.3	6.6	39.8	5.0	45.6 ± 0.9	44.7	320	-2.0	16.9	24.8	-26.5	-44.9	36.1	34.8	82.2	1.8	-6.0	5.6	-5.8
13-B	2.24	266	-4.5	21.1	100-320	7	0.27	0.77	3.6	13.5	5.0	7.8	41.2	14.9			37.4 ± 1.5														
14-A	0.79	134	-1.5	14.9	100-320	7	0.35	0.72	4.1	6.9	4.7	7.3	40.0	14.5			60.5 ± 3.7														
15-A	0.61	218	-7.8	7.0	100-290	6	0.74	0.78	23.7	4.3	1.1	3.9	41.2	14.4	44.8	14.2	46.2 ± 0.9	43.4	290	11.3	13.6	3.3	65.0	-4.1	154.8	84.7	193.6	0.2	-1.7	0.9	0.9

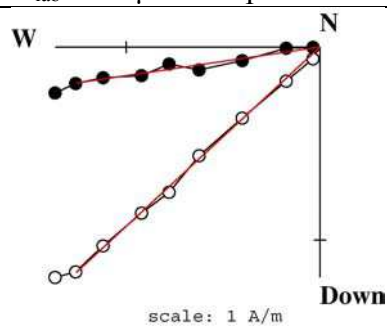
Without anisotropy correction. 11 samples:								With anisotropy and cooling rate correction. 7 samples:										
1-A. 2-A. 3-A. 4-A. 5-A. 6-A. 7-B. 8-A. 11-A. 12-A. 15-A								3-A. 4-A. 5-A. 6-A. 11-A. 12-A. 15-A										
F _m ± sd	F _{po}	I _{ms}	D _{ms}	F _{pa}	I _{pa}	D _{pa}	VDM	F _m ± sd	F _{po}	F _{pocr}	I _{ms}	D _{ms}	F _{pa}	I _{pa}	D _{pa}	VDM	VADM	
(μT)	(μT)	($^{\circ}$)	($^{\circ}$)	(μT)	($^{\circ}$)	($^{\circ}$)	($10^{22} A/m$)	(μT)	(μT)	(μT)	($^{\circ}$)	($^{\circ}$)	(μT)	($^{\circ}$)	($^{\circ}$)	($10^{22} A/m$)	($10^{22} A/m$)	
51.8 ± 5.1	53.2	42.3	14.0	61.4	55.1	16.6	11.2	9.4	49.9 ± 5.9	51.4	51.1 ± 7.9	41.7	15.2	59.0	54.6	18.0	10.8	8.8
$\alpha_{95} = 2.1$								$\alpha_{95} = 4.1$								$F_{ma\ 24h}$		
k = 466								k = 215								(μT)		
54.5								52.3								(°)		
44.7								44.0								(°)		
13.6								14.8										

Rejected samples:

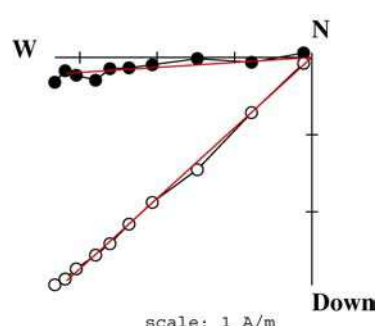
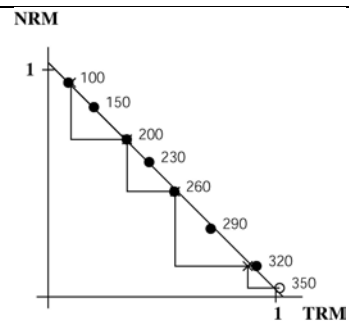
1A (dM_{an}>15%). 2A (bad correction of anisotropy); 7B and 8A (no correction of anisotropy); 13B and 14A (no correction of anisotropy and f < 0.4).

MURI. Age of the structure: 1100-1200 A.D.

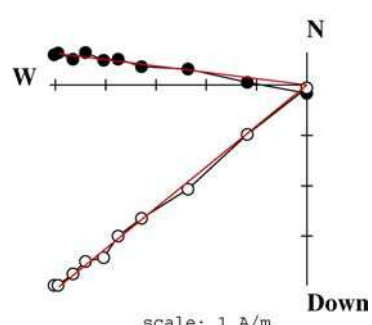
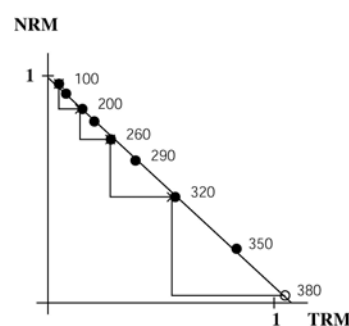
$H_{lab} = 60 \mu\text{T}$. Sample coordinates.



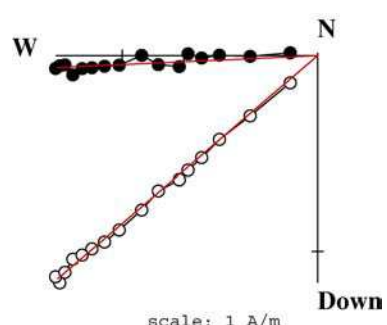
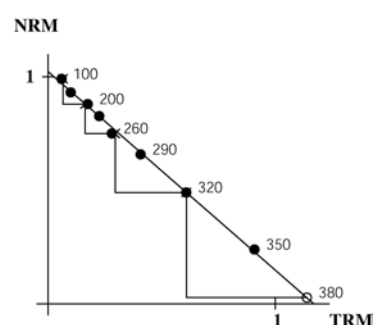
MURI1A
Without correction of
anisotropy
 $\text{NRM}_0 = 1.83 \text{ A/m}$
 $F = 60.0 \mu\text{T}$
 $q = 33.4$



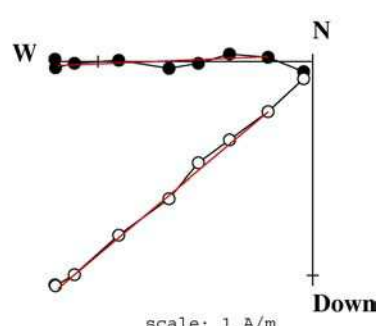
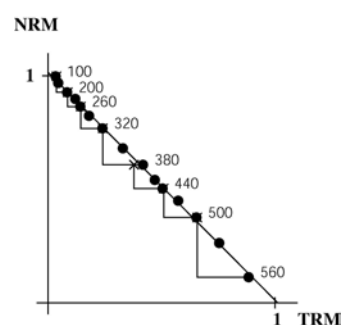
MURI2A
Without correction of
anisotropy
 $\text{NRM}_0 = 4.45 \text{ A/m}$
 $F = 58.1 \mu\text{T}$
 $q = 30.6$



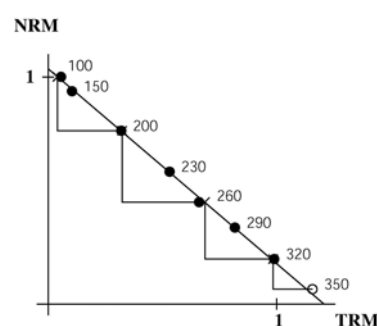
MURI3A
With correction of anisotropy
 $\text{NRM}_0 = 6.65 \text{ A/m}$
 $F = 52.5 \mu\text{T}$
 $q = 24.3$

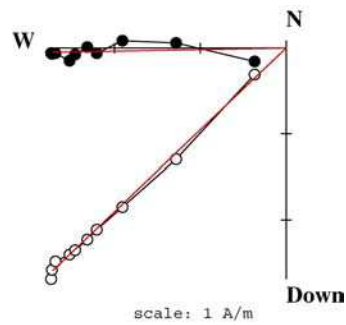


MURI4A
With correction of anisotropy
 $\text{NRM}_0 = 1.78 \text{ A/m}$
 $F = 60.2 \mu\text{T}$
 $q = 79.7$

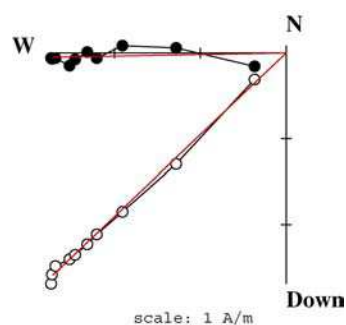
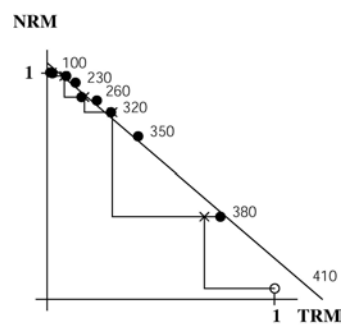


MURI5A
With correction of anisotropy
 $\text{NRM}_0 = 1.63 \text{ A/m}$
 $F = 51.5 \mu\text{T}$
 $q = 38.4$

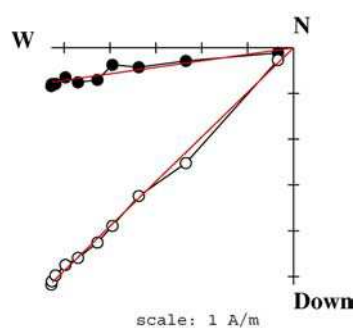
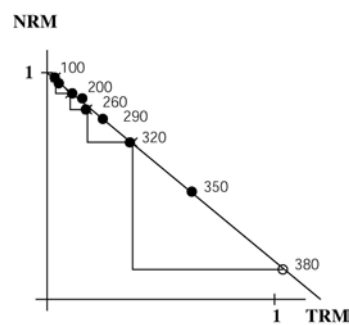




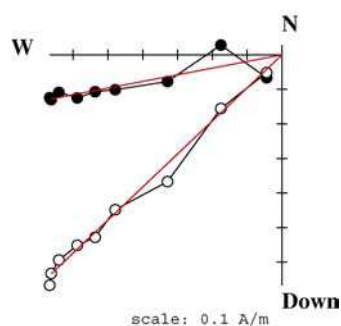
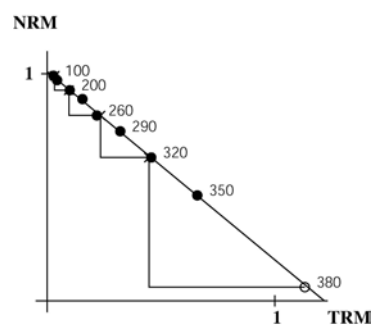
MURI6A
With correction of anisotropy
 $NRM_0 = 6.00 \text{ A/m}$
 $F = 51.8 \mu\text{T}$
 $q = 9.4$



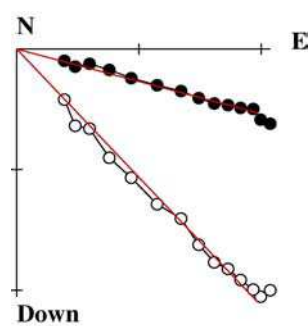
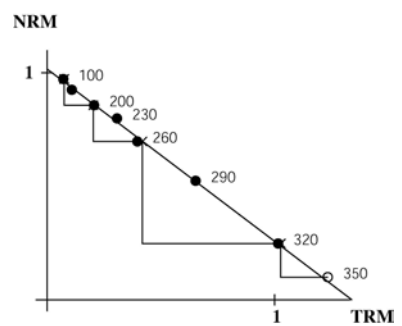
MURI7B
Without correction of
anisotropy
 $NRM_0 = 3.84 \text{ A/m}$
 $F = 49.9 \mu\text{T}$
 $q = 14.5$



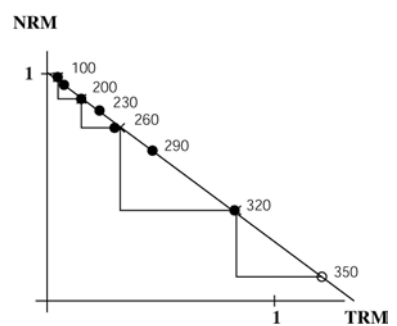
MURI8A
Without correction of
anisotropy
 $NRM_0 = 7.44 \text{ A/m}$
 $F = 49.8 \mu\text{T}$
 $q = 31.6$

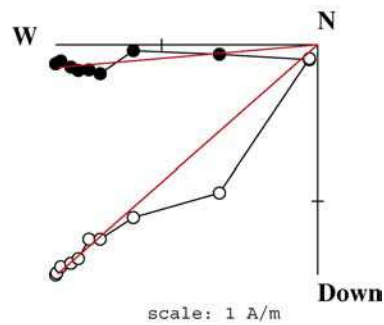


MURI11A
With correction of anisotropy
 $NRM_0 = 0.97 \text{ A/m}$
 $F = 45.5 \mu\text{T}$
 $q = 27.3$

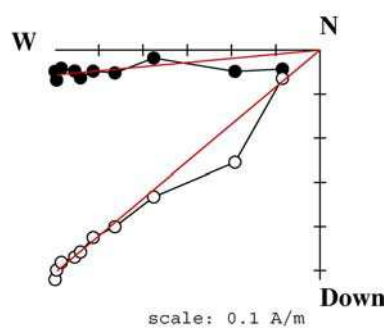
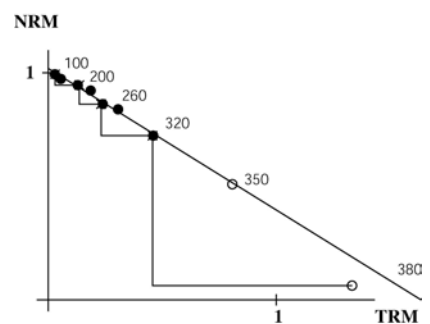


MURI12A
With correction of anisotropy
 $NRM_0 = 0.92 \text{ A/m}$
 $F = 44.7 \mu\text{T}$
 $q = 16.2$

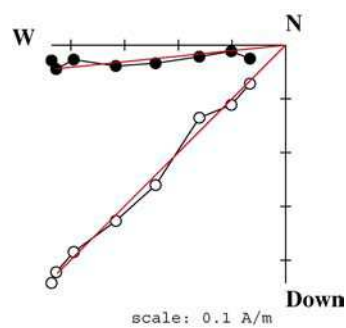
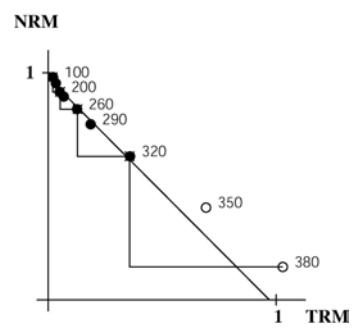




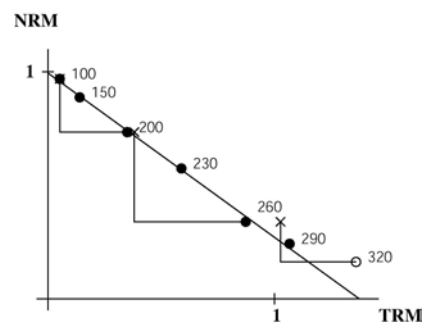
MURI13B
Without correction of
anisotropy
 $NRM_0 = 2.24 \text{ A/m}$
 $F = 37.4 \mu\text{T}$
 $q = 3.6$



MURI14A
Without correction of
anisotropy
 $NRM_0 = 0.79 \text{ A/m}$
 $F = 60.5 \mu\text{T}$
 $q = 4.1$



MURI15A
With correction of anisotropy
 $NRM_0 = 0.61 \text{ A/m}$
 $F = 43.4 \mu\text{T}$
 $q = 23.7$



MURH: 1100-1200 A.D.

Latitude = 37° 59' N Longitude = 1° 07' W

H_{lab} = 50.0 µT

Spl	NRM (A/m)	anisotropy												T _{an} (°C)	dM _{an} (%)	k ₁ /k ₃ (%)	Direction of anisotropy axes				Cooling rate gain											
		no		yes		no		yes		k1		k2					k3		24 h		48 h											
		I	D	I _e	D _e	F ± σF	F _e	(°)	(°)	(°)	(°)	(°)	(°)	(°)	(°)	(°)	(°)	(°)	(%)	(%)	(%)	(%)										
1-A	4.72	544	-10.7	21.8	100-325	6	0.80	0.57	12.8	4.7	4.4	16.1	46.9	11.0	37.3	10.7	62.6 ± 2.8	75.4	325	-39.7	43.8	-80.5	13.9	-7.6	156.7	5.7	67.5	0.2	-0.6			
1-B	4.03	486	-15.0	20.8	100-350								45.5	13.0																		
2-A	1.23	205	-15.6	15.1	100-550	15	0.94	0.91	72.7	1.6	0.3	3.7	46.7	12.2	42.0	17.3	59.8 ± 0.8	64.7	325	-7.9	23.2	-59.0	25.5	30.8	31.6	2.7	-60.0	3.7	-0.1	3.5	1.1	
2-B	1.66	325	-18.2	12.8	100-600								46.7	16.3																		
3-A	0.04	13	23.1	7.7	100-550	15	0.89	0.92	16.2	3.4	1.5	5.8	47.6	15.7	40.6	13.2	53.2 ± 2.8	60.7	325	-11.7	32.2	-80.0	-10.3	-9.9	158.5	1.9	68.9	3.0	2.7	4.6	-0.2	
3-B	0.04	13	23.1	7.7	100-550								47.4	13.4																		
5-A	0.45	76	5.3	14.9	100-600	17	0.99	0.91	91.8	1.2	0.5	1.6	46.3	18.6	48.1	21.7	56.9 ± 0.6	54.4	475	-4.7	10.8	-21.2	60.0	16.2	143.5	62.9	19.1	2.8	-0.6	3.1	0.6	
7-A	0.49	54	-9.3	22.8	100-475	12	0.70	0.88	34.1	2	0.4	2.9	45.5	19.3	43.4	20.4	58.5 ± 1.2	60.6	475	-8.7	10.1	87.2	-23.2	-0.6	55.1	2.7	145.1	3.1	-3.8	2.9	0.5	
8-B	0.77	92	-4.3	21.0	100-600								47.5	18.3																		
8-C	0.23	26	11.5	22.2	100-600	17	0.80	0.93	57	1.6	0.7	1.7	46.3	17.1	45.9	17.8	62.2 ± 1.0	61.3	475	-3.6	5.3	-40.8	51.0	-32.5	174.3	32.3	108.0	4.4	-2.3	6.2	-0.5	
9-A	0.39	49	-16.3	20.0	100-525	14	0.93	0.89	75.2	2.2	0.2	2.4	48.1	13.8	46.0	15.2	61.9 ± 0.9	63.9	475	-4.6	9.4	-80.6	48.3	-9.0	210.0	2.9	120.5	2.5	-6.0	12.0	9.1	
11-A	0.50	197	-23.4	6.4	100-450	9	0.86	0.82	28.1	2.3	3.3	9.8	53.2	17.3	52.3	17.4	54.2 ± 1.5		475	2.1	20.9	31.4	49.8	26.7	157.6	46.6	-80.3	-5.9	1.2			
11-B	0.58	211	-19.9	6.9	100-600								52.7	20.8																		
12-A	0.16	141	-12.8	2.9	100-450	9	0.74	0.83	11.5	5.0	0.9	10.3	51.4	11.6	52.6	20.3	45.0 ± 2.1	42.9	325	1.6	29.3	-34.6	20.4	-7.5	115.6	54.4	36.1	-4.5	-2.2	1.3	-6.9	
12-B	0.17	291	-11.0	1.5	100-450								50.7	15.0																		
13-A	0.32	9	22.2	89.4	100-600								54.2	14.8																		
13'-A	0.04	12	16.7	8.4	100-600	17	0.94	0.93	42.5	2.2	0.4	1.9	51.1	9.3	48.0	14.2	59.0 ± 1.4	60.8	475	-4.1	20.8	-66.6	47.0	-23.4	225.0	0.7	135.3	1.2	-1.6	0.7	-1.0	
14-A	0.10	21	-14.3	12.0	100-600	17	0.97	0.92	69.5	1.7	0.4	1.3	49.9	14.3	45.2	19.9	58.0 ± 0.9	62.1	475	-6.9	24.9	-69.8	32.1	19.9	43.2	3.6	-48.1	5.7	-2.8	6.8	-2.6	
14-B	0.79	17	5.9	116.8	100-600								50.5	16.0																		
15-A	0.38	95	-17.9	10.1	100-450	9	0.88	0.79	37.3	1.6	0.7	2.8	49.7	14.6	51.6	12.8	47.7 ± 0.9	45.0	325	0.6	11.3	13.2	-48.4	-26.3	35.0	60.1	65.6	-0.6	-1.4	1.0	-3.2	

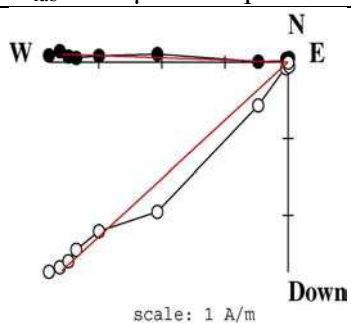
Without anisotropy correction. 12 samples: 1-A. 2-A. 3-A. 5-A. 7-A. 8-C. 9-A. 11-A. 12-A. 13'A. 14-A. 15-A										With anisotropy and cooling rate corrections. 10 samples: 2-A. 3-A. 5-A. 7-A. 8-C. 9-A. 12-A. 13'A. 14-A. 15-A.									
F_m ± sd	F_{po}	I_{ms}	D_{ms}	F_{pa}	I_{pa}	D_{pa}	VDM	VADM	F_m ± sd	F_{po}	F_{pocr}	I_{ms}	D_{ms}	F_{pa}	I_{pa}	D_{pa}	VDM	VADM	
(µT)	(µT)	(°)	(°)	(µT)	(°)	(°)	(10 ²² A/m)	(10 ²² A/m)	(µT)	(µT)	(µT)	(°)	(°)	(µT)	(°)	(°)	(10 ²² A/m)	(10 ²² A/m)	
56.5 ± 5.6	57.6	48.6	14.6	65.6	59.3	17.3	11.3	10.2	57.6 ± 7.7	58.9	57.1 ± 6.4	46.4	17.3	65.6	58.1	20.5	11.5	10.1	
$\alpha_{95} = 1.7$		F_{ma}	I_{ma}	D_{ma}					$\alpha_{95} = 2.7$		F_{ma}	I_{ma}	D_{ma}						
k = 637		(µT)	(°)	(°)					k = 330		(µT)	(°)	(°)						
		59.0	50.7	119.4							58.4	48.4	17.1						

Rejected samples:

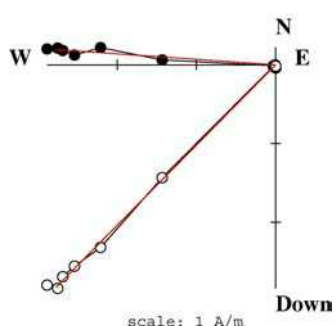
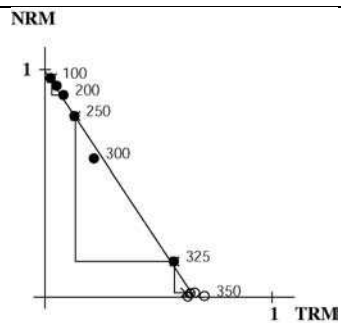
Sister specimens without Thellier experiments and 1A (dz and crm>15%); 11A (bad correction of anisotropy)

MURH. Age of the structure: 1100-1200 A.D.

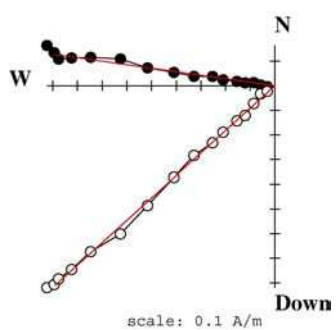
$H_{lab} = 50 \mu T$. Sample coordinates.



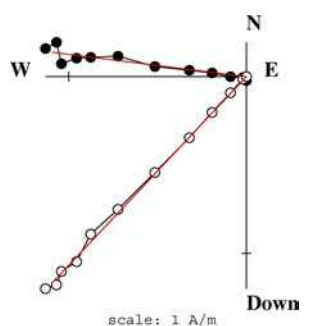
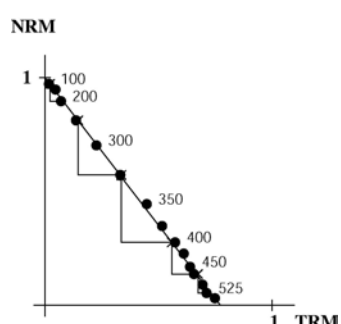
MURH1A
Without correction of anisotropy
 $NRM_0 = 4.72 \text{ A/m}$
 $F = 62.6 \mu T$
 $q = 12.1$



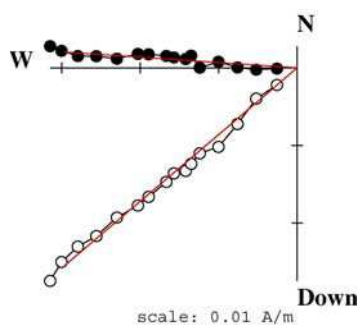
MURH1B
With correction of anisotropy
 $NRM_0 = 4.03 \text{ A/m}$



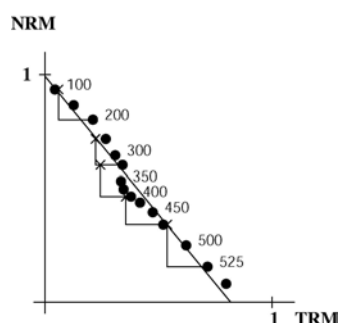
MURH2A
With correction of anisotropy
 $NRM_0 = 1.23 \text{ A/m}$
 $F = 64.7 \mu T$
 $q = 72.7$

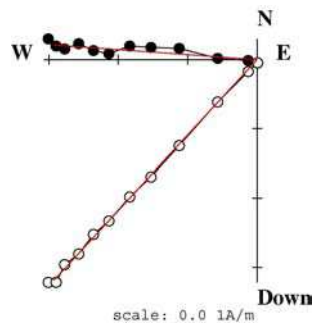


MURH2B
With correction of anisotropy
 $NRM_0 = 1.66 \text{ A/m}$

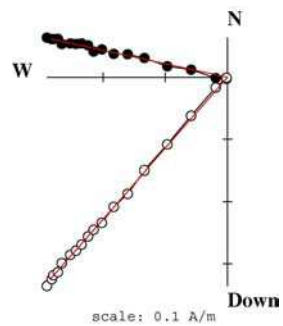


MURH3A
With correction of anisotropy
 $NRM_0 = 0.04 \text{ A/m}$
 $F = 60.7 \mu T$
 $q = 16.2$

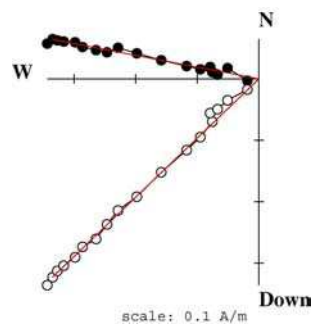
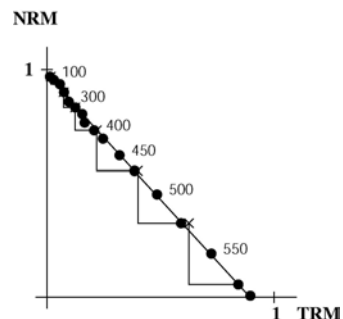




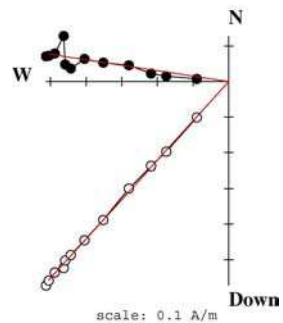
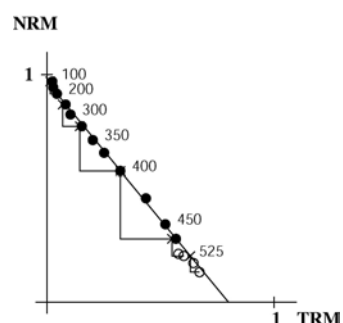
MURH3B
With correction of anisotropy
 $NRM_0 = 0.04 \text{ A/m}$



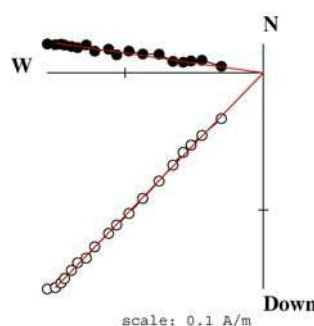
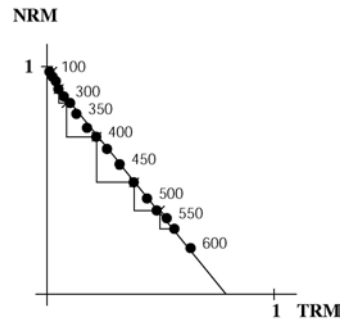
MURH5A
With correction of anisotropy
 $NRM_0 = 0.45 \text{ A/m}$
 $F = 54.4 \mu\text{T}$
 $q = 91.8$



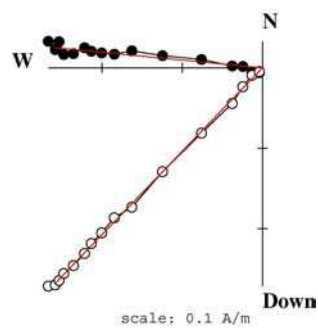
MURH7A
With correction of anisotropy
 $NRM_0 = 0.49 \text{ A/m}$
 $F = 60.6 \mu\text{T}$
 $q = 34.1$



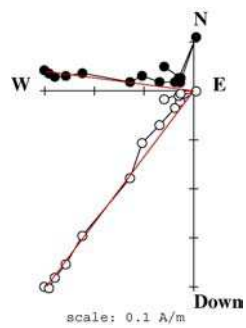
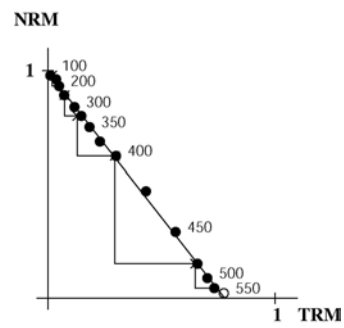
MURH8B
With correction of anisotropy
 $NRM_0 = 0.77 \text{ A/m}$



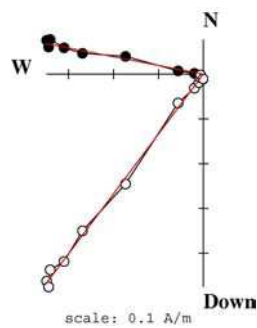
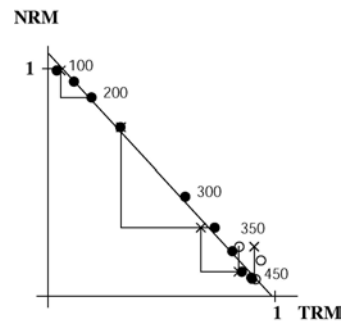
MURH8C
With correction of anisotropy
 $NRM_0 = 0.23 \text{ A/m}$
 $F = 61.3 \mu\text{T}$
 $q = 57.0$



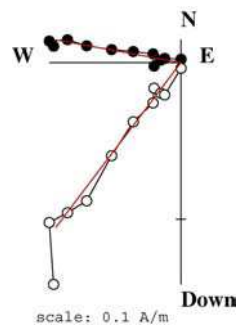
MURH9A
With correction of anisotropy
 $NRM_0 = 0.39 \text{ A/m}$
 $F = 63.9 \text{ T}$
 $q = 75.2$



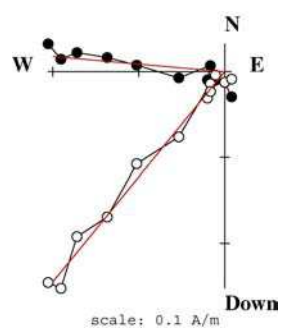
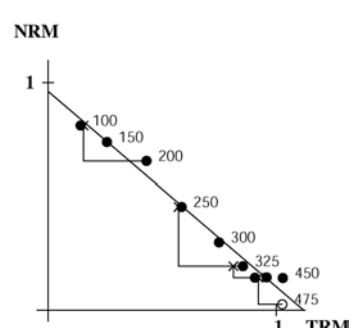
MURH11A
Without correction of anisotropy
 $NRM_0 = 0.50 \text{ A/m}$
 $F = 54.2 \mu\text{T}$
 $q = 29.1$



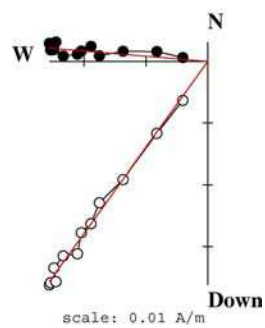
MURH11B
With correction of anisotropy
 $NRM_0 = 0.58 \text{ A/m}$



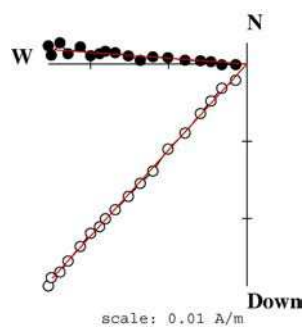
MURH12A
With correction of anisotropy
 $NRM_0 = 0.16 \text{ A/m}$
 $F = 42.9 \mu\text{T}$
 $q = 11.5$



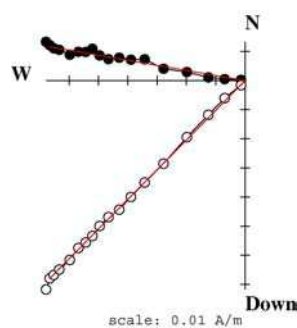
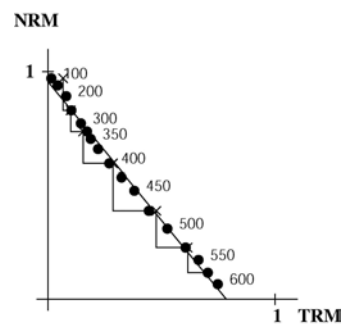
MURH12B
With correction of anisotropy
 $NRM_0 = 0.17 \text{ A/m}$



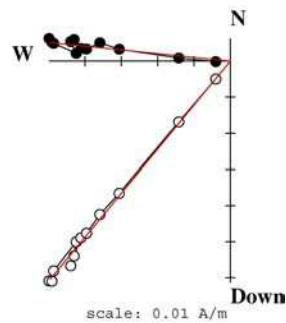
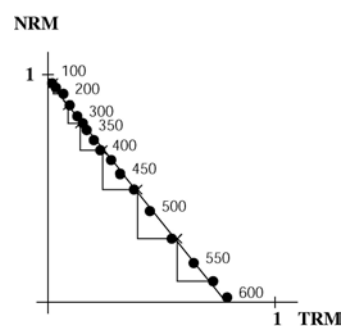
MURH13A
With correction of anisotropy
 $NRM_0 = 0.32 \text{ A/m}$



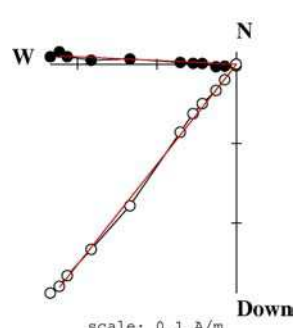
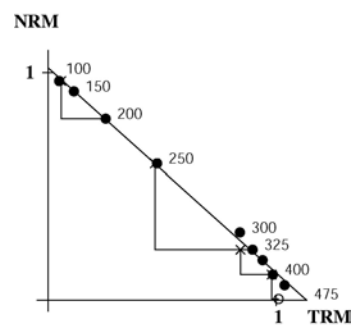
MURH13'A
With correction of anisotropy
 $NRM_0 = 0.04 \text{ A/m}$
 $F = 60.8 \mu\text{T}$
 $q = 42.5$



MURH14A
With correction of anisotropy
 $NRM_0 = 0.10 \text{ A/m}$
 $F = 62.1 \mu\text{T}$
 $q = 69.5$

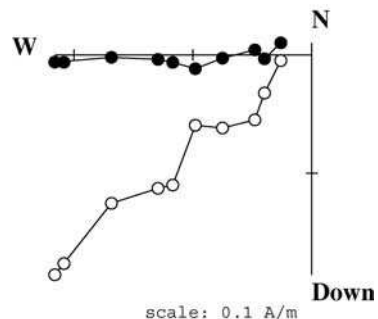


MURH14B
With correction of anisotropy
 $NRM_0 = 0.79 \text{ A/m}$

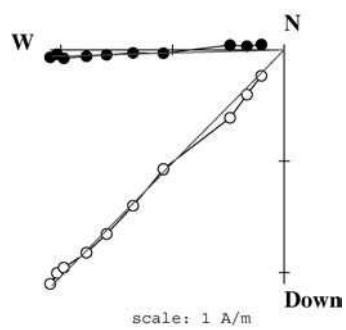
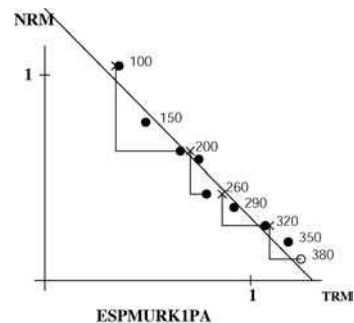


MURH15A
With correction of anisotropy
 $NRM_0 = 0.38 \text{ A/m}$
 $F = 47.7 \mu\text{T}$
 $q = 37.3$

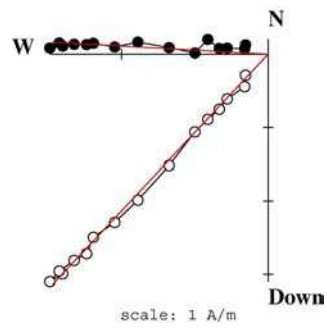
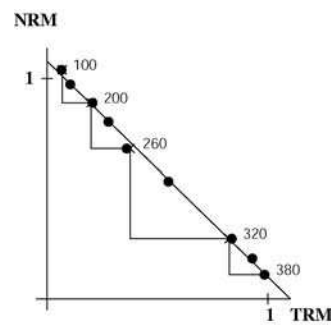
MURK. Age of the structure: 1100-1200 A.D.
 $H_{lab} = 60 \mu T$. Sample coordinates.



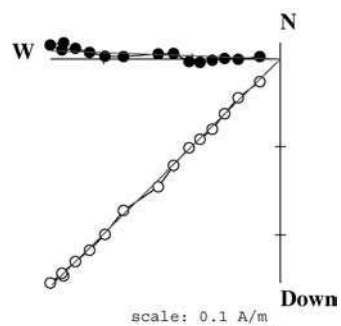
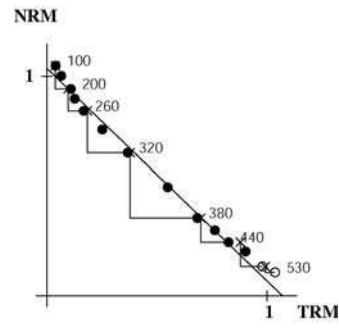
MURK1A
 With correction of anisotropy
 $NRM_0 = 0.29 \text{ A/m}$
 Rejected



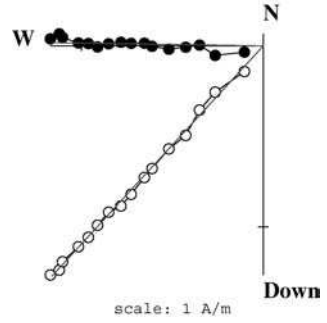
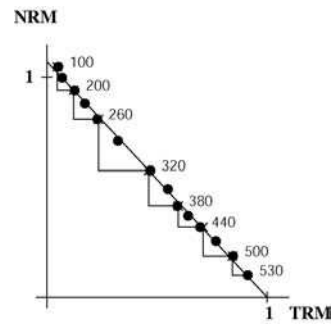
MURK2A
 Without correction of
 anisotropy
 $NRM_0 = 3.08 \text{ A/m}$
 $F = 58.7 \mu T$
 $q = 32.6$



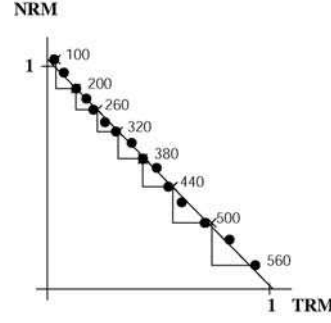
MURK3B
 With correction of anisotropy
 $NRM_0 = 4.43 \text{ A/m}$
 $F = 58.0 \mu T$
 $q = 24.7$

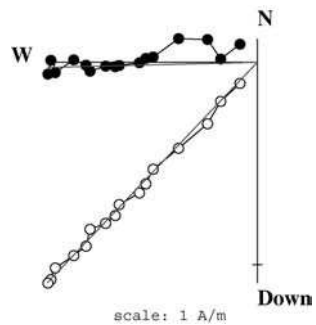


MURK4A
 With correction of anisotropy
 $NRM_0 = 0.38 \text{ A/m}$
 $F = 64.2 \mu T$
 $q = 58.3$

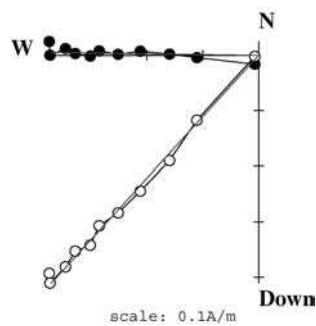


MURK5A
 With correction of anisotropy
 $NRM_0 = 1.81 \text{ A/m}$
 $F = 60.9 \mu T$
 $q = 44.8$

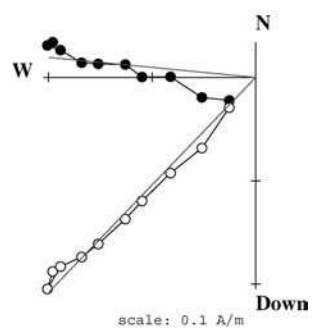




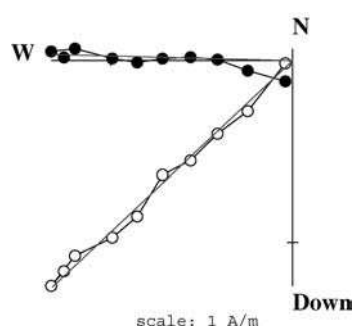
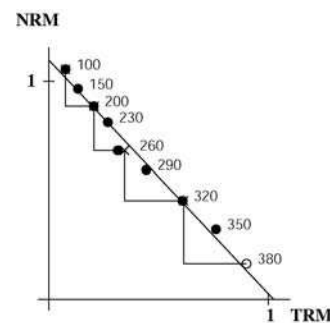
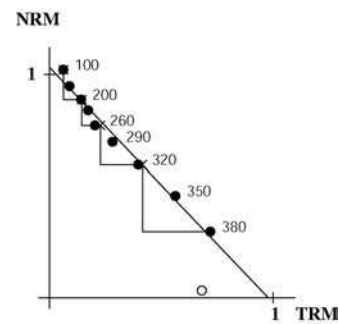
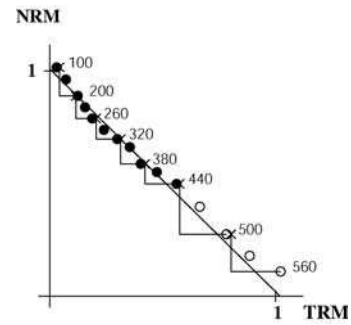
MURK7A
With correction of anisotropy
 $NRM_0 = 1.60 \text{ A/m}$
 $F = 59.3 \mu\text{T}$
 $q = 8.6$



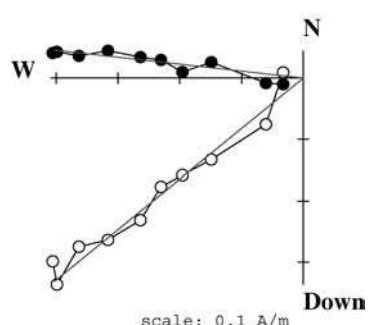
MURK8B
With correction of anisotropy
 $NRM_0 = 0.59 \text{ A/m}$
 $F = 63.2 \mu\text{T}$
 $q = 11.6$



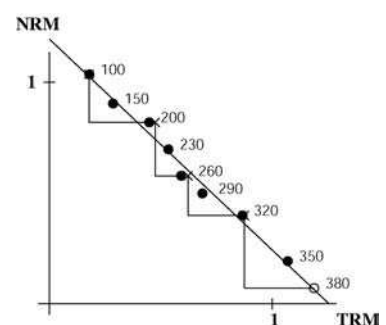
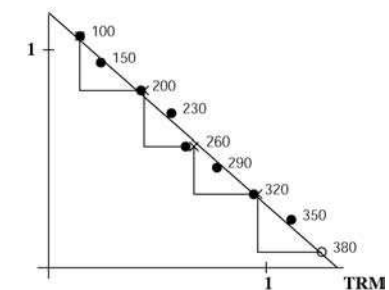
MURK9A
With correction of anisotropy
 $NRM_0 = 0.30 \text{ A/m}$
Rejected

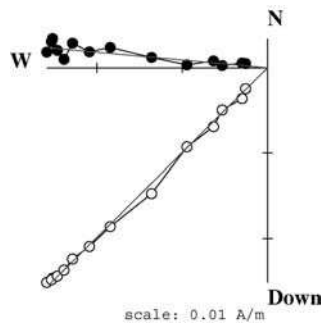


MURK10B
With correction of anisotropy
 $NRM_0 = 1.84 \text{ A/m}$
 $F = 53.0 \mu\text{T}$
 $q = 13.7$

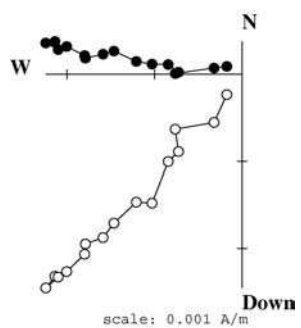
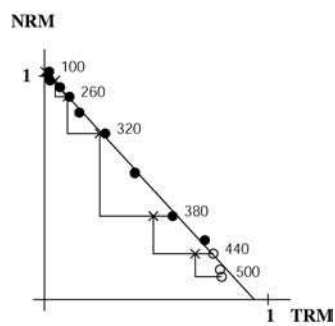


MURK11B
With correction of anisotropy
 $NRM_0 = 0.55 \text{ A/m}$
 $F = 57.1 \mu\text{T}$
 $q = 11.3$

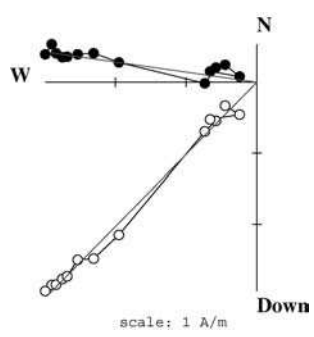
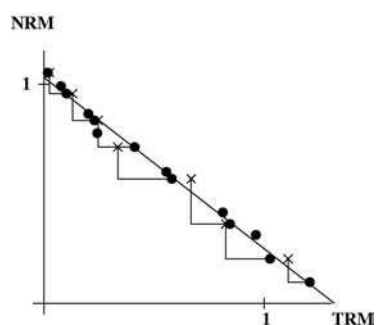




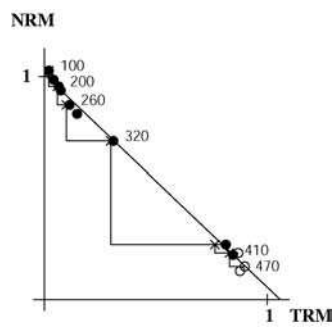
MURK12A
With correction of anisotropy
 $NRM_0 = 0.04 \text{ A/m}$
 $F = 65.4 \mu\text{T}$
 $q = 27.9$



MURK13B
Without correction of anisotropy
Rejected



MURK14A
With correction of anisotropy
 $NRM_0 = 4.44 \text{ A/m}$
 $F = 57.2 \mu\text{T}$
 $q = 18.1$



CALA: 1275-1300 A.D.

Latitude = 39° 01' N Longitude = 3° 49' W

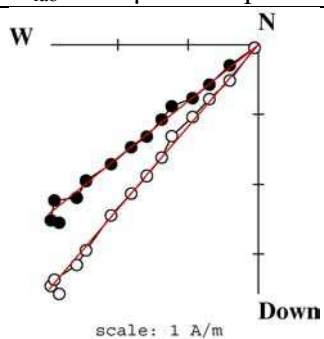
 $H_{lab} = 60.0 \mu T$

Spl	NRM (A/m)	anisotropy												T_{an} (°C)	dM_{an} (%)	k_1/k_3 (%)	Direction of anisotropy axes				Cooling rate gain										
		no		yes		no		yes		k1		k2					k3		24 h		48 h										
		I	D	I_e	D_e	$F \pm \sigma F$	F_e	(°)	(°)	(°)	(°)	I_e	D_e	$F \pm \sigma F$	F_e	(°)	(°)	(°)	(°)	ΔMz_{24} (%)	dz_{24} (%)	ΔMz_{48} (%)	dz_{48} (%)								
2-A	5.65	859	-9.8	16.5	100-530	12	0.83	0.90	38.2	2.6	0.6	3.1	42.6	16.4	42.4	17.3	58.7 ± 1.1	57.7	440	-1.2	6	-48.8	23.5	18.2	91.5	35.5	-12.0	3.5	0.73	-0.6	-1.8
4-A	3.07	530	2.3	14.6	100-560	13	0.88	0.90	160.0	1.6	0.5	1.4	41.1	18.2	40.1	18.1	57.0 ± 0.3	57.6	500	-4.1	14	-16.7	-51.5	-64.4	77.3	18.8	32.6	5.1	2.4	5.5	-3.5
6-A	2.15	597	-16.9	9.1	100-560	13	0.88	0.91	56.1	2.3	0.4	4.1	44.8	15.0	45.2	13.5	60.0 ± 0.8	62.8	440	-2.1	15	-42.0	39.2	29.2	99.0	34.1	-13.1	1.8	3.0	2.1	-2.0
7-A	2.49	655	-7.5	9.6	100-560	13	0.84	0.91	116.1	1.6	0.3	1.7	45.5	12.0	44.9	10.4	55.8 ± 0.3	58.3	440	-3.0	11	-54.3	29.1	25.2	78.2	23.6	-23.6	2.4	4.2	1.7	-2.5
8-A	3.03	610	-7.4	12.5	100-500	11	0.88	0.89	54.7	1.4	0.4	2.0	45.6	2.3	46.8	3.7	61.4 ± 0.9	61.7	360	-1.7	8	-28.9	75.7	-4.4	168.2	60.7	86.0	1.5	-1.6	-0.6	-1.4
10-A	2.32	263	10.6	22.2	100-500	11	0.91	0.89	113.6	1.1	0.4	1.8	46.3	6.4	47.6	8.7	57.7 ± 0.3	58.7	440	-0.8	13	-33.6	78.6	-12.0	176.7	53.8	103.6	0.8	-1.1	-0.4	-2.1
11-A	1.52	441	-12.2	8.7	100-560	13	0.85	0.91	45.2	2.5	0.9	3.0	45.3	11.8	45.9	11.1	57.8 ± 0.9	60.4	440	-0.2	12	-38.7	44.6	7.1	128.9	50.4	30.2	0.9	5.2	-0.1	-1.5
13-A	7.54	1241	-9.8	15.3	100-530	12	0.85	0.90	40.6	1.9	0.5	2.2	44.5	8.4	45.4	6.9	55.8 ± 0.9	57.0	440	0.7	10	-35.4	15.9	6.9	101.0	53.7	1.6	1.8	3.1	1.5	-1.0
14-A	2.11	500	-15.2	10.6	100-360	7	0.50	0.83	26.8	1.6	3.4	1.8	44.3	-1.1	45.7	-4.1	65.7 ± 1.1	65.3	360	-1.4	10	4.1	62.4	37.1	155.4	52.7	-33.0	3.3	0.4	0.2	0.0

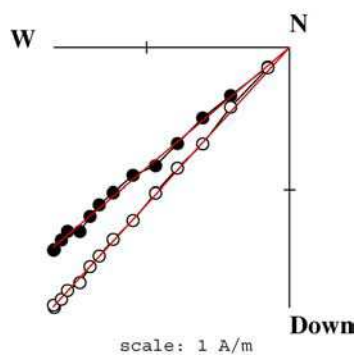
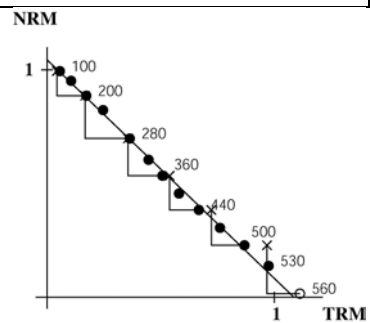
Without anisotropy correction. 9 samples:								With anisotropy and cooling rate corrections. 9 samples:																		
2-A. 4-A. 6-A. 7-A. 8-A. 10-A. 11-A. 13-A. 14-A.				2-A. 4-A. 6-A. 7-A. 8-A. 10-A. 11-A. 13-A. 14-A.				F _m ± sd				F _{po}				F _{pocr} ± sd				I _{ms}						
(μT)	(μT)	(°)	(°)	(μT)	(°)	(°)	(°)	(10 ²² A/m)	(10 ²² A/m)	(μT)	(μT)	(μT)	(°)	(°)	(μT)	(μT)	(°)	(°)	(μT)	(°)	(°)	(10 ²² A/m)	(10 ²² A/m)			
58.9 ± 3.1	58.1	44.6	10.0	66.4	56.2	12.8	11.9	10.2		59.9 ± 2.8	59.3	58.4 ± 3.1	45.1	9.7	66.8	56.6	12.5	11.9								
$\alpha_{95} = 3.1$		F_{ma}	I_{ma}	D_{ma}																$\alpha_{95} = 3.4$		F_{ma}	I_{ma}	D_{ma}		
k = 270		(μT)	(°)	(°)																k = 225		(μT)	(°)	(°)		
		59.2	46.3	10.2																	59.5	46.8	9.9			

CALA. Age of the structure: 1275-1300 A.D.

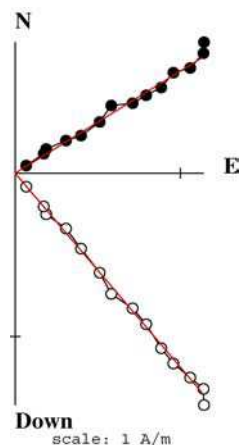
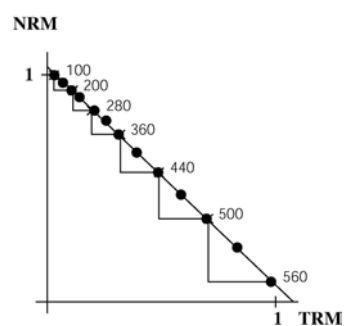
$H_{lab} = 60 \mu\text{T}$. Sample coordinates.



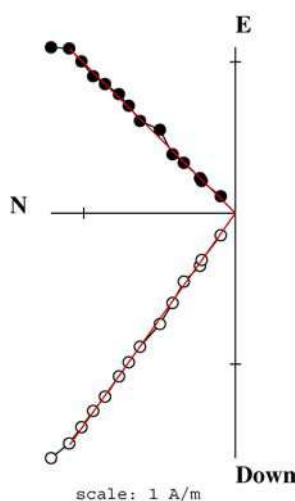
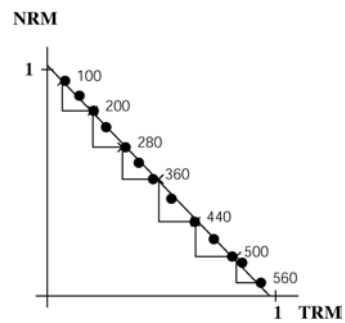
CALA2A
With correction of anisotropy
 $\text{NRM}_0 = 5.65 \text{ A/m}$
 $F = 57.7 \mu\text{T}$
 $q = 38.2$



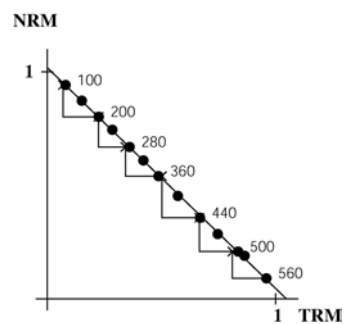
CALA4A
With correction of anisotropy
 $\text{NRM}_0 = 3.07 \text{ A/m}$
 $F = 57.6 \mu\text{T}$
 $q = 160.0$

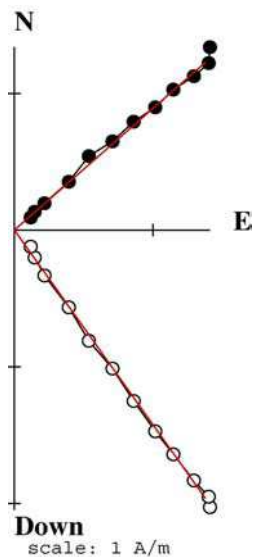


CALA6A
With correction of anisotropy
 $\text{NRM}_0 = 2.15 \text{ A/m}$
 $F = 62.8 \mu\text{T}$
 $q = 56.1$

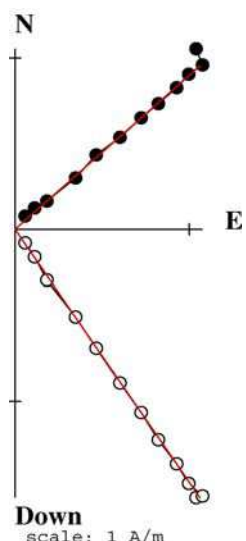
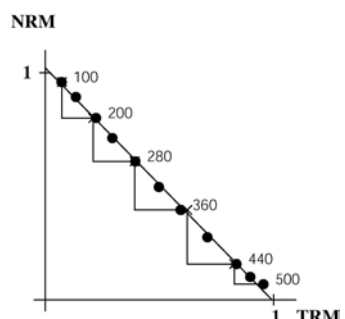


CALA7A
With correction of anisotropy
 $\text{NRM}_0 = 2.49 \text{ A/m}$
 $F = 58.3 \mu\text{T}$
 $q = 116.1$

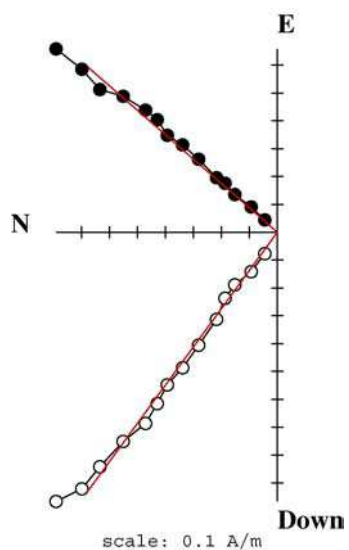
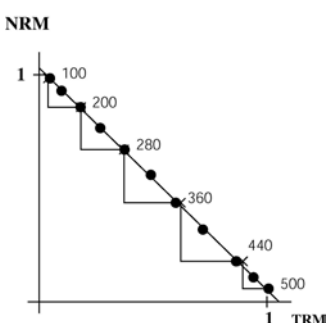




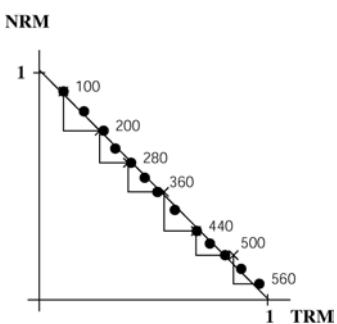
CALA8PA
With correction of anisotropy
 $NRM_0 = 3.03 \text{ A/m}$
 $F = 61.7 \mu\text{T}$
 $q = 54.7$

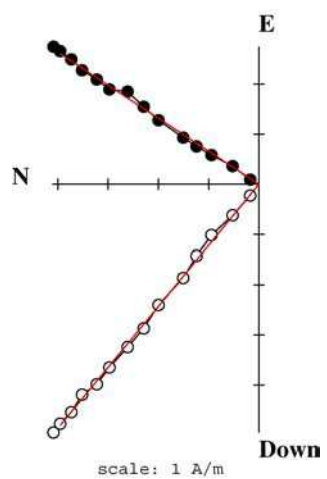


CALA10A
With correction of anisotropy
 $NRM_0 = 2.32 \text{ A/m}$
 $F = 58.7 \mu\text{T}$
 $q = 113.6$

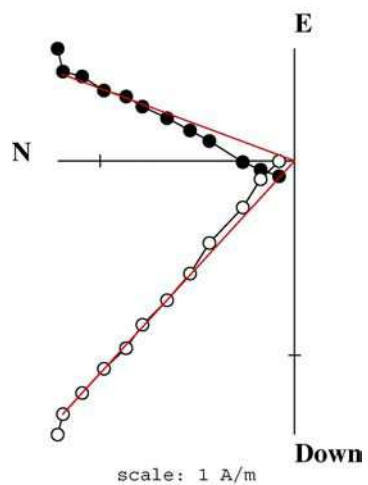
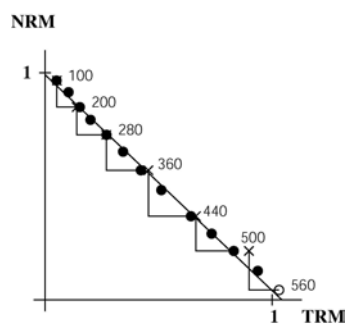


CALA11A
With correction of anisotropy
 $NRM_0 = 1.52 \text{ A/m}$
 $F = 60.4 \mu\text{T}$
 $q = 45.2$

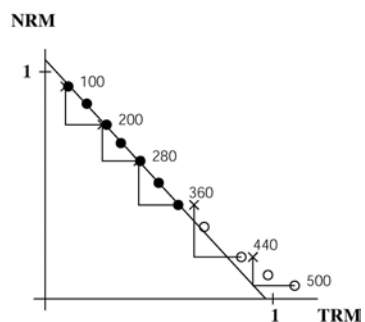




CALA13A
With correction of anisotropy
 $NRM_0 = 7.54 \text{ A/m}$
 $F = 57.0 \mu\text{T}$
 $q = 40.6$



CALA14A
With correction of anisotropy
 $NRM_0 = 2.11 \text{ A/m}$
 $F = 65.3 \mu\text{T}$
 $q = 26.8$



CALB: 1275-1300 A.D.

Latitude = 39° 01' N Longitude = 3° 49' W

H_{lab} = 60.0 µT

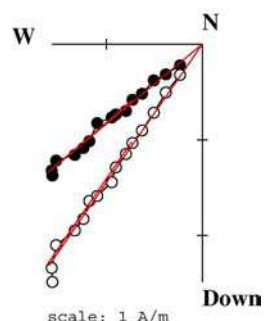
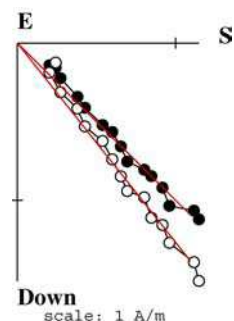
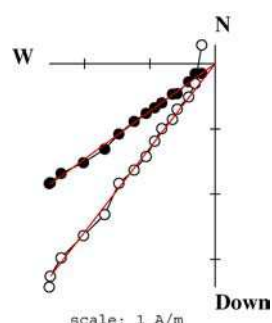
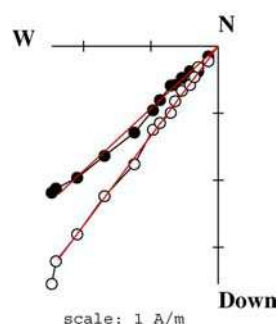
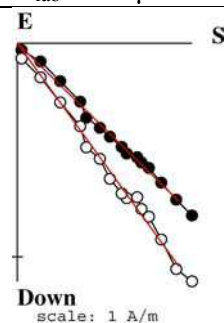
Spl	NRM (A/m)	χ (10 ⁻⁵)	Δχ (%)	Q _I	T _{min-T_{max}} (°C)	n	f	g	q	mad	dang	crm	anisotropy				T _{an} (°C)	dM _{an} (%)	k _{1/k₃} (%)	Direction of anisotropy axes				Cooling rate gain							
													no		yes		no		yes		k1		k2		k3		24 h		48 h		
													I	D	I _e	D _e	F ± σF	F _e (µT)	I	D	I	D	I	D	ΔMz ₂₄ (%)	dz ₂₄ (%)	ΔMz ₄₈ (%)	dz ₄₈ (%)			
1-B	1.60	614	-9.3	6.6	100-530	14	0.83	0.91	30.9	2.7	1	4.5	45.0	5.9	44.7	3.7	56.2 ± 1.4	57.1	410	-2.1	7	49.0	53.5	-36.6	84.8	15.8	162.6	5.3	3.7	11.1	-4.7
2-B	4.89	983	-15.3	12.5	100-410	10	0.75	0.86	28.7	2.8	0.2	3.2	45.7	7.6	44.4	6.5	63.9 ± 1.5	64.7	290	-3.3	6	57.1	-66.6	-31.4	-47.2	8.9	37.3	3.2	0.4		
3-A	4.73	871	-19.5	13.7	100-500	13	0.85	0.91	61.4	2.0	0.5	1.9	45.0	11.4	46.2	13.3	63.1 ± 0.8	61.0	320	-4.1	8	-21.0	33.1	39.6	104.6	43.0	-35.9	4.2	3.7	7.0	-2.2
4-A	2.22	555	-9.5	10.1	100-500	13	0.80	0.92	45.3	3.1	1.9	2.9	41.7	4.3	41.9	4.6	55.7 ± 0.9	55.6	410	-1.1	4	21.9	15.1	-60.5	59.9	18.8	112.9	3.9	4.0	6.7	1.7
5-B*	3.24	742	-12.5	11.0	100-410	10	0.51	0.89	16.5	5.2	0.6	8.8	48.0	9.8	55.9	36.0	65.4 ± 2.0	49.2	410	-1.4	20	-31.9	32.5	38.0	93.4	35.8	-30.9	4.2	5.3	5.9	-2.6
6-A	1.70	383	-6.3	11.2	100-530	14	0.85	0.92	17.4	3.9	0.8	8.8	50.6	-2.5	50.6	-0.7	56.2 ± 2.5	55.0	410	-1.7	11	-43.1	20.7	-46.7	193.5	3.6	107.3	2.8	5.8	4.9	-1.1
7-B	1.18	257	9.3	11.5	100-530	14	0.87	0.92	61.8	4.1	0.5	4.1	49.4	10.3	48.3	13.2	53.5 ± 0.7	53.6	410	-1.0	13	-57.7	21.6	-32.3	200.6	0.3	110.8	3.7	4.3	4.4	0.4
8-B	1.50	330	11.2	11.4	100-500	13	0.87	0.92	47.8	5.0	0.5	2.7	41.7	6.3	42.0	8.2	51.9 ± 0.8	50.4	410	-1.4	10	-35.5	-31.4	-10.2	65.9	52.6	-10.5	0.6	3.2	1.1	0.8
9-A	3.09	766	-8.0	10.1	100-560	15	0.86	0.91	69.5	3.4	1.6	3.4	41.8	2.4	45.1	3.9	58.7 ± 0.7	54.9	410	-1.4	27	-2.2	38.0	85.7	96.7	3.7	-51.9	9.2	-1.4		
12-A	0.17	56	-3.6	7.6	rejected																										
13-A	1.29	227	-7.5	14.3	100-560	15	0.82	0.81	33.8	3.6	3.4	2.4	40.7	9.6	38.4	11.6	61.1 ± 1.3	60.4	500	-9.8	14	-55.0	9.4	-15.3	122.4	30.6	41.7	11.5	-0.9		
14-B	1.61	579	-15.4	7.0	100-560	15	0.83	0.92	36.9	3.2	0.4	3.5	40.9	7.3	41.1	6.4	53.4 ± 1.1	53.7	410	-0.1	6	44.1	13.4	-28.6	71.5	32.4	141.3	4.3	-4.8		

Without anisotropy correction. 11 samples:										With anisotropy and cooling rate corrections. 10 samples:									
1-B, 2-B, 3-A, 4-A, 5-B, 6-A, 7-B, 8-B, 9-A, 13-A, 14-B										1-B, 2-B, 3-A, 4-A, 6-A, 7-B, 8-B, 9-A, 13-A, 14-B									
F _m ± sd	F _{po}	I _{ms}	D _{ms}	F _{pa}	I _{pa}	D _{pa}	VDM	VADM	F _m ± sd	F _{po}	F _{pocr}	I _{ms}	D _{ms}	F _{pa}	I _{pa}	D _{pa}	VDM	VADM	
(µT)	(µT)	(°)	(°)	(µT)	(°)	(°)	(10 ²² A/m)	(10 ²² A/m)	(µT)	(µT)	(µT)	(°)	(°)	(µT)	(°)	(°)	(10 ²² A/m)	(10 ²² A/m)	
58.1 ± 4.6	57.7	44.6	6.6	65.9	56.1	9.0	11.8	10.1	56.6 ± 4.2	56.4	54.4 ± 3.7	44.4	7.1	62.2	55.9	9.6	11.2	9.5	
α ₉₅ = 2.6										α ₉₅ = 2.9									
k = 321										k = 284									
(µT)										(µT)									
58.7										55.5									
46.3										46.2									
6.7										7.2									

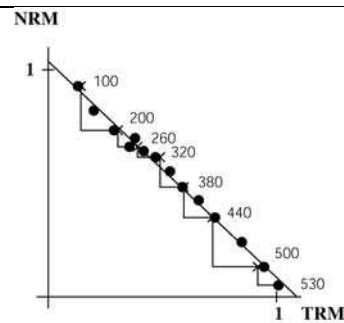
Rejected: 5B bad correction of anisotropy

CALB. Age of the structure: 1275-1300 A.D.

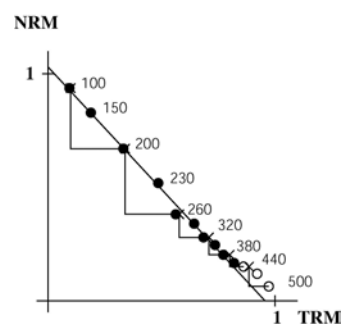
$H_{lab} = 60 \mu\text{T}$. Sample coordinates.



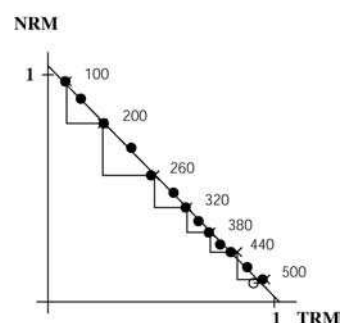
CALB1B
With correction of anisotropy
 $\text{NRM}_0 = 1.73 \text{ A/m}$
 $F = 57.1 \mu\text{T}$
 $q = 30.9$



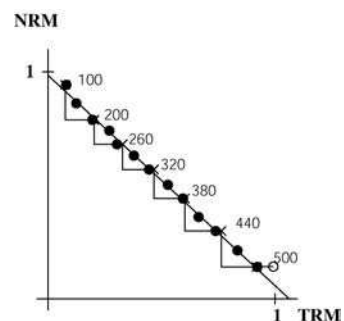
CALB2B
With correction of anisotropy
 $\text{NRM}_0 = 5.23 \text{ A/m}$
 $F = 64.7 \mu\text{T}$
 $q = 28.7$



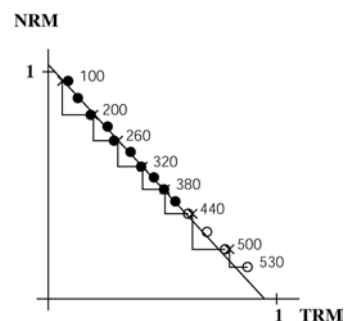
CALB3A
With correction of anisotropy
 $\text{NRM}_0 = 5.02 \text{ A/m}$
 $F = 61.0 \mu\text{T}$
 $q = 61.4$

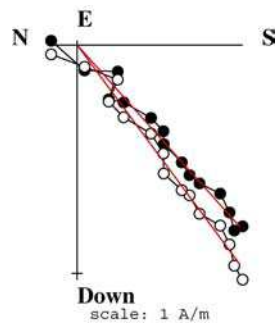


CALB4A
With correction of anisotropy
 $\text{NRM}_0 = 2.38 \text{ A/m}$
 $F = 55.6 \mu\text{T}$
 $q = 45.3$

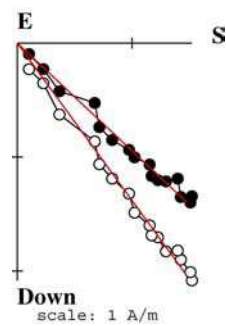


CALB5B
Without correction of anisotropy
 $\text{NRM}_0 = 3.50 \text{ A/m}$
 $F = 65.4 \mu\text{T}$
 $q = 16.5$

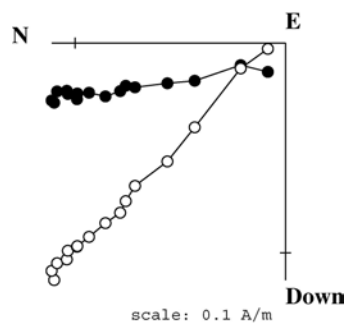




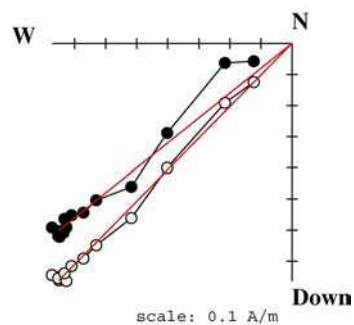
CALB7B
With correction of anisotropy
 $NRM_0 = 1.23 \text{ A/m}$
 $F = 53.6 \mu\text{T}$
 $q = 61.8$



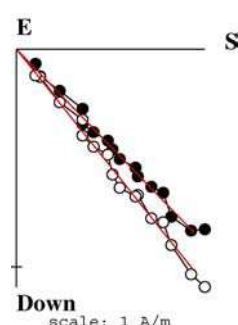
CALB9A
With correction of anisotropy
 $NRM_0 = 3.14 \text{ A/m}$
 $F = 54.8 \mu\text{T}$
 $q = 69.5$



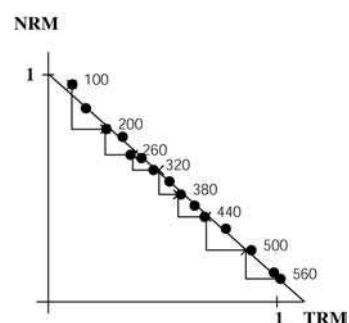
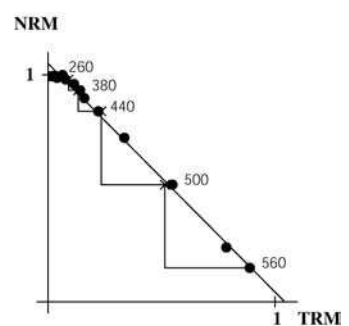
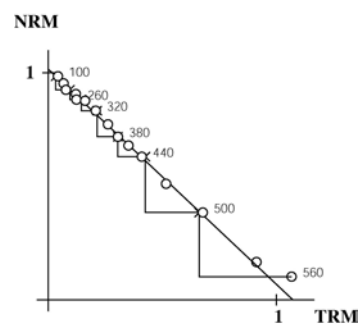
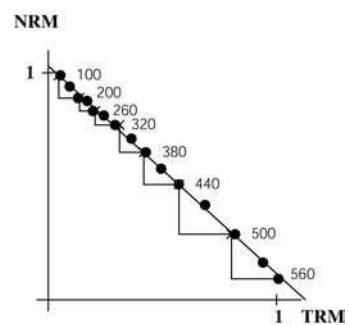
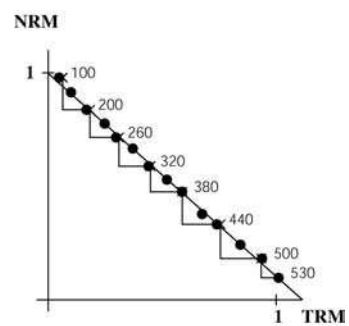
CALB12A
With correction of anisotropy
 $NRM_0 = 0.17 \text{ A/m}$
Rejected
not to the origin



CALB13A
With correction of anisotropy
 $NRM_0 = 1.33 \text{ A/m}$
 $F = 60.4 \mu\text{T}$
 $q = 33.8$



CALB14B
With correction of anisotropy
 $NRM_0 = 1.74 \text{ A/m}$
 $F = 53.7 \mu\text{T}$
 $q = 36.9$



CERCALB: 1275-1300 A.D.

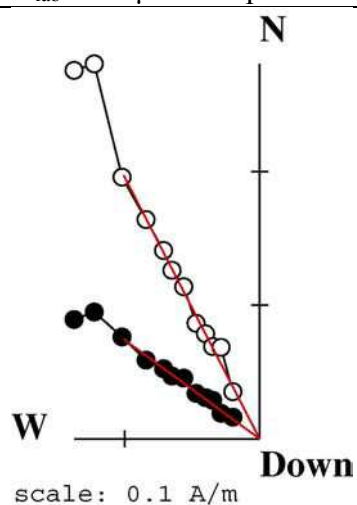
Latitude = $39^{\circ} 01' \text{ N}$ Longitude = $3^{\circ} 49' \text{ W}$

$$H_{lab} = 60.0 \text{ } \mu\text{T}$$

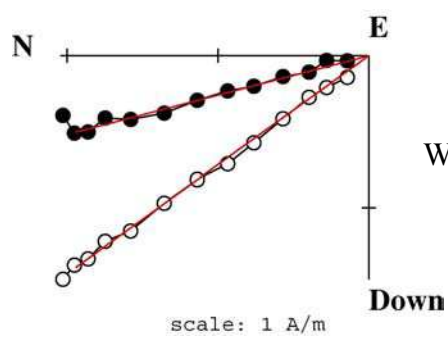
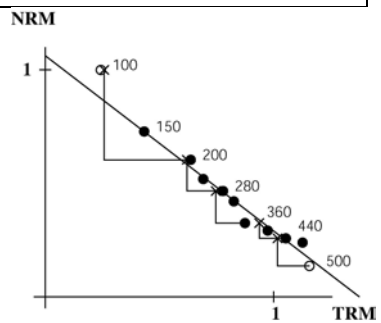
H _{lab} = 60.0 µT													anisotropy						Direction of anisotropy axes				Cooling rate gain				
																			no		yes		k1		k2		k3
Spl	NRM	χ	Δχ	Q _I	T _{min} -T _{max}	n	f	g	q	mad	dang	crm	F ± σF	F _e	T _{an}	dM _{an}	k ₁ /k ₃	I	D	I	D	I	D	ΔMz ₂₄	dz ₂₄	ΔMz ₄₈	dz ₄₈
(A/m)	(10 ⁻⁵)	(%)		(°C)						(°)	(°)	(%)	(µT)	(µT)	(°C)	(%)	(%)	(°)	(°)	(°)	(°)	(°)	(°)	(%)	(%)	(%)	(%)
1-A	0.35	257	-18.3	3.4	150-470	9	0.48	0.85	5.8	3.6	1.1	7.0	46.0 ± 2.5	46.3	360	-0.4	22	1.1	45.5	-21.3	135.1	68.7	138.4	2.6	-5.7		
2-A	2.74	404	-10.1	17.0	100-530	12	0.85	0.90	34.9	1.8	0.9	2.1	49.2 ± 1.0	52.4	440	-4.4	12	-39.0	-54.1	-39.7	78.1	26.3	12.3	0.9	0.5		
4-A	1.83	292	-12.3	15.8	200-440	7	0.54	0.83	9.9	4.7	1.7	3.1	51.3 ± 2.4	56.6	440	-4.5	20	-20.3	59.5	-61.4	192.2	19.3	142.1	1.4	0.2		
6-A	0.63	119	5.9	13.3	320-600	10	0.58	0.88	22.9	2.7	2.4	5.7	71.1 ± 1.5	62.9	530	-8.7	26	-10.9	-81.9	-9.6	10.0	75.4	-39.6	1.6	-3.5		
7-A	0.85	151	4.6	14.1	280-600	11	0.57	0.89	18.1	4.6	3.7	12.2	77.7 ± 2.0	65.6	530	-19.1	28	3.6	83.0	-7.4	172.6	81.8	198.8	4.0	-6.3		

Without anisotropy correction. 4 samples:				With anisotropy and cooling rate corrections. 4 samples:				
1-A.	2-A.	4-A.	6-A.	1-A.	2-A.	4-A.	6-A.	VADM
F _m ± sd	F _{po}	F _{pa}	VADM	F _m ± sd	F _{po}	F _{pocr}	F _{pa}	(10 ²² A/m)
(μT)	(μT)	(μT)	(10 ²² A/m)	(μT)	(μT)	(μT)	(μT)	(10 ²² A/m)
54.4 ± 11.3	56.1	62.3	10.9	54.6 ± 7.0	55.9	55.6 ± 7.0	61.8	9.7
$\overline{F_{ma}}$ <hr/> (μT)				$\overline{F_{ma}}$ <hr/> (μT)				
57.0				56.5				

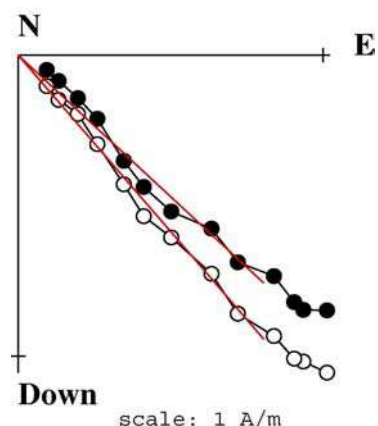
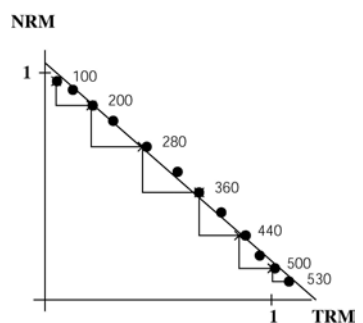
CERCALB. Pottery of the kiln CALB dated between: 1275-1300 A.D.
 $H_{lab} = 60 \mu T$. Sample coordinates.



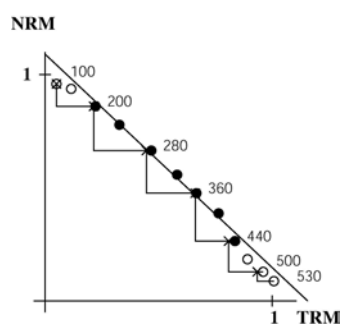
CERCALB1A
 With correction of anisotropy
 $NRM_0 = 0.35 \text{ A/m}$
 $F = 51.5 \mu T$
 $q = 2.6$

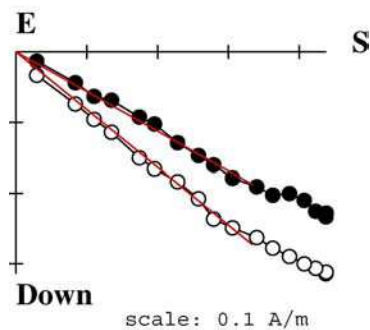


CERCALB2A
 With correction of anisotropy
 $NRM_0 = 2.74 \text{ A/m}$
 $F = 52.4 \mu T$
 $q = 34.9$

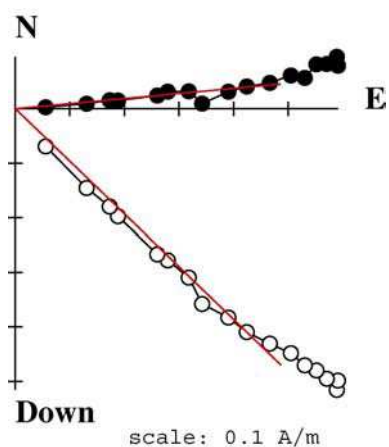
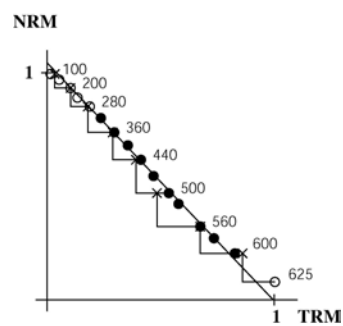


CERCALB4A
 With correction of anisotropy
 $NRM_0 = 1.83 \text{ A/m}$
 $F = 56.6 \mu T$
 $q = 9.9$

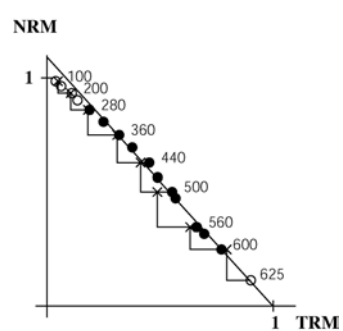




CERCALB6A
With correction of anisotropy
 $NRM_0 = 0.63 \text{ A/m}$
 $F = 62.9 \mu\text{T}$
 $q = 22.9$



CERCALB7A
With correction of anisotropy
 $NRM_0 = 0.85 \text{ A/m}$
 $F = 65.6 \mu\text{T}$
 $q = 18.1$



VALN: 1238-1350 A.D.

Latitude = 39° 28' N Longitude = 0° 22' W

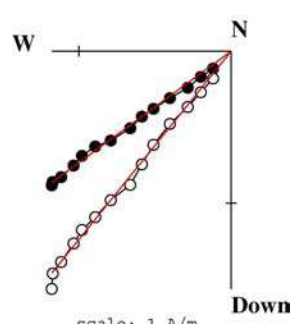
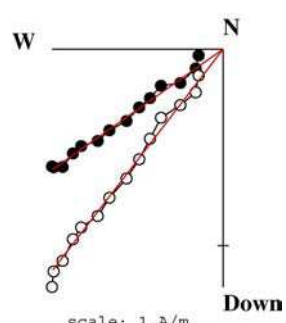
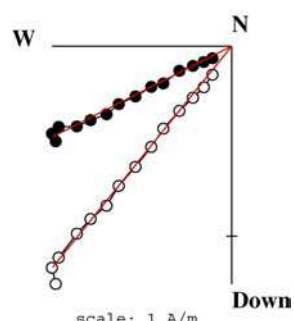
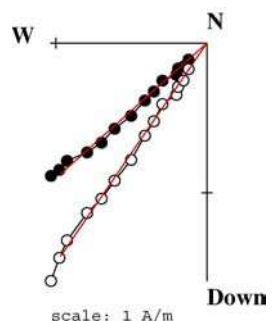
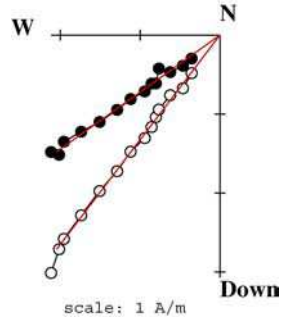
H_{lab} = 50.0 µT

Spl	NRM (A/m)	anisotropy																Direction of anisotropy axes					Cooling rate gain								
		no				yes				no				yes				k1		k2		k3		24 h		48 h					
		χ (10 ⁻⁵)	$\Delta\chi$ (%)	Q _l	T _{min-T_{max}} (°C)	n	f	g	q	mad	dang	crm	I	D	I _e	D _e	F ± σF	F _e (µT)	T _{an} (°C)	dz _{an} (%)	k _{1/k₃}	I	D	I	D	I	D	ΔMz ₂₄ (%)	dz ₂₄ (%)	ΔMz ₄₈ (%)	dz ₄₈ (%)
1-A	3.96	1090	-2.5	9.14	100-540	13	0.77	0.91	102.1	2.7	0.4	2.7	46.7	2.2	47.1	1.3	53.1 ± 0.4	52.7	420	-2.0	2	12.8	-89.2	37.4	10.8	49.7	165.2	5.7	3.7	9.5	1.8
2-A	2.09	624	-6.6	8.40	100-540	13	0.81	0.91	43.1	2.1	0.7	3.6	46.0	-2.6	47.5	-4.9	50.2 ± 0.9	49.9	420	0.9	15	25.8	36.1	-47.1	94.8	31.6	143.4	0.4	2.1	2.1	0.8
4-A	1.71	383	12.8	11.21	100-540	13	0.83	0.91	57.2	2.0	0.9	2.1	46.7	6.6	48.0	10.4	46.2 ± 0.6	44.5	420	-2.9	19	-15.1	39.5	74.9	40.7	0.3	-50.5	1.5	1.8	4.6	0.5
5-A	1.70	420	6.4	10.17	100-540	13	0.82	0.91	69.1	2.7	1.0	3.2	44.8	1.9	46.8	2.2	48.9 ± 0.5	45.6	420	-0.6	19	-17.7	45.3	-61.4	171.1	21.7	128.0	5.8	3.1	6.3	0.0
6-A	2.21	536	5.8	10.36	100-540	13	0.83	0.91	68.4	1.7	0.9	2.2	45.8	1.6	45.0	1.5	49.1 ± 0.5	49.0	420	-1.1	10	66.6	-50.7	-6.8	23.2	22.3	110.4	4.0	2.4	4.9	0.4
7-A	2.07	469	4.5	11.09	100-540	13	0.80	0.92	57.5	2.6	1.7	3.1	44.9	2.7	44.9	3.1	50.5 ± 0.7	50.7	420	-1.0	3	36.4	27.0	-53.3	36.6	4.6	120.4	4.4	1.8	5.3	0.4
8-B*	3.10	906	1.5	8.61	100-390	8	0.56	0.85	27.4	2.3	0.7	4.4	46.7	3.6	39.8	-4.1	50.8 ± 0.9	57.2	420	-1.5	46	5.0	-60.8	-84.9	-49.1	1.0	29.3	3.4	2.3	4.8	1.3
9-A	3.12	934	1.5	8.40	100-540	13	0.78	0.90	76.7	3.5	1.5	4.6	47.0	0.6	46.9	0.6	52.6 ± 0.5	52.6	420	-1.8	2	31.2	-17.7	-47.3	31.3	26.0	89.5	5.6	2.1	6.5	0.3
12-A	2.89	791	-3.3	9.19	100-540	13	0.85	0.91	82.4	1.8	1.2	3.7	47.0	4.0	46.0	2.6	50.3 ± 0.5	50.9	420	-5.8	5	57.4	-51.3	32.6	126.7	0.9	217.3	1.9	1.3	1.6	-0.3
14-A	3.60	1004	-1.7	9.02	100-540	13	0.79	0.91	102.9	3.1	2.2	4.5	48.9	4.3	49.5	6.6	55.8 ± 0.4	54.6	420	-0.9	12	-23.2	36.4	-66.8	215.1	0.5	126.2	5.3	2.0	6.1	0.0
16-A	2.80	1228	-7.2	5.72	100-540	13	0.73	0.91	36.9	4.3	3.2	7.8	46.8	2.6	46.3	1.1	51.9 ± 1.0	52.2	420	-2.0	5	38.1	-46.3	41.0	86.7	25.8	201.5	9.1	1.6	9.7	0.0
18-A	2.63	1066	-5.6	6.19	100-540	13	0.79	0.92	52.2	3.2	3.3	6.1	45.6	-0.9	46.4	0.1	53.1 ± 0.8	51.9	420	-4.4	9	-11.4	41.6	77.4	67.2	5.3	-47.4	6.6	1.5	6.3	-0.4

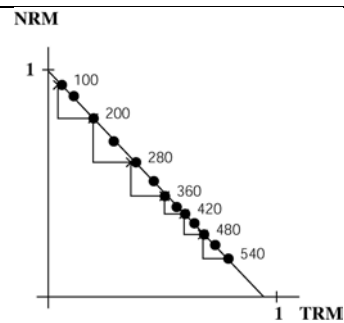
Without anisotropy correction. 12 samples:										With anisotropy and cooling rate corrections. 11 samples:									
1-A. 2-A. 4-A. 5-A. 6-A. 7-A. 8-B. 9-A. 12-A. 14-A. 16-A. 18-A					1-A. 2-A. 4-A. 5-A. 6-A. 7-A. 9-A. 12-A. 14-A. 16-A. 18-A					F _m ± sd					F _{po} F _{pocr} ± sd I _{ms} D _{ms} F _{pa} I _{pa} D _{pa} VDM VADM				
(µT)	(µT)	(°)	(°)	(µT)	(°)	(°)	(10 ²² A/m)	(10 ²² A/m)	(µT)	(µT)	(µT)	(°)	(°)	(µT)	(µT)	(°)	(°)	(10 ²² A/m)	(10 ²² A/m)
51.1 ± 2.5	51.5	46.4	2.1	58.1	56.6	3.0	13.3	9.0	50.4 ± 3.1	50.7	48.5 ± 2.6	46.8	2.2	54.7	56.9	3.1	9.7	8.4	
$\alpha_{95} = 1.1$ k = 1626										$\alpha_{95} = 1.6$ k = 778									
(µT)	(°)	(°)								(µT)	(°)								
52.1	47.4	1.3								48.5	47.8								

VALN. Age of the structure: 1238-1350 A.D.

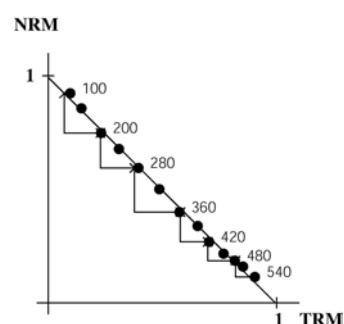
$H_{lab} = 50 \mu\text{T}$. Sample coordinates.



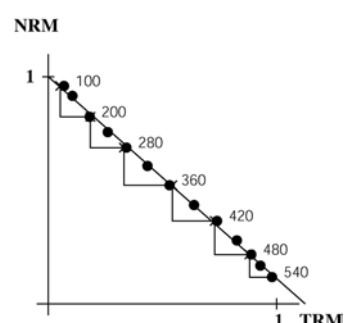
VALN1A
With correction of anisotropy
 $\text{NRM}_0 = 3.96 \text{ A/m}$
 $F = 52.7 \mu\text{T}$
 $q = 102.1$



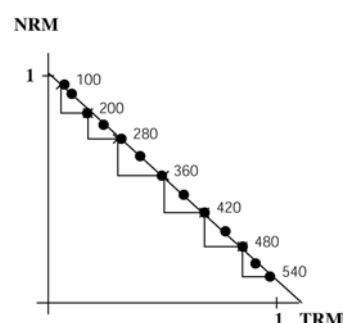
VALN2A
With correction of
anisotropy
 $\text{NRM}_0 = 2.09 \text{ A/m}$
 $F = 49.9 \mu\text{T}$
 $q = 43.1$



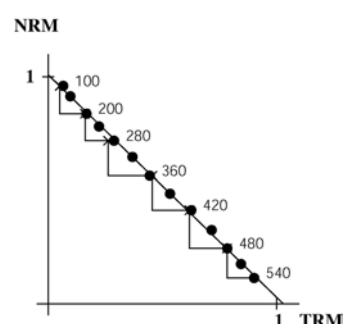
VALN4A
With correction of anisotropy
 $\text{NRM}_0 = 1.71 \text{ A/m}$
 $F = 44.5 \mu\text{T}$
 $q = 57.2$

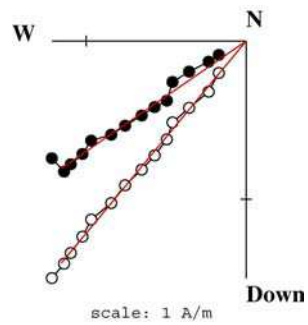


VALN5A
With correction of anisotropy
 $\text{NRM}_0 = 1.70 \text{ A/m}$
 $F = 45.6 \mu\text{T}$
 $q = 69.1$

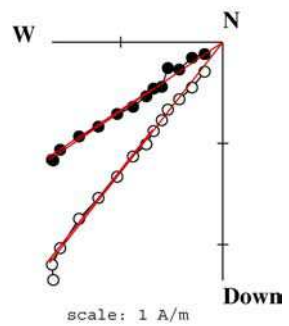
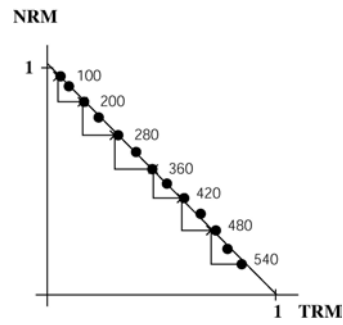


VALN6A
With correction of anisotropy
 $\text{NRM}_0 = 2.21 \text{ A/m}$
 $F = 49.0 \mu\text{T}$
 $q = 68.4$

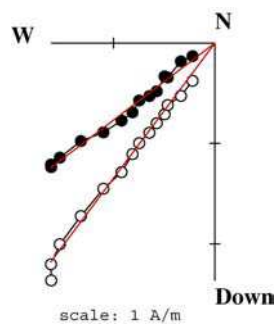
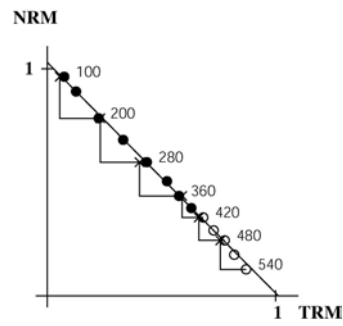




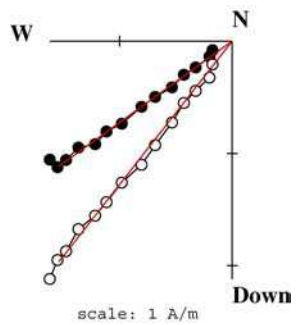
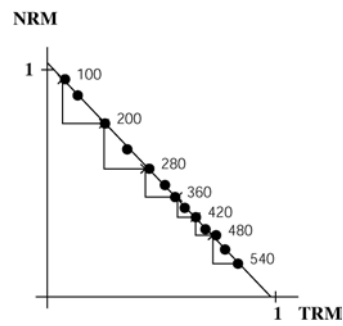
VALN17A
With correction of anisotropy
 $NRM_0 = 2.07 \text{ A/m}$
 $F = 50.7 \mu\text{T}$
 $q = 57.5$



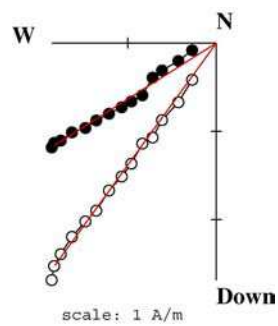
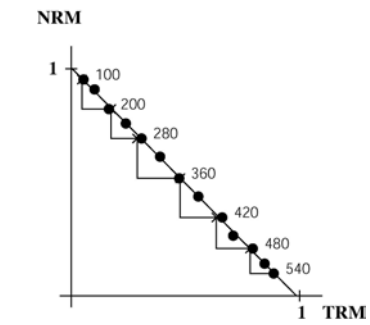
VALN8B
Without correction of anisotropy
 $NRM_0 = 3.10 \text{ A/m}$
 $F = 50.8 \mu\text{T}$
 $q = 27.4$



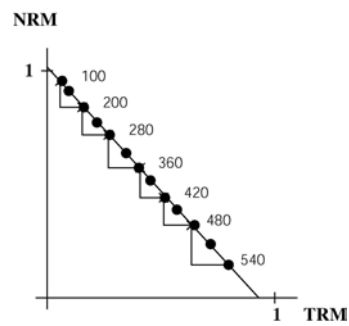
VALN9A
With correction of anisotropy
 $NRM_0 = 3.12 \text{ A/m}$
 $F = 52.6 \mu\text{T}$
 $q = 76.7$

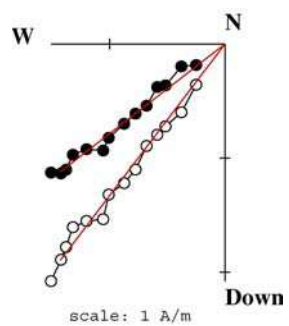


VALN12A
With correction of anisotropy
 $NRM_0 = 2.89 \text{ A/m}$
 $F = 50.9 \mu\text{T}$
 $q = 82.4$

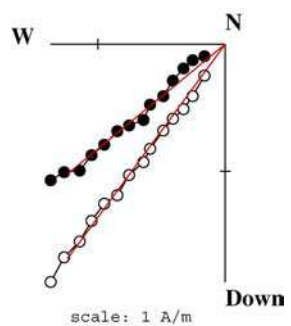


VALN14A
With correction of anisotropy
 $NRM_0 = 3.60 \text{ A/m}$
 $F = 54.6 \mu\text{T}$
 $q = 102.9$

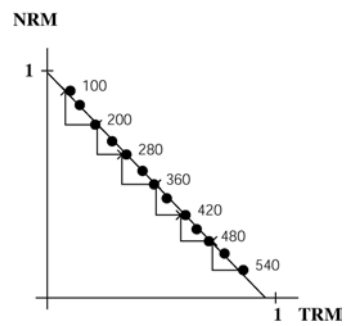
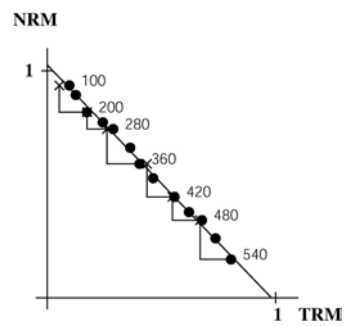




VALN16A
With correction of anisotropy
 $NRM_0 = 2.80 \text{ A/m}$
 $F = 52.2 \mu\text{T}$
 $q = 36.9$



VALN18A
With correction of anisotropy
 $NRM_0 = 2.63 \text{ A/m}$
 $F = 51.9 \mu\text{T}$
 $q = 52.2$



VALID: 1238-1400 A.D.

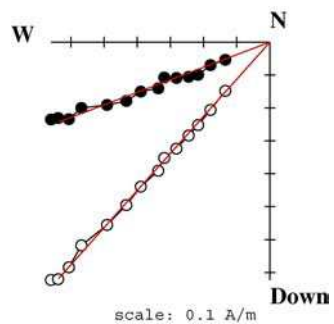
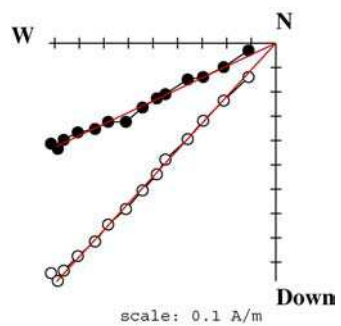
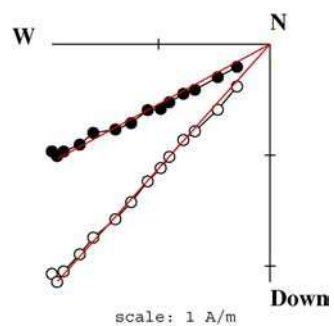
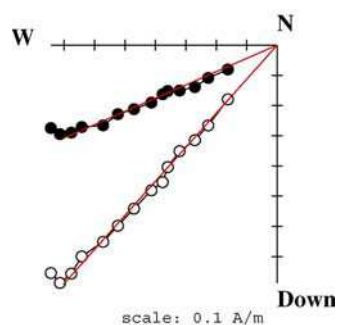
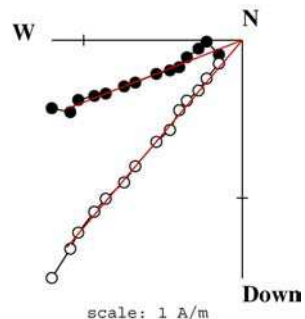
Latitude = $39^{\circ} 28' \text{ N}$ Longitude = $0^{\circ} 22' \text{ W}$

$$H_{lab} = 50.0 \text{ } \mu\text{T}$$

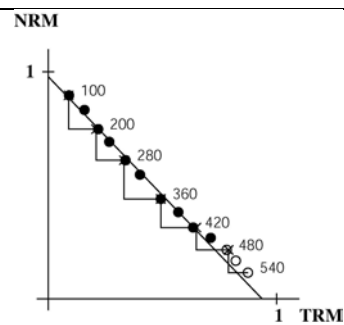
H _{lab} = 50.0 µT																anisotropy								Direction of anisotropy axes								Cooling rate gain							
Spl	NRM	no		yes		no		yes		k1		k2		k3		24 h		48 h																					
		I	D	I _e	D _e	F ± σF	F _e	T _{an}	dM _{an}	k ₁ /k ₃	I	D	I	D	I	D	ΔMz ₂₄	dz ₂₄	ΔMz ₄₈	dz ₄₈																			
5-A	2.03	810	-8.2	6.3	100-450	10	0.65	0.89	20.9	2.8	0.7	3.5	46.6	6.1	47.9	7.6	54.6 ± 1.5	52.2	420	0.4	9	-27.6	56.7	36.3	124.1	41.3	-27.6	6.5	1.4	8.0	-1.9								
6-A	1.12	396	-7.8	7.1	100-540	13	0.72	0.91	22.8	2.5	1.5	4.6	47.4	5.4	45.9	5.7	57.0 ± 1.6	57.8	420	-2.3	6	-78.1	40.9	9.9	74.6	6.5	-78.1	9.9	2.3	11.8	-1.7								
8-A	3.01	1031	-7.3	7.4	100-540	13	0.77	0.91	32.2	1.6	1.9	1.7	44.4	2.6	44.6	1.1	57.5 ± 1.3	57.1	420	-0.7	4	27.4	-71.3	40.5	45.1	37.2	27.4	7.0	2.8	8.7	-2.1								
11-A	1.37	540	4.6	6.4	100-540	13	0.80	0.91	71.4	2.1	0.8	2.3	45.8	4.7	44.7	4.5	52.9 ± 0.5	54.2	420	-1.3	4	80.2	73.6	-3.3	144.2	9.2	80.2	8.5	2.5	9.5	-1.3								
12-A	1.01	218	11.9	11.6	100-540	13	0.76	0.91	40.7	2.3	1.0	3.1	46.5	8.4	46.5	9.1	55.9 ± 1.0	56.4	420	0.9	5	37.1	47.7	52.7	221.1	3.2	37.1	8.7	3.7	9.9	-0.2								
13-A	1.58	360	-12.2	11.0	100-480	11	0.67	0.90	29.8	2.2	2.3	4.5	48.5	-2.0	47.2	0.1	57.2 ± 1.1	58.3	420	-0.2	9	45.5	8.8	-44.4	14.1	2.7	45.5	8.1	2.0	9.0	-0.7								
14-B	2.98	898	-11.3	8.3	100-510	12	0.73	0.90	24.1	5.3	4.7	7.2	50.0	5.2	49.8	7.6	58.2 ± 1.6	58.4	420	-1.9	14	1.6	44.7	-88.2	74.6	0.9	1.6	13.0	2.0	14.8	0.2								
17-B	0.89	272	3.7	8.2	100-510	12	0.77	0.91	52.1	2.8	0.8	1.9	46.3	7.6	45.2	6.9	48.1 ± 0.6	49.2	420	-1.9	7	77.9	8.6	-5.9	70.0	10.5	77.9	4.3	0.8	5.4	-0.6								
18-A	2.20	845	-7.8	6.5	100-510	12	0.78	0.91	35.1	2.3	0.9	3.2	46.3	2.7	45.0	3.0	51.7 ± 1.1	53.0	420	-1.8	7	74.8	9.9	-14.3	31.0	5.3	74.8	5.8	2.3	7.1	-0.9								
19-A	0.62	227	-5.3	6.9	100-510	12	0.64	0.91	27.2	3.2	1.5	4.4	49.1	-4.5	47.4	-3.0	50.6 ± 1.1	51.8	420	-4.7	15	86.1	-78.8	1.2	29.4	3.7	86.1	5.0	0.8	6.6	-1.9								
21-A	0.90	308	-7.8	7.3	100-510	12	0.62	0.90	31.6	2.9	3	7.1	47.0	4.7	45.6	5.4	55.0 ± 1.0	56.9	420	-3.0	11	78.4	47.4	11.6	227.3	0.0	78.4	9.0	1.9	10.1	-1.8								

VALI. Age of the structure: 1238-1400 A.D.

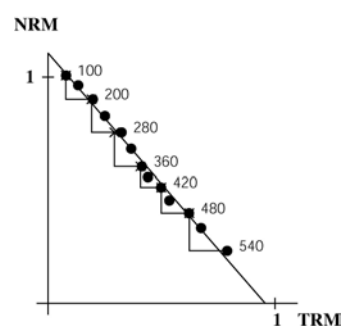
$H_{lab} = 50 \mu T$. Sample coordinates.



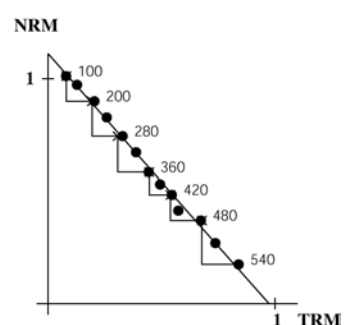
VALI5A
With correction of anisotropy
 $NRM_0 = 2.03 \text{ A/m}$
 $F = 52.2 \mu T$
 $q = 20.9$



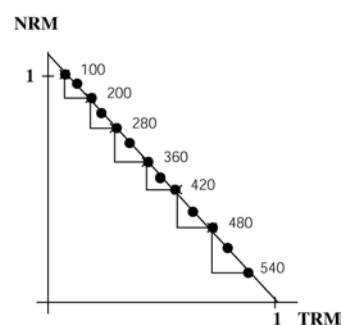
VALI6A
With correction of
anisotropy
 $NRM_0 = 1.12 \text{ A/m}$
 $F = 57.8 \mu T$
 $q = 22.8$



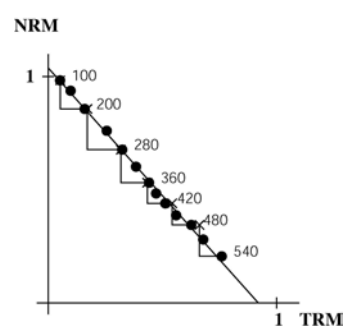
VALI8A
With correction of anisotropy
 $NRM_0 = 3.01 \text{ A/m}$
 $F = 57.1 \mu T$
 $q = 32.2$

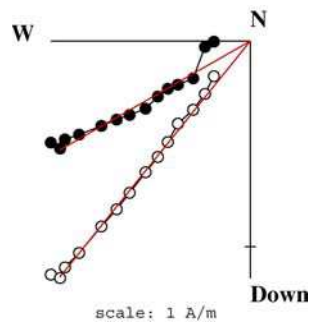


VALI11A
With correction of anisotropy
 $NRM_0 = 1.37 \text{ A/m}$
 $F = 54.2 \mu T$
 $q = 71.4$

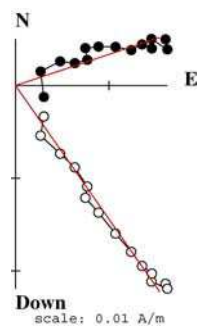


VALI12A
With correction of anisotropy
 $NRM_0 = 1.01 \text{ A/m}$
 $F = 56.4 \mu T$
 $q = 40.7$

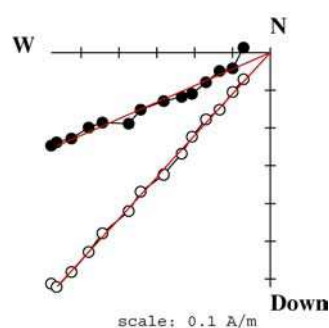




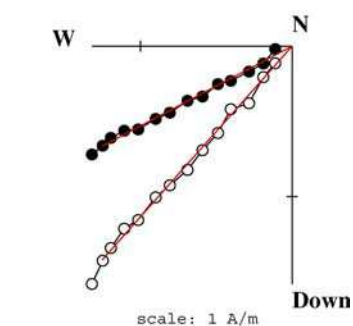
VALI13A
With correction of anisotropy
 $NRM_0 = 1.58 \text{ A/m}$
 $F = 58.3 \mu\text{T}$
 $q = 29.8$



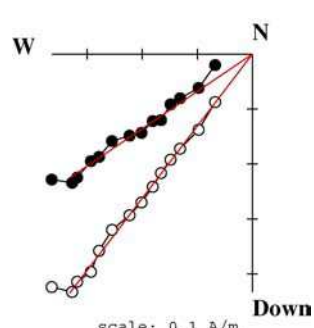
VALI14B
With correction of anisotropy
 $NRM_0 = 2.98 \text{ A/m}$
 $F = 58.0 \mu\text{T}$
 $q = 24.1$



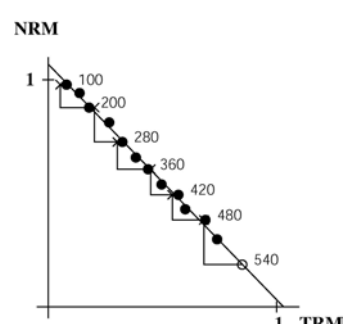
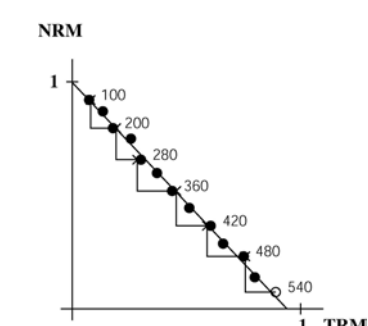
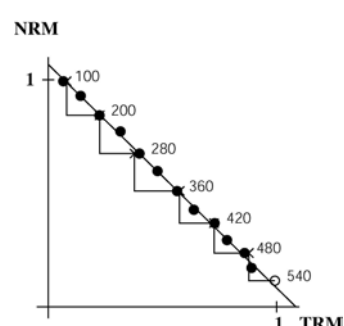
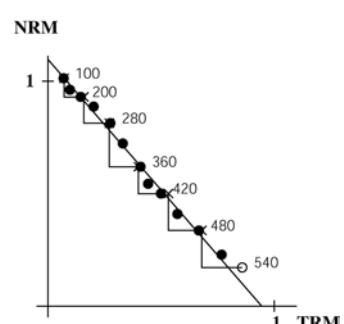
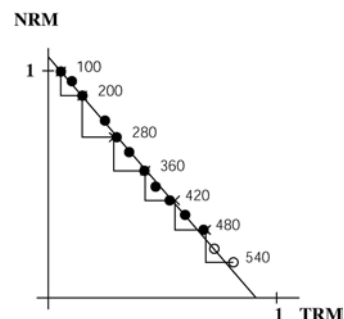
VALI17B
With correction of anisotropy
 $NRM_0 = 0.89 \text{ A/m}$
 $F = 49.2 \mu\text{T}$
 $q = 52.1$

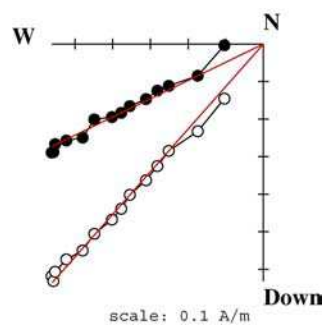


VALI18A
With correction of anisotropy
 $NRM_0 = 2.20 \text{ A/m}$
 $F = 53.0 \mu\text{T}$
 $q = 35.1$

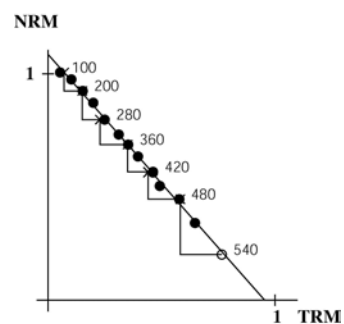


VALI19A
With correction of anisotropy
 $NRM_0 = 0.62 \text{ A/m}$
 $F = 51.8 \mu\text{T}$
 $q = 27.2$





VALI21A
With correction of anisotropy
 $NRM_0 = 0.90 \text{ A/m}$
 $F = 56.9 \mu\text{T}$
 $q = 31.6$



VALK: 1300-1450 A.D.

Latitude = 39° 28' N Longitude = 0° 22' W

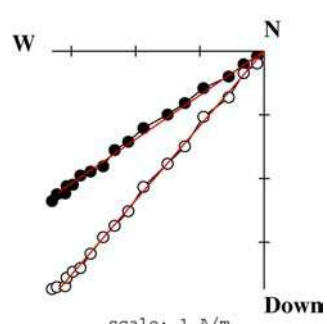
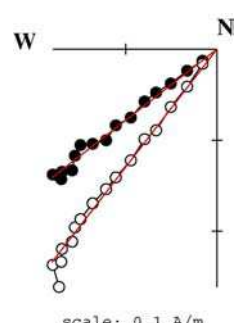
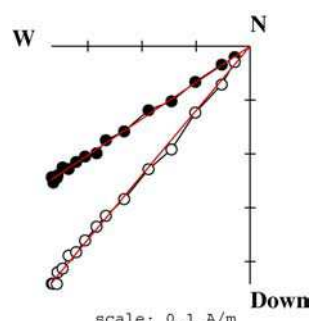
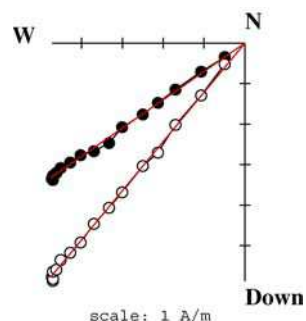
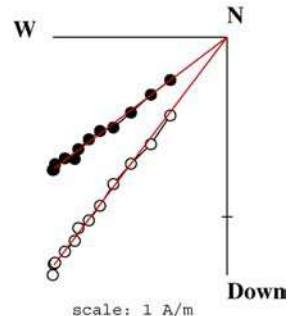
H_{lab} = 60.0 µT

Spl	NRM (A/m)	χ (10 ⁻⁵)	Δχ (%)	Q _l	T _{min-T_{max}} (°C)	n	f	g	q	mad	dang	crm	anisotropy				F _{± σF} (µT)	F _e (µT)	T _{an} (°C)	dM _{an} (%)	k _{1/k₃} (%)	Direction of anisotropy axes		Cooling rate gain							
													no		yes					k1		k2		k3		24 h	48 h				
													I	D	I _e	D _e	(°)	(°)	(°)	(°)	(°)	(°)	(°)	(°)	(%)	(%)					
1-A	1.94	579	4.15	8.4	100-450	10	0.52	0.87	19.9	3.5	0.8	4.0	43.5	-0.2	46.4	1.4	57.6 ± 1.15	54.0	450	-1.0	14	-4.6	61.6	28.9	149.0	60.7	-20.3	3.8	1.0	7.1	-5.7
2-A	8.91	1128	-5.67	19.9	100-560	15	0.88	0.90	65.4	0.6	0.0	1.5	43.0	3.5	44.9	3.8	57.3 ± 0.63	55.9	500	-2.3	8	8.6	44.1	-17.8	131.4	70.1	158.8	8.8	8.3	9.0	-1.8
4-A	0.67	236	-4.66	7.1	100-560	15	0.87	0.90	53.6	0.8	0.0	2.4	42.3	3.0	44.8	4.8	60.7 ± 0.85	56.4	500	-3.1	12	-17.1	26.8	4.0	115.6	72.4	12.8	8.0	4.0	9.6	-2.3
5-A	0.37	134	-6.72	6.9	100-560	15	0.85	0.92	64.0	1.3	0.0	3.4	43.2	-1.0	45.6	1.0	60.5 ± 0.73	56.4	500	-1.9	12	-16.8	26.4	-1.0	116.7	73.2	30.1	8.0	7.7	11.0	-2.8
11-A	5.95	1433	-19.8	10.4	100-580	16	0.89	0.92	83.6	0.8	0.0	2.5	42.6	4.7	43.9	4.9	57.2 ± 0.51	56.0	500	-2.1	7	9.5	18.9	-19.5	105.5	68.1	133.4	-6.1	-14.0	-1.7	-9.4
12-A	0.24	74	-9.46	8.2	200-560	13	0.77	0.91	59.9	1.6	0.5	2.5	43.0	3.7	44.7	4.8	61.2 ± 0.67	59.8	450	1.9	20	-19.5	-55.9	-15.6	39.8	64.7	-14.2	8.7	1.7	9.8	-3.2
13-A	2.34	811	-11.2	7.3	100-560	13	0.75	0.91	60.3	2.1	1.2	2.5	44.1	4.8	44.1	2.8	58.2 ± 0.64	57.2	450	0.5	6	30.2	-81.0	-51.3	-37.4	21.9	22.5	7.5	1.5	8.9	-3.0
14-B	7.51	1417	-3.95	13.3	100-560	15	0.87	0.92	55.8	1.8	0.9	2.1	40.1	0.7	42.0	2.3	52.3 ± 0.63	49.6	500	-2.8	9	-14.3	18.5	7.1	106.7	74.0	-9.0	7.8	-0.4	7.2	-0.1
15-B	2.64	505	11.1	13.1	100-500	12	0.69	0.90	34.8	2.5	1.9	2.9	38.2	7.2	41.2	5.2	51.8 ± 0.78	48.6	500	-1.2	13	-5.0	73.2	-20.3	165.1	69.0	150.2	11.3	0.3	10.9	-4.6

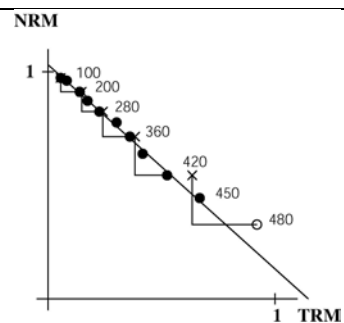
Without anisotropy correction. 9 samples:								With anisotropy and cooling rate corrections. 9 samples:								F _{m ± sd}		F _{po}		I _{ms}		D _{ms}		F _{pa}		I _{pa}		D _{pa}		VDM		VADM	
F _m	± sd	F _{po}	I _{ms}	D _{ms}	F _{pa}	I _{pa}	D _{pa}	VDM	VADM	(µT)	(µT)	(°)	(°)	(µT)	(µT)	(°)	(°)	(µT)	(µT)	(°)	(°)	(10 ²² A/m)	(10 ²² A/m)										
57.4 ± 3.4	57.7	42.3	3.0	65.2	53.4	4.1	12.1	10.0	54.9 ± 3.6	55.4	51.6 ± 4.1	44.2	3.0	58.3	54.9	4.1	10.6	9.0	9.0	9.0	9.0	9.0	9.0	9.0									
$\alpha_{95} = 1.7$								$\alpha_{95} = 1.3$								F _{ma}		I _{ma}		D _{ma}		F _{ma}		I _{ma}		D _{ma}							
k = 889								k = 1606								(µT)		(°)		(°)		52.1		45.2		2.2							
58.3																																	

VALK. Age of the structure: 1300-1450 A.D.

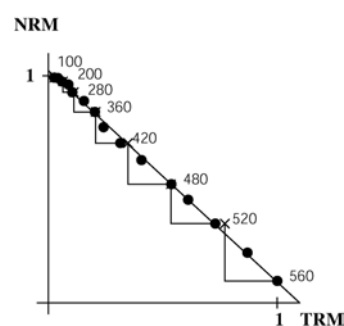
$H_{lab} = 60 \mu T$. Sample coordinates.



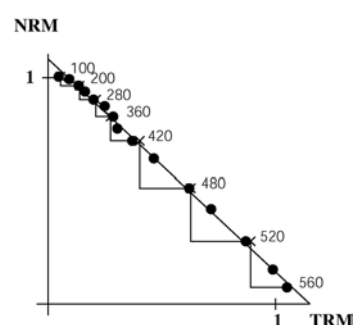
VALK1A
With correction of anisotropy
 $NRM_0 = 1.94 \text{ A/m}$
 $F = 54.0 \mu T$
 $q = 19.9$



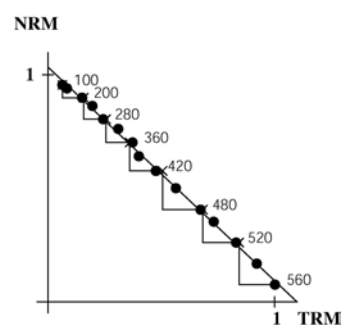
VALK2A
With correction of anisotropy
 $NRM_0 = 8.91 \text{ A/m}$
 $F = 55.9 \mu T$
 $q = 65.4$



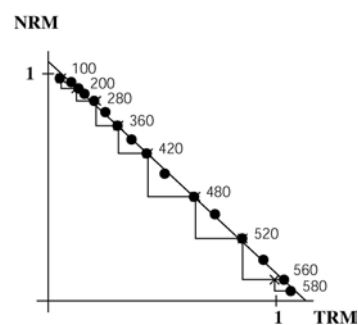
VALK4A
With correction of anisotropy
 $NRM_0 = 0.67 \text{ A/m}$
 $F = 56.4 \mu T$
 $q = 53.6$

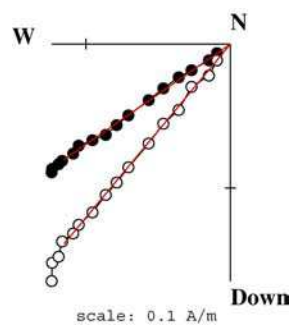


VALK5A
With correction of anisotropy
 $NRM_0 = 0.37 \text{ A/m}$
 $F = 56.4 \mu T$
 $q = 64.0$

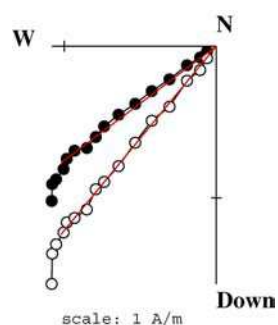


VALK11A
With correction of anisotropy
 $NRM_0 = 5.95 \text{ A/m}$
 $F = 56.0 \mu T$
 $q = 83.6$

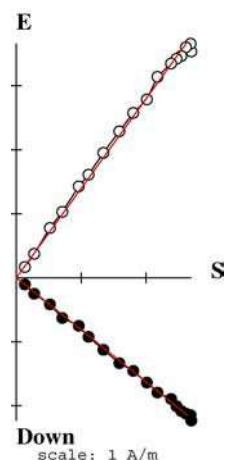




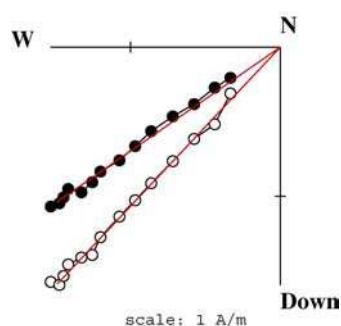
VALK12A
With correction of anisotropy
 $NRM_0 = 0.24 \text{ A/m}$
 $F = 59.8 \mu\text{T}$
 $q = 59.9$



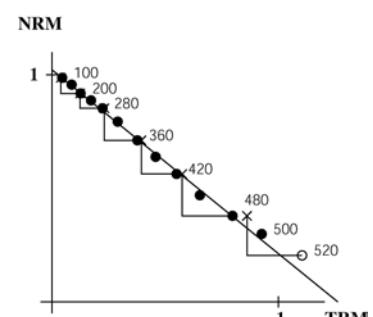
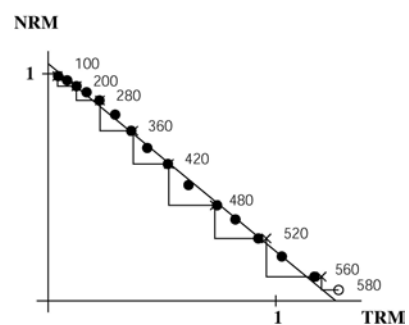
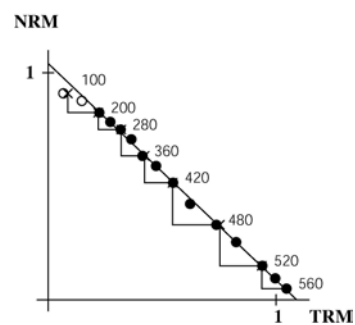
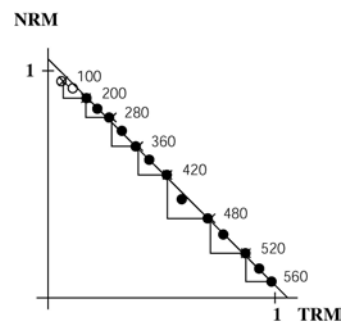
VALK13A
With correction of anisotropy
 $NRM_0 = 2.34 \text{ A/m}$
 $F = 57.2 \mu\text{T}$
 $q = 60.3$



VALK14A
With correction of anisotropy
 $NRM_0 = 7.51 \text{ A/m}$
 $F = 49.6 \mu\text{T}$
 $q = 55.8$



VALK15A
With correction of anisotropy
 $NRM_0 = 2.64 \text{ A/m}$
 $F = 48.6 \mu\text{T}$
 $q = 34.8$



VALM: 1300-1450 A.D.

Latitude = 39° 28' N Longitude = 0° 22' W

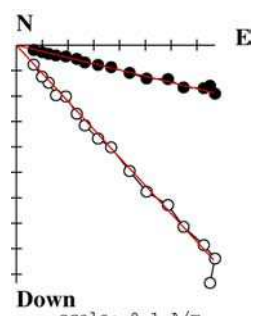
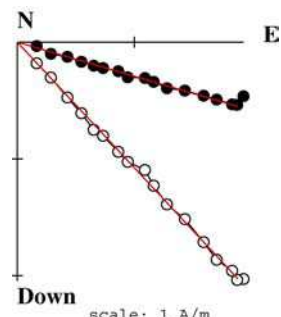
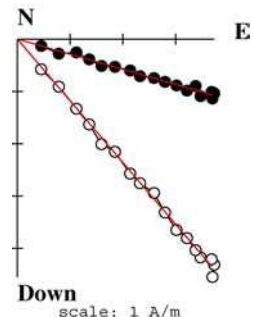
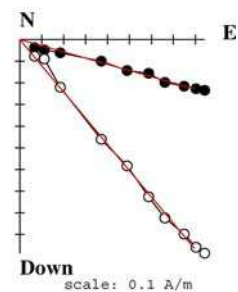
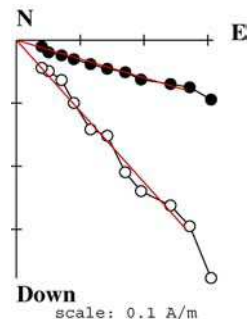
H_{lab} = 60.0 µT

Spl	NRM (A/m)	anisotropy																Direction of anisotropy axes					Cooling rate gain								
		no				yes				no				yes				k1		k2		k3		24 h		48 h					
		χ (10 ⁻⁵)	$\Delta\chi$ (%)	Q_l	T _{min-T_{max}} (°C)	n	f	g	q	mad	dang	crm	I	D	I _e	D _e	F ± σF	F _e (µT)	T _{an} (°C)	dM _{an} (%)	k _{1/k₃}	I	D	I	D	I	D	ΔMz ₂₄ (%)	dz ₂₄ (%)	ΔMz ₄₈ (%)	dz ₄₈ (%)
1-A	0.53	281	-11.7	4.7	100-450	10	0.71	0.88	12.5	4.0	1.2	6.3	46.5	5.7	47.2	8.3	58.2 ± 2.3	58.6	360	-5.3	11	-12.5	64.1	-58.4	175.1	28.5	147.2	13.7	6.4	10.2	0.4
2-A	1.42	537	-8.2	6.6	100-420	9	0.82	0.84	33.3	1.9	1.2	3.4	48.7	10.2	49.4	7.7	46.8 ± 0.8	46.8	360	-1.8	9	30.1	-85.5	-39.0	-23.5	36.5	29.8	7.4	-0.6	3.8	-4.0
3-A	6.45	1590	-9.8	10.2	100-560	15	0.76	0.92	32.8	2.5	0.4	2.5	48.3	11.2	48.6	7.9	46.2 ± 0.8	47.4	500	-1.9	12	-25.3	15.0	-28.9	120.1	49.9	70.9	11.4	-3.7	8.7	2.1
4-A	3.07	897	-8.6	8.6	100-560	15	0.80	0.92	56.4	1.6	0.5	3.1	44.3	8.8	45.9	8.5	53.8 ± 0.7	53.9	500	-2.6	9	-22.0	74.5	-7.0	167.3	66.8	94.1	6.3	-0.1	5.4	1.1
6-A	1.31	642	9.5	5.1	100-560	15	0.84	0.92	65.1	1.5	0.9	2.4	45.0	6.5	47.0	6.1	54.8 ± 0.6	52.7	360	-1.0	9	-6.9	29.9	8.3	118.9	79.2	-21.0	-0.3	3.7	-1.8	-2.1
7-A	3.41	1235	-8.6	6.9	100-560	15	0.86	0.93	66.3	1.9	0.9	2.5	44.1	4.0	45.8	4.3	50.4 ± 0.5	48.6	450	-3.0	7	0.1	57.6	10.7	147.7	79.3	-32.9	-0.4	3.9	-2.0	-2.3
8-A	5.99	1695	-10.3	8.9	100-560	15	0.82	0.93	54.0	2.1	0.6	2.3	45.5	11.3	47.0	7.0	49.8 ± 0.6	49.0	500	-2.0	13	-30.3	-8.6	-19.9	93.6	52.6	31.7	5.9	-0.1	2.8	0.1
12-A	2.91	1065	6.6	6.9	100-480	11	0.68	0.89	26.8	2.6	2.0	3.5	43.8	8.2	46.5	7.0	48.6 ± 0.9	47.3	450	-1.8	11	13.1	-79.9	-16.8	6.0	68.5	46.2	11.5	-1.3	13.5	0.1
14-A	3.18	1067	3.7	7.5	100-480	11	0.68	0.89	21.0	2.5	3.0	4.6	43.7	7.0	45.8	7.9	47.5 ± 1.1	44.9	450	-0.9	9	-12.4	-81.1	16.9	5.1	68.8	223.5	9.6	-1.1	7.2	-0.1

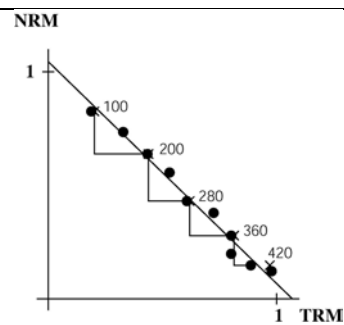
Without anisotropy correction. 9 samples:										With anisotropy and cooling rate correction. 9 samples:									
1-A. 2-A. 3-A. 4-A. 6-A. 7-A. 8-A. 12-A. 14-A										1-A. 2-A. 3-A. 4-A. 6-A. 7-A. 8-A. 12-A. 14-A									
F _m ± sd	F _{po}	I _{ms}	D _{ms}	F _{pa}	I _{pa}	D _{pa}	VDM	VADM	F _m ± sd	F _{po}	F _{pocr}	I _{ms}	D _{ms}	F _{pa}	I _{pa}	D _{pa}	VDM	VADM	
(µT)	(µT)	(°)	(°)	(µT)	(°)	(°)	(10 ²² A/m)	(10 ²² A/m)	(µT)	(µT)	(µT)	(°)	(°)	(µT)	(°)	(°)	(10 ²² A/m)	(10 ²² A/m)	
50.7 ± 4.1	50.8	45.6	8.1	57.4	56.1	9.7	10.3	8.8	49.9 ± 4.3	49.9	47.1 ± 4.5	47.0	7.2	53.2	57.2	8.6	9.4	8.2	
α ₉₅ = 1.6										α ₉₅ = 1.0									
k = 996										k = 2733									

VALM. Age of the structure: 1300-1450 A.D.

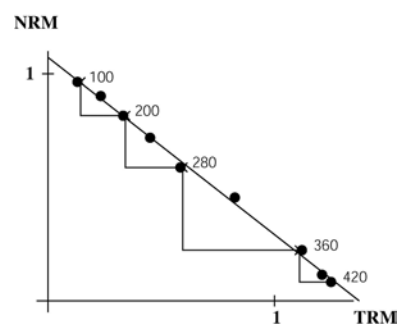
$H_{lab} = 60 \mu T$. Sample coordinates.



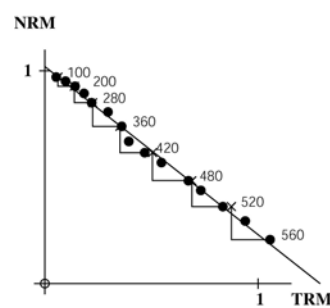
VALM1A
With correction of anisotropy
 $NRM_0 = 0.53 \text{ A/m}$
 $F = 58.6 \mu T$
 $q = 12.5$



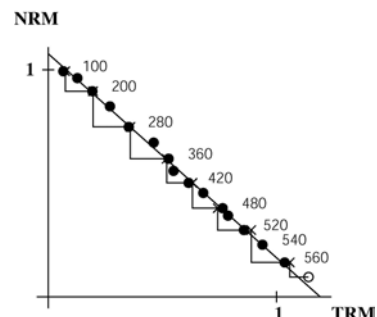
VALM2A
With correction of anisotropy
 $NRM_0 = 1.42 \text{ A/m}$
 $F = 46.8 \mu T$
 $q = 33.3$



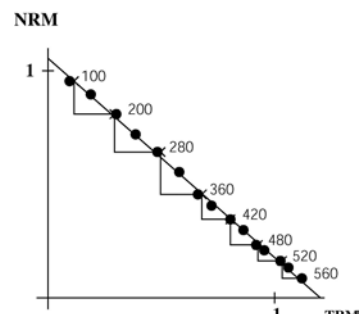
VALM3A
With correction of anisotropy
 $NRM_0 = 6.45 \text{ A/m}$
 $F = 47.4 \mu T$
 $q = 32.8$

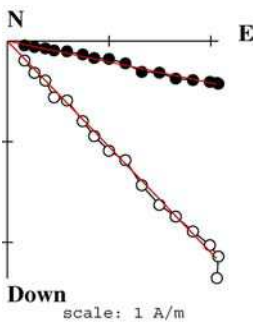


VALM4A
With correction of anisotropy
 $NRM_0 = 3.07 \text{ A/m}$
 $F = 53.9 \mu T$
 $q = 56.4$

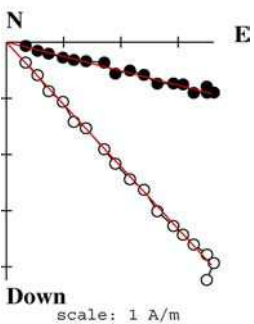


VALM6A
With correction of anisotropy
 $NRM_0 = 1.31 \text{ A/m}$
 $F = 52.7 \mu T$
 $q = 65.1$

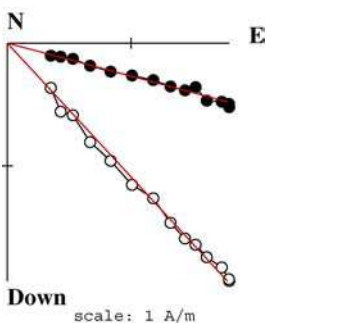




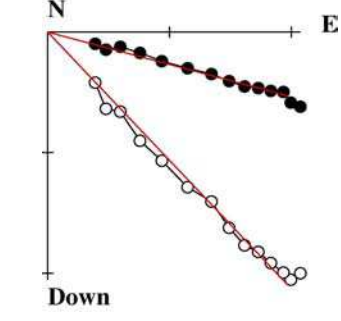
VALM7A
With correction of anisotropy
 $NRM_0 = 3.41 \text{ A/m}$
 $F = 48.6 \mu\text{T}$
 $q = 66.3$



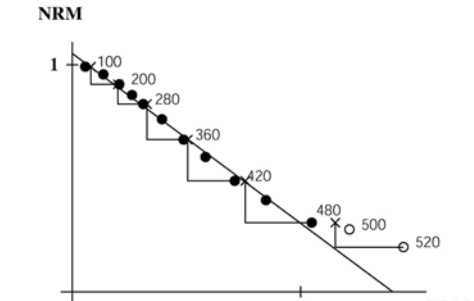
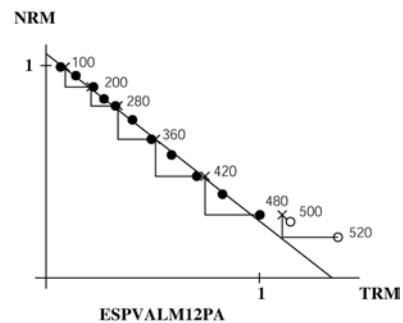
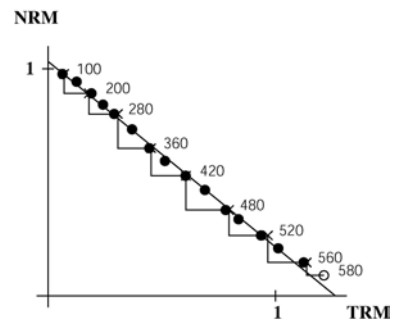
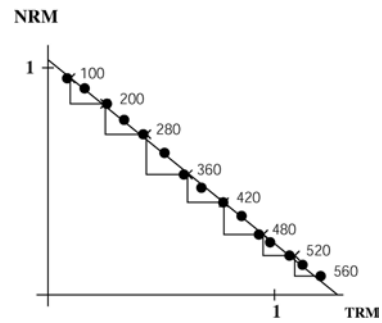
VALM8A
With correction of anisotropy
 $NRM_0 = 5.99 \text{ A/m}$
 $F = 49.0 \mu\text{T}$
 $q = 54.0$



VALM12A
With correction of anisotropy
 $NRM_0 = 2.91 \text{ A/m}$
 $F = 47.3 \mu\text{T}$
 $q = 26.8$



VALM14A
With correction of anisotropy
 $NRM_0 = 3.18 \text{ A/m}$
 $F = 44.9 \mu\text{T}$
 $q = 21.0$



CALC: 1400-1420 A.D.

Latitude = 39° 01' N Longitude = 3° 49' W

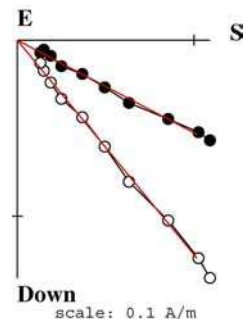
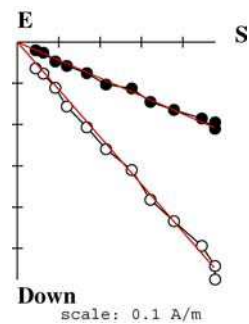
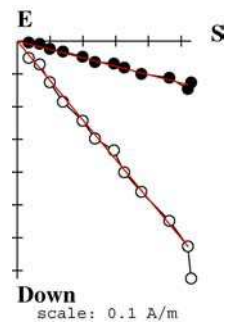
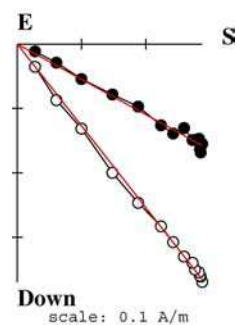
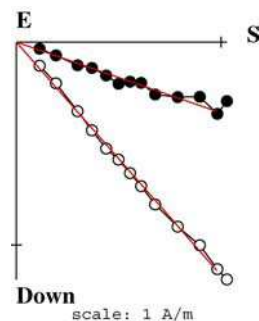
 $H_{lab} = 60.0 \mu T$

Spl	NRM (A/m)	anisotropy																Direction of anisotropy axes						Cooling rate gain							
		no				yes				no				yes				k1			k2			k3			24 h		48 h		
		χ (10^{-5})	$\Delta\chi$ (%)	Q_i	$T_{min}-T_{max}$ (°C)	n	f	g	q	mad	dang	crm	I	D	I_e	D_e	$F \pm \sigma F$	F_e (μT)	T_{an} (°C)	dM_{an} (%)	k_1/k_3 (%)	I	D	I	D	I	D	ΔM_{24} (%)	dz_{24} (%)	ΔM_{48} (%)	dz_{48} (%)
1-A	1.71	176	2.8	24.4	100-530	12	0.88	0.90	62.4	2.6	0.4	1.3	46.2	1.1	47.3	-0.9	50.5 ± 0.6	50.1	440	-2.7	8	7.2	50.0	-62.0	126.3	26.9	143.7	4.1	1.0	1.4	1.0
2-A	0.51	118	-5.1	10.9	100-530	12	0.74	0.86	50.1	3.0	1.8	3.8	44.9	6.0	48.1	8.8	53.9 ± 0.6	49.0	500	-13.9	18	-23.5	-11.0	2.2	78.1	66.4	-16.9	9.6	3.3	10.2	-0.3
4-A	0.98	371	-12.7	6.6	100-500	11	0.82	0.89	73.9	1.9	0.9	2.3	48.9	-1.4	49.4	-0.1	56.0 ± 0.5	54.2	360	-2.5	14	1.0	-56.5	-45.8	32.4	44.2	34.5	4.2	-1.4	1.3	-3.1
8-A	0.83	332	-8.4	6.3	100-500	11	0.83	0.89	57.3	1.7	1.2	2.3	46.3	3.2	46.5	2.3	54.9 ± 0.7	53.0	360	-2.4	9	-26.4	88.1	31.4	160.4	46.7	29.9	0.4	-0.8	-1.9	-2.7
9-A	0.20	131	-3.8	3.8	100-440	9	0.76	0.84	62.1	1.9	0.1	1.7	47.2	6.5	47.2	6.1	52.1 ± 0.5	51.8	360	-3.2	2	15.0	-84.7	-50.5	-13.7	35.5	16.3	2.5	4.5	-1.5	0.8
10-A	1.06	327	13.1	8.1	100-500	11	0.82	0.90	45.8	1.8	0.2	1.1	49.8	-0.7	50.2	-0.3	48.5 ± 0.6	47.7	360	-1.7	4	-18.4	42.1	42.0	114.6	42.3	-30.3	2.7	3.9	2.9	0.2
11-A	0.82	127	-7.1	16.2	100-440	9	0.66	0.87	72.6	2.0	3.8	3.6	46.7	0.3	46.8	-0.7	48.5 ± 0.3	47.2	440	-1.7	8	-40.3	37.2	44.2	71.8	18.1	-36.7	2.7	-1.7	1.6	-3.1
16-A	0.56	57	5.3	24.7	100-500	11	0.83	0.89	75.4	1.8	0.8	1.7	44.6	1.8	44.7	1.9	52.7 ± 0.5	51.3	440	-1.6	7	-43.6	22.2	29.0	80.3	32.5	-30.4	6.2	-1.0	6.7	-2.4
17-A	1.42	115	7.0	31.0	100-500	11	0.86	0.89	110.2	1.8	0.7	2.2	45.7	7.8	45.8	6.5	47.8 ± 0.3	48.0	440	-2.0	4	38.3	30.6	-42.5	74.2	23.5	140.7	1.7	-1.3	1.4	-0.6

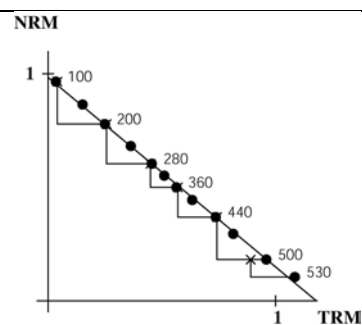
Without anisotropy correction. 9 samples:								With anisotropy and cooling rate corrections. 9 samples:											
1-A. 2-A. 4-A. 8-A. 9-A. 10-A. 11-A. 16-A. 17-A.								1-A. 2-A. 4-A. 8-A. 9-A. 10-A. 11-A. 16-A. 17-A.											
$F_m \pm sd$	F_{po}	I_{ms}	D_{ms}	F_{pa}	I_{pa}	D_{pa}	VDM	VADM	$F_m \pm sd$	F_{po}	$F_{po cr}$	I_{ms}	D_{ms}	F_{pa}	I_{pa}	D_{pa}	VDM	VADM	
(μT)	(μT)	($^\circ$)	($^\circ$)	(μT)	($^\circ$)	($^\circ$)	($10^{22} A/m$)	($10^{22} A/m$)	(μT)	(μT)	(μT)	($^\circ$)	($^\circ$)	(μT)	($^\circ$)	($^\circ$)	($10^{22} A/m$)	($10^{22} A/m$)	
51.7 ± 3.0	51.4	46.7	2.8	58.4	57.4	4.6	10.3	9.0	50.3 ± 2.5	50.2	48.7 ± 3.0	47.4	2.6	55.3	58.0	4.3	9.7	8.5	
$\alpha_{95} = 1.8$ k = 809								$\alpha_{95} = 1.9$ k = 726											
F_{ma} (μT)								F_{ma} (μT)											
I_{ma} ($^\circ$)								I_{ma} ($^\circ$)											
D_{ma} ($^\circ$)								D_{ma} ($^\circ$)											
52.4								49.6											
48.4								49.0											
2.9								2.7											

CALC. Age of the structure: 1400-1420 A.D.

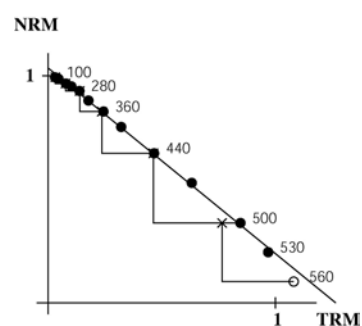
$H_{lab} = 60 \mu T$. Sample coordinates.



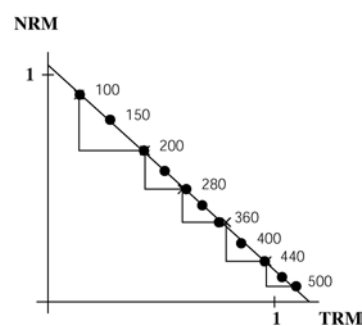
CALC1A
With correction of anisotropy
 $NRM_0 = 1.71 \text{ A/m}$
 $F = 50.1 \mu T$
 $q = 62.4$



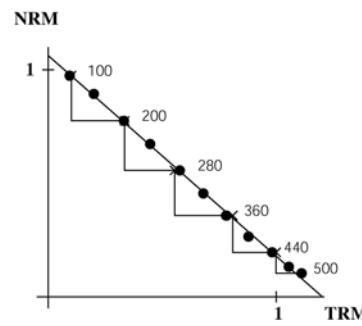
CALC2A
With correction of anisotropy
 $NRM_0 = 0.53 \text{ A/m}$
 $F = 49.0 \mu T$
 $q = 50.1$



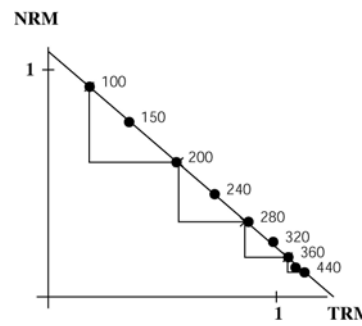
CALC4A
With correction of anisotropy
 $NRM_0 = 0.98 \text{ A/m}$
 $F = 54.2 \mu T$
 $q = 73.9$

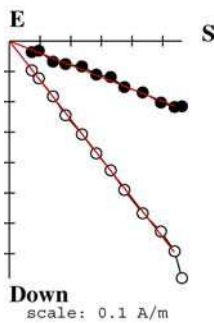


CALC8A
With correction of anisotropy
 $NRM_0 = 0.83 \text{ A/m}$
 $F = 53.0 \mu T$
 $q = 57.3$

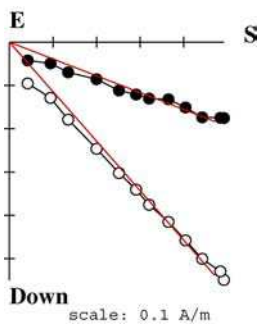


CALC9A
With correction of anisotropy
 $NRM_0 = 0.20 \text{ A/m}$
 $F = 51.8 \mu T$
 $q = 62.1$

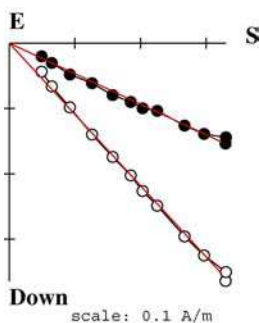




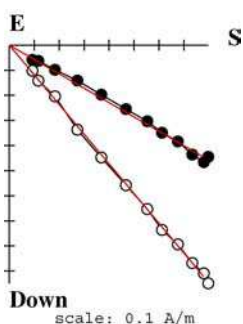
CALC10A
With correction of anisotropy
 $NRM_0 = 1.06 \text{ A/m}$
 $F = 47.7 \mu\text{T}$
 $q = 45.8$



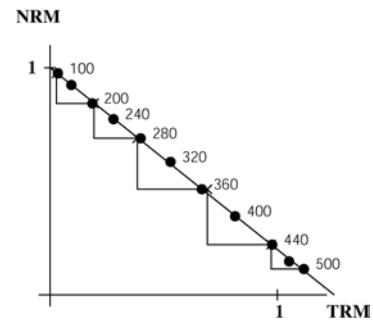
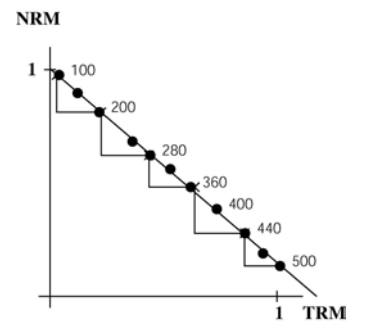
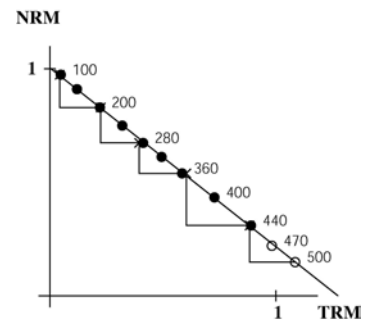
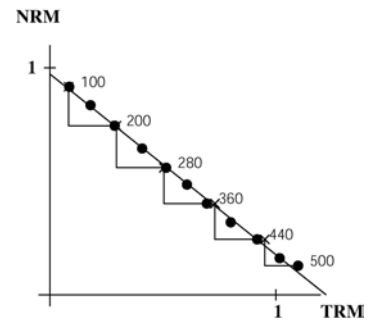
CALC11A
With correction of anisotropy
 $NRM_0 = 0.82 \text{ A/m}$
 $F = 47.2 \mu\text{T}$
 $q = 72.6$



CALC16A
With correction of anisotropy
 $NRM_0 = 0.56 \text{ A/m}$
 $F = 51.3 \mu\text{T}$
 $q = 75.4$



CALC17A
With correction of anisotropy
 $NRM_0 = 1.42 \text{ A/m}$
 $F = 48.0 \mu\text{T}$
 $q = 110.2$



PATH: 1450-1600 A.D.

Latitude = 39° 30' N Longitude = 0° 26' W

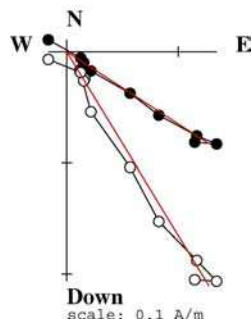
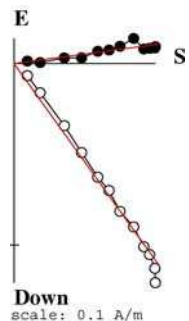
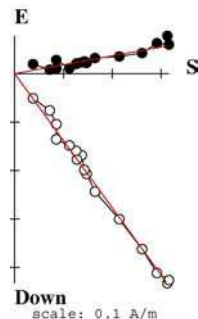
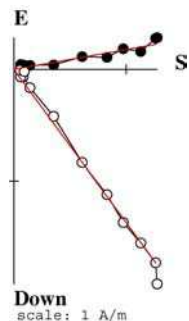
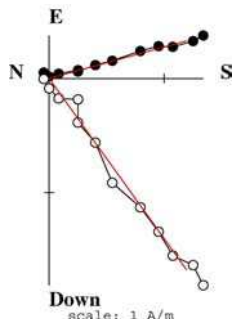
H_{lab} = 50.0 µT

Spl	NRM (A/m)	anisotropy												Direction of anisotropy axes						Cooling rate gain										
		no				yes				no				yes				k1			k2			k3			24 h		48 h	
		I	D	I _e	D _e	F ± σF	F _e (µT)	T _{an} (°C)	dM _{an} (%)	k ₁ /k ₃	I	D	I	D	I	D	I	D	I	D	ΔMz ₂₄ (%)	dz ₂₄ (%)	ΔMz ₄₈ (%)	dz ₄₈ (%)						
1-A	2.35	831	-23.9	7.1	100-400	9	0.81	0.86	22.9	4.6	0.4	11.3	55.0	7.2	53.6	3.1	54.1 ± 1.7	54.4	325	-5.2	12	-50.2	45.9	39.8	47.2	0.7	-50.2	-0.7	-0.6	
1-B	2.33	882	-22.8	6.6									53.5	8.5																
3-B	0.54	318	-19.2	4.3	100-400	9	0.52	0.83	12.5	3.4	1.0	8.3	54.5	9.3	53.7	9.7	64.3 ± 2.9	64.3	325	2.1	7	12.6	-84.0	-68.4	-28.3	17.3	12.6	2.4	-2.5	
3-C	0.14	54	-16.7	6.5									54.5	12.4																
4-A	0.22	357	-17.4	1.5	100-325	6	0.69	0.78	11.5	4.3	2.4	11.3	56.9	6.4	54.2	7.0	59.7 ± 3.5	62.0	325	9.2	16	0.9	36.0	-87.3	105.3	2.5	0.9	0.8	-1.0	
5-B	0.24	112	-8.9	5.4	100-550	15	0.81	0.92	40.3	2.6	1.3	4.6	55.0	2.8	56.4	5.6	54.7 ± 1.1	54.7	475	-6.9	18	22.4	-45.8	50.5	74.2	30.6	22.4	6.2	-1.2	
6-A	1.02	339	-7.4	7.6	100-550	15	0.83	0.92	53.6	2.9	1.1	2.8	52.8	13.5	52.8	14.7	51.9 ± 0.8	51.6	475	-3.2	8	6.1	51.2	58.3	151.1	31.0	6.1	4.1	4.0	
6-B	1.28	384	-7.6	8.4									51.7	2.6																
7-A	3.11	906	-21.2	8.6	100-400	9	0.84	0.85	30.4	2.8	0.8	3.1	54.1	5.4	53.9	1.9	53.7 ± 1.3	54.2	325	-0.2	9	-45.1	16.8	-2.7	109.5	44.8	-45.1	-1.3	0.7	
7-B	3.02	988	-17.3	7.7									53.5	7.9																
8-'A	0.16	44	-9.1	9.1	100-600	17	0.88	0.93	59.5	2.5	3.2	5.1	51.9	9.2	51.8	10.0	57.1 ± 0.9	55.3	475	-2.6	10	53.1	85.7	-2.2	172.8	36.8	53.1	8.1	-2.1	
9-A	2.13	391	-10.7	13.7	100-400	9	0.22	0.87	4.5	10.2	1.5	17.2	54.8	7.0	53.4	8.5	69.1 ± 4.1	69.4	475	-1.7	12	69.5	62.8	-10.4	123.4	17.5	210.1	3.0	-3.6	
10-A	4.13	895	-18.8	11.6	100-450	10	0.88	0.87	36.5	1.2	1.5	1.8	55.0	8.8	55.7	7.6	51.3 ± 1.1	51.2	325	-2.1	7	-1.1	-16.9	-18.4	73.4	71.6	-1.1	0.0	0.9	
10-B	3.23	718	-18.4	11.3									53.0	8.5																
11-A	0.14	54	-9.3	6.5	100-475	12	0.67	0.90	19.0	4.9	2.3	4.3	53.0	6.2	50.8	5.7	53.8 ± 1.8	55.1	475	-5.9	10	86.4	49.9	-0.7	129.1	3.5	86.4	9.2	-2.5	
12-A	0.12	45	-13.3	6.7	100-600	17	0.92	0.93	50.3	2.0	0.6	2.5	54.6	4.1	51.5	7.7	48.9 ± 0.8	52.3	475	-5.4	15	57.8	-23.4	-27.7	25.5	21.3	57.8	5.3	-1.4	
12-B	0.15	45	-4.4	8.4									53.1	11.2																

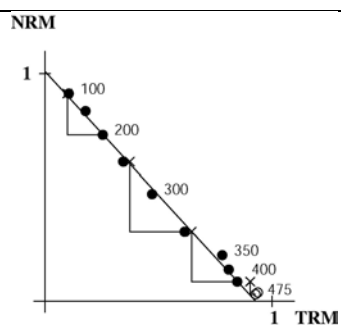
Without anisotropy correction. 10 samples: 1-A. 3-B. 4-A. 5-B. 6-A. 7-A. 8-'A. 10-A. 11-A. 12-A										With anisotropy and cooling rate corrections. 10 samples: 1-A. 3-B. 4-A. 5-B. 6-A. 7-A. 8-'A. 10-A. 11-A. 12-A									
F_m ± sd	F_{po}	I_{ms}	D_{ms}	F_{pa}	I_{pa}	D_{pa}	VDM	VADM	F_m ± sd	F_{po}	F_{pocr}	I_{ms}	D_{ms}	F_{pa}	I_{pa}	D_{pa}	VDM	VADM	
(µT)	(µT)	(°)	(°)	(µT)	(°)	(°)	(10 ²² A/m)	(10 ²² A/m)	(µT)	(µT)	(µT)	(°)	(°)	(µT)	(°)	(°)	(10 ²² A/m)	(10 ²² A/m)	
54.9 ± 4.4	54.0	54.3	7.3	60.3	62.9	8.7	9.9	9.4	55.5 ± 4.3	54.4	52.4 ± 4.9	53.5	7.3	58.7	62.3	8.7	9.8	9.1	
$\alpha_{95} = 1.4$										$\alpha_{95} = 1.7$									
$k = 1255$										$k = 831$									
F_{ma}										F_{ma}									
(µT)										(µT)									
54.3										52.9									
54.8										54.1									
7.1										(54.8)									

PATH. Age of the structure: 1450-1600 A.D.

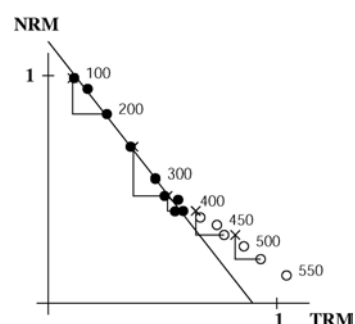
$H_{lab} = 50 \mu T$. Sample coordinates.



PATH1A
Without correction of anisotropy
 $NRM_0 = 2.35 \text{ A/m}$
 $F = 54.4 \mu T$
 $q = 22.9$

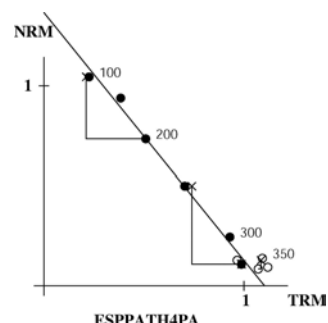


PATH1B
Without correction of anisotropy
 $NRM_0 = 2.33 \text{ A/m}$

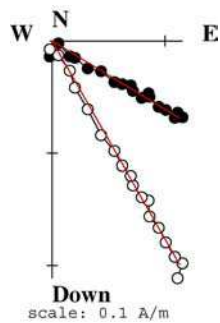


PATH3B
With correction of anisotropy
 $NRM_0 = 0.54 \text{ A/m}$
 $F = 64.3 \mu T$
 $q = 12.5$

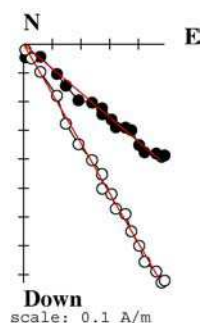
PATH3C
Without correction of anisotropy
 $NRM_0 = 0.14 \text{ A/m}$



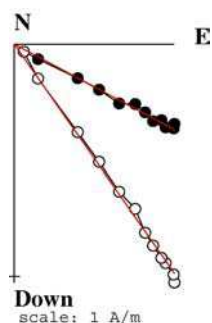
PATH4A
With correction of anisotropy
 $NRM_0 = 0.22 \text{ A/m}$
 $F = 62.0 \mu T$
 $q = 11.5$



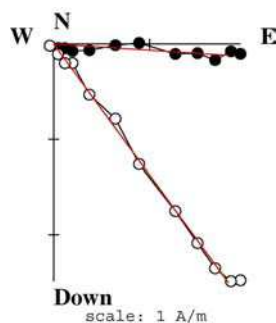
PATH5B
With correction of anisotropy
 $NRM_0 = 0.24 \text{ A/m}$
 $F = 54.7 \mu\text{T}$
 $q = 40.3$



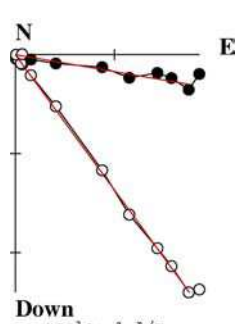
PATH6A
With correction of anisotropy
 $NRM_0 = 1.02 \text{ A/m}$
 $F = 51.6 \mu\text{T}$
 $q = 53.6$



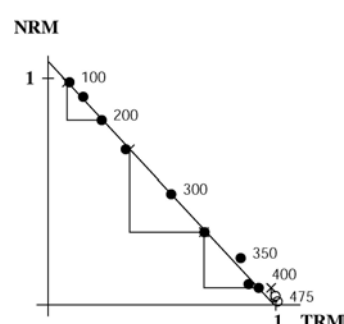
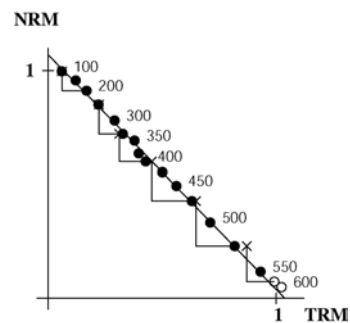
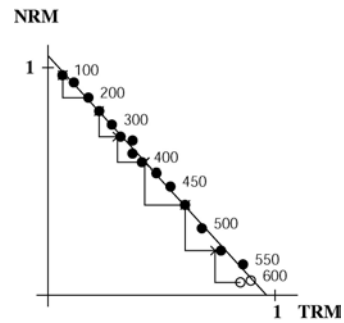
PATH6B
Without correction of anisotropy
 $NRM_0 = 1.28 \text{ A/m}$

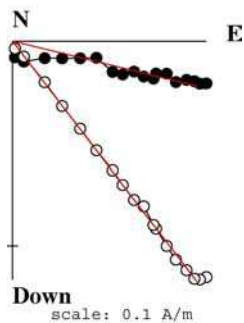


PATH7A
With correction of anisotropy
 $NRM_0 = 3.11 \text{ A/m}$
 $F = 54.2 \mu\text{T}$
 $q = 30.4$

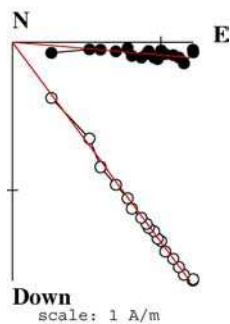


PATH7B
Without correction of anisotropy
 $NRM_0 = 3.02 \text{ A/m}$

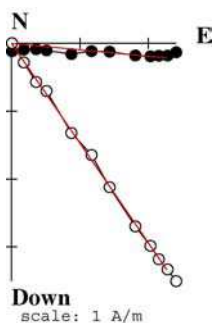




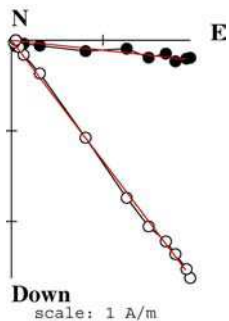
PATH8'A
With correction of anisotropy
 $NRM_0 = 0.16 \text{ A/m}$
 $F = 57.1 \text{ T}$
 $q = 59.5$



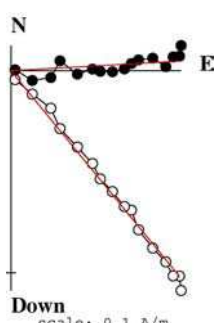
PATH9A
With correction of anisotropy
 $NRM_0 = 2.13 \text{ A/m}$
Rejected



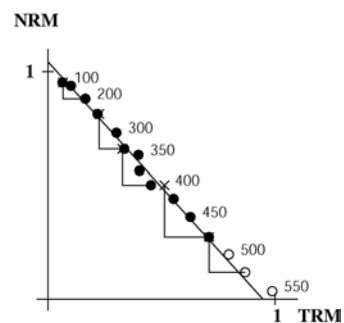
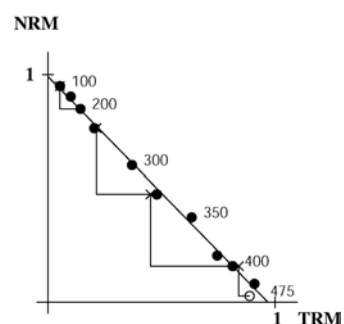
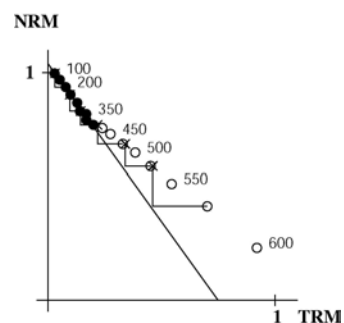
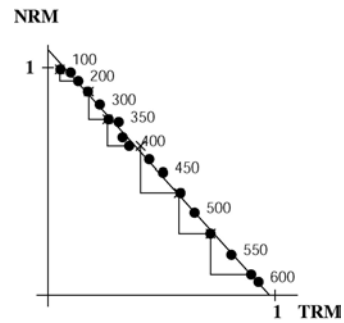
PATH10A
With correction of anisotropy
 $NRM_0 = 4.13 \text{ A/m}$
 $F = 51.2 \text{ T}$
 $q = 36.5$

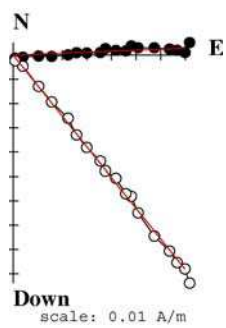


PATH10B
Without correction of anisotropy
 $NRM_0 = 3.23 \text{ A/m}$

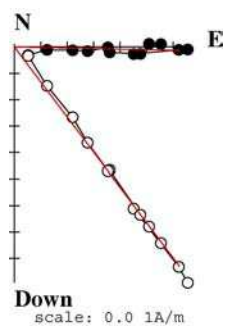
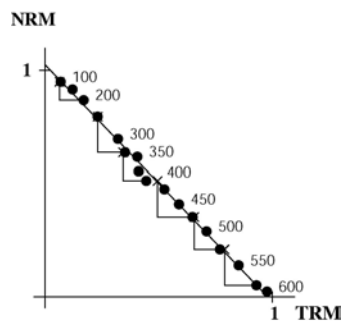


PATH11A
With correction of anisotropy
 $NRM_0 = 0.14 \text{ A/m}$
 $F = 55.5 \text{ T}$
 $q = 19.0$





PATH12A
With correction of anisotropy
 $NRM_0 = 0.12 \text{ A/m}$
 $F = 52.3 \text{ T}$
 $q = 50.3$



PATH12B
Without correction of anisotropy
 $NRM_0 = 0.15 \text{ A/m}$

PATA: 1450-1500 A.D.

Latitude = 39° 30' N Longitude = 0° 26' W

H_{lab} = 50.0 µT

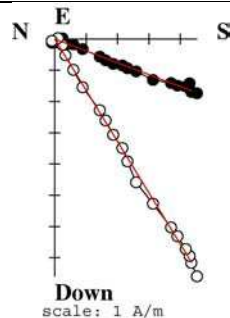
Spl	NRM (A/m)	χ (10 ⁻⁵)	Δχ (%)	Q _I	T _{min-T_{max}} (°C)	n	f	g	q	mad	dang	crm	anisotropy				T _{an} (°C)	dM _{an} (%)	k _{1/k₃} (%)	Direction of anisotropy axes				Cooling rate gain							
													no		yes		no		yes		k1		k2		k3		24 h		48 h		
													I	D	I _e	D _e	F ± σF	F _e (µT)	T _{an} (°C)	dM _{an} (%)	k _{1/k₃} (%)	I	D	I _e	D _e	I	D	ΔMz ₂₄ (%)	dz ₂₄ (%)	ΔMz ₄₈ (%)	dz ₄₈ (%)
50'-A	9.48	1683	-18.7	14.2	100-525	15	0.89	0.92	64.4	2.0	0.5	4.2	57.2	4.6	56.9	2.6	55.4 ± 0.8	55.1	325	-6.1	14	-58.2	38.4	31.8	41.1	1.2	-49.7	1.5	2.7		
50'-B	8.11	1544	-19.0	13.2	100-550	17	0.68	0.92	54.8	2.9	0.8	3.8	55.8	-4.0	59.3	-4.7	48.4 ± 0.5	45.5	475	-6.1	15	-18.1	11.3	-34.7	114.5	49.5	78.8	4.5	1.4		
51'-A	10.25	1381	-10.3	18.7	100-550	13	0.75	0.86	30.3	2.2	1.0	5.0	57.8	3.4	56.3	4.0	52.4 ± 1.2	53.6	325	-3.8	10	66.7	-32.8	-22.9	-21.5	4.1	66.7	-0.5	-3.6	broken	
52-A	5.75	1390	-20.6	10.4	100-450	12	0.66	0.88	28.0	3.7	2.0	6.9	59.4	6.4	58.0	3.1	50.0 ± 1.1	50.8	325	-4.6	19	-80.2	62.2	-9.0	217.5	7.0	128.1	0.9	1.3		
52-B	6.10	1474	-18.4	10.4	100-500	12	0.63	0.88	17.3	4.2	1.7	9.7	55.3	3.1	57.3	2.8	48.2 ± 1.4	45.2	325	-5.6	15	-35.9	25.7	41.3	76.3	28.1	-41.6	2.0	0.4		
53-A	3.39	1366	-23.6	6.2	100-425	12	0.66	0.88	28.0	3.7	2.0	6.9	59.4	6.4	58.0	3.1	50.0 ± 1.1	50.8	325	-4.6	19	-42.6	40.5	-41.6	185.2	18.6	112.6	0.0	2.3	Broken	
54-A	4.42	1770	-20.2	6.3	100-425	12	0.63	0.88	17.3	4.2	1.7	9.7	55.3	3.1	57.3	2.8	48.2 ± 1.4	45.2	325	-5.6	15	-28.8	-54.7	60.7	113.3	5.1	212.5	0.3	-2.0		
55-A	6.05	1905	-17.5	8.0	100-575	18	0.88	0.86	57.9	3.8	3.1	7.9	53.6	5.4	54.5	1.6	47.2 ± 0.6	45.2	325	-1.9	16	-45.6	-4.5	-33.0	47.0	26.1	115.4	0.3	-2.5		
56-A	3.30	1150	-17.6	7.2	100-450	11	0.83	0.81	38.6	2.4	0.4	4.2	57.8	12.1	56.8	11.7	55.5 ± 1.1	56.3	325	-1.3	5	-42.6	40.5	-41.6	185.2	18.6	112.6	0.0	2.3		
57-B	7.09	1702	-14.9	10.5	100-350	9	0.77	0.79	45.5	1.9	0.9	5.3	55.8	2.6	55.3	1.9	56.3 ± 0.8	57.7	325	-2.2	6	-42.6	40.5	-41.6	185.2	18.6	112.6	0.0	2.3		
57-C	7.49	1796	-11.5	10.5	100-500	12	0.66	0.88	28.0	3.7	2.0	6.9	59.4	6.4	58.0	3.1	50.0 ± 1.1	50.8	325	-4.6	19	-42.6	40.5	-41.6	185.2	18.6	112.6	0.0	2.3		
58-A	5.51	1025	-7.7	13.5	100-600	19	0.92	0.92	105.6	2.2	0.8	4.3	57.1	6.5	55.1	8.8	56.2 ± 0.5	56.4	475	-4.0	16	-64.7	-21.8	-21.9	126.4	12.0	41.4	8.0	-1.4	broken	
60'-B	3.80	1130	-23.7	8.5	100-550	11	0.46	0.88	13.0	3.6	2.3	6.9	56.8	4.1	57.6	5.6	49.0 ± 1.5	47.9	475	-1.2	9	-16.4	-35.0	-52.4	77.5	32.7	44.1	3.7	3.0		
60'-C	3.15	1110	-21.8	7.1	100-400	11	0.56	0.89	15.9	3.4	1.0	5.7	55.9	5.6	59.9	5.3	56.5 ± 2.0	52.4	475	-6.9	19	-7.5	-38.7	-22.8	54.5	65.9	34.3	10.9	-2.0		
61-A	2.89	1910	-4.3	3.8	100-450	13	0.56	0.89	15.9	3.4	1.0	5.7	55.9	5.6	59.9	5.3	56.5 ± 2.0	52.4	475	-6.9	19	-49.0	43.1	40.8	216.3	3.4	-50.8	10.3	-1.5		
62-A	3.31	769	-2.7	10.8	100-525	16	0.70	0.90	39.3	3.4	1.2	4.8	55.2	5.6	54.1	3.7	50.8 ± 0.8	51.8	475	-6.4	14	-42.6	40.5	-41.6	185.2	18.6	112.6	0.0	2.3		
62-B	3.90	812	-2.7	12.1	100-550	12	0.66	0.88	28.0	3.7	2.0	6.9	59.4	6.4	58.0	3.1	50.0 ± 1.1	50.8	475	-4.6	19	-42.6	40.5	-41.6	185.2	18.6	112.6	0.0	2.3		
64-B	1.72	819	-17.0	5.3	100-400	12	0.66	0.88	28.0	3.7	2.0	6.9	59.4	6.4	58.0	3.1	50.0 ± 1.1	50.8	475	-4.6	19	-42.6	40.5	-41.6	185.2	18.6	112.6	0.0	2.3		

Without anisotropy correction. 12 samples: 50'-A. 51'-A. 52-A. 53-A. 54-A. 55-A. 56-A. 57-B. 58-A. 60'-C. 61-A. 62-A								With anisotropy and cooling rate corrections. 10 samples: 50'-A. 51'-A. 52-A. 53-A. 54-A. 55-A. 56-A. 57-B. 58-A. 62-A											
F_m ± sd	F_{po}	I_{ms}	D_{ms}	F_{pa}	I_{pa}	D_{pa}	VDM	VADM	F_m ± sd	F_{po}	F_{pocr}	I_{ms}	D_{ms}	F_{pa}	I_{pa}	D_{pa}	VDM	VADM	
(µT)	(µT)	(°)	(°)	(µT)	(°)	(°)	(10 ²² A/m)	(10 ²² A/m)	(µT)	(µT)	(µT)	(°)	(°)	(µT)	(°)	(°)	(10 ²² A/m)	(10 ²² A/m)	
52.2 ± 3.6	52.9	56.5	4.6	58.7	64.6	5.6	9.5	9.2	51.8 ± 4.9	52.7	51.2 ± 5.3	56.4	3.6	56.9	64.6	4.3	9.2	8.9	
$\alpha_{95} = 1.4$	F_{ma}	I_{ma}	D_{ma}						$\alpha_{95} = 1.7$	F_{ma}	I_{ma}	D_{ma}							
k = 1024	(µT)	(°)	(°)						k = 790	(µT)	(°)	(°)							
	53.3	57.1	4.5							51.7	57.1	3.5							

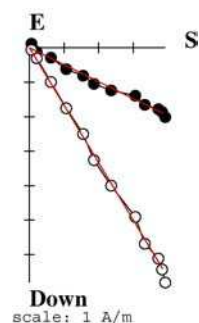
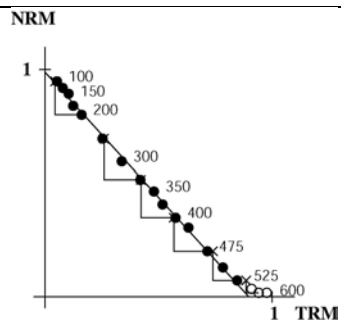
* Samples 60°C and 61-A rejected: Tmax<Tan

PATA. Age of the structure: 1450-1500 A.D.

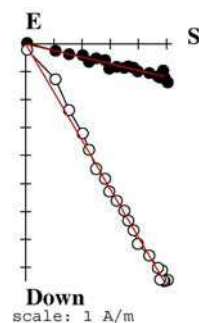
$H_{lab} = 50 \mu T$. Sample coordinates.



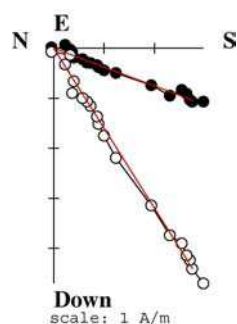
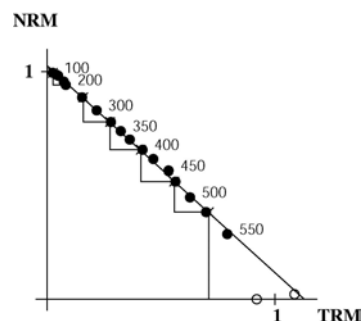
PATA50'A
With correction of anisotropy
 $NRM_0 = 9.48 \text{ A/m}$
 $F = 55.1 \mu T$
 $q = 64.4$



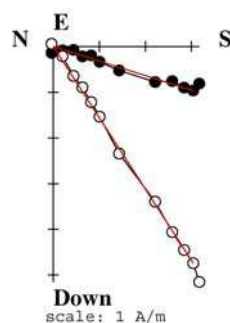
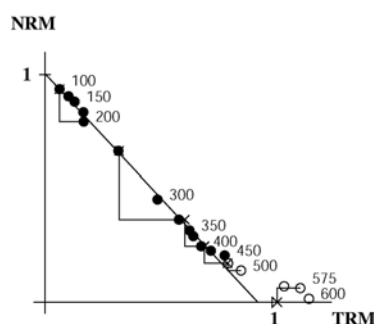
PATA50'B
With correction of anisotropy
 $NRM_0 = 8.11 \text{ A/m}$



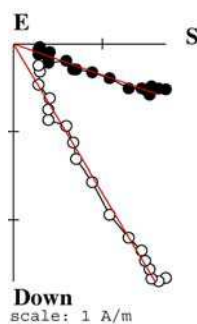
PATA51'A
With correction of anisotropy
 $NRM_0 = 10.25 \text{ A/m}$
 $F = 45.5 \mu T$
 $q = 54.8$



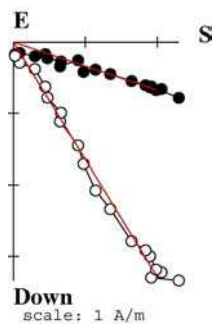
PATA52A
With correction of anisotropy
 $NRM_0 = 5.75 \text{ A/m}$
 $F = 53.6 \mu T$
 $q = 30.3$



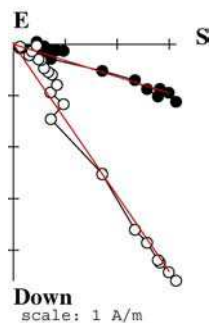
PATA52B
With correction of anisotropy
 $NRM_0 = 6.10 \text{ A/m}$



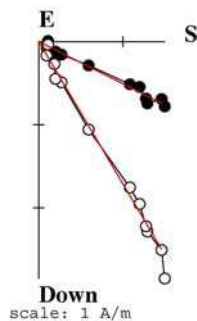
PATA53A
With correction of anisotropy
 $NRM_0 = 3.39 \text{ A/m}$
 $F = 50.8 \mu\text{T}$
 $q = 28.0$



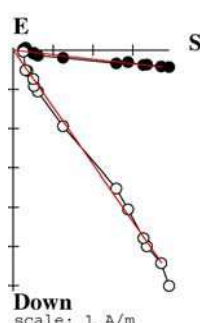
PATA54A
With correction of anisotropy
 $NRM_0 = 4.42 \text{ A/m}$
 $F = 45.2 \mu\text{T}$
 $q = 17.3$



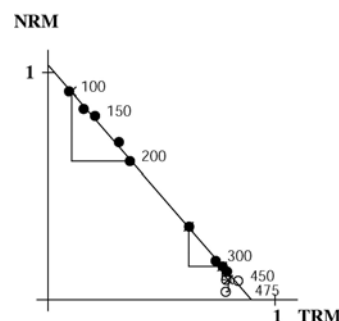
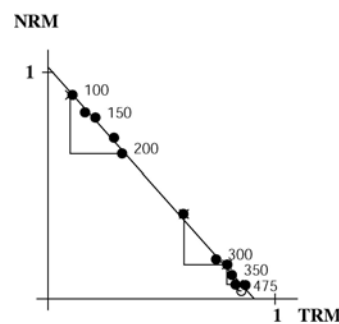
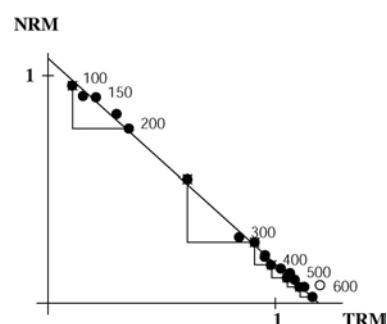
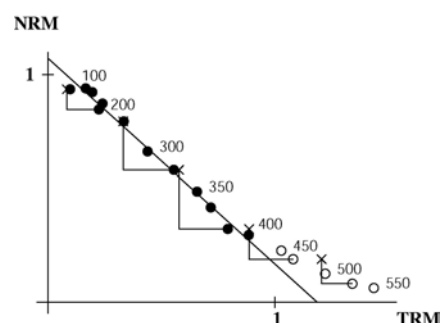
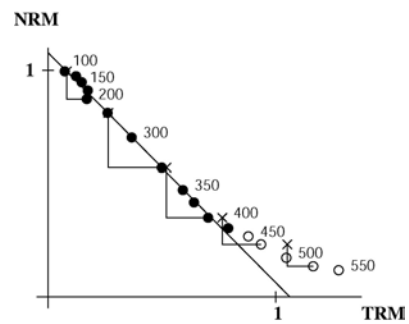
PATA55A
With correction of anisotropy
 $NRM_0 = 6.05 \text{ A/m}$
 $F = 45.2 \mu\text{T}$
 $q = 57.9$

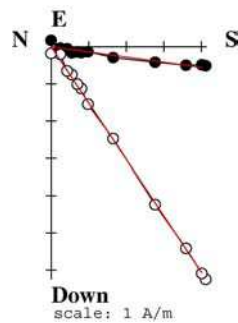


PATA56A
With correction of anisotropy
 $NRM_0 = 3.30 \text{ A/m}$
 $F = 56.3 \mu\text{T}$
 $q = 38.6$

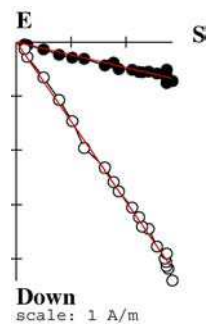


PATA57B
With correction of anisotropy
 $NRM_0 = 7.09 \text{ A/m}$
 $F = 57.7 \mu\text{T}$
 $q = 45.5$

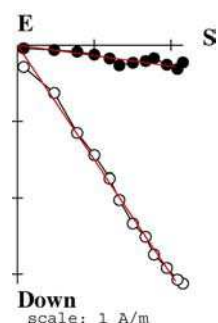
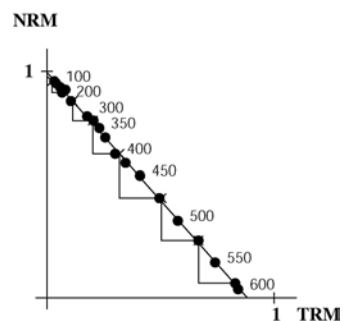




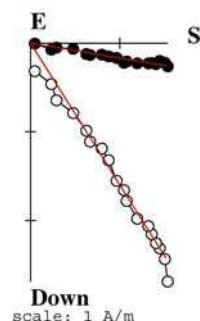
PATA57C
With correction of anisotropy
 $NRM_0 = 7.49 \text{ A/m}$



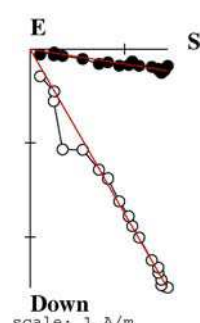
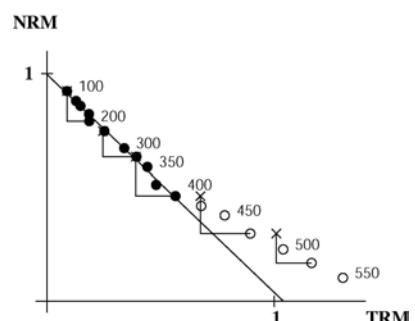
PATA58A
With correction of anisotropy
 $NRM_0 = 5.51 \text{ A/m}$
 $F = 56.4 \mu\text{T}$
 $q = 105.6$



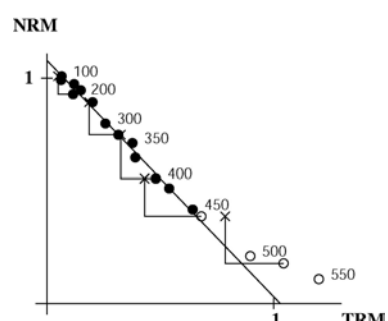
PATA60'B
With correction of anisotropy
 $NRM_0 = 3.80 \text{ A/m}$

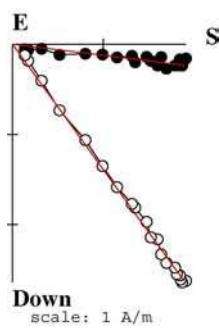


PATA60'C
Without correction of anisotropy
 $NRM_0 = 3.15 \text{ A/m}$
 $F = 49.0 \mu\text{T}$
 $q = 13.0$

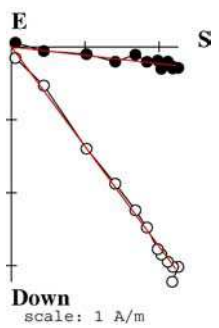


PATA61A
Without correction of anisotropy
 $NRM_0 = 2.89 \text{ A/m}$
 $F = 56.5 \mu\text{T}$
 $q = 15.9$

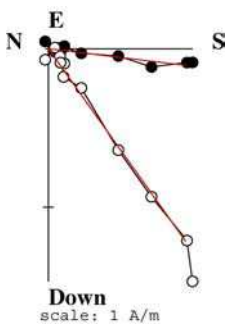




PATA62A
With correction of anisotropy
 $NRM_0 = 3.31 \text{ A/m}$
 $F = 50.8 \mu\text{T}$
 $q = 39.3$



PATA62B
With correction of anisotropy
 $NRM_0 = 3.90 \text{ A/m}$



PATA64B
With correction of anisotropy
 $NRM_0 = 1.72 \text{ A/m}$

FOUR ESPPATB: 1525-1650 A.D.

Latitude = 39° 30' N Longitude = 0° 26' W

Hlab = 50.0 µT

anisotropy

Direction of anisotropy axes

Cooling rate gain

no

yes

no

yes

k1

k2

k3

24 h

48 h

Spl	NRM (A/m)	χ (10^{-5})	$\Delta\chi$ (%)	Q _I	T _{min} -T _{max} (°C)	n	f	g	q	mad	dang	crm	I (°)	D (°)	I _e (°)	D _e (°)	F ± σF (µT)	F _e (µT)	T _{an} (°C)	dM _{an} (%)	k ₁ /k ₃ (%)	I (°)	D (°)	I (°)	D (°)	I (°)	D (°)	ΔMz ₂₄ (%)	dz ₂₄ (%)	ΔMz ₄₈ (%)	dz ₄₈ (%)
1-A	2.14	394	9.4	13.62	100-500	12	0.67	0.88	23.8	2.0	1.4	7.2	63.4	14.2	65.1	16.0	48.8 ± 1.2	47.9	500	-1.5	8	-6.4	27.1	5.6	116.5	81.5	-14.6	-0.6	0.0	-4.1	
2-A	1.94	451	-11.3	10.82	100-590	15	0.87	0.91	60.5	2.2	1.5	3.7	64.2	9.9	64.6	7.5	47.3 ± 0.6	47.6	500	-1.6	6	25.9	-9.4	-4.9	78.2	63.6	158.2	1.4	1.5	-4.2	
3-A	4.54	1308	-22.2	8.71	100-390	8	0.52	0.85	10.4	2.1	3.2	8.4	61.6	9.3	63.5	5.6	60.4 ± 3.1	59.0	390	-0.3	12	-7.3	36.4	-45.7	133.9	43.4	119.4	-0.1	-0.3		
4-A	4.74	932	-12.4	12.78	100-480	11	0.83	0.88	33.0	1.3	0.8	6.3	63.0	-0.5	64.3	2.4	50.6 ± 1.2	49.9	390	-1.7	8	-18.6	-32.2	0.6	57.6	71.4	-34.1	-4.0	0.0		
5-B	2.35	512	-14.5	11.54	100-530	13	0.86	0.91	31.8	4.3	1.2	11.5	59.3	7.0	62.0	7.1	48.3 ± 1.1	46.5	500	0.1	10	-17.9	31.4	-7.8	124.0	70.4	56.7	4.3	1.4	-0.3	
6-A	1.83	1035	-10.2	4.45	100-330	6	0.52	0.80	6.3	4.0	1.4	8.5	64.5	-4.7	66.0	-4.0	52.8 ± 3.7	52.3	330	0.9	12	9.0	31.8	23.7	125.8	64.4	-77.6	-3.0	-0.5	1.3	-1.3
7-A	4.53	520	-14.4	21.89	150-390	7	0.78	0.78	41.8	1.1	1.2	3.4	63.0	9.8	63.7	7.6	49.2 ± 0.7	49.2	390	-2.4	8	12.9	24.6	-39.1	103.9	48.0	129.3	-1.2	-3.3	-1.0	-6.3
8-A	4.09	894	-24.9	11.50	100-330	6	0.69	0.75	15.1	1.2	1.4	3.0	62.0	3.1	62.9	3.9	58.6 ± 2.3	58.4	330	1.1	7	13.0	37.6	16.0	131.4	69.2	-89.8	6.9	0.7	6.6	0.0
10-A	3.03	681	-15.6	11.19	100-330	6	0.55	0.69	9.7	4.6	6.5	22.9	61.1	8.4	62.3	0.7	55.8 ± 2.4	54.8	330	-2.2	15	-29.2	78.8	-20.2	180.7	53.2	120.3	4.6	-30.4		
11-A	4.97	968	-19.3	12.89	100-390	8	0.55	0.85	9.6	2.1	3.2	5.7	61.0	10.3	63.2	14.6	54.3 ± 2.9	51.6	390	-2.1	12	-32.6	7.9	3.0	96.0	57.2	1.4	5.4	0.1	-4.2	4.0
12-A	2.76	713	-20.9	9.72	100-480	11	0.78	0.89	23.9	2.8	1.5	5.6	64.9	1.8	65.7	0.4	53.2 ± 1.6	51.9	390	-5.8	10	-45.9	59.7	34.3	105.0	24.1	-2.8	-2.1	-26.4	broken	
14-A	4.45	904	-9.4	12.36	100-480	11	0.84	0.90	34.4	3.0	1.0	6.1	61.6	-0.8	62.9	2.2	50.0 ± 1.2	48.3	390	-5.2	12	-41.7	-5.4	-19.6	103.1	41.9	31.7	-1.6	-1.2	-0.7	1.8
20-A	3.06	1019	-16.9	7.53	100-330	6	0.74	0.79	12.0	2.9	1.3	8.0	62.3	7.5	60.9	3.1	58.1 ± 3.3	60.1	330	-5.3	17	1.4	69.3	-60.4	156.8	29.6	160.2	broken			

Without anisotropy correction. 12 samples:

1-A. 2-A. 3-A. 4-A. 5-B. 6-A. 7-A. 8-A. 11-A. 12-A. 14-A. 20-A

F _m ± sd (µT)	F _{po} (µT)	I _{ms} (°)	D _{ms} (°)	F _{pa} (µT)	I _{pa} (°)	D _{pa} (°)	VDM (10^{22} A/m)	VADM (10^{22} A/m)	F _m ± sd (µT)	F _{po} (µT)	F _{pocr} (µT)	I _{ms} (°)	D _{ms} (°)	F _{pa} (µT)	I _{pa} (°)	D _{pa} (°)	VDM (10^{22} A/m)	VADM (10^{22} A/m)
52.6 ± 4.4	51.2	62.7	5.6	56.1	69.8	6.4	8.5	8.9	51.9 ± 4.2	50.6	50.4 ± 4.0	63.8	5.6	55.1	70.7	6.4	8.2	8.8

$$\alpha = 1.6 \quad F_{ma} \quad I_{ma} \quad D_{ma}$$

$$k = 705 \quad (\mu T) \quad (°) \quad (°)$$

$$51.5 \quad 63.2 \quad 6.0$$

$$\alpha = 1.5$$

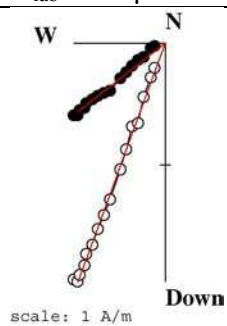
$$k = 798$$

$$(\mu T) \quad (°) \quad (°)$$

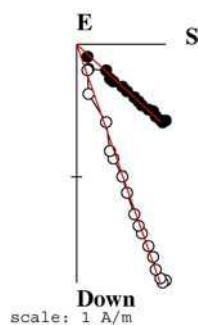
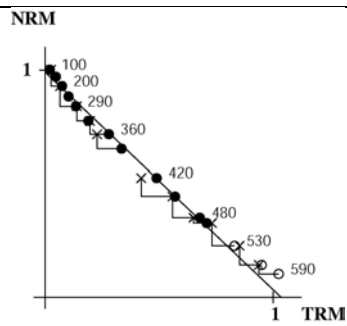
$$50.7 \quad 64.3 \quad 6.2$$

PATB. Age of the structure: 1525-1650 A.D.

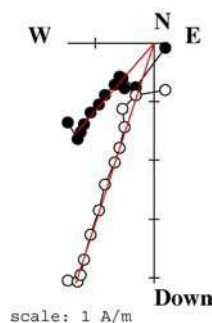
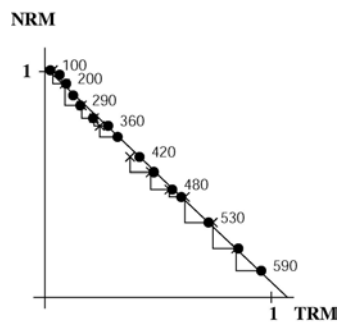
$H_{lab} = 50 \mu\text{T}$. Sample coordinates.



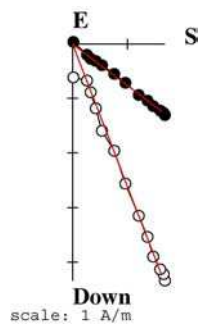
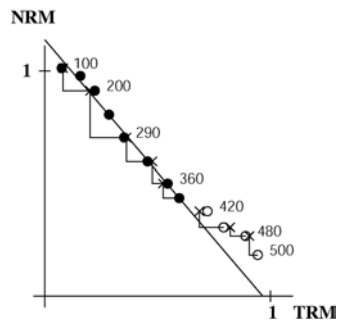
PATB1A
With correction of anisotropy
 $\text{NRM}_0 = 2.14 \text{ A/m}$
 $F = 47.9 \mu\text{T}$
 $q = 23.8$



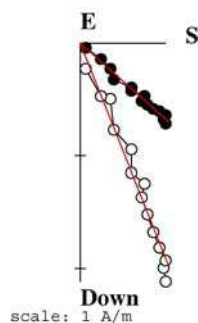
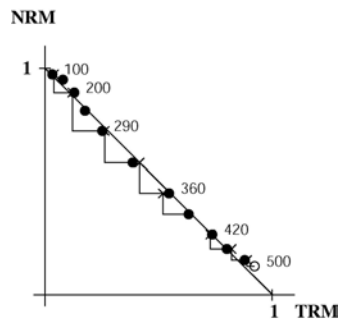
PATB2A
With correction of anisotropy
 $\text{NRM}_0 = 1.94 \text{ A/m}$
 $F = 47.6 \mu\text{T}$
 $q = 60.5$



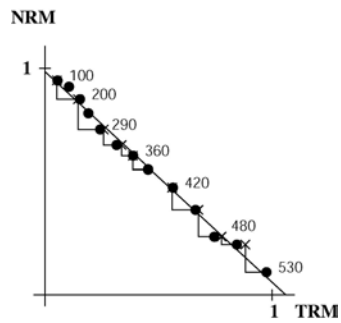
PATB3A
With correction of anisotropy
 $\text{NRM}_0 = 4.54 \text{ A/m}$
 $F = 59.0 \mu\text{T}$
 $q = 10.4$

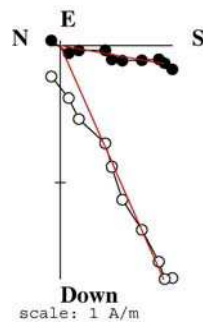


PATB4A
With correction of anisotropy
 $\text{NRM}_0 = 4.74 \text{ A/m}$
 $F = 49.9 \mu\text{T}$
 $q = 33.0$

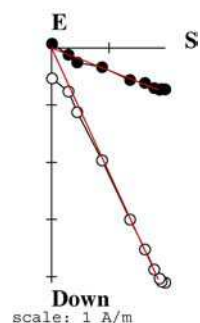


PATB5B
With correction of anisotropy
 $\text{NRM}_0 = 2.35 \text{ A/m}$
 $F = 46.5 \mu\text{T}$
 $q = 31.8$

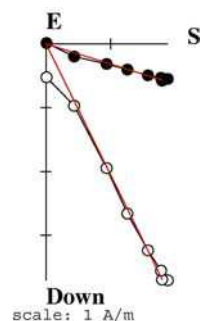




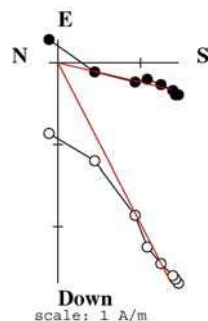
PATB6A
With correction of anisotropy
 $NRM_0 = 1.83 \text{ A/m}$
 $F = 52.3 \mu\text{T}$
 $q = 6.3$



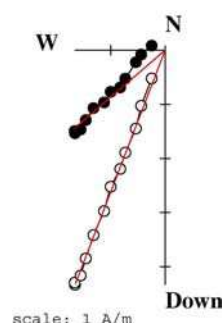
PATB7A
With correction of anisotropy
 $NRM_0 = 4.53 \text{ A/m}$
 $F = 49.2 \mu\text{T}$
 $q = 41.8$



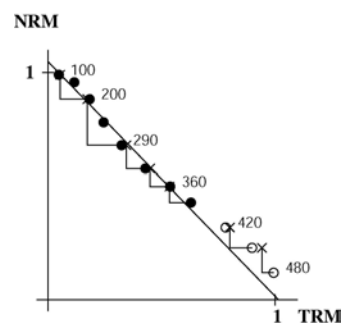
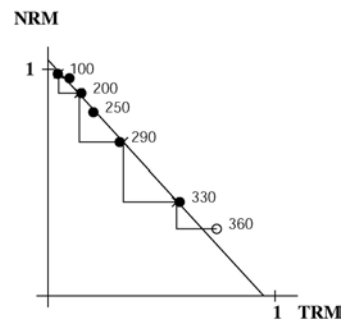
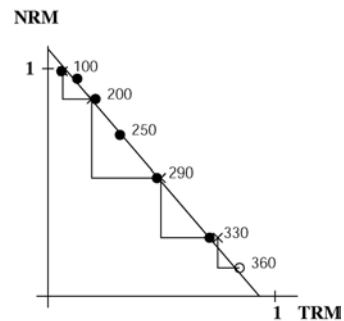
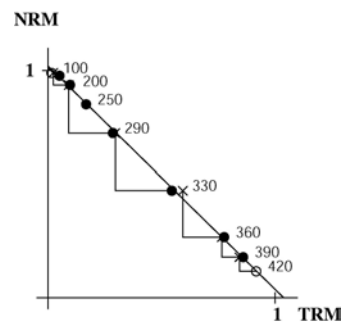
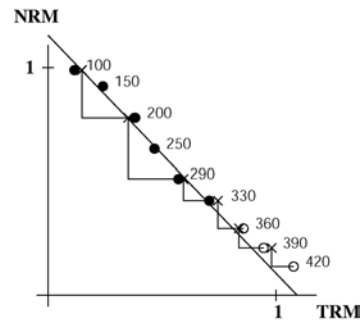
PATB8A
With correction of anisotropy
 $NRM_0 = 4.09 \text{ A/m}$
 $F = 58.4 \mu\text{T}$
 $q = 15.1$

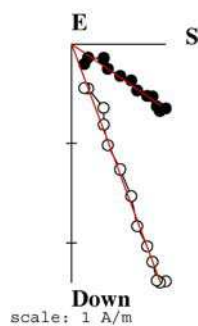


PATB10A
With correction of anisotropy
 $NRM_0 = 3.03 \text{ A/m}$
Rejected

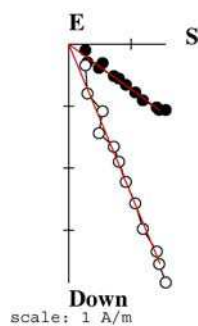


PATB11A
With correction of anisotropy
 $NRM_0 = 4.97 \text{ A/m}$
 $F = 51.6 \mu\text{T}$
 $q = 9.6$

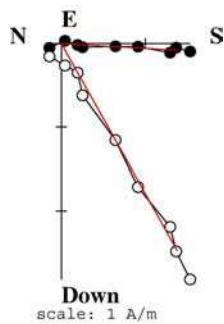




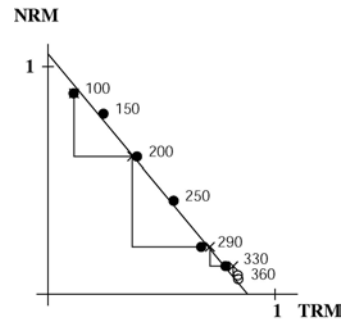
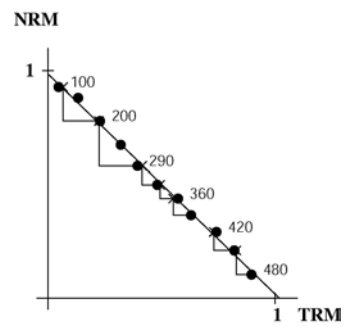
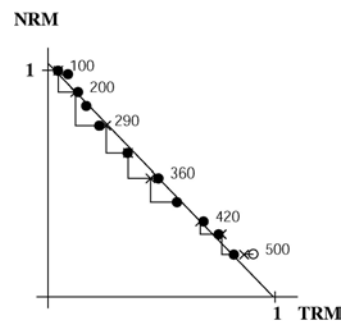
PATB12A
With correction of anisotropy
 $NRM_0 = 2.76 \text{ A/m}$
 $F = 51.9 \mu\text{T}$
 $q = 23.9$



PATB14A
With correction of anisotropy
 $NRM_0 = 4.45 \text{ A/m}$
 $F = 48.3 \mu\text{T}$
 $q = 34.4$



PATB20A
With correction of anisotropy
 $NRM_0 = 3.06 \text{ A/m}$
 $F = 60.1 \mu\text{T}$
 $q = 12.0$



PATJ: 1429-1611 A.D.

Latitude = 39° 30' N Longitude = 0° 26' W

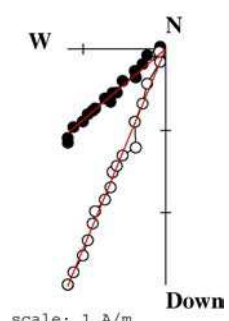
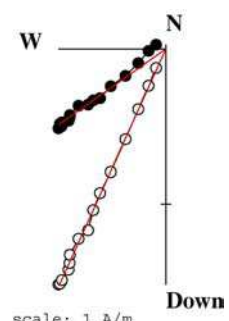
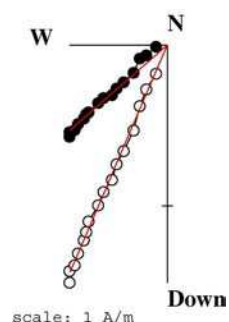
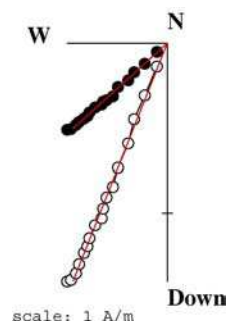
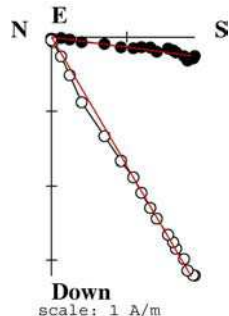
H_{lab} = 50.0 µT

Spl	NRM (A/m)	χ (10 ⁻⁵)	Δχ (%)	Q _I	T _{min-T_{max}} (°C)	n	f	g	q	mad	dang	crm	anisotropy				F _e (µT)	T _{an} (°C)	dM _{an} (%)	k _{1/k₃} (%)	Direction of anisotropy axes				Cooling rate gain						
													no		yes		no		yes		k1		k2		k3		24 h		48 h		
													I	D	I _e	D _e	F ± σF	(µT)	I	D	I	D	I	D	ΔMz ₂₄ (%)	dz ₂₄ (%)	ΔMz ₄₈ (%)	dz ₄₈ (%)			
40-A	3.57	654	-8.4	13.72	100-525	14	0.82	0.90	48.3	2.1	1.9	6.9	60.7	2.5	59.8	0.9	51.2 ± 0.8	52.8	500	-8.2	9	27.4	48.3	-31.6	119.8	45.8	170.6	3.4	3.7		
41-A	1.50	256	5.5	14.74	100-575	16	0.88	0.92	122.5	1.4	0.4	4.5	63.6	1.3	61.9	6.5	50.6 ± 0.4	52.6	500	-0.3	18	-24.6	-52.5	36.4	17.8	43.5	243.3	4.1	-3.4		
42-A	1.71	350	10.3	12.26	100-475	12	0.61	0.90	41.0	1.8	2.0	6.5	59.9	10.2	60.4	7.7	51.9 ± 0.7	50.9	450	-3.6	12	23.0	-48.2	-40.5	20.6	40.7	63.3	1.1	-0.3		
43-B	1.68	474	-11.4	8.90	100-500	13	0.70	0.88	33.2	2.2	1.2	7.1	58.3	10.4	61.1	13.8	61.6 ± 1.4	58.8	500	-1.8	15	-17.3	-44.4	-15.9	50.7	66.2	0.7	6.3	-2.2		
44-A	3.31	1070	-19.0	7.78	100-450	11	0.53	0.89	11.5	3.9	1.1	9.3	61.4	5.2	61.5	8.3	62.1 ± 3.2	61.9	450	-4.4	6	-27.9	-13.8	37.5	52.3	39.8	-77.5	5.4	0.1	5.9	0.0
45-B	1.91	584	-13.5	8.24	100-550	15	0.79	0.92	44.9	2.1	1.6	4.6	61.9	-1.5	60.9	5.7	53.4 ± 0.9	54.5	500	-0.2	18	-28.5	-46.4	34.8	21.5	41.9	252.8	3.9	-0.2		
46-A	2.50	880	-18.3	7.13	100-375	8	0.73	0.83	15.6	2.0	1.3	4.7	60.6	9.4	62.6	9.6	60.2 ± 2.8	58.3	300	3.7	15	-3.1	-54.4	-24.3	37.0	65.5	28.7	2.9	4.0		
47-B	0.79	192	-5.7	10.36	100-600	17	0.89	0.92	131.8	2.3	2.5	6.0	62.7	3.4	63.2	3.1	52.7 ± 0.4	52.5	500	0.4	6	12.3	-10.8	-24.4	73.6	62.3	103.8	3.4	-1.4		
48-A	4.35	613	-5.9	17.84	100-525	14	0.84	0.90	38.0	2.1	1.4	6.9	62.1	7.4	62.1	6.0	57.3 ± 1.3	56.9	450	-6.4	6	-57.0	71.0	-32.8	245.3	2.6	157.0	4.6	-0.7		
49-A	0.52	109	4.6	11.99	100-600	17	0.91	0.92	95.8	2.9	0.4	5.5	62.0	1.3	62.5	3.8	52.5 ± 0.5	52.7	500	-0.2	9	18.9	44.9	52.6	161.5	30.9	-57.0	4.4	-0.4		
50-A	4.03	707	-10.0	14.31	100-425	10	0.66	0.86	18.9	3.1	1.9	11.0	62.3	4.1	60.6	3.5	62.1 ± 2.3	62.3	400	-8.8	13	-76.3	53.4	4.0	127.0	13.1	36.1	3.7	-2.4		
51-A	0.73	291	-7.9	6.27	100-350	7	0.63	0.73	8.6	3.0	1.0	7.9	61.9	6.6	55.7	8.4	53.6 ± 2.9	56.6	350	-25.7	.31	-84.3	6.7	-4.3	145.4	3.7	55.7				
52-A	3.73	677	-8.6	13.85	100-550	15	0.85	0.91	73.1	2.1	0.7	6.1	61.7	3.6	62.9	5.5	59.5 ± 0.7	58.1	500	-3.1	6	-32.6	23.2	20.7	99.2	49.9	-17.5	8.4	-0.8		
53-B	3.98	1020	-7.1	9.81	100-525	14	0.74	0.92	27.4	2.2	1.3	7.4	63.2	10.9	64.7	7.3	53.9 ± 1.4	52.8	450	-5.5	11	-18.2	63.3	-59.8	187.7	23.2	145.2	5.0	0.0		
54-A	2.83	594	2.9	11.99	100-550	15	0.85	0.92	60.6	1.3	0.9	3.5	59.6	2.6	61.9	6.5	54.2 ± 0.8	52.6	450	-3.6	13	-15.0	-16.6	1.6	73.0	74.9	-23.0	3.8	-0.3		
55-'A	3.04	822	-9.1	9.28	100-475	12	0.60	0.90	14.9	4.2	1.4	7.2	62.9	6.4	64.9	1.5	52.5 ± 2.0	50.4	450	-2.9	14	31.5	-58.2	-16.0	21.6	53.8	88.6	6.0	0.0		
56-A	7.68	1274	-13.8	15.14	100-425	10	0.74	0.87	33.6	2.0	0.1	6.3	61.8	10.8	62.9	15.6	62.9 ± 1.4	60.6	350	-6.2	16	-52.5	19.2	13.7	90.7	34.1	-8.8	-2.9	-1.3		

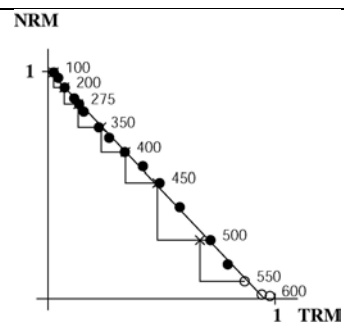
Without anisotropy correction. 16 samples:									With anisotropy and cooling rate corrections. 16 samples:									
$F_m \pm sd$	F_{po}	I_{ms}	D_{ms}	F_{pa}	I_{pa}	D_{pa}	VDM	VADM	$F_m \pm sd$	F_{po}	F_{pocr}	I_{ms}	D_{ms}	F_{pa}	I_{pa}	D_{pa}	VDM	VADM
(μT)	(μT)	($^\circ$)	($^\circ$)	(μT)	($^\circ$)	($^\circ$)	($10^{22} A/m$)	($10^{22} A/m$)	(μT)	(μT)	(μT)	($^\circ$)	($^\circ$)	(μT)	($^\circ$)	($^\circ$)	($10^{22} A/m$)	($10^{22} A/m$)
40-A. 41-A. 42-A. 43-B. 44-A. 45-B. 46-A. 47-B. 48-A. 49-A. 50-A. 52-A. 53-B. 54-A. 55'-A. 56-A									40-A. 41-A. 42-A. 43-B. 44-A. 45-B. 46-A. 47-B. 48-A. 49-A. 50-A. 52-A. 53-B. 54-A. 55'-A. 56-A									
56.2 \pm 4.5	54.9	61.6	5.5	60.4	68.9	6.4	9.2	9.5	55.5 \pm 4.0	54.5	52.4 \pm 4.2	62.2	6.6	57.6	69.3	7.6	8.7	9.1
$\alpha_{95} = 1.1$				F_{ma}	I_{ma}	D_{ma}					$\alpha_{95} = 1.1$	F_{ma}	I_{ma}	D_{ma}				
$k = 1175$				(μT)	($^\circ$)	($^\circ$)					$k = 1201$	(μT)	($^\circ$)	($^\circ$)				
				55.3	62.6	5.9						52.8	62.7	6.9				

PATJ. Age of the structure: 1429-1611 A.D.

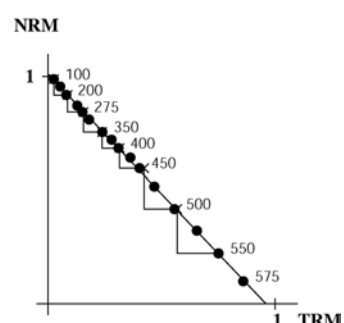
$H_{lab} = 50 \mu\text{T}$. Sample coordinates.



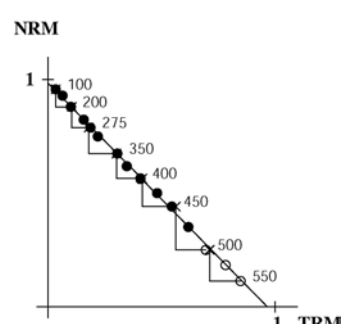
PATJ40A
With correction of anisotropy
 $\text{NRM}_0 = 3.57 \text{ A/m}$
 $F = 52.8 \mu\text{T}$
 $q = 48.3$



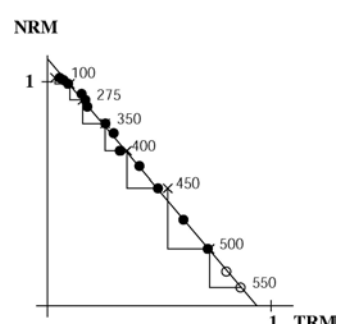
PATJ41A
With correction of anisotropy
 $\text{NRM}_0 = 1.50 \text{ A/m}$
 $F = 52.6 \mu\text{T}$
 $q = 122.5$



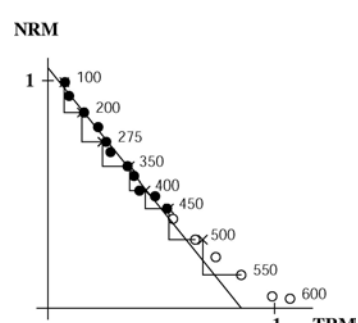
PATJ42A
With correction of anisotropy
 $\text{NRM}_0 = 1.71 \text{ A/m}$
 $F = 50.9 \mu\text{T}$
 $q = 41.0$

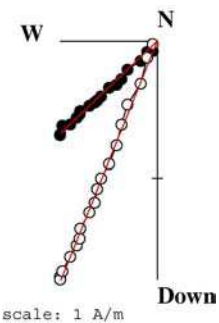


PATJ43B
With correction of anisotropy
 $\text{NRM}_0 = 1.68 \text{ A/m}$
 $F = 58.8 \mu\text{T}$
 $q = 33.2$

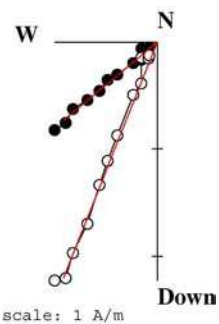


PATJ44A
With correction of anisotropy
 $\text{NRM}_0 = 3.31 \text{ A/m}$
 $F = 61.9 \mu\text{T}$
 $q = 11.5$

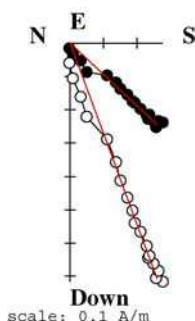




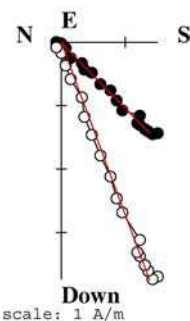
PATJ45B
With correction of anisotropy
 $NRM_0 = 1.91 \text{ A/m}$
 $F = 54.5 \mu\text{T}$
 $q = 44.9$



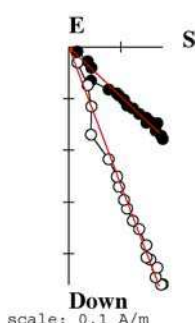
PATJ46A
With correction of anisotropy
 $NRM_0 = 2.50 \text{ A/m}$
 $F = 58.3 \mu\text{T}$
 $q = 15.6$



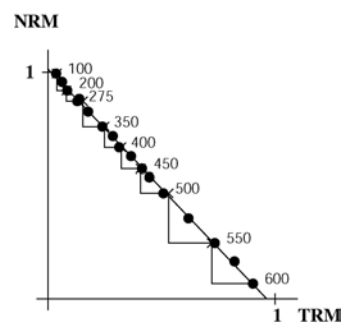
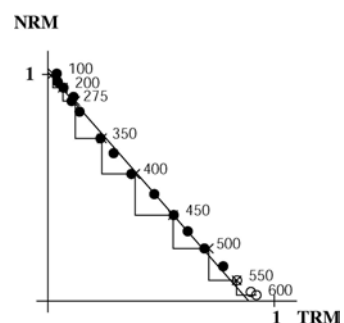
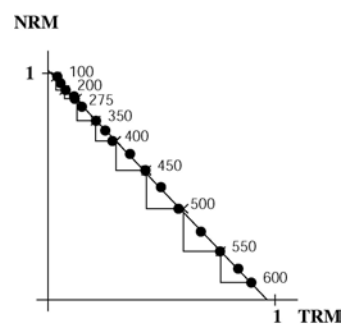
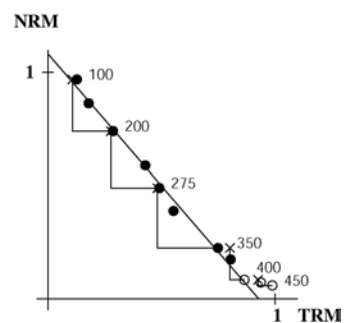
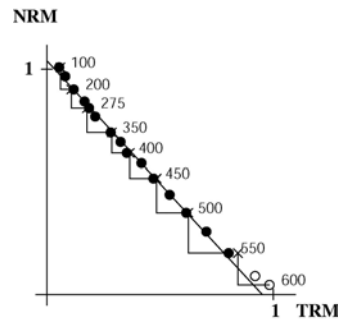
PATJ47B
With correction of anisotropy
 $NRM_0 = 0.79 \text{ A/m}$
 $F = 52.5 \mu\text{T}$
 $q = 131.8$

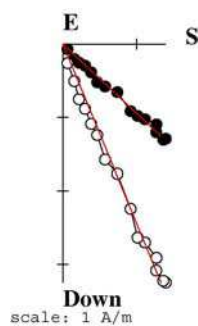


PATJ48A
With correction of anisotropy
 $NRM_0 = 4.35 \text{ A/m}$
 $F = 56.9 \mu\text{T}$
 $q = 38.0$

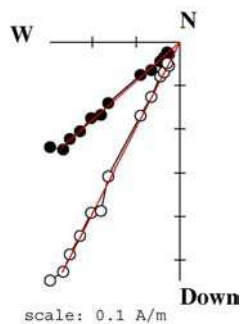


PATJ49A
With correction of anisotropy
 $NRM_0 = 0.52 \text{ A/m}$
 $F = 52.7 \mu\text{T}$
 $q = 95.8$

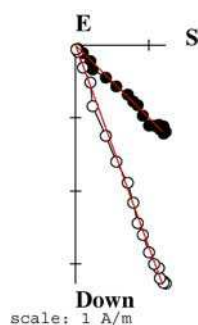




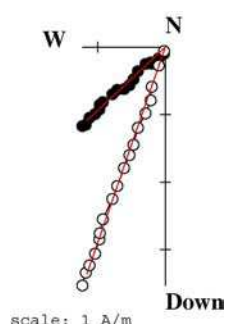
PATJ50A
With correction of anisotropy
 $NRM_0 = 4.03 \text{ A/m}$
 $F = 62.3 \mu\text{T}$
 $q = 18.9$



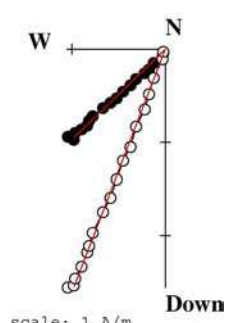
PATJ51A
With correction of anisotropy
 $NRM_0 = 0.73 \text{ A/m}$
 $F = 56.6 \mu\text{T}$
 $q = 8.6$



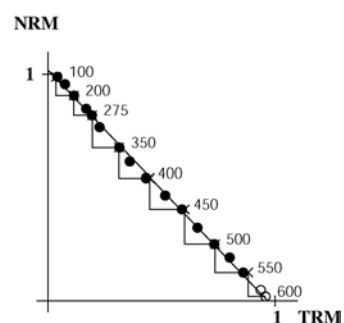
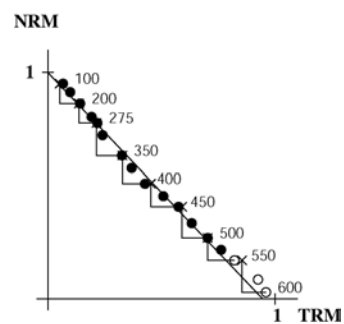
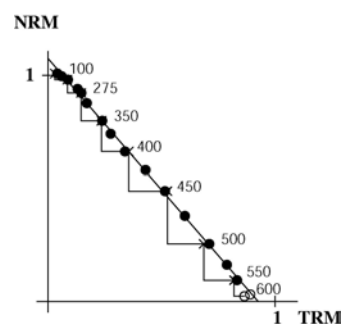
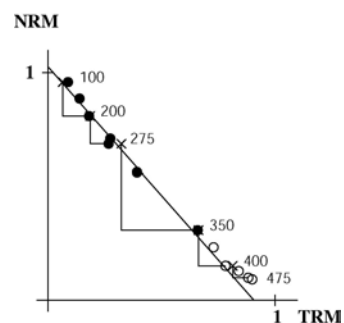
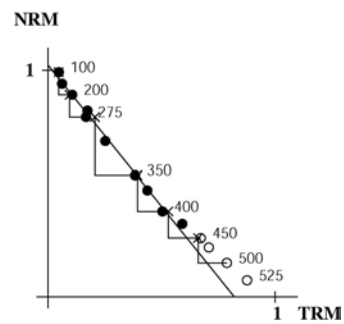
PATJ52A
With correction of anisotropy
 $NRM_0 = 3.73 \text{ A/m}$
 $F = 58.1 \mu\text{T}$
 $q = 73.1$

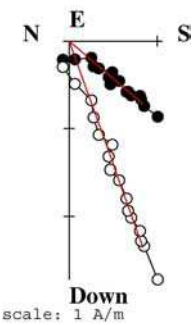


PATJ53B
With correction of anisotropy
 $NRM_0 = 3.98 \text{ A/m}$
 $F = 52.8 \mu\text{T}$
 $q = 27.4$

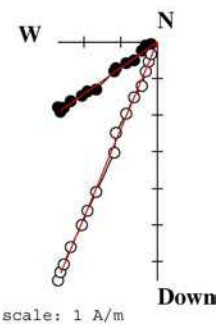


PATJ54A
With correction of anisotropy
 $NRM_0 = 2.83 \text{ A/m}$
 $F = 52.6 \mu\text{T}$
 $q = 60.6$

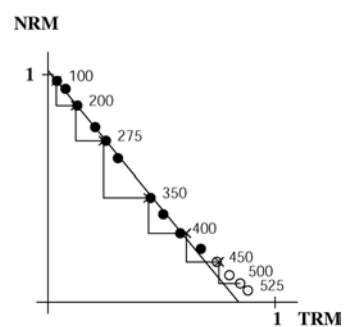
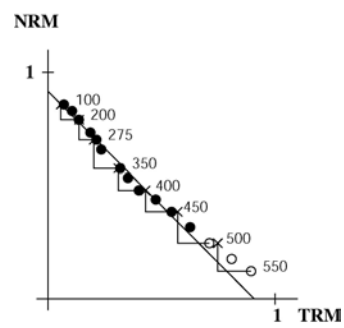




PATJ55'A
With correction of anisotropy
 $NRM_0 = 3.04 \text{ A/m}$
 $F = 50.4 \mu\text{T}$
 $q = 14.9$



PATJ56A
With correction of anisotropy
 $NRM_0 = 7.68 \text{ A/m}$
 $F = 60.6 \mu\text{T}$
 $q = 33.6$



VALL: 1575-1625 A.D.

Latitude = 39° 28' N Longitude = 0° 22' W

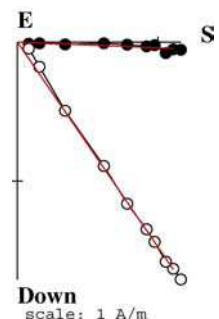
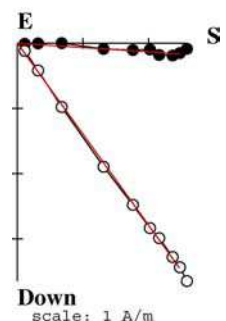
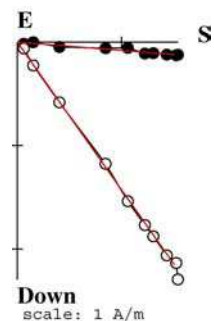
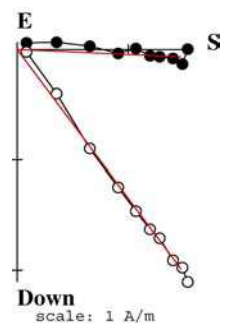
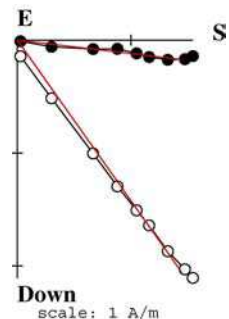
H_{lab} = 50.0 µT**anisotropy****Direction of anisotropy axes****Cooling rate gain****no yes no yes****k1 k2 k3****24 h 48 h**

Spl	NRM (A/m)	χ (10 ⁻⁵)	$\Delta\chi$ (%)	Q _l	T _{min} -T _{max} (°C)	n	f	g	q	mad	dang	crm	I (°)	D (°)	I _e (°)	D _e (°)	F ± σF (µT)	F _e (µT)	T _{an} (°C)	dM _{an} (%)	k ₁ /k ₃ (%)	I (°)	D (°)	I (°)	D (°)	I (°)	D (°)	ΔM _{24h} (%)	dz _{24h} (%)	ΔM _{48h} (%)	dz _{48h} (%)
1-A	2.63	456	-7.2	14.51	100-390	8	0.85	0.83	69.4	1.3	2.2	5.4	54.3	11.7	54.7	12.5	61.5 ± 0.8	60.9	360	-6.7	3	-21.3	-13.7	54.6	43.0	26.8	267.7	1.8	-2.8	7.1	-6.5
2-A	2.60	454	-17.4	14.38	100-420	9	0.91	0.83	26.8	2.3	3.0	5.3	54.3	7.9	53.5	8.5	54.5 ± 1.6	55.4	360	-3.3	4	58.7	65.7	-27.1	98.5	14.5	180.9	2.1	-0.9	4.0	-1.1
3-A	2.73	481	-13.1	14.28	100-420	9	0.90	0.82	46.2	1.2	0.1	2.7	54.8	8.9	54.9	10.8	59.3 ± 1.1	59.7	360	-4.9	6	9.3	-34.5	61.7	73.3	26.4	230.8	0.5	-2.5	1.5	-3.9
4-A	4.47	669	-13.0	16.79	100-420	9	0.90	0.83	74.0	1.2	0.4	2.0	53.1	9.6	54.3	10.4	57.3 ± 0.6	56.3	360	-3.1	5	-2.7	-18.8	-22.8	72.3	67.1	64.8	1.6	-2.8	2.2	-1.9
5-A	2.04	293	-9.2	17.52	100-420	9	0.90	0.83	88.0	1.5	1.1	4.6	54.9	7.4	55.8	9.2	58.7 ± 0.6	58.1	360	-3.8	6	-3.6	-38.0	23.8	50.4	65.9	240.0	4.6	-1.8	4.6	-3.1
7-A	1.45	272	-13.2	13.38	100-420	9	0.70	0.86	38.7	4.5	1.9	4.1	55.1	16.5	56.7	16.0	56.8 ± 1.0	55.2	360	-0.6	6	-13.7	17.2	-3.9	108.2	75.8	33.9	7.2	-1.5	8.3	-2.8
8-A	1.13	236	-8.9	11.99	100-390	8	0.86	0.84	47.8	1.0	3.8	8.8	61.1	10.9	61.9	9.5	48.3 ± 0.7	47.8	360	-0.2	5	19.2	-55.6	-20.7	26.9	61.2	73.6	1.8	-2.6	4.7	-1.6
12-A	2.89	791	5.2	9.19	rejected																										
14-A	2.87	503	-15.1	14.33	100-420	9	0.92	0.84	33.1	1.5	0.4	3.7	59.3	5.6	58.8	4.3	55.9 ± 1.5	57.2	360	-4.7	8	40.7	-16.4	-22.3	52.9	41.0	122.0	-1.3	-1.9	0.4	-2.1
16-A	3.65	852	-16.1	10.77	100-390	8	0.84	0.83	19.1	3.1	3.2	8.1	58.6	5.2	57.9	-1.8	53.3 ± 1.9	51.7	360	-3.9	31	-16.3	46.7	68.5	88.8	13.7	-39.3	4.4	-3.8	5.6	-4.0
17-A	2.70	1429	-21.8	4.75	100-390	8	0.73	0.83	18.2	2.8	1.7	6.4	56.4	10.7	56.6	10.6	50.7 ± 1.7	50.9	360	-1.3	2	24.6	6.8	-53.4	58.7	25.2	109.3	5.6	-5.0	7.4	-2.8
18-A	3.93	518	-12.9	19.07	100-390	8	0.89	0.79	50.6	2.1	3.0	5.0	59.4	9.4	56.9	9.1	55.6 ± 0.8	57.6	360	-16.2	16	85.1	-17.4	-4.8	-1.8	1.3	88.1	1.1	-6.6	2.7	-4.2
19-A	3.04	452	-11.1	16.91	100-360	7	0.78	0.72	24.1	1.7	0.4	1.5	58.1	11.4	55.3	10.5	51.7 ± 1.2	52.9	360	-24.4	20	-82.7	-21.5	4.5	30.6	5.7	-59.9	0.5	-6.6		

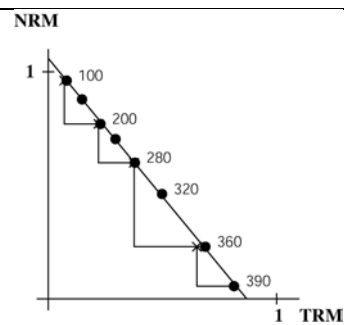
Without anisotropy correction. 12 samples:										With anisotropy and cooling rate corrections. 11 samples:									
1-A. 2-A. 3-A. 4-A. 5-A. 7-A. 8-A. 14-A. 16-A. 17-A. 18-A. 19-A										1-A. 2-A. 3-A. 4-A. 5-A. 7-A. 8-A. 14-A. 16-A. 17-A. 18-A.									
F _m ± sd	F _{po}	I _{ms}	D _{ms}	F _{pa}	I _{pa}	D _{pa}	VDM	VADM	F _m ± sd	F _{po}	F _{pocr}	I _{ms}	D _{ms}	F _{pa}	I _{pa}	D _{pa}	VDM	VADM	
(µT)	(µT)	(°)	(°)	(µT)	(°)	(°)	(10 ²² A/m)	(10 ²² A/m)	(µT)	(µT)	(µT)	(°)	(°)	(µT)	(°)	(°)	(10 ²² A/m)	(10 ²² A/m)	
55.3 ± 3.8	56.3	56.6	9.7	62.6	64.8	9.9	10.1	9.8	55.5 ± 4.0	56.4	55.4 ± 4.6	56.6	9.1	61.6	64.8	10.7	9.9	9.6	
$\alpha_{95} = 1.7$										$\alpha_{95} = 1.9$									
k = 697										k = 557									
$\frac{(µT)}{56.7}$										$\frac{(µT)}{55.8}$									
$\frac{(°)}{57.1}$										$\frac{(°)}{57.1}$									
$\frac{(°)}{9.6}$										$\frac{(°)}{9.0}$									

VALL. Age of the structure: 1575-1625 A.D.

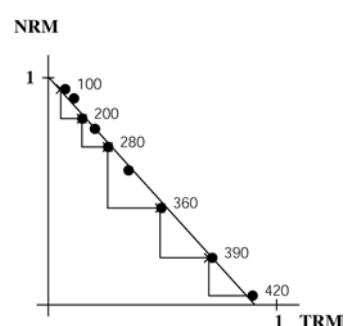
$H_{lab} = 50 \mu\text{T}$. Sample coordinates.



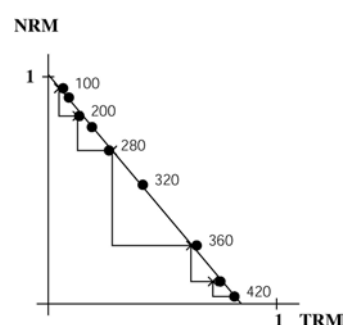
VALL1A
With correction of anisotropy
 $\text{NRM}_0 = 2.63 \text{ A/m}$
 $F = 60.9 \mu\text{T}$
 $q = 69.4$



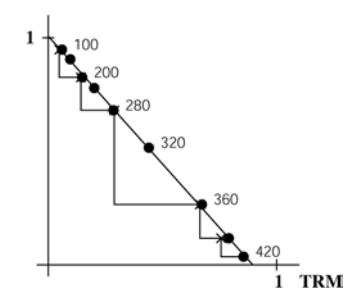
VALL2A
With correction of
anisotropy
 $\text{NRM}_0 = 2.60 \text{ A/m}$
 $F = 55.4 \mu\text{T}$
 $q = 26.8$



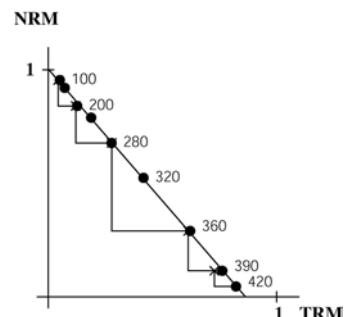
VALL3A
With correction of anisotropy
 $\text{NRM}_0 = 2.73 \text{ A/m}$
 $F = 59.7 \mu\text{T}$
 $q = 46.2$

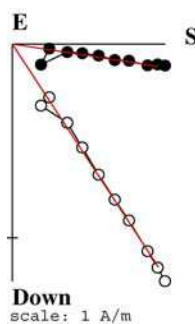


VALL4A
With correction of anisotropy
 $\text{NRM}_0 = 4.47 \text{ A/m}$
 $F = 56.3 \mu\text{T}$
 $q = 74.0$

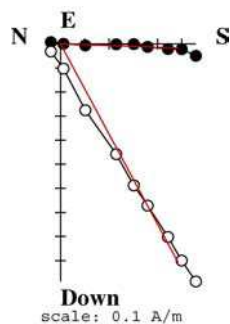


VALL5A
With correction of anisotropy
 $\text{NRM}_0 = 2.04 \text{ A/m}$
 $F = 58.1 \mu\text{T}$
 $q = 88.0$

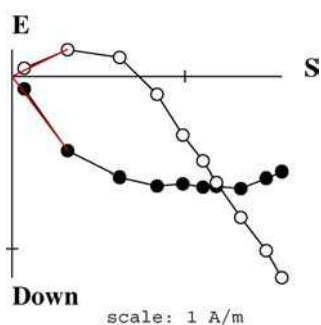




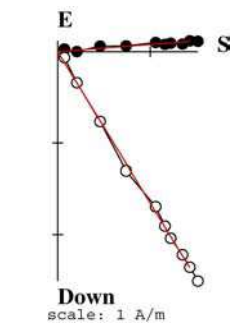
VALL7A
With correction of anisotropy
 $NRM_0 = 1.45 \text{ A/m}$
 $F = 55.2 \mu\text{T}$
 $q = 38.7$



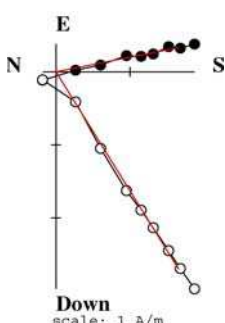
VALL8B
With correction of anisotropy
 $NRM_0 = 1.13 \text{ A/m}$
 $F = 47.8 \mu\text{T}$
 $q = 47.8$



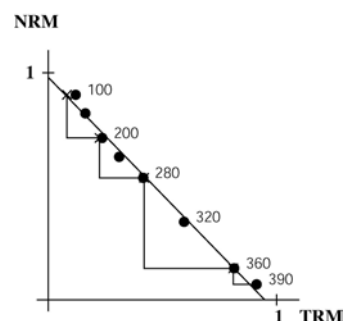
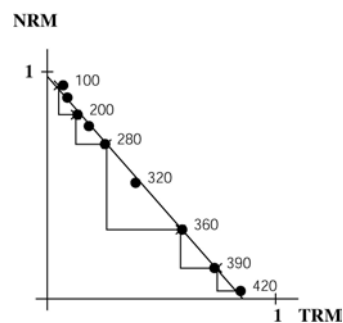
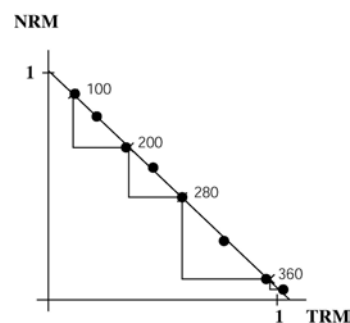
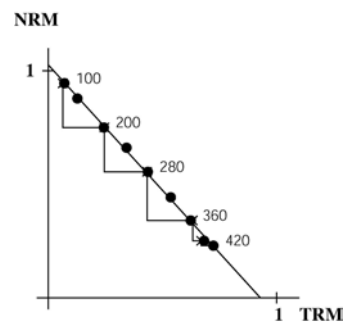
VALL12A
With correction of anisotropy
 $NRM_0 = 2.89 \text{ A/m}$
Rejected

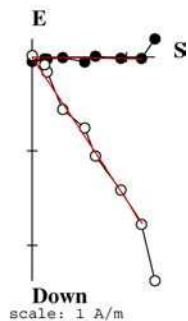


VALL14A
With correction of anisotropy
 $NRM_0 = 2.87 \text{ A/m}$
 $F = 57.2 \mu\text{T}$
 $q = 33.1$

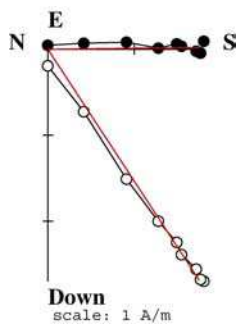


VALL16A
With correction of anisotropy
 $NRM_0 = 3.65 \text{ A/m}$
 $F = 51.7 \mu\text{T}$
 $q = 19.1$

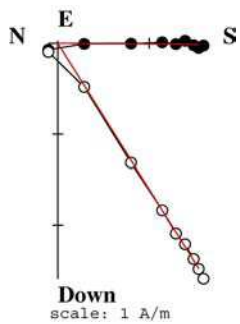




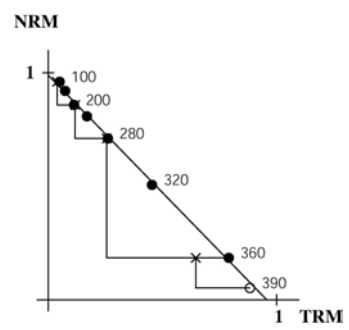
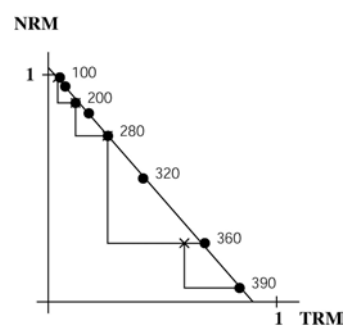
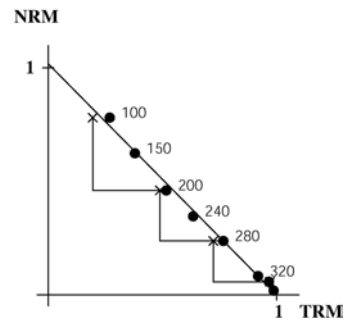
VALL17A
With correction of anisotropy
 $NRM_0 = 2.70 \text{ A/m}$
 $F = 50.9 \mu\text{T}$
 $q = 18.2$



VALL18A
With correction of anisotropy
 $NRM_0 = 3.93 \text{ A/m}$
 $F = 57.6 \mu\text{T}$
 $q = 50.6$



VALL19A
Without correction of anisotropy
 $NRM_0 = 3.04 \text{ A/m}$
 $F = 51.7 \mu\text{T}$
 $q = 24.1$



FOUR GUA2: 1825-1845 A.D.

Latitude = 40° 38' N Longitude = 3° 10' W

Hlab = 60.0 µT

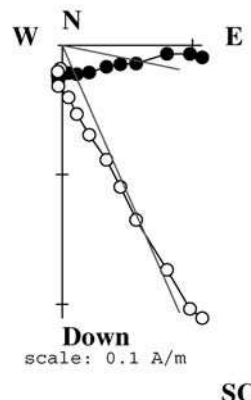
Spl	NRM (A/m)	χ (10 ⁻⁵)	Δχ (%)	Q _i	T _{min-T_{max}} (°C)	n	f	g	q	mad	dang (°)	crm (%)	anisotropy		T _{an} (°C)	dM _{an} (%)	k _{1/k₃} (%)	Direction of anisotropy axes				Cooling rate gain				
													no	yes				k1	k2	k3	24 h	48 h				
1-A	0.26	315	-3.5	2.1	100-400	8	0.70	0.84	65.4	1.4	11.7	5.9	47.4 ± 0.3	46.9	360	-0.2	12	1.2	39.1	-10.9	128.9	79.0	135.0	-0.8	-1.1	
2-A	3.99	1012	7.2	9.9	100-500	11	0.90	0.89	44.2	2.5	0.3	3.0	44.6 ± 0.6		440	4.2							2.6	-2.4		
3-A	0.23	283	-8.1	2.0	100-560	12	0.82	0.90	67.4	2.3	0.7	2.6	48.2 ± 0.4	44.3	440	1.5	11	-0.1	5.5	-5.7	95.5	84.4	94.1	4.1	3.3	
4-A	2.34	184	4.9	32.0	100-400	8	0.80	0.85	59.9	1.7	0.9	0.8	49.3 ± 0.4	46.7	360	-1.2	15	-19.4	16.6	-16.1	112.4	64.4	59.3	-4.3	1.0	
5-A	0.67	650	-6.0	2.6	100-400	8	0.44	0.85	20.8	2.2	6.6	16.8	49.1 ± 0.7	48.6	440	-2.0	8	-37.0	24.5	-40.7	154.9	27.5	91.4	6.9	3.4	
6-A	3.22	744	15.3	10.9	100-470	10	0.84	0.88	37.0	2.1	0.7	1.6	49.2 ± 0.7	45.6	360	3.1	26	9.0	9.1	-1.2	98.9	80.9	181.1	1.5	-1.7	
7-A	0.15	30	-13.3	12.6	100-600	15	0.85	0.91	116.7	1.9	1.6	4.5	53.7 ± 0.3	50.2	530	10.0	41	6.8	71.3	3.3	161.7	82.5	-82.4	3.7	-2.3	
7-B	0.17	31	-9.7	13.8	100-580	14	0.71	0.90	89.4	2.0	1.3	3.6	54.1 ± 0.3	50.2	530	20.5	38	1.2	38.0	4.8	128.1	85.1	-65.5	4.0	-2.5	
8-A	0.19	123	-12.2	3.9	100-530	12	0.79	0.88	67.0	3.0	1.3	1.5	53.8 ± 0.4	46.7	500	-8.0	16	6.6	-48.0	4.1	42.5	82.2	163.8	6.8	3.6	
9-A	7.59	659	10.6	28.9	100-400	8	0.83	0.83	68.2	0.9	0.5	1.3	49.9 ± 0.4	48.4	360	-1.7	13	-13.7	-22.4	-16.4	71.7	68.4	29.7	-2.3	0.8	

Without anisotropy correction. 7 samples:						With anisotropy and cooling rate corrections. 6 samples:									
2-A. 3-A. 4-A. 6-A. 7-A. 8-A. 9-A.			3-A. 4-A. 6-A. 7-A. 8-A. 9-A.			F _m ± sd		F _{po}		F _{pocr}		F _{pa}		VADM	
F _m ± sd	F _{po}	F _{pocr}	F _{pa}	VADM	(µT)	(µT)	(µT)	(µT)	(µT)	(µT)	(µT)	(µT)	(10 ²² A/m)		
49.8 ± 3.2	50.3	54.8		8.6		47.0 ± 2.1	47.4	46.8 ± 2.9		51.0		(51.7)			
			F _{ma}							F _{ma}					
			(µT)							(µT)					
			50.2							46.7		(47.3)			

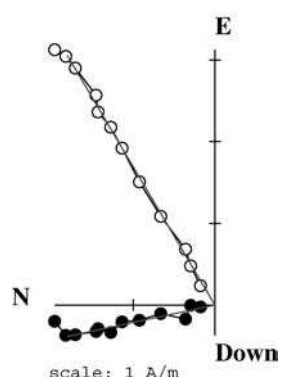
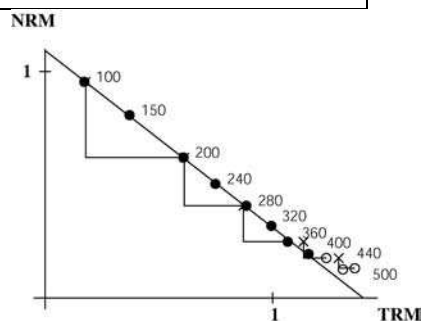
Rejected: 1A and 5A dang>10 and crm>15. 2A: bad correction of anisotropy

GUA2. Age of the structure: 1825-1845 A.D.

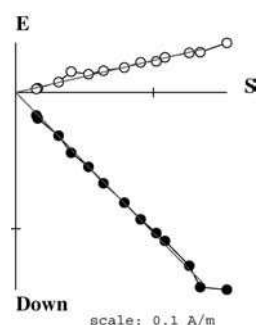
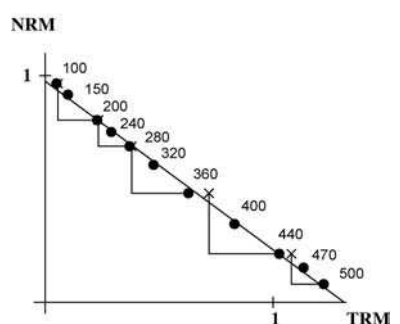
$F_{lab} = 60 \mu T$. Sample coordinates.



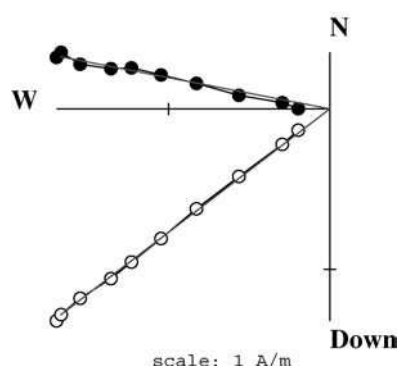
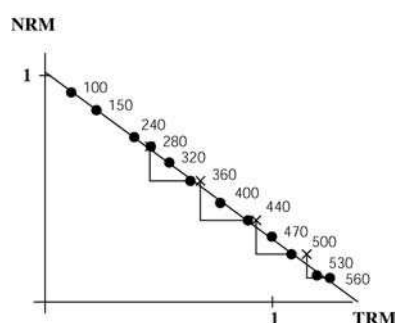
GUA2-1A
With correction of anisotropy
 $NRM_0 = 0.26 \text{ A/m}$
 $F = 46.9 \mu T$
 $q = 65.4$



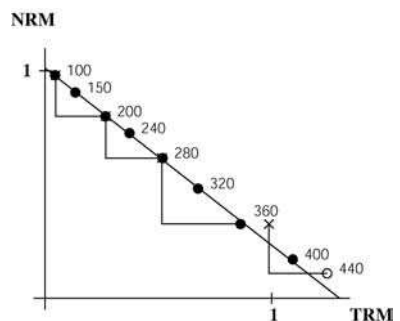
GUA2-2A
Without correction of anisotropy
 $NRM_0 = 3.99 \text{ A/m}$
 $F = 44.6 \mu T$
 $q = 44.2$

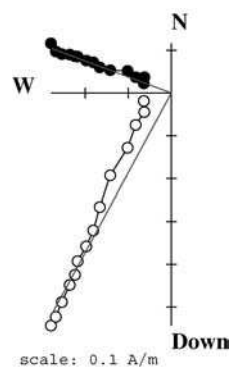


GUA2-3A
With correction of anisotropy
 $NRM_0 = 0.23 \text{ A/m}$
 $F = 44.3 \mu T$
 $q = 67.4$

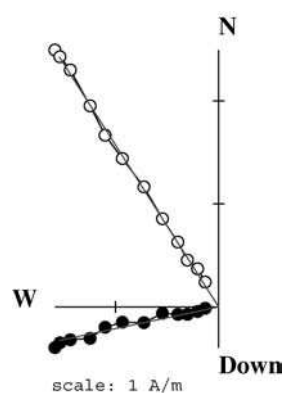
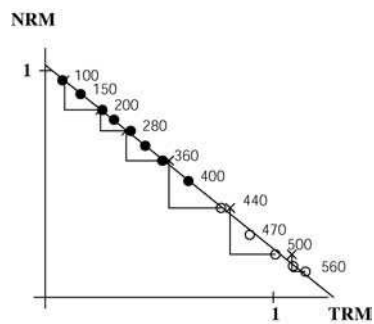


GUA2-4A
With correction of anisotropy
 $NRM_0 = 2.34 \text{ A/m}$
 $F = 46.7 \mu T$
 $q = 59.9$

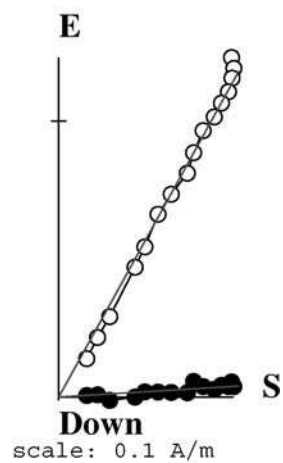
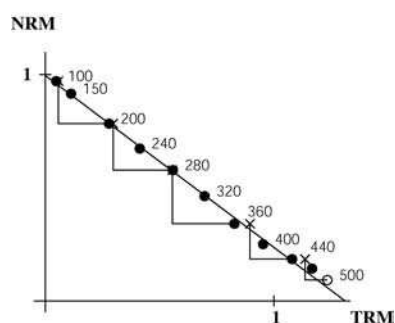




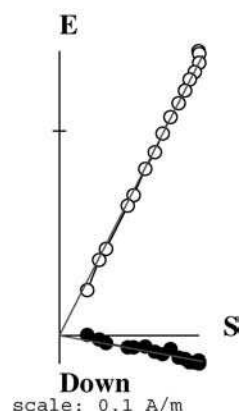
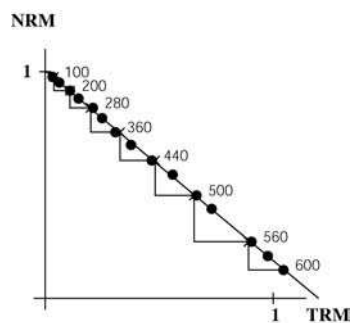
GUA2-5A
With correction of anisotropy
 $NRM_0 = 0.67 \text{ A/m}$
 $F = 48.6 \mu\text{T}$
 $q = 20.8$



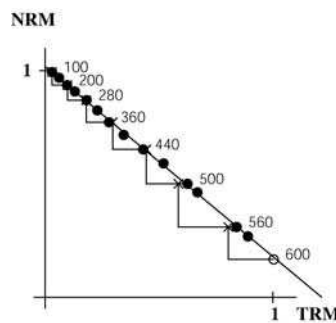
GUA2-6A
With correction of anisotropy
 $NRM_0 = 3.22 \text{ A/m}$
 $F = 45.6 \mu\text{T}$
 $q = 37.0$

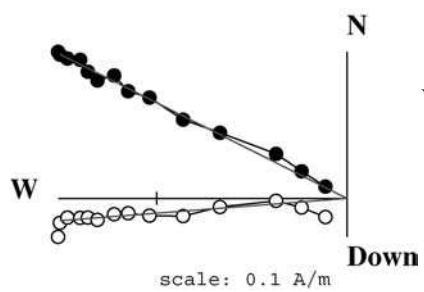


GUA2-7AA
With correction of anisotropy
 $NRM_0 = 0.15 \text{ A/m}$
 $F = 50.2 \mu\text{T}$
 $q = 116.7$

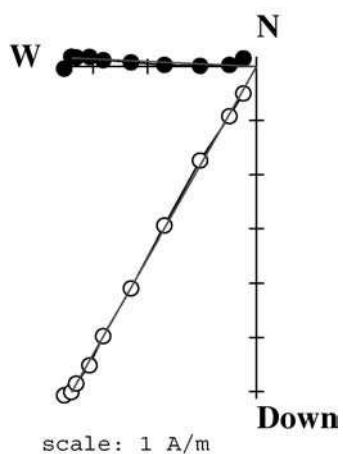
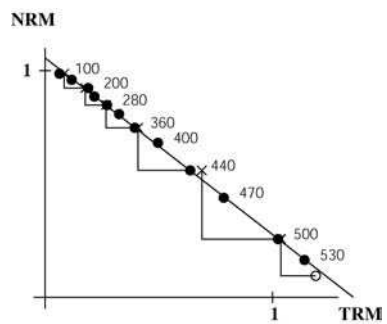


GUA2-7B
With correction of anisotropy
 $NRM_0 = 0.17 \text{ A/m}$
 $F = 50.2 \mu\text{T}$
 $q = 89.4$

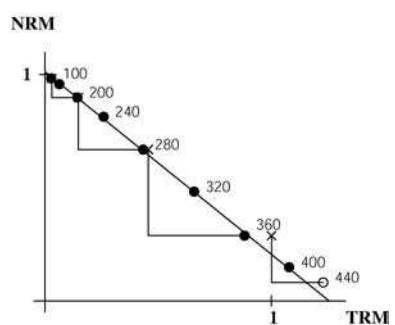




GUA2-8A
With correction of anisotropy
 $NRM_0 = 0.19 \text{ A/m}$
 $F = 46.7 \mu\text{T}$
 $q = 67.0$



GUA2-9A
With correction of anisotropy
 $NRM_0 = 7.59 \text{ A/m}$
 $F = 48.4 \mu\text{T}$
 $q = 68.2$



YUSTE: 1959 A.D.

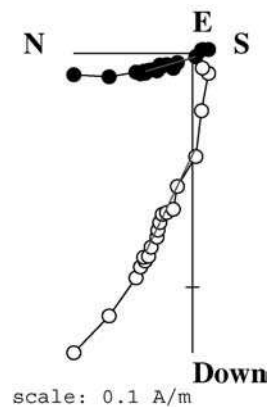
Latitude = 40° 6' N Longitude = 5° 42' W

 $H_{lab} = 60.0 \mu T$

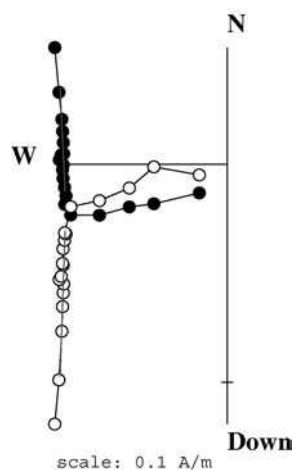
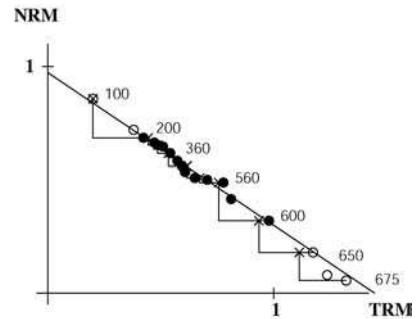
Spl	NRM (A/m)	χ (10^{-5})	$\Delta\chi$ (%)	Q _I	T _{min} -T _{max} (°C)	n	f	g	q	anisotropy		Direction of anisotropy axes						Cooling rate gain						
										no	yes	F _a (μT)	F _e (μT)	T _{an} (°C)	dM _{an} (%)	k ₁ /k ₃ (%)	I (°)	D (°)	I (°)	D (°)	I (°)	D (°)	ΔMz ₂₄ (%)	dz ₂₄ (%)
11A3	0.14	17	-5.9	20.7	100-580	14	0.62	0.85	12.8	43.3									10.3	0.6	18.6	7.4		
13A3	0.15	23	-8.7	16.4	100-580	14	0.99	0.86	27.7	43.2									12.9	0.0	21.2	-1.3		
23A1	0.8	86	-3.5	23.4	100-560	13	0.90	0.83	151.8	56.0	53.8	500	6.7	28	-8.3	-14.8	-55.2	87.3	33.6	69.6	-0.2	2.6	-1.4	-3.8
41A1	1.6	69	8.7	58.3	100-530	12	0.84	0.67	24.0	45.7	43.1	530	2.5	15	-1.9	40.8	-17.3	131.4	72.6	124.9	5.0	3.1	-0.7	-2.4
41A2	0.8	47	2.1	42.8	100-530	12	0.92	0.74	25.3	46.0	44.1	530	9.1	8	16.2	-38.5	4.9	53.0	73.0	159.2	5.3	3.6	0.4	-2.0
43A3	13	888	6.6	36.8	100-530	12	0.99	0.87	43.4	42.1	42.0	440	2.6	23	-17.9	-37.3	-34.0	65.3	50.4	29.8	2.3	1.2	1.8	-1.9

Mean Intensity: 48.69 ± 4.41 (all with and without correction of anisotropy). 47.43 ± 5.82 (after cooling rate correction. 24 h)Mean Intensity: 49.22 ± 4.83 (all EXCEPT 41A2 with and without correction of anisotropy). 48.05 ± 6.47 (after cooling rate correction. 24 h)

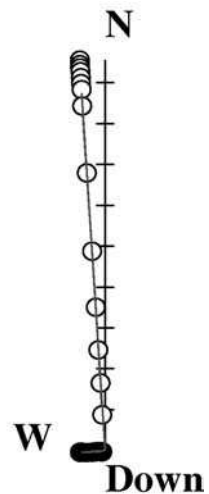
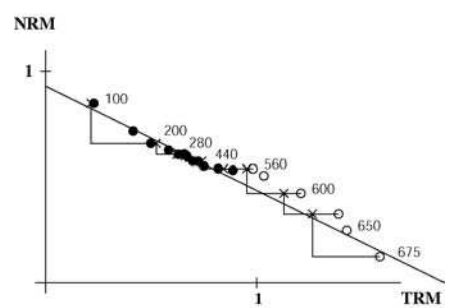
YUS2. Age of the structure: 1959 A.D.
 $F_{lab} = 60 \mu T$. Sample coordinates.



YUS2-11A3
 Without correction of anisotropy
 $NRM_0 = 0.14 \text{ A/m}$
 $F = 43.3 \mu T$
 $q = 12.8$

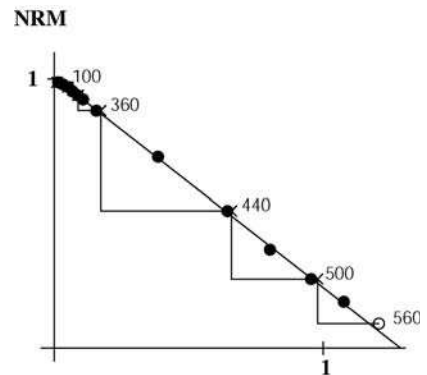


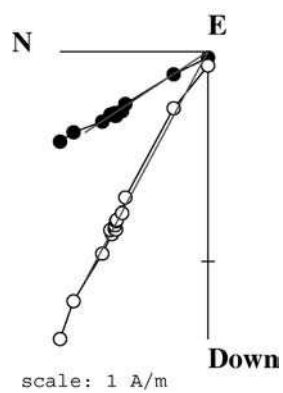
YUS2-13A3
 Without correction of anisotropy
 $NRM_0 = 0.15 \text{ A/m}$
 $F = 43.3 \mu T$
 $q = 27.7$



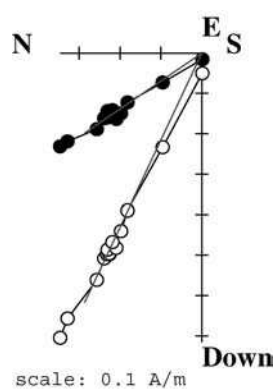
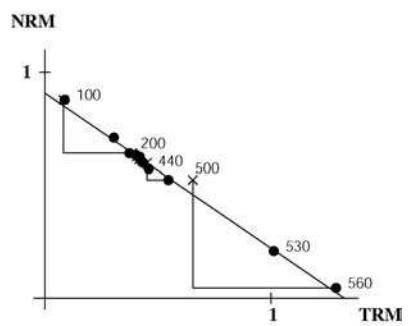
scale: 1 A/m

YUS2-23A1
 With correction of anisotropy
 $NRM_0 = 0.80 \text{ A/m}$
 $F = 151.8 \mu T$
 $q = 150$

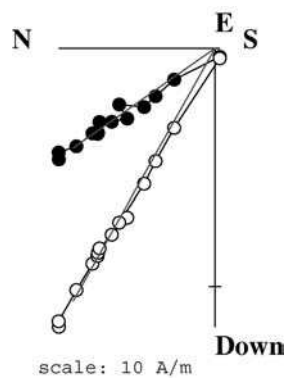
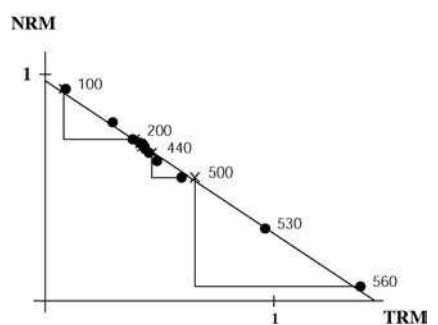




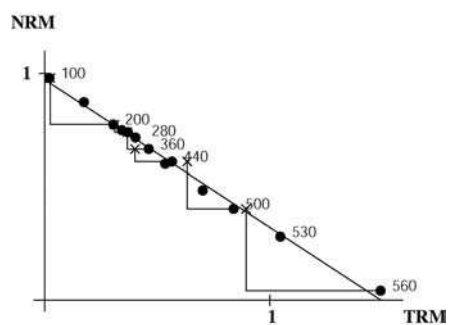
YUS2-41A1
With correction of anisotropy
 $NRM_0 = 1.60 \text{ A/m}$
 $F = 43.2 \mu\text{T}$
 $q = 24.0$



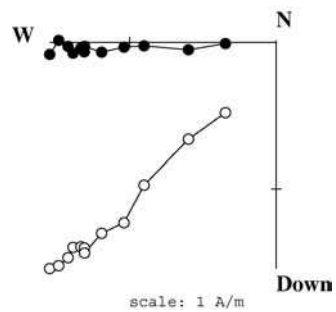
YUS2-41A2
With correction of anisotropy
 $NRM_0 = 0.80 \text{ A/m}$
 $F = 44.1 \mu\text{T}$
 $q = 25.3$



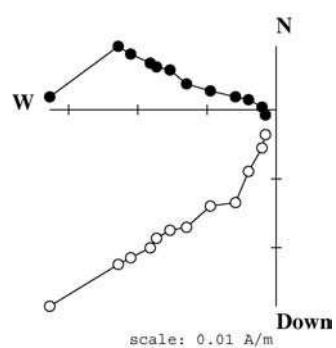
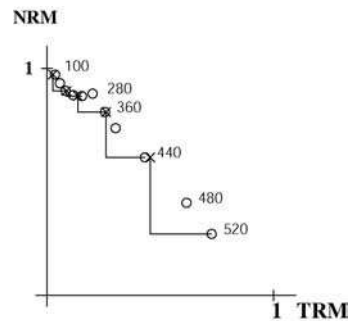
YUS2-43A3
With correction of anisotropy
 $NRM_0 = 13.0 \text{ A/m}$
 $F = 42.0 \mu\text{T}$
 $q = 43.4$



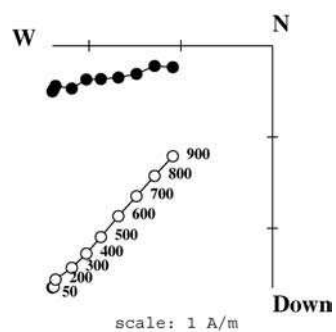
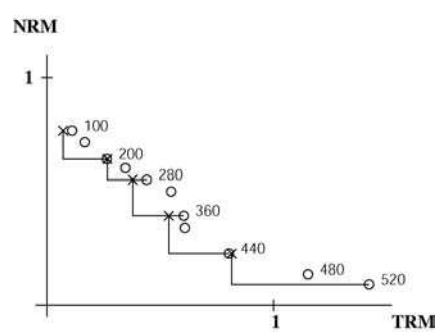
ESPCDAP. Age of the structure : 1010-1220 A.D.
 $F_{lab} = 60 \mu T$. Sample coordinates.



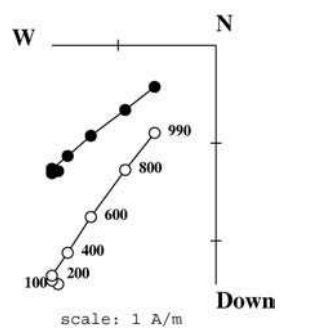
ESPCDAP04A
 Rejected
 $NRM_0 = 2.19 \text{ A/m}$



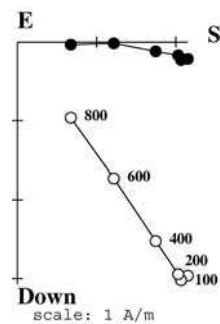
ESPCDAP5B
 Rejected
 $NRM_0 = 0.04 \text{ A/m}$



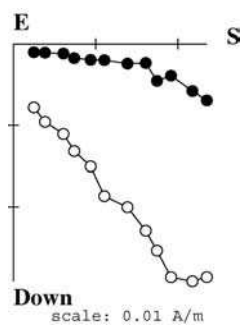
ESPCDAP6C
 AF demagnetization



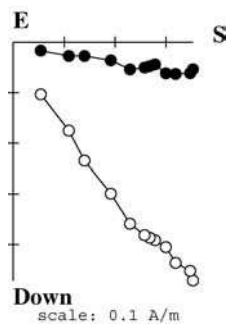
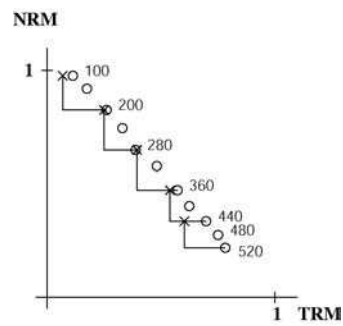
ESPCDAP07B
 AF demagnetization



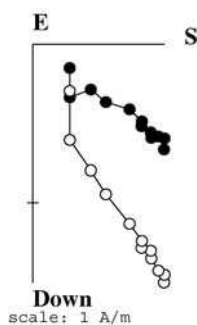
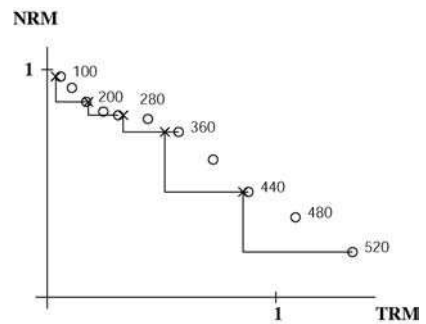
ESPCDAP8B
 AF demagnetization



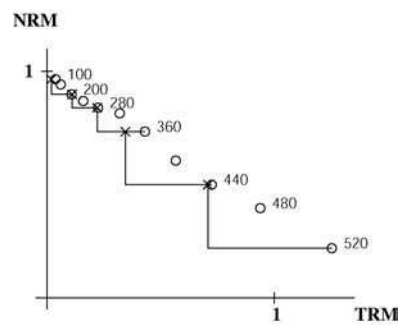
ESPCDAP9B
Rejected
 $NRM_0 = 0.04 \text{ A/m}$



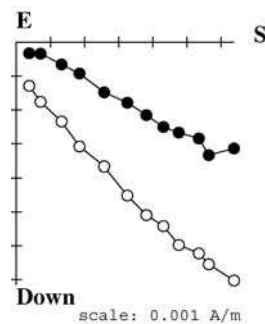
ESPCDAP10A
Rejected
 $NRM_0 = 0.59 \text{ A/m}$



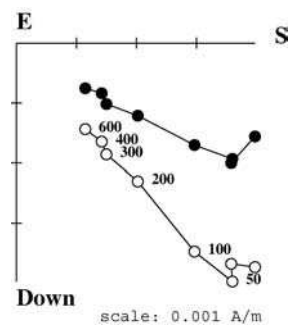
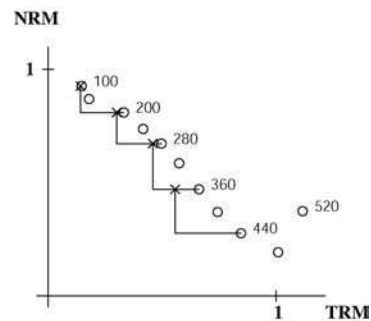
ESPCDAP11A
Rejected
 $NRM_0 = 1.84 \text{ A/m}$



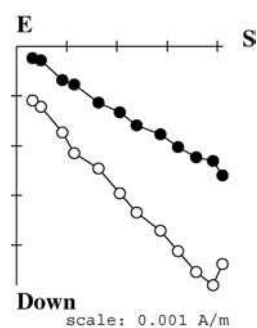
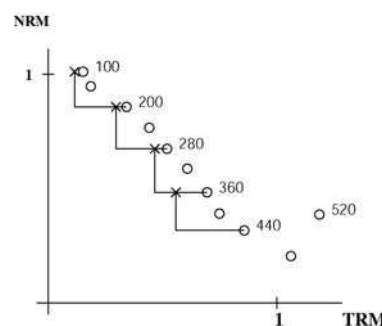
ESPCDAU. Age of the structure : 1029-1203 A.D.
 $F_{lab} = 60 \mu T$. Sample coordinates.



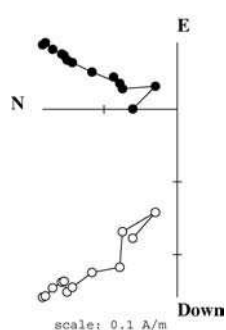
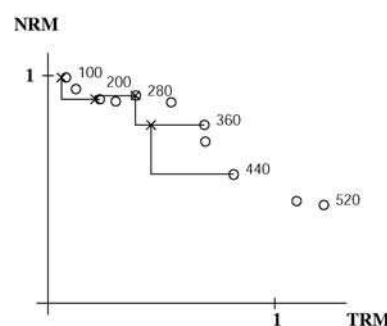
ESPCDAU01A
 Rejected
 $NRM_0 = 0.01 \text{ A/m}$



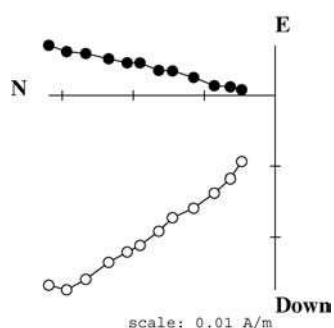
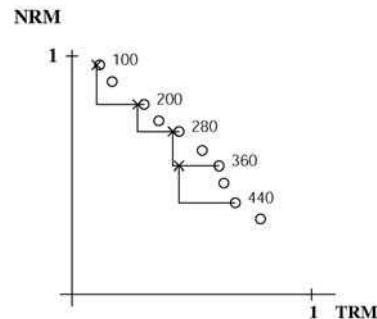
ESPCDAU02A
 AF demagnetization



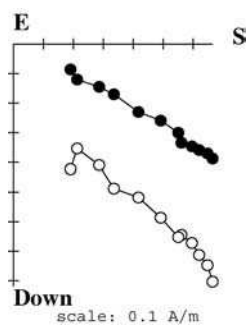
ESPCDAU3A
 Rejected
 $NRM_0 = 0.01 \text{ A/m}$



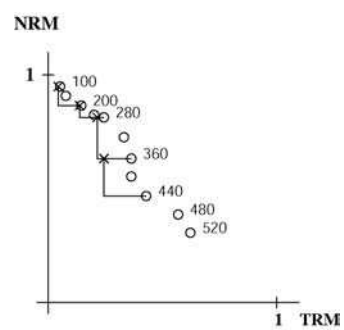
ESPCDAU4A
 Rejected
 $NRM_0 = 0.33 \text{ A/m}$



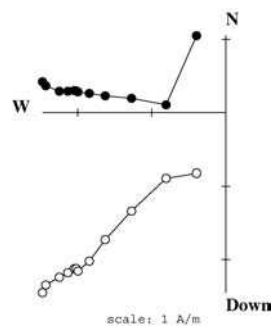
ESPCDAU10B
 Rejected
 $NRM_0 = 0.04 \text{ A/m}$



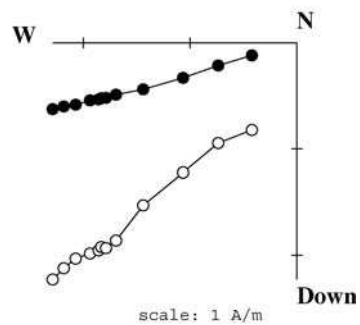
ESPCDAU12A
Rejected
 $NRM_0 = 1.11 \text{ A/m}$



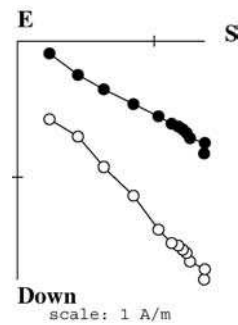
ESPCDAJ. Age of the structure : 1056-1262 A.D.
 $F_{lab} = 60 \mu T$. Sample coordinates.



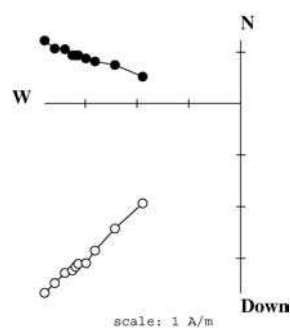
ESPCDAJ02A
 Rejected
 $NRM_0 = 3.51 \text{ A/m}$



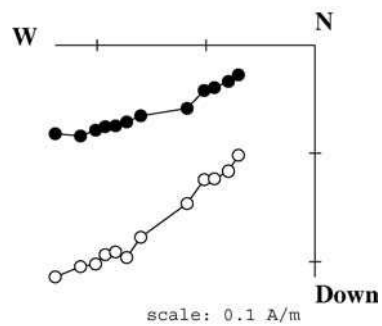
ESPCDAJ05A
 Rejected
 $NRM_0 = 3.25 \text{ A/m}$



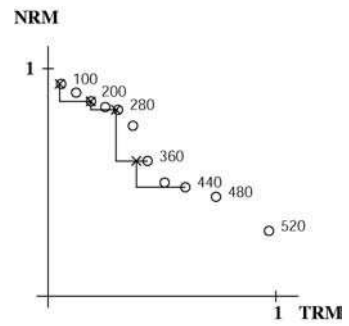
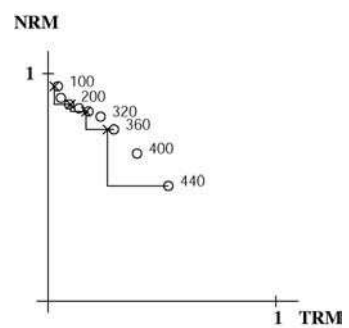
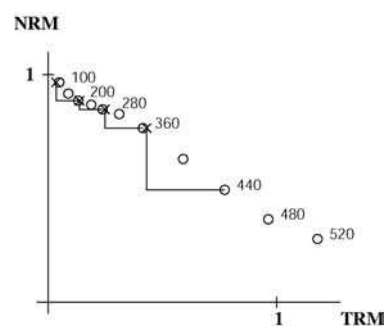
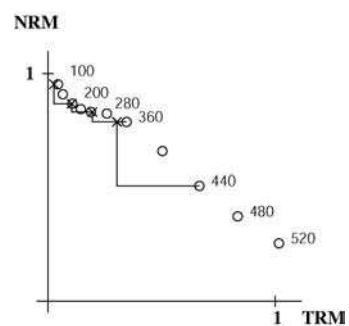
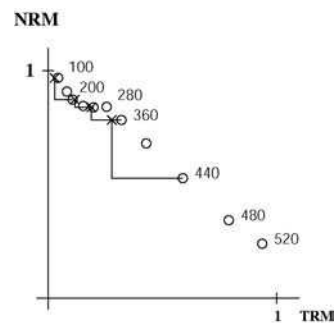
ESPCDAJ07A
 Rejected
 $NRM_0 = 2.37 \text{ A/m}$

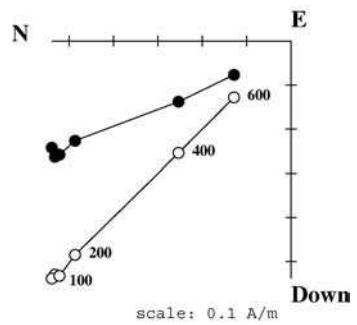


ESPCDAJ08A
 Rejected
 $NRM_0 = 5.42 \text{ A/m}$

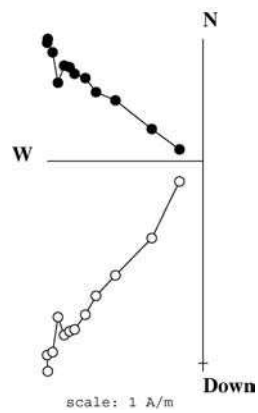


ESPCDAJ09A
 Rejected
 $NRM_0 = 0.33 \text{ A/m}$

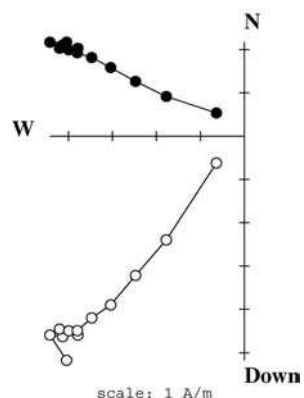
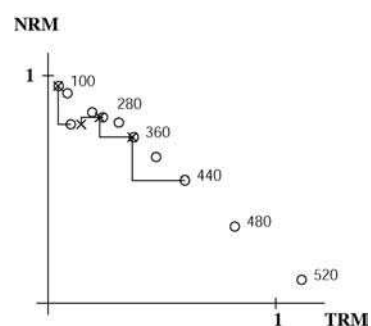




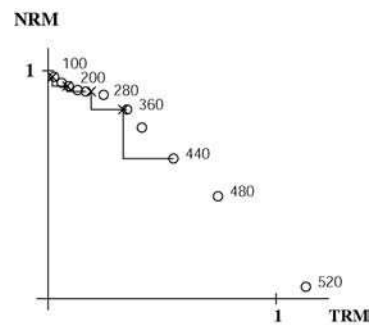
ESPCDAJ10C
AF demagnetization



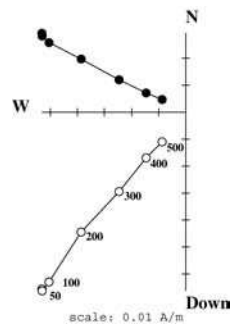
ESPCDAJ11A
Rejected
 $NRM_0 = 1.43 \text{ A/m}$



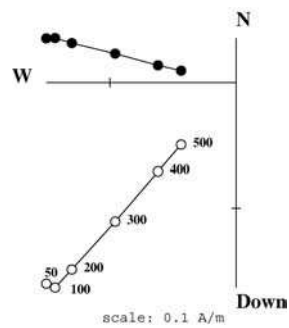
ESPCDAJ12A
Rejected
 $NRM_0 = 6.92 \text{ A/m}$



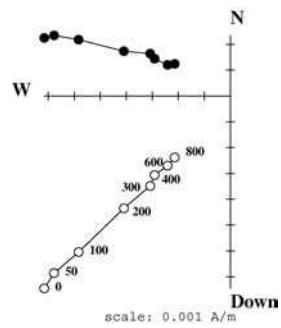
ESPCDAH. Age of the structure : 1043-1281 A.D.
 $F_{lab} = 60 \mu T$. Sample coordinates.



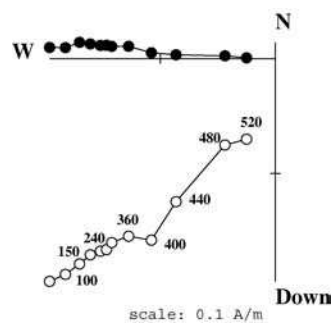
ESPCDAH02A
AF demagnetization



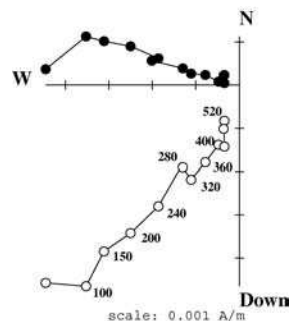
ESPCDAH04B
AF demagnetization



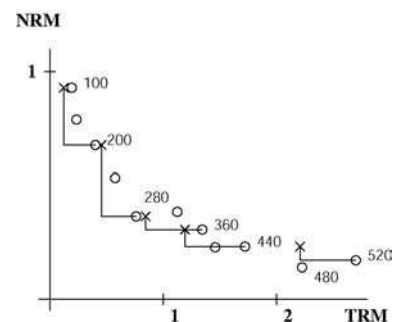
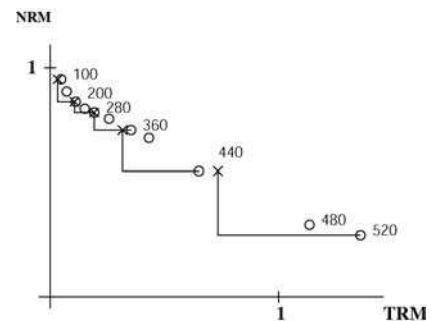
ESPCDAH05C
AF demagnetization

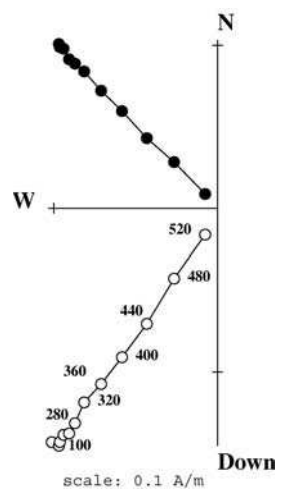


ESPCDAH6PA
Rejected
 $NRM_0 = 0.28 \text{ A/m}$

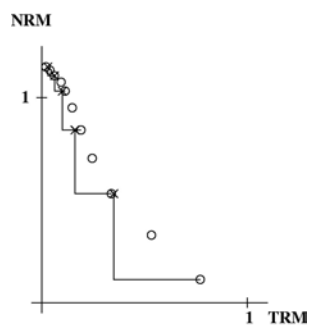


ESPCDAHA10A
Rejected
 $NRM_0 = 0.01 \text{ A/m}$





ESPCDAHXA
Rejected
 $NRM_0 = 0.18 \text{ A/m}$



Annexe II: Anisotropie de l'aimantation thermorémanente

Dans cette annexe on présente les résultats de l'anisotropie de l'aimantation thermorémanente. Les directions des axes principaux du tenseur d'anisotropie obtenus ainsi que le diagramme de Flinn pour chacun des sites étudiés sont présenté dans l'ordre suivant :

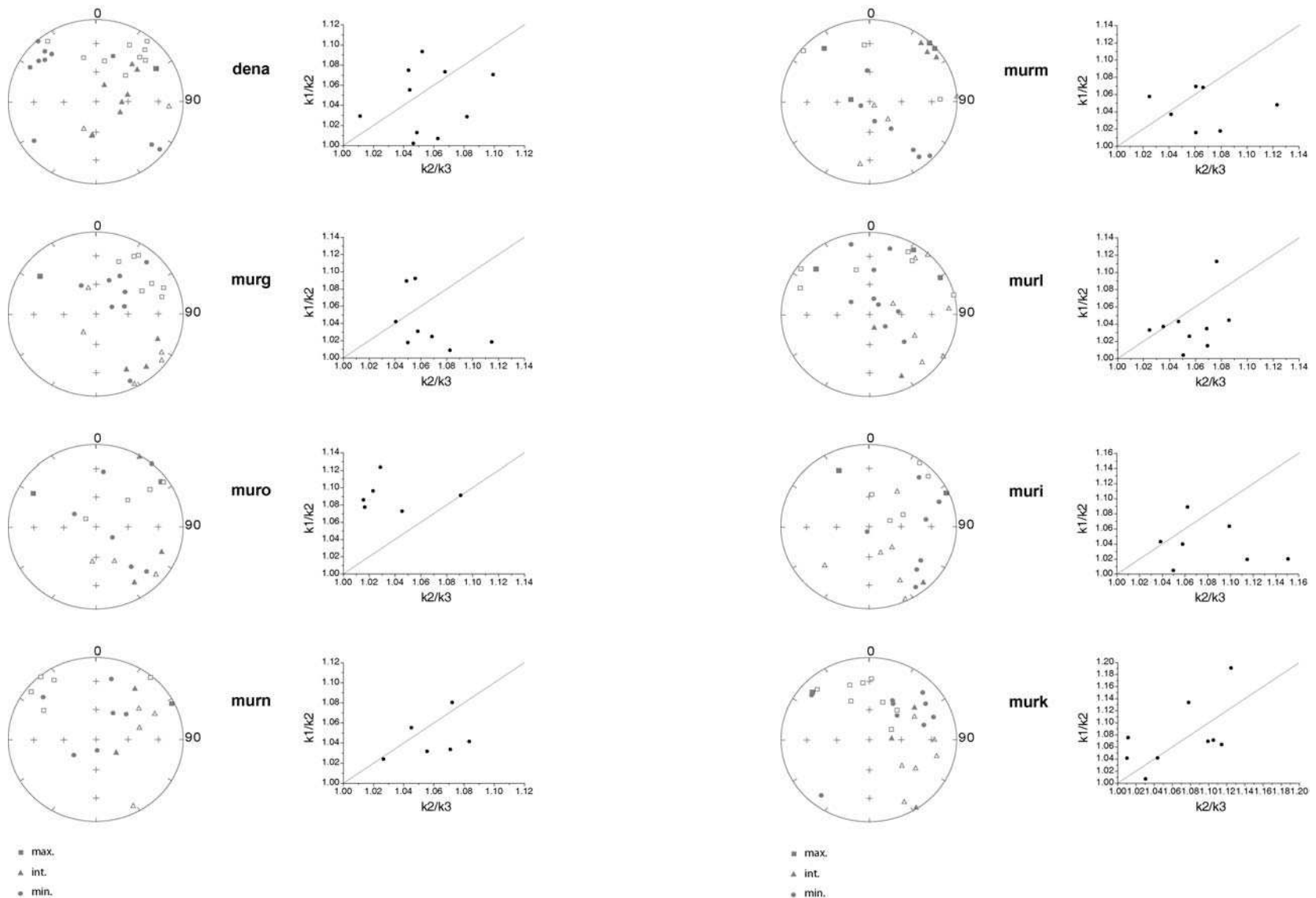
L'ordre de présentation des résultats obtenus par site est le suivant :

DEN	p301
MURG	p301
MURO	p301
MURN	p301
MURM	p301
MURL	p301
MURI	p301
MURK	p301
MURH	p302
CALA	p302
CALB	p302
CERCALB	p302
VALN	p302
VALI	p302
VALK	p302
VALM	p302
CALC	p303
PATA	p303
PATJ	p303
PATH	p303
PATB	p303

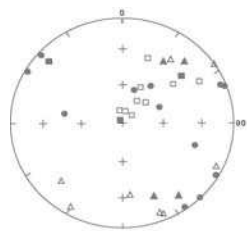
Annexe II

VALL	p303
GUA2	p303
YUS2	p303

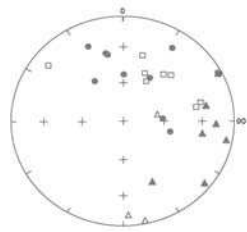
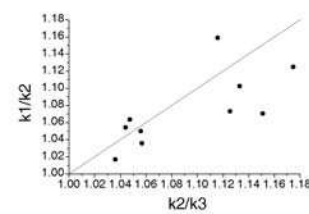
Annexe II



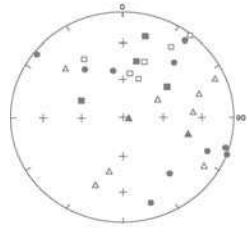
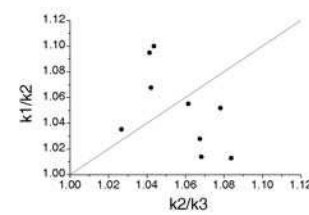
Annexe II



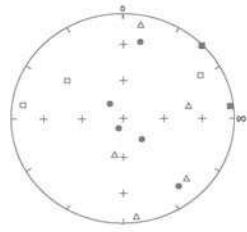
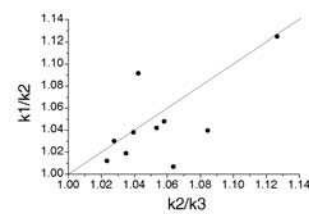
murh



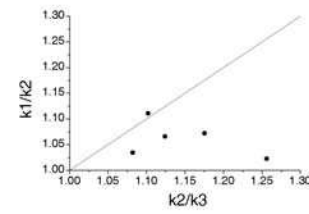
cala



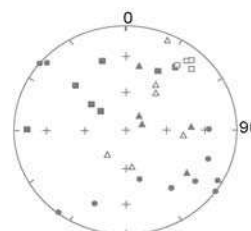
calb



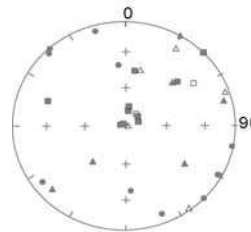
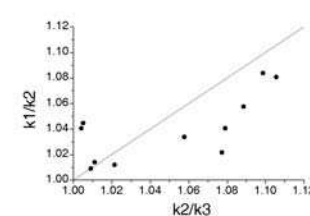
cercalb



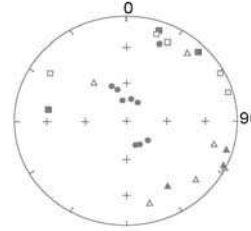
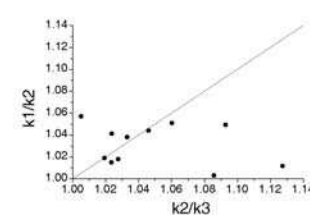
■ max.
△ int.
● min.



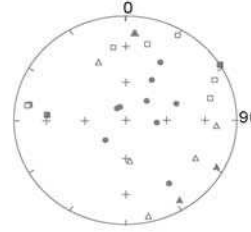
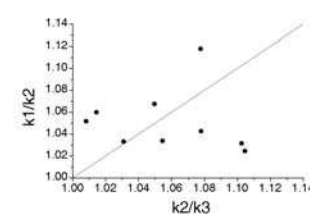
valn



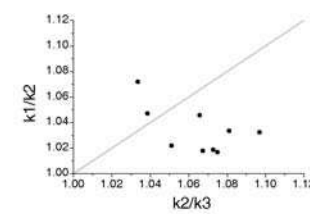
vali



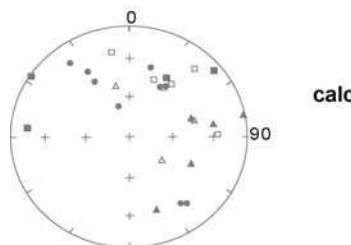
valk



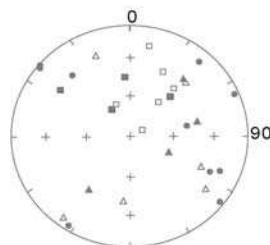
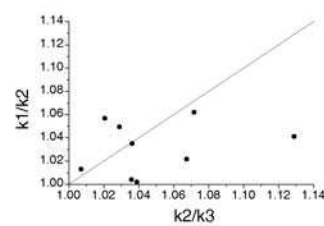
valm



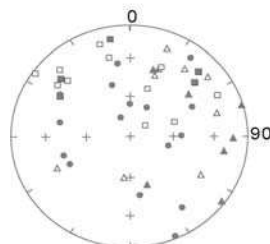
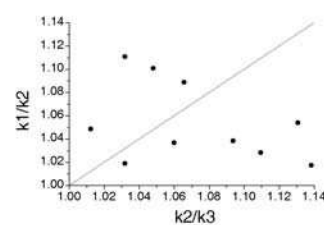
■ max.
△ int.
● min.



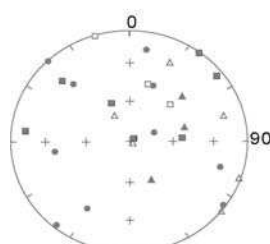
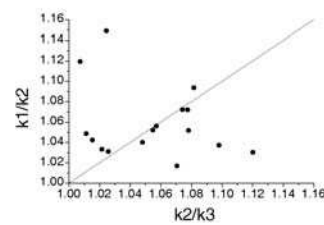
calc



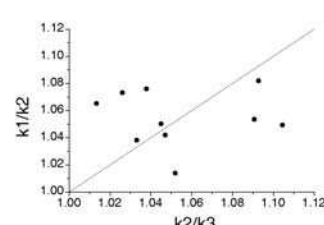
pata



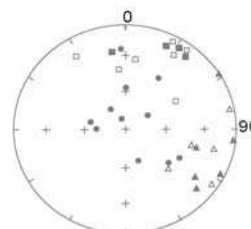
patj



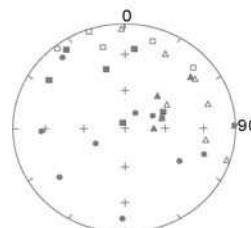
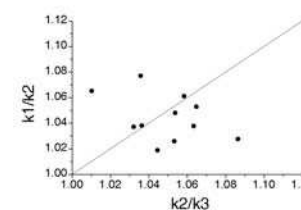
path



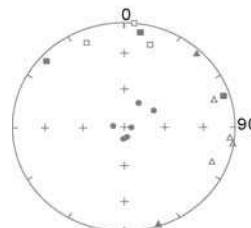
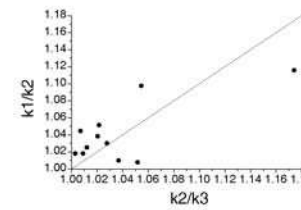
■ max.
▲ int.
● min.



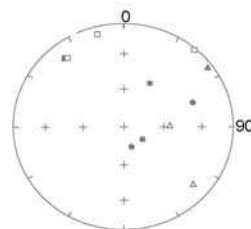
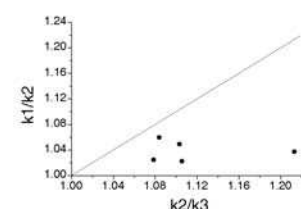
patb



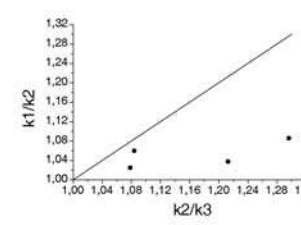
vall



guaa



yuste



■ max.
▲ int.
● min.

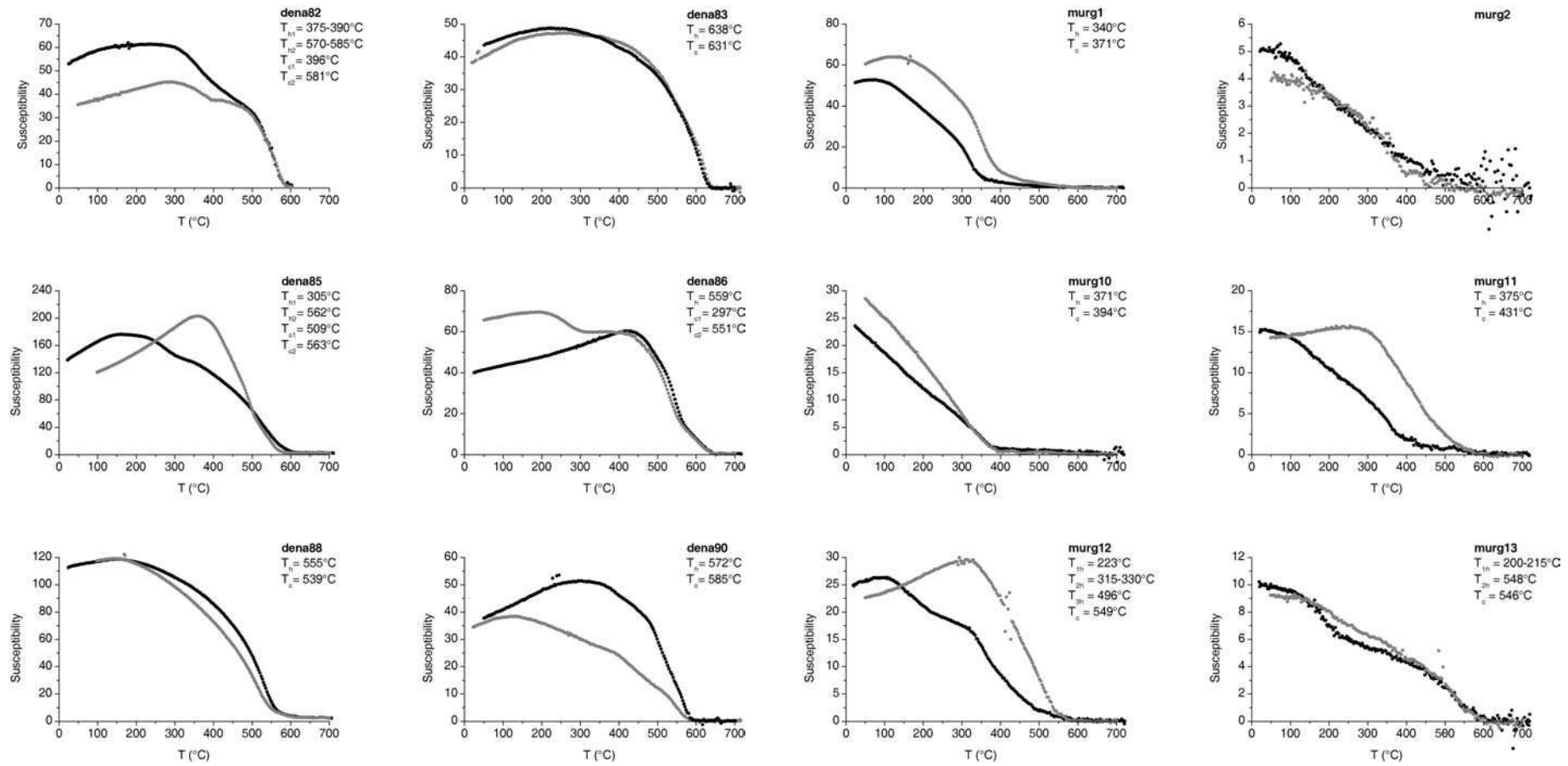
Annexe III: Détermination de températures de Curie

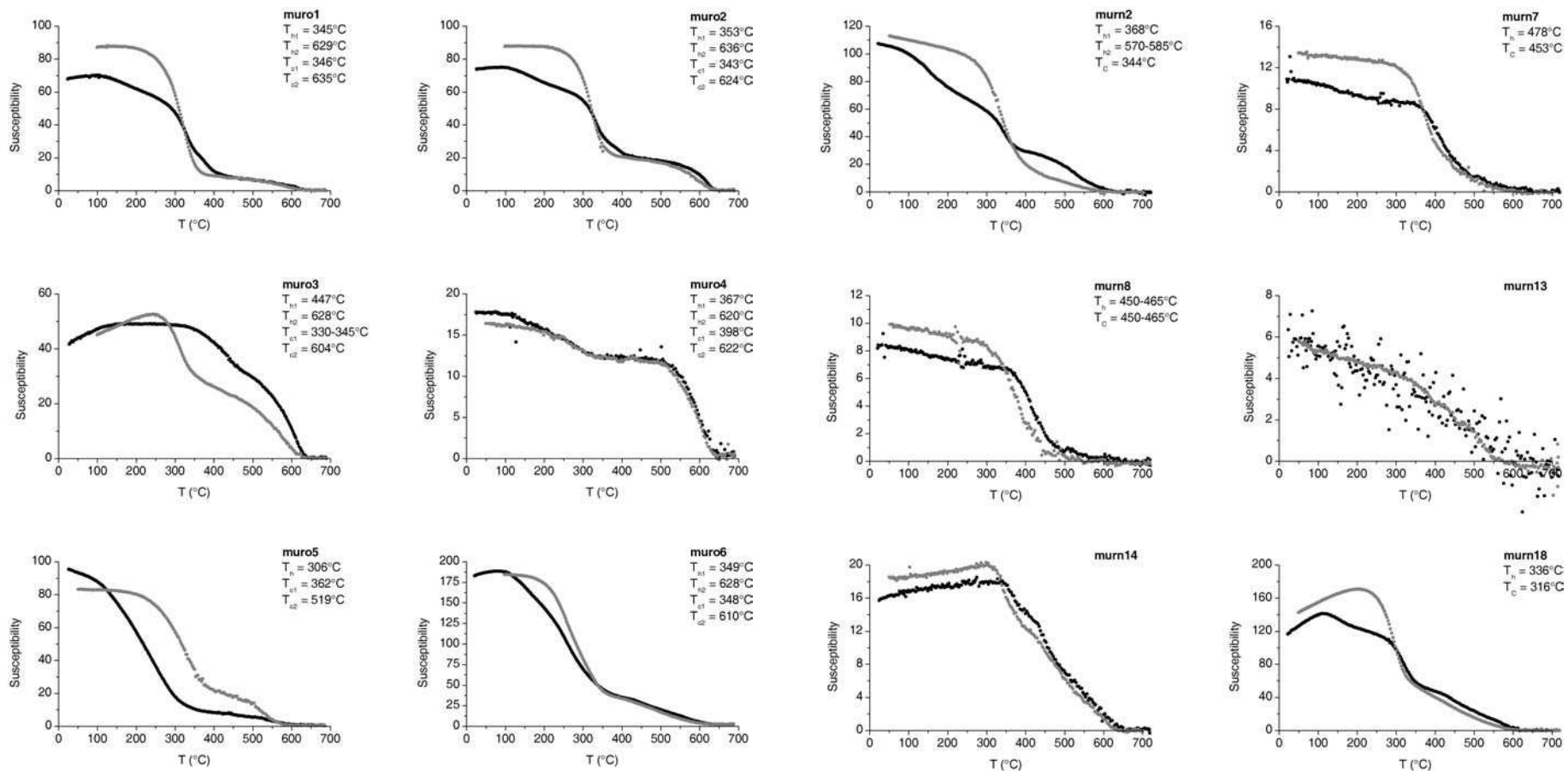
Dans cette annexe sont réunies, pour quelques échantillons caractéristiques de chacun des sites étudiés, les courbes de susceptibilité magnétique en fonction de la température en champ faible (KT-curves). Celles-ci nous ont permis de déterminer les principaux porteurs magnétiques dans nos échantillons. Les annotations sur les graphiques, T_h et T_c , désignent respectivement les températures de Curie déterminées lors de la montée en température de l'échantillon (courbe noire) et lors du refroidissement de l'échantillon (courbe grise). Les températures de Curie ont été déterminées suivant la méthode Tauxe (voir les articles pour la référence).

L'ordre de présentation des résultats obtenus par site est le suivant :

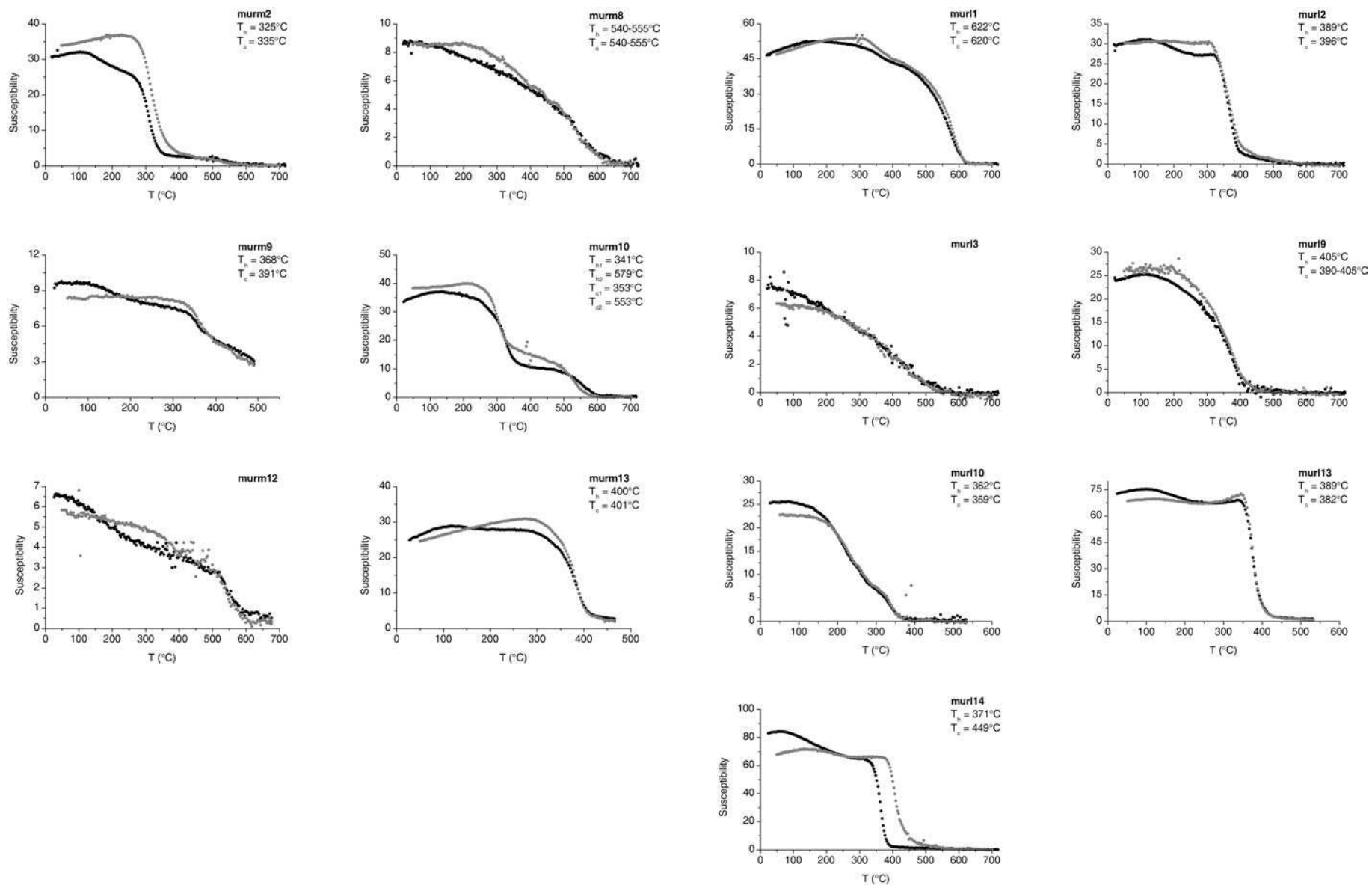
DENA	p307
MURG	p307
MURO	p308
MURN	p308
MURM	p309
MURL	p309
MURI	p310
MURH	p310
MURK	p311
CALA	p311
CALB	p312
CERCALB	p312
VALN	p313
VALI	p313
VALK	p314
VALM	p314

CALC	p315
PATH	p315
PATA	p316
PATB	p316
PATJ	p317
VALL	p317
GUA2	p318
YUS2	p318

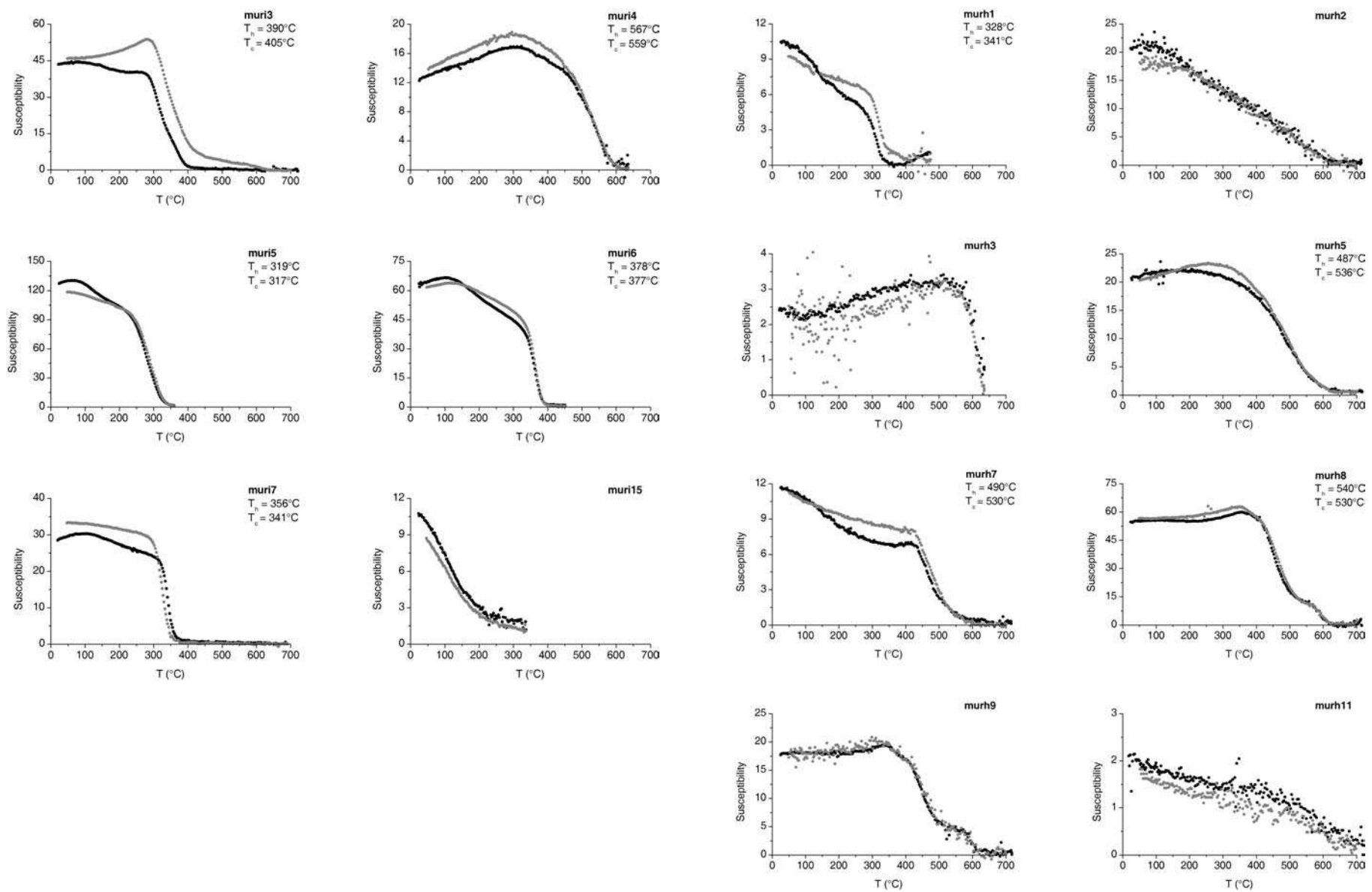




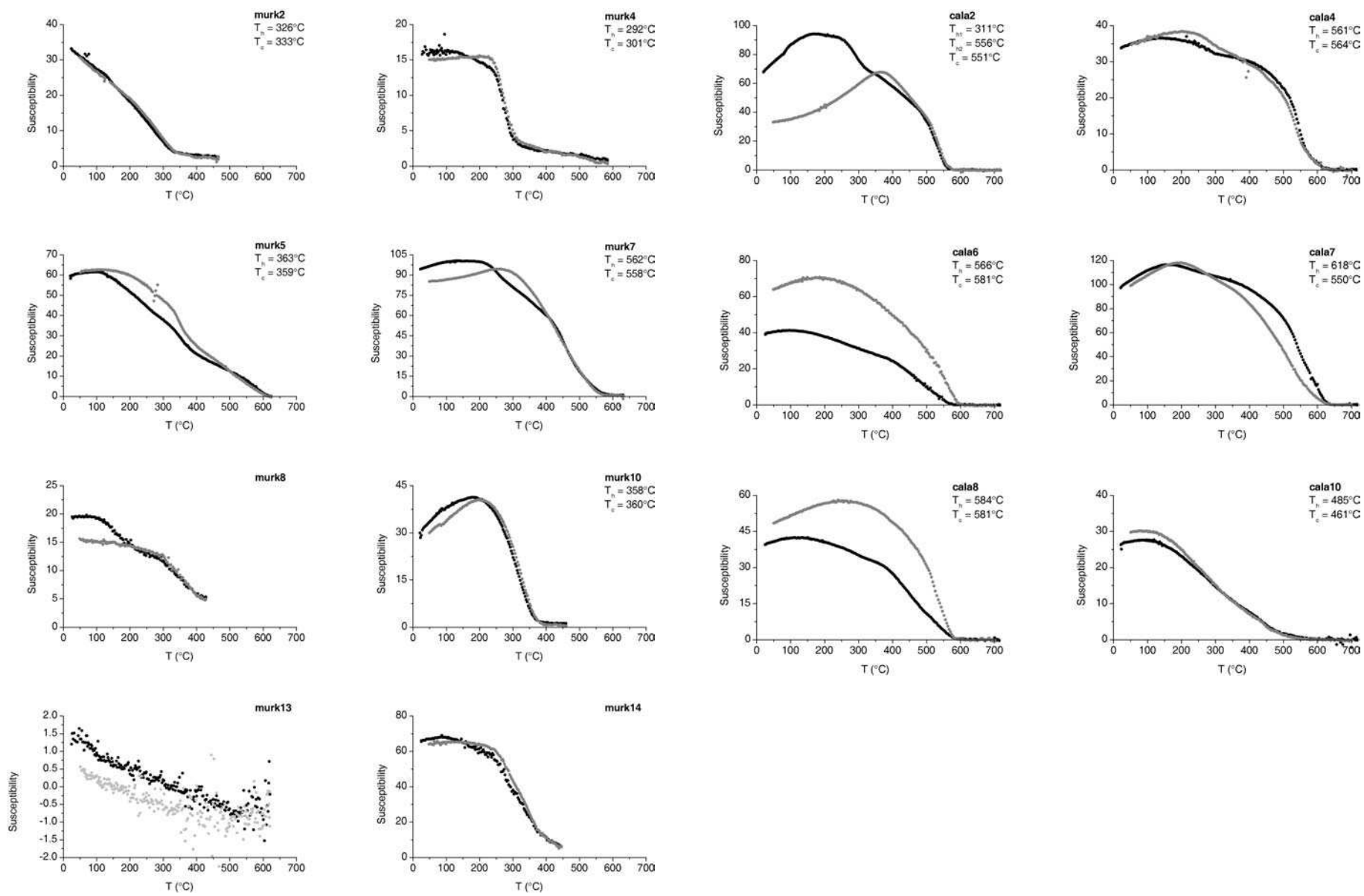
Annexe III



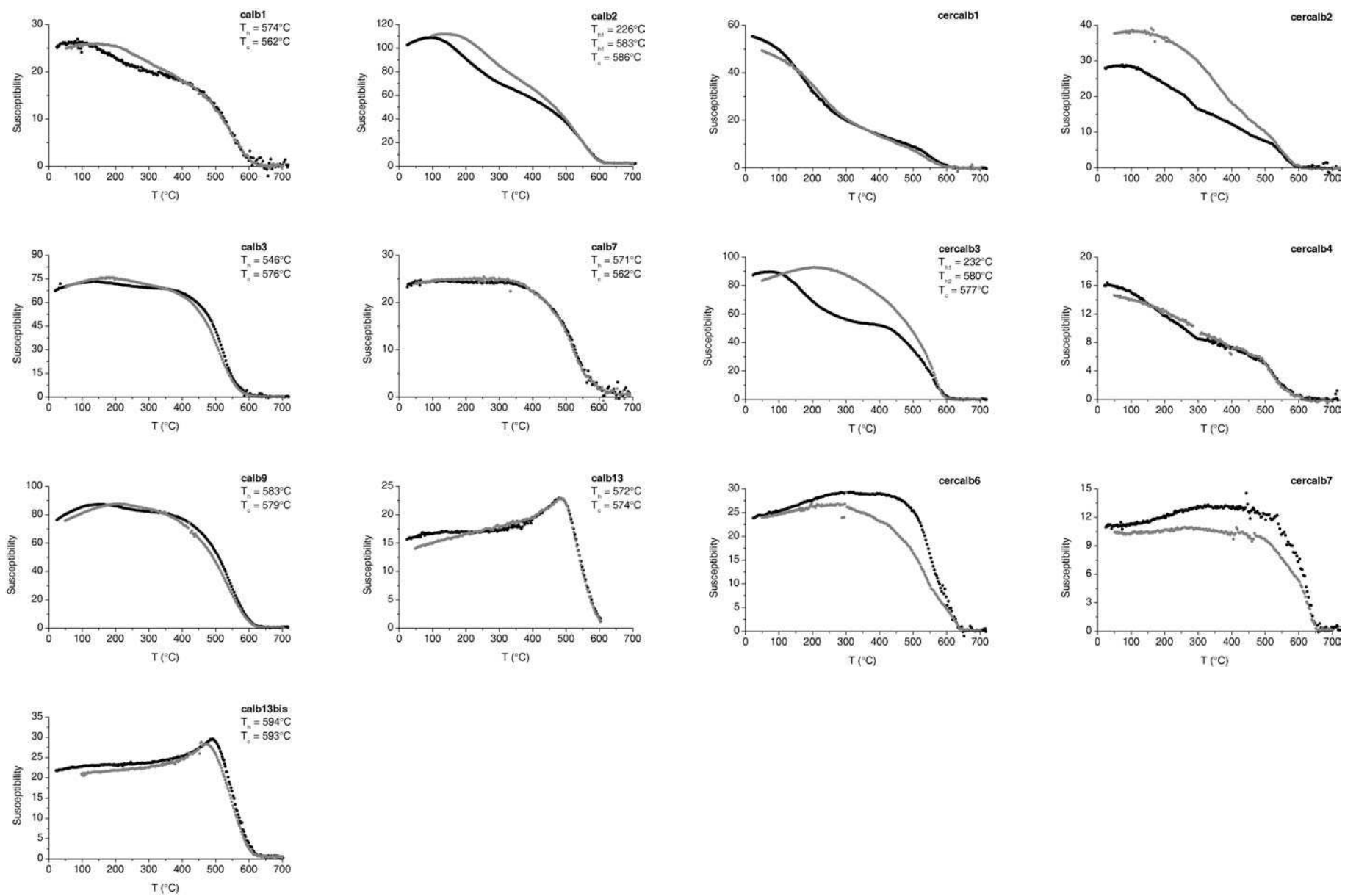
Annexe III

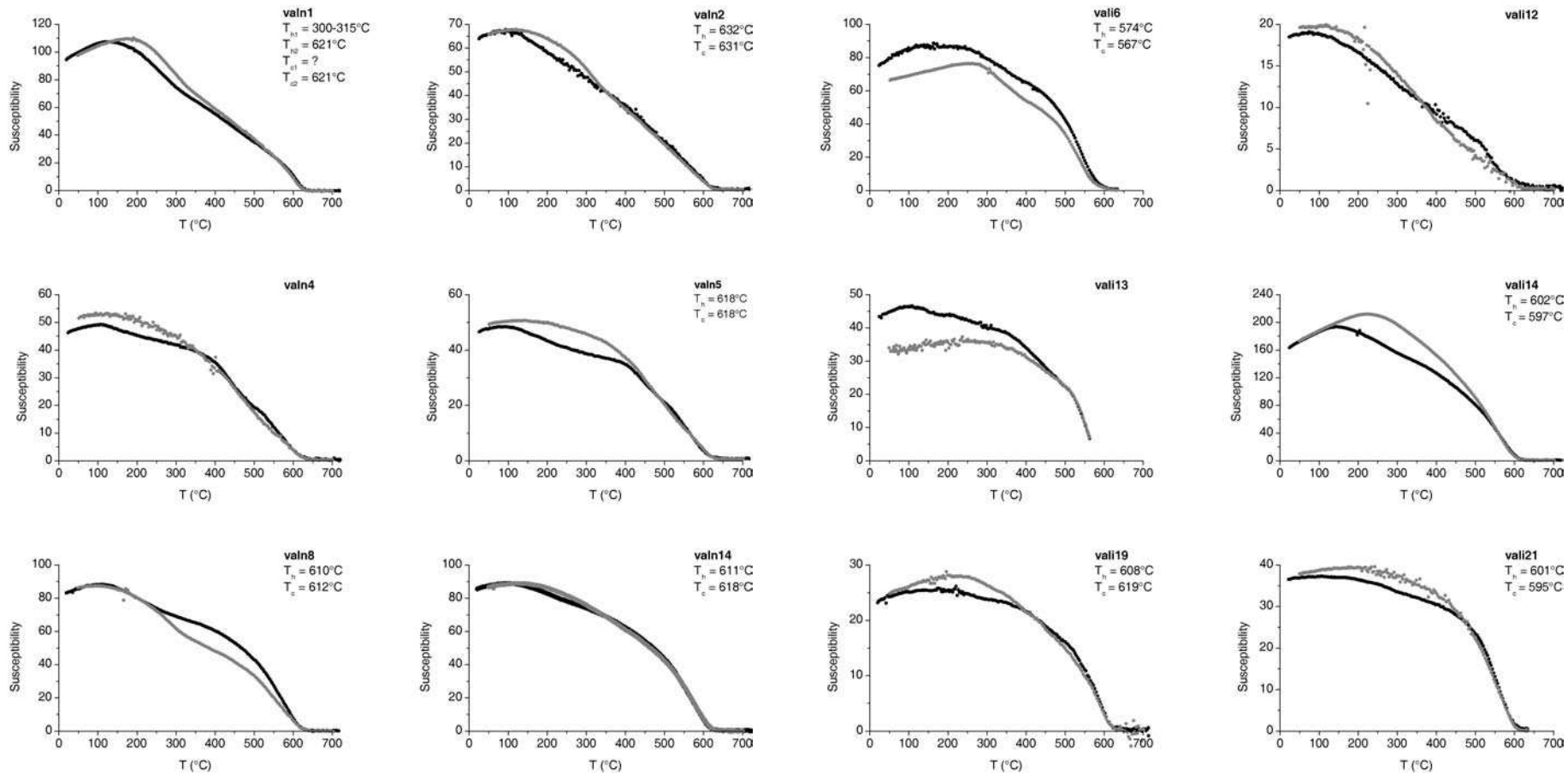


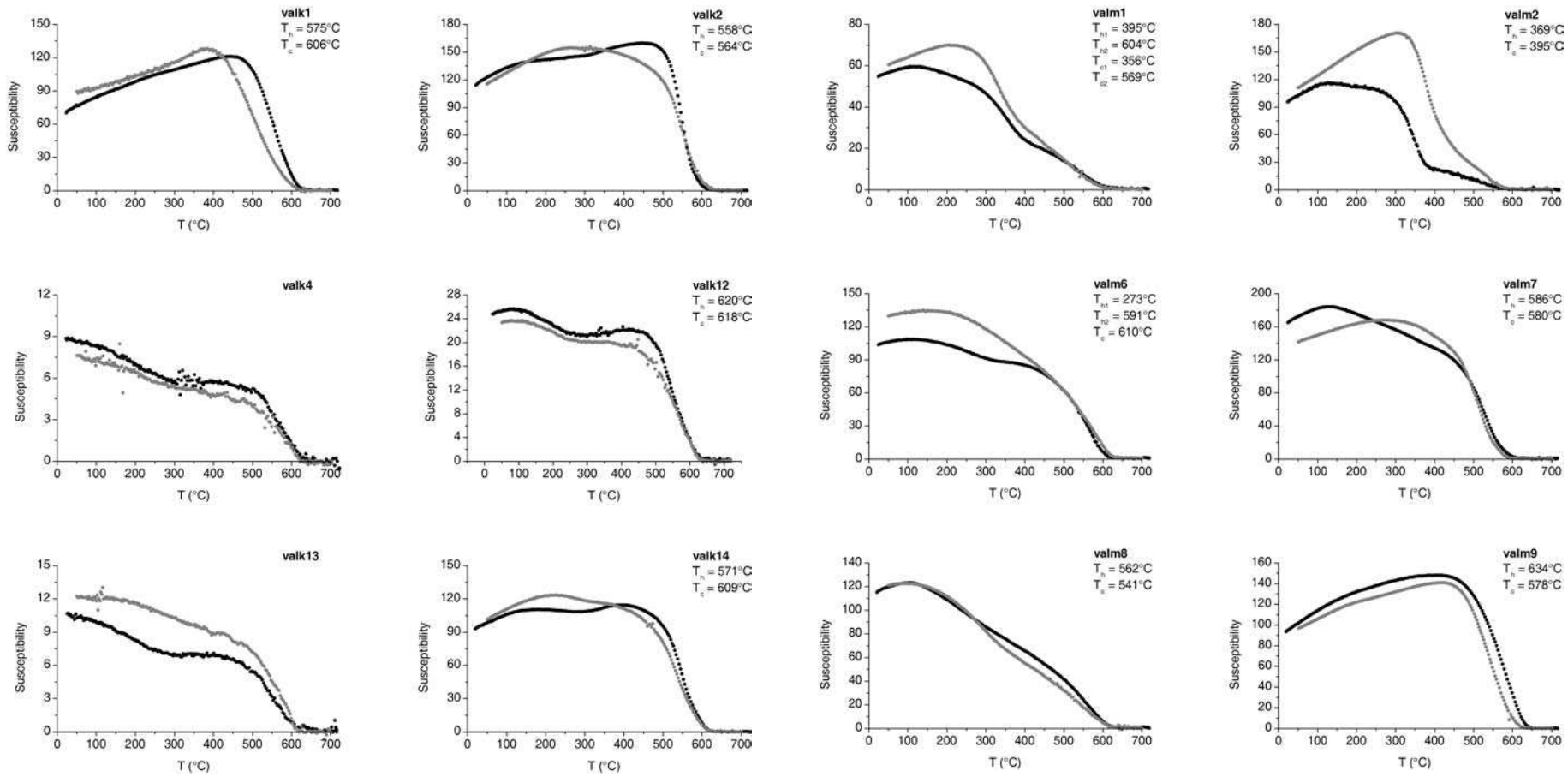
Annexe III

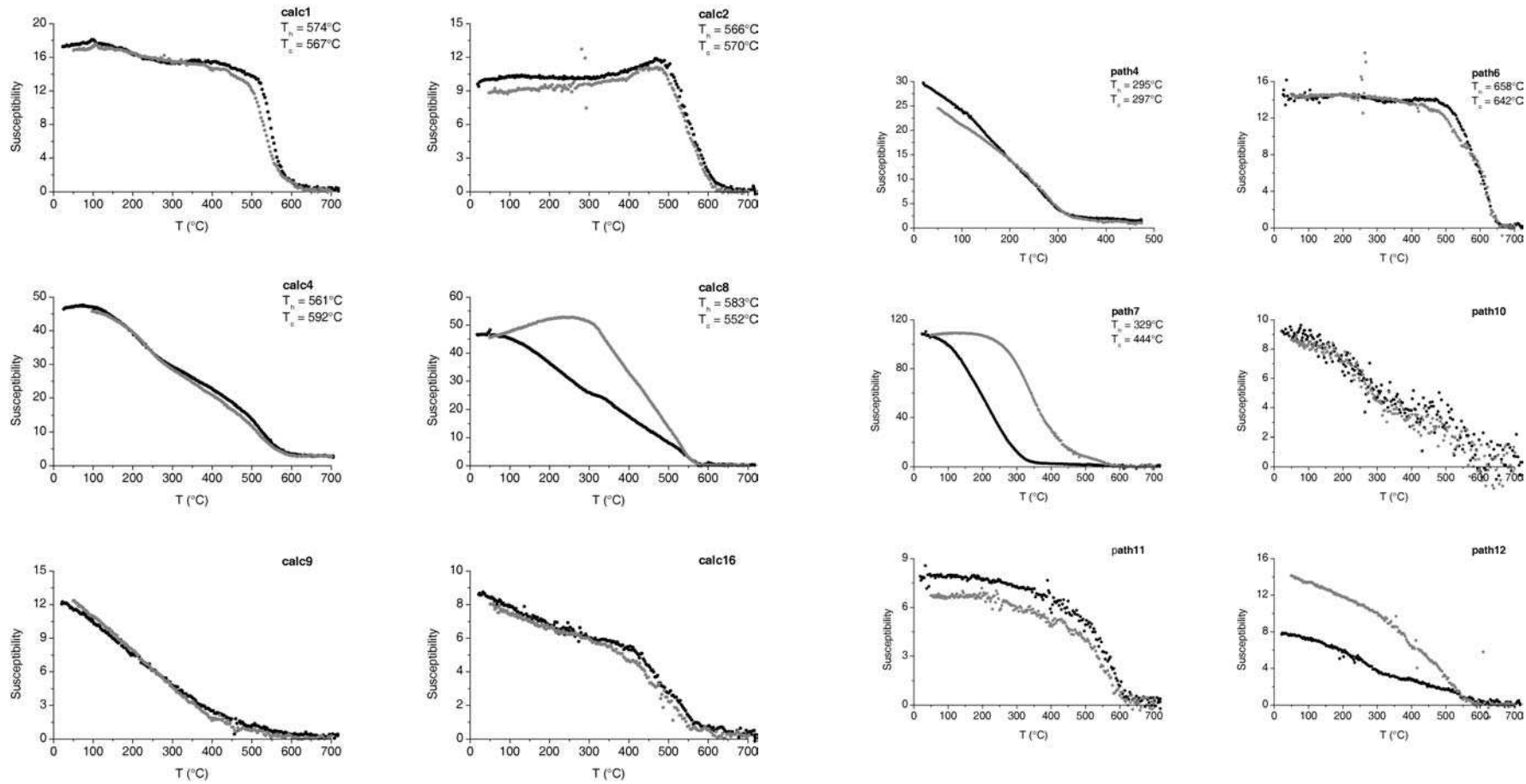


Annexe III

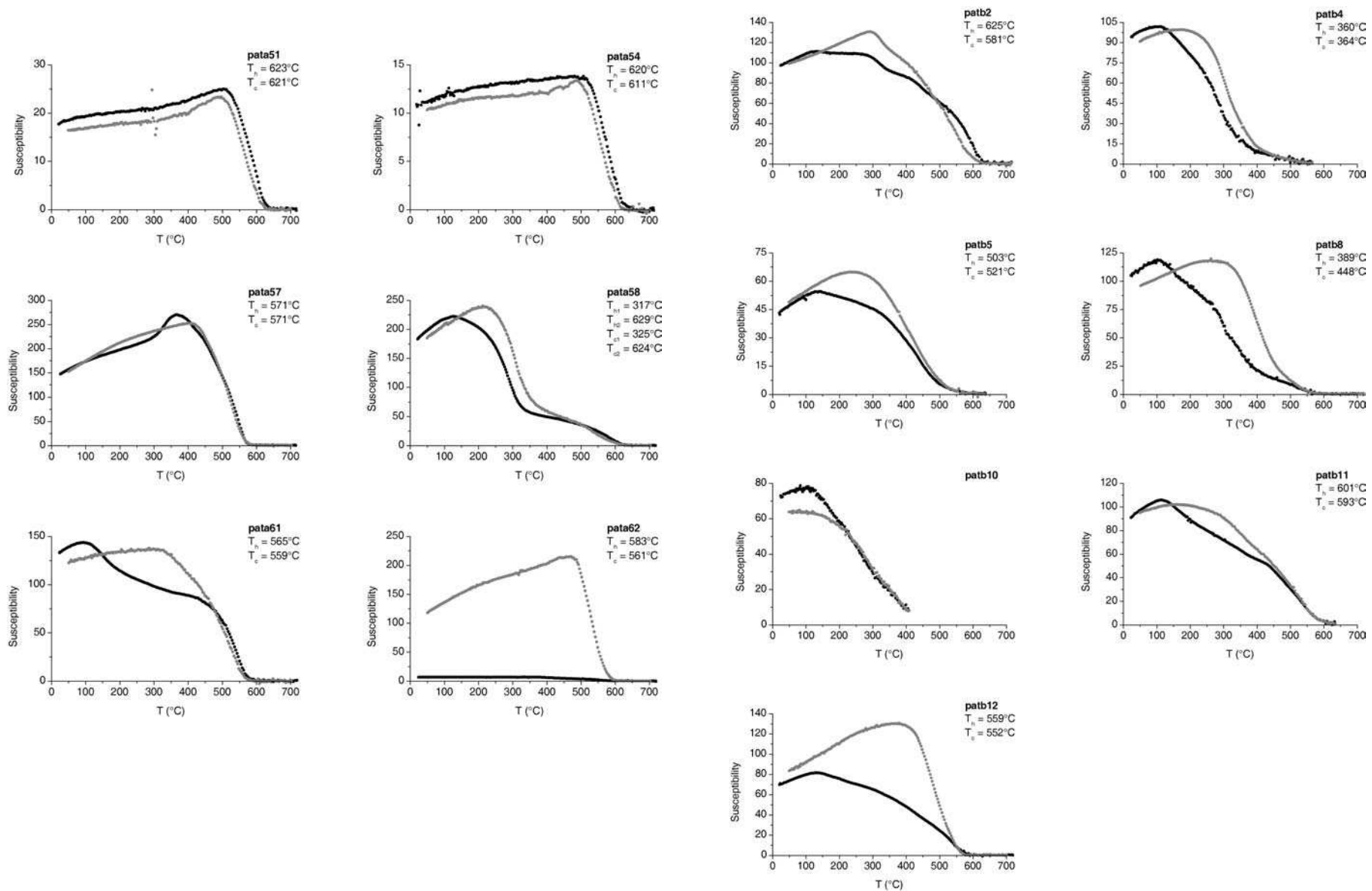




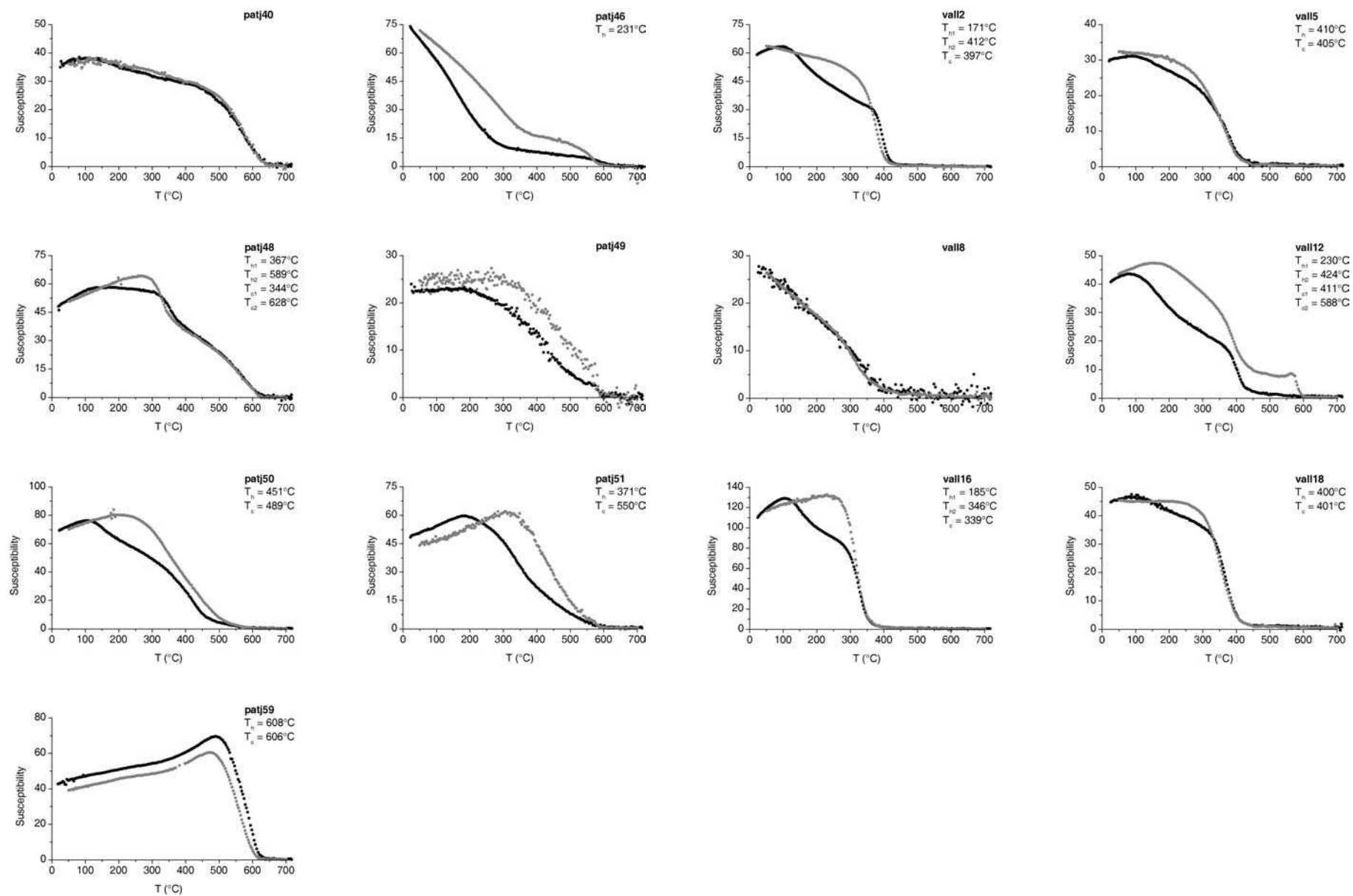




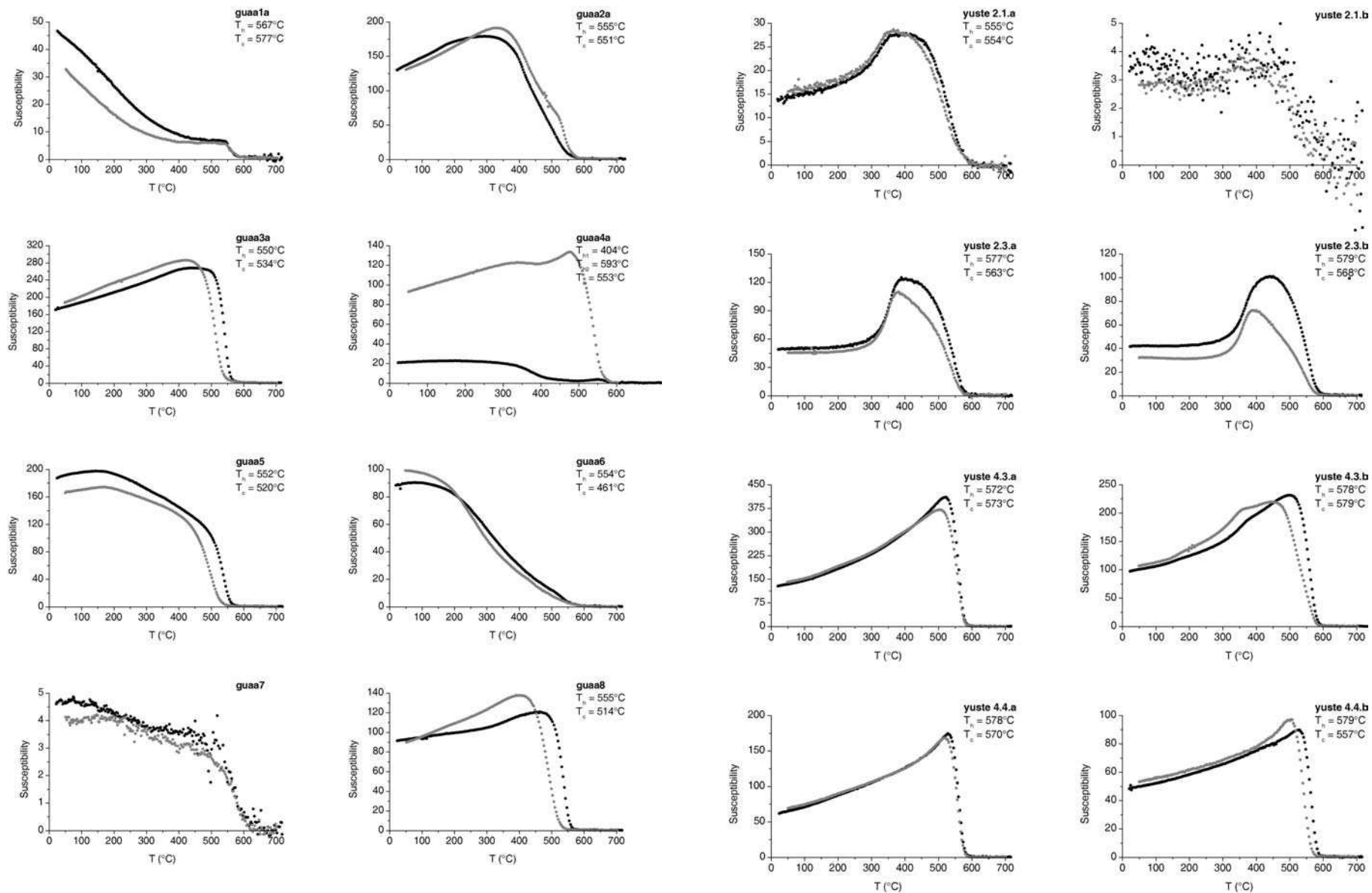
Annexe III



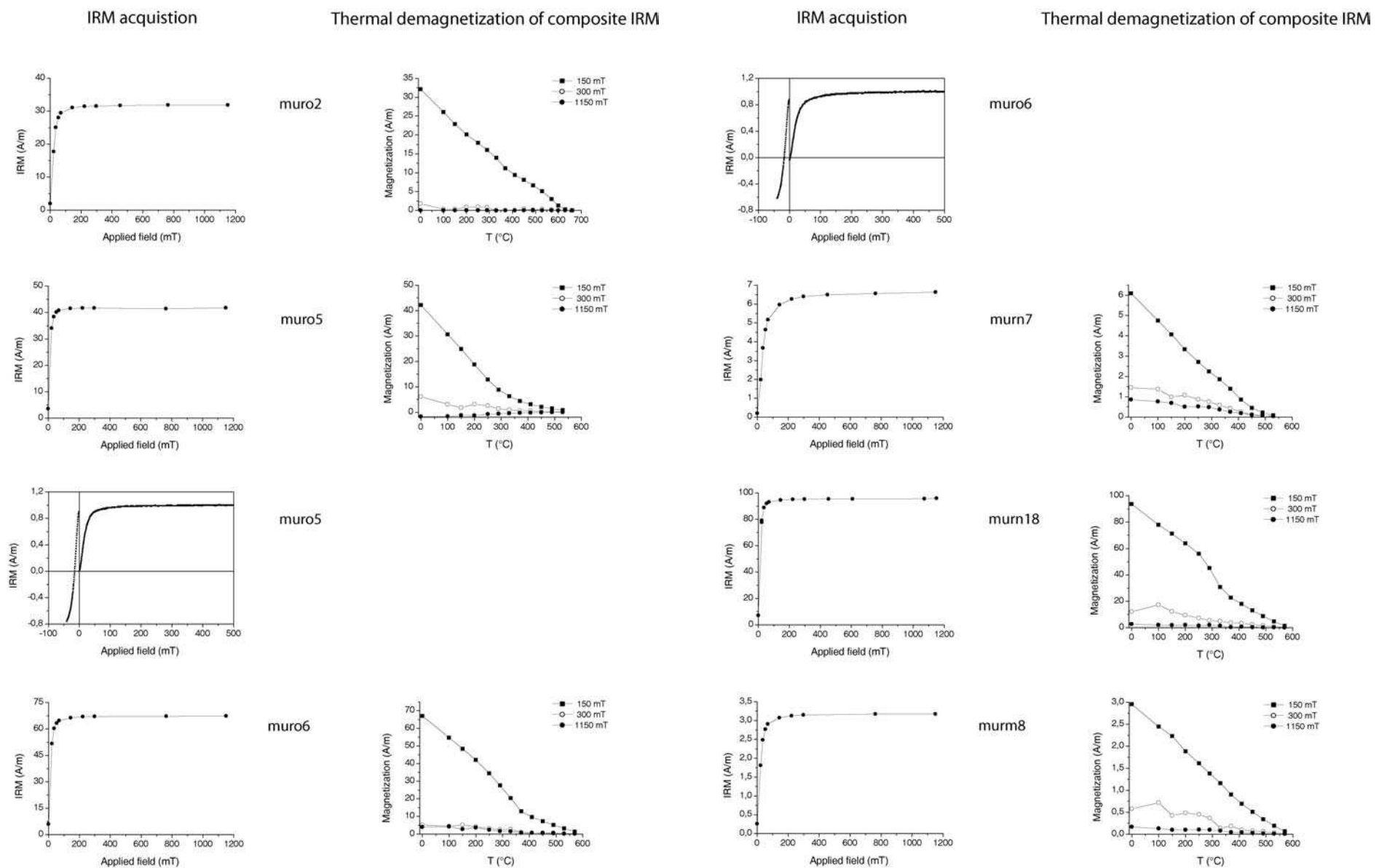
Annexe III

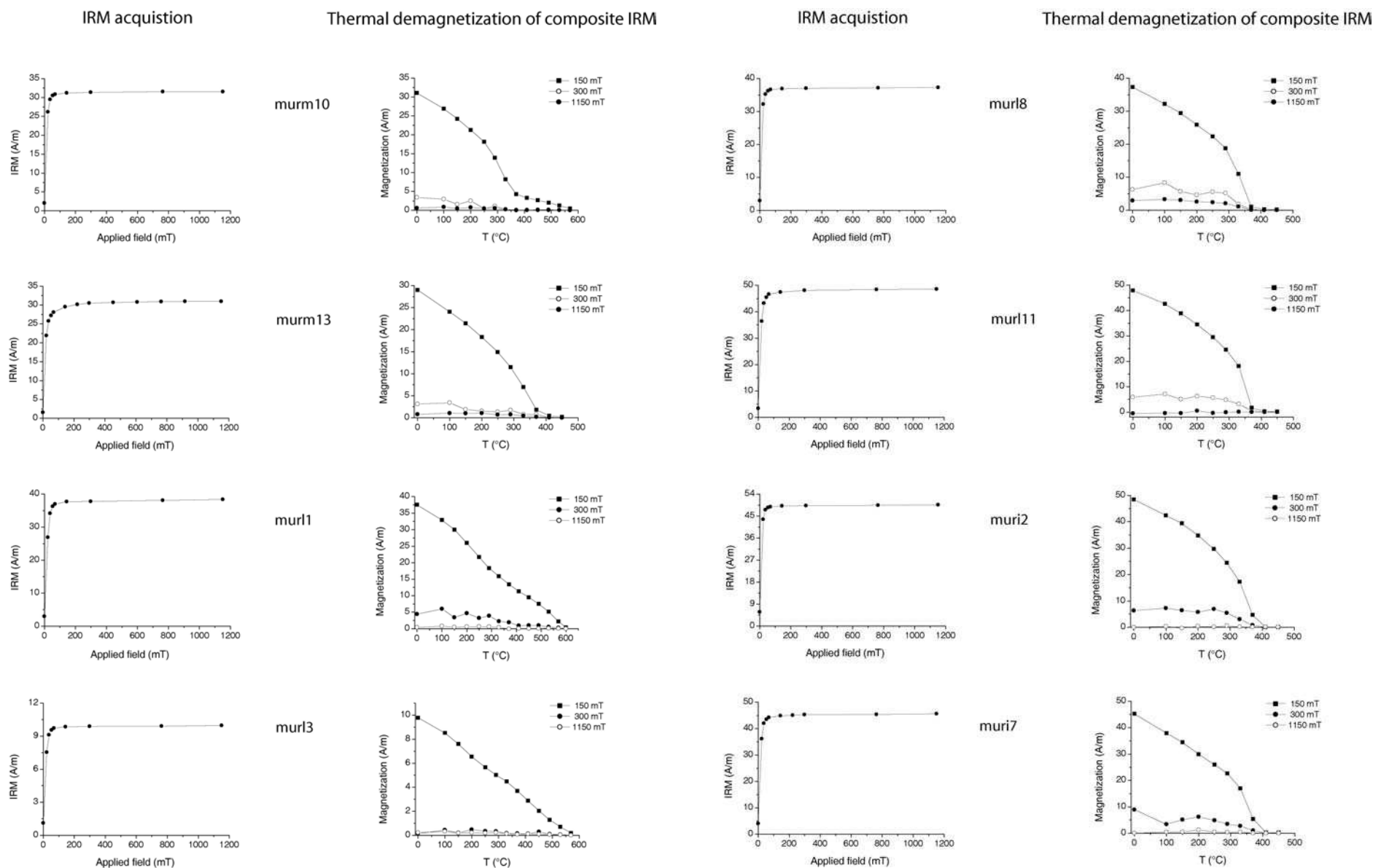


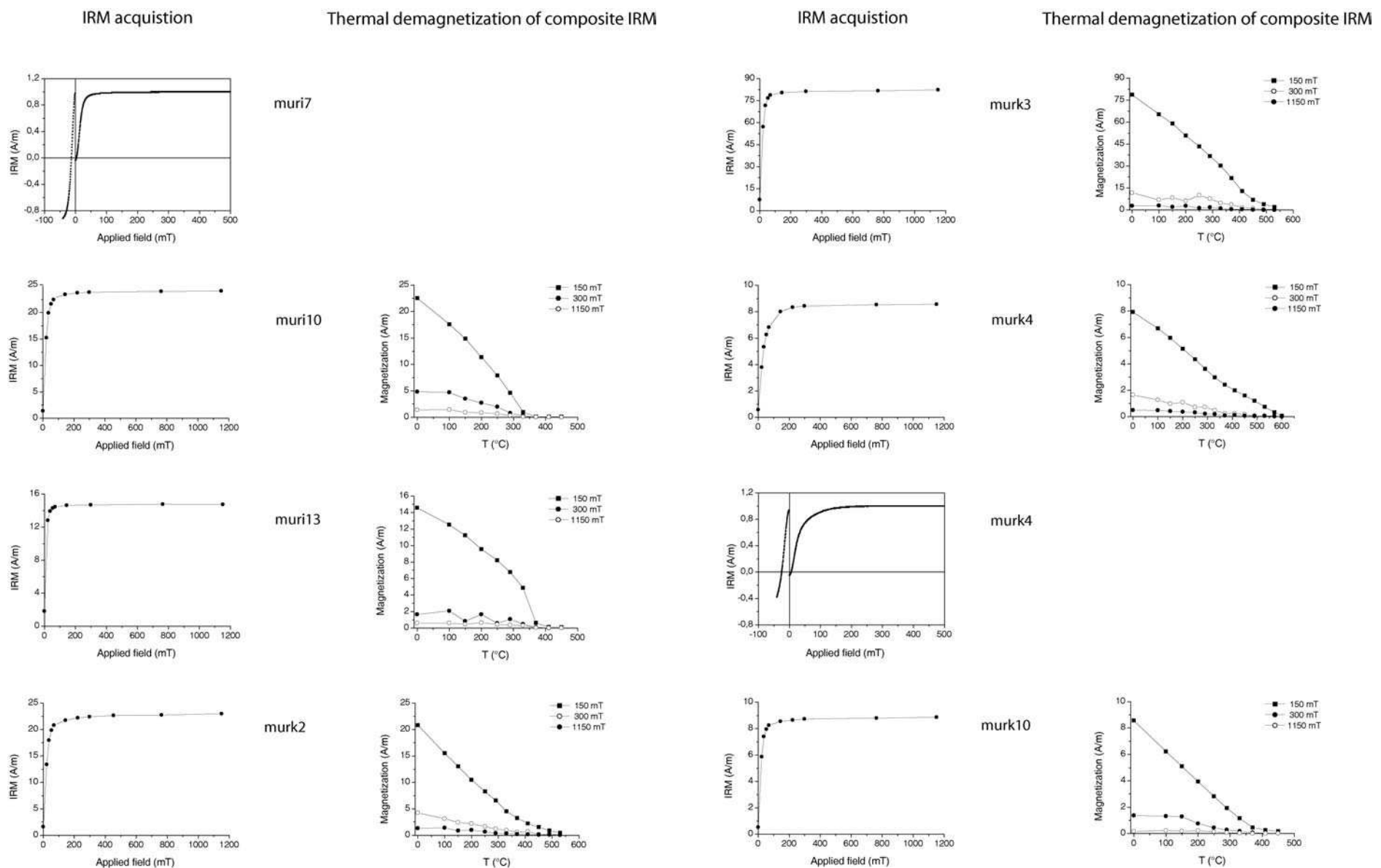
Annexe III

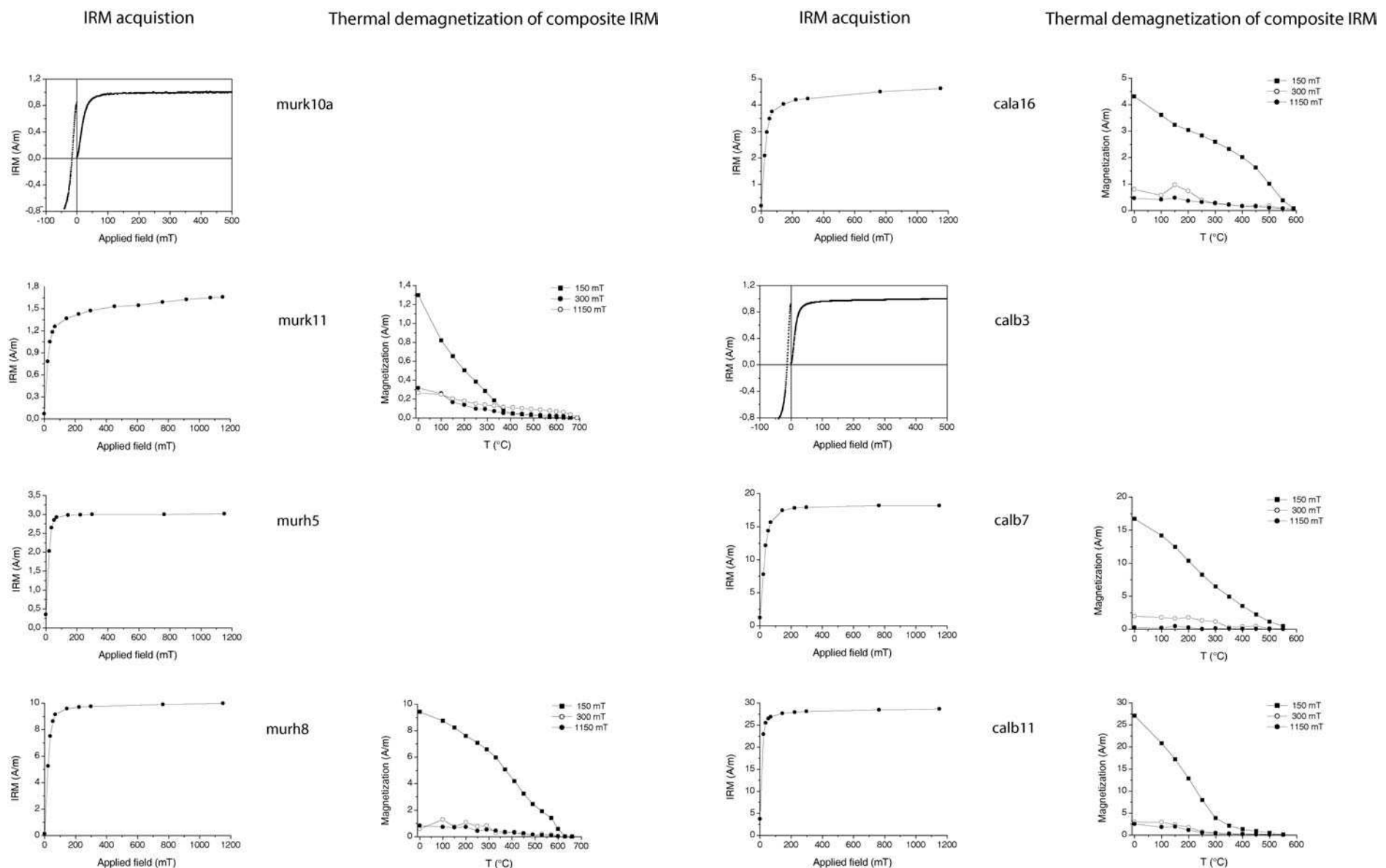


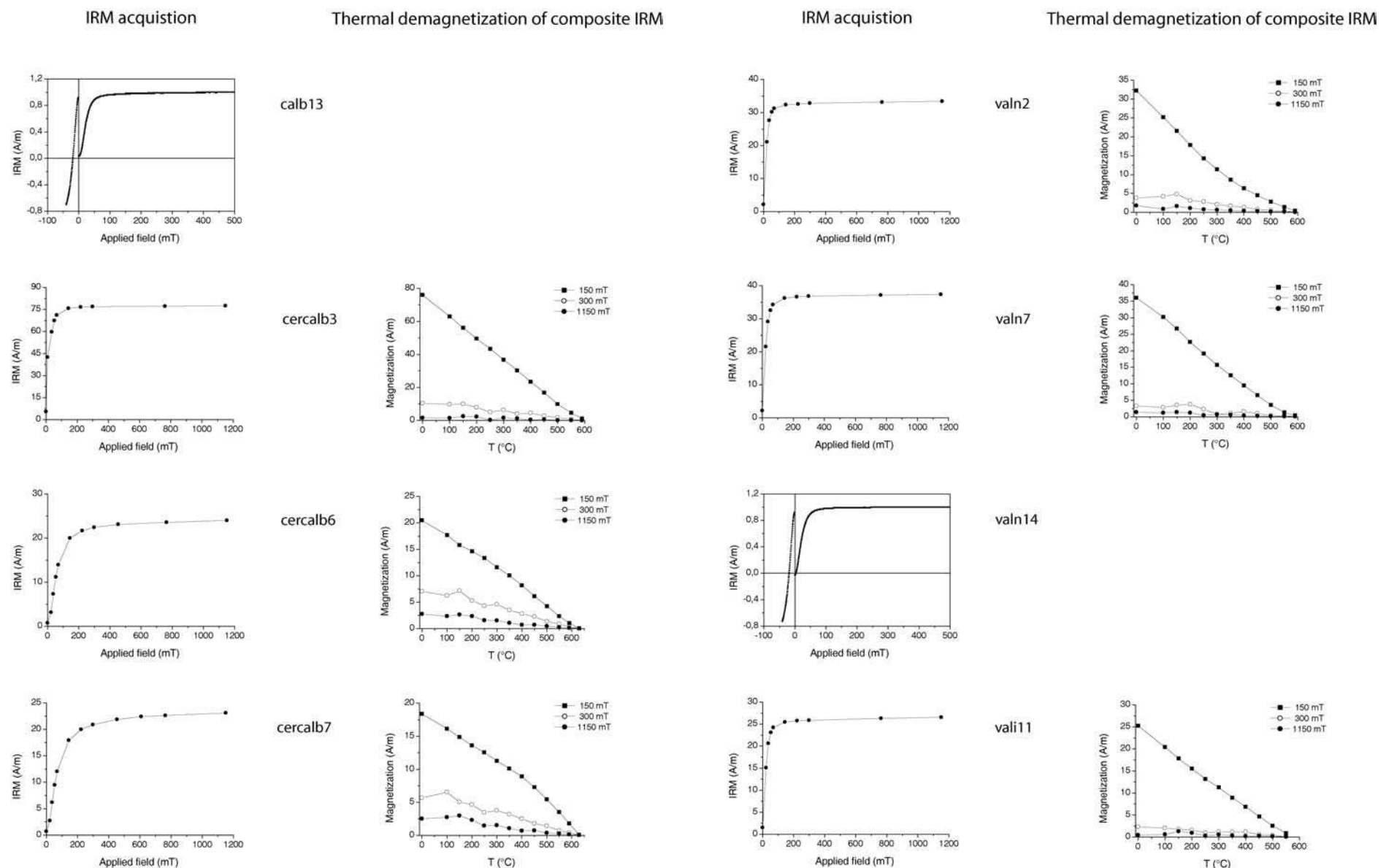
Annexe IV: Acquisition d'aimantation rémanente isotherme (ARI) et désaimantation thermique des ARI croisées

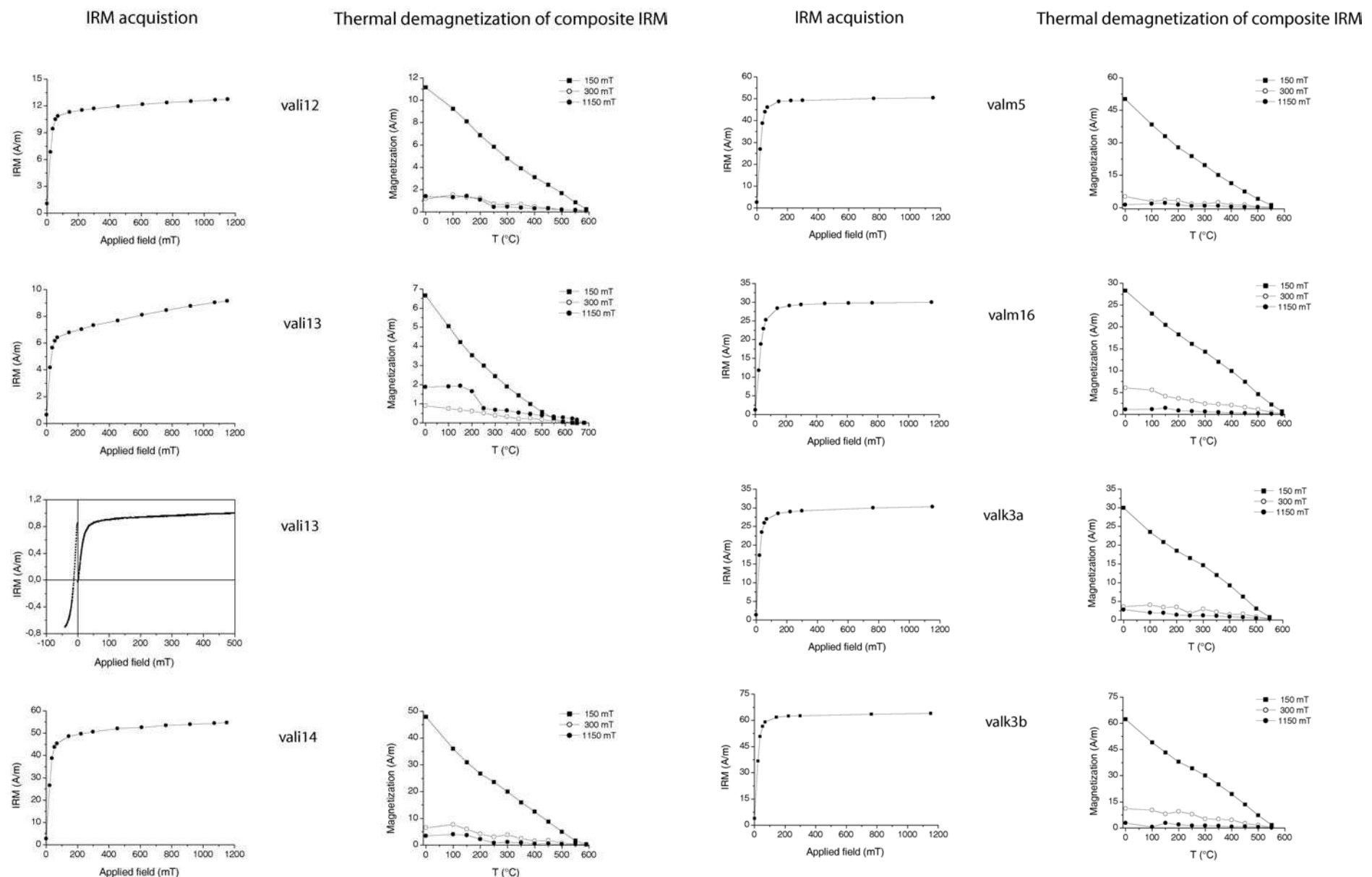


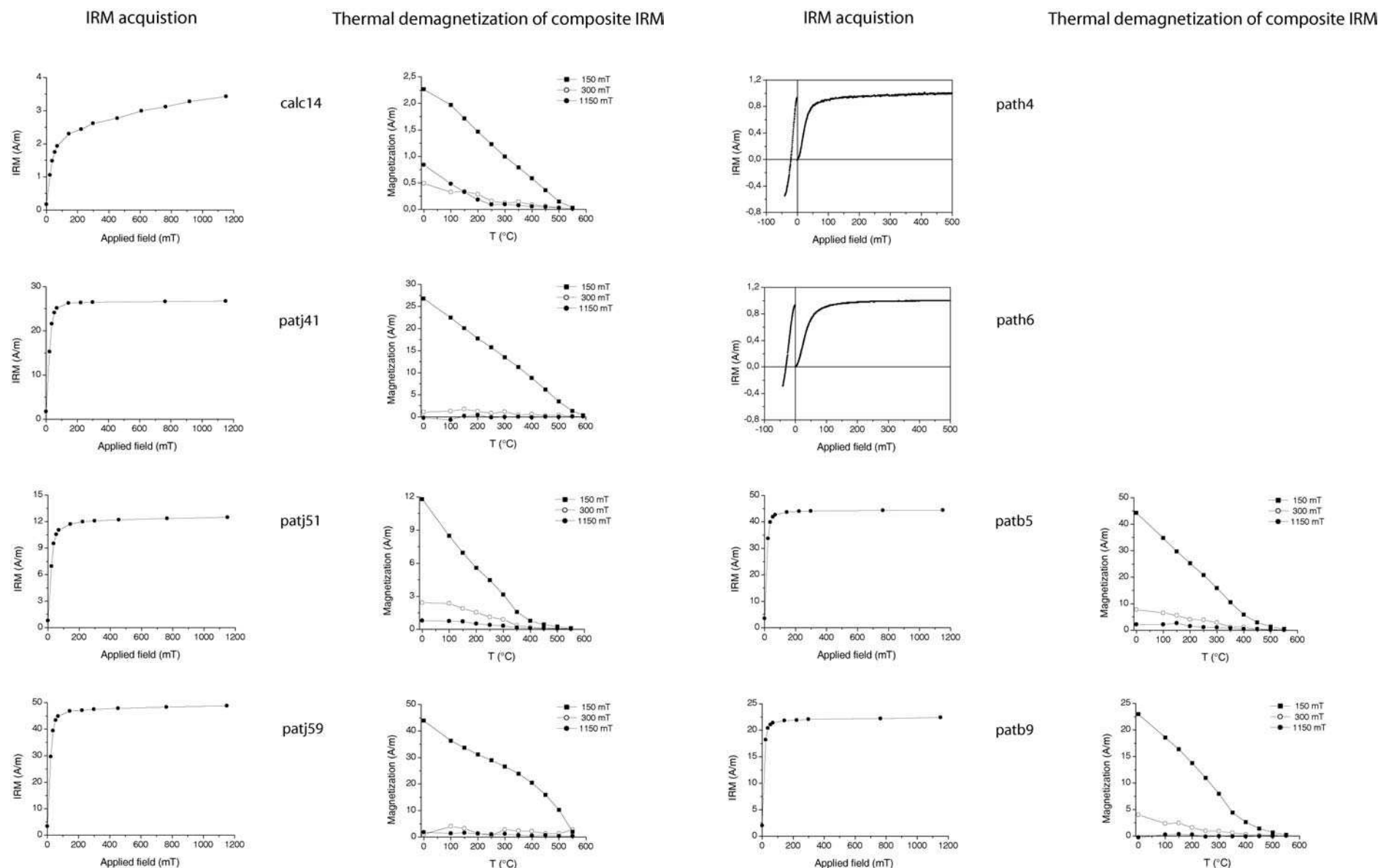


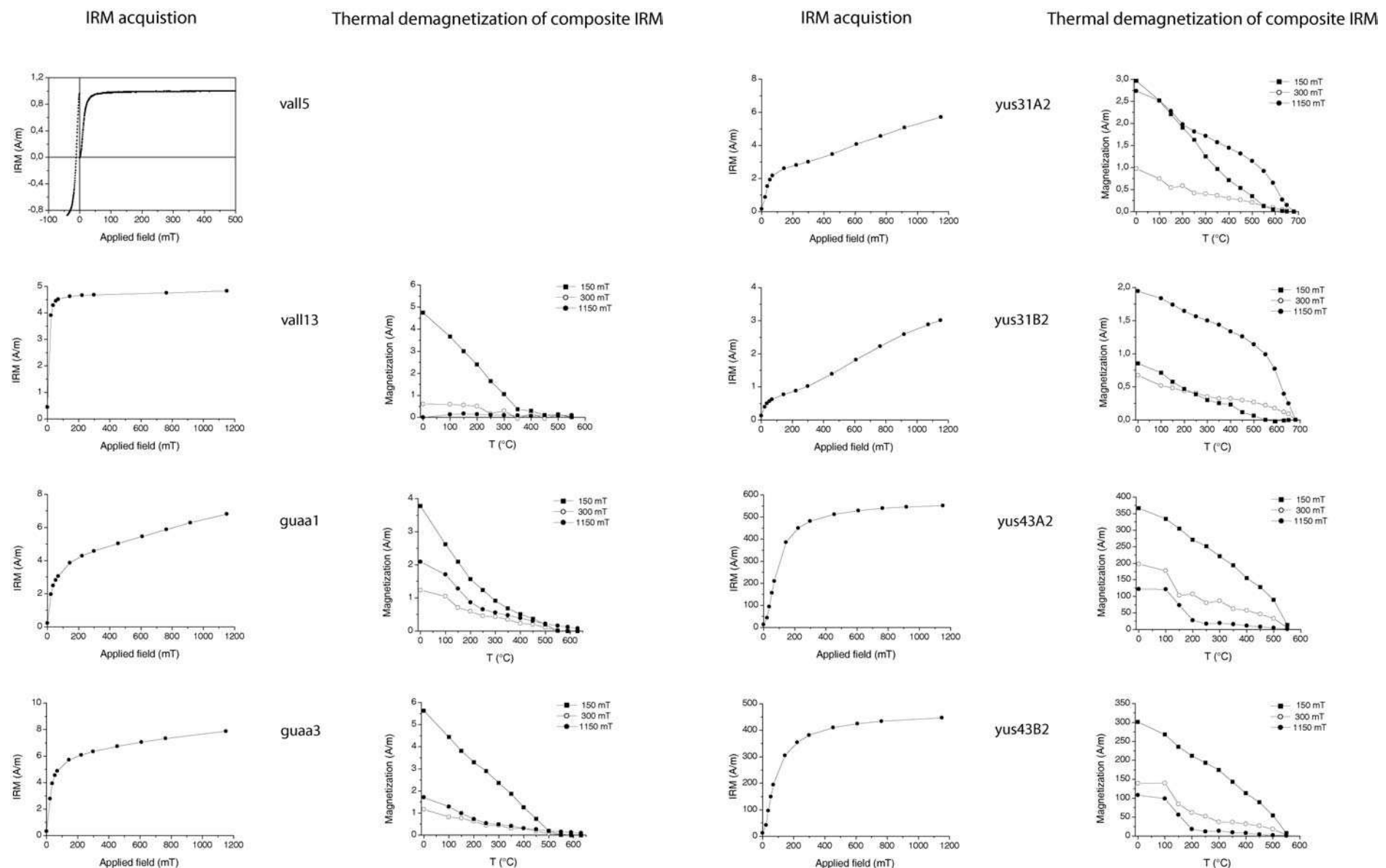












Annexe V: Fiches archéologiques des fours étudiés

Dans cette annexe sont réunies les renseignements archéologiques les plus importants des structures qui ont servi à déterminer l'archéointensité dans le cadre de cette thèse. Toutes les structures décrites dans cette annexe ont été prélevées par Jacques Thiriot.

L'ordre de présentation par fouille archéologique est le suivant :

DENIA	p331
MURCIA CALLE SAGASTA	p333
MURCIA CALLE PUXMARINA	p336
CALATRAVA LA VIEJA	p344
VALENCIA VELLUTERS	p350
PATERNA CALLE DE LOS HUERTOS	p359
PATERNA TESTAR DEL MOLI	p362
CABRERA D'ANOIA	p365

DENIA (L'ALMADRAVA)

Arqueólogo responsable de la excavación: Josep A.Gisbert

Fecha de la excavación: Junio 1986

Contexto: El horno muestreado es uno de los tres de la batería de hornos cerámicos existentes junto a cuatro estructuras de taller del alfar de l'Almadrava, en el municipio de Els Poblets (Setla-Mirarosa-Miraflor). El complejo alfarero es parte del sector artesanal de una gran vila situada junto al mar, unos siete kilómetros al norte de Denia.

Bibliografía:

Han participado en la escritura y revisión de este documento escrito Josep A. Gisbert y Jacques Thiriot.

Gisbert Santonja, Josep Antoni, "La producció de vi al territori de Dianum durant l'Alt Imperi: el taller d'àmfores de la vil·la romana de l'Almadrava (Setla-Mirarosa-Miraflor)", en *I Col·loqui Internacional d'Arqueologia Romana: el vi a l'Antiguitat. Economia, producció i comerç al Mediterrani occidental* (Badalona 1887), Badalona 1987, pàg. 104-107.

Gisbert Santonja, Josep Antoni, "La Almadrava (Setla-Mirarosa-Miraflor)", en *Memòries Arqueològiques de la Comunitat Valenciana, 1984-1985*. València 1988, pàg. 21-24.

Gisbert Santonja, Josep Antoni, "El alfar romano de l'Almadrava (Setla-Mirarosa-Miraflor) y la producción de ánforas en el territorio de *Dianum*", en Aranegui Gascó, C. (coord.), *Saguntum y el Mar*, València 1991, pág. 114-116.

Gisbert Santonja, Josep Antoni, "El alfar de l'Almadrava (Setla-Mirarosa-Miraflor) –Dianum. Materiales de construcción cerámicos. Producción y aproximación a su funcionalidad en la arquitectura del complejo artesanal", en M. Bendala, Ch. Rico, L. Roldán (eds.), *El ladrillo y sus derivados en la época romana*, Madrid 1999, pág. 65-102.

Gisbert Santonja, Josep Antoni, "El Territorium de *Dianum* –Dénia- en el Alto Imperio. La Marina Alta: producción agrícola y poblamiento", en Abascal, J. M. y Abad, L. (coord.) *Canelobre. Las ciudades y los campos de Alicante en época romana*. Revista del Instituto de Cultura "Juan Gil-albert", núm. 48. Alicante, 2003, pág. 121-143.

Fotos y planos de los hornos: Jacques Thiriot

Horno II Setla-Miraflore-Mirarosa, L'Almadrava (DENIA)

Toma de muestras realizada por: Jacques Thiriot

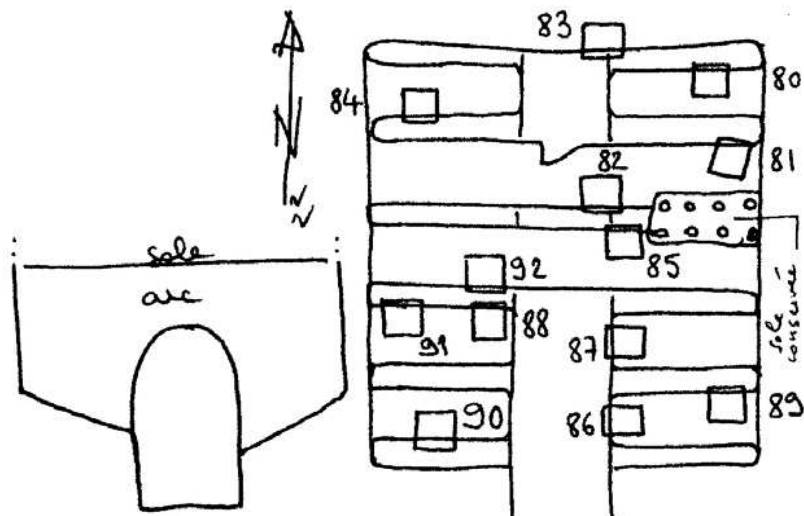
Fecha del muestreo arqueomagnético: 27 Junio 1986

Tipo de estructura y contexto: Gran horno rectangular con 5 arcos. Construido a base de ladrillos. Muy buen estado de conservación. Del horno se conoce el *praefurnium*, o boca del horno, y la cámara de fuego (inferior). Conserva buena parte de los arcos y escasos vestigios de la parrilla perforada (suelo de la cámara de cocción o superior).

Foto :



Plano de la estructura:



Número de muestras y tipo de material:

N	T	N	T
80	M	87	B
81	M	88	B
82	B	89	B
83	M	90	B
84	M	91	M
85	M	92	M
86	B		

Tabla: Número de muestra N y tipo de material T de las mismas: B, ladrillo y M, mortero

Criterios de datación arqueológicos:

Cerámica	Los materiales arqueológicos del estrato que acreditan la actividad del horno evidencian una producción de ánforas de base plana, tipo "Almadrava IV", conjuntamente con cerámicas comunes.
Monedas	No
Estratigrafía y cronología relativa	<p>El registro arqueológico consta, por un lado, de un estrato inferior con abundantes cenizas y fragmentos cerámicos pertenecientes a su periodo de actividad. Sobre el mismo, un potente estrato documenta su proceso de destrucción, con arcilla y materiales constructivos cerámicos pertenecientes a su superestructura.</p> <p>El período de actividad del horno coincide con el de la Fase III, documentado en el Taller I del Alfar de l'Almadrava; cronología precisa fundamentada en el hallazgo de cerámicas "African Red Slip Ware", tipo C, y de piezas numismáticas</p>

Otros métodos:

C14	No
Termoluminescencia	No
Dendrocronología	No

Datación del abandono: 220-250 AD

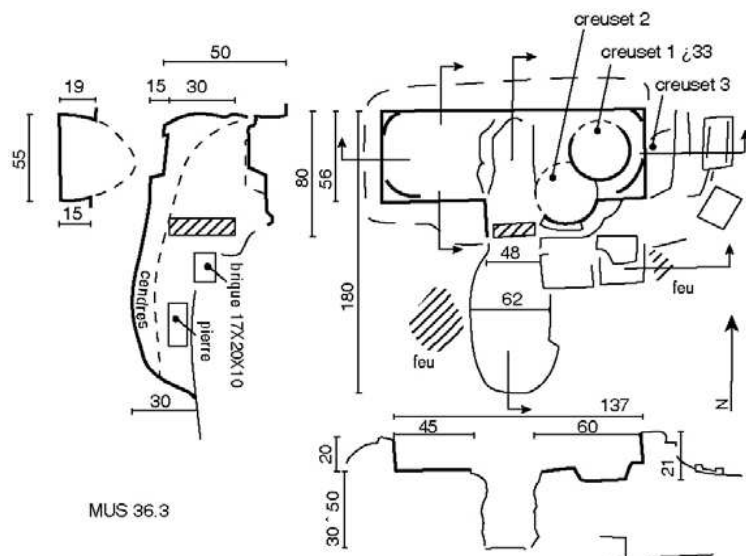
El marco cronológico de la actividad del horno estudiado es 220-250 d. C., es decir, el segundo tercio del siglo III d. C.

MURCIA C/SAGASTA

Arqueólogos responsables de la excavación: J. Navarro y F. Muñoz

Fecha de la excavación: Diciembre 1997 - Enero 1998

Contexto: Por debajo de un barrio de casas andaluzas que se podría fechar a fines del s. XI o principios del XII se documentó una ocupación de carácter artesanal de la que formaría parte el horno.



Bibliografía: La memoria de esta excavación se encuentra actualmente (marzo 05) en prensa; será publicada en las *Memorias de Arqueología. Región de Murcia*. La información procede del informe inédito y nos ha sido facilitado por los directores. Hemos completado dicha información con la que nos facilitó oralmente Jacques Thiriot. Han participado en la escritura y revisión de este documento escrito Pedro Jiménez y Jacques Thiriot.

Fotos y planos de los hornos: Jacques Thiriot

MUS-36.3 (MURG)

Toma de muestras realizada por: Jacques Thiriot

Fecha del muestreo arqueomagnético: 23 Enero 1998

Tipo de estructura y contexto: Parcialmente conservado y construido a base de adobes de distinto tamaño, 19 x 22 x 10 y 17 x 20 x 10 cm. Aunque de planta irregular, las dimensiones internas del horno serían 1.36 de ancho por 0.82 de fondo. Se conservaban las huellas del fondo de dos crisoletas, uno de 28 y otro de 22 cm de diámetro de base, y por la forma que presenta cabe suponer que acogía tres crisoletas: dos de 28 cm y uno de 22 cm.

El elemento más destacable de los encontrados en este área artesanal fue este horno utilizado para la fusión de vidrio y empleado para la fabricación de objetos de este material o para obtener vedrío para la cubierta de la cerámica, a juzgar por la total ausencia de los restos de producción que suelen acompañar los hornos para fabricar vidrio. Estaba realizado en una fosa excavada en el terreno y recubierta de una gruesa capa de arcilla. Su forma es aproximadamente ovalada, presentando tres partes: dos banquetas en los extremos, donde se situaban los crisoletas, y una cubeta central, alargada, en donde se situaría la materia prima para una primera cocción, que era una prolongación del fogón. Éste último era una fosa excavada en el terreno, de forma ovalada y colocada en posición axial. Presentaba señales de numerosas reparaciones a base de arcilla y con fragmentos de crisoletas. Apareció colmatado con abundantes fragmentos de crisoletas.

Foto :



Número de muestras y tipo de material:

N	T	N	T
1	B	12	B
2	B	13	B
3	B	14	B
4	B	15	B
5	B	16	B
6	B	17	C
7	B	18	C
8	B	19	C
9	B	20	C
10	B	21	C
11	B		C

Plano de la estructura:

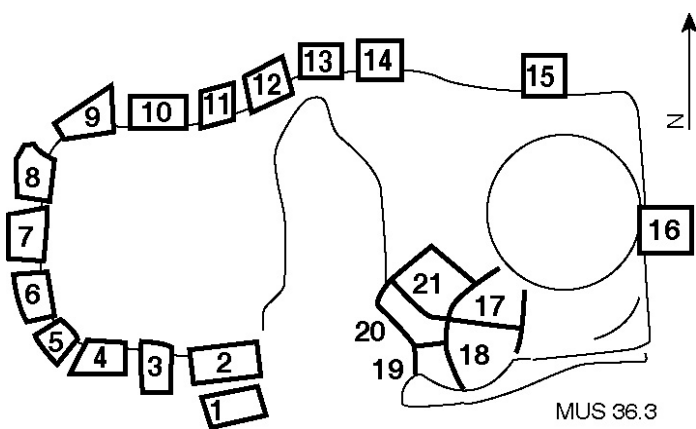


Tabla: Número de muestra N y tipo de material T de las mismas: B, ladrillo y C, vitrificado.

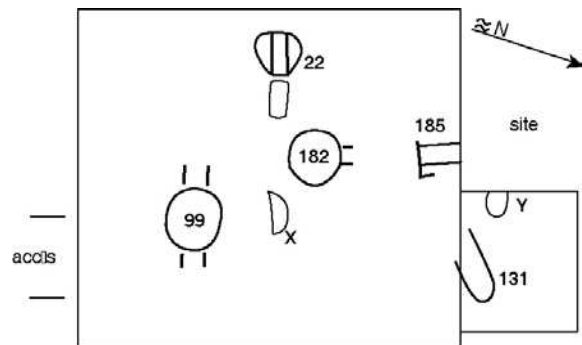
Criterios de datación arqueológicos:	
Cerámica	Asociado al contexto arqueológico del horno se halló un testar con cerámicas del s. XI
Monedas	No
Estratigrafía y cronología relativa	<p>Por debajo de un barrio de casas andalusíes que se podría fechar a fines del s. XI o principios del XII se documentó una ocupación de carácter artesanal de la que formaría parte el horno. (<i>Terminus Ante quem</i> de la estructura: 1100 A.D.)</p> <p>Asociado a este nivel destaca un pequeño testar con cerámicas datables en el siglo XI, y que debió de originarse al llenarse una fosa excavada anteriormente.</p>
Otros métodos:	
C14	No
Termoluminescencia	No
Dendrocronología	No
Datación del abandono: 1000-1100 AD	

MURCIA C/PUXMARINA

Arqueólogos responsables de la excavación: P. Jimenez, J. Navarro

Fecha de la excavación: Julio 1998 - Agosto 1998

Contexto arqueológico: El área estudiada revela un área artesanal particularmente interesante datada del s.XII. A algo más de 100 m de la mezquita y en el interior de las murallas, este espacio está situado al norte de una calle frente al zoco y a proximidad de diversos hábitats. El espacio no parece cortado por muros en el momento de su función artesanal, los muros conservados son posteriores.



Bibliografía: Comunicación oral con Pedro Jimenez y Jacques Thiriot. Participación en la escritura y revisión de este documento escrito de Pedro Jimenez y de Jacques Thiriot.

Jiménez, P., Muñoz-López, F. & Thiriot, J., 2000. Les ateliers urbains de verriers de Murcia au XIIe s. (C. Puxmarina et Pl. Belluga). In : Pétrequin, P., Fluzin, Ph., Thiriot, J., Benoit, P. dir.— Arts du feu et productions artisanales. XXèmes Rencontres internationales d'Antibes, 1999. Editions APDCA, Antibes, 2000, p. 433-452.

Fotos y planos de los hornos: Jacques Thiriot.

MUP-22 (MURH)

Toma de muestras realizada por: Jacques Thiriot

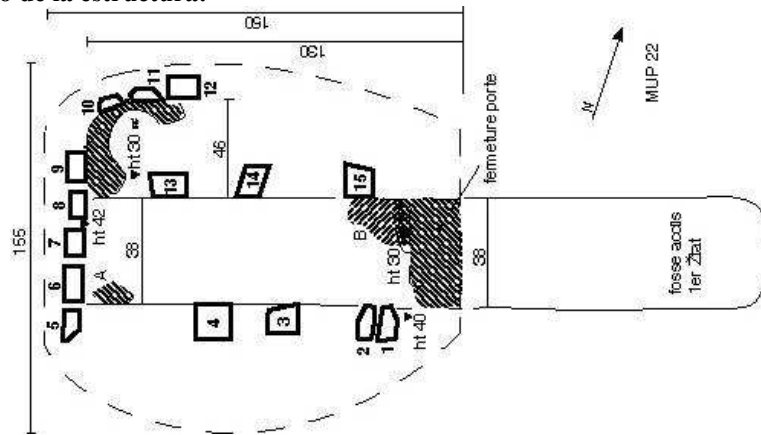
Fecha del muestreo arqueomagnético: 16 Julio 1998

Tipo de estructura y contexto: Pequeño horno de orientación oeste-este adosado a uno de los muros de cierre del espacio artesanal parcialmente conservado. Construido a base de ladrillos aparentemente cocidos trabados con arcilla.

Foto :



Plano de la estructura:



Número de muestras y tipo de material:

N	T	N	T
1	B	9	B
2	B	10	M
3	M	11	M
4	B	12	B
5	B	13	B
6	B	14	B
7	B	15	B
8	B		

Tabla: Número de muestra *N* y tipo de material *T* de las mismas: *M*, mortero y *B*, ladrillo.

MUP-131 (MURI)

Toma de muestras realizada por: Jacques Thiriot

Fecha del muestreo arqueomagnético: 16 Julio 1998

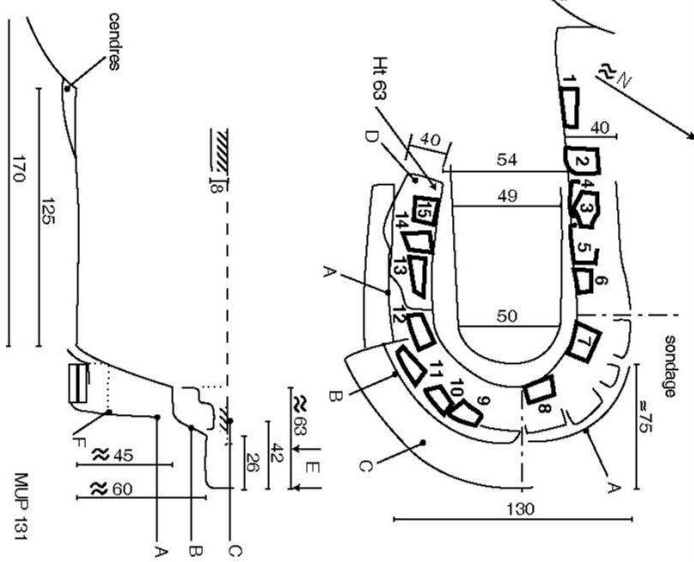
Tipo de estructura y contexto:

Horno alargado (ver dimensiones exactas en el plano de la estructura) construido a base de adobe.

Foto :



Plano de la estructura:



Número de muestras y tipo de material:

N	T	N	T
1	B	9	B
2	B	10	B
3	B	11	B
4	B	12	B
5	B	13	B
6	B	14	B
7	B	15	B
8	B		

Tabla: Número de muestra N y tipo de material T de las mismas: B, ladrillo.

MUP-185 (MURK)

Toma de muestras realizada por: Jacques Thiriot

Fecha del muestreo arqueomagnético: 16 Julio 1998

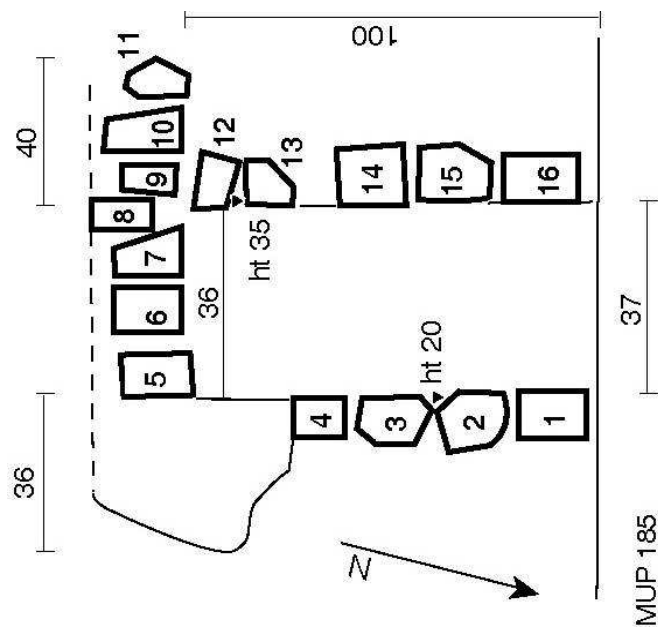
Tipo de estructura y contexto:

Del mismo tipo que el horno MUP-22 (MURH). Con una orientación norte-sur su estado de destrucción no permite saber si posee exactamente la misma morfología que dicho horno. Construido a base de ladrillos. El entorno ha sido destruido por fosas posteriores.

Foto :



Plano de la estructura:



Número de muestras y tipo de material:

N	T	N	T
1	B	9	B
2	B	10	B
3	B	11	B
4	B	12	B
5	B	13	B
6	B	14	B
7	B	15	B
8	B	16	B

Tabla: Número de muestra N y tipo de material T de las mismas: B , ladrillo.

MUP-99A-B-D-E (MURL-M-N-O)

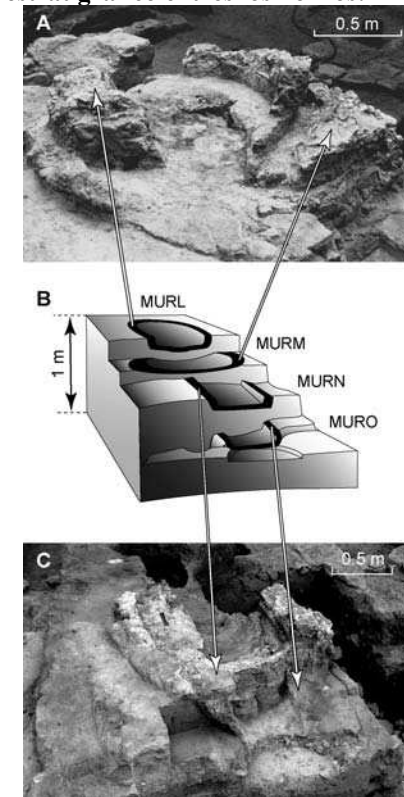
Toma de muestras realizada por: Jacques Thiriot

Fecha del muestreo arqueomagnético: Agosto 1998

Tipo de estructura y contexto:

Situado en las proximidades de dos muros aparentemente posteriores al sur y al oeste. Horno con fases sucesivas que han sido numeradas según el orden de la excavación, contrario al orden cronológico.

Esquema del orden estratigráfico entre los hornos:

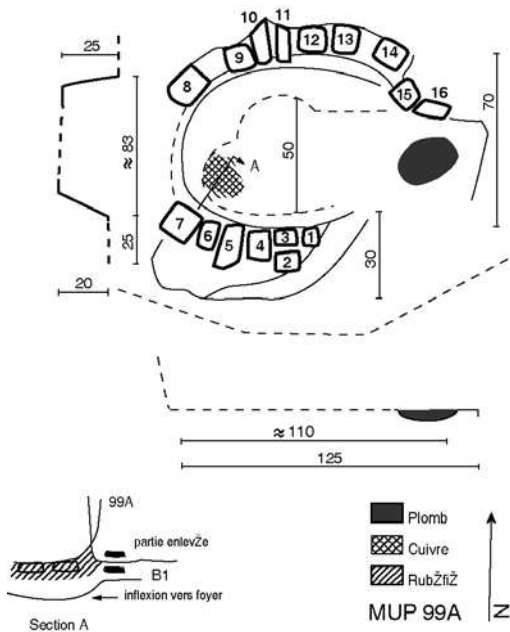


MUP-99A (MURL)

Foto:



Plano de la estructura:



Número de muestras y tipo de material:

N	T	N	T
1	A	9	A
2	A	10	A
3	A	11	A
4	A	12	A
5	A	13	A
6	A	14	A
7	A	15	A
8	A	16	A

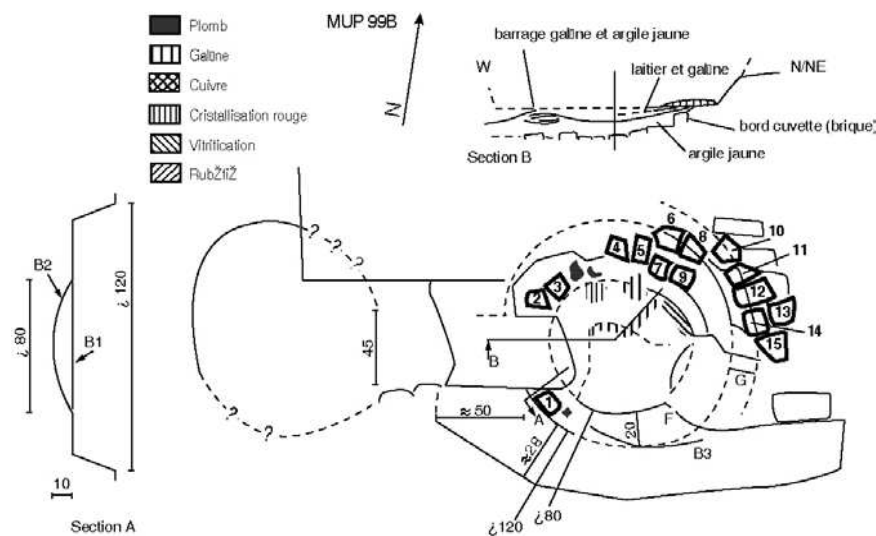
Tabla: Número de muestra N y tipo de material T de las mismas: A, arcilla.

MUP-99B (MURM)

Foto:



Plano de la estructura:



Número de muestras y tipo de material:

N	T	N	T
1	A	9	A
2	A	10	B
3	A	11	A
4	A	12	A
5	A	13	A
6	A	14	A
7	A	15	A
8	A		

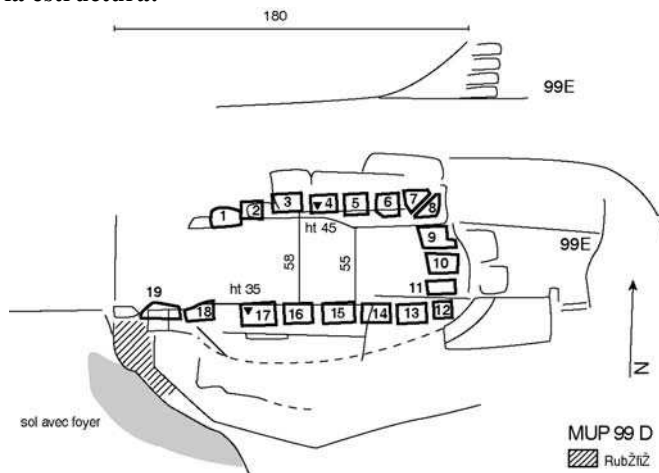
Tabla: Número de muestra N y tipo de material T de las mismas: A, arcilla y B, ladrillo

MUP-99D (MURN)

Foto:



Plano de la estructura:

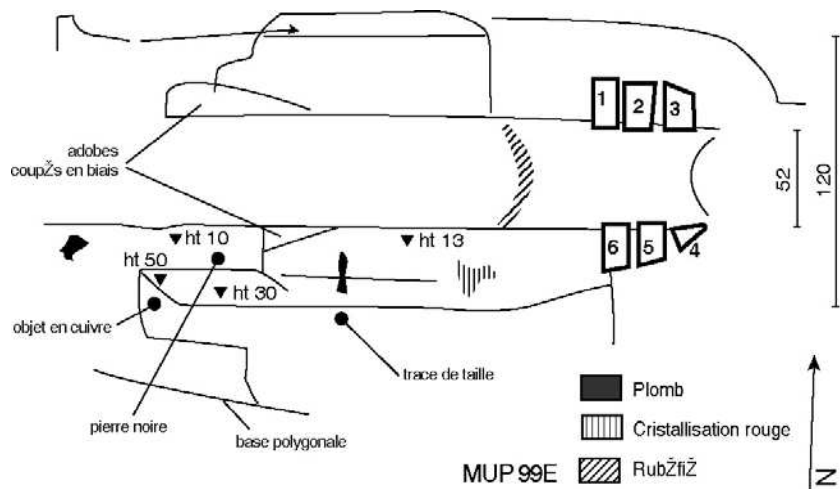


Número de muestras y tipo de material:

N	T	N	T
1	B	11	B
2	B	12	B
3	B	13	B
4	B	14	B
5	B	15	B
6	B	16	B
7	B	17	B
8	B	18	B
9	B	19	B
10	B		

Tabla: Número de muestra N y tipo de material T de las mismas: B, ladrillo

Plano de la estructura:



MUP-99E (MURO)

Foto:



Número de muestras y tipo de material:

N	T
1	A
2	A
3	A
4	A
5	A
6	A

Tabla: Número de muestra N y tipo de material T de las mismas: A, adobe

Criterios de datación arqueológicos (MURO-N-M-L-H-I-K):	
Cerámica	No
Monedas	No
Estratigrafía y cronología relativa	Por orden cronológico del más antiguo al más moderno: muro<murn<murm<murl. Esquema del orden estratigráfico:
Otros métodos:	
C14	No
Termoluminescencia	No
Dendrocronología	No
Datación del abandono: 1100-1200 AD	

CALATRAVA LA VIEJA

Arqueólogos responsables de la excavación: Manuel Retuerce Velasco y Miquel Ángel Hervás Herrera.

Fecha de la excavación: 1997-1998

Contexto arqueológico: Calatrava la Vieja (Carrión de Calatrava, Ciudad Real) está situada a orillas del río Guadiana, a unos 13 km al este de la capital provincial. Instaladas en una colina, la alcazaba y la medina están rodeadas de murallas (unas 4 ha) y de arrabales de unas 15 ha con, entre otras cosas, talleres de cerámica y un molino datado como del s.X. La población de este área disminuye mucho a partir de la definitiva conquista cristiana de 1212 A.D., después de una breve ocupación almohade (1195-1212 A.D.), este hecho fue favorizado por la el carácter insalubre de las aguas del Guadiana. El abandono definitivo tiene lugar a principios del s. XV tras haber sido una Encomienda de la orden de Calatrava (con una iglesia y un poblamiento en el interior del castillo). Análisis de microscopía óptica prueban la producción local de reflejo metálico en lo que fue la Calatrava almohade. Tres hornos han sido muestreados: los hornos CV: 218 (CALA) y 250 (CALB), que se encuentran situados al norte de la alcazaba, en las cercanías de lo que fue una sala de audiencias de época islámica, y el horno 252 (CALC), situado más al este, y cuya datación puede estar cercana al abandono definitivo de Calatrava a principios del s.XV.

Bibliografía: Comunicación oral con Manuel Retuerce y Jacques Thiriot. Participación en la escritura y revisión de este documento escrito de Manuel Retuerce y de Jacques Thiriot.

Retuerce Velasco. Manuel & Hervás, Miguel Ángel (2004): "Excavaciones arqueológicas en Calatrava la Vieja. Planteamientos y principales resultados". *Investigaciones arqueológicas en Castilla-La Mancha. 1996-2002*. Patrimonio Histórico-Arqueología. Castilla-La Mancha, 18. Toledo.
Hervás, Miguel Ángel & Retuerce, Manuel (2000): "Calatrava la Vieja, capital islámica de la región". *El patrimonio arquelógico de Ciudad Real. Métodos de trabajo y actuaciones más recientes*. Luis de Benítez de Lugo Enrich (coord.). p. 297-322. Valdepeñas.

Hervás, Miguel Ángel, Retuerce, Manuel & Thiriot, Jacques (2000): "La fabrication du plâtre au début du XX^e siècle à Calatrava-la-Vieja. (Castilla-La Mancha, Espagne). Maison et installations de la plâtrière Juana la «Perdida»". *Arts du feu et productions artisanales. XX^e Rencontres Internationales et d'Histoire d'Antibes*. (1999). Antibes.

Retuerce Velasco. Manuel & Hervás, Miguel Ángel (2000): "Calatrava. Capital de La Mancha". *La Aventura de la Historia*. 21 (julio, 2000), p. 84-91.

Retuerce Velasco. Manuel (1999): "Calatrava la Vieja". *Itinerario cultural de Almorávides y Almohades. Magreb y Península Ibérica*. Fundación El Legado andalusí. Granada.

Retuerce Velasco. Manuel & Hervás, Miguel Ángel (1999): "Calatrava la Vieja. Fortificación de una ciudad islámica de la Meseta". *Castillos de España*, 113, p. 23-43.

Hervás, Miguel Ángel & Retuerce, Manuel (1999): "La gran sala con piscina. ¿Un baño árabe en el alcázar de Calatrava la Vieja?. I Jornadas de Patrimonio Histórico en Ronda: "Baños árabes. Arqueología y Restauración" (Ronda, 1998). Eds.: Manuel Acién; Pedro Aguayo & José Manuel Castaño. p. 129-161. Ronda.

Retuerce Velasco. Manuel (1996): "Documentación arqueológica de una ciudad almohade de la Meseta: Calatrava". *Alarcos, 1195. Actas del congreso internacional conmemorativo del VIII centenario de la batalla de Alarcos*. (Ciudad Real, 1995). p. 211-222. Ciudad Real.

Zozaya, Juan, Retuerce, Manuel & Aparicio, Alberto (1995): "Cerámica andalusí de reflejo dorado: 1195-1212". *5ème Colloque sur la Céramique Médiévale* (Rabat, 1991). p. 121-124. Rabat.

Fotos y planos de los hornos: Jacques Thiriot.

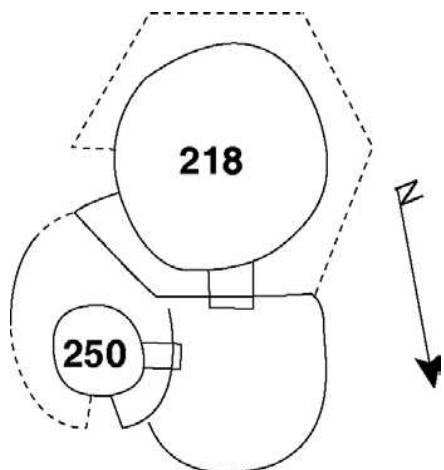
CV-218 (CALA)

Toma de muestras realizada por: Jacques Thiriot

Fecha del muestreo arqueomagnético: Octubre-Noviembre 1998

Tipo de estructura y contexto:

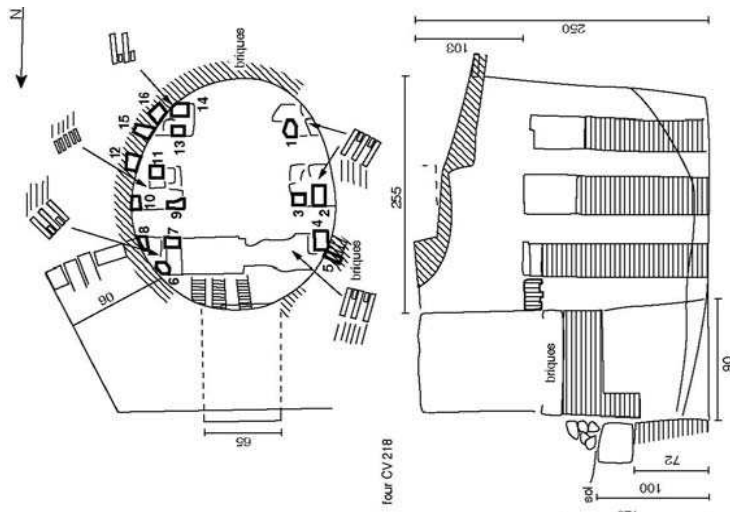
Horno circular de unos 255 cm de diámetro construido, en una fosa excavada en rellenos antrópicos procedente de los derrumbes de la sala de audiencias islámica situada al oeste y del echadizo de basura arrojado desde una fragua cercana. Fue construido a base de ladrillos aparentemente cocidos y trabados con arcilla y se localiza en la parte occidental del alcázar. El fondo del horno está cubierto por una capa de arcilla cocida por la utilización del horno. La puerta del horno comunica con una fosa de acceso común a esta estructura y al horno vecino CV-250 (CALB).



Posición relativa de los hornos CV 218 y CV 250

Foto del horno CV-218 :



Plano de la estructura CV-218:**Número de muestras y tipo de material CV-218:**

N	T	N	T
1	B	9	B
2	B	10	B
3	B	11	B
4	B	12	B
5	B	13	B
6	B	14	B
7	B	15	B
8	B	16	B

Tabla: Número de muestra N y tipo de material T de las mismas: B, ladrillo.

Criterios de datación arqueológicos:

Cerámica	Cerámica de época cristiana, compuesta mayoritariamente de grandes fragmentos de tinajas.
Monedas	No
Estratigrafía y cronología relativa	<p>-Horno con acceso común al horno CV-250 (CALB). Por tanto, muy probablemente, ambos hornos fueron construidos a la vez para la realización de piezas diferentes y utilizados simultáneamente: piezas grandes, como tinajas, en el horno CV-218, y piezas más pequeñas, en el CV-250.</p> <p>-Horno cristiano-mudéjar correspondiente al dominio de la Encomienda de la orden de Calatrava que fue construido en un momento posterior a la conquista cristiana de la ciudad, acaecida en 1212 A.D. (<i>Terminus Post Quem</i> de la estructura: 1212 A.D.)</p>
Otros métodos:	
C14 No	
Termoluminescencia No	
Dendrocronología No	
Datación del abandono: 1275-1300 AD	

CV-250 (CALB)

Toma de muestras realizada por: Jacques Thiriot

Fecha del muestreo arqueomagnético: Octubre-Noviembre 1998

Tipo de estructura y contexto:

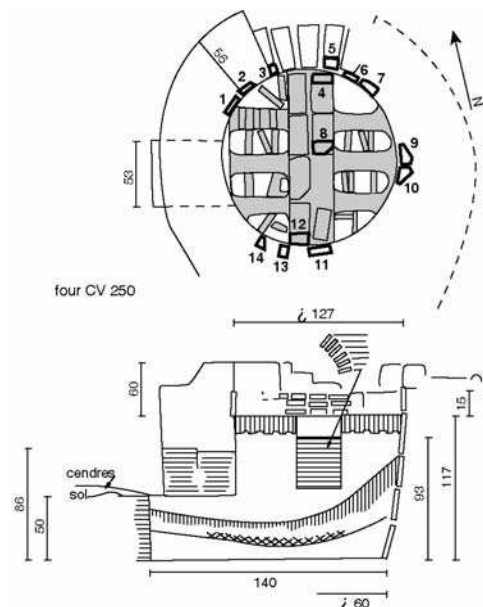
Horno también circular y con las mismas características que el anterior, CV-218 (CALA), el diámetro es de unos 127 cm. Situado en la mitad Norte de la Alcazaba en las cercanías de un gran edificio islámico abandonado e identificado como una sala de audiencias.

La puerta del horno comunica con una fosa de acceso común a este horno y al horno CV-250 (CALB).

Foto del horno CV-250 :



Plano de la estructura CV-250:



Número de muestras y tipo de material CV-250:

N	T	N	T
1	B	8	B
2	B	9	B
3	B	10	B
4	B	11	B
5	B	12	B
6	B	13	B
7	B	14	B

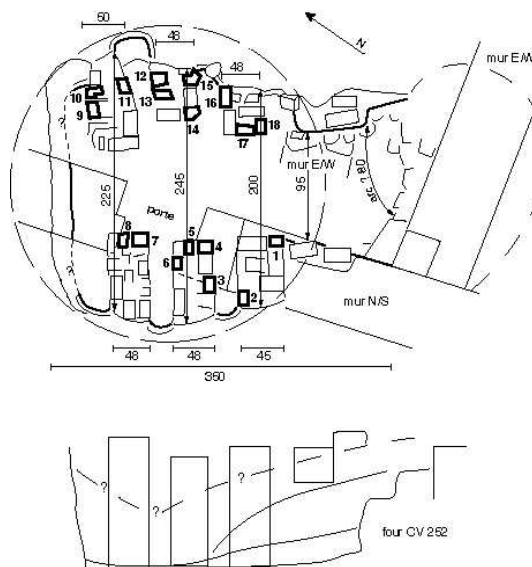
Tabla: Número de muestra N y tipo de material T de las mismas: B, ladrillo.

Criterios de datación arqueológicos:	
Cerámica	Cerámica de época cristiana, compuesto de piezas con un fuerte componente hereditario de época anterior islámica (almohade)—en cuanto a las formas y a los acabados—, que son mayoritarias, y de ejemplares, en menor cantidad, de clara ascendencia castellana normeseteña.
Monedas	No
Estratigrafía y cronología relativa	<p>-Horno con acceso común al horno CV-218 (CALB). Por tanto, muy probablemente, ambos hornos fueron construidos a la vez para la realización de piezas diferentes y utilizados simultáneamente: piezas grandes, como tinajas, en el horno CV-218, y más pequeñas, en el CV-250.</p> <p>-Horno cristiano-mudéjar correspondiente al dominio de la Encomienda de la orden de Calatrava que fue construido en un momento posterior a la conquista cristiana de la ciudad, sucedida en 1212 A.D. (<i>Terminus Post Quem</i> de la estructura: 1212 A.D.)</p>
Otros métodos:	
C14	No
Termoluminescencia	No
Dendrocronología	No
Datación del abandono: 1275-1300 AD	

CV-252 (CALC)**Toma de muestras realizada por:** Jacques Thiriot**Fecha del muestreo arqueomagnético:** Agosto 2000**Tipo de estructura y contexto:**

Horno también circular de unos 250 cm de diámetro construido a bases de piedras y ladrillos trabados con arcilla.

Foto del horno CV-252:

Plano de la estructura CV-252:**Número de muestras y tipo de material CV-252:**

N	T	N	T
1	B	10	B
2	B	11	B
3	B	12	B
4	B	13	B
5	B	14	B
6	B	15	B
7	B	16	B
8	B	17	B
9	B	18	B

Tabla: Número de muestra N y tipo de material T de las mismas: B, ladrillo.

Criterios de datación arqueológicos:

Cerámica	Exclusivamente grandes fragmentos de tinajas bajomedievales. S. XIV-XV.
Monedas	No
Estratigrafía y cronología relativa	El horno se levantó en la zona oriental del alcázar, junto a unas estancias abovedadas bajomedievales. Y en concreto, en un espacio que estaba abandonado. La excavación de la oquedad de la cámara de fuego afectó a estructuras constructivas de época islámica que, en parte, fueron aprovechadas como elementos de apoyo.
Otros métodos:	
C14	
Termoluminescencia	
Dendrocronología	
Datación del abandono: 1400-1420 AD	

VALENCIA VELLUTERS

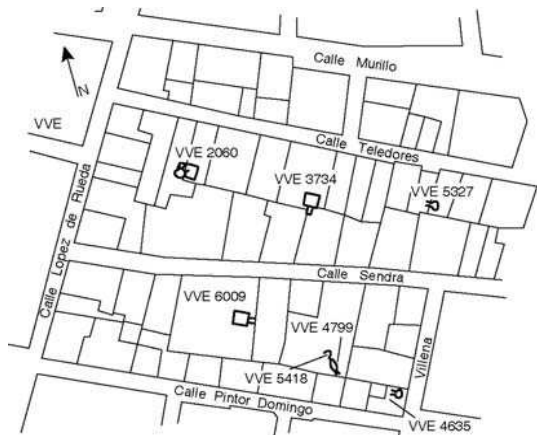
Arqueólogos responsables de la excavación:

Dirección científica: M. Isabel García Villanueva, Carmen Marín y Remedios Martínez.

Excavación de las estructuras: Enrique Ruiz Val (VALI y VALL), Lourdes Roca Fernández (VALK y VALM) y Javier Máñez Rodero (VALN).

Fecha de la excavación: Febrero-Agosto 2000.

Contexto arqueológico: La excavación, de 5097 m², está situada entre las murallas islámica y cristiana de la parte oeste de Valencia en las cercanías de la puerta de Quart (puerta de la muralla cristiana). Este recinto estuvo ocupado en todos los períodos medievales y modernos por hábitats y construcciones de diversos usos. Se encontraron numerosos hornos domésticos y artesanales, tanto de vidrio como alfareros, correspondientes a las distintas actividades realizadas durante la ocupación del territorio.



Bibliografía: Comunicación oral con Isabel García Villanueva y Jacques Thiriot. Participación en la escritura y revisión de este documento escrito de Isabel García Villanueva y de Jacques Thiriot.

Fotos y planos de los hornos: Jacques Thiriot.

VVE-3734 (VALI)

Toma de muestras realizada por: Jacques Thiriot

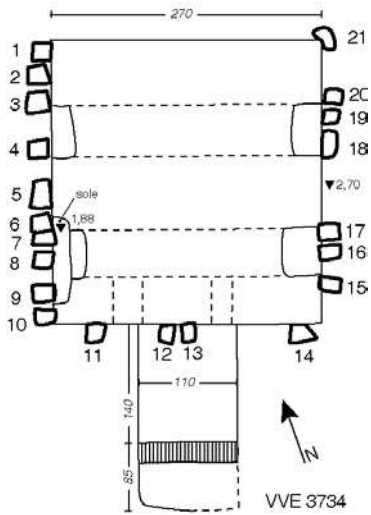
Fecha del muestreo arqueomagnético: Agosto 2000

Tipo de estructura y contexto:

Gran horno de ladrillos excavado en el sustrato geológico. Las dimensiones del horno conservado son 2.50 × 2.70 m por 2.70 m de altura, posee únicamente dos arcos transversales construidos a base de ladrillos. La parrilla se situaría a unos 1.88 m desde la base del horno. Para obtener la estructura completa habría que restituir, al menos, 2 m de altura. La cámara de cocción, probablemente no se hallaría cubierta y poseería una puerta lateral de carga. El fogón, cuyo suelo se encuentra aproximadamente al mismo nivel que la base del horno, posee 2.25 m de longitud y se abre a la cámara de combustión mediante un arco de 1.10 m de largo y 1.60 m de altura.

Foto:



Plano de la estructura:**Número de muestras y tipo de material:**

N	T	N	T
1	A	12	A
2	B	13	A
3	B	14	A
4	B	15	A
5	B	16	A
6	B	17	A
7	B	18	A
8	B	19	A
9	B	20	A
10	B	21	A
11	A		

Tabla: Número de muestra N y tipo de material T de las mismas:
A, arcilla del sustrato geológico y B, ladrillo.

Criterios de datación arqueológicos:

er á- m ic	No
Mo ne- das	No
Estratigrafía y cronología relativa	<ul style="list-style-type: none"> -No se poseemos datos para la datación de la creación de esta estructura ya que se halla excavada directamente en el substrato geológico. En cuanto a su momento final de uso, tan sólo sabemos que el horno, destruido hasta la cámara de combustión y colmatado parcialmente con sus escombros en fechas indeterminadas, se llenó en el siglo XIII con tierras en las que se recuperaron fragmentos de cerámica con barniz de plomo, cerámica común bizcochada y cerámica de cocina de pasta gris. Este conjunto es propio de época ya cristiana en Valencia, concretamente del s. XIII. -En excavaciones posteriores realizadas en el mismo barrio de Velluters y situadas al sur de la que nos ocupa, se han localizado tres nuevos hornos del mismo tipo cuya excavación apunta una cronología para la instalación alfarera (a la que debieron pertenecer este horno y el VVE-6009) de época islámica almohade, es decir, fines del s.XII e inicios del s.XIII ya que la conquista cristiana de Valencia se efectúa en el año 1238 AD. -Proximidad de hábitat de nueva planta de época cristiana (s.XIII). -Se excavó un suelo de la 2ª mitad del s.XIV sobre la fosa de acceso al horno. (<i>Terminus Ante Quem</i> del abandono: 1400 A.D.) -Atendiendo a la cerámica podemos pensar que probablemente el horno se colmató en algún momento dentro del s. XIII, entre 1238 y 1300 AD), en cualquier caso, a partir de fechas ya cristianas. (<i>Terminus Post Quem</i> del abandono: 1238 A.D.)
Otros métodos:	
C14	No
Termoluminescencia	No
Dendrocronología	No
Datación del abandono: 1238-1400 AD	
Horno posiblemente islámico abandonado a partir de fechas ya cristianas dentro del siglo XIII, entre 1230 y 1300 AD.	

VVE-6009 (VALN)

Toma de muestras realizada por: Jacques Thiriot

Fecha del muestreo arqueomagnético: Agosto 2000

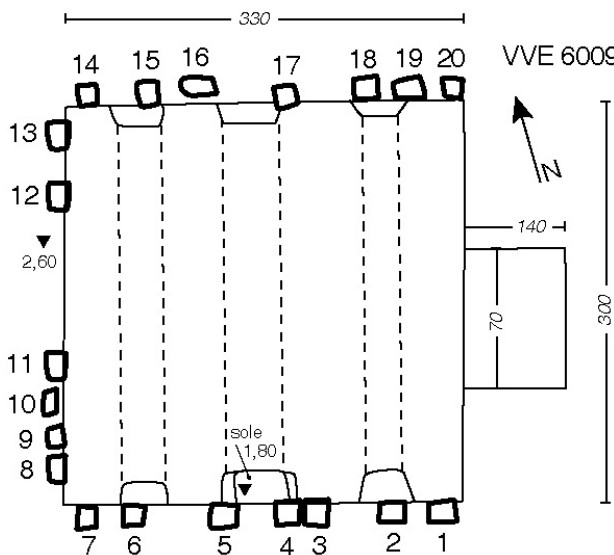
Tipo de estructura y contexto:

-Gran horno de ladrillos excavado en el sustrato geológico. Las dimensiones del horno conservado son de $3 \times 3.30 \text{ m} \times 2.60 \text{ m}$ de profundidad, posee tres grandes arcos transversales y espaciados construidos a base de ladrillos. Horno de características similares al horno VVE-3734. Este horno presentaba paredes excepcionalmente cocidas. Este hecho está sin duda relacionado con el gran volumen útil del horno, estimado en unos 30 m^3 , y con la larga duración de utilización del horno, deducida a partir de las múltiples reparaciones realizadas tanto en la cámara de cocción como en la cámara de combustión.

Foto:



Plano de la estructura:



Número de muestras y tipo de material:

N	T	N	T
1	A	12	A
2	A	13	A
3	A	14	A
4	A	15	A
5	A	16	A
6	A	17	A
7	A	18	A
8	A	19	A
9	A	20	A
10	A		
11	A		

Tabla: Número de muestra N y tipo de material A de las mismas. A, adobe.

Criterios de datación arqueológico:		Otros métodos:
Cerámica	No	C14 No
Monedas	No	Termoluminescencia No
Estratigrafía y cronología relativa	<p>-Sobre la última capa de cenizas de producción del horno, se creó un estrato resultante del derrumbe parcial de la superestructura sobre el que, a su vez, se formó un estrato de tierra arcillosa de escaso espesor que contenía cerámicas de los s. XI-XII. Finalmente, la cámara de combustión fue rellenada con deshechos de la destrucción del horno mezclados con cerámicas de la primera mitad del s.XIV (<i>Terminus Ante Quem</i> del abandono: 1350 A.D.)</p> <p>-La fosa de acceso al horno aparece colmatada con tierra arenosa mezclada con abundantes restos de ladrillo, tierra quemada y tejas, entre la que se recuperó un alto porcentaje de cerámica de cronología almohade y escasos fragmentos de cántaro, lebrillo, mortero y cerámica con barniz de plomo de época ya cristiana. Estos resultados podrían indicar que la fosa de acceso al horno pudo estar en activo hasta, al menos, época almohade o, incluso, en momentos posteriores a la conquista cristiana de Valencia acaecida en 1238 AD. La fosa se colmó en algún momento dentro del s. XIII, entre 1238 y 1300 AD), en cualquier caso, a partir de fechas ya cristianas. (<i>Terminus Post Quem</i> del abandono: 1238 A.D.)</p> <p>-En superficie aparecía cubierto por niveles de la primera mitad del s. XIV y afectado por una fosa rellena con tierras entre las que también aparecía cerámica datada en la 1ª mitad del s.XIV. (<i>Terminus Ante Quem</i> del abandono: 1350 A.D.)</p> <p>-En excavaciones posteriores realizadas en el mismo barrio de Velluters y situadas al sur de la que nos ocupa, se han localizado tres nuevos hornos del mismo tipo cuya excavación apunta una cronología para la instalación alfarera, a la que debieron pertenecer este horno y el VVE-3734, de época islámica almohade, es decir, fines del s.XII e inicios del s.XIII ya que la conquista cristiana de Valencia se efectúa en el año 1238 AD.</p> <p>-Proximidad de hábitat de nueva planta de época cristiana (s.XIII).</p>	Dendrocronología No
		Datación del abandono: 1238-1350 AD
		Horno posiblemente islámico abandonado probablemente a partir de fechas ya cristianas dentro del s. XIII, entre 1238 y 1300 AD.

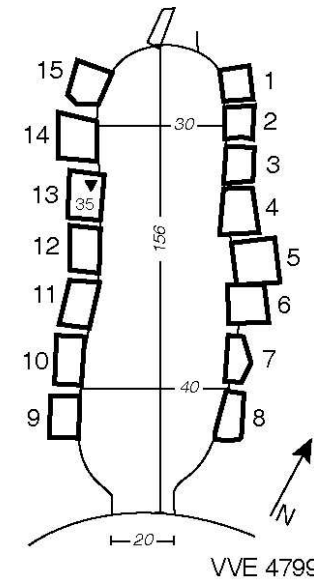
VVE-4799 (VALK)

Toma de muestras realizada por: Jacques Thiriot

Fecha del muestreo arqueomagnético: Agosto 2000

Tipo de estructura y contexto: Horno utilizado para la fusión y realización de piezas de vidrio. Construido a base de adobes perpendiculares a la pared y trabados con mortero realizado con la misma arcilla del adobe. La puerta del horno es de pequeño tamaño, unos 20 cm de largo y una posible altura de 30 cm. Una fosa posterior ha destruido el acceso al horno, en el relleno de la misma encontramos múltiples testimonios de su utilización para fabricación de vidrio. El tamaño del horno es de unos 40 cm de ancho por 156 cm de longitud, la altura restituida del mismo es de unos 45 cm.

Foto:

**Plano de la estructura:****Número de muestras y tipo de material:**

N	T	N	T
1	A	9	A
2	A	10	A
3	A	11	A
4	A	12	A
5	A	13	A
6	A	14	A
7	A	15	A
8	A		

Tabla: Número de muestra N y tipo de material T de las mismas: A, adobe.

Criterios de datación arqueológico:

Cerámica	No
Monedas	No
Estratigrafía y cronología relativa	<ul style="list-style-type: none"> -Horno construido en un estrato de la 1^a mitad del s. XIV. (<i>Terminus Post Quem</i> del abandono: 1300 A.D.) -Anulado por un suelo de mediados del s.XV. (<i>Terminus Ante Quem</i> del abandono: 1450 A.D.) -Anulado asimismo por el horno VVE.5418 (VALM)
Otros métodos:	
C14	No
Termoluminiscencia	No
Dendrocronología	No
Datación del abandono: 1300-1450 AD	

VVE-5418 (VALM)

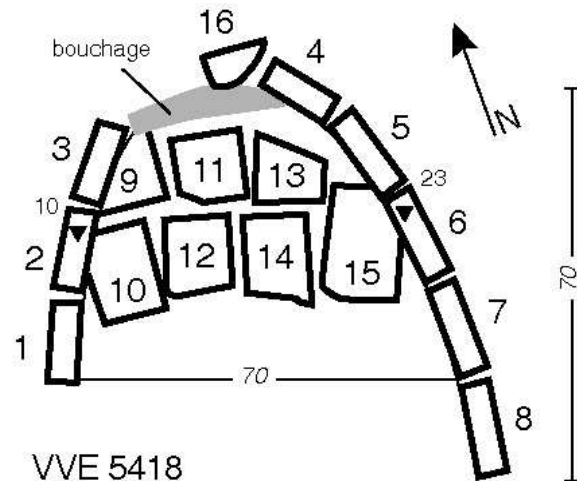
Toma de muestras realizada por: Jacques Thiriot

Fecha del muestreo arqueomagnético: Agosto 2000

Tipo de estructura y contexto: Horno utilizado para la fusión y realización de piezas de vidrio. Construido a base de pequeños ladrillos dispuestos sin orden y trabados con abundante mortero. Sólo se ha conservado la mitad de la estructura: la anchura de unos 70 cm y la mitad conservada de una longitud de unos 70 cm.

Foto:



Plano de la estructura:**Número de muestras y tipo de material:**

N	T	N	T
1	B	9	A
2	B	10	A
3	B	11	A
4	B	12	A
5	B	13	A
6	B	14	A
7	B	15	A
8	B	16	B

Tabla: Número de muestra N y tipo de material T de las mismas: A, adobe. B, ladrillo.

Criterios de datación arqueológicos:	
Cerámica	No
Monedas	No
Estratigrafía y cronología relativa	<ul style="list-style-type: none"> -Horno construido en un estrato de la 1^a mitad del s. XIV. (<i>Terminus Post Quem</i> del abandono: 1300 A.D.) -Anulado por un suelo de mediados del s.XV. (<i>Terminus Antet Quem</i> del abandono: 1450 A.D.) -Anula al horno VVE.4799 (VALK)
Otros métodos:	
C14	No
Termoluminescencia	No
Dendrocronología	No
Datación del abandono: 1300-1450 AD	

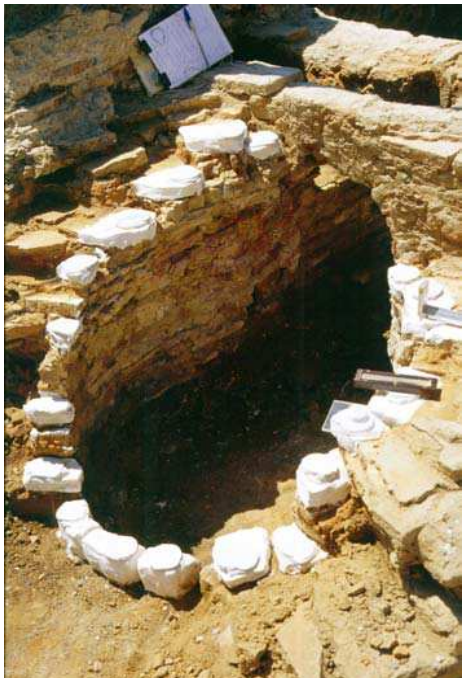
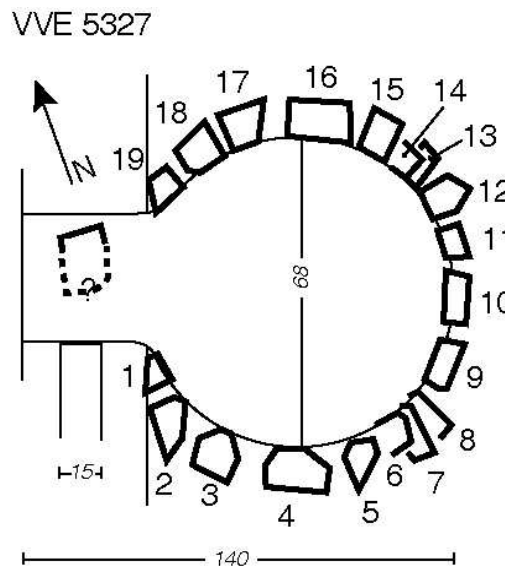
VVE-5327 (VALL)

Toma de muestras realizada por: Jacques Thiriot

Fecha del muestreo arqueomagnético: Agosto 2000

Tipo de estructura y contexto: Horno, probablemente artesanal, construido con ladrillos trabados con arcilla excepto la hilada de base realizada con adobes. La cámara de combustión es cilíndrica, de 68 cm de diámetro, y el acceso se haría a través de un arco de 32 cm de ancho y 50 cm de altura.

Foto:

**Plano de la estructura:****Número de muestras y tipo de material:**

N	T	N	T
1	B	11	A
2	B	12	B
3	B	13	B
4	B	14	B
5	B	15	B
6	B	16	B
7	B	17	B
8	B	18	B
9	A	19	B
10	A		

Tabla: Número de muestra N y tipo de material T de las mismas: A, adobe y B, ladrillo.

Criterios de datación arqueológicos:	
Cerámica	Loza valenciana con motivo de las solfas (fines del s.XV- inicios del s.XVI) recuperada en una capa de cenizas depositada en el fondo del horno.
Monedas	No
Estratigrafía y cronología relativa	<p>La construcción del horno afecta a niveles de ocupación anteriores fechados en la 1^a mitad del siglo XV. (<i>Terminus Post Quem</i> del abandono: 1400 AD)</p> <p>Anulando la escalera de acceso al horno se excavó un estrato de fines del s.XVI- primer cuarto del s.XVII datado a partir de la loza dorada valenciana con el motivo de las espirales achataadas y loza italiana con decoración a berettino. (<i>Terminus Ante Quem</i> del abandono: 1625 A.D.)</p>
Otros métodos:	
C14	No
Termoluminiscencia	No
Dendrocronología	No
Datación del abandono: 1575-1625 AD	
<p>Probablemente el horno se construye en la segunda mitad del s.XV y es usado durante el s.XVI, siendo abandonado a finales de esta centuria o inicios de la siguiente.</p>	

PATERNA (CALLE DE LOS HUERTOS)

Arqueólogos responsables de la excavación: Mercedes Mesquida

Fecha de la excavación: 1997

Contexto:

En la Edad Media, durante la dominación musulmana, Paterna fue un pueblo dominado por un castillo o alcázar que formaba parte del círculo de defensas de la capital, Valencia. Las primeras noticias que conocemos son de 1064 cuando el Conde de Barcelona derrotó a los musulmanes de Paterna y puso sitio a la ciudad de Valencia pero no consiguió tomarla. En 1238 los musulmanes rinden a Jaime I de Aragón.

Bibliografía: Comunicación oral con Mercedes Mesquida y Jacques Thiriot.
Mesquida-García, M., 2002. La cerámica de Paterna, Reflejos del Mediterraneo, Museo de Bellas Artes de Valencia.
Mesquida-García, M., López-Peris, J.E., Prados, S. & Smolka R., 2001. Las Ollerías de Paterna. Tecnología y producción, Volumen I. Siglos XII y XIII, Ajuntament de Paterna.

Fotos y planos de los hornos: Jacques Thiriot.

H21A (PATA)

Toma de muestras realizada por: Jacques Thiriot

Fecha del muestreo arqueomagnético: Julio 1997

Tipo de estructura y contexto:

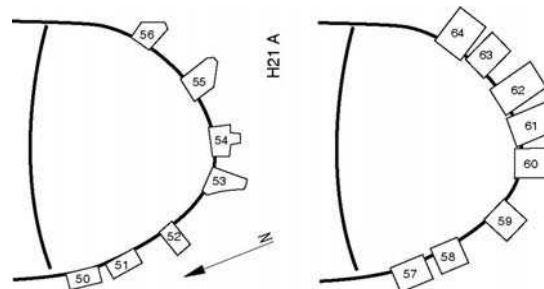
Se han estudiado dos fases del mismo horno, PATA and PATB, siendo PATB la fase más moderna. Se encontraron cerámicas del s. XV asociadas a la primera fase de la estructura. El abandono de la primera fase está datado por contrastes arqueológicos (cerámicas) entre el 1450-1500 AD. Lo que sitúa el *Terminus Ante Quem*

Quem de la primera fase en 1500 AD. La segunda fase se cree que estuvo en uso durante, al menos, 75 años (Mesquida-García, comunicación oral), aunque no es posible establecer el *Terminus Ante Quem* de la segunda fase. Para evitar cualquier error en la datación de las estructuras se ha propuesto un intervalo de edad amplio para el abandono de la segunda fase entre 1525-1650 AD.

Foto:



Plano de la estructura:



Número de muestras y tipo de material:

N	T	N	T
50	B	58	B
51	B	59	B
52	B	60	B
53	B	61	B
54	B	62	B
55	B	63	B
56	B	64	B
57	B		

Tabla: Número de muestra N y tipo de material T de las mismas: B, ladrillo.

H21B (PATB)

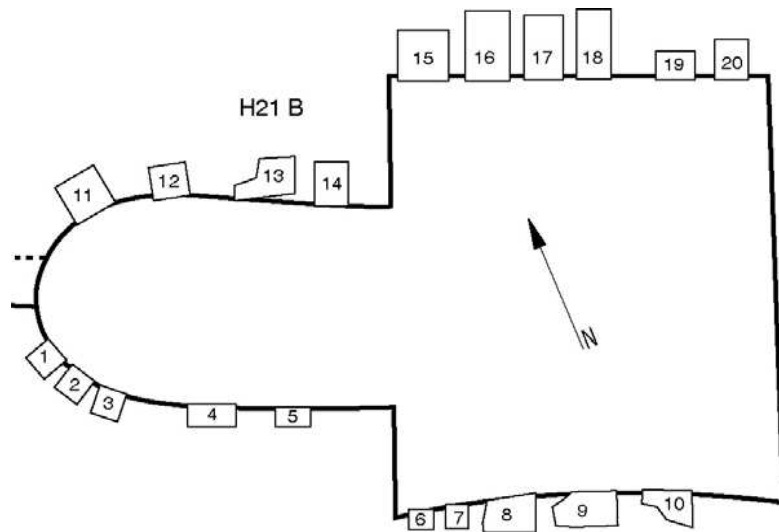
Toma de muestras realizada por: Jacques Thiriot

Fecha del muestreo arqueomagnético: Julio 1997

Foto:



Plano de la estructura:



Número de muestras y tipo de material:

N	T	N	T
1	B	11	B
2	B	12	B
3	B	13	B
4	B	14	B
5	B	15	B
6	B	16	B
7	B	17	B
8	B	18	B
9	B	19	B
10	B	20	B

Tabla: Número de muestra N y tipo de material T de las mismas: B, ladrillo.

Criterios de datación arqueológico (PATA y PATB):

Cerámica	Si
Monedas	No
Estratigrafía y cronología relativa	PATA anterior a PATB

Otros métodos:

C14	No
Termoluminescencia	No
Dendrocronología	No

**Datación del abandono primera fase: 1300-1450 AD
Datación del abandono segunda fase: 1525-1650 AD**

PATERNA (TESTAR DEL MOLI)

Arqueólogos responsables de la excavación: Mercedes Mesquida y François Amigues

Fecha de la excavación: Junio 1986

Contexto arqueológico:

En la Edad Media, durante la dominación musulmana, Paterna fue un pueblo dominado por un castillo o alcázar que formaba parte del círculo de defensas de la capital, Valencia. Las primeras noticias que conocemos son de 1064 cuando el Conde de Barcelona derrotó a los musulmanes de Paterna y puso sitio a la ciudad de Valencia pero no consiguió tomarla. En 1238 los musulmanes rinden a Jaime I de Aragón.

Bibliografía: Comunicación oral con Mercedes Mesquida y Jacques Thiriot
Mesquida-García, M., 2002. La cerámica de Paterna, Reflejos del Mediterraneo,
Museo de Bellas Artes de Valencia.

Mesquida-García, M., López-Peris, J.E., Prados, S. & Smolka R., 2001. Las
Ollerías de Paterna. Tecnología y producción, Volumen I. Siglos XII y XIII,
Ajuntament de Paterna.

Fotos y planos de los hornos: Jacques Thiriot.

41A (PATH)

Toma de muestras realizada por: Jacques Thiriot

Fecha del muestreo arqueomagnético: 23 Junio 1986

Tipo de estructura y contexto: Horno de mesa construido a base de ladrillos

Foto :



Número de muestras y tipo de material:

N	T	N	T
1	B	7	B
2	B	8	B
3	B	9	B
4	B	10	B
5	B	11	B
6	B	12	B

Tabla: Número de muestra N y tipo de material T de las mismas: B; ladrillo.

Criterios de datación arqueológicos:

Cerámica	Cerámicas comunes pintadas de finales del s.XIV, principios del s. XV, lo que permite situar el <i>Terminus Post Quem</i> de la estructura en 1375 AD.
Monedas	No
Estratigrafía y cronología relativa	No

Otros métodos:

C14	No
Termoluminescencia	No
Dendrocronología	No

Datación del abandono: 1450-1600 AD

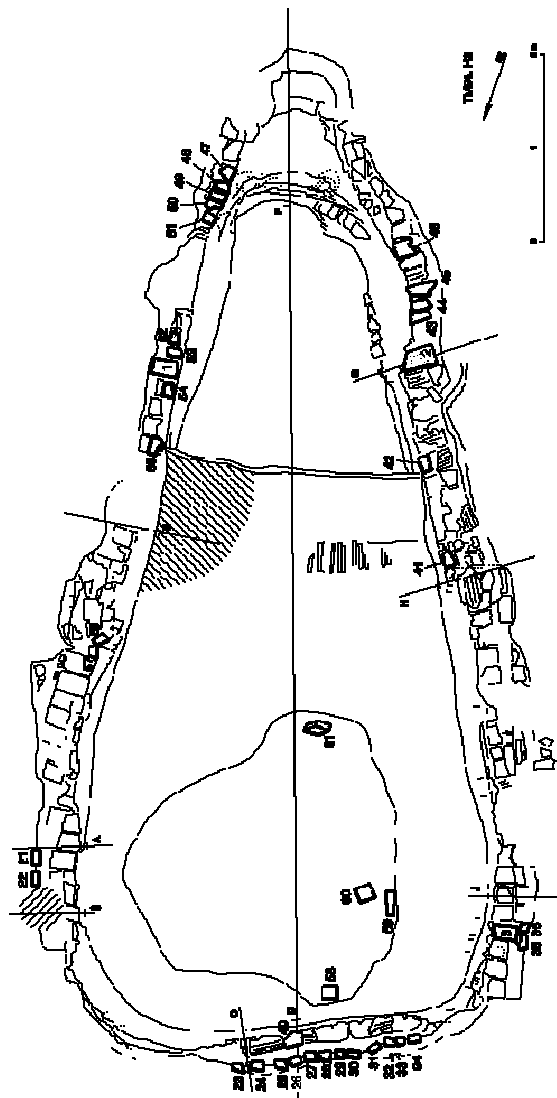
El abandono se ha datado por contrastes arqueológicos entre 1450-1500 AD. Debido a la falta de información arqueológica precisa se ha añadido un siglo a esta datación del abandono.

H3B (PATJ)

Tipo de estructura y contexto: Horno de dimensiones excepcionales (unos 5 m de largo y unos 3 m de profundidad) en muy buen estado de conservación. Construido a base de ladrillos. Existen dos fases de la estructura, la segunda de ellas, más moderna, ha sido estudiada en este trabajo.

Foto:

Plano de la estructura:



Número de muestras y tipo de material:

N	T	N	T
40	B	51	B
41	B	52	B
42	B	53	B
43	B	54	B
44	B	55	B
45	B	56	B
46	B	57	M
47	B	58	M
48	B	59	M
49	B	60	M
50	B		

Tabla: Número de muestra N y tipo de material T de las mismas: B, ladrillo, M, mortero

Criterios de datación arqueológico:	
Cerámica	No
Monedas	No
Estratigrafía y cronología relativa	Se ha estudiado la segunda fase del horno
Otros métodos:	
C14	Si
Termoluminescencia	No
Dendrocronología	No
Datación del abandono: 1429-1611 AD	

CABRERA D'ANOIA

Arqueólogos responsables de la excavación: J. Thiriot, I. Padilla

Fecha de la excavación: Julio 1989

Contexto arqueológico:

El contexto arqueológico de los hornos estudiados (CDAU, H, P y U) puede encontrarse en el artículo citado a continuación. La datación de los hornos está basada en estudios de C14.

Bibliografía: Comunicación oral con Jacques Thiriot

Datation par le radiocarbone des ateliers de potiers médiévaux de Cabrera d'Anoia en Catalogne, I. Padilla, J. Thiriot, J. Evin y J. Mestres. *Actes du colloque C14 Archéologie*, 1998, 419-423.